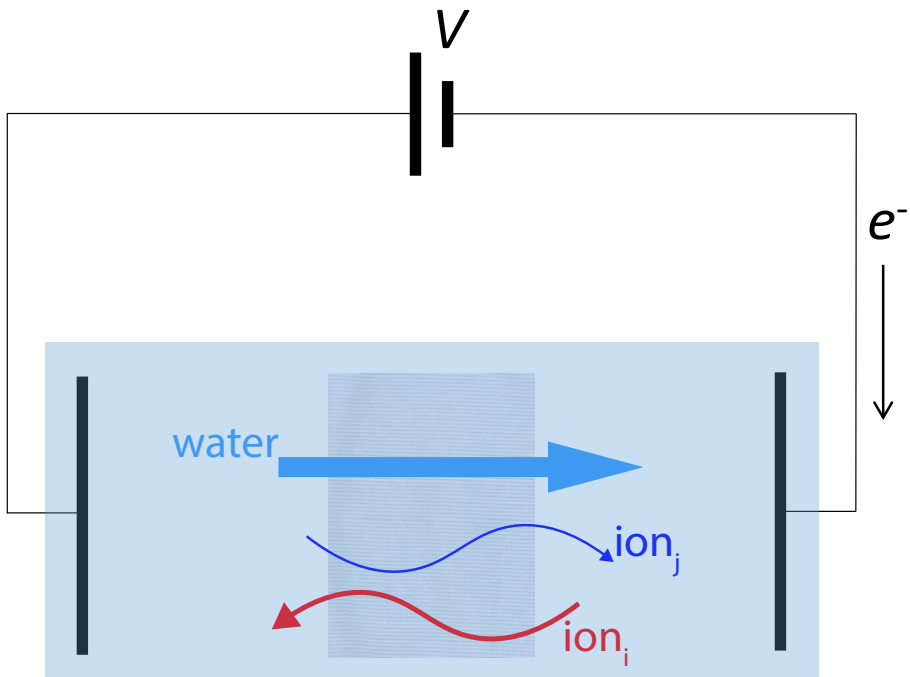


Physics of Electrochemical Processes



P.M. Biesheuvel and J.E. Dykstra

Physics of Electrochemical Processes

P.M. Biesheuvel and J.E. Dykstra

Copyright © 2020 by P.M. Biesheuvel and J.E. Dykstra

All rights reserved.

Version May 16, 2023.

The most recent version can be downloaded from:

<http://www.physicsofelectrochemicalprocesses.com>

ISBN 978-90-9033258-1

This book can be cited as:

Biesheuvel, P. M., & Dykstra, J. E. (2020). *Physics of Electrochemical Processes*.

<http://www.physicsofelectrochemicalprocesses.com>

Contents

I	The Electrical Double Layer	13
1	The extended Frumkin isotherm for the EDL in intercalation materials	21
1.1	The equation of state for gases	22
1.2	The equation of state for a charged film	26
1.3	The Frumkin isotherm for molecular adsorption	27
1.4	The extended Frumkin equation for the EDL structure in intercalation materials	30
1.5	Extensions of the extended Frumkin isotherm for multi-ionic solutions or multi-region electrodes	32
2	The Donnan model: the EDL in small pores	35
2.1	Introduction	36
2.2	Simplified Donnan model	36
2.3	Donnan model including Stern layer	41
2.4	Donnan model for electrodes with chemical charge	43
2.5	Donnan model with ionizable chemical charge	44
2.6	The EDL at the interface between two porous layers of opposite charge . . .	45
2.7	Donnan equilibrium for a mixture of cations: ‘anomalous’ Ca^{2+} -adsorption in collagen	47
2.8	Donnan equilibrium at the membrane/solution interface	49

3	The EDL for a planar surface: The Gouy-Chapman-Stern model	55
3.1	Introduction	56
3.2	The Gouy-Chapman-Stern model	58
3.3	Incorporation of ion volume in the GCS model	70
3.4	Incorporation of polarization in EDL models	75
3.5	EDL structure in solid polymer with fixed charge	76
3.6	The GCS model for mixtures of salt	77
3.7	Surface ionization in the GCS model	79
4	Ion volume effects in electrochemical processes	91
4.1	Introduction	92
4.2	Effect of ion volume on the partitioning into a porous medium	92
4.3	Ion-ion Coulombic interactions in electrolytes	100
5	The energy of an electrical double layer	107
5.1	Wetting of titania: The free energy of an EDL with ionizable surface charge	108
5.2	Electrowetting: The EDL surface pressure on an electrode	112
5.3	The harvesting of electric energy from EDL changes due to the motion of electrical wires	124
6	The interaction forces between colloidal particles	131
6.1	Introduction	132
6.2	Colloidal interaction of particles with a fixed surface charge	135
6.3	Theory of colloidal interaction for ionizable materials	141
6.4	Theory of colloidal interaction for surfaces that are very near - the Donnan limit	146
6.5	Donnan theory for hetero-interaction	147
II	Transport Phenomena & Reactions	153
7	Solute Transport	157
7.1	Diffusion and dispersion towards a surface	158
7.2	Ionic current and transport and transference numbers	165
7.3	General balances for binary electrolytes	172
7.4	Boundary equations for binary salts	176
7.5	Simplified solutions for a symmetric 1:1 salt	180

7.6	Electrolytic conduction across a planar channel	184
7.7	Transient solute transport to an interface for electrolyte solutions	190
7.8	From a force balance to the Nernst-Planck equation	194
8	Electrokinetics	205
8.1	The Navier-Stokes equation for flow in charged porous media	206
8.2	Flow of fluid across a charged membrane	214
8.3	Osmosis and electro-osmosis in charged membranes	224
8.4	Mechanical forces between colloidal particles and charged media	237
9	Heating and cooling in electrochemical systems	245
9.1	Introduction	246
9.2	The heat balance	247
9.3	The current density in an electrolyte bulk phase and membrane	248
9.4	Heat production due to current in a steady-state EDL	250
9.5	Heat production in a capacitive electrode	251
9.6	The relation between the heat production rate and the free energy of an EDL	258
10	Combined mass transport and chemical reactions	261
10.1	Introduction	262
10.2	Theory of ion transport and acid-base reactions	265
10.3	Example calculation: chemical adsorption of CO ₂ in water with MEA	272
10.4	Example calculation: ion transport with multiple pairs of ionizable ions	276
III	Membrane Processes for Water Desalination	281
11	Reverse Osmosis and Nanofiltration	291
11.1	Introduction	292
11.2	One-dimensional model of pressure-driven membrane separation for neutral solutes	293
11.3	RO module calculation for neutral solutes	303
11.4	1D RO module calculation in convection-only limit	306
11.5	2D module calculation for RO and NF	309
11.6	RO and NF with charged membranes - Ion transport inside the membrane	311
11.7	RO and NF with charged membranes - analytical solutions	313

12	Electrodialysis	321
12.1	General introduction to electrodialysis	322
12.2	The Sonin-Probstein approach for electrodialysis	327
12.3	1D model for an ED cell for non-unity current efficiency	333
12.4	2D model for an ED cell for non-unity current efficiency	340
12.5	Selectivity in electrodialysis with a three-ion mixture	344
IV	Electrode Processes	347
13	The difference between Faradaic and non-Faradaic electrode processes	357
14	Electrode Kinetics	367
14.1	Introduction	368
14.2	The Nernst equation, role of EDL structure, and surface transport	370
15	Porous electrodes	373
15.1	Introduction	374
15.2	Faradaic reactions in a porous electrode	376
15.3	Porous electrodes for water desalination	391
16	Combined Faradaic and non-Faradaic (capacitive) processes	397
16.1	Introduction	398
16.2	A single electrode	398
16.3	A Faradaic electrode going to steady-state	400
16.4	Two capacitive electrodes with Faradaic charge loss	403
V	Bio-electrochemical processes	407
17	Ion transport in bioelectrochemical systems	411
17.1	Ion transport in bioelectrochemical systems	412
17.2	Ion transport in ion-exchange membranes	414
17.3	Mass balances for the anolyte and catholyte compartments	417
17.4	Electrode reactions	418
17.5	Example of a membrane-electrode assembly with gas evolution	419

18 Transport and reactions in electroactive biofilms	427
18.1 Introduction	428
18.2 Mass transport across the biofilm	429
18.3 Oxidation of substrate in the bacteria	432
18.4 Electron transfer to the matrix of conductive pili	434
18.5 Charge transport to the anode	435
19 Redox reactions in environmental chemistry	437
19.1 Introduction	438
19.2 Calculating the redox potential of a solution	439
VI Methods	443
20 Overview of electrochemical water desalination	445
20.1 Introduction	446
20.2 Core technologies for electrochemical water desalination	447
20.3 Non-electrochemical methods of water desalination	452
20.4 Non-core methods of water desalination	452
21 Numerical methods in electrochemical processes	455
21.1 Introduction	456
21.2 Solving a set of algebraic equations for a steady state transport problem	458
21.3 Solving a dynamic problem	465
21.4 Including Acid-Base equilibria	468
22 Experimental methods	471
22.1 Membrane Potential	472
22.2 Polarization curve for Faradaic processes	477
22.3 Galvanostatic titration for capacitive processes	478
22.4 Cyclic Voltammetry	481
22.5 Electrochemical Impedance Spectroscopy (EIS)	483
VII Bibliography	485

Preface

The fields of electrochemistry and electrochemical engineering as scientific disciplines have a long tradition, dating back about two and a half centuries (Laidler, 1997). A two-volume book titled “Electrochemistry: History and Theory” by W. Ostwald, with over 1000 densely printed pages, was published in Leipzig in ... 1896!

In addition to its long history, there is much active research in our field which shapes a vibrant scientific community, of importance to society, and positioned at the forefront of modern developments in energy, sustainability, and hightech devices. Methods of electrochemistry play important roles in understanding many processes in physiology and microbiology as well.ⁱ

Much relevant scientific literature and many important textbooks have been published over the years describing key aspects of electrochemistry, and these sources are of significant importance to new students and specialists alike. We hope that our book is a relevant addition to this important body of literature.

In our book we focus on certain aspects of electrochemical processes more than on other aspects. Our general aim and focus is captured by the words in the title, ‘physics’ and ‘processes’. These words highlight that our aim is to describe the underlying physical principles of transport, adsorption, and reaction kinetics in electrochemical processes.

Because of our personal background and interests, the theoretical level we consider is that of the ‘mean field’, which is a modeling philosophy where physical reality is described using

ⁱWhen we use the term ‘electrochemistry’ in this book, we also refer to ‘electrochemical engineering’ and vice-versa.

continuum equations, formulated as mass balances and flux equations, based on averaged-out properties such as concentrations, pressures, and various potentials. In our experience, mean field theories are extremely powerful in describing physical reality, and their study provides extensive insight in the problem at hand. Mean-field theories are very flexible and can always be adjusted to incorporate knowledge from experiments, from other theories, and from detailed (theoretical) analysis at atomistic scales.

In our book we describe for transport processes in and around electrodes, and membranes, combined with models for the electrical double layer. Typical elements of the theory are the Poisson-Boltzmann equation (or, electroneutrality), mass and charge balances, and ion flux equations based on force balances. We focus on electrolytes where the solvent is water, i.e., we study solutions of water containing dissolved molecules such as ions. Ions can be fully dissociated and unreactive, or associate with other ions to ion pairs, or (de-)protonate and become neutral.

The theoretical models often assume the solute molecules or ions to be ideal ‘point charges’, but the volume of hydrated ions is also addressed in several chapters.

It is important to explain how the water (or other solvent) is described in our book. In brief, water is the incompressible continuum fluid that fills up all space between (hydrated) ions and other dissolved solutes and structures. Thus, in the theories that we use, the water has no molecular structure of any importance except for its viscosity (relevant for transport) and the dielectric constant (relevant in some EDL theories). Thus, in this book, the molecular volume of a water molecule, or the concentration of water, is not part of the theory. Related, the theories in this book are not based on molar fractions, x , of water, or of ions, in starting equations for thermodynamics or transport. Instead, the theory is based on *concentrations* of ions and other solutes, each of which may or may not have a non-zero molecular volume. The molecular volume of an ion includes the solvent molecules that are tightly bound in the ion’s solvation shell. Thus, at various points, right from the start, the continuum water is treated differently from how we treat ions and other solutes. Thus, in summary, there are dissolved solutes such as molecules and (hydrated) ions, and there are also larger (colloidal) particles, and we often have a porous medium through which all solutes and water flow. The water is the continuum fluid occupying all space in between these entities and structures.

A technical clarification of choices of certain words and mathematical conventions is provided at the very end of this book, starting at p. 507.

Part I

The Electrical Double Layer

The electrical double layer (EDL) is at the heart of many topics in this book, and therefore several chapters in this book discuss the structure of the EDL.

The EDL is a concept which has both a structural (microscopic) side to it, and an experimental (observable, phenomenological) side. The structural side refers to how we think the EDL ‘looks like’, how ions and other charges are distributed within the EDL and what are the associations between them. On the other hand, the experimental side refers to what we can measure about the EDL, its behavior that is of importance in a description of an electrochemical process, such as the EDL capacitance, and the dependence of ion adsorption on EDL voltage. These two aspects can be well distinguished but in a discussion of the EDL one often switches repeatedly between these two perspectives.

The structural part of the EDL concept relates to the concentration profiles of charge carriers (ions, electrons) inside the EDL, and the details of charge separation between different regions inside the EDL, where we have an excess of positive charge in one region and an excess of negative charge in another region. This charge distribution, or separation, results in a voltage difference across the EDL.

An EDL can form when two or more phases (materials) come in contact with ions being mobile in at least one phase, i.e., an electrolyte. The other phase can also have mobile charge carriers (ions, electrons), or only provides a surface to which ions can adsorb. This surface will then be part of the EDL. Thus there can be multiple bulk phases coming into contact and forming an interface, which is the EDL, or one bulk phase and a surface.

Let us briefly discuss the word *interface*. We use it in this book to describe the layer (of unknown thickness) where two phases or materials come in contact and an EDL forms. *Inside* the EDL there are regions of positive charge and negative charge (which microscopically can often be associated with one of the phases or materials that are in contact). Thus the word interface is not used in the sense of a perfect ideal 2D ‘mathematical’ *surface* or plane, i.e. a plane or surface without thickness, which tracks for instance the outer positions of the atoms in a piece of metal. We do not use the word interface in this sense of an ideal plane, because it turns out that various aspects of an EDL are better understood when the word interface is taken as equivalent to the EDL, referring to the entire layer that encompasses regions with positive and negative charge, with electroneutral bulk phases adjacent to the EDL. Instead, the idea of an ideal surface is useful in constructing a microscopic theory, for instance for ion and electron distributions in the EDL, because we can for instance state that electronic charge can only come up to a certain surface and not beyond.

The difficulty with the concept of an ideal plane or surface also shows up with EDLs formed in porous materials: is the surface to be drawn around such a porous structure, or wrapped around the atomic structure of the solid constituents inside the crystal lattice? Thus,

the concept of a surface or plane is not very obvious to define. This is why 'interface' is more useful – and it is synonymous to the EDL as a whole.

If we look at the charge of an EDL, we know that the EDL is a region which as a whole is electroneutral, but includes two or more regions of different charge. Across the EDL a voltage difference develops. With two such regions, 'the charge of the EDL' then refers to the charge in one of those regions, with the charge in the other region of the same magnitude but of opposite sign.

An EDL forms in two types of situations:

- (I) An EDL forms at the interface between two bulk (volumetric) phases, where both these bulk phases participate in the EDL structure, and at least one of the ions can move between the two bulk phases, or electrons can do that.
- (II) The same as situation I, but without ions or electrons transferring between the two bulk phases. i.e., there might be two bulk phases that form an interface (the EDL) but none of the ions, and neither the electrons, are able to transfer from one to the other bulk phase. Or, an EDL forms at the interface between one bulk (volumetric) phase, and a material of which the surface participates in EDL formation (for instance the surface of a silica particle or protein molecule), or, a material will simply in its totality become part of the EDL, such as the polymer network of a polyelectrolyte gel. In these latter cases, there is no second bulk phase 'in the background'.

The two categories, I and II, described above, are explained in more detail in the preamble to part III on page 349.

—

An EDL forms when any pair of the following types of phases is brought in contact:

1. A metal, or other electron-conducting phase, which stores and transports electronic charge;
2. A solid material which contains chemical groups on its surface that carry a charge. This class includes many types of materials, ranging from globular protein molecules, to virus nanoparticles, to oxidic inorganic surfaces such as silica and alumina;
3. A liquid electrolyte, for instance an aqueous solution, which is a phase which allows the transport and storage of ions;
4. A solid electrolyte, which can be the ion-conducting materials used in certain fuel cells, or as another example the solid salt of AgCl or AgI;
5. A charged polymer network of which the pores fill up with electrolyte. Ion-exchange membranes have a more dense and rigid network, while the network of a polyelectrolyte

gel is more dilute and can expand and contract;

6. An intercalation material that allows the absorption and free movement of ions (often cations) through the (often solvent-filled) interstitial pores that are inside the lattice structure of the material. The intercalation materials can store electronic charge in their crystal lattice structure.

When two such phases or materials are brought in contact (also when both are from the same class), an EDL is formed. Inside the EDL there will be regions that are positively charged, and regions that are negatively charged. The EDL is overall electroneutral, and thus the charges in the two or more regions sum up to zero. With some exceptions that we discuss below, in the EDL all ions and other solutes are in chemical equilibrium in the EDL, from one 'end' of the EDL to the other. Thus their chemical potential is the same at each position in the EDL. This requirement is generally met because EDLs are very thin, no more than a few nm in most cases, and as a consequence concentrations quickly equilibrate, relative to transport and reaction rates in the overall electrochemical process. Thus, inside this type of EDL, profiles in potential and concentration can be calculated as if there is no transport, thus we have local chemical equilibrium. Because of chemical equilibrium, concentrations at one position in the EDL (or just on the outside) directly relate to concentrations at another position in the EDL (or just on the other side). Because of this equilibrium, the EDL can then often be treated separately from transport processes outside this very thin layer, in the charge-neutral bulk solutions (or 'reservoirs') where transport takes place over distances of microns, millimeters, and more. In an EDL we also have mechanical equilibrium, which implies that the change in osmotic pressure across the EDL equals the change in hydrostatic pressure. (Thus, a total pressure, defined as the difference between hydrostatic and osmotic pressure, is invariant across the EDL.) So there can be current running across an EDL, and ion transport, but these flows are low enough for the structure of the EDL to be unperturbed: the structure of the EDL is the same as if there is no current.ⁱⁱ An interesting situation is when in the EDL reactions take place that have a finite rate, such as an electrode reaction which involves the combination of an ion with an electron to another ion (or neutral solutes). Even though this reaction is off-equilibrium, with the reacting species not at equilibrium with one another, the entire structure around the reaction plane, is an EDL where ions in the EDL are at chemical equilibrium with those in an adjacent bulk solution. Another important situation is when we have a porous material of macroscopic dimensions, such as a porous electrode or ion-exchange membrane, all in contact with an external electrolyte phase. When

ⁱⁱOf course the flows change conditions right next to the interface, and this changes properties such as the EDL charge, or ion adsorption in the EDL, but the equations that describe the EDL remain the same, and that is meant with 'the EDL structure stays the same.'

this structure is at equilibrium with an outside solution (so no flows through the material, no changes in time), then the entire porous structure and the boundaries, can be described as an EDL (for instance for titration studies). Now, when there is flow of ions and solvent through such a porous medium, along a coordinate z , then the situation changes. For a porous medium where all transport pathways are of nanoscopic dimensions, such as for an ion-exchange membrane, or a membrane for reverse osmosis, then on the outsides of the membrane we have Donnan equilibrium (an EDL structure), the same as described above. Inside the membrane at each z -position, there is a kind of EDL structure where locally ions and wall charge are in chemical equilibrium with concentrations in a *virtual solution*. Concentrations in the virtual solution, $c_{v,i}$, change gradually from one to the other end of the membrane. During transport, with $c_{v,i}$ a function of z , we do not refer to the inner structure of a membrane as an EDL, because this structure is described by transport equations. Only when $c_{v,i}$ is invariant across the membrane is the entire structure an EDL.

When the porous layer is connected from one end to the other by larger transport pathways, such as for a porous electrode, with porous particles of electrode material (carbon, intercalation material) ‘lining’ these pathways, or ‘macroscopic pores’, then also with flow through these pores, ion adsorption, pressure, charge, and voltages, in each porous particle are described by an EDL.ⁱⁱⁱ The structure of the EDL is the same at each z -position, i.e., the *equations* are the same, though the actual value of charge, etc., will be dependent on z . So for the nanoscopic porous material discussed in the previous paragraph, we do not have an EDL inside the layer when there is transport across it, while we do for a porous material with larger (locally charge neutral) transport pathways, such as for a porous electrode, when the particles that form the porous electrode each by themselves have an equilibrium structure.

—

In the above, examples were provided of an EDL at the interface between two bulk phases, and inside the EDL it was implied in some cases that there are two regions of opposite charge, because overall the EDL is charge-neutral. However, it is also possible that an EDL forms at the interface between three or more phases, for instance when two metals touch while submerged in water with salt. Or inside a fuel cell electrode it is possible that electrolyte, catalyst, conducting substrate, and gas phase, are in contact at distinct points.

ⁱⁱⁱAt least, when inside these particles transport does not change the EDL structure, for instance because the particles are small enough, thus across its volume there are no gradients in concentration. But when inside these particles transport limitations (between its outer surface and more inner regions) influence the distribution of ions and charge, then such an individual particle is not (described by) an EDL, see West *et al.*, “Modeling of porous insertion electrodes with liquid electrolyte,” *J. Electrochem. Soc.* **129**, 1480–1485 (1982).

It is furthermore possible that the EDL has more than two regions which are charged. For instance inside a pore in a porous carbon particle, charged surface groups are attached to the carbon surface, while the pore is filled with ions and water. Thus we have a region of electronic charge in the carbon, (chemical) surface charge on pore walls, and a region of ionic charge in the electrolyte that fills the pores. Even though we now have more than two charged regions in the interface, still the term EDL is used, because from an experimental perspective, the same macroscopic information can be derived such as capacitance, salt adsorption, etc. Instead, details of the theoretical models are always up for discussion, such as the question of whether there are two or three or more charged regions.

We now turn our attention to the experimental (observable) side of the EDL. Here, focus is on the relations between various attributes of an EDL that are measurable, such as charge, voltage, ion adsorption, and surface pressure. For instance, when applying a force to squeeze a gel-like charged polymer material, filled with water and ions, thereby bringing charged polymer groups closer together, we increase the internal energy of the EDL, and this opposes the applied force, and that force can be measured. Another example is when charged molecules are adsorbed at the interface of a gas and liquid, and they are squeezed together by reducing the available surface area. And in capacitive electrode processes we can store ions and charge, depending on the electrode voltage (an electrode is a special type of EDL). We can derive data for the capacitance, which is the change in electrode charge over electrode potential. This property, often with unit Farad, is a key feature of a capacitive electrode process.

Important is the realization that we can record these data of voltage, charge, capacitance, and pressure, and in this way describe the performance of an EDL (the experimental side of the EDL), and we can do so irrespective of the chosen structural theory of what are the chemical, microscopic or atomistic details of what we believe might take place exactly inside the EDL. An example is that for certain electrodes we can calculate a capacitance by measuring the electrode charge and voltage. And we can then conclude that this electrode (EDL) is capacitive, and we can come to that conclusion irrespective of what is the proposed theory for the electrostatic and chemical mechanism of how ions and charge are stored (and that microscopic theory can always change). Data of capacitance can be used to construct or test a microscopic EDL model for the storage of ions and charge as function of electrode voltage.

Also for non-capacitive electrode processes an EDL forms at the interface between electrode and electrolyte, with a separation of charge between different regions inside the EDL, and resulting profiles of ions and electrons. However, it is much more difficult to obtain experimental data of this EDL structure, because the electrode does not have a capacitance.

These non-capacitive, i.e., Faradaic, electrodes are not described by an extended isotherm (see Ch. 1), but a more simple theory suffices to describe key electrode features, relating the voltage across the electrode to the concentrations of the ions that participate in the electrode reaction (concentrations just outside the electrode). This is the Nernst equation used in Faradaic processes (which are processes that can run forever because they do not store charge or ions in the electrode) when the electrode reaction has sufficiently fast kinetics. In the Nernst equation there is no dependence on stored amount of charge or ions in the EDL, which is the ‘additional electrical variable’ that defines a capacitive electrode process, as identified by Mohilner (1966).

In the preamble to Part II, starting on p. 349, we continue our discussion of different types of EDL structures (theories for the EDL).

Let us end with some words by Mohilner (1966):

Mohilner (1966) on the EDL: [The e]lectrical double layer is a term used to denote the arrays of charged particles and/or oriented dipoles believed to exist at every material interface [such as] interfaces formed by metals in contact with electrolyte solutions.

Strictly speaking, EDL is a misnomer, in view of modern ideas about the structure of the interfacial region. A more descriptive term would be electrochemical multilayer, since (a) the forces which lead to its formation include, in addition to long-range electrostatic forces, shorter-range forces of types usually considered chemical, and (b) the interfacial region consists of not two, but at least three, and sometimes more, distinct subregions or layers. However, the old name has persisted for so long and has been used so widely in the electrochemical literature that an attempt to change it now would lead to confusion. Hence EDL will refer to the interfacial region formed by a metal electrode dipping into an electrolyte solution, regardless of the actual structural complexity of the phase boundary.

The extended Frumkin isotherm for the EDL in intercalation materials

The extended Frumkin isotherm is one of the most elegant electrical double layer (EDL) models, and we show how it closely relates to the classical Van der Waals equation of state. We demonstrate how this isotherm accurately describes the capacitance of intercalation materials, and discuss extensions to multi-cation mixtures and materials with a distribution of sites with different adsorption energies.

Models for the electrical double layer (EDL) in capacitive electrodes relate three properties: solution conditions (ion concentrations in solution), adsorbed amounts of ions and charge, and the EDL potential, i.e., the change in (electrical) potential across the interface (i.e., across the electrode, across the EDL), which is the potential (voltage) in the electron-conducting bulk phase (e.g., metal) near the interface, relative to the potential in the nearby bulk electrolyte phase (solution). This difference is the electrode potential.

EDL models for capacitive electrodes are equilibrium models and we can also interpret them as extensions of adsorption isotherms, extended because they include the electrode potential as a variable. They are also an equation of state (EOS) because via measurable capacitances they describe the dependence of charge density and concentration on pressure and voltage.

In this chapter we derive and use one particular EDL model, the extended Frumkin isotherm. This is a very elegant EDL model and it also has practical relevance, because it accurately describes cation adsorption in intercalation materials, which are promising materials for water desalination by capacitive deionization (CDI). As an introduction to the extended Frumkin equation, we start with the Van der Waals equation of state.

1.1 The equation of state for gases

One of the most successful equations of state (EOS) for gases is the classical Van der Waals (VdW) equation which describes the pressure of a gas, \bar{P} , as

$$\left(\bar{P}^{\text{VdW}} + \frac{a}{v^2}\right)(v - b) = RT \quad (1.1)$$

where a is a force of attraction between molecules, b a measure of the molecular volume, and v a volume available per molecule, i.e., an inverse concentration, while R and T have their usual meaning of the gas constant and temperature (in K). We use an overbar notation to indicate that pressure is dimensional, i.e., it has a unit, which in this case is Pa. We can rearrange Eq. (1.1) to

$$\bar{P}^{\text{VdW}} = \frac{cRT}{1 - bc} - ac^2 \quad (1.2)$$

where we implemented that $v = 1/c$, with c the concentration of the (gas) molecules. Eq. (1.2) shows that the pressure of a VdW gas has an ideal part, $\bar{P}^{\text{id}} = cRT$ (which we obtain from Eq. (1.2) when we insert that $a = b = 0$), modified by a volume exclusion effect (often called an ‘excess’ term, abbreviated as ‘exc’), related to the term $1 - bc$, and in addition there are intermolecular attractions. The strength of the attraction between the molecules is described by the parameter a . Because of this last part, when $a > 0$ the VdW equation predicts that

phase separation is possible, with a gas and liquid coexisting. The same can happen in the (extended) Frumkin isotherm that we discuss later on in this chapter, if the attraction between adsorbed species is high enough.

In a solution, the chemical potential of a solute, $\bar{\mu}_i$, relates to osmotic pressure, $\bar{\Pi}$, by the Gibbs-Duhem (GD) equation, which is given by

$$\frac{\partial \bar{\Pi}}{\partial c} = \sum_i c_i \frac{\partial \bar{\mu}_i}{\partial c} \quad (1.3)$$

where c is a summation over all concentrations, and differentiations with respect to c are at constant composition of the solution (ratios between concentrations fixed).ⁱ It is not easy to derive this equation for a mixture. But for a single type of solute, this derivation can be easily made, because in that case $c = c_i$. For a single component, the GD equation follows from combining how the chemical potential relates to the free energy density, f , by $\bar{\mu}_i = \partial f / \partial c_i$, and how osmotic pressure relates to f according to $\bar{\Pi} = -\partial (f \cdot V) / \partial V = -f + c_i \cdot \partial f / \partial c_i$.ⁱⁱ In this differentiation, the total number of molecules, N_i , in the volume V , is fixed ($N_i = c_i V$); thus, in this derivation we make the replacement $dV = -N_i / c_i^2 dc_i$. We now arrive at $\bar{\Pi} = c_i \bar{\mu}_i - f$, and if we again take the derivative with respect to c_i , and again insert $\bar{\mu}_i = \partial f / \partial c_i$, we arrive at

$$\frac{\partial \bar{\Pi}}{\partial c_i} = c_i \frac{\partial \bar{\mu}_i}{\partial c_i} \quad (1.4)$$

which is the Gibbs-Duhem equation for a solution containing a single solute at concentration c_i . In a gas, pressure \bar{P} functions similarly to what is the osmotic pressure $\bar{\Pi}$ in a solution. Thus $\bar{\Pi}$ in Eq. (1.3) can be replaced by \bar{P} to describe the thermodynamic properties of a gas phase. In a solution, osmotic pressure $\bar{\Pi}$ is not like a hydrostatic pressure in that it can be measured directly as a force on an external object, but it is solely a ‘mathematical’ function of solute concentrations. Only under certain conditions will it lead to a hydrostatic pressure, for instance when a membrane that blocks some solutes is placed between two solutions of unequal solute concentration (J.L. Anderson and D.M. Malone, “Mechanism of osmotic flow in porous membrane,” *Biophys. J.* **14**, 957–982, 1974).

If we first analyze the ideal gas law for a system with a single component, $\bar{P}_{id} = RTc_i$, and use the GD equation, Eq. (1.4), what do we arrive at? Inserting the ideal gas law and

ⁱHere the GD equation is written with the ‘overbar’-sign, which is used for dimensional pressures and potentials.

However, Eq. (1.3) equally applies when non-dimensional pressures and energies are used.

ⁱⁱIn a mixture, in the derivation of μ_i , we differentiate f with respect to c_i while we keep all other concentrations constant. For osmotic pressure, in case of a mixture, when we do the differentiation $\partial f / \partial c$, the composition is kept the same (i.e., the ratios between the concentrations of all solutes stay the same).

making the differentiation on the left we arrive at

$$RT = c_i \frac{\partial \bar{\mu}_i}{\partial c_i} \quad (1.5)$$

and then integrating from c_{ref} to c_i , and from $\bar{\mu}_{\text{ref},i}$ to $\bar{\mu}_i$, we obtain

$$\bar{\mu}_i = \bar{\mu}_{\text{ref},i} + RT \ln (c_i/c_{\text{ref}}) \quad (1.6)$$

which immediately provides us with a reference term (relevant for chemical reactions) and the ideal entropy-term. The only assumption was the ideal gas law, and this derivation equally applies to molecules in a gas, and to solutes in a solvent. Thus, the ideal gas law is all we need to derive the entropic contribution to the chemical potential, $\ln c_i$, and we do not need a derivation based on the entropy of a lattice of sites that are occupied or not, Stirling's equation, etc.

For the Van der Waals equation, if we apply Eq. (1.4) we obtain from Eq. (1.2)

$$\mu^{\text{vdW}} = \mu_{\text{ref}} + \ln c/c_{\text{ref}} + \ln \frac{bc_{\text{ref}}}{1-bc} + \frac{bc}{1-bc} - 2a'c \quad (1.7)$$

where we introduce the non-dimensional chemical potential μ_i , which is the dimensional chemical potential, $\bar{\mu}_i$, divided by RT . The attraction term is now $a' = a/RT$ with unit m^3/mol . In Eq. (1.7) the third and fourth terms together relate to volume exclusion, and unfortunately they do not have a clear physical interpretation. This relates to the empirical manner in which the Van der Waals EOS was derived.

It is therefore better to use the Langmuir and Frumkin equations of state, which are models that have a microscopic, atomistic, background, namely they assume that there is a finite number of lattice sites that can be occupied or not. These two models are closely related, with Frumkin an extension of Langmuir by including a term describing attraction between molecules. For the chemical potential, for the Frumkin equation of state, we obtain

$$\mu^{\text{Frumkin}} = \mu_{\text{ref}} + \ln c/c_{\text{ref}} - \ln (1 - \nu c) - 2a'c \quad (1.8)$$

where ν is the molecular volume (in m^3/mol) in the context of such a lattice model, not to be confused with the factor ν in Eq. (1.1)! For the Langmuir equation, the chemical potential is also given by Eq. (1.8) but with $a' = 0$. In Eq. (1.8) we have a reference term, an ideal term, the Langmuir excess term due to volume exclusion, and an attraction between molecules. In Eq. (1.8), the third term, which describes volume exclusion, has a logical appearance, related to a derivation in which the chemical potential of a solute is $\ln c^*/c_{\text{ref}}$ with c^* the concentration per *available*, not total, volume. And the available volume, relative to the total, is $1 - \nu c$, see also p. 50. Thus, $c^* = c/(1 - \nu c)$.

Based on Eq. (1.4) we can rewrite Eq. (1.8) to a pressure according to the Frumkin equation of state (EOS), or according to the Langmuir equation of state ($a=0$), resulting in

$$P^{\text{Frumkin}} = -v^{-1} \cdot \ln(1 - vc) - a'c^2 \quad (1.9)$$

where pressure P relates to pressure \bar{P} according to $P = \bar{P}/RT$. The dimension of pressure P is mol/m^3 , the same as for concentration. Pressures P can always be multiplied by RT to obtain a pressure, \bar{P} , with the conventional unit of Pa. (We use this convention for pressures P and Π throughout this book.) Eq. (1.9) can be rewritten to

$$P^{\text{Frumkin}} = P^{\text{id}} + P^{\text{exc}} + P^{\text{int}} \quad (1.10)$$

where ‘int’ refers to a molecular interaction (e.g., attraction), with $P^{\text{id}} = c$, and $P^{\text{int}} = -a'c^2$. The excess pressure, which relates to the volumes of the molecules, is given in the Frumkin equation by

$$P^{\text{exc,Frumkin}} = -v^{-1} \cdot \ln(1 - vc) - c = 1/2vc^2 + 1/3v^2c^3 + O(c^4). \quad (1.11)$$

It is interesting to compare the volumetric part of the Van der Waals EOS, with that in the Langmuir/Frumkin EOS. We obtain the best correspondence if we relate the factor b in the VdW EOS to the molecular volume v in the Langmuir/Frumkin equation according to $v=2b$. Then the second virial coefficients match (i.e., the EOS matches up until the term c^2 in pressure), though for higher concentrations Eq. (1.9) increases faster than the VdW EOS.

The chemical potential according to the Frumkin EOS, Eq. (1.8), is the basis of the derivation of the Frumkin isotherm in §1.3, and later on for the extended Frumkin isotherm for intercalation materials in §1.4.

Volume effects in the Carnahan-Starling equation of state. To describe volume (excess) effects more accurately than in the VdW or Langmuir/Frumkin EOS, the Carnahan-Starling (CS) EOS is best used. The CS EOS very accurately describes pressures in a ‘hard sphere fluid,’ i.e., a gas in which we describe all molecules as hard spheres. In the CS equation the term $1/(1 - bc)$ of Eq. (1.2) is then replaced by $(1 + \eta + \eta^2 - \eta^3)/(1 - \eta)^3$ where η is the volume fraction occupied by the (gas) molecules, given by $\eta = vc$, where v is the ‘real’ molecular volume of a solute or gas molecule. Now we can elegantly separate the ideal contribution, $P^{\text{id}} = c$, from the excess contribution to the pressure, which then becomes

$$P^{\text{exc,CS}} = \frac{2\eta(2 - \eta)}{(1 - \eta)^3} c = 4vc^2 + O(c^3).$$

Comparison of these equations shows that to make the VdW EOS match the CS EOS, at least in the dilute limit, the parameter b in the VdW equation must be interpreted as $4\times$ the molecular volume, i.e., $b = 4v$. And thus, in the dilute limit, the Langmuir equation predicts an $8\times$ lower pressure effects because of volume exclusion than the Carnahan-Starling equation, if we would treat v and v as equivalent.

The CS model is an extremely powerful starting point because it can be extended in many ways, for instance when the molecules, instead of being considered as spheres, are better described as doublets or triplets (or as a long string of connected spheres). The CS EOS can also be extended to mixtures of molecules of all kinds of sizes and shapes, see the next section, and see Ch. 4. And finally, the equation allows for all of these interactions to take place inside a porous medium. The porous medium we describe as if it is built from a large array of connected beads.

1.2 The equation of state for a charged film

Next we apply these equations of state to the problem of a charged film. Here, charged molecules are adsorbed in an interface (liquid-gas, or liquid-liquid) and because they are mobile *within the interface* they exert a surface pressure, P_s , i.e., a pressure directed along the surface (unit $\text{J/m}^2 = \text{N/m}$), similar to how a gas exerts a pressure volumetrically (unit $\text{Pa} = \text{J/m}^3$). For the pressure of these molecules adsorbed in the interface, Eq. (1.2) is often used, with a surface concentration c_s in mol/m^2 generally translated to a concentration in numbers per area, $n_s = c_s \cdot N_{\text{av}}$, and then n_s is replaced by $1/A$ with A the area available for one molecule, while b is now equal to the area occupied by one molecule, A_0 (i.e., this is the minimum area that a molecule needs). We then arrive at

$$P_s = \frac{k_B T}{A - A_0} - \frac{a}{(N_{\text{av}} A)^2}. \quad (1.12)$$

To this surface pressure a contribution can be added when the adsorbed molecules are charged and a ‘diffuse layer’ of counterions forms in one of the two bulk (electrolyte) phases. According to Gouy-Chapman theory, which we will discuss further on, this contribution is given by Eq. (5.13) with the required surface potential ϕ_D given by the GC-equation, Eq. (3.15). In these equations, surface charge Σ relates to A according to $\Sigma = e n_s = e/A$ when each molecule carries one e charge.

—

To improve on Eq. (1.12), we set up a modified equation of state for a charged film where we model the surfactant molecules in the interface as the short polymer chains that they often are. We use the modified CS equation for the volume exclusion of packing these (relatively short) polymer chains, which has as inputs the cross-sectional area of each of these polymer chain, A_{ch} , and the number of monomers in a chain, \mathcal{N} (i.e., in one surfactant molecule). For instance, based on a chain diameter of $D_{\text{ch}}=0.36$ nm, we have $A_{\text{ch}}=0.10$ nm², and $\mathcal{N} \sim 10$ can be a reasonable number for moderately long surfactant molecules. (\mathcal{N} does not have to coincide exactly with the number of monomers, but can be chosen more freely.)

The excess contribution to the surface pressure due to packing these surfactant molecules is now given by

$$P_{\text{ch}}^{\text{exc}} \frac{A_{\text{ch}}}{\mathcal{N} k_{\text{B}} T} = 3\eta^2 + 9\eta^3 + \mathcal{O}(\eta^4) \quad (1.13)$$

in which the volume fraction η relates to surface concentration according to $\eta = n_{\text{s}} A_{\text{ch}}$. This expression shows how the volumetric exclusion depends on the number of monomers in the molecule, and their cross-sectional area.

The full equation of state for a charged film now becomes

$$P_{\text{s}} = c_{\text{s}} RT + P_{\text{ch}}^{\text{exc}} + P_{\text{elec}} - a\mathcal{N}c_{\text{s}}^2 \quad (1.14)$$

where we implement the electrostatic contribution, P_{elec} , given by Eq. (5.13) or Eq. (5.14) (noting that charge is $\Sigma = Fc_{\text{s}}$, when we assume one charge per surfactant molecule).

In Eq. (1.14) the ideal contribution to the surface pressure, $c_{\text{s}}RT$, and the electric contribution, do not depend on the length of the surfactant molecules (assuming the charge per molecule remains the same), while the volumetric excess term, and the attraction between chains, they do. We highlight this length-dependence for the attractive term (last term in Eq. (1.14)), by multiplying with \mathcal{N} . For so-called ‘theta-conditions’, the first virial coefficient, $3\eta^2$ in Eq. (1.13) and the attraction term exactly cancel which happens when $a/(N_{\text{av}}^2 A_{\text{ch}}) = 3$ kT.

1.3 The Frumkin isotherm for molecular adsorption

In the previous sections we discussed the equation of state, first for a volume of gas, and after that for molecules adsorbed at an interface. We now continue with a more complicated situation, which is the isotherm. An isotherm describes the exchange of molecules between multiple phases. We first discuss the exchange of one type of molecule between bulk solution and a layer in which molecules adsorb. This layer can be modelled as a two-dimensional surface or a three-dimensional volume.

To derive an isotherm one must equate the chemical potential of the molecule in bulk solution (often denoted by ‘ ∞ ’), with that in the surface, i.e., in the adsorption layer, thus $\mu_{i,\infty} = \mu_{i,\text{ads}}$. For the solution phase we only use the first two terms on the right side of Eq. (1.8), while in the adsorption layer we use the same equation but now we use all terms, with the adjustment that the reference concentration becomes the maximum concentration in the layer, thus $c_{\text{ref}} \rightarrow c_{\text{max}} (= 1/v)$.ⁱⁱⁱ We also add to both sides an ‘affinity’ term, which is a chemical interaction of the species with the respective phase. This relates to the solubility in that phase. There are no volume- or charge-effects included in this affinity. Leaving out index i , the result of this equality of chemical potential is

$$\mu_{\text{ref}} + \mu_{\text{aff},\infty} + \ln c_{\infty}/c_{\text{ref}} = \mu_{\text{ref}} + \mu_{\text{aff}} + \ln \vartheta - \ln(1 - \vartheta) + g' \vartheta \quad (1.15)$$

where the volume fraction occupied by the molecules in the adsorption layer is $\vartheta = c_{\text{ads}}/c_{\text{max}} = v c_{\text{ads}}$, and we use a factor g' for the interaction energy which is negative when the molecules within the adsorption layer attract each other. This factor relates to the earlier used parameter a' according to $g' = -2a' c_{\text{max}}$.

We rearrange Eq. (1.15) to arrive at the Frumkin adsorption isotherm, which is an implicit relationship between the occupancy of the adsorption layer, ϑ , and the solution concentration, c_{∞} , given by

$$\frac{\vartheta}{1 - \vartheta} = K \cdot c_{\infty} \cdot \exp(g' \vartheta) \quad (1.16)$$

where $K = e^{-\Delta\mu_{\text{aff}}}/c_{\text{ref}}$, in which $\Delta\mu_{\text{aff}} = \mu_{\text{aff,ads}} - \mu_{\text{aff},\infty}$. Eq. (1.16) is also called the Frumkin-Fowler-Guggenheim (FFG) equation. In the FFG equation, instead of g' , the symbol b is used, called the lateral interaction parameter. For sufficiently negative values of g' , Eq. (1.16) predicts that for a range of values of c_{∞} there are multiple solutions for ϑ , i.e., it is possible to have phase separation within the surface. (This does not always occur for many reasons related to the absence of nucleation points, and that lateral transport of molecules can be slow.)

The FFG equation can be simplified to the Langmuir isotherm when $g' = 0$, which results in

$$\vartheta = \frac{c_{\text{ads}}}{c_{\text{max}}} = \frac{1}{1 + K \cdot c_{\infty}} \quad (1.17)$$

which for low adsorptions simplifies to

$$\vartheta = c_{\text{ads}}/c_{\text{max}} = K \cdot c_{\infty} \quad (1.18)$$

ⁱⁱⁱIf the adsorption layer is modelled as a volume, then c_{ads} is a concentration in mol/m³ and v is the volume per molecule (or per mole of molecules). But if the layer is modelled as an area, then c_{ads} is expressed in mol/m² and v is the area per molecule (or per mole of molecules).

and when c_{ads} and c_{max} are defined as concentrations per volume, this can be written as

$$c_{\text{ads}} = \Phi_{\text{aff}} c_{\infty} \quad (1.19)$$

where $\Phi_{\text{aff}} = c_{\text{max}} \cdot K = c_{\text{max}}/c_{\text{ref}} \cdot e^{-\Delta\mu_{\text{aff}}}$ is a partition coefficient, or solubility, of a molecule, due to a difference in affinity, which relates to its preference to be in phase k rather than in phase j , i.e., the factor Φ_{aff} describes the distribution of a certain solute between two phases for chemical reasons (reasons unrelated to ‘excess’ ion volume effects, or to the charge of the species), see p. 503.

A modification of Eq. (1.17) to account for surface heterogeneity is the Langmuir-Freundlich isotherm^{1,2} which is

$$\vartheta = \frac{c_{\text{ads}}}{c_{\text{max}}} = \frac{1}{1 + (K \cdot c_{\infty})^p} \quad (1.20)$$

where p is the width of the affinity distribution ($0 < p < 1$).³

A generalized distribution function based on the the Langmuir equation, Eq. (1.17), is given by

$$c_{\text{ads}} = c_{\infty} \Phi_{\text{aff}} \Phi_{\text{exc}} \quad (1.21)$$

where Φ_{exc} is the partition coefficient related to volume exclusion, which for the lattice model used in this chapter simply is $\Phi_{\text{exc}} = 1 - \vartheta$.

We will encounter Eq. (1.21) multiple times throughout this book, often supplemented with an electrostatic effect –resulting in an extended Boltzmann equation–, and with more sophisticated expressions for the volumetric, excess, contribution considered, for instance described by (modifications of) the Carnahan-Starling approach, see e.g., Eq. (2.34) in Ch. 4.

The Gibbs adsorption isotherm. Interestingly, the simplified Langmuir equation, Eq. (1.18), is compatible with the ‘Gibbs equation for adsorption’, $d\gamma = -RT\Gamma_s d \ln c_{\infty}$, where γ is surface tension and Γ_s surface concentration, i.e., Γ_s is equal to c_{ads} . Surface tension is the negative of the surface pressure, and for an ideal solution $-\gamma = \Pi_s = RTc_{\text{ads}}$, and thus the Gibbs adsorption isotherm becomes $dc_{\text{ads}} = c_{\text{ads}} d \ln c_{\infty}$, which implies $d \ln c_{\text{ads}} = d \ln c_{\infty}$ which is compatible with the simplified Langmuir equation, Eq. (1.18).

The isotherm when adsorbing species are charged. It is possible to extend Eq. (1.16) to include that adsorbing molecules, or for instance nanoparticles, are charged, by adding to Eq. (1.15) a term $z\phi$ with z the valency of the surfactant (particle, ion) and ϕ the electrical potential in the surface, relative to bulk. To solve for ϕ , we need to set up an EDL model that includes surface charge in the absence of surfactant adsorption, the charge of adsorption surfactant molecules, and the diffuse layer of counterions. Ishiguro and Koopal discuss this topic for a diffuse layer model in the low-potential limit.³ When surfactants have a charge opposite to that of the surface, then at one surfactant concentration in bulk, the influence of salt concentration on adsorption vanishes; below this concentration, we have more surfactant adsorption when salt concentration decreases, while above this point the situation is reversed. More advanced models include how (counter-)ions can also adsorb, and then H^+ and OH^- are of special relevance.

1.4 The extended Frumkin equation for the EDL structure in intercalation materials

We can now use the general expression that was derived for equilibrium, thus for equality of chemical potential in two adjacent phases, Eq. (1.15), and add to both sides an electrostatic term. Assuming that the absorbing species are monovalent cations, the additional term on the left is $+\phi_\infty$ and on the right is $+\phi_{\text{ads}}$. We continue to use $\vartheta = \nu c_{\text{ads}} = c_{\text{ads}}/c_{\text{max}}$, which from this point onward we call the intercalation degree, and we rearrange Eq. (1.15) to obtain for the electrode potential

$$\phi_e = \phi_{\text{ref}} - \ln \frac{\vartheta}{1 - \vartheta} + \ln \frac{c_\infty}{c_{\text{ref}}} - g' (\vartheta - 1/2) \quad (1.22)$$

where $\phi_e = \phi_{\text{ads}} + \phi_{\text{extra}} - \phi_\infty$ and $\phi_{\text{ref}} = \mu_{\text{aff},\infty} - \mu_{\text{aff,ads}} - \ln c_{\text{max}} - \phi_{\text{extra}} - 1/2g'$. In dimensional voltages, with $V_e = V_T \phi_e$, we obtain

$$V_e = V_{\text{ref}} - V_T \left(\ln \frac{\vartheta}{1 - \vartheta} - \ln \frac{c_\infty}{c_{\text{ref}}} \right) - g (\vartheta - 1/2) \quad (1.23)$$

where $g = V_T \cdot g'$ with $V_T = RT/F$ the thermal voltage, which at room temperature is $V_T \sim 25.6$ mV. In using Eqs. (1.22) and (1.23) it must be recalled that an attraction between ions within the adsorption layer means that g is negative.

The equation just derived is the extended Frumkin isotherm (here for monovalent cations), which is a very accurate and elegant EDL model, for instance for intercalation materials, which are promising capacitive materials for desalination in capacitive deionization (CDI). Intercalation materials are charged porous materials into which ions can enter, or intercalate, moving into the small micropores that are inside the framework of the intercalation ‘host compound’, or ‘active material’. Ions are free to move within these interstitial spaces and will be expelled from the material, or attracted inside, dependent on the charge of the host structure. In some well-known examples only cations adsorb (not anions) because the host compound structure is strongly negative charged. These examples are Prussian Blue Analogues (PBA) and sodium manganese oxide (NMO).

Using Eq. (1.23) we can evaluate the electrode charge, $-\vartheta c_{\max}$, which is a concentration per volume of intercalation host compound, as function of electrode potential. Here a minus-sign is implemented because electrode charge is the negative of the cation concentration in the pores of the material. It is interesting to analyze the derivative of charge with electrode potential, which is the capacitance of the intercalation material. Based on Eq. (1.23) capacitance is given by

$$C = -\frac{F c_{\max}}{\rho} \frac{\partial \vartheta}{\partial V_e} = \frac{F^2 c_{\max}}{RT \rho} \left\{ \frac{1}{\vartheta} + \frac{1}{1 - \vartheta} + g' \right\}^{-1} \quad (1.24)$$

where ρ is the mass density of the intercalation material. The maximum in capacitance is obtained when the material is occupied for 50% with cations ($\vartheta = 1/2$), i.e., the other half of available sites is still unoccupied. Then the term within brackets is $4 + g'$. We can have an infinite capacitance when ions are so attracted to one another that they (almost) phase separate, and we arrive in this situation when the attraction term is $g' = -4$ or more negative. For water als electrolyte, for the two materials mentioned above, PBA and NMO, which are both often used in CDI, the factor g' is negative, but not so negative that phase separation takes place. We discuss these materials in more detail in §15.2.1.

In Fig. 1.1 we compare data and theory based on Eq. (1.24) and notice the good fit of theory to the data, especially in reproducing the broad plateau and symmetric behavior around $\vartheta \sim 1/2$, i.e., when the material is halfway charged, when capacitance is at a maximum. Theory is in agreement with data that these high capacitances, beyond 1000 F/g, can be obtained in a large window of charge (~ 150 C/g). The capacitance of other capacitive materials is generally lower. For instance for microporous carbons typical values for capacitance are in the range of 50–100 F/g.

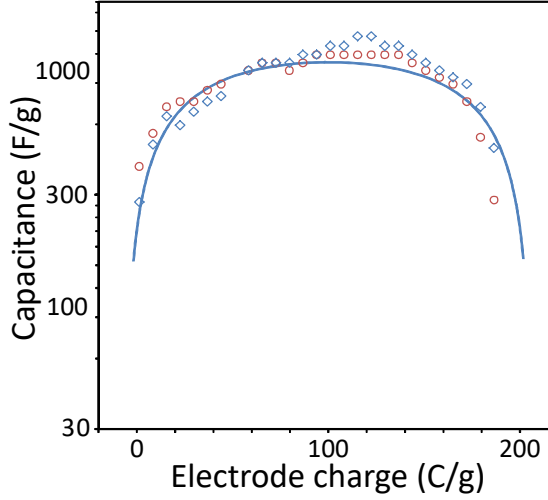


Fig. 1.1: The capacitance of an intercalation material in 1 M Na_2SO_4 in water. The material is a Prussian Blue Analogue (nickel hexacyanoferrate) ($\rho = 2.0$ g/mL, $c_{\max} = 4.40$ M, $g = -90$ mV).

1.5 Extensions of the extended Frumkin isotherm for multi-ionic solutions or multi-region electrodes

The extended Frumkin isotherm, Eq. (1.23), can be further extended to describe the simultaneous adsorption of multiple ionic species in the electrode. It is often the case that the attraction for one ion is higher than for another, which leads to differences in $V_{\text{ref},i}$. For two types of monovalent cations, it is possible to use the following ‘multicomponent extended Frumkin isotherm,’ which in effect are two equations that must be solved jointly to calculate the intercalation degree of each cation, ϑ_i , for a given value of V_e and for a given solution composition, i.e., for known cation concentrations in solution, $c_{\infty,i}$. This equation is

$$V_e = V_{\text{ref},i} - V_T \left(\ln \frac{\vartheta_i}{1 - \vartheta_i - \vartheta_j} - \ln \frac{c_{\infty,i}}{c_{\text{ref}}} \right) - g_i (\vartheta_i - 1/2) - g_{\text{avg}} \vartheta_j \quad (1.25)$$

where g_{avg} is the average of the two g -values of the two cations, based on the assumption that that value is representative of the mutual attraction i - j between these two cations inside the electrode. Eq. (1.25) simplifies to Eq (1.23) for ion i when the other ion j is absent ($c_{\infty,j}=0$, and therefore $\vartheta_j=0$).

Another modification of Eq. (1.23) is to consider a single adsorbing cation, but to realize that not all sites in the intercalation material have the same adsorption energy. Instead, there can be a distribution in energy amongst the sites in the material, with the values of V_{ref} and g different in different regions of the material.

We set up a model based on Eq. (1.23) where we assume three types of sites, $j = 1, 2, 3$ (each with a concentration $1/3^{\text{rd}}$ of the total number of adsorption sites), with a difference in V_{ref} between the three types of sites of 50 mV. Thus we simultaneously solve Eq. (1.23) three times with three different values of $V_{\text{ref},j}$ while ϑ in Eq. (1.23) is replaced by ϑ_j (we assume no interaction between the three types of sites). The total occupancy as presented in Fig. 1.2 is $1/3^{\text{rd}}$ the summation of the three values of ϑ_j , obtained at the same electrode potential, V_e .

What is the most relevant in Fig. 1.2 is that the predicted sequence of multiple plateaus has similarities to observed charging curves for certain intercalation materials, especially NMO (but not observed for PBA). And we can note that when the number of different adsorption sites (with different energies) increases, the resulting curve will become smoother and smoother, and finally it can be described by the extended Frumkin equation as if there is only a single region, but now with a much larger (more positive) g -value than the value used in the more precise multi-region calculation that considers many types of sites with different energies. So this ‘new g ’ has an empirical character; it no longer really describes the attraction energy between cations in the material.

Or in other words, by adjusting g in a model based on only a single Frumkin isotherm, one can in good approximation simulate a material that in reality has many regions with different absorption energies. This may also suggest that an intercalation material that shows a relative steep change $\partial V_e / \partial \vartheta$ may on closer inspection contain multiple regions with different adsorption energies, $V_{\text{ref},j}$.

references

1. R. Sips, “On the structure of a catalyst surface,” *J. Chem. Phys.* **16**, 490–495 (1948).
2. E. Spruijt, P.M. Biesheuvel, and W.M. de Vos, “Adsorption of charged and neutral polymer chains on silica surfaces: The role of electrostatics, volume exclusion, and hydrogen bonding,” *Phys. Rev. E* **91**, 012601 (2015).
3. M. Ishiguro and L. K. Koopal, “Surfactant adsorption to soil components and soils,” *Adv. Colloid Interface Sci.* **231**, 59–102 (2016).

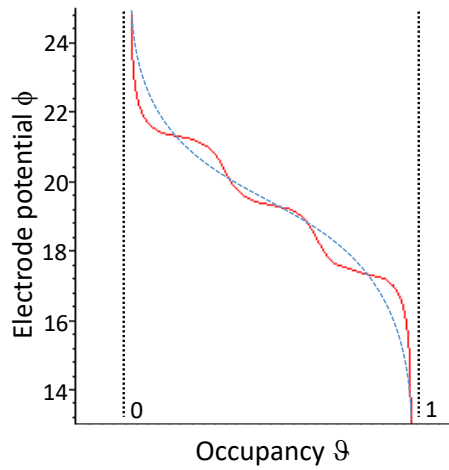


Fig. 1.2: The extended Frumkin adsorption isotherm for an intercalation material with three types of sites with a 50 mV difference in adsorption energy for cation adsorption (for all three sites, $g = -80$ mV). Electrode potential, ϕ , versus total cation adsorption degree, θ . Dashed blue curve is based on an effective ‘single region’ Frumkin model with more positive g -value, approximating the three-region Frumkin prediction.

The Donnan model: the EDL in small pores

The Donnan model is an elegant model for the electrical double layer (EDL) which extends the Frumkin isotherm equation by allowing both anions and cations in the pores of a charged material. The Donnan model has many applications in describing ion adsorption and voltages in membranes and porous electrodes. It is not difficult to extend the Donnan model and include both electronic charge and/or chemical charge, as well as ion volume effects and other contributions to the partitioning of ions. Just like the extended Frumkin isotherm, it can be readily included in models for the transport of ions across porous electrodes and membranes.

2.1 Introduction

As already discussed in the preamble to Part I, the concept of the electrical double layer (EDL) has two sides to it. On the one hand it is the microscopic structure of how we envision the interface to look like which is formed when two bulk phases or materials are in contact, and on the other hand it is the set of mathematical equations that describe measurable properties of the EDL such as a voltage difference across the EDL, ion adsorption, and surface pressure.

The EDL is formed between two bulk phases, of which one can be a metal (conductor of electronic charge) and the other can be electrolyte (conductor of ionic charge). It is also possible that the EDL includes a material that contributes (a surface with) chemical charges, such as a charged polymer network, or the surface of a globular protein molecule. Overall, the EDL is electroneutral. There can be multiple regions with charge, but they all add up to an overall zero charge. Also, the EDL is generally in equilibrium: even when ions are transported across the EDL, for instance when an electrode process is going on, the EDL structure in almost all cases can be assumed to be at chemical and mechanical equilibrium.

In the present chapter we extend the Frumkin isotherm that was discussed in Ch. 1 by allowing adsorption of both anions and cations in the EDL. We furthermore include a constant-capacity element (the Stern layer), and include the possibility of fixed (i.e., immobilized) chemical charge in the pores. This chemical charge can be a function of local pH. We call this approach the Donnan model. The Donnan model is a very powerful modelling approach and has applications in many problems in physiology, hydrogel materials, membrane technology, and ion adsorption in the pores of carbon electrodes.

2.2 Simplified Donnan model

The same as for the extended Frumkin isotherm for intercalation materials, the Donnan model is based on the idea that within a certain small volume, which in this section we call a pore, that is a few nm across at most, with charges on the pore walls, that within this volume ions have a concentration that is different from what it is outside the pore, but within the pore volume, their concentration is independent of position. Related, in this model it is assumed that at all positions in the pore the electrical potential is the same, and likewise other forces and energies are independent of exactly where we are in the pore.

To describe ion concentrations in the pore, relative to outside the pore, we use a general Boltzmann equation, which describes the partitioning of an ion between two phases due to effects such as affinity and volume exclusion, and also includes an electrostatic term which

leads to an attraction or repulsion of the ion into the pore dependent on the charge of the ion and of pore walls (neutral species are not affected)

$$c_i = c_{\infty,i} \Phi_i e^{-z_i \phi_D} \quad (2.1)$$

where z_i is the valency of the ion (e.g., $z_i = +1$ for a monovalent cation), and ϕ_D is the jump in electrostatic potential upon entering the pore (electrical potential in the pore, minus that outside). These dimensionless potentials ϕ can always be multiplied by the thermal voltage, $V_T = RT/F \sim 25.6$ mV at room temperature, to arrive at a dimensional potential or voltage, V , with unit V. We use the index ‘ ∞ ’ to describe (concentrations at) a position outside the pore where we have neutral electrolyte bulk solution.ⁱ We include in Eq. (2.1) a partition coefficient, Φ_i , due to contributions to the chemical potential of an ion in a pore other than the Boltzmann, electrostatic, effect. Examples of forces that are included in Φ_i are an affinity (to be in the pore, rather than outside), and another example is the effect of ion volume (excess term). Affinity is a general term encompassing many effects that can lead to a solute-medium interaction energy. The partition coefficient will be discussed in detail in §2.8, Ch. 4 and Ch. 11. In a multi-ion problem, differences in Φ_i between different ions can be the reason why out of several ionic species with the same charge, one adsorbs more than another. We assume $\Phi_i = 1$ until §2.8, and with that assumption arrive at the most common version of the Boltzmann equation, given by

$$c_i = c_{\infty,i} e^{-z_i \phi_D} . \quad (2.2)$$

Within the pore we have overall electroneutrality, thus the charge on the walls of the pore, and the charge of ions in the pore volume, add up to zero (the possibility of additional chemical charge will be discussed further on). This can be expressed as

$$F V_{\text{pore}} \sum_i z_i c_{\infty,i} e^{-z_i \phi_D} + A_{\text{wall}} \Sigma_{\text{wall}} = 0 \quad (2.3)$$

where F is Faraday’s constant ($F = 96485$ C/mol), V_{pore} is pore volume, A_{wall} pore wall area, and Σ_{wall} pore wall charge in C/m². The summation over i includes all ions in the system.

Next we introduce σ_w , which is the charge on the pore walls, defined as a charge density per unit pore volume (thus it has unit mol/m³)

$$\sigma_w = \Sigma_{\text{wall}} A_{\text{wall}} / (V_{\text{pore}} F) . \quad (2.4)$$

ⁱThis can also be the electroneutral ‘macropore’ electrolyte that fills the larger (transport) pores in a porous electrode, see Ch. 15.

The ratio of pore volume over pore area, $V_{\text{pore}}/A_{\text{wall}}$, is the characteristic pore dimension, h_p , which depends on pore size and pore geometry: for a planar slit, $h_p = 1/2 \cdot w$, where w is the width of the slit, while for a cylindrical pore, $h_p = d/4$ with d the pore diameter. Combination of Eqs. (2.3) and (2.4) leads to

$$\sum_i z_i c_{\infty,i} e^{-z_i \phi_D} + \sigma_w = 0. \quad (2.5)$$

Eq. (2.5) can be simplified when we only have monovalent ions (a 1:1 salt solution, see p. 495). In that case we have a salt solution with cations and anions that all have a charge of $z_i = +1$ or $z_i = -1$, and we arrive at

$$-2c_{\infty} \sinh \phi_D + \sigma_w = 0 \quad (2.6)$$

where c_{∞} is the salt concentration outside the pore, which for a 1:1 solution is equal to the total cation concentration (the sum of the concentrations of all monovalent cations), which is also the total anion concentration. Eq. (2.6) can be rewritten to express the Donnan potential as function of σ_w and c_{∞} ⁱⁱ

$$\phi_D = \sinh^{-1} \frac{\sigma_w}{2c_{\infty}}. \quad (2.7)$$

At very high wall charge density (relative to the external salt concentration), Eq. (2.7) simplifies to

$$\phi_D = \ln \frac{\sigma_w}{c_{\infty}}. \quad (2.8)$$

The wall charge density can have various origins, for instance it can be due to electronic charge in a porous electrode, or it can be the chemical fixed charge of the polymer material of which an ion-exchange membrane is made. In the latter case, the charge of the polymer material is generally denoted by the symbol X , defined as membrane charge per volume of pores in the material, which for membranes used in reverse osmosis is predicted to be a few mM, while many commercial ion-exchange membranes have charge densities as high as $X \sim \pm 5$ M. The sign of the membrane charge can be denoted by a symbol ω , which is $\omega = +1$ or $\omega = -1$ for a membrane with positive or negative fixed charges, respectively. A membrane with positive fixed charges provides easy access to anions, and is therefore called an anion-exchange membrane (AEM), while a membrane with $\omega = -1$ is a cation-exchange membrane (CEM). Rewriting Eq. (2.8) for such a membrane, thus making the replacement

ⁱⁱOn the notation of hyperbolic functions \sinh , \cosh and \tanh : index $^{-1}$ implies that the inverse function is used, thus $\sinh^{-1}(x) = \text{arsinh}(x)$. However, index 2 implies the function as a whole is squared. See p. 512 for details on these functions.

$\sigma_w = X = \omega|X|$, where $| \cdot |$ refers to taking a positive quantity, we obtain

$$\phi_D = \sinh^{-1} \frac{\omega|X|}{2c_\infty}. \quad (2.9)$$

While Eqs. (2.7)–(2.9) describe the relation between Donnan potential and wall charge, another element of an EDL model, i.e., a property that an EDL model must predict, is the concentration of ions in the pores. For each individual ion, this is given by the Boltzmann relation, Eq. (2.2). The total concentration of all anions plus cations in the pore, c_T , assuming a 1:1 solution, is given by

$$c_T = 2c_\infty \cosh \phi_D. \quad (2.10)$$

Making use of $\cosh(\sinh^{-1}(x)) = \sqrt{x^2 + 1}$, Eqs. (2.9) and (2.10) can be combined to arrive at a direct relation between c_∞ , X , and c_T , given by

$$c_T^2 = 4c_\infty^2 + X^2 \quad (2.11)$$

independent of the sign of the membrane charge. For the same analysis as in this section but generalized to $\Phi_i \neq 1$, see §2.8.

For applications in ion-exchange membranes, the above equations often suffice. Modifications are required when the membrane charge is pH-dependent, which we will discuss in §2.4. Other modifications account for electronic charge and are discussed in the next section. Other contributions to the partitioning of ions (for instance due to volume exclusion, because of an energy penalty for ions to fit in the narrow pores) are discussed in §2.8, Ch. 4, and Ch. 11.

Effect of temperature on electric double layer structure. An interesting topic is the effect of temperature on the EDL structure, for instance according to the just-discussed Donnan model. Often chemical potentials are described as ' $RT \ln c_i$ ' which suggests for this entropic part a significant temperature effect, while the electrostatic part, $F \cdot V$, is not temperature dependent. However, when converting to a dimensionless electrical potential, ϕ , we notice the same RT -term in both contributions and thus temperature turns out to not matter. Indeed, an equation such as Eq. (2.11) correctly does not include temperature. Volumetric effects can be included too, and still temperature does not play a role. Instead, 'chemical' affinity effects, such as described by the constants a and g in the last chapter, have a strong dependence on temperature.

Interestingly, EDL models based on the Poisson equation, evaluated for ions in water, see the next chapter, are also quite temperature-insensitive, for the coincidental reason

that the factor $\varepsilon \cdot T$ is quite independent of temperature. This is because the dielectric constant of water decreases with temperature in such a way that after multiplication with temperature T (in K), the result is an almost T -independent factor. When we have transport, the effect of temperature is interesting too, which we discuss in a box on p. 197.

For capacitive processes where small pores are used to store ions, the concept of *charge efficiency*, Λ , plays a key role. Charge efficiency on the one hand is an experimental parameter, obtained from experiments with an electrochemical cell pair, and on the other hand it is a theoretical property of an EDL model. Here we focus on the second aspect, and define charge efficiency as the additional number of ions incorporated in a pore when the charge goes from zero to a particular value, and then divided by that final charge. In this case charge efficiency is given by

$$\Lambda = A^{-1} \left(\sqrt{A^2 + 1} - 1 \right) = \tanh (|\phi_D|/2) \quad (2.12)$$

where $A = |\sigma_w|/(2c_\infty)$ is a dimensionless pore wall charge. The charge efficiency Λ is a number between 0 and 1, and quantifies how much salt is adsorbed when an electrode is charged. Clearly, a number above unity is not possible, and numbers close to this ideal maximum require that the electrode charge, or Donnan potential, is high.

The simple Donnan model discussed above, is completed by consideration of one final property, the difference in pressure between inside and outside the pore. When the assumptions of the Boltzmann equation are valid, as in the above equations, then the osmotic pressure in the pore is given byⁱⁱⁱ

$$\Pi = c_T \quad (2.13)$$

while the osmotic pressure of a 1:1 solution outside the pore is given by $\Pi = 2c_\infty$. Now, because of mechanical equilibrium that we can assume in an EDL, it is the case that the total pressure, P^{tot} , is invariant across the EDL. Because this total pressure has two contributions,

$$P^{\text{tot}} = P^{\text{h}} - \Pi \quad (2.14)$$

where P^{h} is the hydrostatic (hydraulic) pressure, combination of Eqs. (2.13) and (2.14) leads to the conclusion that the increase of the osmotic pressure across the EDL equals the increase in hydrostatic pressure

$$\Delta P^{\text{h}} = P_{\text{pore}}^{\text{h}} - P_{\infty}^{\text{h}} = \Pi_{\text{pore}} - \Pi_{\infty} = c_T - 2c_\infty . \quad (2.15)$$

ⁱⁱⁱThroughout most of this book, ‘reduced’ pressures Π and P^{h} are used, as well as a reduced (chemical) potential μ_i . These parameters can be multiplied by RT to obtain pressures in $\text{J/m}^3 = \text{Pa}$ and potentials in J/mol .

This result is of importance in describing the flow of fluid through a porous medium, such as a membrane, see Chs. 11 and 12, or to calculate the forces that an EDL exerts on particle (pore) walls, which can lead to swelling or fracture of porous charged materials (Biesheuvel, 2017). We will discuss this relation in more detail in Ch. 8.

Mixtures of different ions. Electrolytes generally contain mixtures of ions (e.g., different types of cations), and this situation is described at several points in this book: in §1.5 we provided the theory to describe differences in absorption between two cations in an intercalation material, and in §2.7 we discuss mixtures of ions of different valencies. The Donnan model is particularly useful because it leads to equations that are tractable and describe many relevant situations.

Here we only address an almost trivial, but very relevant point. Namely, in the Donnan model, and neglecting partition effects due to affinity and ion volume, thus only considering ion charge, then the ratio of concentration of a certain ion i in the pore over that in solution, relates in a very simple way to the same ratio for all other ions j (the other ions can have the same valency, $z_i = z_j$, or have a different valency) by

$$\left(\frac{c_i}{c_{\infty,i}} \right)^{z_i} = \left(\frac{c_j}{c_{\infty,j}} \right)^{z_j} . \quad (2.16)$$

This result is used in §2.7 to describe the absorption of two cations of a different valency (and one anion) in a negatively charged porous material.

2.3 Donnan model including Stern layer

The Donnan model of the last section is a very suitable framework that can be extended in multiple ways. The first relevant extension is the inclusion of a Stern layer, which is a layer envisioned to be located between the charged wall and the ionic solution in the pore. This is a layer (also called Helmholtz layer) that is uncharged. Assuming this layer to be planar, the voltage difference that arises across the Stern layer is proportional to the charge density on either side (which are equal in magnitude, but opposite in sign), according to

$$V_T \phi_S = \Sigma_{\text{wall}} F / C_{S,A} \quad (2.17)$$

where $C_{S,A}$ is the areal Stern (layer) capacitance, with unit F/m^2 . In Eq. (2.17), ϕ_S is the difference in electric potential across the Stern layer, defined as that at the wall minus that

in the pore solution. Within the context of the Donnan model, where concentrations and charge are defined per unit pore volume, it is useful to make use of $C_S = C_{S,A}/h_p$, after which Eq. (2.17) becomes

$$V_T \phi_S = \sigma_w / C_S \quad (2.18)$$

where C_S is a Stern capacitance with unit F/m^3 .

Note that the Stern layer, or Helmholtz layer, is a layer free of charge. That is why a (linear) relationship describes the charge (on either side) to the voltage drop across it. In many textbooks, erroneously, the Stern layer is conceived of as a ‘layer of condensed counterions’ (and pictorially represented in that way) but this depiction is not correct. A plane of condensed charge mathematically leads to a change in field strength, but not necessarily to a voltage difference. That is very different from the Stern layer concept.

The total potential across the EDL, from outside the pore, to right at the wall, now becomes

$$V_{EDL} = V_T (\phi_D + \phi_S) . \quad (2.19)$$

This finalizes the introductory discussion of the Donnan layer, including also the Stern layer. The Stern layer concept is very relevant in the modelling of ion adsorption in carbon micropores, and has also been successfully implemented in a transport model for nanofiltration with conductive pore walls (Zhang et al., 2019).

Donnan model in an electrochemical cell with capacitive electrodes. In this box we explain how to use the Donnan model for an electrochemical cell with two capacitive electrodes, operated at equilibrium, thus neglecting any voltage drops between the electrodes due to transport. In this case the voltage between the two metal wires, which is called the cell voltage, V_{cell} , is equal to

$$V_{\text{cell}} = V_{\text{EDL}|_1} - V_{\text{EDL}|_2}. \quad (2.20)$$

Important for an EDL model for capacitive electrodes is the ability to describe capacity and capacitance. The capacity of an electrode is the charge of an electrode relative to the charge at another condition, expressed per area, volume, or mass. If charge is zero at that other condition, it can be given the symbol σ_e . In that case capacity is defined per unit pore volume, and to obtain it per unit mass of an electrode, information of the pore volume per electrode mass, v_{pore}^* , is required. To calculate capacity in a Donnan-Stern model, the Donnan part of the EDL model must be combined with the Stern part, and jointly solved, often numerically.

Different from capacity, the capacitance of an electrode, of an EDL, C_{EDL} , is the change in electronic charge over a change in V_{EDL} , $C_{\text{EDL}} = \partial \Sigma_e / \partial V_{\text{EDL}}$. When charge Σ_e has unit C/m^3 , then capacitance is in F/m^3 (per m^3 pore volume). For the Donnan-Stern model (as well as the GCS model), it relates in a simple manner to the capacitances of the separate sub-elements of the EDL model, namely by

$$\frac{1}{C_{\text{EDL}}} = \frac{1}{C_{\text{S}}} + \frac{1}{C_{\text{D}}} \quad (2.21)$$

where the capacitance of the diffuse, Donnan, part, C_{D} , is given by

$$C_{\text{D}} \cdot \frac{RT}{F^2} = \frac{\partial \sigma_w}{\partial \phi_{\text{D}}} = 2c_{\infty} \cosh \phi_{\text{D}} \quad (2.22)$$

All capacitances in F/m^3 can be multiplied by v_{pore}^* to obtain a capacitance with dimension F/g . Because C_{D} is not a constant but is a function of ϕ_{D} , the entire Donnan-Stern model must be numerically solved when a Stern layer is included.

2.4 Donnan model for electrodes with chemical charge

The charge of ions in solution (in the diffuse layer, in a pore) can be compensated by charge in the Stern plane (i.e., at the interface between Stern and diffuse layers) which can be ‘fixed charge’ or can be due to ion adsorption there (see Eq. (3) in Stern, 1924). Beyond the Stern layer is the ‘0-plane’ which is also charged, which is either because of chemical groups there,

or electronic charge, or both.

In this section we describe the Donnan model for a porous carbon electrode, considering both electronic wall charge and chemical ‘fixed’ charge. This chemical charge is assumed to be located in the Stern plane, and is due to the acidic and basic groups inside the carbon pores. In such an electrode, all of the equations of the previous section remain valid, with just a few modifications. In all equations previously discussed, σ_w must be replaced by the summation of two separate terms, σ_e for the electronic charge, and σ_c for the fixed chemical charge due to the acidic and basic groups. The overall charge balance, Eq. (2.5), now contains three terms

$$\sum_i z_i c_{\infty,i} e^{-z_i \phi_D} + \sigma_c + \sigma_e = 0. \quad (2.23)$$

The other modification is in the equations for the voltage across the Stern layer, Eqs. (2.17) and (2.18). Here, σ_w must be replaced by the electronic charge, σ_e , because the electronic charge is located at one side of the Stern layer, and the chemical charge, together with ionic charge, on the other side. Exactly this model has shown to be extremely powerful in predicting various non-intuitive operational modes found in CDI, such as inverted operation, and inversion peaks (Biesheuvel et al., 2015).

A further modification is to include that the porous carbon contains two different regions, where one region carries negative chemical charge, and the other region contains positive chemical charge. This amphoteric Donnan model successfully describes many data sets for CDI as function of cell voltage and salt concentration, also for mixtures of salts with monovalent and divalent cations (Biesheuvel, 2015). It also describes how much salt is adsorbed by carbon powder when it is mixed with electrolyte solution. In the next section we briefly address how this chemical charge often does not have a fixed value, but the charge depends on the local concentration of ions in the pores, most notably the H^+/OH^- -ions.

2.5 Donnan model with ionizable chemical charge

In most cases, the chemical charge in an electrode, or at the surface of a colloidal particle, or inside a porous membrane or gel, does not have a fixed value, but it can change because ions can adsorb to it. Focusing on the ions H^+ and OH^- , their concentration determines the degree of protonation/deprotonation of acidic and basic groups.^{iv} Thus the charge of chemical groups is not fixed (or ‘quenched’ in the terminology of polyelectrolyte theory) but is ionizable (‘annealed’). Next we discuss a gel or ion-exchange membrane with such

^{iv}It is common to write H^+ for the hydronium ion, even though more chemically correct is H_3O^+ .

ionizable groups and make a simple analysis of ionization degree and osmotic pressure. We neglect the Stern layer.

Outside the charged porous structure (i.e., outside the EDL), we have a certain bulk pH and salt concentration, c_∞ (we consider a 1:1 salt), while the surface has a charge X that depends on pH_p (the pH in the pore) according to

$$X/X_{\max} = \alpha = \frac{1}{1 + 10^{-(\text{pK}-\text{pH}_p)}} = \frac{1}{1 + 10^{-(\text{pK}-\text{pH})} e^{\phi_D}} \quad (2.24)$$

where we introduce the ionization degree, α , which has a value between 0 and 1. (Note that without an index, pH refers to that outside the EDL, in the nearby bulk phase.) In Eq. (2.24) we assumed the material to be basic, thus to be either neutral (at very high pH) or positively charged (at lower pH). In Eq. (2.24), pH_p is pH in the pore, which relates at equilibrium to the pH outside the pore by $10^{\text{pH}_p} = 10^{\text{pH}} \cdot e^{\phi_D}$. We can jointly solve Eqs. (2.10), (2.11), (2.15) and (2.24) to obtain the results presented in Figure 2.1 for the ionization degree and hydrostatic pressure in a charged porous material.

We here present Eq. (2.24) without a derivation. In Ch. 1 the related Langmuir equation was derived for adsorption of neutral species, Eq. (1.17), while in §3.7 the Langmuir equation is derived for materials that are acidic, basic, or amphoteric.

Fig 2.1 shows that the ionization degree of a material with high pK (relative to pH) stays close to unity also at low salt concentration. For all values of pK, the pressure is low at high salt concentration and increases when c_∞ decreases. But only for the material with high pK will the pressure stay at a high value. For materials with lower values of pK, thus with pH closer to the pK of the material, at very low salt concentration the pressure starts to drop off again, because the ionization degree also goes down, i.e., the material discharges at low c_∞ . Thus, a gel with ionizable charge will have an internal pressure (pushing against the polyelectrolyte structure, to make it swell) which will be at a maximum at an intermediate salt concentration. Similar phenomena are also found in the theory of swelling of ionizable polyelectrolyte brushes.

2.6 The EDL at the interface between two porous layers of opposite charge

It is quite interesting to evaluate what happens when two charged porous materials, such as ion-exchange membranes, which have a difference in the sign of the fixed charges, are

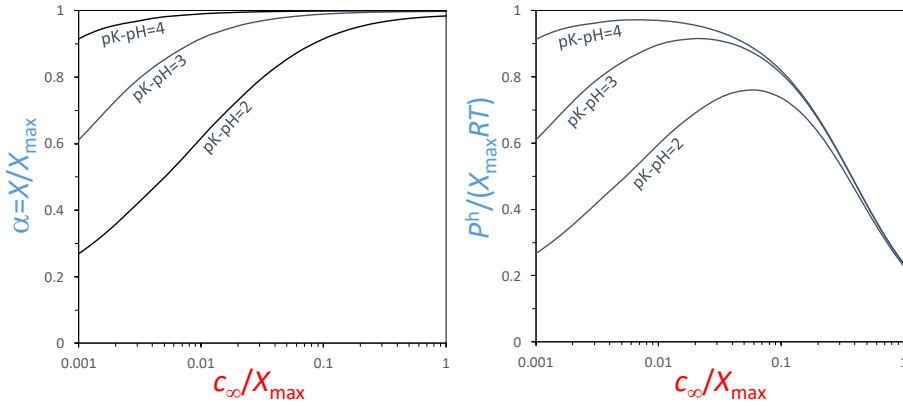


Fig. 2.1: The ionization degree α and hydrostatic pressure P^h in a charged gel as function of salt concentration c_∞ , pH, and membrane charge density, X_m (The charge of the gel is positive, i.e., it is a basic material).

placed in direct contact (while submersed in water). This happens for instance in bipolar membranes (BPMs), where a porous layer with a fixed positive charge, and one with fixed negative charge, are placed in direct contact, forming an EDL at the interface. Thus we have two adjacent layers with an opposite value of X . The cation-exchange layer contains many cations, and few anions, and the reverse is the case for the anion-exchange layer. At the interface, where these two layers are in contact, an EDL forms with a very large EDL voltage drop ΔV , the value of which depends on the charge density X in the two layers. How to solve for ΔV ?

One method is to solve Eq. (2.9) twice, once for each layer, and adding up the two Donnan potentials. But the question then is, how to find the value of salt concentration outside the EDL, c_∞ , that is required in this calculation? And what does c_∞ even mean? This question arises because there is no bulk electrolyte phase in between these two layers. The mathematical solution is that though there may indeed not be such a reservoir in reality, we can still conceive of a *virtual* reservoir here that has a certain salt concentration. Indeed, the calculation outcome will be the same if there really is a reservoir (the two layers are slightly apart) or when they are in close contact and we use the concept of a virtual reservoir.

But how to find the unknown concentration c_∞ in this (virtual) reservoir? If the BPM is in equilibrium, surrounded on all sides by water of the same salt concentration and composition, thus without imposed driving forces such as current or a pressure difference, then c_∞ in this (virtual) reservoir is the same as outside the membrane. If instead the BPM is operated in a

process, with ions and water flowing through the BPM, then determination of c_∞ is part of the full calculation of transport of ions through the two layers of the BPM. For instance when a current is applied, then dependent on the magnitude and direction of the current, the salt concentration in the virtual reservoir at the interface between the two layer can dramatically change from very high values (in the mol/L range) to values in the nM-range. The first case leads to repulsion between the layers and that may lead to the layers coming apart, while in the reverse situation, the layers are being firmly pressed onto one another (Pärnamäe et al., 2023).

2.7 Donnan equilibrium for a mixture of cations: ‘anomalous’ Ca²⁺-adsorption in collagen

Collagen is a natural polymer and this material is a porous (water-filled) structure of charged polyelectrolytes and protein. Overall this polymer is negatively charged. One observation in the study of collagen is that when it is submersed in water with monovalent and divalent cations, say Na⁺ and Ca²⁺, that when the electrolyte is diluted, that the material not simply desorbs ions, like in any regular adsorption/desorption process, but that while the monovalent cations desorb, the divalent cations are *taken up*. That is indeed a quite remarkable result, and unexpected at first sight. But when we realize that collagen is charged, we can make sense of these observations.¹

Though collagen is a complex mixture with many different surface groups, both acidic and basic, with different pK-values, here we use a fixed value of the charge density $|X|$, with $\omega = -1$ the sign of charge of the collagen. We also neglect expansion or contraction of the collagen, and we assume Boltzmann’s law to hold for all ions.

So, what happens when a negatively charged material is equilibrated with a solution containing monovalent and divalent cations, for instance Na⁺ and Ca²⁺, and containing Cl⁻ as anions, and then this mixture is diluted by a certain fraction? The charge balance for a negatively charged gel in equilibrium with an electrolyte solution is

$$\omega|X| + c_{\text{Na}^+}^c + 2c_{\text{Ca}^{2+}}^c - c_{\text{Cl}^-}^c = 0 \quad (2.25)$$

where superscript ‘c’ refers to concentrations inside the collagen gel.

To analyze this problem, we use c_∞ for the concentration of Cl⁻ in bulk solution, and define α as the Ca²⁺/Na⁺ mixing ratio in bulk solution, thus $\alpha = c_{\infty, \text{Ca}^{2+}} / c_{\infty, \text{Na}^+}$. Then the concentrations of the cations in bulk solution are $c_{\infty, \text{Ca}^{2+}} = c_\infty \cdot \alpha / (2\alpha + 1)$ and $c_{\infty, \text{Na}^+} = c_\infty / (2\alpha + 1)$. We also define $\beta = |X| / c_\infty$. If the membrane charge is fixed, β can be

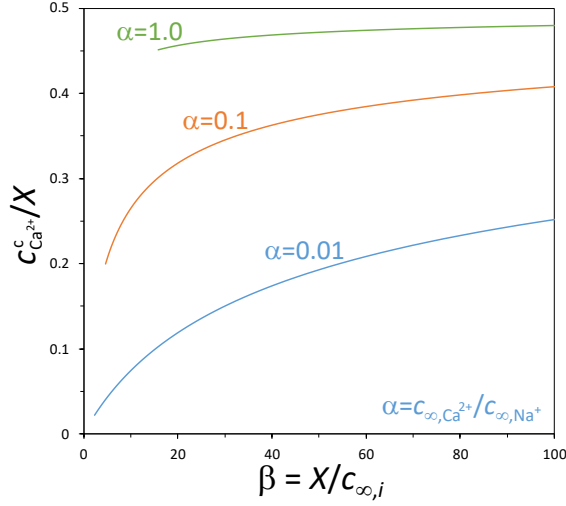


Fig. 2.2: The concentration of Ca^{2+} -ions inside a negatively charged hydrogel such as the natural polymer collagen, as function of dilution, β . The salt solution contains both monovalent and divalent cations in a concentration ratio $\alpha = c_{\infty, \text{Ca}^{2+}} / c_{\infty, \text{Na}^+}$. At low α , then with dilution (increasing β), the Ca^{2+} -concentration in the hydrogel steadily increases; thus, while the water around the material is diluted, Ca^{2+} -ions are absorbed.

interpreted as a degree of dilution: if we dilute the solution, then β increases (while dilution keeps the ratio α constant). We implement these definitions and Boltzmann's law, Eq. (2.2), in Eq. (2.25), after which we obtain a relation between α , β , and the Donnan potential, ϕ_D

$$\beta = (2\alpha + 1)^{-1} \left(e^{-\phi_D} + 2\alpha e^{-2\phi_D} \right) - e^{+\phi_D} \quad (2.26)$$

which can be solved numerically in ϕ_D after which the ion concentrations in the collagen can be calculated with Boltzmann's law. An analytical solution is possible but is complicated. To obtain a more insightful analytical solution, we assume that ϕ_D is sufficiently negative (which is the case when $\omega = -1$ and $|X|$ is sufficiently large), and then we can leave out the coion Cl^- from Eq. (2.26), i.e., we omit the term $-e^{+\phi_D}$. We then solve Eq. (2.26), see [here](#), and obtain

$$c_{\text{Ca}^{2+}}^c = X \cdot \left(\sqrt{1 + \gamma} - 1 \right)^2 / (2\gamma) \quad (2.27)$$

where $\gamma = 8 \cdot |X| \cdot c_{\infty, \text{Ca}^{2+}} / c_{\infty, \text{Na}^+}^2 = 8\alpha\beta(2\alpha + 1)$.

The dependence of the Ca^{2+} -concentration on α and β as described by Eq. (2.27) is analyzed in Fig. 2.2 which shows that especially at a low mixing ratio α , when the solution

is diluted (and thus β goes up), that the Ca^{2+} -concentration in the collagen matrix increases. Thus one will observe that Ca^{2+} is absorbed from solution into the collagen matrix, even when the solution is diluted.^v This result shows how absorption in a porous material such as a polyelectrolyte gel, in which charge neutrality must be maintained, is fundamentally different from the absorption of neutral molecules in a neutral material. In aqueous systems most if not all absorbents carry a charge and thus Donnan effects such as just discussed play a key role in absorption.

2.8 Donnan equilibrium at the membrane/solution interface

In this section we discuss the Donnan layer at the interface between a solution phase (electrolyte) and a charged gel or membrane, where we derive and then use the general Boltzmann equation, Eq. (2.1). Thus we now combine the electrostatic Donnan effect with partitioning due to volume effects or due to the affinity of an ion with a certain phase, but other contributions are possible too. Solute partitioning is of importance for instance in Ch. 11 that deals with ion adsorption in charged membranes and transport across them. For some membranes the water-filled pore phase is highly constricted, thus partitioning because of size exclusion plays an important role besides Donnan electrostatics.

We can derive the general Boltzmann equation from an expression for the chemical potential of an ion i , including an affinity term, and an excess (volume exclusion) term, which for an ion in each separate phase is written as

$$\mu_{i,j} = \mu_{\text{ref},i} + \ln(c_{i,j}/c_{\text{ref}}) + \mu_{\text{aff},i,j} + \mu_{\text{exc},i,j} + z_i\phi_j \quad (2.28)$$

where $\mu_{\text{aff},i}$ includes all possible effects not related to charge or ion volume, generally called affinity, which can include contributions such as dielectric exclusion, image forces, and ion dehydration energy. In Eq. (2.28) index j refers to position, which can be in solution, ‘ ∞ ’, or in the membrane, ‘ m ’.^{vi,vii} If we equate the chemical potentials in solution with that just

^vAt very low β we must include the anions in the charge balance, i.e., Eq. (2.27) is not valid at low β . At very low β , $c_{\text{Ca}^{2+}}^c/X$ increases again. The lines in Fig. 2.2 are for β high enough that anions have a low concentration in the collagen and Eq. (2.27) is valid.

^{vi}See p. 507 for an explanation how each μ -term in Eq. (2.29) can be multiplied by a term RT to arrive at a dimensional potential with unit of J/mol.

^{vii}EDL models are solved for conditions of *chemical* equilibrium, and then *mechanical* equilibrium is also established. In problems of flow of solutes, these equilibria conditions do not apply, and then Eq. (2.28) has an additional term, $v_i P^{\text{tot}}$ that is discussed in several upcoming chapters. At mechanical (and thus also at chemical) equilibrium, this term is zero.

inside the membrane, we arrive at

$$\ln c_{\infty,i} + \mu_{\text{aff},\infty,i} + \mu_{\text{exc},\infty,i} + z_i \phi_{\infty} = \ln c_{\text{m},i}^* + \mu_{\text{aff},\text{m},i} + \mu_{\text{exc},\text{m},i} + z_i \phi_{\text{m}} \quad (2.29)$$

where constant terms $\mu_{\text{ref},i}$ and $\ln c_{\text{ref}}$, that show up on both sides, are cancelled. On the right side of Eq. (2.29), we use a term $c_{\text{m},i}^*$ to denote a concentration of ions or other solutes defined per unit total membrane volume (i.e., for the totality of the water- and ions-filled pores together with the solid polymer membrane matrix structure). When we are not at mechanical equilibrium, an ion's chemical potential also includes the insertion pressure (a term which is zero at equilibrium), which is the last term in Eq. (7.63) in Ch. 7.

One contribution to $\mu_{\text{exc},\text{m},i}$ relates to the exclusion of ions from the membrane matrix, where by 'matrix' we refer to the polymer network and structure of which the membrane is made. This exclusion effect simply implies: where there is polymer (membrane structure), there can not be an ion (and neither a water molecule). We can quantify this excess term by using the Carnahan-Starling equation of state (CS-EOS), or any of its extensions to multicomponent systems, and to porous structures, such as Eq. (4.11) in Ch. 4. When we assume that the ions do not have any volume, i.e., they are point charges, only being excluded from the volume occupied by the membrane structure, the consequence of the CS equation of state is that $\mu_{\text{exc},\text{m},i} = -\ln p_{\text{m}}$ where p_{m} is the porosity of the membrane, i.e., the fraction of the total volume that is available to water and ions, i.e., the fraction of the total volume that consists of pores, see Fig. 7.7. If we combine this term with the concentration term, we have

$$\mu_{\text{exc},\text{m},i} + \ln c_{\text{m},i}^* = -\ln p_{\text{m}} + \ln c_{\text{m},i}^* = \ln c_{\text{m},i} \quad (2.30)$$

where the ion concentration per unit pore volume, $c_{\text{m},i}$, is given by $c_{\text{m},i} = c_{\text{m},i}^*/p_{\text{m}}$. We include this result in Eq. (2.29), and we can do the same for an ion in solution, where $p_{\infty} = 1$ and thus the related term is $\mu_{\text{exc},\infty,i} = 0$. In general there is still an excess contribution on top of the effect just described, so the conversion just discussed does not make volume effects go away, and thus in the equations below, there still is an excess term. Detailed expressions for these excess, volume, effects will be discussed in §4.2, §7.8, and §8.1. Volume is important to consider because it has a significant effect on ion partitioning and thus on ion selectivity in membrane processes.

To further simplify Eq. (2.29), we implement the definition of the Donnan potential, $\Delta\phi_{\text{D}} = \phi_{\text{m}} - \phi_{\infty}$, and we use the notation of $\Delta\mu_{k,i}$ to describe a difference in each of the $\mu_{k,i}$ -contributions between inside the membrane, and in solution. We then arrive at

$$\ln c_{\infty,i} = \ln c_{\text{m},i} + \Delta\mu_{\text{aff},i} + \Delta\mu_{\text{exc},i} + z_i \Delta\phi_{\text{D}}. \quad (2.31)$$

Now, all of these contributions to an ion's chemical potential (except the $\ln c$ -term) can be rewritten to a contribution to the partition coefficient, $\Phi_{k,i}$, where k refers to the type of energy (excess, affinity, etc.), and i to the species, according to

$$\Phi_{k,i} = \exp(-\Delta\mu_{k,i}) \quad , \quad \Delta\mu_{k,i} = \mu_{k,m,i} - \mu_{k,\infty,i} \quad (2.32)$$

and if we apply it to the affinity and volume (excess) terms, we then have

$$\Phi_{\text{aff},i} = \exp(-(\mu_{\text{aff},m,i} - \mu_{\text{aff},\infty,i})) \quad , \quad \Phi_{\text{exc},i} = \exp(-(\mu_{\text{exc},m,i} - \mu_{\text{exc},\infty,i})) \quad (2.33)$$

Including these conversions in Eq. (2.31) we arrive at a detailed general Boltzmann equation

$$c_{m,i} = c_{\infty,i} \cdot \Phi_{\text{aff},i} \cdot \Phi_{\text{exc},i} \cdot \exp(-z_i\phi_D) \quad (2.34)$$

and if we combine the contributions to the partitioning of a species across an interface (those that we identified here) into a single term, Φ_i , thus $\Phi_i = \prod_k \Phi_{k,i}$ (except for the term $\exp(-z_i\phi_D)$), then Eq. (2.34) simplifies to the general Boltzmann equation, Eq. (2.1). In Eq. (2.34), and throughout this book, we described the Donnan (Boltzmann) term separately, and only subsume non-Donnan effects into the Φ_i -function. However, one can also define a Donnan (contribution to the) partition function, $\Phi_D = \exp(-z_i\phi_D)$ and consider this Donnan partitioning as another contribution to Φ_i .

In a real membrane process, there are many types of ions to consider, and for all of them we evaluate Eq. (2.1). All ions have a different value for Φ_i , and will also have different valencies, z_i . Also for neutral species such as carbonic acid and ammonia we use Eq. (2.1), with $z_i=0$. All of these Donnan equations for each ion separately are solved simultaneously with local electroneutrality in the solution phase just outside the membrane, as well as local electroneutrality just inside the membrane (just 'beyond' the Donnan layer), where local EN inside the membrane also includes the membrane charge, X , and thus we have

$$\sum_i z_i c_{m,i} + X = 0. \quad (2.35)$$

For all ions, Eq (2.1) can be inserted in Eq. (2.35), to arrive at a relation between membrane charge X , solution concentrations, and Donnan potential, ϕ_D . Note that the membrane charge, X , is defined –like ion concentrations– as a concentration per unit pore volume. The resulting Donnan potential can be used again in Eq. (2.1) to calculate for each ion the concentration just inside the membrane. When membrane charge is a function of local pH (just in the membrane) or dependent on any other ion concentration, this adds an additional relation to the set of equations to be solved simultaneously, such as $X = f(c_{m,H^+})$, but otherwise this addition does not change the Donnan model equations.

Thus we can insert the general Boltzmann equation, Eq. (2.1), in Eq. (2.35) and that leads to

$$\sum_i z_i c_{\infty,i} \Phi_i \exp(-z_i \phi_D) + X = 0 \quad (2.36)$$

which can always be solved if for all ions we know Φ_i . [Note that in the derivation which follows Φ_i is assumed to be independent of ion concentrations. Equations until the present point did not require that assumption.] If we have a symmetric salt (with $z=1$ for a 1:1 salt, $z=2$ for a 2:2 salt, etc.), and all cations have the value Φ_+ , and all anions Φ_- , this simplifies to

$$z c_{\infty} (\Phi_+ \exp(-z \phi_D) - \Phi_- \exp(z \phi_D)) + X = 0 \quad (2.37)$$

which can be rewritten to

$$z c_{\infty} \sqrt{\Phi_+ \Phi_-} (\exp(-(z \phi_D + \frac{1}{2} \ln(\Phi_-/\Phi_+))) - \Phi_- \exp(z \phi_D + \frac{1}{2} \ln(\Phi_-/\Phi_+))) + X = 0 \quad (2.38)$$

and thus

$$-2z c_{\infty} \sqrt{\Phi_+ \Phi_-} \sinh(z \phi_D + \frac{1}{2} \ln(\Phi_-/\Phi_+)) + X = 0 \quad (2.39)$$

and thus

$$z \phi_D + \frac{1}{2} \ln(\Phi_-/\Phi_+) = \sinh^{-1} \left(\frac{X}{2\sqrt{\Phi_+ \Phi_-} c_{\infty}} \right). \quad (2.40)$$

We can write an equation for the total ions concentration in the membrane, $c_{T,m} = c_{m,+} + c_{m,-}$, similar to Eq. (2.40), which leads to

$$z \phi_D + \frac{1}{2} \ln(\Phi_-/\Phi_+) = \cosh^{-1} \left(\frac{c_{T,m}}{2\sqrt{\Phi_+ \Phi_-} c_{\infty}} \right) \quad (2.41)$$

and thus combination of Eqs. (2.40) and (2.41) leads to

$$c_{T,m}^2 = (X/z)^2 + \Phi_+ \Phi_- (2c_{\infty})^2 \quad (2.42)$$

and this relation depends on the geometric mean partition coefficient, $\sqrt{\Phi_+ \Phi_-}$, but not on the individual factors Φ_- and Φ_+ . It turns out that the same holds for the cation and anion concentration in the membrane, as long as X is fixed and as long as $\sqrt{\Phi_+ \Phi_-}$ is the same. Thus, even when for one ion the factor Φ_i is increased, if we lower that for the other ion such that the geometric mean stays the same, the cation and anion concentrations stay the same. This result implies that for a symmetric binary solution, with one value of Φ_i for all cations, one for all anions, the only property of relevance is the geometric mean partition coefficient, $\sqrt{\Phi_+ \Phi_-}$. This implies that we cannot experimentally distinguish between the two values,

and theory only requires consideration of the geometric mean.^{viii} So from this point onward, we use Φ_i as if both ions have the same partition coefficient, or as the geometric mean in case they are different.

In that latter case, differences between Φ_i for cat- and anions (as long as the geometric mean is the same) will influence the Donnan potential ϕ_D , and this will influence proton adsorption thus pH, and then individual values for Φ_i do matter, but except for such indirect effects, the use of one Φ_i -value for both ions does not influence the predicted EDL structure, thus does not influence $c_{T,m}$ and neither does it influence co- and counterion concentrations just in the membrane. So we continue now using Φ_i as the geometric mean of the individual partition coefficients, or, in a simplified situation, we just assume it is the same for all ions. When all ions are monovalent (or some are zero-valent, i.e., neutral), and we now use the same Φ_i for all ions, then the Donnan potential follows from

$$X = 2c_\infty\Phi_i \sinh \phi_D \quad (2.43)$$

and the total ions concentration (anions *plus* cations) in the membrane becomes

$$c_{T,m} = \sqrt{X^2 + (2\Phi_i c_\infty)^2} \quad (2.44)$$

which is always larger than $|X|$. With $\alpha = X/(2\Phi_i c_\infty)$, the counterion ('ct') concentration in the membrane is given by

$$\frac{c_{m,ct}}{\Phi_i c_\infty} = \sqrt{1 + \alpha^2} + |\alpha| \quad (2.45)$$

which is always larger than $|X|$, just like $c_{T,m}$, while the coion ('co') concentration is

$$\frac{c_{m,co}}{\Phi_i c_\infty} = \frac{\Phi_i c_\infty}{c_{m,ct}} = \left(|\alpha| + \sqrt{1 + \alpha^2}\right)^{-1} = \frac{c_{T,m} - c_{m,ct}}{\Phi_i c_\infty} = \sqrt{1 + \alpha^2} - |\alpha|. \quad (2.46)$$

which is smaller than $|X|$ as long as c_∞ is smaller than $\sqrt{2}|X|/\Phi_i$.

This concludes the description of the Donnan layers formed at the interface of membrane and solution. These results are used again in Ch. 11 to describe desalination of water.

references

1. M. Higa, A. Kira, A. Tanioka, and K. Miyasaka, "Ionic partition equilibrium in a charged membrane immersed in a mixed ionic solution," *J. Chem. Soc. Faraday Trans.* **89**, 3433–3435 (1993).

^{viii}To find the individual values we need very precise experiments with at least three different ions.

The EDL for a planar surface: The Gouy-Chapman-Stern model

The most well-known electrical double layer (EDL) model is the one named after Gouy, Chapman, and Stern, abbreviated as the GCS-model. This EDL model describes the ion distributions, and potential profile, in a thin layer next to a planar surface in contact with electrolyte with free ions. We also discuss extensions of the GCS-model that include ion volume effects and fixed background charge.

3.1 Introduction

The Gouy-Chapman-Stern (GCS) model is the textbook example of an EDL model. It may even be the case that some have come under the impression that the concept of an EDL is equivalent to the GCS model. This is of course not correct: the EDL is a much broader concept than just the GCS approach and the GCS model is just one example amongst many (see previous chapters) of EDL models. In practice, the GCS model is not very widely used in electrochemical process modelling, where preference is given to the Donnan- and isotherm-based models of earlier chapters. What the GCS model does is to describe the EDL of a planar charged surface in contact with an electrolyte phase where other surfaces are absent or sufficiently far away (for instance, at 10 mM salt concentration in water, far enough away would be a separation of more than ~ 20 nm), see Fig. 3.1. In the electrolyte, ions –mainly of a charge sign opposite to the charge of the surface, i.e., counterions– reside near the surface in the diffuse layer (DL). The DL is a theoretical element of the GCS EDL model. Sometimes the DL is called the space charge region.

In the DL, concentrations of ions change from a bulk value outside the DL to a different value near the surface. In bulk solution, the electrolyte is charge neutral (for a 1:1 solution this means we have equal concentrations of cations and anions) but coming nearer to the surface, ‘entering’ the DL, the concentration of counterions (those ions with a charge sign opposite to that of the surface) increases gradually, while the concentration of co-ions (ions with the same charge sign as that of the surface) decreases. Thus a local charge density, ρ , develops (positive when the counterions are cations), and integrated over the DL, this charge density will exactly compensate the charge of the surface, Σ , thus $\int_D^\infty \rho \, dx + \Sigma = 0$ where ‘D’ refers to the Stern plane, see Fig. 3.1, and where ‘ ∞ ’ refers to a position outside the DL. The EDL as a whole is electroneutral.

The DL has a certain thickness, describing the distance over which the ion concentration profiles are clearly different from those in bulk solution, and this thickness is a few times the Debye length, λ_D , which is a number that is inversely proportional to the square root of salt concentration. For instance, for a 1:1 solution, at 10 mM salt concentration, at room temperature, in water, $\lambda_D \sim 3.1$ nm (at 1 mM it is ~ 10 nm, at 100 mM it is ~ 1 nm). For the GCS model to be accurate, the separation between two surfaces must at least be several times the Debye length. ‘Overlap’ of diffuse layers (also called overlap of EDLs, i.e., interaction of two EDLs) is discussed in Ch. 6, as well as the resulting disjoining pressure, which describes the problem of colloidal stability.

The GCS model is of relevance in electrochemistry where it is involved in models for electrochemical reactions at flat electrodes, and in porous electrodes when the material is

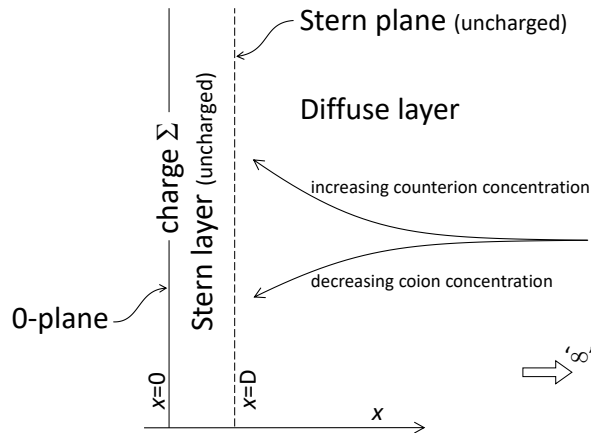


Fig. 3.1: The Gouy-Chapman-Stern (GCS) model consists of a charged 0-plane, an uncharged Stern layer, an uncharged Stern plane, and a charged diffuse layer. The diffuse layer contains counterions and coions distributed over space. The Stern plane, or ‘D-plane’ is uncharged and functions as a closest-approach distance for (the centers of) the ions to come near the surface. In the standard GCS model there is no layer of ‘condensed’ counterions in the Stern layer or on the Stern plane.

sufficiently flat and there is not much EDL overlap (for instance for a porous electrode made of isolated graphene sheets, or the EDL on the outside of carbon nanotubes with sufficiently large diameters.) Otherwise deviations from the Cartesian geometry must be included in the EDL model, or the overlap of the EDLs. The GCS model is also of use for the EDL structure on ‘hard’ surfaces in water, for instance oxidic materials such as silica, alumina and titania, or a material such as mica or glass. And also for the EDL structure around spherical nano-particles such as micelles or globular protein molecules, a (spherical version of) GCS theory can be used.

In the present chapter we focus on the structure of the single planar EDL, and describe microscopic aspects (such as profiles of concentration), as well as phenomenological aspects (for instance, ion adsorption as function of EDL voltage). Application of the GCS model to the surface pressure of an ionizable surface, and the EDL forces involved in electrowetting of an electrode, these two topics are discussed in Ch. 5.

3.2 The Gouy-Chapman-Stern model

To describe the distribution of ions in the diffuse layer (DL), the starting point is Maxwell's first law, also called Gauss's law in differential form, or the Poisson equation

$$\nabla \cdot (\varepsilon \mathbf{E}) = \rho \quad (3.1)$$

where ε is the dielectric permittivity of the electrolyte, given by $\varepsilon = \varepsilon_r \varepsilon_0$, where for water the dielectric constant is $\varepsilon_r \sim 78$, while ε_0 is the permittivity of vacuum, given by $\varepsilon_0 = 8.854 \cdot 10^{-12} \text{ C}/(\text{V} \cdot \text{m})$. In Eq. (3.1), \mathbf{E} is the field strength, which is minus the gradient of the electric potential, $\mathbf{E} = -\nabla V$, and ρ is the local charge density in C/m^3 . Assuming ε to be a constant, we arrive atⁱ

$$\frac{\partial^2 V}{\partial x^2} = -\frac{\rho}{\varepsilon} \quad (3.2)$$

where we also assumed a one-dimensional planar (Cartesian) geometry, with a single coordinate axis, x . Next we replace the dimensional voltage V with the nondimensional electrical potential ϕ , according to $\phi = V/V_T$, where $V_T = RT/F$ is the thermal voltage, which at room temperature is $V_T \sim 25.6 \text{ mV}$, and we arrive at

$$\frac{\partial^2 \phi}{\partial x^2} = -\frac{F}{\varepsilon RT} \rho. \quad (3.3)$$

The ionic charge density ρ has contributions from all free ions in the electrolyte, $\rho = F \sum_i (z_i c_i)$, and thus Eq. (3.3) becomes

$$\frac{\partial^2 \phi}{\partial x^2} = -\frac{F^2}{\varepsilon RT} \sum_i z_i c_i. \quad (3.4)$$

Up to this point the equation we considered is the Poisson equation, valid irrespective of whether (locally) the system is at equilibrium or not. When equilibrium can be assumed for the EDL, and for ions as ideal point charges, the Boltzmann equation, Eq. (2.1), applies, which can be written as

$$c_i = c_{\infty,i} e^{-z_i \phi} \quad (3.5)$$

ⁱIt is a major assumption to set ε as a constant, independent of composition and frequencies of changes in the electric field. Many fundamental physical theories, for instance to describe the Van der Waals energy of the interaction between polarizable materials across another medium, consider the entire spectrum of the ε -dependence on the frequency of changes in the electrical field due to dipole effects. This is beyond the scope of this book.

where ϕ is the potential at some position x in the DL relative to a position just outside the EDL in a charge neutral bulk phase. This outside position is often identified with an index ∞ . We describe here the ion distribution within the same phase, water in most cases, and thus a non-electrostatic contribution to the chemical potential of an ion, which would be described by a partition coefficient Φ_i , can be left out in Eq. (3.5). Combining Eqs. (3.4) and (3.5), we obtain a general form of the Poisson-Boltzmann (PB) equation

$$\frac{\partial^2 \phi}{\partial x^2} = -\frac{F^2}{\varepsilon RT} \sum_i z_i c_{\infty,i} e^{-z_i \phi}. \quad (3.6)$$

When we have a symmetric salt solution (1:1, 2:2, etc.) with $|z|$ the magnitude of the valency of the ions in the salt pair, i.e., $|z| = \{1, 2, \text{etc.}\}$, then Eq. (3.6) becomes

$$\frac{\partial^2 |z| \phi}{\partial x^2} = \kappa^2 \sinh |z| \phi \quad (3.7)$$

where κ , which is the inverse of the Debye length, is given by Eq. (3.19) that is discussed below. For a 1:1 solution (all ions monovalent), $|z| = 1$, and thus Eq. (3.7) becomes

$$\frac{\partial^2 \phi}{\partial x^2} = \kappa^2 \sinh \phi. \quad (3.8)$$

The charge-voltage relationship in the GCS model can be derived from Eq. (3.6), by multiplying both sides with $\partial \phi / \partial x$ and integrating, to

$$\frac{1}{2} \frac{\partial}{\partial x} \left(\frac{\partial \phi}{\partial x} \right)^2 = +\frac{F^2}{\varepsilon RT} \sum_i c_{\infty,i} \frac{\partial}{\partial x} e^{-z_i \phi}. \quad (3.9)$$

Now, with the potential ϕ set to zero far away, where $x = \infty$, and with the gradient $\partial \phi / \partial x$ zero there as well, we arrive at

$$\left(\frac{\partial \phi}{\partial x} \right)^2 = +\frac{2F^2}{\varepsilon RT} \sum_i c_{\infty,i} (1 - e^{-z_i \phi}). \quad (3.10)$$

This equation is valid at each point in a DL. At the Stern plane, which is boundary of the DL, denoted with label 'D', we have an additional condition, which is Gauss's law

$$\Sigma = \varepsilon E \quad (3.11)$$

where Σ is the surface charge density (unit C/m²), and where we assume we only have to consider the electric field in x -direction. With x pointing from the surface into solution, then

$E = -V_T \cdot \partial\phi/\partial x$. Gauss's law, Eq. (3.11), does not depend on the structure of the diffuse layer, such as ion concentration or valencies of ions. Eq. (3.11) can be rewritten to

$$\Sigma = -\frac{\varepsilon RT}{F} \left. \frac{\partial\phi}{\partial x} \right|_D. \quad (3.12)$$

We combine Eqs. (3.10) and (3.12) and obtain

$$\Sigma = \text{sgn}(\phi_D) \sqrt{2\varepsilon RT \sum_i c_{\infty,i} (e^{-z_i \phi_D} - 1)} \quad (3.13)$$

where ϕ_D is the diffuse layer potential, i.e., the potential at the Stern plane, relative to the potential in bulk solution, $\phi_\infty=0$. The Stern plane is the position nearest to the surface up to which we still consider the PB-equation to hold.ⁱⁱ Eq. (3.13) is a generalized Gouy-Chapman equation, valid for mixtures of salts, within the PB framework. The sign of Σ is the same as that of ϕ_D . When we have a symmetric salt solution (all ions monovalent, or all ions divalent, etc.), then Eq. (3.13) simplifies to

$$\Sigma = \text{sgn}(\phi_D) \sqrt{4\varepsilon RT c_\infty} \sqrt{\cosh(|z|\phi_D) - 1} = \sqrt{8\varepsilon RT c_\infty} \sinh(|z|\phi_D/2) \quad (3.14)$$

and when we only have monovalent ions, i.e., a 1:1 solution, then Eq. (3.14) simplifies to

$$\Sigma = \sqrt{8\varepsilon RT c_\infty} \sinh(\phi_D/2). \quad (3.15)$$

This is the classical Gouy-Chapman (GC) equation for a 1:1 solution, which can be inverted to

$$\phi_D = 2 \cdot \sinh^{-1} \left(\frac{\Sigma}{\sqrt{8\varepsilon RT c_\infty}} \right). \quad (3.16)$$

We can also express Eq. (3.15) as (here presented in way valid only for 1:1 salt solution)

$$\Sigma = 4F c_\infty \lambda_D \sinh(\phi_D/2) = 2\varepsilon V_T \kappa \sinh(\phi_D/2) \quad (3.17)$$

where λ_D is the Debye length and κ is the inverse of λ_D . The general definition of κ is

$$\kappa = \lambda_D^{-1} = \sqrt{\frac{2F^2 I}{\varepsilon RT}} \quad (3.18)$$

where I is the ionic strength, which is given by $I = \frac{1}{2} \sum_i z_i^2 c_{\infty,i}$, in which we sum over all ions. For a symmetric salt solution this expression simplifies to

$$\kappa = \lambda_D^{-1} = \sqrt{\frac{2|z|^2 F^2 c_\infty}{\varepsilon RT}}. \quad (3.19)$$

ⁱⁱPoisson's equation still holds beyond the Stern plane, but we assume there are no more (centers of) ions.

For a 1:1 solution, a linearised version of the GC equation for low ϕ_D is

$$\Sigma = \sqrt{2\varepsilon RT c_\infty} \phi_D = 2Fc_\infty \lambda_D \phi_D = \varepsilon V_T \kappa \phi_D. \quad (3.20)$$

Gouy-Chapman equation based on 1:1 salt solution. When we assume from the start that we have a 1:1 salt solution, then Eq. (3.8) applies where we can again multiply each side with $\partial\phi/\partial x$, and integrate by parts, resulting in

$$\frac{1}{2} \frac{\partial}{\partial x} \left(\frac{\partial\phi}{\partial x} \right)^2 = \kappa^2 \frac{\partial}{\partial x} \cosh \phi. \quad (3.21)$$

With the same boundary conditions that potential $\phi = 0$ and $\partial\phi/\partial x = 0$ when $x \rightarrow \infty$, the relation at the Stern plane (position ‘D’) between potential and potential gradient becomes

$$\left(\frac{\partial\phi}{\partial x} \Big|_D \right)^2 = 2\kappa^2 (\cosh \phi_D - 1) \quad (3.22)$$

in which we implement Eq. (3.12), resulting in

$$\Sigma = \text{sgn}(\phi_D) \frac{\varepsilon RT}{F} \sqrt{2\kappa^2 (\cosh \phi_D - 1)} = \text{sgn}(\phi_D) \sqrt{8c_\infty \varepsilon RT} \sinh \phi_D / 2 \quad (3.23)$$

which for $|z|=1$ is equal to Eq. (3.14).

Gauss’s law. In the above derivation we made use of Gauss’s law, Eq. (3.11). This law is an integral version of the Poisson equation, Eq. (3.1), but in Eq. (3.11) some assumptions are made in the integration about the electric field outside the EDL on either side (namely that they are zero). No such assumptions are involved in Eq. (3.1).

To explain this, we start with Eq. (3.1) and integrate over a planar layer from one x -position to another (from position 1 which is the Stern plane, to a position 2 which is outside the DL in the electrolyte; thus we assume a Cartesian, i.e., planar, geometry, with only one coordinate, x ; the system is invariant in directions that are at right angles to x), resulting in

$$(\varepsilon E)_2 - (\varepsilon E)_1 = \int_1^2 \rho dx. \quad (3.24)$$

The right side is equal to the diffuse layer charge, Σ_{DL} , when we identify position ‘1’ with the Stern plane and position ‘2’ with the solution outside the DL (‘ ∞ ’). (When

two equal diffuse layers overlap, in a problem of colloidal interaction, then we have $E = 0$ at a midplane located halfway between the two particles.) If outside the DL we can assume that the field strength is zero, the first term on the left is zero, and we obtain Eq. (3.11) when we realize that the surface charge Σ is equal to minus the diffuse layer charge Σ_{DL} because the EDL as a whole is electroneutral.

We can also integrate Eq. (3.1) from a position 0^* (which is just left of the surface charge Σ which is located in the 0-plane) and then across the Stern layer to position 1, and then we obtain

$$(\varepsilon E)_1 - (\varepsilon E)_{0^*} = \int_{0^*}^1 \rho dx. \quad (3.25)$$

Now on the right is the surface charge Σ , because there is no charge in the Stern layer. On the left side we can implement that the field strength at position 0^* is zero. Thus we again arrive at Eq. (3.11).

Under which conditions is the field strength zero at position 0^* , i.e., just left of the 0-plane? This is the case when for symmetry reasons the field strength inside the charged material (e.g., a colloidal particle or polymer network) is zero (for instance because ‘on its other end’ there is the same EDL structure). A zero field strength at position 0^* is also the case for a metallic phase, because in a metal the charge will reside at the surface (such as at plane 0) and thus just inside a metal the field strength is zero.

There are also situations that the surface charge is not concentrated in plane 0, but it is volumetrically distributed to the left of plane 0, possibly ‘mixed’ with fixed charges in the network (e.g., polymeric charges, or the p- and n-dopants in a semi-conductor). This can be modelled with an extra ‘layer of diffuse and fixed charge’ to the left of $x = 0$. Exactly at $x = 0$ we now have continuity in potential and chemical potential (like before), and we have Gauss’s law applied to this surface, *now without charge in this very 0-plane*, which becomes (based on an integration of Eq. (3.1) across this plane)

$$(\varepsilon E)_{\text{just right of } x=0} - (\varepsilon E)_{\text{just left of } x=0} = 0. \quad (3.26)$$

Based on this understanding we can now model various problems in this book where we have ‘twin’ diffuse layers where one layer is inside a charged polymer network (such as inside an ion-exchange membrane or gel), another in a semi-conductor or other ion-conducting solid state material, or the DL is in a liquid electrolyte such as water.

We continue with the Gouy-Chapman equation, and unless otherwise noted, we consider

a 1:1 solution. A very elegant way to write the GC equation is

$$\frac{Q}{2} = \sinh \frac{\phi_D}{2} \quad (3.27)$$

where Q is a dimensionless charge density

$$Q = \frac{\Sigma \lambda_D}{\varepsilon V_T}. \quad (3.28)$$

The diffuse layer potential ϕ_D is the potential at the Stern plane. The Stern *plane* is the plane that separates the diffuse layer from the Stern *layer*. The Stern layer we discuss later. In the standard GCS model the Stern plane is uncharged. It is solely the plane that borders the region in which (the centers of) the ions in the DL can reside. Thus, the Stern plane can best be considered a plane of ‘closest approach’ of (the centers of) ions to the surface. They cannot approach the hard surface (the 0-plane) any closer. Thus, all ions are volumetrically distributed in the DL, all the way up to the Stern plane, but without any specific adsorption in the Stern plane or Stern layer. In a graphical representation of the GCS model, it would be erroneous to draw even a few, let alone many, counterions as if adsorbed in the Stern plane. In the DL the charge is volumetrically distributed (charge density has unit C/m^3), but this does not imply that charge resides in the Stern plane. Nevertheless, we can speak of an (integrated) DL charge, where the volumetric charge over the DL is integrated from the Stern plane out to infinity, to obtain a DL charge with unit C/m^2 . The Stern layer is a layer between the Stern plane and the ‘hard’ surface (which is the 0-plane). The Stern layer is a dielectric layer not containing any charges.

Eqs. (3.10) and (3.15) provide relationships between potential ϕ and gradient $\partial\phi/\partial x$, which at the Stern plane leads to a relation between surface charge Σ and potential ϕ_D , which is the (generalized) GC-equation. However, this is not yet an explicit solution for the profile $\phi(x)$. This can be obtained by integrating Eq. (3.10) once again, which results in

$$\phi(x) = 4 \cdot \tanh^{-1} \{e^{-\kappa x} \cdot \tanh(\phi_D/4)\} \quad (3.29)$$

with the coordinate x starting at zero at the Stern plane and pointing into solution. For values of ϕ_D below unity, Eq. (3.29) can be approximated to

$$\phi(x) = \phi_D \cdot e^{-\kappa x} \quad (3.30)$$

which can also be derived when we combine Eqs. (3.12) and (3.20) (and implement $\phi_D \rightarrow \phi$) which results in

$$\lambda_D \frac{\partial\phi}{\partial x} = -\phi \quad (3.31)$$

which can be rewritten to

$$\int_{\phi_D}^{\phi} \frac{1}{\phi} d\phi = -\kappa \int_0^x dx \quad (3.32)$$

which after integration leads to Eq. (3.30). Even though Eq. (3.30) is not exact at higher potentials, it illustrates well the exponential-like decay of electrical potential with increasing distance x from the surface. The charge-voltage relationship compatible with Eq. (3.30) is Eq. (3.20).

An alternative version of Eq. (3.29) is

$$\frac{\exp(\frac{1}{2}\phi(x)) + 1}{\exp(\frac{1}{2}\phi(x)) - 1} \cdot \frac{\exp(\frac{1}{2}\phi_D) - 1}{\exp(\frac{1}{2}\phi_D) + 1} = \exp(\kappa x) \quad (3.33)$$

which is easy to solve in commercial spreadsheet software as we explain next. For a certain value of ϕ_D we make a list of values for ϕ between 0 and ϕ_D and we use Eq. (3.33) to calculate the corresponding value of x , and then we plot $\phi(x)$ vs. x . We can implement this x -dependent potential, $\phi(x)$, in the Boltzmann relation, Eq. (3.5), and directly calculate the profiles in concentration of cations and anions versus x -position, which we can again do in spreadsheet software. This calculation will show that the concentration of counterions goes up towards the surface, to reach a maximum value at the surface (i.e., at the Stern plane), while the concentration of coions drops the closer one approaches the surface, to values that at high voltage are almost zero. [Let it be reiterated that the high concentration of counterions near the Stern plane (expressed as a volumetric concentration in mol/m³) does not imply there are ions adsorbed *in* the Stern plane (which would have the unit mol/m²). In the GCS theory, there are no ions adsorbed *in* the Stern plane.]

In the limit of low ϕ_D , we can combine the Boltzmann equation with Eq. (3.30) and obtain for the profile of ion concentration

$$c_i(x) = c_{\infty,i} \cdot \exp(-z_i \phi_D \cdot \exp(-\kappa x)) \quad (3.34)$$

Just as Eq. (3.30), Eq. (3.34) is not exact, but illustrates counterion and coion concentration profiles. It is also in agreement with the fact that when the Boltzmann equation applies, for a 1:1 salt, we have at each position in the EDL the relationship $c_+ c_- = c_{\infty}^2$.

In Fig. 3.2 we compare concentration profiles according to the exact GC-equation with Eq. (3.34), for the same surface charge of $\Sigma = 20$ mC/m² and for $c_{\infty} = 10$ mM. For the GC model, this surface charge recalculates to a diffuse layer potential, ϕ_D , of 67 mV, about 2.5× the thermal voltage. However, in the linearised model, the same surface charge leads to a potential of ϕ_D of 88 mV, about 30% more. The concentration at the Stern plane changes dramatically even though the change in ϕ_D is only 30%: namely it changes from 135 mM to

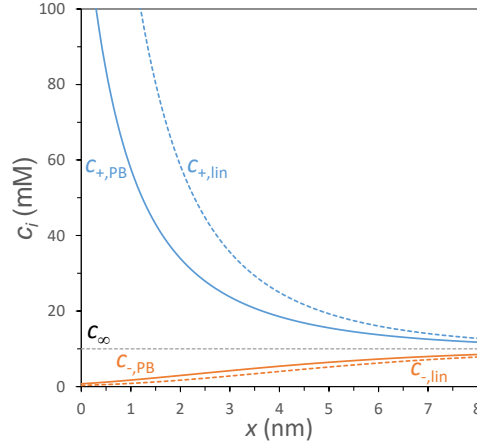


Fig. 3.2: Ion concentration profiles next to a planar charged surface according to the Gouy-Chapman equation (denoted by ‘PB’), and according to a linearised solution, Eq. (3.34). (Surface charge density $\Sigma = 20 \text{ mC/m}^2$. Salt concentration $c_\infty = 10 \text{ mM}$.)

305 mM, a $2.3\times$ increase. Thus in the linearised model, even though at the surface $\partial\phi/\partial x$ is the same as for the non-linearised GC-equation, the counterion concentration starts off at a $2.3\times$ larger value. For the coions, the two models give similar results in the presentation of Fig. 3.2, but also here, the relative difference in concentration (between the two models, for a certain position) going up to a factor of 2.3, with the prediction by the linearised model now closer to zero than for the non-linearised model. The total excess ions adsorption integrated over the DL is overestimated in the linearised model by about 65%. These are significant deviations, and thus, when using any linearisation of the PB-equation, be careful that potentials do not exceed a value of $\sim 30 \text{ mV}$ to have sufficient accuracy.

—

Now that we know the profile of $\phi(x)$, we can calculate the excess adsorption of cations and anions in the diffuse layer. Here, ‘excess’ means the ion adsorption beyond the situation that the surface were uncharged and the concentration at each position in the DL would be equal to the bulk concentration c_∞ . First we calculate the excess adsorption of cations and anions combined in the DL (note, we only consider a 1:1 salt)

$$\Gamma_{\text{ions}} = c_\infty \int_0^\infty \sum_i \left(e^{-z_i \phi(x)} - 1 \right) dx = 2c_\infty \int_0^\infty (\cosh \phi(x) - 1) dx \quad (3.35)$$

where the summation is over anions and cations, and Γ has unit mol/m². The solution to Eq. (3.35) is (Bazant *et al.*, Phys. Rev. E, 2004)

$$\Gamma_{\text{ions}} = 8\lambda_{\text{D}}c_{\infty} \sinh^2(\phi_{\text{D}}/4). \quad (3.36)$$

Each individual ion's excess adsorption (negative for the coion), can be calculated from the above equations, Eqs. (3.15) and (3.36), by making use of

$$\Gamma_{\text{ions}} = \sum_i \Gamma_i \quad \& \quad \Sigma = -F \sum_i z_i \Gamma_i \quad (3.37)$$

where as before the summation runs over the cations and anions. This evaluation results for both ions in the excess adsorption

$$\Gamma_i = 2\lambda_{\text{D}}c_{\infty} \left(e^{-z_i \phi_{\text{D}}/2} - 1 \right). \quad (3.38)$$

Just as in Ch. 2, see Eq. (2.12), we can take the ratio of excess salt adsorption over charge, to calculate the charge efficiency, Λ , of an electrode,

$$\Lambda = \frac{\Gamma_{\text{ions}}}{|\Sigma|/F} = \tanh \frac{|\phi_{\text{D}}|}{4} \quad (3.39)$$

which, like in Ch. 2 for the Donnan model, increases from zero to unity when the surface charge, thus ϕ_{D} , increases. This implies that in the GCS-model (just as in the Donnan model of Ch. 2), the surface charge (when expressed in moles/area) is always larger than the excess number of ions in the diffuse layer.

Does an EDL absorb or desorb salt? Now that we have expressions for the excess adsorption of counterions and coions, we can consider a related, and very interesting, question: does formation of EDLs lead to adsorption or desorption of salt? ¹

When we charge an electrode, we know that we adsorb more counterions than we desorb coions and thus one could say an electrode adsorbs salt. However, we cannot consider just one electrode, we also have a second electrode, from where the charge came. So in this analysis we consider a system without transport of charge.

We analyze how a surface charges up spontaneously when it is brought in contact with water. We consider two scenarios. In the first scenario, ions that were already adsorbed to the material in the dry state, are now released when the material is brought in contact with water ('is wetted'). In the second scenario, the material is already wetted and one of the ions in the water 'specifically' adsorbs to the surface.

So for the formation of an EDL when a dry material is wetted, the first scenario is similar to how we will describe the charging of titania in Ch. 5. In this scenario, we start with a neutral surface, neutralized because of counterion adsorption. For instance the material has COO^- -groups on its surface and they are neutralized by Na^+ -ions adsorbed to these groups.ⁱⁱⁱ This is how many materials can be envisioned when dry. When the material is wetted, the Na^+ -ions release from the surface, and the surface becomes negatively charged, i.e. the EDL is formed. What happens now with the bulk salt concentration? So these Na^+ -ions desorb, and a diffuse layer builds up. Do part of the desorbed Na^+ -ions go there and another part ‘moves on’ to the bulk? This would mean the bulk salt concentration increases. Or, do they go to the DL, to be joined there by extra counterions coming from solution? Then we have desalination of the bulk water. The answer is easily found by evaluating not these Na^+ -ions, but by considering movement of the co-ions: before Na^+ -desorption, all water volume was available to them as a bulk phase, and there was no diffuse layer. Now, the diffuse layer forms, and the coions are expelled from the DL (they have a negative excess adsorption). Thus their bulk concentration goes up. Because of charge neutrality in the bulk, this will also be the case for the counterions. So the answer is that the first hypothesis is correct: formation of the EDL (by the chemical mechanism that we described above) expels salt from the EDL and the bulk salt concentration goes up.

The second scenario is that a neutral surface is brought in water and then charges up because one type of ion adsorbs ‘specifically’ to the surface, and in this way an EDL forms. Note that the adsorbing ion will become the coion. [In the first scenario, just discussed, the desorbing ion became the counterion.] Because, for instance, if the adsorbing ion is a cation, then the surface becomes positively charged, and anions become counterions. Thus the cation becomes the coion, and in the final equilibrium situation its concentration in the diffuse layer will be lower than in bulk. So does the bulk water become more concentrated, like we concluded would happen in the first scenario? To find the answer, it is best to consider the non-adsorbing ion. This is the counterion (in this example an anion). So this counterion (anion) is adsorbed in the diffuse part of the EDL. And thus in bulk its concentration goes down. And the same will happen for the cation, and thus also for the salt as a whole. Thus in this second scenario, EDL formation leads to desalination of the bulk water.

Thus we have two different outcomes based on two scenarios, whether (scenario 1) charging of a surface is because of ion release, or (scenario 2) because of ion adsorption.

Classical experimental data are that EDL formation, when materials such as colloids or polyelectrolytes are brought in contact with water, that this leads to ‘salt expulsion’. Thus, the experimental evidence is that EDL formation leads to expulsion of salt into solution (Lyklema, 2005). These data are in agreement with the first scenario discussed above (related to the example of Na^+ -desorption from COO^- -groups). Thus, the scenario supported by the data is that an adsorbed ion is released when a dry material is contacted with water. The data do not support the second scenario where upon wetting of a material an ion already in the water adsorbs to the surface.

The GCS-model is completed when we add to the diffuse layer, described by Eq. (3.27), the Stern layer. The Stern layer is a charge-free layer that sustains a voltage drop, ϕ_S , proportional to the charge at the surface, Σ , see Eq. (2.17). These two voltages can be added together to arrive for each value of charge at the full EDL voltage drop, ϕ_0 , from Eq. (2.19), resulting in

$$\phi_0 = \phi_D + \phi_S = 2 \sinh^{-1} \left(\frac{\Sigma \lambda_D}{2 \varepsilon V_T} \right) + \frac{\Sigma}{C_S V_T} . \quad (3.40)$$

Interestingly, if we know the value of Σ and are only interested in the diffuse layer potential, ϕ_D , we do not need to evaluate the Stern layer. Vice-versa, the Stern layer does not need to be analysed if the aim is to calculate the charge Σ if we know the diffuse layer potential, ϕ_D . The Stern layer only becomes of relevance if the charge Σ is a function of the potential in the 0-plane, because of ionization reactions, for instance the (de-)protonation reaction of an acidic surface which takes place at the 0-plane. This requires solution of the full GCS-model, Eq. (3.40). In general, the Stern layer plays an important role in capacitive processes (electrowetting, desalination) and in Faradaic electrode processes, such as for the kinetics of anode and cathode reactions in fuel cells.

—

Just as in Ch. 1 also for the GCS model the capacitance of the EDL is given by the differential of charge Σ over EDL voltage V_{EDL} , and this is now an areal capacitance with unit F/m^2 . The capacitance of the Stern layer is a constant, while the capacitance of the diffuse layer is the classical result, obtained from Eq. (3.15), that

$$C_D = \frac{1}{V_T} \frac{\partial \Sigma}{\partial \phi_D} = \frac{\varepsilon}{\lambda_D} \sqrt{1 + \frac{1}{4} Q^2} = \frac{\varepsilon}{\lambda_D} \cosh \frac{\phi_D}{2} . \quad (3.41)$$

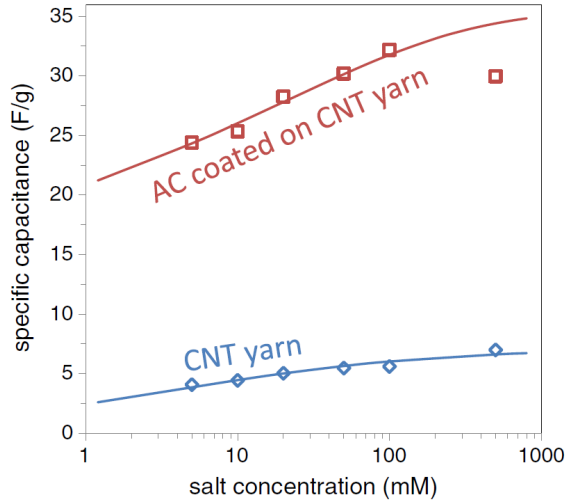


Fig. 3.3: The capacitance of ConyarTM carbon nanotube (CNT) yarns as predicted by the GCS model, as well as the capacitance of CNT yarn coated with a layer of microporous activated carbon, predicted by the Donnan model.

Taylor expansion of Eq. (3.41) around zero charge leads to

$$C_D \cdot \frac{\lambda_D}{\varepsilon} = 1 + \frac{1}{8}Q^2 + \mathcal{O}(Q^4) \quad (3.42)$$

and thus in the limit that charge goes zero, the diffuse layer capacitance is simply $C_D = \varepsilon/\lambda_D$, i.e., the permittivity of water divided by the Debye length. Just as in Ch. 2, the Stern layer capacitance and diffuse layer capacitance can be combined to obtain an EDL capacitance, see Eq. (2.21).

In Fig. 3.3 we give an example of the EDL capacitance according to the GCS model applied to the charging behaviour of carbon nanotube (CNT) yarns from ConyarTM (Arnhem, The Netherlands). CNT yarns are materials that are highly conductive, tough and flexible, and are projected to replace metallic conductors such as copper in many applications (also in electrochemical technology) because they are more conductive, lighter, and sustainable. Fig. 3.3 also shows how the Donnan model of Ch. 2 describes the capacitance of a CNT yarn coated with a layer of microporous activated carbon (Liu *et al.*, 2015).

Debye-Hückel equation for low potentials. The full PB-equation, Eq. (3.6), is valid at both low and high potentials, ϕ (assuming ions as point charges, validity of the mean field approximation, ...) When potentials remain low, $|\phi| < 1$, the Debye-Hückel (DH) equation can be used, which is a modification of Eq. (3.6) by making the replacement $\exp(x) \rightarrow 1 + x$, resulting directly in

$$\frac{\partial^2 \phi}{\partial x^2} = \kappa^2 \phi \quad (3.43)$$

where we implemented electroneutrality in bulk solution, $\sum_i z_i c_{\infty,i} = 0$ and we used the generalized definition of κ for multi-ionic solutions, Eq. (3.18) with ionic strength defined as $I = 1/2 \sum_i z_i^2 c_i$. For a 1:1 solution, Eq. (3.43) can also be directly derived from Eq. (3.8) by noting that for low ϕ , $\sinh \phi \rightarrow \phi$. For the planar diffuse layer, this Debye-Hückel equation has as solution Eq. (3.30). And as discussed above, this profile for potential is useful as a qualitative description. However, within the derivation of Eq. (3.43) is included the idea that we can linearise the Boltzmann equation, Eq. (3.5), to $c_i = c_{\infty,i} (1 - z_i \phi)$. If this linearisation of concentration is used, then the description of the diffuse layer starts to deviate very much, with concentrations of coions predicted to be negative when the potential increases to beyond the thermal voltage of ~ 25 mV, and counterion concentrations are underestimated. The adsorption of counterions is now the same as the desorption of coions, thus summed over these two species, the diffuse layer does not adsorb ions at all. And this would also imply there is no increase of osmotic pressure, thus no EDL interaction. . . These erroneous predictions underpin that the use of Eq. (3.30) for the potential profile is fine in a first approximation, but should be combined with the Boltzmann equation, Eq. (3.5), to avoid negative concentrations, which then results in Eq. (3.34). For the charge-voltage relationship, also for this general case of mixtures of ions, we can use Eq. (3.20) at low enough diffuse layer voltages.

3.3 Incorporation of ion volume in the GCS model

Ion volume effects are discussed in many chapters of this book, either using a Langmuir/lattice gas approach or based on the Carnahan-Starling equation-of-state. The Stern layer (thickness) is also an approach to incorporate ion volume effects in an EDL model, as it can be interpreted as a layer next to the surface that is inaccessible to ions because ions have a size. To be more precise, in this approach it is a layer which is

inaccessible to the *centers* of the (hydrated) ions, where we envision the charge to reside, and its thickness is then equal to the radius of the (hydrated) ions. With a dielectric constant in the Stern layer set to $\varepsilon_r \sim 7$ (instead of the value in bulk water of ~ 78), and the thickness of the Stern layer equal to the radius of a typical hydrated ion, say 0.3 nm, then a Stern layer capacitance follows of $C_S \sim 0.2 \text{ F/m}^2$, a value in line with data for C_S in an EDL model of oxidic materials in water.

In this section we describe ion volume effects in the diffuse layer (DL) of the GCS EDL model using the Langmuir isotherm, a model with a long history.^{iv,v} In this approach, using the Langmuir-description for the excess volume term, the Langmuir-Boltzmann chemical potential of an ion is

$$\mu_i = \mu_{\text{ref},i} + \ln c_i - \ln(1 - \nu c_{\text{tot}}) + z_i \phi \quad (3.44)$$

where we assume that all ions in the system have the same molecular volume, ν , and where c_{tot} is the total ion concentration (summation over all ions, not including water molecules).^{vi} In this approach all ions can pack to fill all space up to 100%, when $c_{\text{tot}} \rightarrow 1/\nu$.

If we set $\mu_i = \mu_{i,\infty}$, and just as in §1.3, we use ϑ for the volume fraction occupied by all solutes (in the context of the Langmuir model), thus $\vartheta = \nu c_{\text{tot}}$ and $\vartheta_\infty = \nu c_{\text{tot},\infty}$, Eq. (3.44) can be developed into ($\phi_\infty = 0$)

$$c_i = c_{i,\infty} \frac{1 - \vartheta}{1 - \vartheta_\infty} e^{-z_i \phi}. \quad (3.45)$$

If we now have a 1:1 solution we have $\vartheta = \nu(c_+ + c_-)$, while in bulk solution we have $c_{i,\infty} = c_\infty$ and $\vartheta_\infty = 2\nu c_\infty$. We can now solve Eq. (3.45) for both ions, and arrive at

$$\vartheta = \frac{\vartheta_\infty \cosh \phi}{1 - \vartheta_\infty (1 - \cosh \phi)} = \frac{\vartheta_\infty \cosh \phi}{1 + 2 \vartheta_\infty \sinh^2(\phi/2)} \quad (3.46)$$

which we can once again combine with Eq. (3.45) and implement in the modified PB equation to obtain

$$\frac{\partial^2 \phi}{\partial x^2} = \kappa^2 \frac{\sinh \phi}{1 + 2 \vartheta_\infty \sinh^2(\phi/2)} \quad (3.47)$$

which results in the Langmuir-Gouy-Chapman (LGC) equation for the charge Σ as function of diffuse layer potential, ϕ_D , given by

$$Q = \frac{\Sigma \lambda_D}{\varepsilon V_T} = \text{sgn}(\phi_D) \sqrt{\frac{2}{\vartheta_\infty} \ln \left(1 + 2 \vartheta_\infty \sinh^2(\phi_D/2) \right)} \quad (3.48)$$

^{iv}For a full historical overview, see §3.1.2 in ref. ²

^vFor a brief discussion of other possible contributions to the EDL structure, see [here](#).

^{vi}To include that ions have different sizes, an extension of the Carnahan-Starling equation-of-state can be used, see for instance §4.2.

where we use the same dimensionless surface charge Q that we introduced in Eq. (3.27). For $\vartheta_\infty \rightarrow 0$, Eq. (3.48) simplifies to the GC equation, Eq. (3.15). Eq. (3.48) can be rewritten to

$$\phi_D = \operatorname{sgn}(Q) \cosh^{-1} \left(\vartheta_\infty^{-1} (\alpha + \vartheta_\infty - 1) \right) \quad (3.49)$$

where $\alpha = \exp(\vartheta_\infty/2 \cdot Q^2)$.

The Bikerman-Freise (BF) capacitance, based on Eq. (3.48), is

$$C_D = \frac{\varepsilon}{\lambda_D} \frac{\sinh \phi_D}{\alpha Q} = \frac{\varepsilon}{\lambda_D} (\alpha|Q|)^{-1} \sqrt{(\vartheta_\infty^{-1} (\alpha + \vartheta_\infty - 1))^2 - 1} \quad (3.50)$$

which for $\vartheta_\infty \rightarrow 0$ simplifies to the GC capacitance, Eq. (3.41). The expansion of the BF capacitance around zero charge is

$$C_D \cdot \frac{\lambda_D}{\varepsilon} = 1 + \frac{1}{8} (1 - 3\vartheta_\infty) Q^2 + \mathcal{O}(Q^4) \quad (3.51)$$

where the additional negative term $-3\vartheta_\infty$ (which is not in Eq. (3.42)) shows that volume effects reduce the capacitance compared to situation that ions have no volume. Indeed, with ions having a volume, with increasing charge the capacitance will level off and come down again (in the GC model it only increases without limit), see Fig. 3.4.

For high charge, Eq. (3.50) simplifies to

$$C_D = \frac{\varepsilon}{\lambda_D \vartheta_\infty} Q^{-1} = \frac{\varepsilon F}{v \Sigma} \quad (3.52)$$

which shows how at high charge, and with ions having some volume, the capacitance no longer increases as the GC capacitance predicts, but decreases with charge following a -1 power dependence. Bazant *et al.* show an inverse square root-dependence of capacitance on diffuse layer potential, which as Eq. (3.55) shows (to be discussed further on; take the last term on the right side) also leads to a -1 dependence on charge. In agreement with Bazant *et al.*, Eq. (3.52) shows no dependence on salt concentration. In Eq. (3.52), parameter v is as before the molar volume of the ions.

We next derive an approximation for the location and maximum of the capacitance curve. First we discuss the charge Q at the maximum. As Fig. 3.4 shows, if we take the intersection of the curves for the GC capacitance, Eq. (3.41), and the high-charge expression, Eq. (3.52), we obtain an excellent prediction for charge Q at the maximum. Assuming (correctly) that $\vartheta_\infty \ll 1$, we then obtain

$$Q|_{\text{maximum capacitance}} \sim \sqrt{\frac{2}{\vartheta_\infty}} \quad (3.53)$$

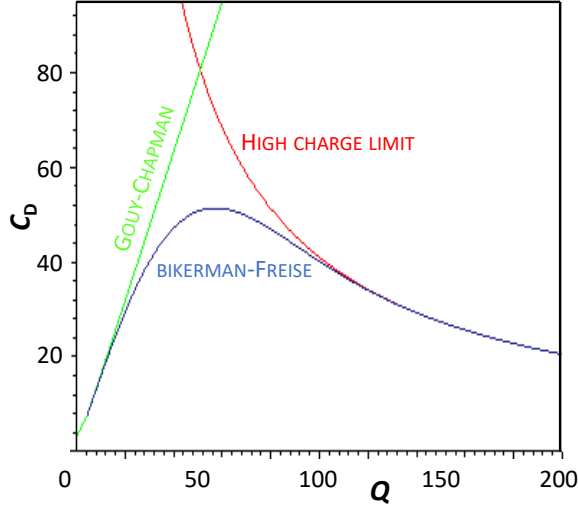


Fig. 3.4: The capacitance of a diffuse layer according to Gouy-Chapman, Bikerman-Freise, and the high-charge limit (ion volume $v = 0.4^3 \text{ nm}^3$, $c_\infty = 10 \text{ mM}$, other conditions apply for water at T_{room}). On the y-axis, C_D is scaled to $\varepsilon / \lambda_D|_{1 \text{ mM}} = 72 \text{ mF/m}^2$.

which indicates that the maximum shifts to lower charge when the ion volume v increases and when salt concentration c_∞ increases (both influence $\vartheta_\infty = 2vc_\infty$), and this is in line with Fig. 6 of Bazant *et al.* (2009)² Eq. (3.53) very accurately describes the charge Q at which C_D is at a maximum.

To find the value of the capacitance at the maximum, we can again take the intersection of the two branches just discussed and implement Eq. (3.53) to obtain

$$C_D|_{\text{maximum capacitance}} \sim c_1 \sqrt{\frac{\varepsilon F^2}{2RT}} \cdot \sqrt{\frac{1}{v}} \quad (3.54)$$

showing that a $10\times$ smaller ion volume, v , should lead to a $\sim 3\times$ larger capacitance maximum. This prediction matches exactly Fig. 5b in Bazant *et al.* (2009)². Furthermore, in their Fig. 6, Bazant *et al.* show how the maximum in C_D does not depend on salt concentration, and Eq. (3.54) also agrees with that.

Because Eq. (3.54) is based on the intersection point of two limiting curves, see Fig. 3.4, compared to the correct BF capacitance it predicts a too high capacitance. The deviation is a constant factor (as far as we can tell independent of c_∞ or v) for which we find a value of $c_1 \sim 0.64$. This correction factor can be implemented in Eq. (3.54) to provide an excellent prediction of the maximum in the diffuse layer capacitance C_D .

In a numerical scheme, it is known that the above equations can be hard to work with at high voltages³ and thus the following approximation to the LGC equation is proposed, which is very close to Eq. (3.49),

$$|\phi_D| \sim 2 \sinh^{-1} (|Q|/2) + \vartheta_\infty/2 \cdot Q^2. \quad (3.55)$$

Eq. (3.55) heuristically puts two terms together, first the GC equation valid in case ions have no volume, and second the high-charge branch as discussed above. That this term must be quadratic in charge is based on the following observation in calculations with the FGC equation (also reported by Bazant *et al.*, Fig. 5a) that beyond a certain charge the counterions form a close-packed layer of which the thickness is proportional to the charge, and proportional to the ion volume (the layer must be thicker the larger is the charge, and the larger are the counterions). The gradient in voltage across this layer is also proportional to charge (Gauss's law), and this together leads to a dependence on Q^2 , and on v , and an inverse dependence on ε .

Based on Eq. (3.55) we can also derive for capacitance

$$C_D^{-1} \sim \frac{\lambda_D}{\varepsilon} \left(\left(1 + 1/4 Q^2\right)^{-1/2} + \vartheta_\infty Q \right) \quad (3.56)$$

which has the correct limits at low and high Q and also has the maximum located at the correct Q -value. However, around this maximum, it underpredicts the capacitance by around 20%. [Note that Taylor expansion of Eq. (3.56) around $Q = 0$ does not give the correct behaviour.]

In the next chapter we discuss in more detail the Carnahan-Starling equation for hard sphere mixtures, and extensions thereof for mixtures of spheres of different sizes, even allowing for molecules that are better described as two or more connected spheres. These more detailed models can also be used in EDL models instead of the lattice-based models discussed above. A typical result is that when volume v in the lattice models is equated to ν in the CS-models, that in the latter models volume exclusion effects are much stronger, thus ions are rejected much more from regions of high ion density (near charged walls).

3.4 Incorporation of polarization in EDL models

Much scientific literature on the theory of EDLs relates to the effect of the dielectric constant (permittivity), ϵ_r , on the EDL structure. One aspect is that because of high electric field strength, E , near a charged plane, water molecules polarize (orient themselves) and thus ϵ_r drops. This effect can be described by the Booth equation and shows up at field strengths of 10 MV/m and more, so this influence can often be neglected. Other effects relate to what is called a Born energy that describes that ions are rejected from regions of lower permittivity. That is likely relevant in models where ions have their own cloud of counterions, and in that case when ϵ_r drops around an ion, that is energetically disadvantageous for the ‘self-energy’ of an ion, and thus one can surmise that a force develops that pushes ions away from such low-permittivity regions. But perhaps that kind of effect does not apply so much in the diffuse layer near a charged plane, and neither inside the pores of an overall charge neutral material. It is also unclear how exactly this type of force can be implemented in a model for the diffuse layer, because we also need to know *why* and *how* ϵ_r changes across space. Thus, this analysis based on the Born energy likely is more applicable to a situation where ϵ_r has distinct values independent of the field strength or ion concentration, and that is not the scenario for a diffuse layer near a charged plane. The use of the Booth equation to ‘generate’ gradients in dielectric constant that are subsequently used in an expression for the Born energy may not be a self-consistent approach.

However, one approach is internally consistent, and that approach is often incorporated, which is ion polarization, which refers to the decrease of the local ϵ_r of the electrolyte, due to the presence of ions. So the decrease of ϵ_r is caused by ions that themselves then are subjected to this lowered ϵ_r , but as we will see, only in regions of a high field strength. Ions that are larger, or orient the water more strongly induce more polarization, thus ϵ_r will go down more for such ions. Let us assume that ϵ_r decreases linearly with the concentration of an ion of type i , and we then define $\beta_i = -1/\epsilon_r^w \cdot \partial\epsilon_r/\partial c_i$. It is now the case that the contribution to the chemical potential of that ion because of polarization is $\mu_{\text{pol},i} = +\beta_i\epsilon_r^w E^2$ (unit J/mol)⁴. This contribution can be added to general expressions for the chemical potential of an ion, such as Eq. (2.28). At the same time, the dependence of ϵ_r on ion concentration must be included on the left side of Eq. (3.1) and thus we do not end up with Eq. (3.2) but we must solve

$$\epsilon_0 \frac{\partial}{\partial x} \left(\epsilon_r \frac{\partial V}{\partial x} \right) = -\rho \quad (3.57)$$

where ϵ_r is for instance described by $\epsilon_r/\epsilon_r^w = 1 - \sum_i \beta_i c_i$, if all β_i ’s are assumed to be independent of concentration. (This linearization can only be used as long as ϵ_r does not

drop below 1.)

For a 1:1 salt with both ions having an equal impact on ε_r , thus for one common value of β_i , Eq. (3.57) can be developed into

$$\varepsilon_0 \varepsilon_r^w \frac{\partial}{\partial x} \left(1 - \beta_i (c_+ + c_-) \frac{\partial \phi}{\partial x} \right) = -\frac{F^2}{RT} \cdot (c_+ - c_-) \quad (3.58)$$

where for each ion the modified Boltzmann equation is

$$\frac{c_i}{c_{\infty,i}} \cdot \exp(+z_i \phi) = \exp \left(-\beta_i \varepsilon_r^w RT / F^2 \left(\frac{\partial \phi}{\partial x} \right)^2 \right). \quad (3.59)$$

We can implement this result in Eq. (3.58) and obtain

$$\frac{\partial}{\partial x} \left(1 - 2\beta_i c_{\infty} \cdot \cosh(\phi) \cdot \text{rhs (Eq. (3.59))} \frac{\partial \phi}{\partial x} \right) = \kappa^2 \cdot \sinh(\phi) \cdot \text{rhs (Eq. (3.59))} \quad (3.60)$$

with κ defined based on the dielectric constant of water, ε_r^w . Solving this modified Poisson-Boltzmann equation will lead to the prediction that ions are rejected from regions of high field strength, and thus the field strength there, near a charged surface, will not go up as fast as otherwise, and thus counterion concentrations do not increase as much as before. Typically, in advanced EDL models the polarization effect is combined with volume (excess) effects and that full EDL model numerically solved.

3.5 EDL structure in solid polymer with fixed charge

In the above theories both ions are assumed to be mobile, i.e., free to move towards and away from the charged surface. However, the situation where one type of ion is mobile and the other is fixed in space, both in the DL and in bulk, is also of relevance. We consider the case when monovalent cations are mobile and in bulk have a concentration c_{∞} , which is then also the concentration of the negative charges that are fixed in place up to the surface. The PB-equation is now

$$\frac{\partial^2 \phi}{\partial x^2} = 1/2 \kappa^2 (1 - e^{-\phi}) \quad (3.61)$$

which can be integrated to

$$Q = \text{sgn}(\phi_D) \sqrt{\exp(-\phi_D) + \phi_D - 1} \quad (3.62)$$

which is asymmetric around $\phi_D = 0$, and that is different from the standard GC equation, Eq. (3.15) which is symmetric around $\phi_D = 0$.

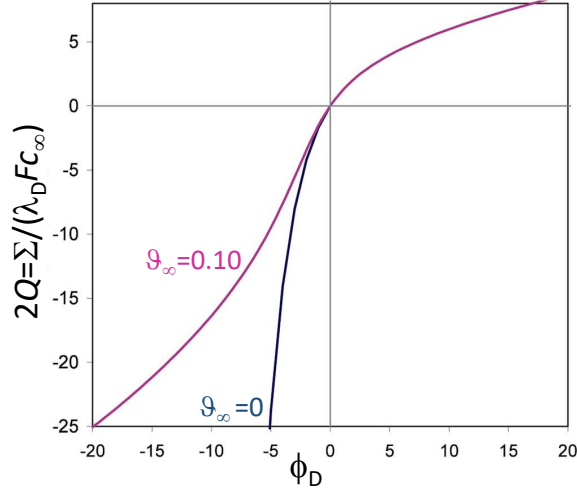


Fig. 3.5: The charge-voltage characteristic for an EDL with only cations mobile, and anionic charge fixed in position, with ($\vartheta_\infty = 0.10$) and without ($\vartheta_\infty = 0$) volume effects.

Often when we encounter this situation with one type of ion fixed in space, then often there are additional effects, such as volume exclusion, for instance in theories of the EDL structure in semiconductors. Including volume effects using a Langmuir/lattice approach (see previous section), we obtain

$$Q = \text{sgn}(\phi_D) \sqrt{\phi_D + \vartheta_\infty^{-1} \cdot \ln \{1 + \vartheta_\infty (\exp(-\phi_D) - 1)\}} \quad (3.63)$$

where $0 < \vartheta_\infty < 1$ is the fraction of lattice sites occupied by a cation in the bulk electrolyte. For $\vartheta_\infty = 0$, Eq. (3.62) is recovered. Eq. (3.63) may also play a role in describing the EDL-structure at the edges of a solid salt such as AgCl and AgI, where it may be the case that only one of the two ions has a concentration that deviates from the bulk composition. Fig. 3.5 compares the predictions of Eqs. (3.62) and (3.63).

The EDL structure when there is a fixed background charge, and both anions and cations are mobile, will be discussed in §5.3.3.

3.6 The GCS model for mixtures of salt

When the electrolyte contains mixtures of ions (and thus the double layer also contains a mixture of ions), for instance when besides monovalent ions there are divalent anions or

cations (or both) in the mixture, some of the above results can still be used. First of all, when in the mixture all ions are monovalent, all of the above equations apply, with c_∞ the summed concentration of all cations in bulk electrolyte, which is equal to the summed concentration of all anions there. In this case the excess adsorption of an ion is proportional to its contribution to c_∞ , and thus

$$\frac{\Gamma_+}{\Gamma_{\text{all cations}}} = \frac{c_{\infty,+}}{c_\infty} \quad (3.64)$$

where “+” refers to one specific type of cation. The same expression applies to the anions. Thus, in solving the GCS-model we can combine all monovalent cations into one group, likewise for all monovalent anions, make the required calculations, and only at a later point we split out the contribution of each ion to the total EDL absorption. This is a general conclusion also when we next move to mixtures with ions with other charge signs. Thus, all ions with the same charge can be grouped together as if they are one ion (e.g., all monovalent cations can be grouped together and be represented by a single monovalent cation). These simplifications are only possible in a calculation of chemical equilibrium, such as for the EDL structure. However, in a multi-ion mixture a difference for instance in diffusion coefficients of cations has a significant effect on the relative ion transport rates of these ions.

Now when besides monovalent ions, also divalent ions are present, the general charge-voltage relationship, Eq. (3.13) is valid, while relationship for ion adsorption vs. voltage exist as analytical solutions, though they can be very awkward, but no expressions at all exist for the exact profile of potential, $\phi(x)$. Indeed, for ion adsorption, analytical solutions do exist even for the most general case where both cat- and anions are present as monovalent and divalent species (E. Spruijt, pers. comm.), and for the simplified case when there is only one type of divalent ion (either anion or cation) and both anions and cations are present in monovalent form (Zhao *et al.*, 2012). However, these expressions are rather cumbersome.

The more tractable case is when we have one monovalent ion (say anion) and one divalent ion of the other charge sign (a divalent cation in this example), i.e., a 2:1 or 1:2 salt (Grahame, 1953; Joshi and Parsons, 1961; Mohilner, 1966). For a 2:1 salt, the excess adsorption of the divalent cation is

$$\Gamma_{2+} = 2\lambda_D c_\infty \left(e^{-\phi_D} \sqrt{1 + 2e^{\phi_D}} - \sqrt{3} \right) \quad (3.65)$$

while the excess adsorption of the monovalent anion is

$$\Gamma_{1-} = 4\lambda_D c_\infty \left(\sqrt{1 + 2e^{\phi_D}} - \sqrt{3} \right) \quad (3.66)$$

where c_∞ is defined as the bulk concentration of the divalent cations.

For the reverse case of monovalent cations and divalent anions (a 1:2 salt), the expression for Γ_{2+} above can be used for divalent anions, Γ_{2-} , when we apply the transformation $\phi_D \rightleftharpoons -\phi_D$, and the same transformation makes the expression for Γ_{1-} applicable for monovalent cations.

3.7 Surface ionization in the GCS model

Surfaces generally do not have a fixed surface charge, described by Σ in the previous sections, but adsorption and desorption of ions adds to, or modifies, the charge, as was already commented on in §1.4 and in §2.2–2.5. For capacitive electrodes, this chemical charge is an extra source of charge besides electronic and ionic charge, see §2.4 and §2.5. Adsorption of ions can also be a precursor to an electrode reaction in a (capacitive or Faradaic) electrode process.

In the present section we focus on ion adsorption to interfaces other than electrodes, for instance to oxidic materials such as alumina and silica. The descriptions can also be applied to more ‘soft’ interfaces such as polyelectrolytes (charged polymers), either in the form of a network (gel, membrane, layer of adsorbed (bio-)polymers), or as more discrete entities such as globular protein molecules or other charged nanoparticles. Though the theories below refer to an ideal surface with only one type of composition, large parts of the texts are also valid when the surface has distinct patches of different surface composition and/or geometry (for rough or wavy surfaces, cylindrical or spherical surfaces, surfaces with protuberances, etc.).

When a surface has patches, a very interesting problem deals with the diffuse layers corresponding to each patch, and the question is to what extent they ‘mix’, i.e., the question is, does each patch have ‘its own’ diffuse layer, or is there one ‘average’ diffuse layer, the same for both patches. We know this problem exists for the micropores in carbon electrodes (see Ch. 15), in the interior of ion-exchange membranes⁵ and for materials such as clays which on their edges have a different chemistry than on the faces of the clay platelets. Many types of bionanoparticles (viruses) have a very heterogeneous surface structure both in terms of charge and shape.

The extent of ‘diffuse layer mixing’ depends on how large are the patches relative to the Debye length: for large patches relative to the Debye length, a treatment with different diffuse layers for each patch is preferable, while for smaller patches relative to the Debye length (low salt concentration), the two diffuse layers mix.

One can also think of setting up a numerical theory with two separate diffuse layers—for instance based on the Poisson-Boltzmann equation for a symmetric salt solution, Eq. (3.7)—and at each x -position from the surface we mix the two concentrations in each layer, and this mixing increases with distance from the surface, so the diffuse layers that were fully distinct at the very surface, become more and more intertwined the further we move away from the surface. In this way we solve two adjacent 1D models, instead of having to set up a full 2D calculation.

Let us discuss now a flat surface with a completely homogeneous composition. Questions are: do we need to include a Stern layer (or further refinements to the Stern layer concept), and where (in which theoretical plane) do ions adsorb. On the topic of the Stern layer—to which we return below—it turns out that we do not need to include a Stern layer at all in many calculations with organic materials (gels, membranes, protein molecules and other polyelectrolytes, either in a ‘brush’ or as an adsorbed layer). Or in any case, it does not seem to be necessary. There is just ‘the’ surface to which protons/hydroxyl ions adsorb (and possibly other ions) and we can assume this plane to be ‘directly next to’ the diffuse layer without a Stern layer in between (which would have a voltage drop across it). For ion adsorption in the intercalation materials discussed in Ch. 1 a Stern layer was also not necessary. On the other hand, in carbon electrode micropores, the Stern layer as a mathematical concept is of key importance to describe data of salt adsorption and charge.^{vii} Also for hard surfaces such as oxides, the Stern layer concept is considered of essential relevance, and often further refined, as discussed below.

We next focus on models that include proton/hydroxyl ion adsorption in the 0-plane, see Fig. 3.1, and a further extension can be the adsorption of ‘indifferent ions’ (in most contexts this refers to all ions except for H^+ and OH^-) in the Stern plane, i.e., the plane located at the interface of Stern layer and diffuse layer, see Fig. 3.1. More refined models are the ‘triple layer model’ which considers that indifferent ions adsorb to a plane ‘inside’ the Stern layer, and in this way an ‘inner Helmholtz plane’ (iHp) is defined where these ions adsorb, in addition to the ‘outer Helmholtz plane’ (oHp), where the diffuse layer starts. This oHp corresponds to the Stern plane that we described before. In the triple layer model there are two capacitances, one between 0-plane and iHp, and one between iHp and oHp.

By now, one wonders perhaps, how do these various planes and their location matter. They

^{vii}In theoretical modeling of the EDLs in carbon micropores, this Stern layer is assumed to be located ‘behind’ the chemical charge. This suggests that in carbon micropores the Stern layer may relate to the space charge region within the carbon material itself, related to the distribution of electrons there.

matter because in the adsorption isotherm for that specific plane there is an electrostatic term (related to the adsorbing ion), and because the capacitances lead to an increase in potential towards the surface, and this higher potential suppresses adsorption.^{viii} Even more detailed models describe the adsorption of large ions, for instance phosphate, PO_4^{3-} , with part of the ion is assumed to adsorb in one plane, and part in another plane.

In the present section, we consider the simplest situation, of adsorption of ‘potential-determining ions’ (often H^+ and OH^-) in the 0-plane, and ‘indifferent ions’ in the Stern plane, with a single Stern capacitance in between these planes.

Two remarks are now in place relating to the ions. First of all, in some cases the ions adsorbing in the 0-plane, the ‘potential-determining ions’, are not H^+ and OH^- , but are other ions, often cations. This is the case for certain complex inorganic materials such as clays and mica. Nevertheless, from this point onward we assume the ions adsorbing in the 0-plane are H^+ and OH^- . The second point is discussed in the next box.

The relationship between H^+ - and OH^- -ions. It is important to discuss the nature of the H^+ - and OH^- -ions. One might have the idea that they are (to be considered as) two separate species. However, a repeating theme in this book is that it is generally not very helpful to consider these ions in this way, as separate entities.

Instead, because of water self-dissociation, a reaction where two water molecules react to H_3O^+ and OH^- , these two ions are intimately connected: knowing the concentration of the one ion, means knowing that of the other. The following example illustrates the relatedness of these ions. The example is, how can one distinguish the situation of an H^+ -ion moving from bulk and adsorbing to a surface, from the situation that a water molecule adsorbs which consequently releases a OH^- -ion which then moves to bulk. We cannot distinguish these two situations: we can set up a theory that focuses on the adsorption/desorption of H^+ , or we can do the same for the OH^- -ion, and these two analyses will give the same results (if correctly done). Reiterating this point: it does not matter whether we consider H^+ -adsorption, or OH^- -desorption. This relates to the assumption underlying this book, that the water is to a large extent an ‘invisible’ solvent, omnipresent in the background. And the equivalence of H^+ and OH^- relates to the assumption of fast enough water self-dissociation. For an equilibrium EDL theory this assumption is valid, and the relation $K_w = [\text{H}^+][\text{OH}^-]$ will be valid. There are many advantages to this approach, and that is why we also use it in Chs. 10, 17, and 18.

^{viii}In a more complicated scheme, charge overcompensation leads to the potential not monotonically going up or down which complicates this analysis.

One example is: if we have a Faradaic reaction at an electrode with for instance carbonate ions reducing to formate ions, in the 'H⁺/OH⁻ are equivalent'-formalism that we advocate, we can use the same model for the Faradaic reaction at all pH values, and we do not need to consider a reaction based on H⁺ at low pH and another formalism using OH⁻ at high pH (and some combination of both at intermediate pH). Instead one and the same model works at all pH-values, see Chs. 17 and 18. Interestingly, in such a model electrode reactions of H⁺ or OH⁻ do not have to be explicitly formulated, but nevertheless after the calculation has completed, one can back-calculate all fluxes of all ions at all position, also of H⁺ and OH⁻.

Important as well is that in this book we often write H⁺ as shorthand for the hydronium ion, H₃O⁺. It is not necessary to explicitly consider that the molecule is actually H₃O⁺ which is formed jointly with an OH⁻-ion from two water molecules. Instead, just like how the water self-dissociation reaction is written, as a reaction of a water molecule to a OH⁻-ion and H⁺-ion, we can use the H⁺-ion as shorthand for the hydronium ion. Thus there is freedom in switching between the notation/concept of a H⁺- and H₃O⁺-ion, and this is only possible because the water is modelled as a continuum fluid around ions. In a more statistical-mechanical framework, this freedom may not exist in this way.

So for adsorption to a surface, we can choose between focusing on H⁺ or on OH⁻. Throughout this book, and this holds for most literature in general, the choice is to focus on the H⁺-ion, and we do so for acidic and basic materials alike. For acidic materials (e.g., a carboxylic acid group -COO⁻ adsorbing/desorbing a proton (protonation/deprotonation) this is rather straightforward. For basic groups this may seem less obvious because they are neutralized because of OH⁻ adsorption, as for the case where a basic group such as an amine, -NH₂⁺, is neutralized because of OH⁻ adsorption. However, as long as we can assume that water self-dissociation is a fast enough reversible reaction, mathematically these two approaches are completely equivalent.

With these elements addressed, what we will arrive at is a situation where we come to one general 'Langmuir' isotherm valid for acidic, amphoteric, and basic surface groups, and they are only distinguished based on a constant reference charge number, which is -1, ½, and 0, for these three cases.

Amphoteric materials. It is very interesting to discuss the word ‘amphoteric’, which is broadly used and has various meanings. For a discussion on the word ‘amphoteric’ in the context of ionic solutions, see p. 511 For surfaces, it means that the material can charge both positively and negatively. At least three levels of detail can be distinguished. On the highest level, the term amphoteric material can be applied to a material with distinct regions (each consisting of 10s-1000s of atoms) differing in surface chemistry and geometric structure (as for a coronavirus or a clay particle).

One level down is a material where each surface group can be different, such as a protein molecule. The surface of a globular protein molecule generally consist of several types of acidic and basic groups, each with their own pK-value. An acidic group can be deprotonated (negatively charged) or neutral. A basic group can be neutral or positively charged. So none of these groups is amphoteric, but the material as a whole is, because the total, effective, average, surface charge can go from negative to positive as function of pH, and this average charge follows from a summation over all the groups at its surface.

The smallest scale at which we can define the term amphoteric, is when one and the same surface group (atom) can go from negative to positive. This is the case for amphoteric oxidic materials such as titania and alumina. There is one type of surface group with one pK-value and this group can go from negative at high pH to positive at lower pH. The fractional charge (charge per group) goes from a minimum of $-1/2$ to a maximum of $+1/2$. (Please see [here](#) for more discussion on the amphoteric behaviour of titania.)

In the present section when discussing an amphoteric material, we refer to this last case, which applies to oxidic material such as alumina and titania. The ionization of protein molecules is discussed in the next box.

We continue with describing these ionizable materials that adsorb and desorb protonic charge, i.e., a material that is charged by (de-)protonation. As discussed, these ions adsorb at the 0-plane, where potential is ϕ_0 (relative to the potential outside the EDL). This potential depends on the diffuse layer potential, ϕ_D , the Stern capacitance, and the charge in the 0-plane, Σ ,^{ix} with $\phi_0 = \phi_D + \phi_S$. As before, ϕ_D is the potential across the diffuse layer, and ϕ_S the potential across the Stern layer (i.e., both are potential differences).

Next we derive the general Langmuir ionization isotherm. The surface has a density of

^{ix}We do not include electronic charge for now, or ions adsorbing in the Stern plane. Instead, we consider solely surface charge in the 0-plane and diffuse charge extending beyond the Stern plane, see Fig. 3.1.

sites to which a proton can adsorb, $c_{s,\max}$, and the Langmuir isotherm considers that a proton either occupies one of these sites, or not. Thus we take the same approach as in §1.3 in that we describe an equilibrium between adsorbed species, and species in solution.^x Thus the equilibrium of a proton exchanging between solution (bulk) and surface is

$$\mu_{\text{aff},\infty} + \ln(c_{\infty,\text{H}^+}/c_{\text{ref}}) = \mu_{\text{aff},\text{ads}} + \ln(c_{0,\text{H}^+}/c_{s,\max}) - \ln(1 - v c_{0,\text{H}^+}) + \phi_0 \quad (3.67)$$

where c_{0,H^+} is the surface concentration of protons, adsorbed in the 0-plane (unit mol/m²). A potential ϕ_{∞} is omitted in Eq. (3.67) because ϕ_0 is already defined as the surface potential relative to that outside the EDL. Note that in Eq. (3.67) we assume equilibrium between the protons in the 0-plane and the same protons outside the EDL, in bulk. However, when the diffuse layer is not at equilibrium with a solution outside the EDL, then Eq. (3.67) must be written as a balance between the proton at the 0-plane and that at the D-plane. Then on the left side ‘ ∞ ’ must be replaced by D, and on the right side ϕ_0 is replaced by the voltage difference across the Stern layer, ϕ_s . Note the equivalence of Eq. (3.67) with Eq. (1.15) in Ch. 1.

Next we define a fractional charge, which is the fraction of how many of the surface sites have an adsorbed H⁺-ion, for which we can use $\vartheta = c_{0,\text{H}^+}/c_{s,\max}$ from Ch. 1, and note that $v \cdot c_{\max} = 1$. This converts Eq. (3.67) into

$$\vartheta = \frac{1}{1 + K \cdot c_{\infty,\text{H}^+}^{-1} \cdot e^{\phi_0}} = \frac{1}{1 + 10^{3-\text{pK}} \cdot 10^{\text{pH}-3} \cdot e^{\phi_0}} = \frac{1}{1 + 10^{\text{pH}-\text{pK}} \cdot e^{\phi_0}} \quad (3.68)$$

where like in §1.3, $K = c_{\text{ref}} \cdot \exp(\mu_{\text{aff},\text{ads}} - \mu_{\text{aff},\infty})$, and where we implement $\text{pH} = 3 - 10 \log(c_{\infty,\text{H}^+})$ and $\text{pK} = 3 - 10 \log(K)$.^{xi,xii}

Eq. (3.68) introduces K and pK of a certain ionization equilibrium. These are what are called *intrinsic* (p)K-values, i.e., they are constants, dependent only on the chemistry of the ion and the surface. Some studies report *apparent* pK-values, which are very different. These apparent pK-values are obtained in an experiment to measure the pH at which a material is charged for 50%.

Eq. (3.68) shows how with increasing pH the coverage of the surface with H⁺-ions will decrease. The same when the surface potential ϕ_0 goes up. This makes sense, because increasing pH (which refers to bulk, outside the EDL) means less protons in solution, thus

^xWe do not derive the Langmuir isotherm as if it is based on a reaction between ‘empty sites’ reacting with a proton to become an ‘occupied site’.

^{xi}Throughout this book, pH without sub- or superscripts refers to bulk, not to pH at the D- or 0-plane.

^{xiii}In our book, concentrations and K -values are in mM (mol/m³) and the conversion here to pH and pK, implementing a factor 3– allows for the traditional definition of pH and pK on a mol/L-basis.

also less adsorption, while a higher surface potential would mean that positive ions, such as H^+ -ions, are pushed away from the surface.^{xiii}

Eq. (3.68) shows how a higher pK-value leads to more H^+ -adsorption. This corresponds to how we understand basic materials, e.g., going from pK7 to pK9 leads to a higher charge, in line with Eq. (3.68). However, for acidic materials, Eq. (3.68) does not seem right, because we know that a material with \sim pK4 (carboxylic acid-type groups) has a lower charge than acid materials with \sim pK2 (sulphate-like) let alone \sim pK1 (phosphate). At a given pH, these latter materials are charged more than, say, carboxylic acid. However, as we will see below, there is no problem because for acidic material, ‘higher charge’ actually refers to the charge being more negative.

Let us repeat that Eq. (3.68) refers to pH in bulk, thus outside the EDL, with ϕ_0 the potential at the surface, defined relative to the potential in bulk.^{xiv} The fractional coverage ϑ times c_{\max} equals the surface concentration of adsorbed protons, with dimension mol/m^2 , and multiplying with Faraday’s number, F , we obtain a charge with unit C/m^2 .

Now, the surface, the material, has of itself a certain number of surface groups, each of which has a ‘natural’ or ‘native’ charge. The surface concentration of these groups is N . The charge density of these groups by themselves, i.e., their native charge, is $F \gamma N$ (in C/m^2), where we introduce the charge sign of the native groups, γ . For an acidic material $\gamma = -1$ (each surface group ‘by itself’ has a $\gamma = -1$ charge). For a basic surface, these N groups are all neutral, i.e., in the native state, they have no charge, and thus $\gamma = 0$. Amphoteric materials cover the range between these two extremes. We will in this section only consider amphoteric materials which have a native fractional charge of $\gamma = -1/2$. For these materials the native charge density of the surface groups is $F \gamma N$. Typical numbers for N are for instance $N = 3 \text{ nm}^{-2}$ for titania to $N = 8 \text{ nm}^{-2}$ for silica (to be divided by N_{av} to go to the unit of mol/m^2).

Now, how to arrive at the charge density of the material? It may be clear this will be a summation of the native charge and the charge due to proton adsorption. This is indeed the case, and this applies to all three material types (acidic, basic, amphoteric). The interesting step is to recognize that c_{\max} is equal to N , i.e., the site density identified in Eq. (3.67), to which the protons can adsorb, c_{\max} , is the same as the density of surface groups of the ionizable material, N .

Thus, when we add these two terms together, set $c_{\max} = N$, and multiply by F , we obtain

$$\Sigma = F \cdot (\gamma + \vartheta) \cdot N . \quad (3.69)$$

^{xiii}See [here](#) for a discussion on the involvement of OH^- -ions.

^{xiv}See [here](#) for two remarks extending the validity and use of Eq. (3.68). These statements also apply to the ionization equilibria given below.

Next we can combine Eqs. (3.68) and (3.69) and obtain the general result

$$\frac{\Sigma}{F \cdot N} = \gamma + \frac{1}{1 + 10^{-(\text{pK}-\text{pH})} e^{\phi_0}} \quad (3.70)$$

which we can develop for the three types of material.

But first let us introduce the parameter α , which is the ionization degree of the surface. First we describe it for *acidic and basic materials*. For these materials (for their surface groups), α describes to what extent the surface is charged, i.e., for $\alpha = 0$ the surface is uncharged, neutral, and for $\alpha = 1$ it is fully charged, i.e., all N groups carry the maximum charge, irrespective of the sign, i.e., whether the material is charged negatively or positively. The ionization degree α refers to the combination of native charge and proton charge, i.e., it is a parameter representing the charge in the 0-plane by the two contributions combined. Thus, the ionization degree α represents the effective charge of a surface (as a fraction of the maximum). For *amphoteric materials* such as titania and alumina, α is defined differently. It has a sign (i.e., can be negative and positive) and it will not reach a value of ± 1 . Instead, it varies from $-1/2$ at high pH, to $+1/2$ at low pH. These values of $-1/2$, $+1/2$ are the maximum values of the charge per surface group in this material. (There are N surface groups.)

Thus, for the three materials the ionization degree is obtained from Eq. (3.70) as follows:

For an *acidic* material ($\gamma=1$):

$$\alpha = \frac{\Sigma}{F N} = \frac{1}{1 + 10^{\text{pK}-\text{pH}} e^{-\phi_0}} \quad (3.71)$$

For a *basic* material ($\gamma=0$):

$$\alpha = \frac{\Sigma}{F N} = \frac{1}{1 + 10^{-(\text{pK}-\text{pH})} e^{+\phi_0}} \quad (3.72)$$

For an *amphoteric* material such as titania or alumina ($\gamma=-1/2$):

$$\alpha = \frac{\Sigma}{F \cdot N} = \frac{1}{2} - \frac{1}{1 + 10^{\text{pK}-\text{pH}} e^{-\phi_0}} \quad (3.73)$$

These are three types of Langmuir adsorption equilibria, which can be used to describe the ionization of a surface, as we will further outline below.

The amphoteric behaviour of a protein molecule. For an amphoteric material such as a protein molecule, with multiple ionizable groups, both acidic and basic, the above

general formulation, Eq. (3.70), is very useful to obtain the general equation for protein charge, because we can sum over all amino acid groups (where some are acidic, some basic) (in a protein molecule there are q_i of each amino acid type), and obtain for the protein charge Z (with unit ‘number’)

$$Z = \sum_i \left\{ q_i \left\{ \gamma_i + \frac{1}{1 + 10^{-(\text{pK}_i - \text{pH})} e^{-\phi_0}} \right\} \right\} \quad (3.74)$$

which often is written in the ‘acid form’ as

$$Z = Z_+ - \sum_i \left\{ \frac{q_i}{1 + 10^{\text{pK}_i - \text{pH}} e^{-\phi_0}} \right\} \quad (3.75)$$

where Z_+ is the maximum charge of a protein molecule, which is

$$Z_+ = \sum_i \{ (\gamma_i + 1) q_i \}$$

to which acidic groups ($\gamma = -1$) do not add, only the basic groups (which have $\gamma = 0$). Thus $Z_+ = \sum_B q_i$ where subscript ‘B’ refers to a summation only over the basic groups in the protein molecule.

A third representation makes use of the definition of the ionization degree, α , and uses the parameter z_i which is the charge sign of the respective amino acid, with $z_i = -1$ for an acidic molecule, and $z_i = +1$ for a basic molecule. Then we arrive at

$$Z = \sum_i z_i q_i \alpha_i . \quad (3.76)$$

Next we show adsorption isotherms, or ‘titration curves’ in Fig. 3.6 for four materials, with the charge Σ divided by $F \cdot N$, plotted as function of bulk pH. For acidic and basic materials, this ratio Σ/FN equals $z \alpha$, and for amphoteric materials it equals α . The four surfaces are the acidic material silica, the amphoteric materials titania and alumina, and the amine group.^{xv} We use here realistic pK-values.^{xvi} Some other pK-values of materials not

^{xv} Amine by itself is not a stand-alone material, but can be the charged group in a polymer network or in an amino acid. Note there are different types of amine groups, one of which is a tertiary amine, which is considered to have a fixed charge (thus it is not ionizable).

^{xvi} The pK-value of 7.5 for silica may look uncommon: isn’t it around pK 3? However, that latter number relates to the erroneous 2-pK approach to describe the ionization of silica. Instead, silica is an acid, described by a single pK-value, and the value is around pK 7.5.

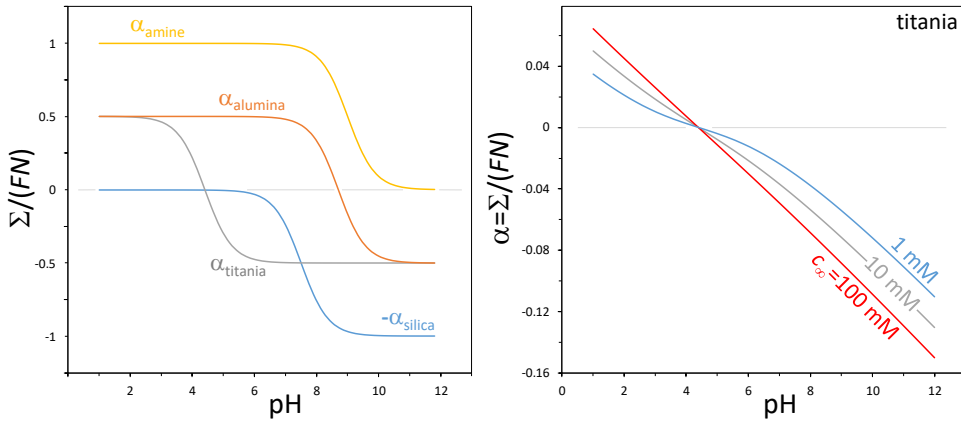


Fig. 3.6: Titration curves as function of pH. (a). Titration in the absence of electrostatic effects ($\phi_0 = 0$) for silica (acidic material, $\gamma = -1$, pK7.5), titania ($\gamma = 1/2$, pK4.4), alumina ($\gamma = 1/2$, pK8.7) and the basic amine group ($\gamma = 0$, pK9), based on Eqs. (3.71)-(3.73). Titania and alumina are amphoteric. (b). Titration curves for titania in a model including a Stern layer ($C_S = 0.2 \text{ F/m}^2$), and a diffuse layer according to the GC equation, for three salt concentrations ($N = 3 \text{ nm}^{-2}$).

considered in Fig. 3.6 are that of carboxylic acid (around pK 4-5), sulphonate groups (around pK 2) and phosphate groups (around pK 1). Note that for a basic material an increase in pK leads to a higher charge (at the same pH value) but for acidic materials it is the opposite: the phosphate group is a very strong acid (typically highly charged, pK ~ 1) while silica ($\sim \text{pK}7.5$) is a very weak acid.

In Fig. 3.6a we show titration curves in the absence of electrostatic effects, thus when $\phi_0 = 0$. We notice how silica is negatively charged, especially for pH values above pH 6, while amine groups are positively charged for pH 10 and lower. Titania and alumina are amphoteric and are positively charged for pH below their pK-value, and negatively charged for pH > pK. For these materials, their pK value is equal to their point of zero charge, PZC. In the absence of specific adsorption of other ions except for H^+/OH^- , titration curves for these materials always intersect the x-axis (i.e., go from positive to negative charge) at the same pH-value, irrespective of which ions are in solution and irrespective of the ion concentration. If we do observe that the pH at which the material goes from positive to negative charge depends on salt type or concentration (this transition point can often be established based on electrokinetic experiments), this is an indication that ions other than H^+/OH^- also adsorb (for instance in the Stern plane).

Fig. 3.6a suggests that these materials go from one limiting value of charge to the other

by varying pH by about 2 points. However, this is not the case in a calculation that includes the diffuse layer and the Stern layer, as shown in Fig. 3.6b. Fig. 3.6b is set up for titania, implementing the GCS model with a Stern layer ($C_S = 0.2 \text{ F/m}^2$) and the Gouy-Chapman equation based on standard values for T and for ϵ of water. We make a calculation for three values of the concentration of a 1:1 solution. We now observe that throughout the entire pH range charge gradually increases without levelling off. All curves are symmetric in the point (pH 4.4, $\alpha = 0$). in Fig. 3.6b shows that the maximum value of the ionization degree, α , reached in the practical pH range, is not more than 0.15 negative or -0.05 positive, at least a factor of three lower than the theoretical maximum that was obtained in Fig. 3.6a. Thus, ionizable materials in many cases do not charge up to their maximum at all.^{xvii}

Another feature of Fig. 3.6b is that we have a higher charge at higher salt concentration, both for the positive branch at low pH, and for the negative branch at high pH. The reason is that at higher c_∞ the diffuse layer (DL) is ‘thinner’, i.e., the potential drop over the DL is less, i.e., ϕ_D is closer to zero, and thus ϕ_0 as well. For the positive branch, where we have a positively charged surface and a positive potential, which ‘pushes away’ the protons, the lower potential at higher c_∞ allows for a higher proton concentration at the surface and thus a higher surface charge. For the negative branch, the surface is negative, the potential as well, and this attracts the protons. At higher salt concentration, this electrostatic attraction is reduced, i.e., protons are less attracted to the 0-plane. This leads to a more negative surface.

references

1. J. Lyklema, “Does electrical double layer formation lead to salt exclusion or to uptake?,” *Phys. Rev. E* **71**, 032501 (2005).
2. M.Z. Bazant, M.S. Kilic, B.D. Storey, and A. Ajdari, “Towards an understanding of induced-charge electrokinetics at large applied voltages in concentrated solutions,” *Adv. Colloid Interface Sci.* **152**, 48–88 (2009).
3. M. van Soestbergen, P. M. Biesheuvel, R. T. Rongen, L. J. Ernst, and G. Q. Zhang, “Modified Poisson-Nernst-Planck theory for ion transport in polymeric electrolytes,” *J. Electrostat.* **66**, 567–573 (2008).
4. P.M. Biesheuvel, “Volume exclusion effects in the ground-state dominance approximation for polyelectrolyte adsorption on charged interfaces,” *Eur. Phys. J. E* **16**, 353–359 (2005).
5. A.H. Galama, J.W. Post, M.A.C. Stuart, and P.M. Biesheuvel, “Validity of the boltzmann equation to describe donnan equilibrium at the membrane–solution interface,” *J. Membr. Sci.* **442**, 131–139

^{xvii}For (globular) protein molecules, this can be different because the potential remains relatively low because of the simultaneous presence of positive and negative amino acids, and the likely absence of a strong Stern layer effect. Thus the individual amino acids are likely charged to a much higher degree.

(2013).

Ion volume effects in electrochemical processes

Ion volume effects play an important role in electrochemical processes, both influencing rates of transport as well as the adsorption of ions (and other species) in the electrical double layer. They contribute significantly to the partitioning of ions between two phases, especially when at least one of the phases is based on small pores. In this chapter we also introduce a simple model for the ion activity coefficient in solution, incorporating a model for Coulombic interactions between ions in solution. We combine it with the correction due to ion volume effects, and thereby explain the typical non-monotonic trend of ' $\ln\gamma$ ' versus salt concentration.

4.1 Introduction

In electrochemical systems, the sizes and shapes of ions and other solutes play an important role, especially inside the pores of electrodes and membranes. For the rate of transport, the dimensions of an ion matter because a larger ion diffuses more slowly due to more friction with the fluid, and this effect is enhanced in a porous network with narrow channels where an ion also has friction with pore walls. The volume of an ion also leads to a driving force related to (gradients in) the excess function, which is a contribution to the chemical potential of an ion due to its volume: solutes tend to move away from crowded regions.

The above effects relate to transport. Besides that, ion volume influences the equilibrium structure of the diffuse part of the EDL, and, related, the distribution, or partitioning, of ions and other solutes between phases, especially when one of the phases consists of narrow pores into which the ions must enter. This was discussed in general in §2.8 and in the present chapter will be further developed with specific expressions for $\Phi_{\text{exc},i}$ presented.

The volume of an ion is not just its bare atomic volume. Instead, as often mentioned in this book, often an ion has a strong association with several tightly bound water molecules, its hydration shell. It is this total entity that is then called an ion (or other solute). Outside this shell, where water freely moves, we have the ‘free’ water, i.e., the solvent or fluid. We will generally refrain from using these adjectives ‘bound’ and ‘free’ etc. and when we write ‘ions’ we refer to hydrated ions, and ‘water’ applies to the free water around the hydrated ions.

Whereas in previous chapters we extensively used the Langmuir/lattice gas approach, in the present chapter the Carnahan-Starling equation of state is introduced. This equation is very exact and highly amendable to describe various situations relating to multi-component and ‘multi-shaped’ particles and porous media. We also provide a theory for the Coulomb interactions between ions in solution, which is of aid in describing the activity coefficients of ions in dilute and moderately concentrated solutions.

4.2 Effect of ion volume on the partitioning into a porous medium

A simple way to introduce the effect of ion size is how for a spherical particle (ion) that enters a perfectly cylindrical pore, not all positions are available. In this case, the partitioning function, $\Phi_{\text{exc},i}$, is the ratio between the area of the pore cross-section that is accessible to

the centre of the ion (with ion size σ_i), over the total cross-sectional area, and is given by

$$\Phi_{\text{exc},i} = \frac{\pi/4 (D_p - \sigma_i)^2}{\pi/4 D_p^2} = (1 - \lambda)^2 \quad (4.1)$$

where λ is the ratio of ion size σ_i over pore size D_p . In Eq. (4.1) it is assumed that the ions are unrestricted in their motion outside the pores, in bulk solution. Eq. (4.1) is based on the idea that an ion's center cannot get closer to the wall of a pore than a distance equal to its own radius, $\sigma_i/2$, or in other words, only a center region with diameter $D_p - \sigma_i$ is available for the center of an ion. This is based on the concept of the ion as a perfect sphere and the pore of a perfect cylindrical shape.

This very elegant equation has only one problem. Which is that most porous materials do not consist of (one type of) perfect cylindrical pores. But fortunately, there are other, more appropriate, approximations of the structure of a porous network that we can make use of. The approach we will use is to approximate the porous structure as a random assembly of more-or-less spherical particles. They can be very close-packed, or form a very dilute assembly. In the theory they are fixed in position, i.e., they form a rigid structure. We can make a structure with mixtures of different fractions of spheres of different sizes, but we will assume one type of sphere in this chapter. We base our derivation on a very accurate equation-of-state (EOS) that was originally developed for hard sphere mixtures, and modify it to make it apply to the case of a porous medium consisting of a network of spheres, where all spherical particles are connected and held rigidly in space.

The starting point is the Carnahan-Starling equation of state (CS EOS), which very accurately describes volumetric interactions in a 'hard-sphere mixture', i.e., for a solution of particles that all have the same size. The osmotic pressure according to the CS EOS is given by

$$\frac{\Pi}{c} = \frac{1 + \eta + \eta^2 - \eta^3}{(1 - \eta)^3} = 1 + \frac{2\eta(2 - \eta)}{(1 - \eta)^3} \quad (4.2)$$

where η is the volume fraction occupied by the spherical particles. Eq. (4.2) includes both an ideal term, which is the factor 1 on the right, and a volumetric excess term, which is the term $2\eta(2 - \dots$ there.¹ The expansion of Eq. (4.2) around $\eta = 0$ leads to

$$\frac{\Pi}{c} = 1 + 4\eta + 10\eta^2 + 18\eta^3 \dots \quad (4.3)$$

¹Here, as throughout this book, pressures and chemical potentials can be multiplied by RT to obtain a dimensional pressure in J/m^3 and potential in J/mol . For the dimensionless potential, μ , it is common to then write that the chemical potential is so many 'kT's, or ' $k_B T$'s.

which shows that the CS virial coefficients are $B_2 = 4$, $B_3 = 10$, $B_4 = 18$, etc., where the 2nd and 3rd virial coefficients are exact for hard sphere mixtures, but higher order virial coefficients are slightly off (18 must be 18.36. . . , etc.).

Based on Eq. (4.2), and the Gibbs-Duhem equation, Eq. (1.4), we can derive the excess contribution to the chemical potential of a species

$$\mu_{\text{exc},i} = \frac{3 - \eta}{(1 - \eta)^3} - 3 \quad (4.4)$$

which has the expansion around $\eta = 0$ of

$$\mu_{\text{exc},i} = 8\eta + 15\eta^2 + \dots \quad (4.5)$$

where the factor 8 can be interpreted as due to a single sphere of volume v excluding $8\times$ its own volume for (the placement of the center of) another sphere of the same size. Note that this $8\times$ larger volume does not imply that (CS predicts that) there is a maximum packing density of $1/8$, or 12.5%. This limit is not there because when two spheres are so close that their *excluded* volumes overlap, then their joint excluded volume is less than the sum of their individual excluded volumes. (It may be good to reiterate that our interest in μ_i -values for volume or other effect is because a difference in μ_i of a solute between two phases leads to a contribution to the partitioning coefficient.)

Besides its exact nature, the elegance of the CS EOS is that it can be extended to multicomponent mixtures of spheres of different sizes. And that equation can be further modified to consider mixtures where some of the particles are connected in pairs, triplets, etc., and even into long strings of particles, to describe polymer molecules, or to represent random porous media. The generalization of the CS EOS to mixtures of spheres of unequal size. is the Boublik-Mansoori-Carnahan-Starling-Leland (BMCSL) equation of state. The complete equation is rather unwieldy, but it is an explicit expression for Π and $\mu_{\text{exc},i}$ as function of the volume fractions and sizes of all the species involved. When the sizes of all particles are the same, the BMCSL EOS simplifies to the CS EOS.

Some useful limits of BMCSL are as follows. When particles of size σ_i are dispersed in a solution containing other particles j that are infinitely small (point charges), then the CS-equations above can be used with η based on particle i , with an additional term based on the osmotic pressure exerted by the small particles j , which results in an additional contribution to the total osmotic pressure of the system of

$$\Pi_{\text{sea of small particles}} = c_j \quad (4.6)$$

where the concentration c_j of the small particles in Eq. (4.6) is based on the volume available

to them, which is the volume not occupied by the large particles i , thus $c_j = c_j^*/(1 - \eta)$, where c_j^* is the concentration per total volume.

The small particles j also modify the chemical potential of species i by a term that is equal to the volume of particle i times the pressure exerted by all the small particles, j

$$\mu_{\text{additional},i} = v_i \cdot \Pi_{\text{sea of small particles}} \quad (4.7)$$

which can be understood as an insertion pressure: it is the energy that must be invested by the large particle to open up a space with the volume v_i against the pressure exerted by the small particles j .

The excess contribution to the chemical potential for the small particles, j , because of the presence of larger particles, i , is

$$\mu_{\text{exc},j} = - \ln(1 - \eta). \quad (4.8)$$

A different limit is when we have N types of particles, i.e., a polydisperse system, and all species can have non-zero sizes, but all particles, indexed as type i in the remainder of section are present at a very low concentration, except for one majority species that is indexed j . All equations below until Eq. (4.18) are valid for such a polydisperse system. In this case we can take the elegant ‘test particle limit’ or ‘tracer limit’ of the BMCSL EOS. For all particles type i , present in low quantities, and with size σ_i in a mixture that predominantly consists of spherical particles j , of size σ_j , with $\alpha = \sigma_i/\sigma_j$, the excess term for molecules i in the tracer limit of the BMCSL equation is given by

$$\mu_{\text{exc},i} = - \left(1 - 3\alpha^2 + 2\alpha^3\right) \ln(1 - \eta) + \eta\alpha \left\{ \frac{\alpha(3 + 2\alpha - 3\eta)}{(1 - \eta)^3} + \frac{3(1 + \alpha - \alpha^2)}{1 - \eta} \right\} \quad (4.9)$$

where η is the volume fraction of total space filled up with particles type j . Eq. (4.9) correctly simplifies to all of the earlier mentioned limits when α is either 0, 1, or ∞ .ⁱⁱ

When now the other species j is to some extent restricted in its movement, by being connected to other spheres of species j , such as when they are combined into doublets, triplets, or into long (polymer) chains, Eq. (4.9) is modified to account for the lower exclusion effect. This is because the entropic contribution to the excess function is reduced or altogether switched off when these species j cannot move as freely as before. We here extend this approach to describe volumetric effects in a porous medium that is described as a dense packing of connected spheres (the j -particles). To account for this connectedness, for the

ⁱⁱNote that in this section we are leaving out an index i in our notation of α , even though α is a factor that for each solute i can be different.

particles type i that move through the porous medium consisting of particles type j that have fixed positions in space, we add to Eq. (4.9) a contribution given by

$$\mu_{\text{additional},i} = -\frac{\eta}{1-\eta} \alpha^3 + \ln(1-\eta) \quad (4.10)$$

which consists of two terms, the first one being a correction because all spheres of type j are connected to one another, and the second term is a constant factor that now allows for concentrations to be defined per unit pore volume. Thus, for all equations that follow in this section, until Eq. (4.24), note that all concentrations in the porous medium are defined per volume of the open fraction (the pores).

Combining these two terms, we can easily group all terms according to their dependency on α , resulting in

$$\mu_{\text{exc},i} = \frac{3\eta}{1-\eta} \alpha + 3 \left(\ln(1-\eta) + \frac{\eta(2-\eta)}{(1-\eta)^2} \right) \alpha^2 - 2 \left(\ln(1-\eta) + \frac{\eta(2\eta^2-4\eta+1)}{(1-\eta)^3} \right) \alpha^3. \quad (4.11)$$

We can analyze this new excess function for a particle of size σ_i in a porous material that has a volume fraction η and is made of spheres of size σ_j . Interestingly, the resulting curves as function of size ratio α can be made to almost overlap when we plot the excess functions $\mu_{\text{exc},i}$ not versus the size ratio as such, but versus the ratio of ion size over an effective pore size. This effective pore size, h_p , or ‘characteristic pore dimension’ (also discussed in §2.2), is equal to the pore volume over the area, and thus h_p is the inverse of the specific ‘liquid phase’ surface area, a_L). For the type of porous medium just discussed, h_p is given by

$$h_p = \frac{\sigma_j}{6} \frac{1-\eta}{\eta}. \quad (4.12)$$

Thus we define a modified size ratio, α' ,

$$\alpha' = \frac{\sigma_i}{h_p} \quad (4.13)$$

and combine Eqs. (4.12) and (4.13) to arrive at

$$\alpha' = \frac{6\eta}{1-\eta} \alpha. \quad (4.14)$$

Combination of Eqs. (4.11) and (4.14) leads to

$$\mu_{\text{exc},i} = \frac{1}{2} \alpha' + \left(\frac{(1-\eta)^2}{12\eta^2} \ln(1-\eta) + \frac{2-\eta}{12\eta} \right) \alpha'^2 - \left(\frac{(1-\eta)^3}{108\eta^3} \ln(1-\eta) + \frac{2\eta^2-4\eta+1}{108\eta^2} \right) \alpha'^3. \quad (4.15)$$

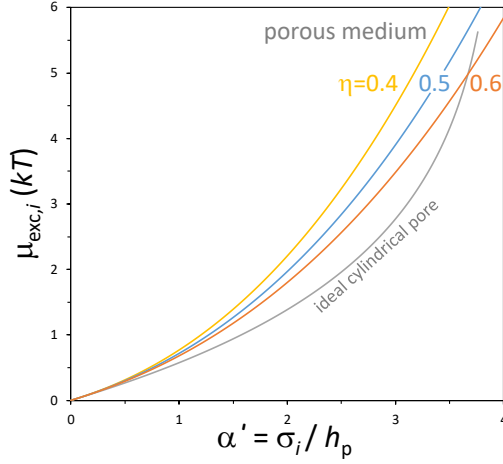


Fig. 4.1: The excess contribution to the chemical potential, $\mu_{\text{exc},i}$, of a spherical particle of size σ_i , inside a dense porous medium with various packing degrees η , as well as comparison with $\mu_{\text{exc},i}$ for the ideal case of a sphere in a cylindrical pore.

For this porous medium approach, we can now plot the excess term $\mu_{\text{exc},i}$ of Eq. (4.11) versus α' in Fig. 4.1 as function of packing degree η . Interestingly, all curves for $\mu_{\text{exc},i}$ vs. α' now start off with the same slope of $\partial\mu_{\text{exc},i}/\partial\alpha' = 1/2$, irrespective of the chosen packing degree of the porous medium, η , just as described by the first term in Eq. (4.15).

And we can now analyze this slope for the classical partitioning function based on the cylindrical pore, Eq. (4.1). Also here we must recalculate, now from the ratio of ion size over pore size, λ , to α' . We must also convert the partitioning function for volume effects, $\Phi_{\text{exc},i}$, from Eq. (4.1), to an excess contribution to the chemical potential, $\mu_{\text{exc},i}$, resulting in

$$\mu_{\text{exc,cyl},i} = -2 \ln(1 - \lambda) \quad (4.16)$$

in which we can implement that for a cylindrical pore $\alpha' = 4\lambda$. Taylor expansion around $\alpha' = 0$ leads to

$$\mu_{\text{exc,cyl},i} = 1/2 \alpha' + 1/16 \alpha'^2 + \dots \quad (4.17)$$

which has the same first term, linear in α' , as for the porous medium approach, Eq. (4.15). Thus, for small enough ions the two approaches overlap, which is a comforting result.

It is advantageous that the new approach based on a porous medium does not depend on a virtual ‘diameter of an ideal cylindrical pore’ but uses the much more accessible and insightful property of the specific surface area, a_L , or its inverse, the characteristic pore

dimension, h_p .

As Fig. 4.1 shows, until around $\alpha' \sim 3$, the new expression for $\mu_{\text{exc},i}$ changes faster than the prior function based on an ideal cylindrical pore, i.e., there is now a larger impact of a size change on $\mu_{\text{exc},i}$. This trend only reverses at larger values of α' when for the cylinder approach the excess function more rapidly increases and diverges when the ion size approaches the diameter of the cylindrical pore. This rapid increase and divergence is not seen with the new approach. Importantly, both approaches give results that are not too different, with very similar $\mu_{\text{exc},i}$ up to $\alpha' \sim 1$, and with a maximum deviation of ~ 1 kT around $\alpha' \sim 3$ (2.5 vs. 3.5 kT).

The new approach has a small dependency of the function $\alpha' - \mu_{\text{exc},i}$ on the packing density of the porous medium, η , as Fig. 4.1 shows, but the effect is relatively small. For further analysis, let us use the curve for 50% packing as an appropriate choice, for which the resulting expression for $\Phi_{\text{exc},i}$ becomes

$$\Phi_{\text{exc},i} = e^{-(\mu_{\text{exc},i} - \mu_{\text{exc},\infty,i})} = \exp \left\{ - \left(1/2 \alpha' + 5/26 \alpha'^2 + 1/40 \alpha'^3 \right) \right\} \quad (4.18)$$

where the first numerical value is exact, the other two are approximations. Note that the predicted partitioning effect is still a function of the density of the porous medium, via the value of h_p , which is a strong function of η , see Eq. (4.12). (In Eq. (4.18) we assumed that $\mu_{\text{exc},\infty,i} = 0$.)

The expressions discussed in this section can also be compared to another empirical method that was used to develop an expression for $\mu_{\text{exc},i}$ for ions inside a slit-shaped pore, results of which compared favorably with full density functional theory (DFT) calculations. Here the standard CS EOS was used, with a dependence on η_i , which is the volume fraction of the spheres *themselves* in the slit. To correct for the presence of the slit-shaped pore walls (to get a good fit to the DFT calculation results), this volume fraction η_i was corrected by adding an extra term $\gamma\alpha'$ that depended on the ratio of ion size over slit size ($\gamma = 0.0725$). Thus to each factor η_i in the CS expression, Eq. (4.5), this extra factor is added to account for pore constriction, which results in

$$\mu_{\text{exc},i} = \frac{3 - (\eta_i + \gamma\alpha')}{(1 - (\eta_i + \gamma\alpha'))^3} - 3. \quad (4.19)$$

If we take the tracer limit, so a dependence on the ion concentration itself is neglected, i.e., we set $\eta_i = 0$, and do a Taylor expansion around $\alpha' = 0$, we obtain

$$\mu_{\text{exc},i} = 8\gamma\alpha' + \mathcal{O}(\alpha'^2) \quad (4.20)$$

and thus we have around $\alpha' = 0$ a linear dependence on α' with a prefactor for $\mu_{\text{exc},i}$ of $8\gamma = 0.58$, which is close to the value of $1/2$ derived for the approaches discussed earlier on.

Eq. (4.19) can also be used to describe the interactions between the ions in the pore, i.e., a dependence of the excess function on η_i , but we use a different function for that later.

Thus, in conclusion, all of these approaches for the effect of ion volume on the excess function in porous media, give similar results, though the original ‘sphere-in-cylinder’ approach has the weakest dependence on pore size below $\alpha' \sim 3$ and after that the effect of pore size increases very steeply. The more gradual dependencies predicted by the two other approaches seem better. Note that all expressions until now (except Eq. (4.19)) assume that the absorbing species is present only in trace quantities, and thus do not interfere with one another. This effect we discuss further on.

—

We can use these expressions to estimate the effect of ion size on ion selectivity, for equilibrium conditions, thus neglecting for now how different transport rates influence selectivity. At equilibrium, ion selectivity describes the difference in ion adsorption in a microporous material (porous electrodes, gel, membrane) between two different ions (Gamaethiralalage *et al.*, 2021). We can define the selectivity between ion 1 and ion 2 as

$$S_{1-2} = \frac{c_1}{c_2} \cdot \frac{c_{\infty,2}}{c_{\infty,1}} \quad (4.21)$$

where index ∞ refers to outside the porous material, while c without an extra index refers to inside the micropores. To find an expression for S_{1-2} as function of the two ion sizes, we use the partitioning coefficient related to volume, given by

$$\Phi_{\text{exc},i} = \exp(-(\mu_{\text{exc},i} - \mu_{\text{exc},\infty,i})) \quad (4.22)$$

If we now combine with Eqs. (2.34) and (4.21), we arrive at

$$S_{1-2} = \exp(\mu_{\text{exc},2} - \mu_{\text{exc},1}) \quad (4.23)$$

where we assumed that for both ions outside the pore $\mu_{\text{exc},\infty,i}$ is zero, which for a sufficiently dilute solution is a valid approximation.

We can now insert any of the above-discussed expressions for $\mu_{\text{exc},i}$ in Eq. (4.23). The expression we will analyze is Eq. (4.15) and thus we obtain

$$S_{1-2} = \exp(-\frac{1}{2} (\sigma_1 - \sigma_2) / h_p) \quad (4.24)$$

which illustrates that when ion 1 is smaller than ion 2, S_{1-2} is larger than unity, i.e., the smaller ion is preferentially adsorbed. As Eq. (4.24) also shows, the effect of ion size increases with decreasing pore size, h_p .

According to Eq. (4.24), a difference in size between the ions of 20%, with the smaller ion having a size equal to h_p , thus $\alpha' = 1.0$, leads to a selectivity of $S_{1-2} \sim 1.11$, which is not very impressive. Using Eq. (4.18) instead of Eq. (4.15) leads to the more correct result that for these parameters, $S_{1-2} \sim 1.22$, which is twice larger but still not very large. But when we analyze the situation beyond the tracer limit, selectivity becomes significantly higher, as we show next. We will now use the full BMCSL approach with two ions modelled as spheres of different sizes, and a third type of particle that represents the porous medium and is modelled as spheres that are all connected to one another. This is Eq. (7.2) in Spruijt and Biesheuvel (2014) where we use $N = \infty$ for this third type of particle ($\eta_3 = 50\%$). We make a calculation of ion selectivity at a 20% total volume fraction of the two ions in the pores (thus the two ions together occupy 10% of the total volume of the porous medium) including that the two types of ions have volumetric interactions with one another. Like in the previous example, the larger ion is only 20% larger than the smaller one.ⁱⁱⁱ Results are that we now have a selectivity factor of $S_{1-2} = 4.44!$ Thus ion volume effect can be very significant in a realistic porous medium, significantly beyond what the simple Eq. (4.24) might suggest.

4.3 Ion-ion Coulombic interactions in electrolytes

An important topic in physical chemistry is the activity coefficient of ions in a salt solution (electrolyte). The activity coefficient is the correction to the concentration required to obtain a good prediction of the chemical potential of an ion, μ_i , as well as of other thermodynamic properties of an electrolyte solution, such as the osmotic pressure and vapour pressure. The activity coefficient γ_i relates to activity a_i and concentration c_i by $a_i = \gamma_i c_i / c_{\text{ref}}$, and for the chemical potential we thus obtain

$$\mu_i = \mu_{\text{ref},i} + \ln a_i = \mu_{\text{ref},i} + \ln (\gamma_i c_i / c_{\text{ref}}) = \mu_{\text{ref},i} + \ln (c_i / c_{\text{ref}}) + \ln \gamma_i. \quad (4.25)$$

Typical results for γ_i are that starting at a value of $\gamma_i = 1$ for a very dilute solution, it first decreases, then reaches a minimum at moderate salt concentration, and then increases again, for very high salt concentration to pass beyond the value $\gamma_i = 1$. The initial decrease in γ_i is because of Coulombic forces between ions of opposite sign, and the increase at higher concentrations is due to an ion volume effect, for which the Carnahan-Starling equation of state, Eq. (4.4), can be used.

When we add salt to water, in most cases the ions fully dissolve, primarily because of an increase in the entropy of the ions in this process. The hydration of ions when they dissolve

ⁱⁱⁱOther calculation parameters: the smaller ion has a size equal to h_p ; the two ions have an equal concentration in bulk solution.

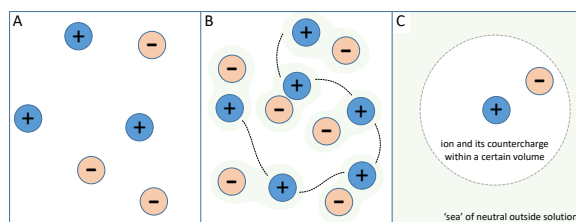


Fig. 4.2: In a dilute electrolyte solution, ions are randomly distributed as depicted in panel A, but the electrostatic energy is lowered when ions of opposite charge stay nearer to one another as illustrated in panel B for a 1:1 salt. There is a distribution of distances between an ion and its nearest countercharge.

is another contributing factor. Another energy term is of electrostatic origin, because ions of like sign repel and of opposite charge sign attract. For dilute solutions the attraction of an ion with its most nearby countercharge is the most relevant, and it is the Coulombic attraction between them which leads to a decrease of the energy of the electrolyte, and thus to a reduction of the activity of the ions. When very dilute, these Coulombic interactions are effectively zero, because the ions remain far apart and the likelihood of an ion starting to orbit its counterpart is small. But if concentrations go up, ions are ‘pushed together’, in a statistical sense, and trajectories of a certain ion more frequently get close to ions of opposite sign. Then it will happen more frequently that these trajectories are further deflected such that ions stay closer for a longer time, i.e., their paths become correlated. A snapshot for a dilute solution would not show ion-ion positional correlations, but a snapshot at higher concentrations shows correlations of cations with anions, see Fig. 4.2. The Coulombic interactions result in a negative contribution to an ion’s chemical potential, i.e., to a value of γ less than unity.

In a calculation of the chemical potential, we can focus on the Coulombic interactions between an ion and its most nearby countercharge, and we do not consider the trajectories of other cations and anions. Thus we can focus on an ion and the most nearby countercharge, and analyze the Coulombic energy of the interaction between them. In this calculation we must consider all possible distances between the two ions, and take into account the likelihood of each separation. First of all, being very close is increasingly unlikely because around any point ‘space’ expands with distance squared, making two ions being further apart more likely than being close. On the other hand, further apart is less likely because the Coulombic energy is less, i.e., because of the higher attraction short distances are favoured by Boltzmann’s distribution law. The minimum distance between the ions in a pair is determined by the sum of their radii, which is then also part of the theory. There is not a sharp maximum for the range of possible distances where the first countercharge is to

found relative to a certain ion, but very large distances for the first countercharge, are very unlikely. A simplification assumes a distinct maximum separation calculated from equally distributing all ions over space, away from one another to a maximum, and then taking this ion-ion distance as the maximum. In the dilute limit this entire calculation can be done analytically for a 1:1 salt and leads to the result that the natural logarithm of γ is given by

$$\ln \gamma_{\pm} = -\alpha \lambda_B \sqrt[3]{N_{\text{av}} c_{\infty}} \quad (4.26)$$

where \pm refers to the mean activity coefficient which is equally attributed to the cation as to the anion, with α a numerical prefactor that we empirically determine to be $\alpha = 1$, and λ_B is the Bjerrum length, at room temperature about $\lambda_B = 0.716$ nm. This expression for the dilute limit, Eq. (4.26), is independent of ion radii, but ion radii do play a role in a full numerical calculation that for non-dilute conditions is more exact. These complete numerical calculations are provided as continuous lines in Fig. 4.3 and accurately describe data of the activity coefficients of several 1:1 salts up to quite high salt concentrations. For a low average ion radius of $\langle a \rangle = 0.18$ nm, the analytical solution, Eq. (4.26) is close to the numerical calculation, certainly in the dilute limit. In Biesheuvel (2020) also an excellent fit of this theory to data is provided for symmetric 2:2 and 3:3 salts, as well as for asymmetric 2:1 and 3:1 salts. In the latter cases, instead of considering only one countercharge, an ‘ion ensemble’ with 3 and 4 ions, respectively, must be numerically evaluated.

—

For a 1:1 fully dissociated salt, the contribution to the osmotic pressure because of this ion-ion Coulombic interaction (i.i.c.i.) is as follows. We can make use of Eq. (1.3) with the right hand side now a summation over two ions, and we can also use the expression for free energy density f that we discuss further on, Eq. (III-14), noting that $\Pi = c^2 \partial (f/c) / \partial c$. For a symmetric salt this relation can be directly used with c twice the salt concentration, c_{∞} .^{iv} We now obtain for the contribution to the osmotic pressure

$$\Pi_{\text{i.i.c.i.}} = -\frac{1}{2} \alpha \lambda_B N_{\text{av}}^{1/3} c_{\infty}^{4/3}. \quad (4.27)$$

At room temperature, this contribution is $\bar{\Pi}_{\text{i.i.c.i.}} \sim -0.03 RT c_{\infty}^{4/3}$, with c_{∞} expressed in mM. Thus at $c_{\infty} = 1000$ mM this contribution reduces the osmotic pressure by 7.7 bar.

The same result can also be expressed as an osmotic coefficient, ϕ , which describes the osmotic pressure relative to the ideal situation that $\bar{\Pi}_{\text{id}} = 2RTc_{\infty}$, thus $\phi = \Pi/\bar{\Pi}_{\text{id}}$. For a 1:1 salt, at room temperature, ϕ is given by $\phi \sim 1 - 0.015 \sqrt[3]{c_{\infty}}$ (Biesheuvel, 2020). Thus at 1 M, the osmotic pressure is reduced because of electrostatic interactions by $\sim 15\%$.

^{iv}For the ideal part, we have $f = 2c_{\infty} (\ln (c_{\infty}/c_{\text{ref}}) - 1)$, and we then correctly end up with $\Pi = 2c_{\infty}$.

It is possible to include the effect of this ion-ion Coulombic interaction in a flux expression for ions where it will be combined with other driving forces acting on an ion, such as diffusion and electromigration. If we combine ion-ion Coulombic interaction with regular diffusion by Fick's law, we arrive for a 1:1 salt at^v

$$J = -D \left(1 + \frac{\partial \ln \gamma}{\partial \ln c_\infty} \right) \frac{\partial c_\infty}{\partial x}. \quad (4.28)$$

The term within brackets becomes $1 - 1/3 \alpha \lambda_B \sqrt[3]{N_{av} c_\infty}$, and that term multiplied with D_i can be called an apparent diffusion coefficient, $D_{app,i}$. A large range of data for the diffusion of KCl, NaCl and LiCl up to concentrations of $c_\infty \sim 200$ mM is excellently described by Eq. (4.28), see Biesheuvel (2020). Due to the activity correction, at ~ 200 mM, the apparent diffusion coefficient, $D_{app,i}$, is about 10% lower than its value at infinite dilution, where $D_{app,i} = D_i$.

A general conclusion of a study of ion activity coefficients is also that certainly for 1:1 salts the correction to an ion's activity due to ion-ion Coulombic interactions is in many cases not very large, and can be neglected. A drop in $\ln \gamma$ by 0.3 points, as shown in Fig. 4.3, relates to an contribution to an ion's chemical potential that is equivalent to the effect of an electrical field with a voltage change of 8 mV, not a very large number. Thus, electromigration, and regular diffusion, are in most cases more important than ion-ion Coulombic interactions. But for 2:2 and 3:3 salts, these energies are much stronger, see Biesheuvel (2020).

Thus, Eq. (4.26) is a first contribution to the activity correction of an ion, $\ln \gamma$, with the effect of ion volume a second contribution, which develops at moderate to high salt concentrations. We describe this volume effect with the Carnahan-Starling equation of state, Eq. (4.4), and take for the anion and cation the same size. The volume fraction η is calculated from multiplying the ion's volume v_i with the total ions concentration, which is two times the salt concentration. We present in Fig. 4.4 curves for $\ln \gamma$ (the summation of the two μ -terms discussed in this section) as function of salt concentration and ion size (the ion

^vThis derivation is based on the solute friction balances that will be extensively discussed in Ch. 7 where the extra contribution to an ion's chemical potential is included in the force acting on an ion which is minus the gradient of the chemical potential.

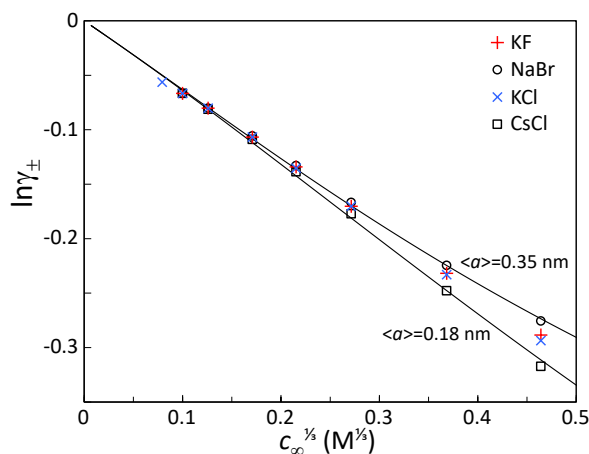


Fig. 4.3: Data and theory for (the natural logarithm of) the mean ion activity coefficient of four 1:1 salts as function of the cube root of salt concentration. Lines are based on a calculation of the Coulombic energy between an ion and its most nearby countercharge, for different values of the average ion radius, $\langle a \rangle$, which for low c_∞ and/or low average ion radius $\langle a \rangle$ has the analytical solution given by Eq. (4.26).

size is only required in the volumetric excess contribution). For ions with a non-zero size, Fig. 4.4 shows that with increasing salt concentration the curves first go down and then up again, and do so much quicker when the ion size is larger.

The effects just discussed, relating to Coulombic interactions and ion volume, have an impact on many aspects of electrochemical processes, including ion transport and thermodynamics, such as the calculation of the minimum energy required for water desalination. The impact of these two non-idealities on this thermodynamic energy for desalination is discussed on p. 288.

Salting in/salting out. The solubility of a salt (ion pair) depends on the chemical potential of the ions, and thus depends on the effects discussed above, the ion pair energy, and volume exclusion. The more that ions of a salt A are ‘stabilized’ (reduced chemical potential), the more they remain dissolved and do not condense into neutral aggregates containing the two ions. If now another salt, X, is added, at low concentration of X the solubility of A increases. This is because extra X reduces the Coulombic energy of the ions of A, and thus the ions of A are stabilized. This is a well-known effect, called ‘salting in’: adding an additional salt X leads to a higher solubility of a salt A. However,

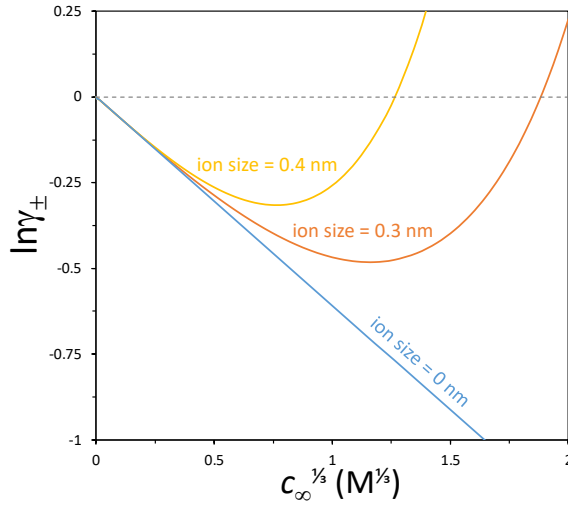


Fig. 4.4: Theory for $\ln \gamma_{\pm}$ in a 1:1 salt solution as function of the cube root of salt concentration including the analytical solution for ion-ion Coulombic interaction, Eq. (4.26), and a volumetric excess effect described by the Carnahan-Starling equation of state.

beyond a certain concentration of X , the effect is reversed: with more X the solubility of A goes down, and this is called ‘salting out’.

One common explanation of salting out is that so few water molecules remain to hydrate the ions, that a significant competition develops, and clustering into neutral salt aggregates becomes more favourable. The other route to explain this reduction in solubility is via an effect of ion volume, because now higher concentrations of salts (of whichever type) increase the energy of the ions, see Fig. 4.4, and clustering into aggregates of salt A is enhanced. Thus in the same way that a reduction of the chemical potential of an ion (i.e., reduction of $\ln \gamma$) leads to salting in, its increase leads to salting out.

The energy of an electrical double layer

In this chapter we discuss three topics in which the energy in an electrical double layer (EDL) plays a key role.

These three topics are as follows:

- The wetting of titania. Titania is an amphoteric ionizable material and the dependence of the contact angle of a water droplet on a titania surface depends in an intricate manner on pH and salt concentration, and requires consideration of electrical and chemical aspects of surface tension and energy.
- Electrowetting. For a vertically placed electrode that is partially wetted, the energy in charging the EDL structure is balanced by the G/L interfacial energy and by gravity. We discuss the maximum rise in a capillary and the topic of contact angle saturation. We demonstrate how the Laplace equation follows from Young's equation.
- Energy from the change in EDL structure around electrode wires. We discuss the structure of the EDL formed at the interface of an electrode and a polyelectrolyte gel, and show how cyclic stretching of the gel leads to changes in the EDL structure which can be a source of electrical energy.

5.1 Wetting of titania: The free energy of an EDL with ionizable surface charge

In previous chapters we discussed the EDL structure according to the Donnan and the GCS models, also including the possibility that surface charge responds to local pH, i.e., an ionizable surface or material, see §2.5 and §3.7. In the present section we use the GCS model for a single surface that does not have a fixed surface charge, but the charge responds to local pH (i.e., at the surface). We analyze the surface energy of the EDL, and describe how this energy impacts the contact angle when a droplet of water is in contact with such an ionizable surface.

EDL theories for single surfaces are often used to calculate properties such as the zeta-potential and charge of a surface as function of pH and salt concentration, as we also do in Ch. 3. However, in this and the next sections we extend the range of applications of EDL theory and demonstrate the use of GCS theory for several very different purposes. In the present section we discuss the pH- and salt-dependence of the contact angle of an air bubble in contact with a flat titania surface submersed in water (Virga *et al.*, 2018). Titania has a surface charge that is strongly pH-dependent, from positive at low pH to negative at high pH, i.e., titania is an amphoteric material, and in the example calculation in this section we show the effect of pH and salt concentration on the EDL structure and how that impacts the contact angle, see Fig. 5.1 for an illustration.

A balance of forces acting on the G/L/S contact line determines the contact angle. In this balance, three forces play a role, one force related to the L/G interface, one to the S/L interface, and one to the S/G interface.

We can define the force by which each surface pulls on the contact line, and this is the surface tension, σ . The reverse is the surface pressure, P_s , which is the force that pushes on the contact line. Because in the present section all three surfaces pull on the contact line, the σ 's are positive and the P_s 's are all negative.

The force balance on the contact line, in the direction along the solid surface, is

$$P_{s,LG} \cdot \cos \theta + P_{s,SL} = P_{s,SG} \quad (5.1)$$

where θ is the contact angle measured in the liquid phase (water).

For each of the three surfaces, the surface pressure is related to the surface energy γ according to

$$P_s = -\frac{\partial(\gamma A)}{\partial A} \quad (5.2)$$

where A is the area of that surface, and γ is an energy density, i.e., defined per unit area.

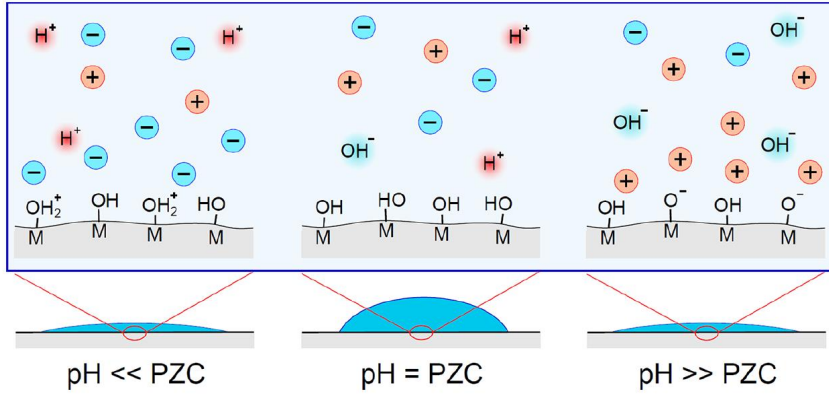


Fig. 5.1: The contact angle of a water droplet on titania. The charge of titania in contact with water changes from positive at low pH, to zero at the point of zero charge (PZC), to negative at high pH. A droplet of water placed on an otherwise dry titania surface would be the most flattened out at very low and very high pH (low contact angle), when the energetic reward of the surface being in contact with water is the highest.

Now, when γ is a constant when we change the area (i.e., when upon stretching the surface there is no internal variable such as concentration or charge that changes), then $P_s = -\gamma$, and we can rewrite Eq. (5.1) to the classical Young's equation,

$$\gamma_{LG} \cdot \cos \theta = \gamma_{SG} - \gamma_{SL} . \quad (5.3)$$

In Eq. (5.3) there is the water/air surface energy which is $\gamma_{LG} \sim 73$ mN/m. The other two energy terms however are yet unknown, though we only need to know the difference between the two, to be able to predict the contact angle.¹ For the dry titania (S/G interface) γ_{SG} is a constant, while for the wetted surface, i.e., titania in contact with water, there is a constant term, $\gamma_{SL}^{\text{unch}}$, which is the energy when the surface is uncharged, and when the surface is charged, there is also a term due to the free energy of EDL formation on this surface.

This term due to the EDL is negative and reduces the surface energy of the S/L interface (the titania in contact with water), and the more so the higher is the charge of the titania, thus at very high and very low pH. Reducing γ_{SL} because of EDL formation will make the contact angle θ smaller, i.e., more of the titania surface will be wetted, see Eq. (5.3).

¹Or vice-versa, data on the contact angle will only provide information on the difference between these two γ -terms.

For titania in contact with water (the S/L interface), the EDL surface energy can be written as the sum of a chemical and an electrical contribution, where the chemical contribution is negative (this actually drives the spontaneous formation of the EDL) while the electrical energy is always positive. The sum is negative because EDL formation is spontaneous in this case.

Instead of a distinction between chemical and electrical work, it is easier to write the EDL energy as a sum of a contribution from the diffuse layer, F^D , and from the surface, F^S (Chan and Mitchell, 1976). These two F -contributions are both added to the surface energy of the S/L interface in the absence of charge, which is γ_{SL}^{unch} , and in this way these two terms end up in Young's equation.

For a single surface, within the GC model for a 1:1 salt, the contribution of the diffuse layer isⁱⁱ

$$F^D = -16c_{\infty}RT\lambda_D \sinh^2(1/4\phi_D) \quad (5.4)$$

where ϕ_D is the electrical potential at the start of the diffuse layer (at the Stern plane), i.e., at the titania surface.ⁱⁱⁱ

For an ionizable material with only acidic or basic groups, the surface contribution to the free energy is

$$F^S = RTN \ln(1 - \alpha) \quad (5.5)$$

where N is the concentration of surface groups (in mol/m²), and where the ionization degree, α , is based on a standard Langmuir model (both for acidic and basic groups, α in Eq. (5.5) is defined as a number between 0 and 1), with the surface charge given by $\Sigma = \pm F \alpha N$.

However, materials such as titania and alumina are amphoteric materials, and the charging degree of each surface group is between $-1/2$ and $+1/2$. For such a material, the isotherm describing the charge as function of surface potential is

$$\alpha = \frac{1}{2} - \frac{1}{1 + 10^{pK - pH} \cdot e^{-\phi_D}} \quad (5.6)$$

where pH is that in bulk solution (sufficiently far away from the surface) and for an amphoteric material pK is the pH at which the material is uncharged, which is the point of zero charge, PZC. For titania, pK = PZC = 4.4.

For a material that obeys Eq. (5.6), the expression for F^S is

$$F^S = 1/2 RTN \ln((1 + 2\alpha)(1 - 2\alpha)) \quad (5.7)$$

ⁱⁱIn this and the next section, pressures and energies are presented with unit N/m or N/m²; in many other parts of the book the term RT is omitted, see p. 507.

ⁱⁱⁱWe neglect the Stern layer in this section, and use ϕ_D instead of ϕ_0 in Eq. (5.6).

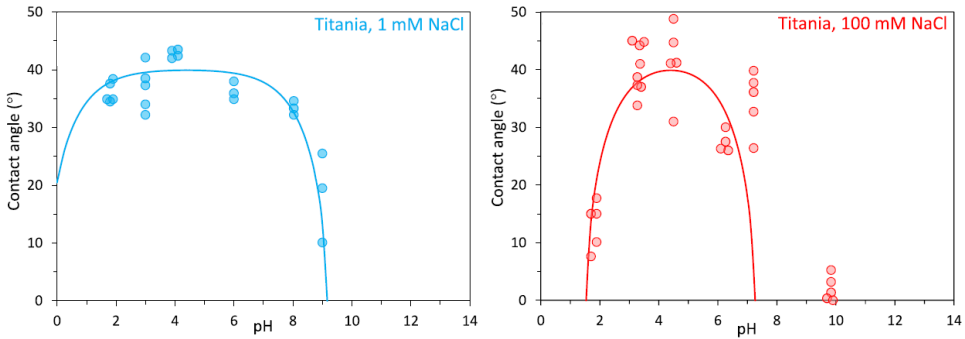


Fig. 5.2: The contact angle of the air-water-titania contact line, as function of pH for two values of salt concentration. The GCS model including surface ionization very well reproduces the experimental data. ($N = 3 \text{ nm}^{-2}$, $\text{pK} = 4.4$, $\gamma_{\text{SG}} - \gamma_{\text{SL}}^{\text{unch}} = 56 \text{ mN/m}$).

which like F^{D} from Eq. (5.4) is negative. Thus, EDL formation will decrease γ_{SL} and thus reduce θ and thus increase the wetted area on the titania.

For each salt concentration and pH, we can solve Eq. (5.6) together with the Gouy-Chapman equation for an isolated surface, Eq. (3.15), to obtain α and ϕ_{D} . These values enter the expressions for F^{D} and F^{S} and these are combined with the S/L surface energy for the uncharged surface, $\gamma_{\text{SL}}^{\text{unch}}$ and jointly used as γ_{SL} in Eq. (5.3).

Results of this theory are presented in Fig. 5.2 as function of pH and c_{∞} and they show a very good agreement with data. The model predicts symmetry of the contact angle θ around the PZC (at $\text{pH} = \text{pK} = 4.4$), and the data corroborate this prediction. The much broader plateau in contact angle at low salinity (1 mM) compared to the situation at high salinity (100 mM), as experimentally found, is also very well reproduced in the theory.^{iv}

^{iv}A very different approach to Young's equation is based on minimization of the total energy in the system, which is a summation of the surface energies of the three areas, times the respective area. This energy is minimized with the constraints that the volume of bubble or droplet is constant, with the shape thereof a (truncated) sphere, and that the solid surface is either wet or dry. This entire minimization (also possible including gravity, resulting in the shape no longer being spherical), leads exactly to Young's equation, without having to explicitly consider forces. This analysis also shows that the L/G interface ideally forms a hemisphere, with θ ideally at 90° , because at this point the L/G area is at a minimum. Thus, the L/G interface always pulls to bring θ closer to 90° . If the solid material is a partially wetted electrode (see next section), this minimization must be done for a fixed total charge. Then we do not end up with Young's law based on surface energies, γ .

5.2 Electrowetting: The EDL surface pressure on an electrode

The previous section discussed EDL formation on titania, and showed that a more negative surface energy of the S/L interface leads to a lower contact angle (more wetting of the surface).

So for titania the surface energy steadily decreases when the titania is increasingly charged, and this leads to more wetting. But this provides us with a puzzle when we consider the problem of electrowetting, a very relevant and important technology where a conducting material (a piece of metal, or metal coating) is increasingly wetted when it is charged. Up to this point, this is all the same as for the example with titania: the higher the charge, the more wetting. However, externally charging an electrode leads to an *increase* in the surface energy because electrical energy must be invested to charge the EDL. So how can it be that for electrowetting we have the same outcome as for titania, that the wetted area expands when we charge the material, even though for electrowetting the surface energy increases, and for titania it decreases?

5.2.1 The surface pressure in electrowetting according to the GC model

To analyze this problem, let us consider the surface energy of such an electrode, which increases when we increase the charge. We know that the energy increases because we need to invest electrical energy to push charge in the electrode and build the EDL. Just as for the titania example in the previous section, the EDL energy has contributions of F^D and F^S . The diffuse contribution, F^D , is the same as before, Eq. (5.4), which is negative, but the surface term is now different. For an electrode which is externally charged, the surface contribution is

$$F^S = V_T \phi_D \Sigma. \quad (5.8)$$

The summation of these two energy terms given by Eqs. (5.4) and (5.8), is F^{EDL} , and this total energy is always positive. The energy F^{EDL} can also be obtained from the energy of charging the electrode,

$$F^{\text{EDL}} = F^D + F^S = \int_0^\Sigma \phi_D d\Sigma \quad (5.9)$$

which indeed results in the summation of F^D and F^S by Eqs. (5.4) and (5.8). That integration

also leads to a novel representation of Eq. (5.4), which is

$$F^D = -2V_T \left(\sqrt{\Sigma^2 + 8\varepsilon RT c_\infty} - \sqrt{8\varepsilon RT c_\infty} \right) \quad (5.10)$$

which mathematically is the same as Eq. (5.4).

Thus, in this case the energy of Eqs. (5.4) and (5.8) combined is positive and thus EDL formation increases the surface energy of the S/L interface, and the more so at higher surface charge. Then, how can it be that charging such an electrode leads to electrowetting, i.e., the spreading of liquid over an electrode, when it increases the surface energy, whereas for titania we had more wetting when the energy of the S/L interface decreased?

The reason is that for electrowetting we cannot use Young's law, Eq. (5.3), but must return to the force balance, Eq. (5.1). For the L/G interface, and for the dry part of the electrode, we can still use as before $P_s = -\gamma$. For the S/L interface, there is again a contribution from the uncharged surface, $\gamma_{SL}^{\text{unch}}$, and in addition we again have a contribution from the EDL. But for this contribution it is no longer the case that surface energy and surface pressure are simply given by $P_s = -\gamma$. Instead of being of opposite sign, they are even of the same sign! All of this is because of a difference in the differentiation of the EDL-contribution to the energy of the S/L interface by Eq. (5.2). For electrowetting, the EDL contribution to the surface energy, γ^{EDL} , is not constant when we expand the surface. Instead, in such an experiment one inserts a certain amount of charge in the *total* electrode, Σ_{tot} (per unit total, dry+wet, area), but the charge can only be stored in the wetted part of the surface.^v Thus it is now the case that when the S/L interface expands, the charge density in the wetted area decreases, and the surface energy, γ , decreases as well. Thus for electrowetting, for a given amount of injected charge, this surface energy depends on how much the surface is stretched, and is not independent of that, which was the key assumption on which Eq. (5.3) is based.

In this case we must use a modification of Eq. (5.3) where we replace the term γ_{SL} by the constant term $\gamma_{SL}^{\text{unch}}$ (the contribution to the surface energy of S/L interface due to its contact with water, which is independent of the charging process), and add to that a term $-P_{s,SL}^{\text{EDL}}$. Thus we obtain for the electrowetting problem

$$\gamma_{LG} \cdot \cos \theta = \gamma_{SG} - \gamma_{SL}^{\text{unch}} + P_{s,SL}^{\text{EDL}}. \quad (5.11)$$

What is the surface pressure of the S/L interface due to the formation of the EDL, $P_{s,SL}^{\text{EDL}}$? The surface pressure can be derived from the total EDL free energy density ($F_{SL}^{\text{EDL}} = F^D + F^S$) by using Eq. (5.2), which can be modified to

$$P_s = \Sigma^2 \frac{\partial (F/\Sigma)}{\partial \Sigma} = \Sigma \frac{\partial F}{\partial \Sigma} - F \quad (5.12)$$

^vIn the dry part of the electrode, the S/G interface, a very tiny charge already leads to a large voltage, and thus hardly any charge will be stored here.

where Σ is the surface charge density. Implementing the two contributions to $F_{\text{SL}}^{\text{EDL}}$ according to Eqs. (5.4) and (5.8), and making the derivation in Eq. (5.12) leads to

$$P_{\text{s,SL}}^{\text{EDL}} = 8c_{\infty}RT\lambda_{\text{D}} (\cosh(1/2\phi_{\text{D}}) - 1) = 16c_{\infty}RT\lambda_{\text{D}} \sinh^2(1/4\phi_{\text{D}}) \quad (5.13)$$

which, after inserting the GC-equation, Eq. (3.15), we can write as function of charge as

$$P_{\text{s,SL}}^{\text{EDL}} = 2V_{\text{T}} \left(\sqrt{\Sigma^2 + 8\varepsilon RTc_{\infty}} - \sqrt{8\varepsilon RTc_{\infty}} \right). \quad (5.14)$$

With this addition, the relevant force balance for electrowetting, Eq. (5.11), will predict that θ goes down when we increase the electrode charge, as expected.

For a sufficiently low surface charge (or low diffuse layer potential), Eq. (5.14) simplifies to

$$P_{\text{s,SL}}^{\text{EDL}} = \frac{\lambda_{\text{D}}}{2\varepsilon} \Sigma^2 + \mathcal{O}(\Sigma^4) \quad (5.15)$$

which has a dependency on salt concentration by a power $-1/2$, and a quadratic dependency on charge.

For a high surface charge (or high diffuse layer potential), instead Eq. (5.14) simplifies to the ‘counterions only’ limit

$$P_{\text{s,SL}}^{\text{EDL}} = 2V_{\text{T}}\Sigma - 8c_{\infty}RT\lambda_{\text{D}} \quad (5.16)$$

which is accurate when the the first term on the right side is at least twice as large as the second term, and thus the criterion to apply Eq. (5.16) is $\Sigma > 8c_{\infty}F\lambda_{\text{D}}$.

5.2.2 Electrowetting and capillary rise

Using electrowetting we can quickly change the shape of a bubble or droplet on an electrode, which is described by the theory of the previous section. In addition, electrowetting is often used to induce fluid motion, for instance against gravity inside a vertical capillary. The question in a study of capillary rise is, how much does a fluid move against gravity inside an electrode-coated capillary that we charge up?

We can solve this problem of capillary rise by considering the two energy contributions involved, which are gravity and electrical energy. The energy in the L/G surface, which is the L/G area \times surface energy γ_{LG} , is actually very low for a thin capillary (around 1% of the other energies in the example we discuss below).^{vi}

^{vi}This is very different in the problem we discuss further on that is about a single vertical plate in contact with water.

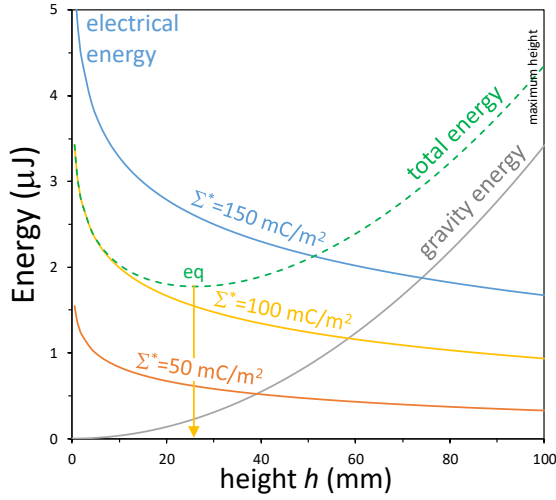


Fig. 5.3: The energies involved in electrowetting, which are electrical energy and gravity, as function of capillary rise (height h). Electrical energy as function of total charge, Σ^* . The maximum fluid rise is $h_{\max} = 100$ mm, and Σ^* is based on $h^* = h_{\max}$ ($\rho_L = 1$ g/mL, $\mathbf{g} = 9.81$ m/s², $a = 147$ μm , $\gamma_{\text{LG}} = 73$ mN/m, $c_\infty = 10$ mM).

The electric energy of charging is given by $F^D + F^S$ of Eqs. (5.8) and (5.10), times the total wetted area, which is height h times $2\pi a$, where a is the capillary radius.^{vii} The gravitational energy of the fluid that is lifted against gravity is $1/2\rho_L\mathbf{g}h^2$ times πa^2 which is the cross-sectional area.^{viii} This total energy, electrical plus gravitational, is minimized by varying h for each value of a total charge, Σ^* . This Σ^* is a charge density (in C/m²) for a certain reference area ($2\pi a h^*$). Thus we make use of $\Sigma \cdot h = \Sigma^* \cdot h^*$.^{ix} For this given total charge, when the wetted area expands, the charge per unit wetted area decreases, and this reduces the electrical energy. Thus, as function of height h , the gravitational energy increases quadratically, while the electrical energy decreases, see Fig. 5.3. The summation of these two terms has a minimum at h_{eq} , which is the height up to which the capillary will be filled with liquid.

The equilibrium height, h_{eq} , can also be found from a force balance acting on the L/G

^{vii}Height h is defined relative to a starting height h_0 when the capillary is uncharged.

^{viii}We use the gravitational constant \mathbf{g} as a positive number in this section.

^{ix}We neglect a technical complication that also for zero charge part of the electrode-coated capillary is below the fluid level, i.e., already wetted. Charge will also go to this region, but the charging of the EDL here will not lead to fluid rise.

interface. The first term relates to gravity and is minus the derivative of the gravitational energy with height, which gives a downward force equal to $\rho_L \mathbf{g} h \times \pi a^2$ by which the liquid column pulls the L/G interface downward. This gravitational force is balanced by the EDL surface pressure given by Eq. (5.13) times the circumference, thus $P_{s,SL}^{EDL} \times 2\pi a$.^x This balance of forces leads to the equilibrium height in the capillary given by

$$h_{eq} = \frac{2 P_{s,SL}^{EDL}}{a \rho_L \mathbf{g}} \quad (5.17)$$

in which we can insert the various expression for the EDL surface pressure, $P_{s,SL}^{EDL}$, given by Eqs. (5.13)-(5.16). The general solution is

$$h_{eq} = 4 V_T (\rho_L \mathbf{g} a)^{-1} \left(\sqrt{\Sigma^2 + 8 \varepsilon R T c_\infty} - \sqrt{8 \varepsilon R T c_\infty} \right) \quad (5.18)$$

which shows that the capillary rise increases with charge and increases when the diameter of the capillary becomes smaller. Eq. (5.18) exactly matches the minimum, or equilibrium, depicted in Fig. 5.3, which was based on an energy analysis. For low charge, we can do a Taylor expansion of Eq. (5.18) around $\Sigma = 0$, resulting in

$$h_{eq} = \lambda_D \cdot (\rho_L \mathbf{g} a)^{-1} \cdot \varepsilon^{-1} \cdot \Sigma^2 + O(\Sigma^4) \quad (5.19)$$

which shows that in this limit height depends quadratically on charge Σ , and depends with a $-1/2$ power on salt concentration.

In the high-charge limit, we can insert Eq. (5.16) in Eq. (5.17), and obtain for the capillary rise

$$h_{eq} - h_{ref} = (a \rho_L \mathbf{g})^{-1} \cdot 4 V_T \cdot \Sigma \quad (5.20)$$

which predicts that the height depends linearly on surface charge, *without any dependence on any EDL property*.^{xi} This is quite remarkable. If correct, then one expects also the same equation for height versus charge when instead of evaluating a GC model for the diffuse layer, we use a more complicated EDL model, or a model only dependent on a constant dielectric, or Stern, capacitance. In that case capillary rise is independent of the Stern capacitance but only depends on the charge injected into the electrode, as described by Eq. (5.20).^{xii}

^xNon-electrostatic contributions to the surface energy are not part of this balance because h is defined relative to the height of the column when the capillary wall is uncharged.

^{xi}Only the constant term h_{ref} (which is small compared to the right side at high charge) has a $1/2$ power dependency on salt concentration.

^{xiii}Of course, the EDL voltage that is required to store a certain charge, depends on properties of the EDL and on the properties of the dielectric coating.

5.2.3 Derivation of the Laplace equation from Young's equation

Can we continue charging the inner surface of the capillary, and thereby have the fluid move up more and more in the capillary? Interestingly, no, we cannot. There is a natural limit, and that follows from the next analysis.

This analysis is based on a combination of the modified Young's equation for the contact angle in case of electrowetting, Eq. (5.11), with the balance of forces given by Eq. (5.17), which results in^{xiii}

$$h_{\text{eq}} = \frac{2}{a\rho_L\mathbf{g}} \cdot \gamma_{\text{LG}} \cdot \cos \theta \quad (5.21)$$

which shows the dependence of height on the capillary radius a , and on contact angle, θ , with height increasing when a goes down or θ goes down. Now, Eq. (5.21) shows that there is a maximum in height arrived at when θ is zero, and for this height we obtain

$$h_{\text{eq,max}} = \frac{2}{a\rho_L\mathbf{g}} \cdot \gamma_{\text{LG}}. \quad (5.22)$$

The maximum height for the calculation settings of Fig. 5.3 was $h_{\text{max}} = 100$ mm, for a capillary radius of $a \sim 150$ μm . This is already a fairly thin capillary and this analysis shows that more than 100 mm capillary rise is not possible for an electrode-coated capillary of this inner diameter filled with water.^{xiv}

We can also derive another result from this analysis. We first note that for thin enough capillaries, the shape of the L/G interface is spherical, i.e., the radius of curvature R is a constant, independent of radial position. In that case we can relate R to the contact angle θ and to the capillary radius a , according to $a = R \cos \theta$, which we can implement in Eq. (5.21), resulting in

$$\rho_L\mathbf{g}h_{\text{eq}} = \gamma_{\text{LG}} \frac{2}{R}. \quad (5.23)$$

Now, the left side of this equation is also equal to the increase in pressure when we go vertically down the capillary, starting at a position in the liquid near the L/G interface down to the height of the bath in which the capillary is positioned. This latter pressure equals the external gas phase pressure.^{xv} Thus, the left side of Eq. (5.23) is the gas pressure minus the pressure in the liquid just below the L/G interface (i.e., the latter is lower than the gas phase

^{xiii}We assume $\gamma_{\text{SG}} - \gamma_{\text{SL}}^{\text{unch}} = 0$ (this term only leads to a constant change in height).

^{xiv}Of course microporous materials such as membranes, gels, or electrodes, can have much smaller pores (down to the nm-range), and thus the wetting of such materials occurs throughout the sample against gravity to a much larger height. Thus water transport against gravity will make use of this microporous phase, not through larger pores if they exist. These will be dry.

^{xv}All of this is correct irrespective of details of the S/L interaction on the capillary wall (such as EDL charging), and of the L/G interface.

pressure). For this pressure difference across the curved G/L interface, ΔP , we therefore arrive at

$$\Delta P = \gamma_{LG} \frac{2}{R} \quad (5.24)$$

and this is the Laplace equation for a thin capillary! Thus, we derived the Laplace equation (for a thin capillary) based on two inputs: 1. A force balance of the G/L/S contact line on the capillary wall; and 2. An overall force balance relating gravity with the surface pressure of the wetted capillary wall. Thus, we derived the Laplace equation –relating curvature and pressure difference across the L/G interface– by combining two previously discussed force balances.

Derivation of Laplace equation. Let us again derive the Laplace equation based on a vertical capillary, but starting with an energy analysis. We bring a vertical capillary in contact with a volume of water. The capillary just touches the upper surface of the water, and this position we assign as height $h=0$. The water will rise in the capillary until an equilibrium height h is reached. The energy has a gravity contribution, $\frac{1}{2}\rho_L \mathbf{g} h^2 \times \pi a^2$, and a contribution from the energy of the wetted surface minus that of the dry surface, $(\gamma_{SL} - \gamma_{SG}) \times 2\pi a h$. Adding up and calculating at which h this total energy is at a minimum, leads to $\rho_L \mathbf{g} h a + 2(\gamma_{SL} - \gamma_{SG}) = 0$. This last equation is a ‘column-based’ force balance, and does not include the G/L interface. It is not a force balance on the G/L/S contact line such as Eq. (5.1) which does include the G/L interface. We can leave out the G/L interface in this balance because the capillary is thin and thus this area small, and thus the energy related to the G/L interface is small too. We implement Eq. (5.3) and the geometrical relationship for a (hemi-)sphere, $a = R \cos \theta$, leading to $\rho_L \mathbf{g} h = 2\gamma_{LG}/R$. The column height h times $\rho_L \mathbf{g}$ equals the pressure in the gas phase minus that just below the curved G/L meniscus, ΔP , and thus we again arrive at the Laplace equation.

A very different derivation of the Laplace equation is based on creating a bubble in a liquid. If we have a bubble and increase the radius R by dR , we must push against the surface energy. The energy required to enlarge the bubble, to push in the extra volume, is $\Delta P \cdot 4\pi R^2 dR$, and the energy increase of the surface is $\gamma_{GL} \cdot 8\pi R dR$. [The increase in area when the radius of a bubble increases by dR is $4\pi (R + dR)^2 - 4\pi R^2$ which for small dR becomes $8\pi R dR$.] Each of these terms is a force, pushing outward and inward on the bubble surface, and the equilibrium condition is when these forces add up to zero. Doing so, we again arrive at the Laplace equation, Eq. (5.24), now derived on the basis of forming a bubble in a liquid. Thus, with γ_{SL} a positive number, the pressure ΔP , measured as that in the gas phase minus in the liquid, is positive for a gas bubble or in any other situation where the G/L surface ‘bends towards the gas phase’, ‘tries to enclose it’. Then ΔP is higher than in the liquid around it, the more so the smaller the bubble, and the more so the higher the surface energy of the G/L interface.

The same result also follows if we minimize the energy of a bubble that is compressible, placed

inside a bath of liquid, water for instance. We start with a small bubble at high pressure which we let expand to end at a size where the pressure inside (which is larger than in the bath) is such that we reach mechanical equilibrium. So the expansion (increase of volume V) leads to a decrease of pressure energy. [If we would compress it against an inside pressure higher than outside, then the energy would go up, so expanding a volume that has higher pressure than outside, means the energy in the object goes down.] Thus counted from the initial volume, the pressure energy is $E_p = - \int \Delta P dV$ with pressure ΔP that inside minus outside (outside must be a large system at constant pressure). The surface energy is $E_s = \int \gamma_{GL} dA$, with A area, and this creation of (more) surface means an energy increase. So what must be minimized is $E_p + E_s$. Making use of $dV = 4\pi R^2 dR$ and $dA = 8\pi R dR$ we indeed end up with the Laplace equation $\Delta P = 2\gamma_{GL}/R$, and thus the pressure inside the bubble is higher than outside. The same result should be arrived at for a water droplet in air, but then the derivation of an expanding droplet is less intuitive.

Charging beyond the maximum. One final question is, what happens in a charged capillary when we charge the surface beyond the maximum value? [In the example of Fig. 5.3, this maximum was at a charge density of $\Sigma = \Sigma^* \sim 1.43 \text{ C/m}^2$ (EDL voltage 283 mV) when we reach a height of $h_{\text{eq,max}} = 100 \text{ mm}$.]

What then happens is that the surface continues to be wetted, but only with a very thin layer forming, just enough for an EDL to form. This layer therefore can be as thin as just a few nm. More and more of the capillary will be coated with a nanoscopic thin layer of fluid, and charge is stored in this EDL. The system ‘pays’ in electric energy that must be invested in forming this EDL, as well as in forming the new L/G interface, while S/G interface is replaced by S/L interface. There can also be a ‘stabilizing’ effect of a repulsive Van der Waals force (repulsive between the dissimilar materials air and metal, interacting across the water film).

For the assumptions made above, charge and potential follow from a force balance for the expansion of the surface. In this balance capillary radius a and height h do not enter. This force balance is $P_{s,SL}^{\text{EDL}} = \gamma_{LG}$, with $P_{s,SL}^{\text{EDL}}$ calculated for instance by Eq. (5.14). Interestingly, we know the answer must be the charge and potential that we have when we reach the maximum capillary height, h^* . And indeed in our previous calculation we again find a value for the EDL voltage of 283 mV as a threshold value beyond which the nanoscopic layer will form. Or in other words, this nanoscopic film starts to form when (the electrostatic contribution to) the surface pressure is about to exceed the air-water surface energy of $\gamma_{SL} = 73 \text{ mN/m}$.

Interestingly, if we run the electrowetting experiment by making steps in voltage, and we now arrive at the EDL threshold voltage identified above (the value required for the nanoscopic layer to start being formed, when the capillary has reached the maximum height, where θ becomes zero), then a further increase in EDL voltage will immediately lead to the rapid formation of the nanoscopic layer until some system limit is reached (e.g., the nanoscopic layer reaches the top of

the capillary). This may look like an electric breakdown or Faradaic loss current, because now suddenly a small increase in voltage leads to a large current spike. But it is the current that goes into charging the nanoscopic surface layer that is rapidly growing beyond the L/G meniscus.

Contact angle saturation. An outstanding problem in the field of electrowetting is contact angle saturation, which is the phenomenon that a droplet deposited on an (often polymer-coated) electrode surface will not expand further when a contact angle of around 25° is reached (i.e., the contact angle will not go down further). It is as if a further expansion of the G/L interface just doesn't pay off anymore, and to accommodate the extra charge, formation of a thin layer on the electrode outside the droplet is preferred. It would be interesting to find out if the electrode voltage –which is measured against a (pseudo-reference) electrode inserted in the droplet– at the point that the lowest contact angle is reached, is the same voltage as measured for the same liquid and same electrode in the geometry of a vertical capillary for the condition that the maximum height h^* is reached. If these voltages coincide, a nanoscopic film can also be expected to form for a droplet on a horizontal electrode when charge continues to be injected after this threshold voltage is reached. In combination with a repulsive Van der Waals force acting across the nanoscopic layer –which stabilizes the layer, i.e., lowers the energy of formation– this may then explain why the macroscopic G/L interface does not further expand, and that may explain the phenomenon of contact angle saturation.

5.2.4 Surface tension effects near a charged vertical wall

The following calculation is of interest to check the theory of electrowetting put forward. Namely, we consider a single vertical electrode placed in a salt solution (electrolyte), without any other surface nearby. At zero charge we assume we have a zero contact angle. The shape of the L/G interface can be solved from the Young-Laplace equation for a two dimensional planar geometry: $z = \lambda^2 \cdot z'' / (1 + z')^2$ where the capillary length is $\lambda = \sqrt{\gamma_{LG} / \rho_L g}$ and where z' and z'' are the first and second derivative of the z -coordinate of the L/G interface with respect to the x -coordinate (z vertical, x horizontal). For a single surface, the analytical solution is $X = \cosh^{-1}(2/z) - \cosh^{-1}(2/H) + \sqrt{4 - H^2} - \sqrt{4 - Z^2}$, where X , Z and H are dimensionless coordinates, each of which can be multiplied by λ to obtain the dimensional coordinates, x , z and h . Height h is the height of the meniscus at the solid surface (at the electrode, where $z=0$), and for a vertical electrode is given by

$$h = \lambda \cdot \sqrt{2(1 - \sin \theta)} . \quad (5.25)$$

Thus the maximum height, reached when $\theta=0$, is $h=\sqrt{2}\lambda$. Water (in contact with air) has a capillary length of $\lambda=2.7$ mm, and thus the maximum height of the meniscus is ~ 3.9 mm. [If the vertical wall is at an angle α , the above remains valid, with α added to θ in Eq. (5.25). When the wall is tilted towards the liquid, the height of the meniscus goes up.]

We make a calculation of the energies involved in charging an electrode that is placed vertically in a salt solution, with the meniscus at a height of 3 mm. A height of $h=3$ mm implies a contact angle of 23.3° , a surface pressure of the wetted electrode of $P_s=67.1$ N/m, a surface potential of $\phi_D=10.83$, a surface charge of $\Sigma=1.317$ C/m², and a corresponding electrical energy of 0.30 J/m² per unit wetted electrode area. By multiplying with the height of 3 mm, we obtain the electrical energy per unit length in the direction along the contact line of 898.2 μ J/m. The gravity energy can also be calculated numerically (in lifting up the fluid from the level of the bulk liquid) and is 45.2 μ J/m, while the surface energy in the extra created L/G interface is 65.6 μ J/m. (This number is the product of γ_{LG} and the extra created line length of 0.899 mm; this is the extra ‘length’ of L/G surface as measured in the direction to the electrode.)

In this example of the shape of the L/G surface near a single vertical wall, we find that gravity and surface energy are about equal in magnitude, while the energy of charging the electrode is about $9\times$ larger than the other two energy terms together. Interestingly, the ratio of these numbers is very different here compared to the case of capillary rise, where surface energy was not more than 1% of 1 μ J, thus negligible compared to the other two energies, see Fig. 5.3, while electrical energy was larger than gravity by a factor of 6–8 (while in the new example the ratio is ~ 20).

Now, for the example of the single vertical wall, there seems to be an error in all energy numbers. Because how can it be that the electrical energy of 898 μ J/m is not the same as the gravitational plus surface energy? Aren’t we investing electrical energy with the aim to raise the liquid against gravity, and expand the surface? But the latter two terms are much lower together, almost a factor of 9. Where is the factor 9 error?

The answer is, there is no error. Instead, we invest electrical energy and that is stored in three ways: 1. charging the surface; 2. lifting up the fluid against gravity; and 3. creating the extra L/G surface. The electrical energy that is *stored* in the electrode (EDL), is the number of 898 μ J/m above.

The electrical energy we invest must be equal to the summation of these three energies, which is 1009 μ J/m. Let us see if we can calculate that number via an independent route. In a first method, for each height (from zero to the 3 mm) we determine the contact angle via Eq. (5.25), thus the surface pressure via Eq. (5.11), and integrate, i.e., we push against the surface pressure along the path to push the contact line up to its final position. Thus we

obtain for the invested energy

$$E_{\text{inv}} = \int_0^h P_s dh = \gamma_{\text{LG}} \int_0^h \cos \theta dh = \gamma_{\text{LG}} \cdot \lambda^{-2} \cdot \int_0^h \sqrt{\lambda^2 h^2 - 1/4 h^4} dh \quad (5.26)$$

which results in a number of $E_{\text{inv}} = 110.8 \mu\text{J/m}$, but this is not the number of $1009 \mu\text{J/m}$ that we are after! Actually it equals the sum of the gravitational and L/G surface contributions. Thus, integration of the surface pressure over height, only gives us the energy in the L/G interface, plus the gravitational energy. In hindsight it makes sense that this last calculation gave an energy that was too low, because when we push charge in an electrode, we are not pushing against the contact line, but we push against the potential of the EDL already formed. Thus we have to make a calculation where we charge an electrode and calculate the energy that is invested by integrating from one charging state to another. In a standard calculation, the electrode has a fixed surface area and thus we integrate from one charge density to another, see Eq. (5.9). However, in the present case, while we charge the wetted part of the electrode expands, and this increase in area must be part of the integration process, because we integrate over charge (C), not charge density (C/m^2). This becomes

$$E_{\text{inv}} = V_T \int_0^S \phi_D dS = V_T \int_0^S \phi_D (hd\Sigma + \Sigma dh) \quad (5.27)$$

where S is a charge with unit C/m, and Σ as before the charge density, $\Sigma = S/h$. For both terms in the integration, we must know how Σ and ϕ_D change with height, which we obtain in a calculation where we combine Eqs. (3.15), (5.11), (5.13), and (5.25). In a numerical calculation, this entire procedure leads to an energy that is invested of ... $1009 \mu\text{J/m}$, exactly the same as the number for total energy arrived at earlier!

It is interesting that this last integration results in the total energy that is invested in the process, although this calculation seems to be about electrostatics only (EDL formation), and nowhere are the gravity and L/G surface energy involved. So how can this calculation also provide us the gravity energy and the energy of the L/G interface? The answer is that ‘information’ of these two energies is included in the dependency of charge on meniscus height, i.e., on the ‘shape’ of the $\Sigma(h)$ -function. This relationship is part of the integration to obtain E_{inv} . For another surface tension or surface shape, this function is different, and thus the outcome of the integration would be different. Thus, the electric work as calculated by Eq. (5.27) was in effect also pushing against the contact line.

In conclusion, we have consistency between all equations that we used in this problem of single electrode electrowetting, and consistency with the same theory applied earlier on for the electrowetting of a capillary.

5.2.5 Influence of Stern layer on contact angle and electrowetting

The above two sections considered several elements of an EDL model, such as the diffuse part of the EDL, described by the Gouy-Chapman equation, the ionization of titania, an amphoteric material, and the related chemical energy of surface (de-)protonation. The next extension of these models would be to include a Stern layer (dielectric layer). As explained before, the Stern layer is a layer of constant capacitance, that can be considered to be located between the diffuse layer and the underlying 0-plane or electrode. This 0-plane is where in the case of titania we assume the surface groups (titania charged groups) to reside. The Stern layer changes the effective pH at the 0-plane, thereby reducing α (pushing it closer to zero), and it adds a term to the surface energy. Also in the case of electrowetting the Stern layer plays a role in EDL surface energy, surface pressure and the resulting capillary rise. Actually, the Lippmann equation of capillary rise assumes only a constant (Stern, Helmholtz) capacitance, and a diffuse layer is not considered. Despite their relevance, we must nevertheless postpone discussion of these Stern layer effects to a later time.

Electrocapillary curves. A problem related to the topics in this section, is the phenomenon of electrocapillarity, where the fluid inside a capillary is a liquid metal, mercury, which can be externally electrified. The mercury column at its lower end is in contact with electrolyte. The EDL structure at this electrolyte/mercury interface can now be studied.

Compared to the electrowetting case discussed above, in this device electronic charge is not injected into the conductive wall of the capillary, but it is injected into the fluid itself, which is a quite different experiment. This electronic charge will move to the mercury/electrolyte interface. The required gas phase pressure applied to the top of the column to keep it in place is a measure of the surface tension of the mercury/electrolyte interface, and data of this surface tension versus voltage are plotted as electrocapillary curves, which have a maximum at a certain voltage (when the interface is uncharged), and they drop off, roughly symmetrically, at lower and higher voltages. [The asymmetry is because when mercury is positively charged it attracts anions as counterions, but when negatively charged cations are the counterions, and these ions may have different properties such as hydrated ion size and shape.] From these curves (which depend moderately on salt concentration) by analysing the slope (first derivative) we obtain the charge for each voltage, and taking a second derivative results in the capacitance of the EDL as function of charge.

Detailed discussion of this methodology in this book must wait for a later moment.

5.3 The harvesting of electric energy from EDL changes due to the motion of electrical wires

5.3.1 Introduction

We have previously discussed the Donnan model which describes the distribution of ions between free solution and a medium with fixed charges that are volumetrically distributed, such as a Donnan model for an electrode micropore, or for the interface between solution and a charged (ion exchange) membrane, see Ch. 2. We also discussed the Gouy-Chapman model for the ion distribution in free electrolyte next to a planar electrode, see Ch. 3.

Next we extend and combine these two models, to describe the EDL structure when an electrode is coated with a charged medium (such as a gel or charged membrane) permeable for ions, see Fig. 5.4, as described in Virga *et al.* (2017).

The study of the EDL at the interface between an electrode and a charged gel or membrane is of importance in various application, for example for membrane electrodes, and for proton-conducting fuel cell membranes. The example we will discuss shows that this EDL structure can be used to harvest energy from motion. The electrode we consider in this section is capacitive, and there are no reactions at the electrode. The coupling of EDL structure with electrode reactions is discussed in Ch. 14.

The charged polymer (for instance a polyelectrolyte gel) contains fixed charges, of a positive or negative sign, and there are free counterions as well as coions inside this network. Such (polyelectrolyte) gels are able to absorb a significant amount of water into its network structure (up to ~ 2000 times the polymer weight). A gel is characterized by a molar concentration of fixed charges, X , similar to the approach in Chs. 2 and 12.

When a gel is coated on an electrode, then both the electrode charge and the gel fixed charge density are responsible for the distribution of ions in the EDL, hence for the profile of the potential, ϕ , see Fig 5.4. As depicted here, it is possible that the potential, ϕ (relative to that in bulk solution outside the gel), flips sign at some position near the electrode. For a positively charged gel, we can then have an excess of cations at the electrode, while in the gel bulk phase we mainly have free anions.

5.3.2 Theory

In this section, we explain the EDL theory of an electrode coated with a charged gel permeable to water and ions. In a later section we show how this EDL theory can be included in a model for an electrochemical cell, to describe harvesting of energy from motion.

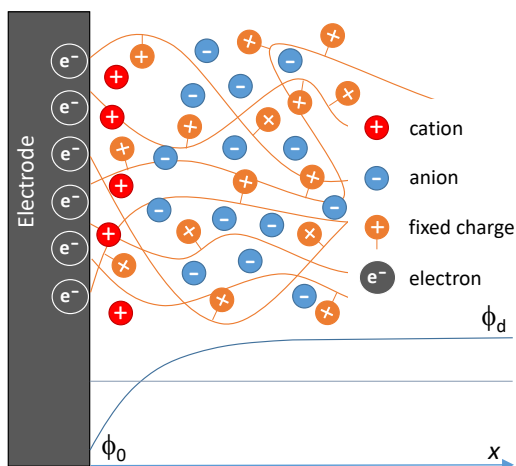


Fig. 5.4: Electrode coated with a positively charged gel layer permeable to electrolyte. The electrode charge and the fixed charges of the gel determine the distribution of free ions in the gel and in the EDL near the electrode, and thus the potential profile, ϕ , as it changes from the value at the electrode to a value in the gel bulk phase. In this case it is possible that while the gel bulk has an excess of anions, right near the surface there is an excess of cations.

We start with a derivation describing the equilibrium EDL profile for the potential and ion concentrations near an electrode covered with a charged gel. Since the EDL is thin we can use the one-dimensional planar form of the Poisson equation, Eq. (3.1) (whatever is the shape of the electrode), and write for the charge density ρ

$$\rho = F (c_\infty (e^{-\phi} - e^\phi) + \omega X) \quad (5.28)$$

where ω is the sign of the fixed charges in the gel ($\omega = +1$ for a positively charged gel and $\omega = -1$ for negative charge). Eq. (5.28) is obtained when the gel is in contact with an electrolyte containing a monovalent salt, with the bulk salt concentration outside the gel given by c_∞ . Furthermore, Eq. (5.28) assumes that the entire gel phase is available for ions and the gel structure does not exclude volume to the ions. Thus, volume effects of ions and of the polymer network are neglected.

Combining Eqs. (3.1) and (5.28), we obtain a modified Poisson-Boltzmann equation^{xvi}

$$\frac{\partial^2 \phi}{\partial x^2} = \kappa^2 (\sinh \phi - A) \quad (5.29)$$

where $A = \omega X / (2c_\infty)$ is a dimensionless gel charge density. Multiplying each side of Eq. (5.29) by $\frac{\partial \phi}{\partial x}$, we obtain

$$\frac{1}{2} \frac{\partial}{\partial x} \left(\frac{\partial \phi}{\partial x} \right)^2 = \kappa^2 \left(\left(\frac{\partial \cosh \phi}{\partial x} \right) - A \frac{\partial \phi}{\partial x} \right) \quad (5.30)$$

which, making use of boundary conditions $\frac{\partial \phi}{\partial x} = 0$ and $\phi = \phi_D$ for $x \rightarrow +\infty$, and $\phi = \phi_0$ for $x = 0$, can be integrated to the modified Gouy-Chapman equation

$$\Sigma^2 = 4\varepsilon RT c_\infty (\cosh(\phi_0) - \cosh(\phi_D) - A(\phi_0 - \phi_D)) \quad (5.31)$$

where $\phi_D = \sinh A$ is the Donnan potential deep within the gel layer (very right in Fig. 5.4), which is defined relative to bulk electrolyte outside the gel. To derive Eq. (5.31), we also made use of Gauss' law at the electrode surface

$$\Sigma = -\varepsilon \left. \frac{\partial V}{\partial x} \right|_0 \quad (5.32)$$

where Σ is the electrode charge in C/m^2 . For $X = 0$, Eq. (5.31) simplifies to the classical Gouy-Chapman equation for a charged surface in contact with an electrolyte, see Eq. (3.15). Fig. 5.5 shows the effect of the dimensionless gel charge, A , and electrode charge, B , on the EDL voltage, ϕ_0 , where $A=0$ represents the Gouy-Chapman solution.

^{xvi}Similar to Eq. (2.11) in Shockley (1949)¹.

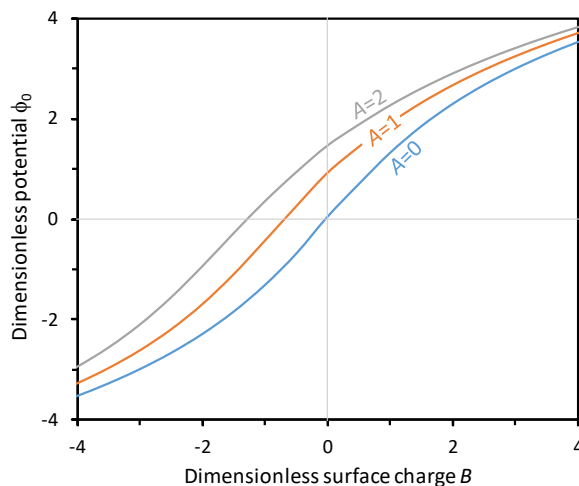


Fig. 5.5: Electrode potential, ϕ_0 , as a function of dimensionless gel charge $A = \omega X / 2c_\infty$ and electrode charge $B = \Sigma / \sqrt{4c_\infty \varepsilon RT}$ (B is $\sqrt{2}$ smaller than Q used in §3.3, i.e., $Q = \sqrt{2} B$).

5.3.3 Electrochemical harvesting of energy from motion

One possible application of an EDL at the interface between a metal and a charged polymer phase such as a polyelectrolyte gel, is the generation of motion of thin flexible electrodes, while in the present example we consider the reverse case: the harvesting of energy from motion, by coiled electrodes embedded in a gel.

If electrode coils embedded in a polyelectrolyte gel are stretched, this will lead to a change in the charge density of the gel, X , right next to the electrode surface.^{xvii} This change in X changes the EDL structure, and thus the electrode potential. Two such electrodes placed in an electrochemical cell (with oppositely charged gel materials used for each electrode) generate electrical current and energy from repeated stretching and relaxation of the entire assembly, see Fig. 5.6.

We evaluate the system of two gel-coated coiled electrodes, one with a gel with positive fixed charge and one with negative fixed charge, which as a whole are dipped in a salt solution of given concentration c_∞ . We analyze how energy is produced from stretching and relaxation of the coils. An external load, R_{EXT} , is placed in the electrical circuit, see Fig. 5.6b, such as a battery or other device, to harvest the electrical energy that is generated. Furthermore, a capacitive element ('external capacitor', or EC) is placed in the circuit.

^{xvii}For details on this statement, see Virga *et al.* (2017).

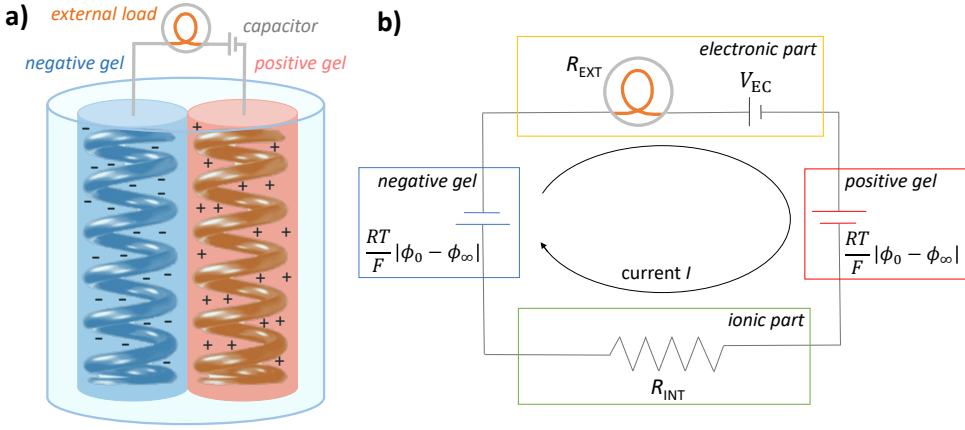


Fig. 5.6: a) Schematic picture of an electrochemical cell consisting of two coiled electrodes coated with a positively and negatively charged polyelectrolyte gel. b) Electrical circuit diagram of the same system, including an ionic resistance, R_{INT} , a load to harvest energy, R_{EXT} , and an external capacitor, V_{EC} .

A dynamic model of this electrochemical cell includes a description of how the gel charge X changes in time, and thus via Eq. (5.31) how the EDL structure changes. This relation is supplemented by Kirchhoff's voltage law

$$V_{cell} + V_{EC} + 2V_T |\phi_0| + V_{INT} = 0 \quad (5.33)$$

where we assume perfect symmetry of the two electrodes (with only the gel charge of each electrode of opposite sign), while V_{cell} , V_{EC} and V_{INT} are the cell voltage (which is the voltage across the load; the load is represented in Fig. 5.6 by R_{EXT}), the voltage across the external capacitor, and a voltage drop because of a resistance for ion transport across the two gel layers. Furthermore, we relate the charge in one of the electrodes to current according to

$$\frac{\partial \Sigma}{\partial t} = \pm I \quad (5.34)$$

where I is the current density in A/m^2 . Combining the above equations, and assuming Ohmic behaviour for the external load and for the ionic transport in the gel, we can calculate the electrical power as function of time according to

$$P_d = V_{cell} \cdot I. \quad (5.35)$$

Details of this calculation and results can be found in Virga *et al.* (2017).

references

1. W. Shockley, "The Theory of p - n Junctions in Semiconductors and p - n Junction Transistors," Bell Syst. Tech. J. **28**, 435–489 (1949).

The interaction forces between colloidal particles

The study of the interaction between colloidal particles is of importance in many environmental and industrial processes, and their understanding requires physical theories of repulsion and attraction between the particles. An important part is the electrostatic force due to the structure of the EDL on each particle and the theory includes a description of surface charge and ionization. Combined with the Van der Waals force that also acts between particles, these two forces together describe the forces and pressures between colloidal surfaces and particles. This balance of forces determines the conditions of stability of a colloidal solution.

6.1 Introduction

The interaction forces between charged surfaces and particles is of key relevance for many environmental and industrial systems and processes. These interactions can be between particles on the one hand, and flat or porous materials on the other, as in studies of particle deposition on surfaces, and in studies of particle capture in porous media. In this case the two materials/particles that are interacting across water will be different in their surface structure or chemistry (and thus have a different charge while in contact with the same bulk solution). This topic is called hetero-interaction and refers to interaction between dissimilar materials or surfaces.

On the other hand, homo-interaction refers to the interaction between materials or surfaces that have the same structure and chemistry (i.e., are similar), and therefore also have the same charge density on their surfaces. When they have different shapes and sizes, the interaction is still classified as homo-interaction. Though hetero-interaction may be more relevant in practice, homo-interaction is a more common topic of scientific study, and already presents many challenges.

Indeed, when particles that are the same are brought in contact, the situation can already be breathtakingly complex, with an attraction changing at some separation to repulsion, again attraction, and again repulsion. This situation is illustrated in Fig. 6.2b for a surface charge density of $\Sigma = 15 \text{ mC/m}^2$ (not shown is the region of weak attraction for distances beyond 10 nm). This example illustrates the complexity of the problem of the interaction of electrostatics, surface ionization, and Van der Waals forces, even when the two surfaces are the same.

It is interesting to notice how these curves for the interaction force versus distance depend on pH and salt concentration, c_∞ . As we will explain, it is possible that at a certain pH or c_∞ two particles are repulsive (the particles are dispersed), but at a different pH or salt concentration, an attraction develops between them (the particles will now ‘coagulate’), but the attraction disappears again when the original pH/salt concentration is reinstated. This behaviour indicates that an attractive ‘minimum’ can be reversed upon changing solution conditions, i.e., in this case coagulation is reversible. This theoretical prediction is also observed experimentally (‘repeptization’).

An interesting problem is to what extent dynamic effects must be incorporated in this theory. Particles that approach a surface, or approach one another, do so with a certain (initial) velocity, and the redistribution of ions in the gap between the particles may not be fast enough for equilibrium to remain established during the entire period of encounter, and likewise the surface charge may not adjust fast enough for there to be equilibrium at each

separation. Thus, during particle collision the surface charge may remain constant even when according to chemical equilibrium the charge would change.¹

This advanced topic of the dynamics of particle interaction will not be discussed here, and we will limit the explanation to the forces between particles, with chemical equilibrium always established. We first explain the interaction of equally charged surfaces, where we first consider surfaces with a fixed, or constant, charge (CC condition), and then analyze the interaction between ionizable surfaces, i.e., surfaces of which the charge changes when particles come closer (charge regulation, CR). After that we address hetero-interaction, i.e., the interaction between different materials, both for CC and CR boundary conditions.

To calculate the electrostatic contribution to the attractive or repulsive forces between colloidal particles, we must solve the Poisson-Boltzmann (PB) equation in the entire space between and around the two charged surfaces. But thanks to the Derjaguin approximation, mathematically we only have to solve a 1D planar geometry to describe the full problem of the interaction between real 3D particles. However, even for a 1:1 salt solution there are no good analytical solutions to the PB equation that work at all separations and charge densities, let alone for asymmetric salts or when ion volume effects are included.

In this chapter we first discuss three approximations to the (1D planar) PB equation: the Gregory approach valid at low potentials, the more general Ettelaie-Buscall approach, and the Donnan approach for surfaces that are very near. In Fig. 6.3 we also show results obtained from numerical solution of the full PB-equation. To analyze colloidal stability, we combine the electrostatic contribution to the interaction force, with the Van der Waals force (attractive for homo-interaction), to describe the total colloidal interaction force. We first discuss the force between flat surfaces (called disjoining pressure), and then move to curved surfaces (particles) and include the Van der Waals force. For flat surfaces we also discuss hetero-interaction.

It was F.G. Donnan who before 1911 was the first to bring up the idea that the stability of colloids is likely due to a repulsive electrostatic pressure because of an increase in ion concentration in the gap between two particles, and that work must be done to bring particles into close contact against this electrical force (reported in R. Ellis, 1912). The complete

¹In AFM studies of the homo-interaction of two charged materials, an intriguing phenomenon is the ‘snap-off’ force: two surfaces that are repulsive all the way until they are pushed into contact, when they are subsequently pulled apart, they are found to adhere. One explanation is that during approach, the particle charge remains non-zero, leading to repulsion, but during contact, the charge decreases to zero or close to zero in the region of contact (a consequence of the establishment of chemical equilibrium and EDL overlap for ionizable surfaces, see §6.3). When the two particles are now pulled apart, the electrostatic repulsion drops away, and only the attractive Van der Waals force remains, so the particles now stick together, hence the required snap-off force to pull them apart (discussed in Biesheuvel, 2002).

theory of colloidal interaction is therefore best called DVDW theory, referring to Donnan and Van der Waals.

The disjoining pressure, P , has the unit of Pa ($=\text{N}/\text{m}^2$) and is the pressure that must be applied to keep two flat surfaces at a certain distance. Thus when the surfaces are attractive, and we actually must pull on them, P is negative. Contributions to P arise from electrostatics (Donnan, ion entropy), P_e , and from the Van der Waals force, P_{vdw} . Integration of the curve of pressure, P , against separation of the surfaces, D , results in an interaction energy, V (unit J/m^2), according to

$$V = \int_D^\infty P dD . \quad (6.1)$$

For curved surfaces, for instance spherical particles with a radius a , this energy of flat surfaces, V , is proportional to the disjoining force, F , between these curved surfaces (unit N) with the proportionality factor dependent on a . This is the Derjaguin approximation, which is valid when the Debye length is small compared to the curvature of the particles, a condition that is almost always applicable.

We can integrate F once again over separation D to obtain the energy between the curved objects (particles), E (unit J), according to

$$E = \int_D^\infty F dD \quad (6.2)$$

And finally, this energy can be integrated one more time over D (involving an exponential dependence on energy E) to obtain the stability ratio W , a property that can be correlated with experiments on the coagulation of a dispersion of small particles. (Other words for coagulation are: flocculation, agglomeration, aggregation, phase separation.) When such a dispersion does not coagulate, i.e., it is 'stable,' the attractive forces are apparently not strong enough to overcome the repulsive forces, or there is an attraction at close distances but there is a repulsive barrier that is large enough.ⁱⁱ

ⁱⁱA dispersion is in between a solution and a suspension in terms of particle size. A solution consists of solvent and smaller molecules, and macromolecules of perhaps a few kDa. The term suspension refers to a mixture of a fluid and suspended larger particles, with sizes at least 100 nm. In a gravity field these particles will sediment over time. A dispersion is in between these two classes, and particles in a dispersion have sizes from a few nm to perhaps 1 μm . They do not sediment due to gravity but remain dispersed.

6.2 Colloidal interaction of particles with a fixed surface charge

Before describing the theory for colloidal interaction in more detail, let us first define certain words for distance. Two surfaces can be pushed together, to any separation D . This D is the distance between (i.e., is the separation of) two flat surfaces. Below we will also use the half-separation, h , i.e., $D = 2h$, which is of use for the symmetric problem of homo-interaction.

The above are definitions for two flat surfaces pushed together. When we go to curved surfaces (either two spherical particles, or the geometry of 'crossed cylinders', or of sphere-surface interaction), then D and h will refer to the (half-)distance at the point where the surfaces are the closest.

There are now three important points to make:

- The first is to realize that D and h represent the separation between the surfaces, i.e., a distance, and they are not the positional coordinate x within the gap region between the surfaces. Thus, with particles separated by a distance D , the coordinate x has values between 0 and D .
- Secondly, all distances relate to the dimensions of the electrolyte region. This means that they relate to the thickness of the region where (the centers of) the ions can be located. This is the region of the (two overlapping) diffuse layers. Thus, distances such as D and h relate to the separation of the Stern planes (the distance between the two Stern planes).
- Finally, it is important to realize that these Stern planes may be located a few Å away from the hard 0-plane (Reerink, 1952). Let us call this extra distance δ . Thus δ is the distance between the 'hard surface' (the 0-plane) and the plane that serves as the start of the ionic region (which is the Stern plane), i.e., δ can be envisioned as the thickness of the Stern layer. Consideration of this point is of importance when we discuss the Van der Waals force. This is because this force (attractive in case of homo-interaction) is due to differences between the permittivity of the material of the surfaces/particles, and that of the water (or other electrolyte) in between. Thus this Van der Waals force 'emanates' from the 0-plane, i.e., it depends on how far the two materials are separated from one another (with water in between). This separation is slightly larger than how far the Stern planes are apart. Thus, when at some point the Stern planes are a distance D apart, the 0-planes are a distance $D + 2\delta$ apart. Thus, the parameter δ will be found in equations involving the Van der Waals force.

From this point onward we write 'distance between surfaces', and use similar terminology,

and this refers to a distance between the two Stern planes, i.e., it is the thickness of the electrolyte (ion containing) region. When we introduce the Van der Waals force, we will specifically refer to the ‘distance between the hard surfaces’, which are a distance 2δ further apart than the thickness of the electrolyte region, i.e., this distance is 2δ larger than the distance between the Stern planes.

For interaction between two equal surfaces, both flat and placed in parallel, the electrostatic contribution to the disjoining pressure, P_e , can best be evaluated at the midplane, ‘m’, in the gap between the two surfaces, and then we obtain

$$P_e = 2 RT c_\infty (\cosh(|z|\phi_m) - 1) . \quad (6.3)$$

which assumes the PB-framework based on ideal point charges for a symmetric salt (1:1, 2:2, etc.) with $|z|$ the magnitude of the charge of the ions ($|z| = \{1, 2, \text{etc.}\}$). Note that in this chapter we include the term ‘ RT ’ for pressures and other energy units. The pressure in Eq. (6.3) is the osmotic pressure due to the ions at the midplane in the gap, $RT \sum_i c_{m,i}$ minus that far away, $2 c_\infty$, and we used the Boltzmann equation to relate $c_{m,i}$ to c_∞ and ϕ_m . Instead of evaluating Eq. (6.3) at the midplane, it can also be evaluated at any other position in the gap, but then we must add the attractive Maxwell pressure as well, $-1/2\epsilon E^2$. This term does not have to be considered at the midplane for equally charged surfaces because there it is zero. For hetero-interaction, this extra term must always be evaluated besides the osmotic pressure of Eq. (6.3). The background to these equations is further discussed in Ch. 8.

To arrive at a simple analytical expression for P_e , we use the result derived by Gregory (1973) to take the low-potential limit of the Poisson-Boltzmann equation and integrate across the gap between two equally charged planar surfaces, which results in

$$Q = \frac{\sum \lambda_D}{\epsilon V_T} = \phi_m \sinh(\kappa h) \quad (6.4)$$

and

$$\phi_D = \phi_m \cosh(\kappa h) . \quad (6.5)$$

These two equations can be used for a 1:1 salt as well as for any asymmetric salt or salt mixture, as long as κ is calculated by Eq. (3.18). Note that Q is a function of the Debye length, $\lambda_D = \kappa^{-1}$, and thus it depends on ion concentrations and valencies. The same definition of Q was used in §3.3.

We assume now a symmetric salt solution (1:1, 2:2, etc.), and combine Eq. (6.3) with Eq. (6.4) to arrive at (Biesheuvel, 2001)

$$P_e = 2 RT c_\infty \left(\cosh \left(\frac{|z| Q}{\sinh(\kappa h)} \right) - 1 \right) . \quad (6.6)$$

A useful simplification can be made for $h \gg \lambda_D$ and then we obtain

$$P_e = \frac{2}{\varepsilon} \Sigma^2 \exp(-\kappa D) \quad (6.7)$$

which indicates that c_∞ and z only have an impact on the pressure via the inverse Debye length, κ . Thus with higher c_∞ or higher z , the Debye length decreases and thus the repulsion goes down. This is a general result for the ‘constant charge’ (CC) approach, also for surfaces that are close. Later on we explain that for ionizable surfaces, at short distances the situation reverses and repulsion can go up with salt concentration.

Based on Eqs. (6.1) and (6.7) we derive an expression for the interaction energy V between flat surfaces (in J/m^2)

$$V_e = \int_D^\infty P_e dD = \frac{2}{\varepsilon \kappa} \Sigma^2 \exp(-\kappa D). \quad (6.8)$$

Having integrated P_e over D to arrive at the interaction energy V in J/m^2 , we can now implement the Derjaguin approximation which is to multiply V by a factor 2π to obtain the ‘force/radius’ (F/R) as often reported in force studies using the atomic force microscope (AFM) and the surface force apparatus (SFA). Or, to find the force, F_e , that acts between two equal spherical particles, each of radius a , we multiply V by πa (unit of force is N),

$$F_e = \frac{2\pi a}{\varepsilon \kappa} \Sigma^2 \exp(-\kappa D) \quad (6.9)$$

which can be integrated to the energy E between particles (unit J), see Eq. (6.2)

$$E_e = \int_D^\infty F_e dD = \frac{2\pi a}{\varepsilon \kappa^2} \Sigma^2 \exp(-\kappa D). \quad (6.10)$$

In Eq. (6.10), the prefactor in E_e depends on $1/|z|^2$ (within κ), but an even more significant dependence on z goes via the exponential term.

We can now combine the above equations for electrostatic repulsion, with the attractive Van der Waals interaction. This attraction depends on the Hamaker constant, A , which for instance for two titania layers interacting across water is $A \sim 6 \cdot 10^{-20}$ J. We can also express this energy in ‘units of kT’, by dividing by $kT = 4.12 \cdot 10^{-21}$ J, resulting in this case in $A = 14.6$ ‘kT’. [This is strictly speaking a non-dimensional number, and ‘kT’ should be omitted.]

For close surfaces (shortest distance between the surfaces much lower than the particle size), the Van der Waals attraction between flat surfaces is given by

$$P_{\text{vdw}} = -\frac{A}{6\pi (D + 2\delta)^3}. \quad (6.11)$$

We can integrate P_{vdw} from Eq. (6.11) over D , and multiply by πa to obtain the force between two particles of radius a

$$F_{\text{vdw}} = -\frac{A a}{12 (D + 2\delta)^2} \quad (6.12)$$

which we can integrate again, to obtain the interaction energy

$$E_{\text{vdw}} = -\frac{A a}{12 (D + 2\delta)}. \quad (6.13)$$

We first analyze results for the force between curved surfaces, focusing on the total interaction force, $F = F_e + F_{\text{vdw}}$. Because often results are reported of experiments with AFM and SFA methods, we present results for the factor F/R . This implies that the force contributions, F_j , in the equations above, are multiplied by a factor 2 and divided by a .

Using Eqs. (6.9) and (6.12), the total interaction force becomes

$$F/R = \frac{4\pi}{\varepsilon \kappa} \Sigma^2 \exp(-\kappa D) - \frac{A}{6 (D + 2\delta)^2}. \quad (6.14)$$

In Fig. 6.1 we analyze the behavior of Eq. (6.14) for various surface charge densities Σ and salt concentrations c_∞ for a 1:1 salt. For zero surface charge the particles (surfaces) attract, and the more so the closer they get, until a limiting value that is reached when the Stern planes touch. With increasing surface charge, a repulsion develops, which for $c_\infty = 10$ mM starts at distances of 5–10 nm, and note how a twice larger surface charge means a four times larger electrostatic repulsion. At some point a maximum is reached in the total interaction curve, and the force decreases again when we push the particles closer. For the conditions in Fig. 6.1 at contact an attraction remains, but for a surface charge larger than $\Sigma_{c1} = \sqrt{A \varepsilon \kappa / 48\pi \delta^2}$, which at $c_\infty = 10$ mM is $\Sigma_{c1} = 22.4$ mC/m², this is different. Even though for $\Sigma > \Sigma_c$ the repulsion goes down just before the surfaces touch, the repulsion stays positive until contact. At an even higher charge, the curve not even comes down again. This happens beyond a charge of $\Sigma_{c2} = \Sigma_{c1} / \sqrt{\kappa \delta}$, which in this case is at 71.2 mC/m².

Though all of this analysis is interesting, at near-contact the Gregory equation, Eq. (6.14), can be very much off, because in reality the electrostatic force is very different (as found by a full Poisson-Boltzmann calculation). The deviation already starts at a distance several times the Debye length. Though at a low charge (say 10 mC/m²) the correctly calculated P_e follows Eq. (6.14) until $D/\lambda_D \sim 2$, nevertheless for lower distances the correct P_e is significantly higher than predicted by the Gregory equation. For instance, Eq. (1.1) underestimates the

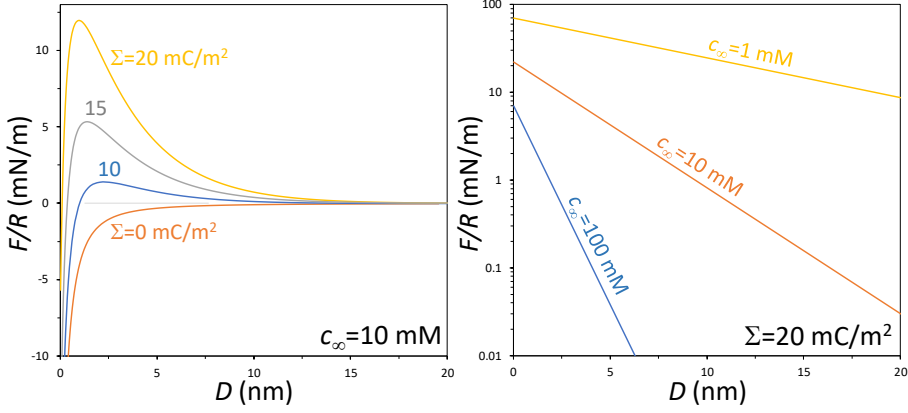


Fig. 6.1: Interaction curves using the analytical DVDW theory, Eq. (6.14), using the Gregory-function that is valid in the limit of $h \gg \lambda_D$ ($\delta = 0.3$ nm, $A = 14.6$ kT, 1:1 salt solution). a) As function of surface charge ($c_\infty = 10$ mM). b) As function of salt concentration ($\Sigma = 20$ mC/m²).

electrostatic pressure P_e by a factor of 5 at $c_\infty = 100$ mM and $\sigma = 10$ mC/m². But intriguingly, at higher charge (already at 20 mC/m²) the correct P_e is no longer larger than predicted by Eq. (6.14), but now is much lower! For instance there is a factor ~ 25 overestimate by Eq. (6.9) compared to the correct pressure at $c_\infty = 10$ mM, $\Sigma = 0.1$ C/m², and $D = 5$ nm separation. In conclusion, the Gregory equation based on this simple analytical solution can be very much off, and must ideally only be used when other calculations have ascertained it is an accurate simplification of the full PB-based solution.

A much better estimate of P_e is provided by the solution of the PB-equation by Ettelaie and Buscall (1995). As long as the charge is not too high (e.g., for a charge less than 20 mC/m²), it is highly accurate, especially for very close surfaces. [Still, ideally we solve the full PB-equation across the gap, either numerically or using the exact solution that is based on the use of elliptic functions, see for instance Biesheuvel, 2004; Eqs. (20) and (21).] The Ettelaie-Buscall (EB) solution is obtained from the PB equation in planar coordinates for a 1:1 salt solution, Eq. (3.8), by linearizing the term $\sinh \phi$ around its midplane value (thus around ϕ_m), leading to

$$\sinh \phi(x) \rightarrow \sinh \phi_m + (\phi(x) - \phi_m) \cdot \cosh(\phi_m) \quad (6.15)$$

which can be inserted in the PB-equation, which can then be integrated to obtain for the surface charge, Σ

$$\Sigma = \sqrt{2c_\infty RT \varepsilon} \cdot \sqrt{\cosh \phi_m} \cdot \tanh \phi_m \cdot \sinh \left(\kappa h \sqrt{\cosh \phi_m} \right). \quad (6.16)$$

This result can be simultaneously solved with Eq. (6.3) for the disjoining pressure

$$P_e = 2c_\infty (\cosh \phi_m - 1)$$

to solve P_e vs. h for a given value of Σ and subsequently calculate F/R versus separation, D .ⁱⁱⁱ

A correct prediction of the EB solution is that for a fixed surface charge, that the pressure P_e does not have a finite limiting value, as wrongly predicted by Eq. (6.6), but the pressure diverges when the Stern layers are about to come into contact ($D \rightarrow 0$). This is due to the fact that in the increasingly narrow gap the concentration of counterions must go to infinity to neutralize the fixed surface charge. (This is different when surfaces are ionizable, i.e., reduce their surface charge upon compression, as we discuss in the next section.) This divergence does not show up in the energy F/R that we will analyze next.

Fig. 6.2 shows results of the full EB-expression for the electrostatic contribution to F/R , in combination with the same Van der Waals attractive force as used in Fig. 6.1. Now the required charge for F/R to stay above zero in the entire range $0 < D$ (nm) < 10 is slightly lower than before. But there is an especially large effect on the charge Σ_{c2} , which is the charge beyond which there is no longer a maximum in the interaction curve, but now upon decreasing D until contact, repulsion monotonically increases. This critical charge was 71 mC/m² in Fig. 6.1 using the Gregory expression, and now –based on the EB equation– drops to a value around 25 mC/m² in Fig. 6.2. So for a value beyond this relatively moderate charge of 25 mC/m², this new analysis predicts that the interaction not only is repulsive until contact, but the interaction force monotonically increases all the way until particles are in contact.

An interesting phenomenon is hysteresis in coagulation/repeptization: as Fig. 6.2 points out, we can coagulate a dispersion when the repulsion barrier is low enough (perhaps around 5 mC/m²) and particles then end up in the deep attractive minimum that we see in Fig. 6.2 located below 1 nm separation. But if we now increase surface charge, in this case to 17 mC/m² or larger, the entire attraction curve becomes repulsive ($F/R > 0$ at all

ⁱⁱⁱIn spreadsheet software a useful method is to make a list of values of ϕ_m , and for each entry calculate P_e as well as h , and after that plot P_e vs. h . In this method, Eq. (6.16) must be inverted to an explicit equation for h . If we make a list of such calculations with index i from 1 to N , where distance h (or, D) increases with index number, then we can now numerically calculate F/R by the iterative ‘summation’ procedure $F/R_i - F/R_{i+1} = \pi (P_i + P_{i+1}) \cdot (D_{i+1} - D_i)$ with $F/R|_N$ set to zero. We must make sure in this list the steps between the D -values are small enough (they don’t have to be equi-distant) and that D_N is large enough, such that P at that separation is much smaller than P ’s at closer separations. This procedure can be used both for the electrostatic part of the force and for the Van der Waals contribution. However, for the latter contribution, analytical solutions are available for its contribution to F/R as function of D , so the Van der Waals contribution can also be added subsequently without being included in the integration based on the summation method.

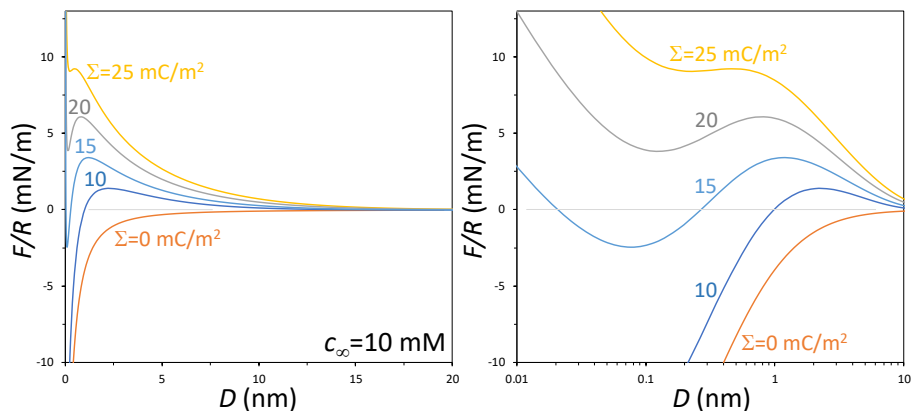


Fig. 6.2: Interaction curves using the Ettelaie-Buscall DVDW theory, Eq. (6.16), for several values of the fixed charge ($c_\infty = 10$ mM). (For other parameters see Fig. 6.1.)

separations up to 10 nm), and the coagulated particles will disperse again and we obtain a stable dispersion. Thus changing the charge to higher than approx. 17 mC/m² (for instance by a pH change) will disperse particles that were coagulated. So interestingly, there is hysteresis: when we start out with a stable dispersion and now decrease the charge, then this dispersion stays stable down to a charge of ~ 5 mC/m² and only below this charge coagulates. On increasing the charge again, we must go beyond 17 mC/m² to stabilize the dispersion. So between the numbers of 5 and 17 mC/m² (these numbers are examples, for the specific calculation made here), the dispersion can be stable or flocculated, dependent on the history of the sample.

6.3 Theory of colloidal interaction for ionizable materials

We next continue with surfaces that are charge regulating (CR), and thus we no longer assume that the surfaces keep their charge at a constant value while particles approach (that was abbreviated as ‘CC’ for ‘constant charge’). Charge regulation is a theoretical description of surface chemistry that takes account of the ionization equilibrium at the surface, and thus when these surfaces are pushed together the surface charge changes. The theory predicts that for homo-interaction (the surfaces are the same), when the two materials are pushed into contact, the surface charge goes down, all the way to zero. This all makes sense because when surfaces are in contact, there is no room left for counterions to compensate the surface

charge; thus the surface charge should go to zero. And this is exactly what CR theory predicts.^{iv}

Until this point, assuming a fixed surface charge density, we did not have to consider the Stern layer (capacitance). This is because with a fixed surface charge, the gradient $\partial\phi/\partial x|_D$ follows directly from the charge density, irrespective of the Stern capacitance.

However, because from this point onward we are including surface ionization, the Stern layer will play a role. But to simplify the discussion from this point forward, we assume an infinitely high Stern capacitance, thus $\phi_0 = \phi_D$, and thus the potential at the 0-plane, ϕ_0 , is the same as ϕ_D , which is the potential where the diffuse layer starts.

As an example of a charge-regulating material, we choose for an amphoteric material, which is a material that can charge both positively and negatively. Examples are alumina and titania, see §3.7, but also many biological materials and protein molecules are amphoteric. For alumina and titania, pK (e.g., pK=4.4 for titania) is equal to the pH at which the material is uncharged (and this pH is called the point of zero charge, PZC, or equivalently, the iso-electric point, IEP, see p. 507). When pH is higher than PZC, the material is negatively charged, and for a lower pH it is positively charged.^v

For this problem of the overlap of two EDLs and an amphoteric charge-regulating surface, there are no analytical solutions that work. We thus show numerical results using the full 1D Poisson-Boltzmann equation, for a 1:1 solution given by Eq. (3.8), evaluated at a range of separations D and subsequently numerically integrated to obtain F/R vs. D , in the same way as discussed for the EB calculation. Thus, we put aside the EB-approach because it does not give very accurate results at high charge, especially when the surfaces are far apart.

But even without solving the equations, we can already predict what happens when two equal charge-regulating materials interact across a thin gap. Let us assume we are at a pH above the iso-electric point of titania, thus titania is negatively charged at this $\text{pH} > \text{pK}$. We thus have cations as counterions in the gap between the surfaces at a larger concentration than outside the gap. Thus pH in the gap is lower because we have more H^+ -ions here than outside (the relative increase in H^+ concentration equals the relative increase in cation concentration, similar to Eq. (2.16) in Ch. 2). When the gap is further narrowed, pH in the gap goes down

^{iv}Instead, for hetero-interaction the charge can both go up and down with separation, but at contact the two materials will have an exactly opposite charge (together they must be charge-neutral because at that point there are no longer ions in the gap between the surfaces to compensate for any charge mismatch).

^vThough this discussion relates to pH right at the surface, let us stress that pH in equations is the pH in bulk solution, outside the overlapping diffuse layers, and is not a pH at the 0- or D-plane.

more, until at contact pH is such that the material has discharged completely, i.e., pH in the gap becomes equal to pK of the material. Thus we know the ‘final’ pH in the gap (i.e., when there is almost or full contact), and thus we can calculate the potential in the gap ϕ when there is contact, and this tells us the electrostatic pressure at contact. This pressure is the maximum value, i.e., with separation D going down, P_e monotonically increases from zero when $D = \infty$, to a maximum value at contact. This increase in pressure occurs even though the surface charge continues to decrease the closer the surfaces come together, down to zero charge at contact, when the repulsive pressure is the highest. Concentration and potential profiles across the gap become more and more ‘flat’ the smaller the gap, because the charge density goes down, and because the gap gets more narrow. [By ‘flat’ we mean that the difference between the potential (concentration) at the surface and in the center of the gap, becomes very small.]

Important to note, even though at contact the surfaces have discharged completely, P_e will not go to zero, not at all! Instead, for equal materials, P_e monotonically increases when we bring the surfaces closer together, not only for a fixed surface charge but also for surfaces that are ionizable. Thus, while the two surfaces are pushed together, and the surfaces discharge, P_e monotonically increases, with a maximum at contact for CR (for CC P_e increases indefinitely, i.e., ‘it is unbounded’).

When the surfaces are far apart, we can calculate charge Σ and surface potential ϕ_0 based on Eqs. (3.69) and (3.70). When far apart, the charge is at its maximum value, while potential ϕ_0 is at a minimum value. When we now push the two materials together, the charge goes down, all the way to zero at contact, while ϕ_0 reaches a maximum value. At that point the potential across the (by now very narrow) gap is almost constant (gradients in potential become negligible).^{vi} This potential at contact is obtained by setting $\alpha = 0$ in Eq. (3.73), which results in

$$\phi_c = \ln 10 \cdot (\text{pK} - \text{pH}) . \quad (6.17)$$

As this equation shows, the potential in the gap when $D \rightarrow 0$ is negative for $\text{pH} > \text{pK}$, and positive for $\text{pH} < \text{pK}$. We will refer to this potential as ϕ_c , where index ‘c’ refers to being in contact. Note that this high potential is only reached at the point where the two materials are pushed together and there is no room left for ions in the gap between the surfaces. For an area on a particle that is still at a slight distance from other surfaces, the surface potential is lower in magnitude than ϕ_c .

At (points of) contact, the electrostatic contribution to the disjoining pressure, $P_{e,c}$, follows

^{vi}Minimum and maximum refer here to the magnitude of these variables, neglecting their sign.

from inserting Eq. (6.17) in Eq. (6.3), which results in

$$P_{e,c} = c_{\infty} \left(10^{pK-pH} + 10^{pH-pK} - 2 \right). \quad (6.18)$$

Eq. (6.18) shows a very relevant phenomenon, that now with charge regulation (CR) included, at contact $P_{e,c}$ increases with salt concentration c_{∞} (the two are exactly proportional). This is the exact opposite of what was predicted for the fixed charge case, where repulsion was always lower when c_{∞} was increased (for the same surface charge), see Fig. 6.1b. The very high repulsive pressure between amphoteric materials that occurs at contact in case of a high c_{∞} , provides a method to keep very concentrated colloidal suspensions in a fluid-like state, with the pressure between particles at contact functioning as a very short-range repulsive force (Yu *et al.*, 2002).

Even though now the repulsion is higher at contact when c_{∞} is higher, the pressure also decreases faster when the distance goes up, and thus there is a cross-over point, i.e., beyond a certain separation, the repulsion is larger for a lower c_{∞} . Thus with CR, the influence of c_{∞} is not as straightforward as how it was for the CC situation.

We show in Fig. 6.3 as function of pH curves for the interaction between two equal titania surfaces, for which surface ionization is described by Eq. (3.73). As might be expected, the further pH is away from the iso-electric point (point of zero charge, when $pH=pK$), the higher is the repulsion. For a pH only 1 point away from pK , the theory predicts only a shallow repulsive barrier, which is likely not enough to inhibit aggregation. However, for a two- and three-point difference between pH and pK , there is repulsion at all distances, and we can expect a dispersion of titania particles to be stable.

Stability ratio W . In this section we analyzed force curves in the ‘ F/R ’ property. To describe the interaction force F between equally sized particles with radius a , we multiply F/R with a and divide by 2. We can then (numerically) integrate F to obtain the interaction energy E in J, see Eq. (6.2) and a footnote on p. 140. Often this number is divided by kT to obtain the energy expressed in so many kT . The energy E can again be integrated to obtain the stability ratio W which describes the stability of a dispersion. For W very large, e.g., $W > 10^4$, a dispersion is expected to be stable, and not to coagulate. But when W is low, e.g. $W = 100$ or less, or even lower than unity, the dispersion (‘sol’) will flocculate/coagulate.

The stability ratio W is given by

$$W = 2a \int_0^{\infty} \frac{\exp(E/kT)}{(2a + D)^2} dD \quad (6.19)$$

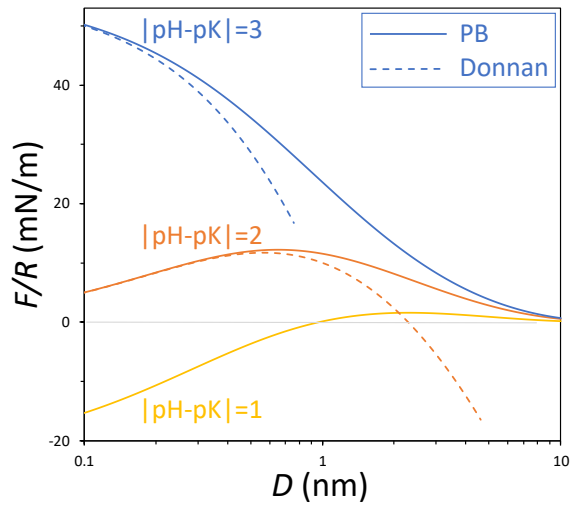


Fig. 6.3: Interaction curves including charge regulation based on the ionization of titania surfaces, making use of the full PB equation (solid lines) and the Donnan approximation (dashed lines), for several values of $|\text{pK}-\text{pH}|$. ($c_\infty = 10$ mM, number of surface sites $N = 3 \text{ nm}^{-2}$, no Stern capacitance. For other parameters see Fig. 6.1.)

and when the interaction energy E is non-zero only when $D \ll a$, this simplifies to

$$W = 1 + \frac{1}{2a} \int_0^\infty (\exp(E/kT) - 1) dD. \quad (6.20)$$

Into Eq. (6.20) we can insert Eq. (6.14) after multiplying by a and dividing by 2, or use any other numerical solution for F versus separation D based on Eq. (6.1), another numerical evaluation to obtain E using Eq. (6.2), and a final numerical evaluation to calculate W , see for a general description a footnote on p. 140, we can evaluate the stability ratio of a dispersion as function of parameters such as pH, Hamaker constant A , surface charge density Σ , and salt concentration c_∞ . Also the valencies of the ions involved, z_i , play a significant role, via their effect on P_e as described by Eq. (6.3).

6.4 Theory of colloidal interaction for surfaces that are very near - the Donnan limit

For very close surfaces, the Donnan approach is highly suitable. In case we also have charge regulation, the equations that must be solved jointly are (here we also include the Stern capacitance, we assume a 1:1 salt solution):

$$P_e = 2RTc_\infty (\cosh(\phi_D) - 1) \quad (6.21)$$

$$\phi_0 = \phi_D + \phi_S \quad (6.22)$$

$$C_S \phi_S V_T = \Sigma \quad (6.23)$$

$$\Sigma = c_\infty F \sinh \phi_D \cdot D \quad (6.24)$$

and if we consider an amphoteric material such as alumina or titania, we have in addition Eq. (3.73).

These equations can be solved jointly in a numerical calculation, and then the Van der Waals pressure can be added to obtain the total interaction pressure. We tried in many ways to come to insightful analytical solutions but were not successful. But numerically solving these equations is not difficult.

Note that the above equations only describe the electrostatic pressure, between flat interfaces. This is useful for the interaction pressure between two entities or layers that form a thin film in between. This can for instance be the interlayer structure in clay particles.

Here a Donnan model including the clay chemistry can predict the disjoining pressure, and this is relevant to understand clay swelling (and collapse) (Koopal *et al.*, 2020). It can also describe the interaction at the flattened interface between two deformable charged droplets or vesicles that only have a thin film in between.

For more rigid objects the above equations cannot simply be used to generate information on the force F , because the Donnan equations for the pressure P_e are only valid at short distances, D , and thus cannot be used for a calculation of integrated properties such as F_e , for which we must integrate from infinity to a certain distance D . This is because for larger distances, the Donnan equations are very inaccurate and deviate strongly from the correct results. Then we better solve the full PB equation, and integrate numerically from ∞ down to a certain small D .

However, we can also integrate the Donnan pressure, P_e , from $D = 0$ outward. But this is of course only possible if we would know the electrostatic contribution to the interaction energy V_e at contact, $V_{e,c}$. Though that property might not seem so readily available, it actually is, see Eqs. (27) and (A.6) in Biesheuvel (2004). With $V_{e,c}$ available, we can then integrate from $D = 0$ outward, making use of P_e from the Donnan model, according to $V_e = V_{e,c} - \int_0^D P_e dD$ to which then the Van der Waals contribution must be added. And we must multiply by π to arrive at ' F/R '. Then we have a Donnan-based model for the interaction force F_e between curved entities for short D . Note that this still does not allow us to integrate once again to an interaction energy E . Results of this Donnan calculation are given in Fig. 6.3 as dashed lines. We must conclude that beyond a separation of 1 nm at the intermediate value of charge, the Donnan prediction starts to fail. For the high charge case, the Donnan approach already fails beyond ~ 0.5 nm. Thus, the Donnan approach can be used to calculate the interaction pressure at contact, and in combination with the calculation of V_c , it can be used to obtain a curve of F/R vs. D , which is accurate for very short distances, but the Donnan approach cannot be used to calculate interaction forces at larger separations.

6.5 Donnan theory for hetero-interaction

In practical situations we often encounter problems that depend on the interaction between dissimilar materials, thus between particles or surfaces that have a different surface chemistry, for instance in the capture of charged nanoparticles by (charged) porous media.

If after reading the previous sections the reader came to the conclusion that interaction of equal surfaces is complicated (and fascinating), then the reader will also appreciate the complexities that arise in the study of the interaction between different surfaces, i.e., hetero-interaction. In this broad class of problems one encounters many special and unexpected

features. For instance, when two materials have an equal sign of the surface charge they are always repulsive, but when they have an equal sign of the surface potential, they repel when further apart but closer together they attract one another. Or, when at least one surface is charge regulating (with the charge dependent on local pH), we can have a sequence of repulsion, attraction, and again repulsion when particles approach one another. And this is only the electrostatic part of the interaction, not yet involving the Van der Waals force. This Van der Waals force can also be attractive and repulsive, and can change sign dependent on the separation. All of these elements together results in what can be a very intricate problem.

In this section we neglect the Van der Waals force, and focus on the electrostatic part of the interaction between particles and materials. We demonstrate that even when we only consider electrostatics, in many problems we readily go from attractive to repulsive and vice-versa. This is different from homo-interaction: in that case the electrostatic contribution to the forces and energies is always repulsive, with or without charge regulation.

The complete problem of hetero-interaction is best addressed by numerically solving the PB-equation in the gap between the (charge regulating) surfaces, with appropriate boundary conditions. The electrostatic component to the disjoining pressure, P_e , follows from evaluating at some point in the gap the sum of the repulsive osmotic part, $RT (c_T - c_{T,\infty})$ (for a $z:z$ -salt), and the attractive Maxwell contribution, $-1/2 \varepsilon E^2$. The result of this calculation will be the same irrespective of where in the gap (at which position x) these pressures are evaluated. This numerical calculation is done at many values of separation D and calculated values of P_e are numerically integrated to obtain the force and energy between curved surfaces, see Eqs. (6.1) and (6.2).

As an example, we consider the interaction of two amphoteric materials, alumina and titania, of which the charge is described by Eq. (3.73) ($j = \{a, t\}$),

$$\Sigma_j = F N_j \left(\frac{1}{2} - \frac{1}{1 + 10^{\text{pK}_j - \text{pH}} e^{-\phi}} \right)$$

where pH refers to bulk solution. For these materials we have a pK of resp. $\text{pK}_a = 8.7$ and $\text{pK}_t = 4.4$. For a pH in between these two pK-values, we can expect an attraction between these oppositely charged interfaces. This is indeed correct for distances that are a few times the Debye length and further apart, but what happens when the surfaces come closer?

In the following calculation we only evaluate the pressure at contact. If this is positive (repulsive) we know that the electrostatic pressure went from attractive to repulsive (because at large distances it is attractive). In the calculation we include that the two surfaces together are charge neutral because there is no space left for ions to contribute to the charge balance, thus

$$\Sigma_t + \Sigma_a = 0. \quad (6.25)$$

This calculation can be done for any pH-value, to calculate the charge of each surface, Σ_j , and the common value of potential in the vanishingly thin gap, ϕ . The charge that follows from this calculation does not depend on salt concentration, and –intriguingly enough– *neither depends on external, bulk, pH* as we discuss further on. Having now calculated the surface charge (opposite for the two surfaces), we can calculate the Maxwell attraction according to

$$P_{e,\text{Maxwell}} = -\frac{1}{2} \varepsilon E^2 = -\frac{1}{2 \varepsilon} \Sigma^2. \quad (6.26)$$

Thus this attractive term directly follows from Eqs. (3.73) and (6.25) and is independent of salt concentration and bulk pH. The osmotic pressure, P_e , can also be directly calculated from Eq. (6.21) because it is a function of ϕ and of c_∞ . Thus the osmotic pressure, which is zero or repulsive, will not be very prominent when c_∞ is low, but will have a larger effect at a higher c_∞ . Thus we can have the situation that for low c_∞ the total electrostatic interaction (osmotic plus Maxwell) at contact is attractive, but becomes repulsive at contact for a higher c_∞ . This prediction is illustrated in Fig. 6.4.

But the situation can be even more interesting. The contact condition, Eq. (6.25), is independent of external pH. The system will always ‘find the pH’ in the gap that is needed to make sure the two surfaces have an opposite charge. In this case this is $\text{pH}_{\text{gap}} \sim 8.1$. And to achieve that value of pH a certain potential in the gap is required, only a function of external pH, namely $\phi = \ln(10) \cdot (\text{pH}_{\text{gap}} - \text{pH}_{\text{ext}})$.

Interestingly, this result shows that also when we are at a pH below the iso-electric point of titania ($\text{pH} < \text{pK}_t$), or likewise, pH is above the pK of alumina, we can also push the surfaces in full contact with the two materials becoming oppositely charged. Thus one of the materials then reverses its sign of charge upon being pushed towards the other material. And for all values of pH and c_∞ at contact the Maxwell attractive term is the same, in this case equal to an attractive force of 41.8 MPa.

At $\text{pH}_{\text{ext}} \sim 8.1$ the osmotic repulsive force is always zero whatever the salt concentration (because in the gap we always have $\phi = 0$ in this case), but away from this pH-value we can make the surfaces less attractive, even repulsive, by adding salt. Fig. 6.4 shows calculation results of the electrostatic pressure at contact for hetero-interaction of alumina and titania. What will be immediately observed is the very high values of pressure, in the 100s of MPa-range! Clearly at a pH between the pK-values of the two materials, when they are overall attractive, this attraction is extremely strong, while if we go sufficiently above pK of alumina, or below pK of titania, especially if we add a sufficient amount of salt, the two materials become highly repulsive. Under these latter conditions they can be mixed without any risk of agglomeration.

Furthermore, note how in Fig. 6.4 the entire curve is symmetric around pH_{gap} , which is close to the pK of alumina. Alumina in this calculation is the material with the higher density of surface groups, N . On this side of the curve, thus for instance at pH 9, pH 10 and even pH 11 (when $c_{\infty} = 10$ mM), both materials are negatively charged when they are far apart, but when pushed together into contact, they are very strongly attractive! This is because the alumina material will reverse its charge when titania and alumina are pushed together, to become positive.

The full interaction curve, for instance at pH 11 and $c_{\infty} = 10$ mM will go from repulsive when the surfaces are far apart to very attractive at contact. Increasing salt concentration to 100 mM, or increasing pH to 12, will disperse the particles again.

But we can also have the reverse situation. For instance at pH 5 and $c_{\infty} = 100$ mM. In this case the two materials will be attractive when far apart, while at contact the total pressure is repulsive! The dashed line in Fig. 6.4 describes the minimum salt concentration to make the interaction at contact repulsive. This curve predicts that between $4.4 < \text{pH} < 6$ the surfaces –which are attractive at large distances– become repulsive at contact, even for moderate c_{∞} . Between pH 8.7 and pH 11, even pH 12, the surfaces are repulsive far apart, but can be turned to attractive at contact when the salt concentration is low enough.

In the last sections, the Stern layer was neglected in the electrostatic description, but in a full description should be included. This layer creates a difference between the surface potential ϕ_0 , and the diffuse layer potential ϕ_D . It is possible to include the Stern capacitance correctly in analytical expressions for the energy between flat surfaces, V (thus for F/R), for which examples are given in Biesheuvel (2004). But it is easier to include them in the numerical 1D Poisson-Boltzmann calculation that creates an output of the function P_e vs. D , and this function is subsequently integrated to $V(F/R)$ and other energies. In conclusion, the problem of hetero-interaction has many intriguing aspects, even when only considering the electrostatic pressure P_e at various conditions. It will be interesting to study the full interaction curve (F/R vs. D), certainly in combination with the Van der Waals force, and understand its dependence on pH , c_{∞} , etc.

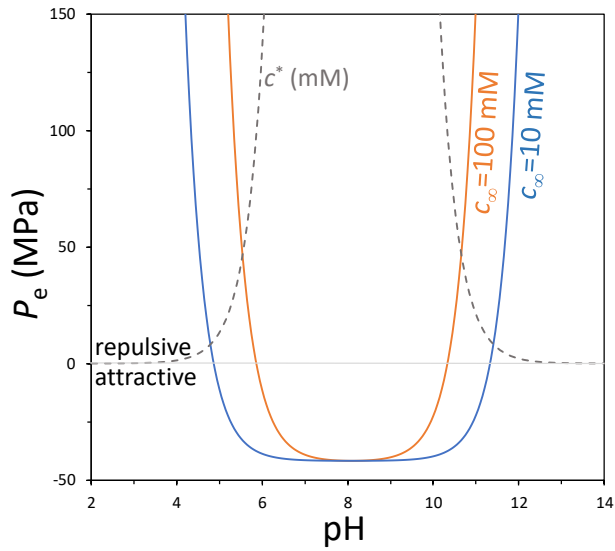


Fig. 6.4: Contact pressure for hetero-interaction between alumina (a) and titania (t) as function of pH and salt concentration, c_∞ . For $\text{pK}_t < \text{pH} < \text{pK}_a$, the two materials are always attractive at large separations, but as can be seen, for high enough c_∞ at contact the interaction can be made repulsive. The dashed line gives the minimum salt concentration c^* (for a 1:1 salt solution) to make the interaction at contact repulsive ($\text{pK}_t = 4.4$, $N_t = 3 \text{ nm}^{-2}$, $\text{pK}_a = 8.7$, $N_a = 5 \text{ nm}^{-2}$).

Part II

**Transport Phenomena
&
Reactions**

Transport of mass and heat, in combination with chemical reactions, is at the basis of the physics of electrochemical processes. Mass and heat are transported in bulk electrolyte phases, in the region near selective or reactive interfaces such as membranes and electrodes, and through porous (charged) materials such as porous electrodes, filters and membranes.

In this part we discuss several aspects of the transport of mass and heat, and chemical reactions. We start in Ch. 7 with the transport of solutes in bulk electrolyte and in porous media. Solute are transported by various driving forces including electrical effects and concentration gradients, and their fluxes depend on friction with other phases (other ions, solvent, membranes), leading to the concept of the hydrodynamic factors $K_{c,i}$ and $K_{d,i}$ that we will analyze in detail. We summarize and develop several approaches to the description of diffusion and dispersion in the region near reactive or selective interfaces.

In Ch. 8 we continue with the description of the forces acting on the fluid (the solvent) which is different from, but complementary to, the theory for the transport of solutes, see an earlier discussion on p. 11. We present the porous medium two-fluid Navier-Stokes equation and show how in several limits it simplifies to classical expressions found in literature. We use this theory to explain the always elusive topic of osmosis, after which we extend the theory to describe electro-osmosis, and briefly describe several cross-effects in electrokinetics, such as the streaming potential. We elaborate how the same theory also describes the various pressures of relevance in a description of colloidal interaction.

We continue in Ch. 9 with the heat balance, in the context of current flow through membranes and into electrodes. In this chapter we also describe the current-voltage relationship for bulk electrolyte and membranes.

Finally, in Ch. 10 we combine mass transport with reactions, a topic of the highest importance in the physics of electrochemical processes, because (certainly in water) there are always many ion types that while being transported participate in ongoing reactions with other ions. These reactions can be of the acid-base type that involve hydronium ions or hydroxide ions, but ions can also react to ion pairs (as mentioned in § 4.3). In this chapter the example of CO_2 -adsorption in amine solutions is further developed, while the relevance of this theory for bio-electrochemical systems will be further demonstrated in Chs. 17 and 18.

Solute Transport

In this chapter we discuss several aspects of transport of solutes (ions, molecules, etc.) through a solvent such as water in electrochemical processes. In the first sections we discuss diffusion to a surface (which can for instance be an electrode or membrane) modified by dispersion, related to the concept of the diffusion boundary layer, both for steady state and for transient situations. We discuss the conductivity of electrolyte solutions and of electrolyte-filled porous media, and explain the difference between transference and transport numbers. We present generalized salt balances for a binary salt, and give examples for the flux of asymmetric salts across a channel and boundary layer. In the final section we discuss how the Nernst-Planck equation and extensions thereof follow from a force balance for solutes, a force balance which includes all possible driving forces acting on a solute as well as all possible frictions of a solute with other phases such as the water and other types of solutes.

7.1 Diffusion and dispersion towards a surface

In electrochemical processes it is very important to describe the transport of solutes from a bulk solution to a surface, and vice-versa. The surface can be selective, which means that one solute or ion can enter it more readily than another ion, while it can also be reactive to some ions, or it can adsorb some of the solutes. This selective transport, reaction and adsorption can be to a 'hard' surface, such as a solid piece of metal, or the solutes transfer into another phase, which for instance is a porous electrode or a membrane. In all cases, the bulk solution from which the solutes come, is stirred with a certain intensity. The theory we derive is not limited to the situation of ions arriving at a surface from solution, but works just as well when the ions flow away from a surface into solution.

The classical approach is the film layer model (diffusion boundary layer model, DBL) which uses the concept of a virtual stagnant layer of a certain thickness through which all matter must diffuse. Diffusion inside this layer is not influenced by stirring of the bulk solution. Stirring only influences the thickness of this layer. In this approach a sharp distinction is made between the film layer and the bulk solution. We will discuss this approach and compare it with other approaches that do not make this sharp distinction but that describe the entire solution phase in a unified way with gradually varying properties.

The theory of transport through a boundary layer is a challenging topic in chemical process engineering, and in electrochemical systems this is even more so because the theory must include the effects of the charge of the ions, and thus electromigration effects. Also convection to the surface is encountered in pressure-driven membrane processes. In this chapter we provide several approaches of how to theoretically describe solute transport towards a surface by combined diffusion and dispersion. In the first section we focus on equations for diffusion and dispersion from a bulk solution towards a certain surface with no other surfaces nearby, but in a later section we also consider dispersion inside a channel.

Solute concentrations can increase towards the surface, which happens for instance when fluid flows towards and through the surface, while the solutes are partially retained there. This is the typical situation for reverse osmosis and nanofiltration. In this case concentrations go up towards the surface and this phenomenon is called concentration polarization (see Ch. 11). When solutes are pulled out of solution, then concentrations will go down towards the surface, and then it is possible that we arrive at a limiting flux (current), as can be the case in electro dialysis (Ch. 12).

7.1.1 The film layer, or diffusion boundary layer

The standard approach to describe diffusion from a bulk solution to an interface is the *film layer model*, which is the concept of a layer through which all matter must be transported before arriving at the surface. The film layer is also called Nernst diffusion layer, stagnant diffusion layer (SDL), diffusion boundary layer (DBL),¹ or concentration polarization (CP) layer (Nernst, 1904; Mackay and Meares, 1959).

The DBL concept in its most general form only introduces the concept that there is a thin layer along the surface across which all matter must be flow before arriving at the surface. The direction of this solute transport is at right angles to the surface. At any position in this layer, a differential mass balance is

$$p \frac{\partial c_i}{\partial t} = -\frac{\partial}{\partial x} J_i \quad (7.1)$$

where p is porosity, which is unity ($p=1$) when there is no other phase or structure occupying part of the region in front of the surface, but porosity can also be less than unity, for instance when a mesh structure partially fills up this space. Flux J_i is a flux of ion type i by diffusion, migration and convection, in the x -direction, which is the direction towards the surface. To describe this flux of ions (and of any other solute), we can use the extended Nernst-Planck (NP) equation

$$J_i = c_i v_F - \varepsilon D_i \left(\frac{\partial c_i}{\partial x} + z_i c_i \frac{\partial \phi}{\partial x} \right) \quad (7.2)$$

in which the first term is convection, which describes that solutes are transported because they are dragged with the fluid (for instance water) towards or away from the surface. The fluid has a velocity v_F . Next is diffusion, sometimes called molecular diffusion, describing solute flow because of a concentration gradient, and the final term is due to migration, also called electromigration, which describes that ions also flow as function of a gradient in electric potential. Migration is absent for solutes that are uncharged, for which $z_i=0$, while it increases when the valency (charge) of an ion is larger (either positive or negative). The diffusion coefficient, D_i , is a molecular diffusion coefficient and is that for an unrestricted electrolyte phase, and when there is a mesh structure, or other porous material with a porosity p , a factor $\varepsilon = p/\tau$ is included, where τ is the tortuosity factor (equal to tortuosity τ squared). When ions (solutes) flow through a nanoporous medium, and have friction with the structure, an additional terms $K_{f,i}$ arises in Eq. (7.2) as well, which will be discussed in § 7.8.

¹This term, *diffusion* layer, is not to be confused with the *diffuse* layer, an element of an EDL model. The diffusion layer has a thickness of many microns, while the diffuse layer only extends a few nms.

In this most general framework, Eq. (7.1) can be solved dynamically for a layer of a certain thickness. However, from this point onward, we will solve Eq. (7.1) assuming steady-state, even when the processes around the film layer are not. The processes around the film layer can be dynamic (i.e., concentrations change in time), for instance when the surface is a porous capacitive electrode. Irrespective of whether the larger-scale processes are dynamic, the steady-state assumption for the film layer is a very good approach. Steady-state in the film is assumed for the remainder of this section.

For the CP-layer in front of a membrane in reverse osmosis and nanofiltration (Ch. 11), we must combine diffusion, migration, and convection, which we will discuss at the end of §7.3. In this case convection, which is due to fluid flow through the membrane, leads to a gradual increase of the concentration of solutes through the DBL towards the membrane. In these pressure-driven membrane processes this higher solute concentration has two adverse effects: it leads to a higher osmotic pressure at the solution/membrane interface, thus less flow of fluid through the membrane when the hydrostatic pressure is the same, and it leads to an increased leakage of solutes through the membrane.

But in the remainder of this section we leave out convection, thus we set $v_F = 0$ in Eq. (7.2). We also set $\varepsilon = 1$ until §7.8, but a factor ε can always be included as an extra term in front of D_i . Then diffusion and electromigration remain as possible driving forces. The combination of diffusion and electromigration is important in examples such as water desalination by electrodialysis (Ch. 12) and ion transport to a reactive electrode (Ch. 14), and we will discuss this problem in §7.3. But first we discuss in this section the situation that we only have neutral solutes. Thus we set $z_i = 0$ in Eq. (7.2) and then arrive at Fick's law

$$J_i = -D_i \frac{\partial c_i}{\partial x} \quad (7.3)$$

which we can integrate across the DBL (from the side of the bulk with concentration c_∞ , to the surface where concentration is c^*), for steady state (thus flux J_i is constant), which leads to the most classical film layer model for the flux of a species i

$$J_i = k_L (c_{\infty,i} - c_i^*) \quad (7.4)$$

where $k_L = D_i/\delta$, where δ is the thickness of the film layer. If there are multiple neutral solutes, this equation can be solved for each of them, because their diffusional processes do not interfere when Fick's law, Eq. 7.3, is valid. Eq. 7.3 shows that for a constant flux J_i the concentration gradient is a constant, thus the concentration changes linearly from the value c_∞ on one side of the film, to c^* on the other side.

7.1.2 Dispersion as an additional ‘diffusion-like’ term

The film model just discussed is very relevant, but a potentially much better approach is to add dispersion, and do so in such a way that we no longer have to make a sharp distinction between a film layer and the bulk solution. Two fundamentally different approaches are discussed, in the present and next sections.

The first approach is to add dispersion to the diffusion in x -direction. In this case, dispersion describes additional local mixing of solutes. Mathematically it behaves the same as molecular diffusion, and thus we now have a dispersion coefficient which we can add to the molecular diffusion coefficient. Thus the combination of diffusion and dispersion becomes

$$J_i = - (D_i + D_{\text{disp}}) \frac{\partial c_i}{\partial x}. \quad (7.5)$$

Note that throughout this book, the parameter D always refers to molecular diffusion, and a dispersion coefficient always has index ‘disp’ included. Unlike the molecular diffusion coefficient, the dispersion coefficient in Eq. (7.5) is not constant, but its value is zero at the surface, and very high away from the surface, in bulk solution. This is because dispersion is due to local ‘circulations’, also called ‘eddies’. Far from the surface these eddies are large (there are larger and more vigorous circulations of fluid), while they dampen out the closer we approach the surface, and just before the surface they are gone, i.e., there is no dispersion right at the surface.

We can postulate a function for D_{disp} that starts at zero at the surface and then rapidly increases moving away from the surface. We propose $D_{\text{disp}} = D_i \cdot (\exp(\tilde{x}/\delta) - 1)$, where δ is an exponential length describing how fast the eddies grow, and where \tilde{x} is a coordinate axis pointing from the surface into solution ($d\tilde{x} = -dx$). Thus, moving a distance δ away from the surface, $D_i + D_{\text{disp}}$ increases by a factor e . We implement this function in Eq. (7.5) and rewrite in integral form, resulting in

$$-J_i \cdot \int_0^\infty \exp(-\tilde{x}/\delta) d\tilde{x} = -D_i \int_{c^*}^{c_\infty} dc \quad (7.6)$$

which we integrate to

$$-J_i \cdot (-\delta) \cdot [\exp(-\tilde{x}/\delta)]_0^\infty = -D_i \cdot (c_\infty - c^*) \quad (7.7)$$

which then becomes

$$-J_i \cdot (-\delta) \cdot (0 - 1) = -D_i \cdot (c_\infty - c^*) \quad (7.8)$$

which has four times a minus-sign, which all cancel out, and then Eq. (7.8) can be rewritten to ... Eq. (7.4), with again $k_L = D_i/\delta$! Thus we obtain the same result as for the basic film

model of §7.1.1, but now we have a different interpretation of δ . It is no longer the distance from the surface where an ad-hoc transition from a stagnant film to a well-stirred bulk is postulated, but now it is a measure of the rate by which dispersion grows when we move away from the surface.

In the new approach, the concentration of solutes no longer changes linearly across the film as in §7.1.1, but now it changes exponentially with \tilde{x} , a result we obtain from integrating Eq. (7.6) from a position \tilde{x} to ∞ , which results in

$$-J_i \cdot (-\delta) \cdot (0 - \exp(-\tilde{x}/\delta)) = -D_i (c_\infty - c(\tilde{x})) \quad (7.9)$$

which we can rewrite to

$$c(\tilde{x}) = c_\infty - J_i/k_L \cdot \exp(-\tilde{x}/\delta) \quad (7.10)$$

which shows that starting at the surface, where $\tilde{x}=0$, the concentration $c(\tilde{x})$ changes rapidly with \tilde{x} , but the further we go away from the surface the more the rate of change of c vs. \tilde{x} decreases.

7.1.3 Dispersion as a convective term parallel to the surface

A very different approach is as follows. In this approach, in the x -direction towards the surface we have the driving forces as before, which are molecular diffusion and convection, and for ions also electromigration, but we no longer add dispersion in this x -direction. Instead, we include dispersion as an effect that works ‘from the side’, with fresh fluid and solutes coming from a bulk phase entering the profile sideways at each position x . Thus, at each position in the DBL, solution is ‘refreshed’ with new solution coming from the bulk ever so often. The difference with the prior approach is that in the approach of §7.1.2 stirring led to a faster equilibration of solutes *with nearby solutes*, and thus gradients in x -direction were increasingly flattened out, but in the new approach the fluid composition at a position x is refreshed every so much time with fresh solution from outside the transport layer. This may be an approach more representative of how eddies near a surface behave, which indeed leads to fluid sweeping along the surface, the more the further away we are from the surface.

The refreshment of fluid-plus-solutes at each position in the DBL is described by a refreshment time τ . Faster stirring will decrease τ . We first describe an approach where τ is constant, independent of distance to the surface. Later we discuss the more realistic situation that τ depends on position x , starting at infinity at the surface (which means no refreshment at all), and going down when we move away from the surface, so more and more refreshment. In this new approach, at any position in a channel (near a surface, in a

DBL), the mass balance for a neutral solute now becomes

$$p \frac{\partial c_i}{\partial t} = D_i \frac{\partial^2 c_i}{\partial x^2} + \frac{c_\infty - c_i}{\tau} \quad (7.11)$$

where the last term represents the refreshment of fluid: fresh bulk solution with concentration c_∞ is inserted at position x in the DBL with a frequency that is the inverse of the refreshment time τ , and it replaces the fluid that was there.ⁱⁱ The refreshment time τ will go down the more vigorously we stir the solution. Eq. (7.11) is valid for neutral solutes, but as we will discuss in §7.2, it also applies to many situations with binary salt solutions, even for the case that the two ions have different diffusion coefficients and valencies (an asymmetric salt).

We consider the steady state, thus set $\partial c_i / \partial t = 0$, and solve this equation with the boundary conditions that at $\tilde{x} = 0$ we have the surface concentration $c_i = c^*$, where index * refers to the surface, and far from the surface we have $c_i = c_\infty$ and $\partial c_i / \partial \tilde{x} = 0$. The solution is

$$c(\tilde{x}) = c^* + (c_\infty - c^*) \left(1 - \exp\left(-\tilde{x}/\sqrt{\tau D}\right) \right). \quad (7.12)$$

Now with the flux of solutes, J_i , at the surface given by $J_i = -D_i \cdot \partial c_i / \partial x|_*$, we obtain

$$J_i = \sqrt{D_i/\tau} \cdot (c_\infty - c^*). \quad (7.13)$$

This is a very interesting and remarkable result. Just as in the previous two models, flux J_i is proportional to the difference between c_∞ and c^* , and we have a constant prefactor, which we can again represent by k_L , and thus for this refreshment model we have $k_L = \sqrt{D_i/\tau}$. But interestingly, in this approach, the transport coefficient k_L is no longer linear in D_i (as it was in the film model of §7.1.1), but k_L now only depend on D_i to the power $1/2$. Though we can define a length scale $\delta = \sqrt{D_i \tau}$, and then, as in the previous models, $k_L = D_i/\delta$.

We can combine Eqs. (7.12) and (7.13) to arrive at the profile $c(\tilde{x})$, given by

$$c(\tilde{x}) = c_\infty - J_i \cdot \sqrt{\frac{\tau}{D_i}} \cdot \exp\left(-\frac{\tilde{x}}{\sqrt{D_i \tau}}\right) \quad (7.14)$$

which we can also write in terms of k_L and δ , and then we exactly obtain Eq. (7.10). Thus the two approaches, of the present and previous sections, give the exact same result for molar flux and concentration profiles, if we group underlying constants in the same factors k_L and δ .

ⁱⁱIn 2D (x, z) models for flow through channels, see Chs. 11 and 12, with z a coordinate along the surface, this refreshment term can be replaced by $-v_z \partial c / \partial z$ describing convection in z -direction. So this refreshment concept, by which we modify a 1D transport model, has similarities to modelling convection along surfaces in a 2D transport model.

7.1.4 Dispersion as a convective term parallel to the surface - varying refreshment rate

In the previous section, the refreshment time τ was a constant factor. However, in a more advanced theory it is made a function of position x : infinite at the surface (no refreshment at that position), and going down to zero or a low value far away from the surface. This relates to the typical profile of the fluid velocity along a surface, v_{\parallel} : this velocity is zero right at the surface (zero wall slip), first linearly increasing the further we move away from the surface, and then gradually levelling off far away. For the calculation outcome it is not very relevant how v_{\parallel} exactly changes far away because there concentration profiles have become flat anyway, and thus it is a good approach to assume that this parallel fluid velocity, v_{\parallel} , continues to linearly increase with x , starting at $v_{\parallel} = 0$ at the surface, without levelling off at some point. For steady-state we can now rewrite Eq. (7.11) to

$$y'' - \xi y = 0 \quad (7.15)$$

where $y = c - c_{\infty}$, $y'' = \partial^2 y / \partial \xi^2$, and the factor ξ is given by $\xi = \tilde{x} / \sqrt[3]{D/\gamma}$. The factor γ in this expression will be explained below; again D is the molecular diffusion coefficient. This differential equation is the Airy function. It can be solved with the boundary condition that far from the surface $y' = 0$, and we then obtain the result that flux J_i at the surface is once again given by Eq. (7.4), but now with the transfer coefficient k_L defined as

$$k_L = \alpha \cdot D^{2/3} \cdot \gamma^{1/3} \quad (7.16)$$

where α is a constant, equal to $\alpha = -\text{Ai}'(0)/\text{Ai}(0)$. This factor includes π and the $\Gamma(2/3)$ -function. Evaluating this function, we find a number $\alpha = 0.729011\dots$. The key result is that once again the flux of solutes into the surface, J_i , is proportional to the difference between bulk concentration, c_{∞} , and surface concentration, c^* . Now the prefactor depends on the molecular diffusion coefficient to the power $2/3$. The factor γ represents the gradient in injection frequency of fresh solution. A numerical example explains this best: if fluid flows along the surface with such a rate that at $100 \mu\text{m}$ above the surface the solution is replaced 10 times every second, then $\gamma = 0.1 (\mu\text{m} \cdot \text{s})^{-1}$. At $10 \mu\text{m}$ above the surface, refreshment is then every second, and at $1 \mu\text{m}$ only once every 10 s, etc. With a typical value of $D = 1 \cdot 10^{-9} \text{ m}^2/\text{s}$, we then have a value of $k_L = 34 \mu\text{m}/\text{s}$, which in the standard film model, with the same diffusion coefficient, would correspond to a diffusion layer thickness of $\sim 30 \mu\text{m}$, a typical number. If stirring intensity is proportional to the factor γ , then according to this equation, if stirring is increased by a factor of say 10, mass transport is only enhanced by the cube root thereof, in this case a factor of ~ 2 more. Thus, even though stirring is

important, and a certain change in $\Delta\gamma$ important to make when γ is low, i.e., a small amount of extra stirring then helps a lot, at some point the incremental effect of stirring is small and the energy costs thereof will surpass the advantage of more stirring. In addition, at some point of increasing stirring intensity, another mass transport limitation in the process will become rate-limiting.

A very accurate approximation to the Airy equation (with the given boundary conditions) for the profile $c(\tilde{x})$ is

$$\frac{c(\tilde{x}) - c_\infty}{c^* - c_\infty} = 1 - \tanh(\alpha \xi) \quad (7.17)$$

where α and ξ are the same as above.

In conclusion, in this section we presented four models to describe steady-state diffusion and dispersion near a reactive or selective surface for neutral solutes. For the relationship between flux and concentration, these models all end up with the same result that flux is proportional to the concentration difference between bulk and surface. However, for the proportionality factor different expressions are obtained, with a dependence on diffusion coefficient that can be to the power $1/2$, $2/3$, or 1 .ⁱⁱⁱ

7.2 Ionic current and transport and transference numbers

In §7.1, we discussed transport of neutral solutes between bulk solution and a surface, and obtained several relations for the flux of a solute, and for the concentration difference between bulk and surface. These equations can also be applied when there are many different neutral solutes, because they do not influence each other. There can even be charged solutes (ions) but all the while the diffusion equations for the neutral solutes are unchanged. But the diffusion of ions must be described in a different manner. In the present and next sections we discuss how to extend the theory to an electrolyte solution, thus when there are ions. In this case there are always at least two types of ions, cations and anions.

Further on we will explain that many of the results of §7.1 also apply to binary electrolytes. But first we give general expressions for the ionic current density, and for transference numbers t_i , and transport numbers, T_i . We start with the Nernst-Planck (NP) equation,

ⁱⁱⁱInterestingly, the theories presented here for mass transport and diffusion equally apply to the important problem of heat transport to a surface by conduction and the effect of mixing/stirring. The diffusion coefficient is then replaced by the thermal conductivity, concentration by temperature, and molar flux by a heat flux.

Eq. (7.2), extended with convection, which describes the molar flux of an ion i by

$$J_i = c_i v_F - D_i \left(\frac{\partial c_i}{\partial x} + z_i c_i \frac{\partial \phi}{\partial x} \right)$$

where D_i is the diffusion coefficient of the ion in the electrolyte phase, and where the potential ϕ relates to a voltage V by $\phi = V/V_T$. In §7.8 we explain how this extended NP-equation derives from a balance of forces acting on ions in solution.

A summation over all ions of their flux J_i times their valency z_i results for current density (unit A/m²) in

$$I = F \sum_i z_i J_i = F v_F \sum_i z_i c_i - F \varepsilon \sum_i \left\{ D_i z_i \frac{\partial c_i}{\partial x} \right\} - \varepsilon \sigma_\infty \frac{\partial V}{\partial x} \quad (7.18)$$

where we introduce the ionic conductivity of a solution (unit S/m, where S=A/V and A=C/m²)

$$\sigma_\infty = \left(F^2 / RT \right) \sum_i z_i^2 D_i c_i \quad (7.19)$$

also called the electrical conductivity of a solution, κ . In bulk electrolyte we have local electroneutrality, $\sum_i z_i c_i = 0$, and thus the convective term in Eq. (7.18) can be omitted, but that is not the case in a charged porous medium. We discuss ion conduction in a porous medium in the next box.

Conductivity in porous media, such as membranes. The conductivity of a porous medium where pores are filled with electrolyte, such as a flow channel that contains a mesh of material, σ_m , is lower than the conductivity of bulk solution by a factor ε , thus $\sigma_m = \varepsilon \sigma_\infty$, see p. 159. The factor ε is porosity, p , divided by the tortuosity factor, τ , i.e., $\varepsilon = p/\tau$. For flow inside a nanoporous medium such as an ion-exchange membrane, ions also have friction with the structure, the matrix. In that case, the conductivity, σ_m is lower again, now by an additional factor $K_{f,i}$ that we discuss at p. 197. Thus $\sigma_m^* = K_{f,i} \sigma_m = K_{f,i} \varepsilon \sigma_\infty$.

An important topic is the electrolyte conductivity inside charged membranes, of special importance for electrodialysis (ED), see Ch. 12. Also here Eq. (7.19) can be directly applied, as conclusively proven by J.C. Díaz and J. Kamcev¹. We illustrate this fact by an extensive data set of Díaz and Kamcev for an AEM with $|X| = 3.1$ M and a CEM with $|X| = 2.5$ M for membranes with several thicknesses, tested with NaCl solutions with salt concentration from 1 mM to 1 M, see Fig. 7.1A for results obtained with an

AEM membrane. From the slope of a trendline running through the origin, we can derive a conductivity of $\sigma_m^* \sim 16$ mS/cm for salt concentrations 1–100 mM and $\sigma_m^* \sim 17$ mS/m for $c_\infty = 1$ M. Thus conductivity is independent of salt concentration, except for a slight increase around 1 M NaCl, see Fig. 7.1B. The constant conductance is in agreement with Eq. (7.19) given that at low enough c_∞ the concentration of counterions in the membrane is almost equal to $|X|$ and the concentration of coions is very low. The increase of σ_m^* at 1 M NaCl is due to the increase in co- and counterion concentrations in the membrane. To describe these data, we extend Eq. (2.11) in Ch. 2 to account for a non-unity partition coefficient, Φ_i (which we use to describe non-electrostatic contributions to the chemical potential of an ion), resulting in $c_{T,m}^2 = X^2 + (2\Phi_i c_\infty)^2$, which relates the total ion concentration in the membrane, $c_{T,m}$, to salt concentration and membrane charge. The counterion concentration in the membrane is then $\frac{1}{2}(c_{T,m} + |X|)$ and the coion concentration $\frac{1}{2}(c_{T,m} - |X|)$. These concentrations are then used in Eq. (7.19) which results in the theoretical lines in Fig. 7.1B ($\Phi_i = 0.6$). To fit to the data we introduce a membrane reduction factor, mrf, which describes by how much the rate of diffusion of ions is reduced in the membrane compared to solution, thus $\text{mrf} = \sigma_\infty / \sigma_m^* = 1 / K_{f,i} \varepsilon$. For the AEM considered in Fig. 7.1B, we then have $\text{mrf} \sim 15$ while for the CEM we derive $\text{mrf} \sim 9.5$. Note that measurement of σ_m^* based on conductivity (current-voltage relationship) is only correct when convection and diffusion can be neglected, see 1st and 2nd term on the right in Eq. (7.18). For a charged membrane, convection is typically non-zero while diffusion is only zero if we can assume the same D_i for all ions.

Interestingly, a similar analysis by Díaz and Kamcev of data for a commercial CEM membrane (Neosepta CMX) with $|X| \sim 5.7$ M, leads to a value of $\sigma_m^* \sim 5$ mS/cm while other literature reports 7–10 mS/cm. These numbers lead to a reduction factor between $\text{mrf} = 30$ – 60 , in line with estimates for the mrf of Neosepta CMX membranes in Tedesco *et al.* (2018).²

We summarize these data of mrf vs. $|X|$ with the empirical function $\text{mrf} = \exp(\alpha_1 |X|^{\alpha_2})$ where $|X|$ has the unit M, with $\alpha_1 = 1.32$ and $\alpha_2 = 0.6$. (For $X = 0$ M, $\text{mrf} = 1$, i.e., no reduction in ion mobility. In this analysis, we use $\text{mrf} = \sqrt{30 \cdot 60} \sim 42$ for the Neosepta membrane.) Data points and the fit line are presented in Fig. 7.2.

A similar relationship between conductivity and membrane charge density is given by Fan *et al.* (2022)³ where effectively mrf is expressed as an exponential function of the ionic valency squared, and with membrane charge density to the power 2/3, i.e., the empirical function above is modified to $\text{mrf} \propto \exp(A \cdot |X|^{3/2})$. The prefactor A is

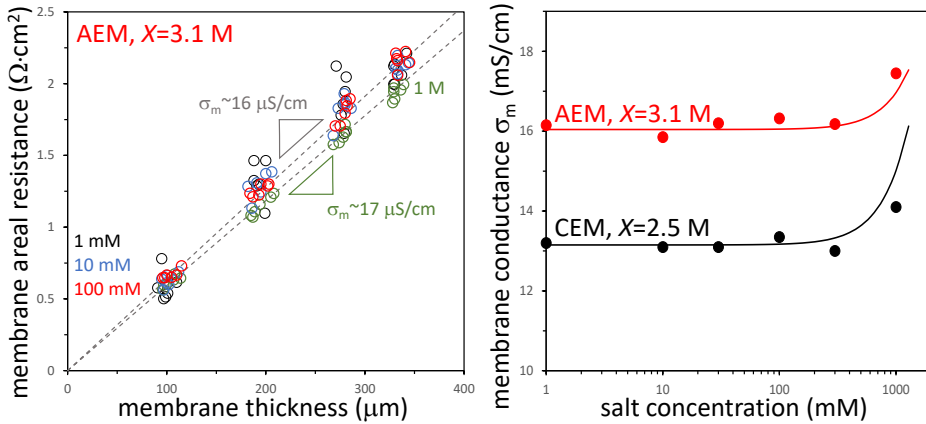


Fig. 7.1: Resistance to ionic transport in an anion and cation exchange membrane (AEM and CEM). A) Resistance as function of membrane thickness for an AEM. B) Ionic conductivity as function of external salt concentration. Data from Díaz and Kamcev (2021), and lines based on Eq. (7.19) and Donnan model, as explained in the nearby box.

inversely proportional to the dielectric constant in the membrane ϵ_r squared, and the equation in Fan *et al.* matches that by us if $\epsilon_r = 32$ is used. Note that mrf as calculated by Fan *et al.* is extremely sensitive to the assumed value of ϵ_r in the membrane.

In Fan *et al.* (2022)³ also an expression is provided for the influence of membrane porosity, or water fraction, p , on the diffusion coefficient in the membrane, which is $\text{mrf} = (2/p - 1)^2$. This expression implies that when $p = 0.48$, $\text{mrf} = 10$, and when $p = 0.18$, $\text{mrf} = 100$, which are realistic predictions. However, it is not known whether this formula relates to an influence on diffusion itself (relating to porosity and tortuosity), or also to ion-membrane friction (resulting in $K_{f,i} < 1$). In §7.8 we discuss approaches to include ion-membrane friction in a transport model.

We can now define the transference number of an ion, t_i , as

$$t_i = \frac{z_i^2 D_i c_i}{\sum_i z_i^2 D_i c_i}. \quad (7.20)$$

The transference numbers, t_i , are positive for all ions, and add up to unity, i.e., $\sum_i t_i = 1$. For a binary $z_+ : z_-$ salt solution (only one cation, one anion), the transference number of each

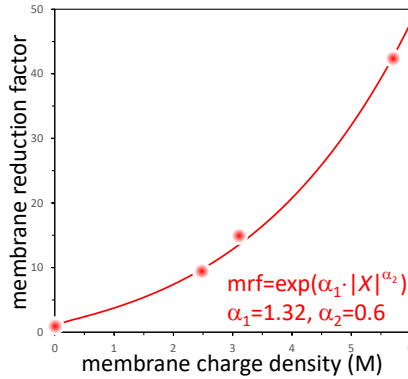


Fig. 7.2: Data for ionic conductivity of an ion-exchange membrane (IEM) recalculated to a membrane reduction factor, mrf, which is the ratio of ion diffusion coefficient in an IEM relative to that in free solution, plotted as function of membrane charge density, $|X|$. An empirical fit for mrf starts at mrf=1 at $X=0$, and increases to above mrf=40 for the Neosepta CMX membrane ($|X| \sim 5.7$ M).

of the ions is

$$t_i = \frac{|z_i|D_i}{z_+D_+ + |z_-|D_-} \quad (7.21)$$

and we have $t_+ + t_- = 1$.

In the absence of concentration gradients we only have electromigration as a driving force for ion transport, and then implementing the above equations in Eq. (7.2) results for the ionic flux in

$$J_i = c_i v_F - \frac{t_i I}{z_i F}. \quad (7.22)$$

This is a very elegant equation, but it must be noted that it has a very small range of application: it is only valid in the complete absence of any concentration gradient, so in the boundary region near a selective surface it cannot be used.

Transference numbers in membranes. In this chapter we discuss transport in bulk electrolyte, where we have charge neutrality based on the ions. However, in a charged membrane, we also have the fixed charge groups, with concentration $|X|$. In a description of transference numbers, these groups are mathematically treated as if they are ions, with a diffusion coefficient of zero. Thus, also in a membrane we can use Eq. (7.20) to calculate transference numbers of all (mobile) ions. Transference numbers will then strongly depend on the concentrations of counterions and of coions, leading to values

of t_i close to zero or unity, even though the diffusion coefficients (mobilities) of the ions are similar. These numbers for t_i in the membrane via their dependence on ion concentration in the membrane, will then depend on the concentrations of ions outside the membrane (because of Donnan equilibrium). But transference numbers have no direct relation to the rates of transport of ions, as we will discuss next.

—

Besides the transference number, t_i , there is the transport number, T_i , and this is a very different parameter. The transference number, t_i , was defined by Eq. (7.20) and can be calculated when we know all ion valencies and diffusion coefficients. It describes the contribution of ions to the current only if the composition of the solution phase is uniform (all concentration gradients are zero). Instead, the transport number describes the actual or ‘real’ contribution of ion transport to the current, thus also when there are concentration gradients, which always is the case near a selective surface, such as near an electrode or membrane. Thus, the transport number T_i is the local contribution of a certain ion flux to the local current, whether or not there are ion concentration gradients. The differences between t_i and T_i can be large, with the transference number, t_i , in a binary salt solution always at the same value, see Eq. (7.21), but the transport number, T_i , changing in time and with position. Only with vigorous stirring, and away from selective interfaces, do the two parameters have the same value. But in general they have different values.

Transport numbers can be used to describe a process where bulk electrolyte is in contact with a selective interface, with current running through this interface. This interface can be an electrode, absorbent material, or membrane. As just mentioned, the transport numbers, T_i , describe the contribution of each ion to the current density, and they are often position-dependent, and for a dynamic process also time-dependent. Only in a one-dimensional steady-state transport problem, without convection along the surface, i.e., without dispersion modelled as a ‘sideways’ refreshment, are they constant, i.e., independent of position. In other situations they vary with position. If the selective layer (for instance a membrane) operates in steady-state, with ion fluxes assumed to cross the membrane in one particular direction x , then inside the membrane the transport number of a certain ion will be the same at each x -position, i.e., T_i will be invariant with x .^{iv} Note that this is only true for inert ions. When we have reactive ions, transport numbers of individual ions will change with position, also for a membrane layer in steady state, see Ch. 10.

^{iv}In a full membrane module, with also a coordinate z directed along the membrane, i.e., through the flow channel from entrance to exit, transport numbers will depend on z .

So how to calculate transport numbers right next to a selective interface, such as a membrane? They are not material properties, or properties of the ionic solution, like the transference number is. They are not membrane properties in the same way that an ion mobility or a membrane charge density is. Instead, they follow from a combination of a transport model for the membrane, with a transport model for the flow channel, and they (i.e., their values) emerge in a calculation that considers the complete membrane-electrolyte system. In some cases we can assume the membrane (or other selective layer) to have a certain transport number for a certain ion, for instance we can assume that a certain membrane is perfectly selective and only allows access to a certain type of ion, so for this ion $T_i = 1$ and for all other ions $T_i = 0$. For a reactive electrode where only a certain species is consumed, for that species the transport number is unity, while it is zero for all other species.^v

The transport number is defined (at any position) as the fraction of the current density carried by a certain ion, i.e., it is the local ion flux times z_i over the local current density

$$T_i = z_i J_i / J_{\text{ch}} \quad (7.23)$$

without any requirements such as uniformity of concentration profiles. Also, because $J_{\text{ch}} = \sum_i z_i J_i$, it is the case that $\sum_i T_i = 1$, just like for transference numbers. However, what is different is that transport numbers can also be < 0 or > 1 , while transference numbers are always between 0 and 1. For instance, in a process called ‘osmotic power generation’, or reverse electrodialysis (RED), both ions have fluxes in the same direction, thus for the coion the transport number is < 0 , while it is > 1 for the counterion.

For solutions with all ions monovalent (a 1:1 salt, but more than one type of cation and anion possible), we can use the concept of the current efficiency, λ , which is the ratio of ions flux into a surface, J_{ions} , over the current density, J_{ch} . This current efficiency, λ , can be used to characterize ion adsorption in porous electrodes, see §15.3, and also describes ion selectivity in membrane transport, see §12.3. Current efficiency is defined as

$$\lambda = \frac{J_{\text{ions}}}{J_{\text{ch}}} = \frac{J_+ + J_-}{J_{\text{ch}}} \quad (7.24)$$

and for a 1:1 salt can be related to transport numbers according to

$$\lambda = T_+ - T_- \quad (7.25)$$

where T_+ is calculated as a summation over the T_i 's of all cations, and the same for T_- and all anions. Thus when all anions together contribute 50% to the current density, and likewise

^vThis is then the case at the very surface, not necessarily at distances $x > 0$, unless there is steady-state, no dispersion, etc.

all cations contribute 50%, then $T_+ = T_- = 1/2$ and then $\lambda = 0$, i.e., there is transport of current, with all cations going in one direction and all anions in the opposite direction, but there is no 'net' transport of ions as a whole.

As mentioned, when both the anions and cations go in the same direction (as is the case for the aforementioned RED-process), then the transport number will be < 0 for the coion and > 1 for the counterion, and consequently $\lambda > 1$. As a metric to define efficiency, numbers beyond unity are not very intuitive, and that is why in RED and similar processes, instead a different efficiency is used, which is the salt transport efficiency, ϑ . This efficiency is defined as $\vartheta = 1/\lambda$ and is a measure of how effectively the salt concentration difference is used to generate electrical current. For a well-designed RED process this ratio is close to unity. However, when membranes are used with large pores (a pore diameter of several nm's or more), or membranes that are too thin (for instance a thickness less than $1 \mu\text{m}$), then the ions flux (leakage of ions, $J_+ + J_-$) is high relative to the generated current, and thus ϑ will be low. On p. 338 we discuss in more detail the low value of ϑ when very thin membranes are used, and the effect thereof on osmotic power production.

7.3 General balances for binary electrolytes

In multicomponent ionic mixtures (electrolytes), in general we must solve mass balances for all ions individually. When there are fast reactions between them, it is possible to combine balances of individual ions to one balance per 'group' of ions, as explained in Ch. 10. But in the absence of such reactions, generally each ion must be considered by a separate balance equation. And this balance then includes diffusion as driving force, electrical potentials, and convection and dispersion. But in this section we explain how for a binary salt, which is a salt with one type of cation and one type of anion, with arbitrary values of diffusion coefficients and valencies, we can derive a general, combined, balance for the salt as a whole, which does not include a dependence on potential gradients. This derivation is for a solution phase without additional charges from a porous medium, and thus includes the electroneutrality condition which is that at each position the concentration of cations times their valency plus that of the anion times their valency, is zero; see p. 203 for more information on the electroneutrality condition.

To evaluate transport of a binary salt, we start with the NP equation for an ion, Eq. (7.2), in combination with a mass balance, Eq. (7.1), to which we also add a dispersion effect

modelled by a refreshment term.^{vi} Reactions in solution are not considered – for that, see Ch. 10. The convection term can be in the x -direction towards a surface or in a direction along a surface, z , and to describe both situations simultaneously we use the general formulation of $\nabla \cdot (c\mathbf{v}_F)$ here. Thus, the ion mass balance becomes

$$p \frac{\partial c_i}{\partial t} = -\nabla \cdot (c_i \mathbf{v}_F) + \frac{\partial}{\partial x} \left(D_i \frac{\partial c_i}{\partial x} \right) + \frac{\partial}{\partial x} \left(D_i z_i c_i \frac{\partial \phi}{\partial x} \right) + \frac{c_{\infty, i} - c_i}{\tau}. \quad (7.26)$$

Now we analyze Eq. (7.26) for a binary salt. We multiply each term in Eq. (7.26) by z_+ for the cation, and by $|z_-|$ for the anion, and define c as the ‘monovalent equivalent’ (m.e.) salt concentration, which is given by $c = z_+ c_+ = |z_-| c_-$. We now arrive both for the cation and for the anion at

$$p \frac{\partial c}{\partial t} = -\nabla \cdot (c \mathbf{v}_F) + \frac{\partial}{\partial x} \left(D_i \frac{\partial c}{\partial x} \right) + \frac{\partial}{\partial x} \left(D_i z_i c \frac{\partial \phi}{\partial x} \right) + \frac{c_{\infty} - c}{\tau} \quad (7.27)$$

where c without index i is the m.e. salt concentration defined above. We evaluate Eq. (7.27) for both ions and equate the two results. We then arrive at the charge balance

$$0 = \frac{\partial}{\partial x} \left((D_+ - D_-) \frac{\partial c}{\partial x} \right) + \frac{\partial}{\partial x} \left((z_+ D_+ + |z_-| D_-) c \frac{\partial \phi}{\partial x} \right). \quad (7.28)$$

Combining Eq. (7.27) (evaluated for one of the ions) with Eq. (7.28), we arrive at the salt mass balance

$$p \frac{\partial c}{\partial t} = -\nabla \cdot (c \mathbf{v}_F) + \frac{\partial}{\partial x} \left(D_{\text{hm}} \frac{\partial c}{\partial x} \right) + \frac{c - c_{\infty}}{\tau} \quad (7.29)$$

which is a quite amazing result: for any binary salt also when it is asymmetric (such as a 2:1 salt, for instance CaCl_2), we can derive a salt balance that includes convection, diffusion, and refreshment, but not electromigration. The ‘harmonic mean’ diffusion coefficient in Eq. (7.29), D_{hm} , is given by

$$D_{\text{hm}} = \frac{(z_+ + |z_-|) D_+ D_-}{z_+ D_+ + |z_-| D_-} \quad (7.30)$$

which for a binary symmetric salt (a 1:1 or 2:2 salt) simplifies to

$$\frac{2}{D_{\text{hm}}} = \frac{1}{D_+} + \frac{1}{D_-}. \quad (7.31)$$

When $D_+ = D_- = D$, also for an asymmetric salt, it follows from Eq. (7.30) that $D_{\text{hm}} = D$.

^{vi}We do not include here dispersion modelled as parallel to molecular diffusion, as discussed in §7.1.2, though the results arrived at in the present section also hold then.

Thus Eq. (7.29) shows how also for any asymmetric binary salt, with the two ions having different diffusion coefficients and different valencies, we have transport of salt as if it is a single neutral molecule. This is only the case for a binary salt solution, i.e., with only one cation and one anion, in a phase without any other (fixed) charge. This equation can be used for electrolyte flow in a channel that is empty or filled with an uncharged mesh structure, or for flow through any other type of uncharged porous medium.^{vii}

Including dispersion in the general balance for binary salts. When Eq. (7.30) is solved in multiple dimensions with flow, then the refreshment term $(c - c_\infty) / \tau$ is not typically used because there is no additional sideways flow that can be the origin of it (convection is already included in the $\nabla \cdot (c \mathbf{v}_F)$ -term). But instead, Eq. (7.30) can be extended with 'dispersion parallel to diffusion' as described in §7.1.2. Then we use a coefficient D_i^\diamond that combines molecular diffusion and dispersion, and this D_i^\diamond is used in the concentration gradient-terms in Eqs. (7.27) and (7.28) instead of just D_i . The electromigration-part only depends on molecular diffusion and thus D_i is used there. Re-analysing Eqs. (7.27) and (7.28) we then find that Eq. (7.30) is replaced by (Newman, 1983)

$$D_{\text{hm}}^\diamond = \frac{z_+ D_+ D_-^\diamond + |z_-| D_- D_+^\diamond}{z_+ D_+ + |z_-| D_-} \quad (7.32)$$

where the D_i^\diamond 's include both molecular diffusion and dispersion. The dispersion coefficient is independent of the ion; it only depends on the hydrodynamic flow pattern near the surface and the resulting fluid mixing. For a symmetric salt (where $z_+ = |z_-|$) and in case $D = D_+ = D_-$, we obtain $D_{\text{hm}}^\diamond = D^\diamond = D + D_{\text{disp}}$. If dispersion is much larger than diffusion, so the D_i^\diamond 's become the same for both ions (because the dispersion coefficient does not depend on the ion), we end up with $D_{\text{hm}}^\diamond = D_{\text{disp}}$ for any binary salt. If this limit applies, then nothing about an ion's charge, valency, or diffusion coefficient matters in determining salt concentration profiles, only the dispersion coefficient. This is correct in a bulk phase sufficiently far away from any surface, but certainly does not apply to the last 10s of μm 's right next to a selective interface, where mass transfer limitations most certainly are important.

The approach described in this box, where D_{hm} depends on a dispersion coefficient, is generally valid whichever expression is used for the dispersion coefficient, irrespective of whether it is invariant or not with position. This is the case when we use the general

^{vii}The presence of which, as we explain in Ch. 12, leads to an additional term p/τ (with τ the tortuosity factor) in front of each factor D , and to the porosity-term p in front of the $\partial c / \partial t$ -term.

form of Eq. (7.29) with D_{hm} ‘inside the differential’. We can only take D_{hm} outside the differential if there is no dependence of it on position or concentration. That will be the approach in the next box.

Simplified approaches to include dispersion in mass transfer modelling in channels. In several cases, especially for a flow channel (not so much for a surface in contact with bulk solution), it is useful to assume the dispersion coefficient is some constant, for instance we set it to a multiple of the diffusion coefficient, thus not x - or c -dependent. We can then simplify Eq. (7.29) (also leaving out refreshment), resulting in

$$p \frac{\partial c}{\partial t} = D_{\text{hm}}^{\diamond} \frac{\partial^2 c}{\partial x^2} - \nabla \cdot (c \mathbf{v}_{\text{F}}) . \quad (7.33)$$

Even though salt transport is enhanced because of dispersion, a calculation of potentials and currents, making use of Eqs. (7.2), (7.18), and (7.28), is based on the molecular diffusion coefficients, D_i , and thus is not directly affected by dispersion. This is a very useful approach to describe transport across the flow channels used in membrane-based water desalination technologies described in Chs. 11 and 12. When this model is evaluated in the limit of a very high dispersion coefficient, then flat concentration profiles are predicted in the direction across the flow channel. This limiting model should then give the same outcome as a simple model where this flat profile is a priori assumed, i.e., where in the x -direction towards an interface concentrations are assumed to be invariant. Of course in this model, all effects of mass transport across the channel that could lead to concentration profiles are gone but this may nevertheless be a realistic first order model for reverse osmosis or electrodialysis when combined with a plug flow reactor (PFR) approach in the z -direction along the membrane. An Ohmic resistance across the channels, relating current and voltage drop, depends on the *molecular* diffusion coefficients, and is still part of the the model even when dispersion is so large that all concentration profiles are equalized out. For a given current, the voltage changes across a channel are less when concentrations are more equalized out, but except for this effect, more stirring does not enhance charge transport or reduce voltages.

Convection in a model for concentration polarization (CP) in membrane transport.

When we make use of the full extended NP equation also including convection, Eq. (7.2), then a DBL model solved for a binary $z_+ : |z_-|$ salt for zero current leads to the result that the ‘monovalent equivalent’ (m.e.) molar flux ($J_{\text{m.e.}} = z_+ J_+ = |z_-| J_-$) is given by

$$J_{\text{m.e.}} = c v_F - D_{\text{hm}} \frac{\partial c}{\partial x} \quad (7.34)$$

where the harmonic mean diffusion coefficient D_{hm} is given by Eq. (7.30). For a 1:1 salt, $J_{\text{m.e.}}$ simply corresponds to the salt flux, J_i (the same molar flux for cations as for anions), and c is simply the salt concentration, at any point in the DBL. In Ch. 11 this expression is integrated to obtain an analytical expression for the DBL in front of a membrane used for water desalination.

7.4 Boundary equations for binary salts

We will explain how the general validity of Eq. (7.29), also for asymmetric salts, has the implication that the various analytical results of §7.1 are valid not just for a neutral solute, but just as much for any binary asymmetric salt with two ions with different valencies and diffusion coefficients. [And even for a system with many more solutes, but all of these then have to be neutral.] The only added complexity is that we must analyze what the flux J used in §7.1 means to in the context of a binary salt solution.

We make this comparison on the basis of a simplification of the binary salt balance, Eq. (7.29), neglecting convection and assuming a constant diffusion coefficient, leading to

$$p \frac{\partial c}{\partial t} = D_{\text{hm}} \frac{\partial^2 c}{\partial x^2} + \frac{c - c_\infty}{\tau} \quad (7.35)$$

which we will analyze for steady state, i.e., we set the left side to zero. Eq. (7.35) is very similar to Eq. (7.11) which was based on a neutral solute with concentration c and diffusion coefficient D , while Eq. (7.35) is for a binary salt with monovalent equivalent concentration c and harmonic mean diffusion coefficient D_{hm} . Thus these equations are completely analogous, and results from §7.1 can also be used for a binary salt, also in the presence of electrical potential gradients and/or non-zero current densities. *Note that this analogy only holds for three out of the four models used in §7.1, namely for the standard DBL model where the term $(c - c_\infty) / \tau$ is zero, and for the two refreshment models, the one with fixed τ and the one with position-dependent τ . Thus, we will not consider the model*

with ‘dispersion parallel to diffusion’ in this section, because it is not exactly described by Eq. (7.35).

We will explain how to make use of results from §7.1. There several results were obtained for the relationship between the boundary flux J in steady state, and the difference in concentration between bulk and surface based on solving Eq. (7.11) with the boundary condition at the surface $J = -D \cdot \partial c / \partial x|_*$ (and $\partial c / \partial x = 0$ far away). First of all, terms J in the expressions in §7.1 must be replaced by $-D \partial c / \partial x|_*$, and we must interpret D now as D_{hm} . Then we have an expression for $c^* - c_\infty$ versus $\partial c / \partial x|_*$ based on Eq. (7.11) with D replaced by D_{hm} . Next we need to know what is $\partial c / \partial x|_*$ in the new model for a binary salt, as function of current, J_{ch} , transport numbers at the surface, T_i , ion valencies, and ion diffusion coefficients. This is the step we make next.

We can evaluate the expression for current density, Eq. (7.18), for a binary salt, use $J_{\text{ch}} = I/F$, assume electroneutrality, thus $\sum_i z_i c_i = 0$, make use of $z_-^2 = |z_-|^2$, define c again as the ‘monovalent equivalent’ salt concentration, and thus obtain

$$J_{\text{ch}} = -(D_+ - D_-) \frac{\partial c}{\partial x} - (z_+ D_+ + |z_-| D_-) c \frac{\partial \phi}{\partial x}. \quad (7.36)$$

Free diffusional potential. When current density J_{ch} is zero, we can derive what is the potential gradient that develops when the asymmetric salt diffuses through ‘free’ solution, or through a porous medium without fixed charges. This ‘free diffusional potential’ (Sasidhar and Ruckenstein, 1982; p. 351)⁴ can be derived from Eq. (7.36) by setting J_{ch} to zero, leading to

$$\frac{\partial \phi}{\partial x} = - \frac{D_+ - D_-}{z_+ D_+ + |z_-| D_-} \frac{\partial \ln c}{\partial x} \quad (7.37)$$

which can be integrated from a position I to II, leading to

$$\phi_{\text{II}} - \phi_{\text{I}} = - \frac{D_+ - D_-}{z_+ D_+ + |z_-| D_-} \ln \frac{c_{\text{II}}}{c_{\text{I}}} \quad (7.38)$$

which we can also rewrite to

$$c = c_\infty \cdot \exp(-\alpha \phi) \quad (7.39)$$

where we replaced c_{II} by just c , c_{I} by c_∞ , set $\phi_{\text{I}} = 0$, replace ϕ_{II} by ϕ , and use $\alpha = (z_+ D_+ + |z_-| D_-) / (D_+ - D_-)$. Eq. (7.39) seems similar to the Boltzmann equation, Eq. (2.2), but this similarity is only superficial and is not real. Because the Boltzmann

distribution exists independent of diffusion coefficients, while here the sign of $D_+ - D_-$ determines the slope of the potential change versus the concentration change, setting this slope to negative, zero, or positive. This different dependence on diffusion coefficients, shows that there is no relation between Eq. (7.39) and Boltzmann's law.

Second, we make use of the definition of the transport number, $T_i = z_i J_i / J_{\text{ch}}$, which we combine with Eq. (7.2) evaluated for one of the ions (we choose the cation), and then combine with Eq. (7.36), resulting finally in

$$\frac{\partial c}{\partial x} \cdot (T_+ D_- + T_- D_+) = c \frac{\partial \phi}{\partial x} \cdot (|z_-| D_- T_+ - z_+ D_+ T_-) . \quad (7.40)$$

This we combine again with Eq. (7.36), resulting in

$$J_{\text{ch}} = - \frac{D_+ D_- (z_+ + |z_-|)}{|z_-| D_- T_+ - z_+ D_+ T_-} \cdot \left. \frac{\partial c}{\partial x} \right|^* = -c \frac{D_+ D_- (z_+ + |z_-|)}{D_- T_+ + D_+ T_-} \cdot \left. \frac{\partial \phi}{\partial x} \right|^* \quad (7.41)$$

reiterating that index * refers to a position at the surface. This general relationship provides for any binary $z_+ : |z_-|$ salt the required boundary condition for $\partial c / \partial x|^*$ at the surface as function of current density J_{ch} , transport numbers, and ion diffusion coefficients and valencies.

Thus when in a certain experiment with a certain binary salt solution we know J_{ch} and the T_i 's, we can use Eq. (7.41) to calculate $\partial c / \partial x|^*$, which is then equal to the related expression for J_i / D_{hm} from §7.1. Below we provide examples of how this works out exactly, but first let us discuss certain simplifications of Eq. (7.41).

As a first simplified case of Eq. (7.41), we can assume that the surface is only accessible to cations (i.e., only cations can cross the surface), and thus we have $T_+ = 1$ and $T_- = 0$ there, and then the general expression, Eq. (7.41), simplifies to

$$J_{\text{ch}} = - \frac{z_+ + |z_-|}{|z_-|} D_+ \left. \frac{\partial c}{\partial x} \right|^* \quad (7.42)$$

which shows that for a certain current density the concentration gradient in solution next to a selective interface (for instance a membrane or electrode) only depends on the diffusion coefficient, D , of the ion that goes through the interface, and not on D of the ion that is blocked.^{viii} For a given current density, the resulting concentration gradient also depends on the valencies of both ions. Note that this result that J_{ch} is independent of D_{coion} , as Eq. (7.42)

^{viii}Eq. (7.42) is the same as Eq. (72-11) in Newman (1983) when we use $u_i \propto D_i$. Note that in Newman, $\nu_+ z_+ = 1$.

shows, is only correct for a membrane or electrode that completely blocks the coions, and is only valid at the very interface. Eq. (7.42) is also valid away from the interface but then only in the simple DBL model of §7.1.1 for steady state. It is not valid away from the surface for the models that include refreshment if only because transport numbers T_i gradually change from their values at the surface (which relate to the selectivity of the interface) to values in bulk where they are equal to the transference numbers, t_i .

For a 1:1 salt, Eq. (7.42) simplifies to the classical result

$$J_{\text{ch}} = -2D_+ \left. \frac{\partial c}{\partial x} \right|^* \left(= -2cD_+ \left. \frac{\partial \phi}{\partial x} \right|^* \right) \quad (7.43)$$

which illustrates that the cation flux (which is equal to the current density, J_{ch} , in this case of a perfectly selective interface) is twice the flux by molecular diffusion, and twice the Ohmic transport of cations. Thus the cation flux is now for 50% due to diffusion, and for 50% due to electromigration. The electrical field that drags the cations (counterions) to and through the surface (which leads to the Ohmic contribution to cation transport), also pushes the coions away from the surface. This leads to the salt concentration near the surface to go down until the concentration gradient becomes steep enough that diffusion attracts the coions with the same force as the force of the electric field pushes them away. That concentration profile –with the concentration now decreasing towards the interface– now acts as a diffusional driving force for the counterions towards the surface. The end result is that the counterion has a twice larger flux than one would guess based on Ohm's law only and assuming only cations to be mobile charge carriers. Instead, the coions, even if they don't go through the interface, play a role, are coupled to the counterions, and for a given current they reduce the voltage drop over a film or channel by a factor of 2 compared to the case that they would be fixed in space, homogeneously distributed. For a 2:1 salt and again a membrane which does not allow anions through, the proportionality between J_{ch} and $-D_+ \partial c_+ / \partial x$ (with $c_+ = c/z_+$) is not 2 but 6. For a 1:2 salt it is a factor 1.5 ($c_+ = c$).

The examples here for an interface that only allows cations through, can be easily modified to represent the opposite case of an interface only allowing access to the anions, by replacing each z_+ by $|z_-|$, and vice-versa. To derive these equations, it is best to start again at Eq. (7.41).

A different simplification is when we have a symmetric $z:z$ salt, with equal diffusion coefficients, $D = D_{\text{hm}}$, but the surface is no longer perfectly selective to one of the ions. We then simplify Eq. (7.41) to

$$J_{\text{ch}} = -\frac{2D}{T_+ - T_-} \left. \frac{\partial c}{\partial x} \right|^* \quad (7.44)$$

and, interestingly, this relationship is independent of the ion valency, i.e., Eq. (7.44) is

equally valid for a 1:1 and a 2:2 salt. Note that for a 2:2 salt, concentration c is twice higher than the salt concentration.

As explained, an important application of the above expressions for J_{ch} as function of $\partial c/\partial x|_*$ is that it allows us to generalize results from §7.1. Thus, for instance, we can use Eq. (7.13) for the convection-along-the-surface-with-constant- τ -model, implement $J = -D_{\text{hm}} \cdot \partial c/\partial x|_*$, and have $\partial c/\partial x|_*$ replaced by an expression involving J_{ch} and the T_i 's based on any of the expressions just discussed, such as Eq. (7.41) in the general case.

Here let us analyze the example of a solution of a 1:1 salt, with equal diffusion coefficients, $D = D_{\text{hm}}$, based on Eq. (7.44). We use Eq. (7.13) and then arrive at

$$J_{\text{ch}} = \sqrt{\frac{D}{\tau}} \cdot \frac{2}{T_+ - T_-} \cdot (c_\infty - c^*) . \quad (7.45)$$

In a different example, again for a 1:1 salt, but now with unequal diffusion coefficients, for a perfectly selective interface (only allowing cations through, thus $T_+ = 1$), combination of Eqs. (7.13) and (7.42) leads to

$$J_{\text{ch}} = 2 \sqrt{\frac{D_+}{\tau}} \sqrt{\frac{D_+}{D_{\text{hm}}}} \cdot (c_\infty - c^*) \quad (7.46)$$

which interestingly still includes a dependence on the coion (anion) diffusion coefficient (via D_{hm}). There will not be such an influence of the coion when we use the classical film model without a refreshment effect from §7.1.1. The two last expressions lead to the same result when we set $T_+ = 1$ and $T_- = 0$ in the first, and $D_{\text{hm}} = D_+ = D$ in the second expression.

Note that when expressions similar to Eqs. (7.45) and (7.46) are derived for 2:1, 2:2, etc., salts, that c_∞ and c^* again refer to bulk and surface, but they are not the salt concentration, in the way that throughout this book c_∞ is defined as a salt concentration of a 1:1 salt. Instead they are monovalent equivalent salt concentrations.

7.5 Simplified solutions for a symmetric 1:1 salt

In this section we consider the simplified situation of a 1:1 salt with the anion and cation having the same diffusion coefficient, D . We first consider the situation of the simple film layer as described in §7.1.1. The current density running across the DBL is given by the general equation, Eq. (7.41), which we solve for $z_+ = |z_-| = 1$ and $D = D_- = D_+$, resulting in

$$J_{\text{ch}} = -\frac{2D}{\lambda} \frac{\partial c}{\partial x} \quad (7.47)$$

where we implemented Eq. (7.25) for current efficiency, λ . And thus according to Eq. (7.24), the ions flux across the DBL is given by

$$J_{\text{ions}} = -2D \frac{\partial c}{\partial x} \quad (7.48)$$

a result we can also have arrived at from adding up J_+ and J_- , based on the NP-equation without convection, Eq. (7.2). We can then integrate Eq. (7.48) across the film layer, thus from bulk to surface, and obtain

$$J_{\text{ions}} = 2 k_L (c_\infty - c^*) \quad (7.49)$$

where as before $k_L = D/\delta$, and δ is the thickness of the film layer (DBL), and c^* is the salt concentration at the surface.

We can also derive an expression for current density from Eq. (7.2) based on $J_{\text{ch}} = I/F = J_+ - J_-$, resulting in

$$J_{\text{ch}} = -2 D c \frac{\partial \phi}{\partial x} \quad (7.50)$$

which can be combined with Eq. (7.47) which then results in

$$\lambda = \frac{\partial \ln c}{\partial \phi} \quad (7.51)$$

and if λ is the same at all positions in the film layer (which is the case for the simple film model of §7.1.1), then Eq. (7.51) can be integrated over the DBL to^{ix}

$$c^* = c_\infty \cdot \exp(\lambda \phi_{\text{dbl}}) \quad (7.52)$$

where ϕ_{dbl} is the potential across the film layer (potential at surface minus that in bulk).

These equations define transport in the film layer, or DBL, when diffusion and electromigration are both important driving forces. In combination with knowledge of ion reactions at the surface, or transport through it, for instance because of a membrane, the factor λ is established at that position, and for a given current J_{ch} we then know J_{ions} , and the above equations provide information on the surface concentration c^* , and potential drop over the DBL.

We can integrate Eq. (7.47) across the film and obtain

$$J_{\text{ch}} = \frac{2k_L}{\lambda} (c_\infty - c^*) \rightarrow c^* = c_\infty - \frac{J_{\text{ch}} \delta}{2D\lambda}. \quad (7.53)$$

^{ix}This equation is an extension of Eq. (2.118b) in Vetter (1967). Many of the equations in the present and former sections can be found there.

If both λ and current J_{ch} are positive, then Eq. (7.53) predicts that the surface concentration is lower than the bulk concentration, thus the concentration of both ions goes down towards the membrane. For a current J_{ch} that is positive in the direction to the surface, the potential over the DBL, ϕ_{DBL} is negative which inspection of Eq. (7.50) also shows, and then Eq. (7.52) shows the same, that for $\lambda > 0$, that $c^* < c_\infty$. This decrease in salt concentration towards the surface is indeed the general observation in (models of) electro dialysis (ED) for the concentration profile of ions near a membrane in the diluate channel. The case of positive J_{ch} and positive λ relates to the surface being a cation exchange membrane. For an anion-exchange membrane, both J_{ch} and λ are negative and again we have the concentration going down towards the membrane in the diluate channel. In the concentrate channels the situation is reversed, and at the membranes the salt concentration is higher than in the center of the flow channels.

If we consider the case of $\lambda = \pm 1$, we have a perfectly selective interface that only allows one type of ion to go through. Then J_{ions} only has a contribution from the ion that reacts at, or moves through, the surface. This ion we can call the counterion. The other ion is the coion and this ion cannot cross the interface, and thus it is at equilibrium throughout the DBL, and thus its concentration profile must follow Boltzmann's law. With $\lambda = 1$ and $J_{\text{ch}} > 0$, then anions are the coions, thus Eq. (7.52) should be the Boltzmann equation for anions, which indeed it is. If the membrane only allows anions through, then $\lambda = -1$ and now Eq. (7.52) results in the Boltzmann distribution for cations. Thus for a perfectly selective surface, the Boltzmann relation is established for the coions over the entire film layer. Note that this is only the case in the classical DBL model of a fixed thickness, that was explained in §7.1.1.

Next we continue with models in which a dispersion effect is included by the refreshment concept of adding a term $(c - c_\infty) / \tau$ in the salt mass balance that was explained in §7.1.3. For neutral solutes this led to the same relationship between J_i and surface concentration as for the standard film model, just with a different definition of k_L . That will then also be the case for a 1:1 salt solution, thus Eq. (7.53) is again valid. But the concentration and voltage profiles are now different. Compared to the basic film model of §7.1.1 where transport is across a layer of thickness δ , the result we arrive at is more elegant because it integrates simultaneously over the entire bulk phase (such as a channel) and the DBL, without an ad hoc dividing plane.

To find the potential across a channel including the DBL, we use Eq. (7.10) in which we implement Eq. (7.47), resulting in

$$c(\tilde{x}) = c_\infty - \frac{J_{\text{ch}} \lambda}{2k_L} \cdot \exp(-\tilde{x}/\delta) \quad (7.54)$$

where $k_L = \sqrt{D/\tau}$ and $\delta = \sqrt{D\tau}$. Eq. (7.54) can be implemented in Eq. (7.50)^x to obtain an expression for the potential, ϕ_{ch} , across a layer or channel with thickness L_{ch} , as function of the current density (directed across the channel) and salt concentration c_∞

$$\phi_{\text{ch}} = -\frac{J_{\text{ch}}}{2k_L c_\infty} \left(\frac{L_{\text{ch}}}{\delta} - \ln \left(1 - \frac{\lambda J_{\text{ch}}}{2k_L c_\infty} \right) \right). \quad (7.55)$$

This ϕ_{ch} is the total voltage drop across the channel, all the way up to the surface; thus it includes the DBL. For low currents, Eq. (7.55) simplifies to

$$\phi_{\text{ch}}|_{\text{Ohmic}} = -\frac{J_{\text{ch}}}{2k_L c_\infty} \frac{L_{\text{ch}}}{\delta} = -\frac{J_{\text{ch}} L_{\text{ch}}}{2D c_\infty} \quad (7.56)$$

which describes the Ohmic potential drop over a channel with concentration c_∞ , independent of refreshment parameters such as τ and δ . In the other limit, Eq. (7.55) leads to a limiting current (LC). For $\lambda = \pm 1$ we arrive at $J_{\text{ch,LC}} = \pm 2k_L \cdot c_\infty$. When the current density approaches this limit, the potential drop over the entire layer, ϕ_{ch} , diverges.^{xi}

In Fig. 7.3 we provide calculation results for voltage versus current across a channel of thickness L_{ch} for a 1:1 salt that is next to a perfectly selectivity interface ($\lambda = 1$). [These results also apply to a ‘half-channel’ with a symmetry plane, with a surface on both sides, as in the diluate channel in the ED-process.] We use the refreshment model, Eq. (7.55), scaled to the Ohmic voltage drop given by Eq. (7.56). We use a value of δ that is 10% of the channel thickness L_{ch} , and we scale J_{ch} to $J_{\text{ch,LC}}$. We also plot the result for the standard DBL model given by Eq. (7.52) for a DBL of thickness δ , to which we must add the Ohmic voltage drop across the remaining channel of thickness $L_{\text{ch}} - \delta$. The standard model with fixed film layer thickness predicts a lower voltage across the channel than Eq. (7.55). This can be understood because in the standard film model 90% of the channel is at the bulk salt concentration, and only 10% is perturbed, while in the refreshment model, the decrease in salt concentration penetrates further into the channel, i.e., the average salt concentration will be somewhat less, implying a higher resistance across the full channel thus a higher voltage. For low currents, the slope of $\phi_{\text{ch}} / \phi_{\text{ch}}|_{\text{Ohmic}}$ vs. $J_{\text{ch}} / J_{\text{ch,LC}}$ in the refreshment model is given by δ / L_{ch} , which in this calculation then has a value of 0.1. The standard film model has a slope in this limit that is exactly half that value. This difference has the consequence that if a transfer coefficient, k_L , is derived on the basis of (the deviation from linearity of) a curve of

^xThis equation is also valid with refreshment included, see Eq. (7.36) for the case considered of a 1:1 symmetric salt.

^{xi}For the refreshment model with variable τ of §7.1.4, the $c(z)$ -function is given by Eq. (7.17) which can be implemented in Eq. (7.50) and then integrated to obtain an expression for ϕ_{ch} . This is possible but the result is a very lengthy expression.

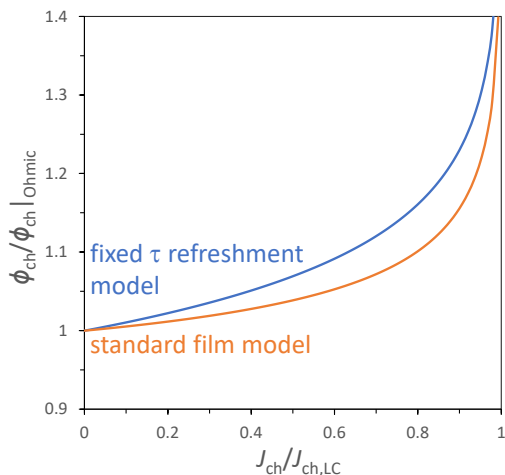


Fig. 7.3: The voltage across a channel that has a selective interface on one side, as function of current density, according to the standard film model, and based on the fixed- τ refreshment theory. For parameter settings see main text.

voltage versus current in the limit of low currents, that we obtain a difference by a factor of two in the predicted value of k_L , depending on the chosen model. The standard film model with fixed thickness would lead to the prediction of a twice lower k_L than when the same data of voltage vs. current are analysed using the constant- τ refreshment model.

7.6 Electrolytic conduction across a planar channel

To illustrate the concepts of previous sections, we will analyze the transfer of charge across a planar channel, a classical experiment in electrochemical engineering, relevant for many applications, for instance metal plating and Li^+ -ion batteries. It is also a good example to show the results of the theory for ion transport and dispersion, and how it affects transport numbers. We discuss the problem of a metallic cation dissolving from one electrode and depositing on the other, with a fixed total concentration of anions in the gap (channel) in between the two electrodes. This problem is discussed for Cu^{2+} dissolution and deposition in Newman (1983), and for Li^+ -ion transport in Lacey (2017). For simplicity, we discuss in this section a system with all ions monovalent, as for the LiX solution described by Lacey (2017).

We first discuss the case of this 1:1 salt without dispersion, thus we only have diffusion

and migration. The two electrodes are planar and parallel and the x -coordinate runs at right angles from the one to the other electrode. We describe the system as if the Li-metal dissolves from one electrode and deposits on the other. In reality in a Li^+ -ion battery, there is no dissolution, but instead Li^+ -ions desorb from and absorb in porous battery electrodes. Thus, we apply a constant current I leading to a flow of Li-ions from one to the other electrode. The total amount of anions in the gap in between the electrodes is conserved, i.e., $\int_0^L [X]dx = L c_0$ with L the width of the gap.

In this theoretical calculation the transport numbers at the two surfaces are $T_+ = 1$ and $T_- = 0$. (With porous battery electrodes on each side of the channel we will not have these ideal numbers.) Based on Eq. (7.43) we then know the gradients in concentration at the two surfaces, only dependent on the cation diffusion coefficient. In between the surfaces we use the salt balance, Eq. (7.29) (with $v_F = 0$ and no refreshment). This salt balance immediately makes clear that in the steady-state the concentration changes linearly. This means that at any position in the channel the concentration gradient will be the same as at the surfaces, thus independent of the anion diffusion coefficient. The anion diffusion coefficient only influences the dynamic part of this process, but not the final steady-state behaviour.

Next we present results for concentration profiles and transport numbers for $D_+ = D_-$, and thus the transference number of both ions is $t_+ = t_- = 1/2$. Results are presented in Fig. 7.4. As discussed in the previous section (and by Newman, 1983), at the start of this process the fraction of the current carried by the two ions is described by their transference number, t_i , but this is no longer the case when concentration gradients develop. When we reach steady state, the transport number of the cation is unity, $T_+ = 1$, at each position in the channel, and for the anion, the transport number has become zero, $T_- = 0$, everywhere. We show the changes in T_- with position and time (T_+ always given by $1 - T_-$) in Fig. 7.4B.

Across the midplane of the channel, concentration profiles are exactly ‘point-symmetric’, with concentrations increasing on the anode, and decreasing on the cathode in an exact mirror-image, also when $D_+ \neq D_-$, like shown in Fig. 7.4A. Initially, we have concentration profiles ‘growing’ from the electrodes into solution, until they ‘meet’ in the middle. In steady state, we arrive at a linear concentration profile, also when $D_+ \neq D_-$. At the midplane, concentrations remain the same as initially, also when $D_+ \neq D_-$.

For equal anion and cation diffusion coefficients, there is an analytical solution for $c(x, t)$ given as Eq. (15) in Van Soestbergen *et al.* (2010). Here, however, we numerically solve the equations: the salt balance, the charge balance, and the boundary conditions for $\partial c / \partial x$ vs. current J_{ch} . We choose a current such that in steady state we just reach the limiting current, i.e., the concentration eventually reaches zero at the cathode, which is on the right in Fig. 7.4A. With that choice, the entire problem is defined.

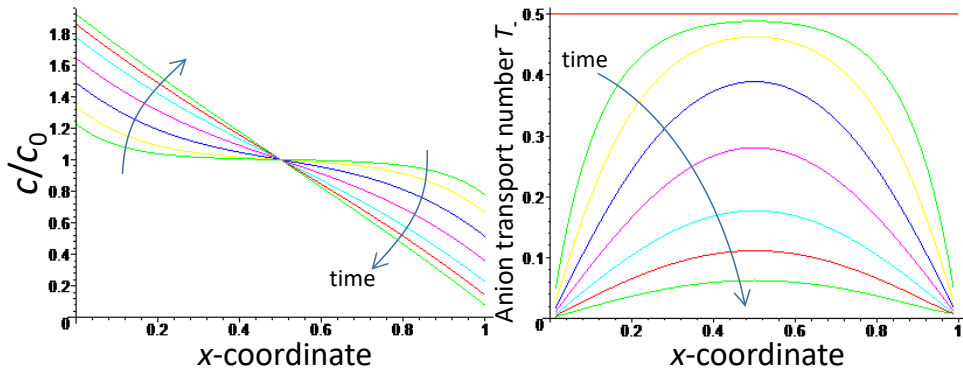


Fig. 7.4: Electrolytic conduction, i.e., the development of concentration profiles across the gap between anode and cathode which are perfectly selective for cations (all ions monovalent; current density equal to the limiting current).

On the anode the salt concentration increases, and on the cathode it goes down, to finally reach a linearly decaying profile in salt concentration. The transport number of the anion, T_- , is plotted in Fig. 7.4B, and we note how it quickly drops from the initial value of $T_- = 0.5$ to values close to zero after some time. The profiles for the cation transport number are a mirror image (vertically mirrored across the horizontal line at $T = 0.5$), and starting at $T_+ = 0.5$ they increase to ultimately reach $T_+ = 1.0$ after some time. Interestingly, these curves for the transport number are symmetric across the midplane of the channel, even though the concentration profiles are not, and neither is the potential profile symmetric. This potential profile decays from left to right, going down steeper and steeper. Still, the plots for the transport numbers vs. position (at various moments in time) remain perfectly symmetric (between left of the midplane, and right of the midplane). This is even the case when the two ions have different diffusion coefficients, which to us is not an immediately intuitive outcome. [With different diffusion coefficients only the ‘starting value’ of T_i shifts. This can be easily derived because at time zero, $T_i = t_i$, and t_i depends via Eq. (7.21) on the diffusion coefficients of the two ions.]

Next we implement dispersion as an additional effect, as also addressed by Newman (1983, p. 11). We implement dispersion by adding to the mass balance the refreshment effect, $(c_0 - c) / \tau$, due to flow parallel to the surface, see §7.1.4. We assume that the parallel fluid velocity, v_{\parallel} , has a parabolic profile, starting at zero at the walls, with a maximum in the middle of the channel. Thus at each point, the salt is mixed up with the average value, c_0 , with a frequency that has a maximum in the middle of the channel and decreases to zero

at the two electrodes.

The outcome is presented in Fig. 7.5A which shows that the higher the refreshment of fluid and ions, the closer the anion transport number remains to the maximum value, which is given by the transference number, which in this case is $t_+ = 0.5$. But in all cases, near the sides of the channel the transport number for the anions drops to zero, also for a high refreshment rate. The profiles remain left-to-right symmetric across the midplane. When we reduce the anion diffusion coefficient, the transport number for the anion decreases, but the profiles of transport number are still symmetric with the maximum for T_- in the center of the channel (and here is the minimum for T_+).

The voltage across the channel (analysed as a positive number) goes down if the refreshment rate (the degree of dispersion) goes up. In the steady state, without any dispersion this voltage becomes infinite because we work at the limiting current, while dispersion leads to a steady drop in voltage the more we mix, though after some point the further reduction in voltage becomes very minor. When we reduce the diffusion coefficient of the anion (for a certain degree of dispersion) the voltage increases (the resistance of the solution goes up), also in steady state. Thus, while without dispersion the anion diffusion coefficient does not play a role in determining the steady state profiles (and neither does it have an effect on the voltage across the channel), it does play a role when there is some mixing.

Effect of indifferent salt. A related topic is the effect of added inert, or ‘indifferent’ salt. Inert salt is added in many electrochemical experiments to reduce voltages across a channel. We make several calculations extending on the example just discussed. In the calculation we add an extra cation that is inert, while for charge balance more (of the same, inert) anions are added. [Note that a very different outcome would be obtained when a third ion (either anion or cation) is added that has zero mobility, i.e., an ion which is homogeneously distributed across the channel. That would actually be a model for flow of ions across a charged gel or membrane.] Theoretical analysis is not straightforward because we have many variables to consider: concentrations, diffusion coefficients, type and intensity of dispersion. . . Some key results we obtain are as follows:

1. In all calculations, the transport number for the anion remains symmetric around the midplane, behaving similarly as above, dropping to zero over time in a calculation without dispersion, and remaining at higher values (except near the surfaces) when there is dispersion.

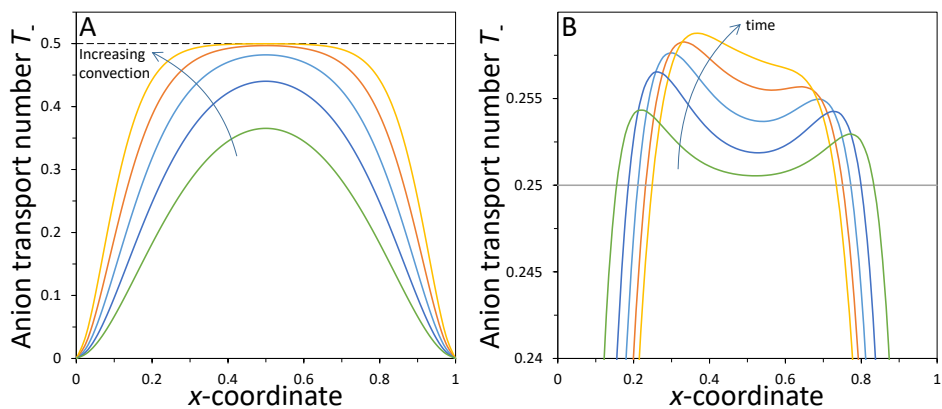


Fig. 7.5: Anion transport number, T_- , for electrolytic conduction of a cation across a channel between two electrodes. a) Steady state profiles at various degrees of refreshment (convective mixing), described by a parabolic profile for the flow velocity along the electrodes. With increasing refreshment, the anion transport numbers more closely approach the maximum value, which is equal to the anion transference number $t_- = 0.5$. (Except for refreshment (convective mixing), this is the same calculation as Fig. 7.4.) b) Development in time of T_- in a three-ion system with an alternative, realistic, mixing model where salt and water are exchanged between positions equally far from the electrode that are on either side of the channel. In this case the transference number is $t_- = 0.25$ while the transport number, T_- , can be both larger and smaller than t_- , and exhibits very non-monotonic profiles.

2. Now with a second cation, the transport number profiles for the cations can become asymmetric.
3. In a small channel, when there is not much mixing, or none at all, adding salt reduces the electric field, which thus reduces the migration term for the reactive cation, and as a consequence—for the same current—its concentration profile must become steeper, and thus the limiting current decreases, i.e., certain high values of current can no longer be realized. (Interestingly, this limiting current in the reactive cation is now arrived at without the voltage across the channel diverging.) Nevertheless, adding this indifferent salt, for any current that can be realized, we obtain a lower voltage.
4. For wider channels, with mixing, adding salt reduces the voltage across the channel for the same current.

An alternative dispersion model for a rotating electrode pair. Interestingly, the calculation with three ions leads to slight errors when dispersion is included, which was considered by adding the term $(c_{0,i} - c_i) / \tau$ to each ion's individual mass balance, where $c_{0,i}$ is the initial concentration in the channel. This works fine, but an interesting effect is that the total amount of the two cations in the channel will no longer be equal to the initial value. This is due to concentration profiles no longer remaining point-symmetric across the midplane. This is fine if the model is meant to represent a channel flow through from a larger container. But otherwise, there are two alternatives. The first is that we do impose mass conservation in the channel, and thus have the convective outflow, which is the term $-c_i / \tau$, slightly corrected by a factor α (the same across the channel, varying in time), such that this convective outflow exactly equals the total inflow, which is always $c_{0,i} / \tau$. The second option is much easier. And this second option is representative of the circulation patterns that are possible between two electrodes when the inner electrode rotates (Newman, 1983). What we do in this second option, mathematically, is to have the fluid (and the ions inside any volume of fluid) at a distance δ from the one electrode, mix with fluid located at the same distance δ from the other electrode. The mixing frequency is related to the velocity profile in the direction parallel to the surface, v_{\parallel} . This velocity, as before, will be zero at the electrode surface, and now is also zero in the center of the channel; thus we assume a parabolic profile in one half of the channel, as well as in the other half, thereby representing the flow pattern presented on p. 7 in Newman (1983). This second model is easily implemented in our numerical code and then works flawlessly. Interestingly, with this corrected model, that keeps all

salt in the channel (no exchange with an outside reservoir), the transport numbers, for instance for the anion, can be both larger and smaller than the transference number, see Fig. 7.5B for one particular example calculation (details [here](#)) in which all three ions have different diffusion coefficients. Fig. 7.5B shows interesting non-monotonic and asymmetric profiles in T_- , until steady state is reached. In steady state, the profile in T_- is symmetric across the midplane with a single maximum value at that position which is around 6% larger than t_- . For the two cations the profiles in transport number are asymmetric during the lead-up to steady state as well as in steady state.

7.7 Transient solute transport to an interface for electrolyte solutions

In §7.1 we discussed boundary layer models for steady state transport towards a selective interface. Dynamic transport was discussed in §7.6 for flow across a channel. In the present section we discuss transient (dynamic, time-dependent) transport in DBL models, thus extending the results of §7.1.

Let us analyze the dynamics of the salt balance, Eq. (7.29), for transport towards a selective interface from a bulk phase that is sufficiently large. We first consider the simplest case of no refreshment (no convection along the surface), thus we have to solve Fick's second law, $\partial c/\partial t = D \cdot \partial^2 c/\partial x^2$, often associated with flow of neutral solutes. But because of the results in §7.2, we know we can apply Fick's law also to any binary salt, symmetric and asymmetric, when we make use of the harmonic mean diffusion coefficient, D_{hm} .

In the context of neutral species, an important dynamic situation involving Fick's second law is the response of the system after a sudden step change in surface concentration. The resulting 'penetration theory' describes the flux at the surface $J = -D \cdot \partial c/\partial x|_*$ as function of the suddenly applied step change Δc . Interestingly, the result of this calculation does not depend on 'where we are in the c -range,' but solely the step change Δc matters, i.e., the value by which the surface concentration is suddenly increased or decreased compared to the concentration c_∞ in a far-away bulk phase. The resulting expression for flux at the surface is then

$$J = \pm \sqrt{\frac{D}{\pi t}} \Delta c \quad (7.57)$$

where t is time after the sudden step change. A step change downward (the surface concentration is suddenly lowered) of course leads to a flux towards the surface, and a step

change upward to flow away from the surface. Thus, as function of time t , the flux starts off infinitely high, and then drops down, ultimately to zero, because the concentration profiles extend further and further away, becoming more and more shallow. The concentration change at each distance x away from the surface, as a fraction of the applied step change Δc , is given by $\text{erf}\left(x/(2\sqrt{Dt})\right)$, where erf is the Error function. Note that penetration theory often uses the flux averaged from time zero to time t . This averaged flux is equal to twice the ‘instantaneous’ flux (i.e., the flux at any time t) that is given by Eq. (7.57).

When instead of a step change in concentration, a step change in boundary flux J is applied from time $t=0$ onward, the solution for the surface concentration vs. time is given by Sand’s equation

$$\Delta c = \pm 2J \sqrt{\frac{t}{\pi D}}. \quad (7.58)$$

In electrochemical processes, we often analyze the situation of a step-change in current J_{ch} from time $t=0$ onward (with current zero before $t=0$). As explained above, together with information on the transport numbers T_i (or λ for a 1:1 salt, and then $\lambda = T_+ - T_-$), we can convert this information into a concentration gradient at the surface, see Eq. (7.41). And results from §7.1 can be rewritten such that they apply to a binary salt solution, by making the replacements $J \rightarrow -D \partial c / \partial x|_*$ and $D \rightarrow D_{\text{hm}}$. Concentration c is the monovalent equivalent (m.e.) salt concentration.

For a 1:1 salt and a perfectly selective interface, i.e., an interface where only one type of ion reacts or moves across (the counterion, abbreviated as ‘ct’), we can use Eq. (7.43), and combination with Eq. (7.58) then results in

$$\Delta c = \pm \frac{J_{\text{ch}}}{D_{\text{ct}}} \sqrt{\frac{D_{\text{hm}}}{\pi}} t \quad (7.59)$$

which shows that the dynamics of the change in surface concentration depend on the diffusion coefficients of both ions, also the one that is completely blocked from the interface.

If we start at a concentration c_∞ , which is the unvarying bulk concentration, and if we remove counterions from solution through the interface for a fixed current (and $\lambda=1$), then the surface concentration drops, first fast then slower, and it reaches zero at the transition time, which we can calculate after rearranging Eq. (7.59) to

$$t = \left(\pi D_{\text{ct}}^2 c_\infty^2 \right) / \left(D_{\text{hm}} J_{\text{ch}}^2 \right). \quad (7.60)$$

At this time, the salt concentration at the interface reaches zero, and the voltage across the solution phase diverges. Measurement of this transition time can be helpful to establish ion

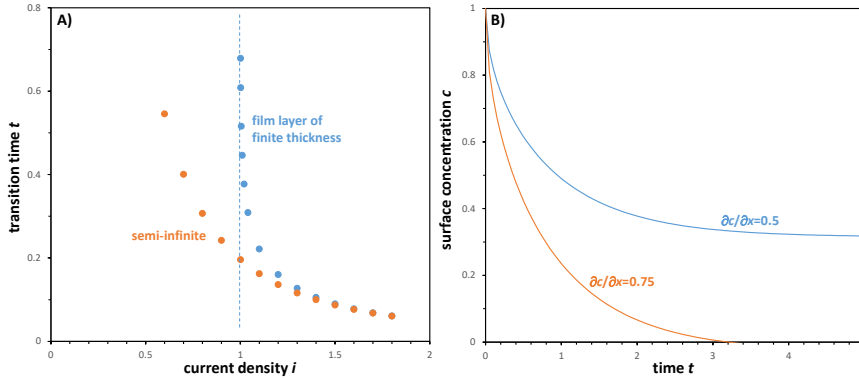


Fig. 7.6: Sand's equation for the transition time for diffusion to a surface. a) Qualitative illustration of the transition time for a semi-infinite layer of electrolyte solution (orange dots), as considered by Eq. (7.61), compared with the case of a film layer of finite thickness, according to Eq. (28) in Van Soestbergen *et al.* (2010) (blue dots). For currents below the limiting current, in this second case (blue dots), we never reach a surface concentration of zero. For high enough currents, the two calculations give the same result, with the transition time dependent on current to the power -2 . b) The surface concentration in a model with diffusion and dispersion with a variable refreshment time τ , all as function of time \tilde{t} . Only when the flux is high enough (resulting in a high enough value of $\partial\tilde{c}/\partial\tilde{x}$) will the concentration at the surface drop to zero at some point. All calculations are based on a 1:1 salt, equal D 's and current efficiency $\lambda=1$.

transport numbers when the measured time for the voltage to diverge is longer than predicted by Eq. (7.60).

Indeed, when the surface is not perfectly selective for counterions, and thus the transport numbers are not either 0 or 1, and when we have a 1:1 salt with both ions having the same diffusion coefficients, $D=D_{\text{hm}}$, then we can combine Eq. (7.44) with Eq. (7.59), and arrive for the relationship between transition time and transport numbers at

$$t = \pi D c_{\infty}^2 / ((T_+ - T_-) J_{\text{ch}})^2 . \quad (7.61)$$

Eq. (7.61) for the transition time predicts that at some time the concentration will always reach zero and the current will diverge, see the orange dots in Fig. 7.6A. This relates to the assumption that we have an unstirred bulk solution that extends to far away. It is, however, more realistic to consider a film layer with a certain thickness, or assume some dispersion. Then for currents that are too low, the concentration will never hit zero and the voltage will not diverge, see the blue dots in Fig. 7.6A. So in the latter case there is a minimum current

required to reach zero concentration after some time. For the standard film layer model with thickness δ , Eq. (28) in Van Soestbergen *et al.*, Phys. Rev. E **81**, 021503 (2010) is used, which as function of δ (for a 1:1 salt, equal ion diffusion coefficients, and for $T_{ct} = 1$), provides the relationship between transition time and current, see the blue dots in Fig. 7.6A.

Next we consider the case where in addition to diffusion and electromigration towards the surface we have dispersion described by the refreshment approach. Here we analyze the case that τ is a decreasing function with distance to the surface, see §7.1.4. For this model we can rewrite the salt balance, Eq. (7.29), to

$$\frac{\partial \tilde{c}}{\partial \tilde{t}} = \frac{\partial^2 \tilde{c}}{\partial \tilde{x}^2} + (1 - \tilde{c}) \tilde{x} \quad (7.62)$$

where $\tilde{c} = c/c_\infty$ and $\tilde{t} = t \cdot \sqrt[3]{D\gamma^2}$. For a given gradient $\partial \tilde{c}/\partial \tilde{x}$ at the surface –proportional to the applied current, J_{ch} , and also dependent on the counterion transport number, T_{ct} – we can analyze how \tilde{c} at the surface drops with time \tilde{t} , see Fig. 7.6B. Results here show that we do not reach a zero concentration at the surface when the current, thus $\partial \tilde{c}/\partial \tilde{x}$, is too low, but for a higher value of the current we do reach zero concentration at the surface after some time. When that happens, the voltage will steeply increase. If the aim is to avoid reaching this limiting situation, and when current is fixed, then we must reduce the mass transfer resistance, i.e., stir more (increase γ), or make the surface more leaky for coions, because that reduces T_{ct} .

This finalizes our discussion of diffusion and electromigration to a selective surface, such as an electrode or membrane, for steady state and for the dynamic approach to steady state, for arbitrary binary salt solutions (i.e., solutions with two ions that can have different valencies and/or diffusion coefficients). We also showed that when we have more than two ions, the situation can become drastically different, and for instance we can reach a limiting current in one of the ions, but not in other ion types.

Sand's equation with background salt. Note that we presented here results of concentration changes in time for an electrolyte with one type of anion and one type of cation, and we include all electric field effects. Instead, the classical analysis of the Sand equation and the transition time (e.g., Bard & Faulkner (1980) p. 252) is based on the absence of electric fields because of addition of indifferent background electrolyte, or because the species moving to the interface is neutral and therefore only experiences a diffusional force. This is why in that literature there is effectively a factor 2 difference with our equations, i.e., their results make use of $J_{ch} = -D_{ct} \partial c/\partial x|^*$. In addition,

because of neglecting electromigration, results in these literature sources never have an influence of the diffusion coefficient of the coion, or a dependence on transport numbers. In an electrochemical experiment indeed the electric field can be cancelled by adding ‘indifferent electrolyte’, but of course this is not generally advisable in an electrochemical process, for instance for water desalination with membranes.

7.8 From a force balance to the Nernst-Planck equation

In this section we explain how the velocity of solutes (such as ions) can be calculated from a force balance that includes all driving forces acting on a certain ion as well as all frictions it experiences with other species that surround it. Driving forces are for instance gradients in concentration and in electrical potential, but also gradients in the total pressure must be incorporated when ions have volume. These driving forces are balanced by friction of the ion with the fluid (often water), with the porous medium (such as the solid structure of a membrane), and with other dissolved solutes. We explain how under certain conditions this force balance simplifies to an extended NP equation including convection. This extended NP equation is used frequently throughout this book.

The molar fluxes of solutes are described by a balance of forces acting on the solutes that includes all driving forces acting on them, and at the same time includes frictions with the water, with other types of ions and solutes, and when flowing through a porous medium, friction with this medium. This friction-based approach for solutes and solvent in a porous medium dates back at least to Spiegler (1958). Fig. 7.7 illustrates the related terminology such as fluid, pore, and porous medium. To find the driving force on an ion or other solute we start with an expression for the chemical potential of an ion, μ_i , including ion entropy and charge, but also including the insertion pressure, i.e., the energy required to free up a volume v_i (the molar volume of the hydrated ions) against the total pressure, P^{tot} , and thus the total chemical potential is

$$\mu_i = \mu_{\text{ref},i} + \ln c_i + z_i \phi + \mu_{\text{exc},i} + v_i P^{\text{tot}} \quad (7.63)$$

where concentrations are defined per unit pore volume, and we leave out a gravitational/centrifugal contribution, an affinity term, and an ion-ion attraction energy discussed in §4.3. The driving force on an ion moving through a tortuous pore is given by the negative of the gradient in the chemical potential, $-\partial\mu_i/\partial x'$, where x' is a coordinate following the tortuous path of a pore, and this driving force is combined with all frictions

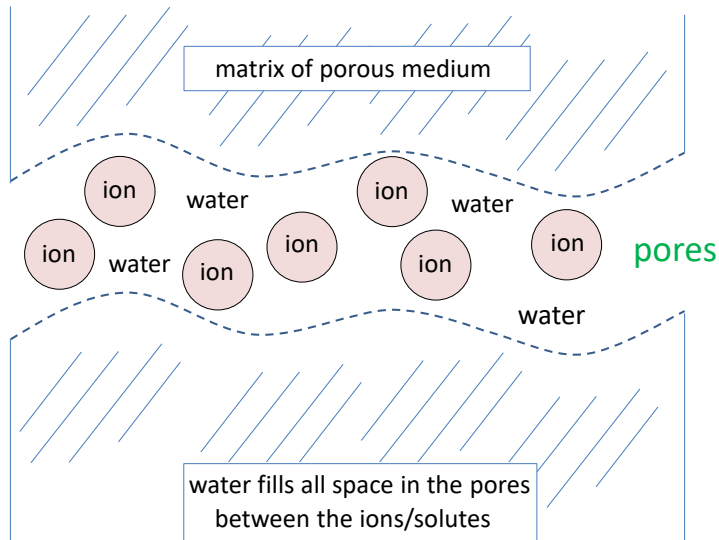


Fig. 7.7: Illustration of the terminology used to describe transport of solvent and solutes in a porous medium. Solutes, such as ions, flow through the pores in the porous medium (also called structure, or matrix), and all space around the solutes which is not occupied by the structure, is filled with solvent (fluid), often water. The porous medium can be a membrane, ion absorbent material, or a porous electrode. When water is the solvent, an ion will be hydrated. A bare ion together with its shell of tightly bound hydration water as a whole is called an ion. The solvent (for instance water) is 'free' and flows through all the space that is not occupied by the (hydrated) ions and other solutes, or occupied by the porous medium.

of the ion with all other phases, and these depend on the velocity difference between the ion and that phase, resulting in

$$-\frac{\partial \mu_i}{\partial x'} + \sum_k f_{i-k} (v'_k - v'_i) = 0 \quad (7.64)$$

where the summation over k is over all phases and species, including the solvent and the porous structure, and where f_{i-k} is a measure of the friction of a mole of ions i with all of phase k present. In Eq. (7.64) we introduce the notation $'$ for movement following a path through a tortuous pore. Velocities v'_k are 'real' interstitial velocities following this path.

When phase k is a species of which the concentration can change, such as for any of the ion types, it is relevant to make the frictional term proportional to the amount (concentration) of that species. Thus for ion-ion friction, acting between ion type i and k , in the force balance for ion type i , Eq. (7.64), f_{i-k} is made a linear function of the concentration of the other type of ion, k . Thus for ion-ion friction, in the force balance for species i , f_{i-k} is replaced by $\beta_{i-k} c_k$, where β_{i-k} is a constant, and c_k is the local concentration of the other solute. (In doing so, there will ultimately be one ion-ion friction coefficient for each ion-ion pair, i.e., $\beta_{i-k} = \beta_{k-i}$.) However, when the other phase 'is simply there', the use of f_{i-k} as a friction factor between ionic species i and that other phase, suffices. This applies for the friction with the porous medium, such as a membrane, and for friction with the fluid, because it surrounds all ions and solutes. There is no 'concentration' to speak of for these other phases. Indeed for friction of an ion with these two phases, there is no need to consider a proportionality with the 'concentration of the porous medium' or with 'the concentration of water'. The porous medium is just there, while each ion is always completely enveloped by water molecules. Of course, for friction of solutes with the porous medium, if we have an open structure with large pores, f_{i-m} will be much lower than for a tight structure with small pores, but for a given porous structure, f_{i-m} can be taken as a constant that describes the ion-matrix friction.

From this point onward, we first leave out ion-ion friction. Including that the porous medium has zero velocity, combination of Eqs. (7.63) and (7.64) results in

$$-\frac{\partial \ln c_i}{\partial x'} - z_i \frac{\partial \phi}{\partial x'} - \frac{\partial \mu_{\text{exc},i}}{\partial x'} - v_i \frac{\partial P^{\text{tot}}}{\partial x'} = -f_{i-F} (v'_F - v'_i) + f_{i-m} v'_i \quad (7.65)$$

where we include the excess term that describes volumetric interactions, and the insertion pressure of a solute that has volume. These last two terms on the left would be zero when we assume the ions to be point charges.

Effect of temperature on transport. We continue here a discussion of temperature effects set up for equilibrium (EDL theory) on p. 39. As explained above, the driving force on (a mole of) ions is minus the gradient of the chemical potential, and in that analysis we should multiply equations given above with the factor RT to obtain a driving force with the correct unit of N/mol, for instance in Eq. (7.65). Then the right side is also multiplied by RT and the resulting friction factors $RT f_{i-F}$ and $RT f_{i-m}$ do not have a specific relation to RT . Below we replace f_{i-F} with $1/D_i$ and thus D_i linearly increases with RT . Thus, in a typical NP equation, such as Eq. (7.67) below, diffusion coefficients linearly depend on temperature, T , and the origin of this effect is in a temperature dependence of driving forces, not in an intrinsic change to its mobility. In addition, there will be such an intrinsic effect because the viscosity of solvent decreases with temperature and thus mobility will go up. So a T -dependence of the diffusion coefficient combines an intrinsic increase in solute mobility, with the RT -term.

In the next step we multiply each side by c_i and we make the replacement $J'_i = v'_i c_i$, because the flux of an ion through a pore J'_i is equal to its own velocity v'_i times its concentration c_i . We make the replacement $f_{i-F} = 1/D_i$ for the ion-fluid friction, resulting in

$$-\frac{\partial c_i}{\partial x'} - z_i c_i \frac{\partial \phi}{\partial x'} - c_i \frac{\partial \mu_{exc,i}}{\partial x'} - c_i v_i \frac{\partial P^{tot}}{\partial x'} = -\frac{1}{D_i} (c_i v'_F - J'_i) + f_{i-m} J'_i \quad (7.66)$$

which we rewrite to an expression explicit in flux J'_i that is

$$J'_i = K_{f,i} c_i v'_F - K_{f,i} D_i \left(\frac{\partial c_i}{\partial x'} + z_i c_i \frac{\partial \phi}{\partial x'} + c_i \frac{\partial \mu_{exc,i}}{\partial x'} + c_i v_i \frac{\partial P^{tot}}{\partial x'} \right) \quad (7.67)$$

where (Spiegler and Kedem, 1966, Eq. 49)

$$K_{f,i} = 1/(1 + f_{i-m}/f_{i-F}) . \quad (7.68)$$

is a factor which describes the importance of ion-matrix friction relative to ion-fluid friction, with $K_{f,i} \rightarrow 1$ for very low ion-matrix friction, and $K_{f,i} \rightarrow 0$ when ion-matrix friction is very large.

In the next step, Eq. (7.67) –in which fluxes and velocities J'_i and v'_F are defined inside a tortuous pore– is converted to an expression with fluxes and velocities defined on the macroscopic scale of the porous material, v_F and J_i , which is the common usage of fluxes and velocities in this book. To this end, we implement that $J_i = J'_i \cdot p/\tau$ where p is porosity and τ is tortuosity. The latter describes that the path through a pore is longer than straight

across a material, because it is constantly at an ever-changing angle to a direct line that goes from one to the other side of a material. If there is a certain flux J'_i along that curvy path, it is less by a factor τ (with τ larger than 1) if we project on the direction straight through the material. The factor p for porosity enters because flux J'_i is per unit pore and with J_i we aim to describe the superficial flux (which is per unit geometrical, i.e., 'total' area). These conversions from J'_i to J_i also apply to the conversion from v'_F to v_F . But for the fluid, also a factor $1-\eta$ enters in the conversion, because inside the pores, a volume fraction η is blocked out for the fluid.^{xii} Thus the interstitial fluid velocity in the pore, along the pore direction, v'_F , relates to the superficial fluid velocity straight across the material, v_F , by $v_F = v'_F \cdot (1-\eta) \cdot p/\tau$. The final implementation is that the coordinate axis straight through the material is shorter than the curved path, and thus $\partial x = \partial x'/\tau$. If we include all of this in Eq. (7.67), we obtain the intermediate result that

$$J_i \frac{\tau}{p} = K_{f,i} c_i v_F \frac{\tau}{p(1-\eta)} - \frac{1}{\tau} K_{f,i} D_i \left(\frac{\partial c_i}{\partial x'} + z_i c_i \frac{\partial \phi}{\partial x'} + c_i \frac{\partial \mu_{\text{exc},i}}{\partial x'} + c_i v_i \frac{\partial P^{\text{tot}}}{\partial x'} \right). \quad (7.69)$$

Multiplying all sides by p/τ , and making use of the variable $\varepsilon = p/\tau^2$, we obtain the most general NP equation^{xiii,xiv}

$$J_i = \frac{K_{f,i}}{1-\eta} c_i v_F - \varepsilon K_{f,i} D_i \left(\frac{\partial c_i}{\partial x} + z_i c_i \frac{\partial \phi}{\partial x} + c_i \frac{\partial \mu_{\text{exc},i}}{\partial x} + c_i v_i \frac{\partial P^{\text{tot}}}{\partial x} \right) \quad (7.70)$$

where the fraction of the pores occupied by solutes is η and the porosity (fraction of total volume that is pores) is p . Fluxes are defined per cross-section of the total material (pores plus matrix), but concentrations are defined per volume of pore phase. Thus, a balance of forces acting on solutes inside a porous medium results in a general NP-equation that includes a group $K_{f,i}/(1-\eta) \rightarrow K'_{c,i}$ and $\varepsilon K_{f,i} \rightarrow K'_{d,i}$, where $K'_{c,i} > K'_{d,i}$. These latter K' -values have similarities to the convective and diffusive hindrance functions derived on the basis of hydrodynamic theories for transport of spherical particles through cylindrical pores, where also the term for convection is larger than for diffusion, as used for instance in SEDE theory (see next box).

If we neglect all possible solute volume effects, Eq. (7.70) simplifies to the extended NP

^{xii}The volume fraction η used here is different from η in Ch. 4 where it relates to the volume fraction of the immobile structure. Here it relates to the fraction of the pores (that themselves have a porosity p) that contains solutes.

^{xiii}Often this term τ^2 is replaced by τ and then called the tortuosity *factor*.

^{xiv}In this book we generally present flux expressions as if there is only one direction, x , to make the equations more insightful. The reader familiar with flow in multiple directions will understand that a gradient $\partial/\partial x$ can be generalized, for instance by using the notation ∇ .

equation

$$J_i = K_{f,i} c_i v_F - \varepsilon K_{f,i} D_i \left(\frac{\partial c_i}{\partial x} + z_i c_i \frac{\partial \phi}{\partial x} \right) \quad (7.71)$$

which is an equation we will use extensively throughout this book. When solutes have no direct friction with a porous medium, then $K_{f,i} = 1$ and Eq. (7.71) simplifies to Eq. (7.2). The complete transport model based on Eq. (7.71), partition functions such as Eq. (2.1), and solvent transport equations given by Eq. (8.2), is called the two-fluid model (TFM), and in the context of membrane transport is called the solution-friction (SF) model.

The DSP model for ion transport in membranes. When the model explained in this section for multicomponent transport of charged and uncharged species through a membrane (which is typically also charged) is combined with a description for the Donnan equilibrium at the membrane-solution interfaces, and also includes contributions to the partitioning of ions at these interfaces such as related to ion volume, as discussed in §2.2, §2.8, and §4.2, we end up with a model called the Donnan Steric (Partitioning) Pore model, or DSP model. The state-of-the-art version is called the extended DSP-model. This ext-DSP model also includes how membrane charge is a function of local ion concentrations (especially pH and absorbing ions such as Ca^{2+}) and also includes how ions react with one another in the pore space, as will be addressed in Ch. 10. For instance, the bicarbonate ion, HCO_3^- , can react with a proton to form carbonic acid, H_2CO_3 , and this reaction is included in the ext-DSP model. And many similar reactions can be included at the same time as well. Also the formation of ion pairs, for instance because Mg^{2+} reacts with Cl^- to MgCl^+ , can be included in the ext-DSP model, see Kimani *et al.*, *J. Chem. Phys.* **154** 124501 (2021), and references therein.

A different line of theory that was specifically developed for nanofiltration, is the SEDE model, which is a very detailed extension to the SF model, as explained in detail in Lanteri *et al.*, *J. Colloid Interface Sci.* **331**, 148–155 (2009). For a comparison of this SEDE model with the SF model of this section, see [here](#).

Finally we explain the theory to describe ion fluxes in five different cases. The first case we consider is to include ion-ion friction in addition to the other frictional forces. Leaving out all effects related to solute volume, we then have an implicit relationship for ion flux,

given by^{xv}

$$f_{i-m}J_i - f_{i-F}(c_i v_F - J_i) - \sum_k \beta_{i-k}(c_i J_k - c_k J_i) = -\varepsilon \left(\frac{\partial c_i}{\partial x} + z_i c_i \frac{\partial \phi}{\partial x} \right) \quad (7.72)$$

where the summation runs over all ion types k that are present. For any problem with k ions, Eq. (7.72) can be inverted resulting in expressions where each flux J_i , with i running from 1 to k , is made an explicit function of the gradients in ion concentration, potential, and of fluid velocity, v_F , but is then no longer related directly to the other fluxes. However, because this problem will be solved numerically anyway –by first discretizing along the space coordinate, which results in several algebraic equations at each gridpoint which are then jointly solved for all gridpoints, together with all boundary conditions, see Ch. 21– there is no use for this mathematical inversion procedure.

The second extension of the theory is with the ion-ion Coulombic energy that was discussed in §4.3. For a 1:1 salt this extra contribution is given by Eq. (4.26), and we can include that in Eq. (7.63). We evaluate the force balance, Eq. (7.64), for a solution inside a porous medium, and we make the following assumptions: no friction of solutes with the porous medium, thus $K_{f,i} = 1$, no ion-ion friction, and no ion volume effects. We then arrive at

$$-\frac{1}{c_i} \frac{\partial c_i}{\partial x} - z_i \frac{\partial \phi}{\partial x} + 1/3 \cdot \alpha \cdot \lambda_B \cdot \sqrt[3]{N_{av} c_\infty} \cdot \frac{\partial \ln c_\infty}{\partial x} = -\frac{1}{\varepsilon D_i} (v_F - v_i) \quad (7.73)$$

where $\alpha = \sqrt[3]{\pi/3}$ and λ_B is the Bjerrum length. Eq. (7.73) can be rewritten to (making use of $J_i = c_i v_i$)

$$J_i = c_i v_F - \varepsilon D_i \left(\frac{\partial c_i}{\partial x} + z_i c_i \frac{\partial \phi}{\partial x} - 1/3 \cdot \alpha \cdot \lambda_B \cdot \sqrt[3]{N_{av} c_\infty} \cdot \frac{\partial c_\infty}{\partial x} \right). \quad (7.74)$$

When we leave out convection and electromigration, Eq. (7.74) leads to Eq. (4.28) if we also implement that for a binary 1:1 salt we have $c_i = c_\infty$. Note that Eq. (7.74) can also be used for mixtures of salts as long as all ions are monovalent.

A third analysis is to include the molecular volume of solutes, diffusing through water inside a porous medium. We consider neutral solutes that have no friction with the porous medium, thus $K_{f,i} = 1$. For the flow of fluid (water), we can now use Eq. (8.11) with $\rho \mathbf{E}$ set to zero. When the overall hydrostatic pressure difference is zero, and in steady state,^{xvi} this

^{xv}Eq. (3) in Tedesco *et al.*, J. Membrane Sci. **531**, 172–182 (2017).

^{xvi}Dynamically, when we started with pure solvent, and now, after adding solutes to the solution on one side of a porous layer (such as a membrane placed between two solutions), and now solutes entering the layer and diffusing to the other side, water will be displaced from the pores of the material, and might either flow left or right, dependent on external conditions. If the overall pressure difference is set to zero, water flows to the left in the left part of the layer, and to the right in the right part; inside the porous layer, the hydrostatic pressure is temporally higher than on the outsides.

Eq. (8.11) predicts that v_F is zero as well. The total volumetric flow rate v_{tot} is only due to the flow of solutes, thus $v_{\text{tot}} = v_i c_i v_i = v_i J_i = \eta v_i$, thus based on Eq. (7.70) we obtain

$$J_i = -\varepsilon D_i \left(\frac{\partial c_i}{\partial x} + c_i \frac{\partial \mu_{\text{exc},i}}{\partial x} - v_i c_i \frac{\partial \Pi}{\partial x} \right) \quad (7.75)$$

where we implemented that $P^{\text{tot}} = P^{\text{h}} - \Pi$ and $\partial P^{\text{h}}/\partial x = 0$. We now assume there is only one type of solute, and thus $\eta = v_i c_i$. We implement the Gibbs-Duhem equation, Eq. (8.9), which we discuss in the next chapter, and we then rewrite Eq. (7.75) to

$$J_i = -\varepsilon D_i (1 - \eta) \left(\frac{\partial c_i}{\partial x} + c_i \frac{\partial \mu_{\text{exc},i}}{\partial x} \right) \quad (7.76)$$

This result shows that in this case we end up with Fick's law for solute diffusion including an excess-term (that describes volumetric interactions), extended with a reduction factor $1 - \eta$.

The fourth example is like the previous one, with one neutral solute, but now the total flowrate v_{tot} is set to zero, and $\partial P^{\text{h}}/\partial x$ is free to adjust itself. For the water flowrate we again have Eq. (8.11), and for J_i Eq. (7.70). Because $v_{\text{tot}} = 0$, thus $v_{\text{tot}} = 0 = v_F + v_i J_i$, we have $J_i = -v_F/v_i$. Thus

$$J_i = -\frac{\eta}{1 - \eta} J_i - \varepsilon D_i \left(\frac{\partial c_i}{\partial x} + c_i \frac{\partial \mu_{\text{exc},i}}{\partial x} + \eta \frac{\partial}{\partial x} (P^{\text{h}} - \Pi) \right). \quad (7.77)$$

After implementing the Gibbs-Duhem equation (again assuming there is only one solute) we obtain

$$J_i = -\varepsilon D_i (1 - \eta) \left((1 - \eta) \frac{\partial \Pi}{\partial x} + \eta \frac{\partial P^{\text{h}}}{\partial x} \right). \quad (7.78)$$

Replacing $\partial P^{\text{h}}/\partial x$ by Eq. (8.11) and implementing $J_i = -v_F/v_i$ we obtain

$$J_i = \left(\frac{\eta v_i}{\mathbb{k}_{F-m}} + \frac{1}{\varepsilon D_i} \right)^{-1} (1 - \eta)^2 \left(\frac{\partial c_i}{\partial x} + c_i \frac{\partial \mu_{\text{exc},i}}{\partial x} \right) \quad (7.79)$$

where \mathbb{k}_{F-m} is a water-matrix friction coefficient that is discussed in the next chapter. When $\mathbb{k}_{F-m} \rightarrow \infty$, Eq. (7.79) simplifies to

$$J_i = \varepsilon D_i (1 - \eta)^2 \left(\frac{\partial c_i}{\partial x} + c_i \frac{\partial \mu_{\text{exc},i}}{\partial x} \right). \quad (7.80)$$

The reduction factor here, $(1 - \eta)^2$, is the same as a factor required in the study of the sedimentation rate of suspensions in a closed container.^{xvii} One contribution $1 - \eta$ is because

^{xvii}P.M. Biesheuvel, *Chem. Eng. Sci.* **55**, 2595–2606 (2000).

diffusion is relative to the fluid velocity, and the fluid now moves opposite to the direction of solute movement, which reduces the diffusion rate in the ‘laboratory frame of reference’, and the other contribution is because of the term $-v_i \partial \Pi / \partial x$.

When we analyze $\mu_{\text{exc},i}$ based on Carnahan-Starling, Eq. (4.4) in Ch. 4, then the derivative $c_i \partial \mu_{\text{exc},i} / \partial x = 2\eta(4 - \eta) / (1 - \eta)^4 \partial c_i / \partial x$ with $\eta = v_i c_i$. If we implement this in Eq. (7.80), for a single solute, we arrive at

$$J_i = -\varepsilon D_i \cdot \frac{1 + 4\eta + 4\eta^2 - 4\eta^3 + \eta^4}{(1 - \eta)^2} \cdot \frac{\partial c_i}{\partial x} \quad (7.81)$$

which for low η simplifies to

$$J_i = -\varepsilon D_i \left(1 + 6\eta + 15\eta^2 + \dots \right) \frac{\partial c_i}{\partial x} \quad (7.82)$$

which predicts that diffusion goes (very slightly) faster at higher η if it were just for the volumetric excess effect.

In the fifth example we discuss ‘free’ diffusion of solutes through water without hydrostatic pressure gradients, and we set $\varepsilon = 1$, and we do not consider an overall volume balance but define a flux of solutes relative to the interstitial, or ‘real’, water velocity, $v_F / (1 - \eta)$. This flux is then $J_i^\dagger = c_i (v_i - v_F / (1 - \eta))$. Then (with $J_i = v_i c_i$) we have

$$J_i^\dagger = J_i - \frac{c_i v_F}{1 - \eta} = -D_i \left(\frac{\partial c_i}{\partial x} + c_i \frac{\partial \mu_{\text{exc},i}}{\partial x} - v_i c_i \frac{\partial \Pi}{\partial x} \right). \quad (7.83)$$

Making use of the Gibbs-Duhem equation, assuming only one type of solute, we obtain

$$J_i^\dagger = -D_i (1 - \eta) \left(\frac{\partial c_i}{\partial x} + c_i \frac{\partial \mu_{\text{exc},i}}{\partial x} \right) \quad (7.84)$$

which is the same as Eq. (7.76). If one would now use a lattice expression for $\mu_{\text{exc},i}$, namely Eq. (1.8) in Ch. 1, which is $\mu_{\text{exc},i} = -\ln(1 - \eta)$, then we end up with

$$J_i^\dagger = -D_i \frac{\partial c_i}{\partial x} \quad (7.85)$$

which is exactly Fick’s law, but now for the case of solutes that do have volume, and expressed relative to the ‘real’ water velocity. Note that this particular result is only arrived at when this specific function is used for the excess-term, for a system with only one type of solute. So in general, Eq. (7.85) does not describe diffusion of solutes when volume effects are included. When there is a hydrostatic pressure gradient, then the solutes in addition experience a force to move relative to the fluid to lower hydrostatic pressure. So when a fluid has friction with a

porous medium through which it is pushed, but dissolved solutes do not have such a friction, but do have volume, they move faster than the fluid through the pores of the medium.

Based on these five examples, what will be clear by now is that dependent on how many driving forces we include, how many types of solutes, and what expressions are used for each term, and dependent on which contributions we consider for the frictions acting on a solute, a range of modified NP-equations is possible, from simple to detailed.

Local electroneutrality. The topic of local electroneutrality (EN), or called charge neutrality, is addressed at many points in this book, stating how this condition of EN can be used at positions away from interfaces, involving the local concentrations of all ions and fixed charges (e.g., those of a membrane structure) in the EN balance. According to EN, all of these contributions to the charge, of all ions and fixed charges, add up to zero. Only in calculating detailed profiles of concentration and potential in an EDL, is it relevant to use the full Poisson equation, $\nabla \cdot (\epsilon \mathbf{E}) = \rho$. It may seem that the use of EN, which leads to a zero charge density ρ , can be implemented in the Poisson equation, and then (when ϵ is constant) we obtain the Laplace equation, $\nabla^2 \phi = 0$, which we can solve to calculate the distribution of ϕ across the system. However, this is not the case! Once we assume EN, i.e., use the local EN-condition, we can no longer use the Poisson equation, or the Laplace equation. Instead, we directly implement EN in the transport equations, as we do throughout this book, see Newman (1983), p. 231, for a detailed discussion. Interestingly, there are instances where the two routes lead to the same result, i.e., that after inserting EN in the ion transport equations, we do arrive at the Laplace equation for the potential field. This for instance occurs when there are no concentration gradients (Newman, 1983, p. 223).

In the next chapter we continue this topic and use the two-fluid model (TFM) to describe the transport of the fluid or solvent, such as water, flowing around the ions inside a porous medium.

references

1. J.C. Díaz, J. Kamcev, “Ionic conductivity of ion-exchange membranes: Measurement techniques and salt concentration dependence,” *J. Membrane Sci.* **618**, 118718 (2021).
2. M. Tedesco, H.V.M. Hamelers, P.M. Biesheuvel, “Nernst-Planck transport theory for (reverse) electrodialysis: III. Optimal membrane thickness for enhanced process performance,” *J. Membrane Sci.* **565**, 480–487 (2018).

3. H. Fan, Y. Huang, I.H. Billinge, S.M. Bannon, G.M. Geise, and N.Y. Yip, “Counterion Mobility in Ion-Exchange Membranes: Spatial Effect and Valency-Dependent Electrostatic Interaction,” *ACS ES&T Engineering* **2**, 1274–1286 (2022).
4. V. Sasidhar, E. Ruckenstein, “Anomalous effects during electrolyte osmosis across charged porous membranes,” *J. Colloid Interface Sci.* **85**, 332–362 (1982).

Electrokinetics

In this chapter on electrokinetics we address the flow of solvent in combination with that of solutes, both in bulk electrolyte phases and inside porous media. We describe the dependence of electrolyte flow on hydrostatic and osmotic pressure gradients, and explain how water-ion frictional forces lead to the electrical body force in the Darcy equation and in the Navier-Stokes equation. We describe electrolyte flow through charged membranes, and discuss the classical experiments of water flow by osmosis and electro-osmosis. In the last section we discuss the various relations between hydrostatic, osmotic, Maxwell, and disjoining pressures, pressures relevant for the interaction between charged surfaces in the study of colloidal interactions, and relevant for the forces that develop between charged layers when a current flows.

8.1 The Navier-Stokes equation for flow in charged porous media

Flow of solutes such as ions was addressed in Ch. 7, both in free solution in the context of transport in a boundary film in front of a reactive or selective surface, as well as in porous media such as membranes. What is addressed in the present chapter is the equally important topic of transport of the fluid, often water, which is the solvent that fills up all space that is not already occupied by the porous medium structure or by the solute particles such as the ions, see Fig. 7.7. To describe fluid flow rates, we use the porous-medium version of the Navier-Stokes (NS) equation for flow of electrolyte solutions. We explain how the electrostatic body force term naturally appears when we include as driving forces on the fluid not only hydrostatic pressure gradients but also osmotic pressure gradients, and when we include that the solvent has friction with the solutes that move through it. We will also present the NS equation in free solution. In §8.4.1 we use these results to describe the forces in EDLs and between charged particles.

The theory for transport of solutes and fluid in porous media that combines the force balance approach for solutes from Ch. 7 with a force balance for the fluid, is called the two-fluid model (TFM) which was originally developed for liquid-solid flows in fluidized beds (Kuipers *et al.*, 1992). In these applications the dispersed particles are macroscopic, i.e., their mass and buoyancy were the most relevant driving forces acting on them. This approach was later extended to encompass colloidal particles and ions by including entropic effects (diffusion), electrostatics, and other effects related to solute volume and affinity (Biesheuvel, 2011).

We will explain the theory of the flow rate of fluids as a function of osmotic and hydrostatic pressures and the frictional forces between the fluid and solutes. The starting point is a force balance for fluid flow inside a porous medium. This balance considers the force per unit pore volume acting on the fluid, which equals minus the gradient in total pressure, P^{tot} , and adds to that the sum of frictional contributions, first a friction of the fluid with the porous medium, and second, frictional forces of the fluid with all solutes that are dispersed in the fluid. The sum-total of the forces is zero. This force balance is

$$-(1 - \eta) \frac{\partial P^{\text{tot}}}{\partial x'} - f'_{\text{F-m}} v'_F + \sum_i f_{i\text{-F}} c_i (v'_i - v'_F) = 0 \quad (8.1)$$

where $f'_{\text{F-m}}$ is a fluid-matrix friction coefficient (defined per unit pore volume, for flow along a tortuous path), while on the right of Eq. (8.1), to calculate the friction of the fluid with the solutes, we sum over all solutes that are in the fluid, inside the porous medium. On the

left, the factor $1-\eta$ is the open fraction of the pore volume available for fluid, i.e., a fraction η is blocked out by solutes (such as hydrated ions). Just like the procedure for Eq. (7.67), Eq. (8.1) can be converted to an expression based on fluxes defined per unit geometrical area, with coordinate x directed straight through the porous medium, to arrive at

$$-(1-\eta) \frac{\partial P^{\text{tot}}}{\partial x} - \frac{f_{\text{F-m}} v_{\text{F}}}{1-\eta} = - \sum_i \frac{1}{\varepsilon D_i} \left(J_i - \frac{c_i v_{\text{F}}}{1-\eta} \right) \quad (8.2)$$

where $f_{\text{F-m}} = f'_{\text{F-m}}/\varepsilon$. Just as in Ch. 7 we use $D_i = 1/f_{i\text{-F}}$, $\partial x' = \tau \partial x$, $v_{\text{F}} = v'_{\text{F}} (1-\eta) p/\tau$ and $v_i = v'_i p/\tau$. The factor ε is again the porosity, p , divided by the tortuosity factor, see p. 198. (This ε relates to the structure of the porous medium, and is unrelated to the fraction of pores, η , that is filled with solutes.) This general force balance can be solved jointly with general expressions for solute flow, such as by the most general NP expression given in Ch. 7 as Eq. (7.70).

A simplification we will often use is to set the volume fraction of solutes inside the pores to zero, i.e., we set $\eta=0$, resulting in

$$-\frac{\partial P^{\text{tot}}}{\partial x} - f_{\text{F-m}} v_{\text{F}} = - \sum_i \frac{1}{\varepsilon D_i} (J_i - c_i v_{\text{F}}) . \quad (8.3)$$

It is interesting to analyze Eq. (8.3) in case we only have neutral solutes that move by convection and diffusion without friction with the porous matrix, so $K_{i,i} = 1$. Thus we can use Eq. (7.2) without the migration-term, because for all species $z_i = 0$. So we analyze the case of ideal thermodynamics, thus with the activity coefficient equal to unity and the osmotic pressure given by $\Pi = \sum_i c_i$. If we combine Eqs. (7.2) and (8.3), we have

$$-\frac{\partial P^{\text{tot}}}{\partial x} - f_{\text{F-m}} v_{\text{F}} = \frac{\partial \sum_i c_i}{\partial x} \quad (8.4)$$

and implementing $P^{\text{tot}} = P^{\text{h}} - \Pi$ we arrive at

$$-\frac{\partial P^{\text{h}}}{\partial x} - f_{\text{F-m}} v_{\text{F}} = 0 \quad (8.5)$$

which we can rewrite to the Darcy equation

$$v_{\text{F}} = -\mathbb{k}_{\text{F-m}} \frac{\partial P^{\text{h}}}{\partial x} \quad (8.6)$$

where fluid only flows as function of a hydrostatic pressure gradient, with $\mathbb{k}_{\text{F-m}} = 1/f_{\text{F-m}}$ describing the permeability of the fluid through the porous medium. As this derivation

shows, even though an osmotic pressure gradient acts on the fluid (for instance water), which would tend to make it flow to more concentrated regions, the diffusion of solutes in the opposite direction exactly cancels this effect, and we arrive at the expected, logical, result, that the flow of fluid is not impacted by diffusion of solutes across that fluid, as long as those solutes only have friction with the fluid, and no further forces act on them. Interestingly, Eq. (8.6) is also arrived at when we do include an activity correction in the expression for convection and diffusion, and at the same time implement the related contribution to the osmotic pressure.

So Darcy's equation that only has a hydrostatic pressure gradient to drive the fluid, follows from a balance of forces on the fluid, which includes frictions with solutes, and a total pressure, which has contributions from a hydrostatic pressure, and osmotic pressure.

Further on, Darcy's law is derived again, and it is also shown that even when the solutes do occupy some volume (thus $\eta \neq 0$), we arrive at the same Darcy equation describing the total volume flow (of solutes and solvent together).

In a steady-state one-dimensional process, for instance for transport across a porous (charged) layer, Eq. (8.3) can be applied in a simplified form. We assume ions are unreactive so just like v_F , their fluxes J_i are invariant with position x . Integration of Eq. (8.3) over the thickness of the layer, from one end to other, staying inside the layer, then leads to

$$-\Delta P^{\text{tot}} - \frac{1}{k_{F-m}} v_F = - \sum_i \frac{1}{k_{m,i}} (J_i - \langle c_i \rangle v_F) \quad (8.7)$$

where $k_{F-m} = 1/(f_{F-m} L_m)$ is a 'clean water permeability', L_m is the thickness of the charged porous layer (membrane), and $k_{m,i} = \varepsilon D_i / L_m$ is a solute mass transfer coefficient in the porous layer. Eq. (8.7) can be used in a numerical model where fluxes and concentrations are calculated. This can be more insightful than implementing all expressions for fluxes, J_i , in Eq. (8.7), though we will follow that approach below.

We can make a significant simplification when for all solutes (ions) we neglect the solute-matrix friction, thus we assume $f_{i-m} = 0$, i.e., $K_{f,i} = 1$. We do not have to assume that the solutes are without volume. We can combine Eq. (7.70) with Eq. (8.2), which results in

$$(1 - \eta) \frac{\partial P^{\text{tot}}}{\partial x} = - \frac{f_{F-m} v_F}{1 - \eta} - \sum_i \left(\frac{\partial c_i}{\partial x} + z_i c_i \frac{\partial \phi}{\partial x} + c_i \frac{\partial \mu_{\text{exc},i}}{\partial x} + c_i v_i \frac{\partial P^{\text{tot}}}{\partial x} \right) \quad (8.8)$$

which we can simplify by implementing $P^{\text{tot}} = P^{\text{h}} - \Pi$, and by making use of the Gibbs-Duhem equation for a multicomponent solution, which in this case relates the osmotic pressure to the sum of ideal and excess contribution of the chemical potential

$$\frac{\partial \Pi}{\partial x} = \sum_i c_i \left\{ \frac{\partial \mu_{\text{id},i}}{\partial x} + \frac{\partial \mu_{\text{exc},i}}{\partial x} \right\} \quad (8.9)$$

where $\mu_{\text{id},i} = \ln c_i$.ⁱ We sum over all solutes (such as ions) that are dispersed in the fluid. Note also that $\eta = \sum_i v_i c_i$, where v_i is the volume per mole of solutes, such as (hydrated) ions. Eq. (8.8) then dramatically simplifies, to

$$\frac{\partial P^{\text{h}}}{\partial x} = -\frac{f_{\text{F-m}} v_{\text{F}}}{1 - \eta} - \sum_i \left(z_i c_i \frac{\partial \phi}{\partial x} \right). \quad (8.10)$$

After multiplying all terms with RT , Eq. (8.10) can be rearranged to

$$v_{\text{F}} = - (1 - \eta) \frac{\mathbb{k}_{\text{F-m}}}{RT} \left(\frac{\partial \bar{P}^{\text{h}}}{\partial x} - \rho \mathbf{E} \right) \quad (8.11)$$

where $\bar{P}^{\text{h}} = RT \cdot P^{\text{h}}$ is a dimensional pressure with unit Pa. On the very right we have the charge density due to all mobile species, $\rho = F \cdot \sum_i z_i c_i$, while $\mathbf{E} = -V_{\text{T}} \cdot \partial \phi / \partial x$ is the field strength (in V/m).

These equations are the porous medium version of the Navier Stokes equation including an electrostatic body force term $\rho \mathbf{E}$ that arises in an EDL or for flow through charged porous media. The permeability $\mathbb{k}_{\text{F-m}}$ can be multiplied by the fluid viscosity μ_{F} (in Pa.s) and divided by RT , to arrive at an intrinsic permeability k_i with unit m^2 , and this factor only depends on the structure of the porous medium, i.e., $k_i / \mu_{\text{F}} = \mathbb{k}_{\text{F-m}} / RT$. For a porous structure consisting of tortuous cylindrical pores, $k_i = p^{3/2} d_{\text{p}}^2 / 32$ (based on Hagen-Poiseuille), where d_{p} is the pore diameter, and where we implemented the Bruggeman equation to relate the tortuosity factor τ to porosity, p , by $\tau = p^{-1/2}$. Using the Bruggeman equation, the factor ε becomes $\varepsilon = p / \tau = p^{3/2}$, while another expression in the membrane literature is $\varepsilon = (p / (2 - p))^2$. In this second expression, ε is predicted to be much lower. For instance, at $p = 0.5$, ε is more than three times lower using the second expression, than when the Bruggeman equation is used.

ⁱThe osmotic pressure and chemical potential can also have other contributions such as an attraction energy between solutes, or the electrostatic interaction energy between ions, as discussed on p. 200.

Expressions for fluid permeability in porous media. For a porous medium, the Carman-Kozeny (CK) equation is often used which we can represent as $k_i/h_p^2 = 1/5 p$, where h_p is the volume/area ratio of the pores, $h_p = \sigma/6 \cdot p/(1-p)$, which depends on the size of the spheres of which the porous medium is constructed, σ , see Eq. (4.12). (There, η is the packing factor, which is replaced here by $1-p$, with p the porosity of the medium.) When we compare with numerical results for the Stokes flow through arrays of spheres (Zick and Homsy, J. Fluid Mech., 1982) we notice that the CK equation is about right for a porosity p less than 35%. However, for more open structures the predicted permeability k_i is too high. Analysing the numerical results in Zick and Homsy (1982) for an FCC packing, we find that the '5' in the above CK-equation is best replaced by $4+1/(1-p)$. This equation fits numerical results very well up to a porosity of 93.5 vol% packing. For even more porous structures, we use

$$\frac{\partial P^h}{\partial x} = -\frac{18 \mu_F (1-p)}{\sigma^2} \left(1 + \alpha (1-p)^{2/3}\right) v_F \quad (8.12)$$

where $\alpha = 12.8$, and σ is again the size (diameter) of the spheres of which the porous medium consists. For a porosity in the limit of 100%, this equation relates to the Stokes drag force on a single isolated sphere. [In that limit, the pressure gradient is given by $\partial P^h/\partial x = -cF$ with c the concentration of immobile obstacles and F the Stokes drag force, $F = -3\pi\mu_F\sigma v_S$, and with $p = 1 - cv$ and $v = \pi/6 \sigma^3$ we indeed get the required result. (In this very dilute limit v_F is equal to the Stokes velocity of the spheres relative to the fluid, v_S .)]

Darcy's law also follows when there are free-flowing inclusions in the fluid.

Interestingly, when there are dispersed particles in the fluid that are uncharged and do not have friction with the pore walls (and thus $K_{f,i} = 1$), and when solute concentration gradients are zero, then Eq. (8.11) results in the Darcy equation for the fluid-plus-solute mixture. And then the term $1 - \eta$ 'disappears' without having to assume the dispersed particles are without volume. This can be derived as follows. Eq. (8.11) describes the superficial velocity of the fluid. If the dispersed entities have no friction with the porous matrix ($K_{f,i} = 1$), and there are no diffusional or electrostatic forces acting on them, then their velocity v_i is the same as the interstitial velocity of the fluid, thus $v_i = v_F/(1 - \eta)$, where η is the fraction of the pore volume blocked out by these solutes. The combined, or total, superficial volumetric flow rate of fluid and

particles together (i.e., their joint superficial velocity as a whole) is $v_{\text{tot}} = v_{\text{F}} + \sum_i v_i c_i v_i$ (with v_i the molar volume of the solutes), and when all solutes have the same velocity v_i , we have $v_{\text{tot}} = v_{\text{F}} + \eta v_i = v_{\text{F}} + \eta/(1 - \eta) v_{\text{F}} = v_{\text{F}}/(1 - \eta)$. Inserting this conversion in Eq. (8.11) and assuming $\rho = 0$, the total volumetric flow rate v_{tot} is then given by the Darcy equation

$$v_{\text{tot}} = -\frac{k_i}{\mu_{\text{F}}} \frac{\partial \overline{P}^{\text{h}}}{\partial x}. \quad (8.13)$$

And thus we have the same results when we press pure water through a porous medium as when in the water there are solutes that just flow along with the water.

[When solutes *do have* a gradient in volume fraction (thus concentration) across the porous medium, then the total volume flow is influenced by their flow, and thus depends on additional factors such as ε and D_i , also when they do not interact with the porous medium directly, so when $K_{\text{f},i} = 1$.]

This long analysis leads to the important result that that the $(1 - \eta)$ -term in Eq. (8.11) is indeed correct there, a term which goes all the way back to the term $f'_{\text{F-m}} v'_{\text{F}}$ in Eq. (8.1) where we did *not* add a term $1 - \eta$ because the fluid-matrix friction does not depend on how much of the pore space is blocked out by solutes. That is a correct approach because it leads ultimately to the Darcy equation for a total fluid flow rate that does not depend on whether we have ‘phantom’ particles in the fluid that move along with it. If they are there, they should not influence a Darcy equation for the measurable total volumetric flow, as described by Eq. (8.13), and correctly, their presence indeed doesn’t.

When we assume that the ions are volumeless point charges (leading to $\eta = 0$), we can simplify Eq. (8.10) to

$$v_{\text{F}} = -\mathbb{k}_{\text{F-m}} \left(\frac{\partial P^{\text{h}}}{\partial x} - X \frac{\partial \phi}{\partial x} \right), \quad v_{\text{F}} = -k_{\text{F-m}} \left(\frac{\partial P^{\text{h}}}{\partial \bar{x}} - X \frac{\partial \phi}{\partial \bar{x}} \right) \quad (8.14)$$

where we also included local charge neutrality, $\sum_i z_i c_i + X = 0$ where X is a membrane charge density. In Eq. (8.14), $\mathbb{k}_{\text{F-m}} = 1/(f_{\text{F-m}})$, and the dimensionless thickness is $\bar{x} = x/L_{\text{m}}$. Remember that Eq. (8.10) and thus also Eq. (8.14) assume $K_{\text{f},i} = 1$. This extension of Darcy’s law is a classical equation in the field of electrokinetics with charged porous media. It can be found first in a paper in 1955 from R. Schlögl and this equation was called *Schlögl’s equation of motion* by Verbrugge and Hill (1990). If X is constant, Eq. (8.14) can be integrated across the layer to arrive at an equation we will discuss further on, Eq. (8.32).

Thus we saw in Eq. (8.11) that the electrical body force $\rho\mathbf{E}$ naturally develops from the general force balance, Eq. (8.1), when combined with the extended NP equation from Ch. 7. In the next box, we present a similar result for the Navier-Stokes equation in an electrolyte phase outside of a porous medium.

The electrostatic body force term in the Navier-Stokes equation. If in the derivation of the Schlögl-equation instead of $-f_{F-m}v_F$ a term $-\mu_F\nabla^2\mathbf{v}_F$ is used, describing viscous dissipation of a fluid, then the exact same derivation that led to the Schlögl-equation, now first leads to

$$\nabla\bar{P}^{\text{tot}} - \mu_F\nabla^2\mathbf{v}_F = RT \sum_i \frac{c_i}{D_{\infty,i}} (\mathbf{v}_i - \mathbf{v}_F) \quad (8.15)$$

where we neglect all solute volume effects and we simply describe flow in a ‘free’ electrolyte. If we implement the extended Nernst-Planck equation for the ionic fluxes, we arrive at the classical Navier-Stokes equation for Stokes flow (low fluid velocities) including an electric body force term

$$\mu_F \nabla^2 \mathbf{v}_F = \nabla \bar{P}^{\text{h}} - \rho \mathbf{E}. \quad (8.16)$$

When solutes do have volume, there are several complications in this derivation that require formal solution of a two-phase viscous flow problem with varying volume fractions. That goes beyond the authors’ expertise.

Thus again, a formulation starting with a total pressure P^{tot} and friction of the fluid with all solutes, leads to the classical Navier-Stokes equation based on the hydrostatic pressure, P^{h} , and an electrostatic body force term. The electrostatic term arises because electrical fields pull on ions, and they in turn pull on the water. [Interestingly, the standard explanation for a term $\rho\mathbf{E}$ in Eq. (8.16) often found in literature is rather that it is a force acting on the electrolyte as a whole, see for instance Harned and Owen (1958), p. 100.]

The above equations are compatible with the fact that at mechanical equilibrium, thus when all velocities are zero relative to one another, we arrive at $\partial P^{\text{tot}}/\partial x = 0$, for instance see Eq. (8.3), and thus $\partial P^{\text{h}}/\partial x = \partial \Pi/\partial x$, and thus $\Delta P^{\text{h}} = \Delta \Pi$, which implies that gradients and thus changes in hydrostatic pressure are the same as those in the osmotic pressure (Schlögl, 1955; Fair and Osterle, 1971; Anderson and Malone, 1974; Sonin, 1976; Sasidhar and Ruckenstein, 1981; Peters *et al.*, 2016). This is the case when mechanical equilibrium can be assumed as is generally the case in an equilibrium EDL structure, such as in the

Donnan layers at the edges of a membrane, when fluxes of solutes and solvent may not be zero, relative to one another, but nevertheless very small to the gradient in pressure-term. Based on Eq. (8.11) we can also derive that at mechanical equilibrium we have $\frac{\partial \bar{P}^h}{\partial x} = \rho \mathbf{E}$, a result we can use to study the structure of an EDL and colloidal interactions. These conditions also hold when there is flow across an interface, as long as the structure is thin, thus gradients are large. This is a local condition, that holds across any interfacial structure of a few nm thickness, or without flows also across thicker layers. The macroscopic corollary is what in the physiology literature is called Starling's equilibrium condition which is that at zero flow of water and of solutes, the hydrostatic pressure difference between two sides of a membrane equals the osmotic pressure difference.

—

An equation such as Eq. 8.14 for the fluid flow through a charged porous structure, such as a membrane, simplified for the case of ions as point charges and no ion-matrix friction, on the one hand seems logical, with an pressure term and an electrostatic term, but on the other hand is also completely mysterious, especially the second part. The first part makes sense, fluid moves because of a pressure gradient inside the membrane. But where is the effect of the osmotic pressure gradient, because doesn't fluid also move because of gradients in osmotic pressure, and why would fluid respond to the product of a membrane charge and a potential gradient? The fluid is uncharged by itself after all. The answers are to be found in the fact that first of all, one of the main driving forces on the fluid is the friction with the ions, and the ions move because they respond to concentration gradients (Fick's law), and because of electrostatic effects (migration). This Fickian driving force on ions exactly cancels the effect of the osmotic pressure gradient acting on the fluid. Thus, the diffusional forces acting on ions to make them move one way, exactly cancels the osmotic pressure gradient that would pull the fluid to higher concentration. What remains then are the electrostatic forces acting on ions, that via their friction with the fluid effectively pull on the fluid. This results in the term $-X \partial \phi / \partial x$ in the fluid force balance. With coions and counterions in a membrane, and even when their fluxes are the same, irrespective of direction, because there are many more counterions (at a concentration close to $|X|$), the migration term $z_i c_i \partial \phi / \partial x$ mainly acts on the counterions, which effectively makes it look as if the electrostatic pull on the water is only due to counterions, even though the flux of counterions may not be much different from that of coions. Thus this intuitive relationship, between the electrostatic force on the fluid, and the migration of counterions, may be misleading. For an intuitive relationship, we should consider Eq. (8.1) (and set $\eta = 0$ and neglect ') where we have first the total driving force on a volume of liquid, next its friction with the membrane matrix, and finally

friction with ions that move through it. If we want an intuitive ‘physical’ starting point, this is where to look. And we should not be surprised when an explanation that instead starts with Eq. (8.14), leads to confusion.

One way to interpret the term $-X\partial\phi/\partial x$ in a membrane is that it relates to net force on the membrane to move relative to the fluid, as if the membrane itself is a (very big) molecule with charge X . At a positive current, $\partial\phi/\partial x$ will be negative. Let us assume a CEM, with $X < 0$, that would mean a force acts on this negative molecule that pulls it left relative to the fluid. [Because a negative charge is drawn to locations of a higher potential, ϕ .] But its position is fixed. Thus instead we will have fluid flow to the right. And indeed, in a derivation that has four times a minus-sign, Eq. (8.14) results in a positive v_F ! In this way we can make some sense of the electro-osmotic term in Eq. (8.14) by relating it to the force acting on the charged material relative to the fluid that moves through it.

8.2 Flow of fluid across a charged membrane

The above derivation of an expression for fluid velocity in a porous layer started with a force balance which includes a *total* pressure gradient balanced by friction with the porous medium and with the free solutes. And when we can neglect friction between ions and the porous medium, this balance leads to a final simple expression where a *hydrostatic* pressure acts on the fluid as well as an electric body force, $X\partial\phi/\partial x$. The derivation demonstrates that the electric body force acting on the fluid originates in the drag of the electric field on the ions, and the ions in turn exert a frictional force on the fluid, i.e., they drag along the fluid. Thus, there is no direct force by the electric field on the solvent. This makes sense, because how could there be such an effect, as the solvent by itself is uncharged. Instead, the above derivation shows that the electric body force on a fluid is *indirect*: it acts on the charge carriers, which then drag along the fluid.

The exact cancellations in Eq. (8.8) that lead to the elegant Eq. (8.10), where the osmotic pressure gradient acting on the fluid cancels against the diffusional driving forces that act on the ions, is of particular interest. *It shows that even though an osmotic force always acts on the fluid, it is the case that when ions are free to move, this force effectively is not operational.* This matches the outcome of an experiment where we bring a high-salt solution in contact with a volume of pure water with the two liquids only separated by a neutral very open filter, or separated by nothing at all. Even though the water feels a natural force to move to the high-salt solution, the ions diffusing away from that region into the pure water act with an opposing drag force on the water, and that force exactly cancels the osmotic ‘attraction’ of the water to go to the high-salinity side. In effect, the water –as we see in such

an experiment— does *not* move to the high-salt side, as correctly predicted by the equations in this section. In such an experiment it is just the ions that diffuse away from the high-salt region, through water that is not moving at all. [This analysis is valid when all solutes are without volume. When they do have volume there is a backflow of water such that the total volumetric flow rate, v_{tot} , stays zero, related to an analysis of diffusion on p. 211.]

It is only when a selective layer, i.e., a membrane, is placed between two salt solutions, i.e., a layer that has a retention for at least one of the ions in the system, that indeed a water flow develops to the high-osmotic pressure side. The same force (of the water to go to that side) was already there without this membrane, but only now it actually leads to water flow. Why it now does lead to water flow is explained in this and the next sections.

Eq. (8.14) shows that a hydrostatic pressure gradient in the membrane can push water across a layer. But how does a pressure gradient develop? The reason is the pressure drops at the two membrane-solution interfaces. Across these Donnan layers, the hydrostatic pressure goes up or down by an amount equal to the difference in osmotic pressure across that same interface, see Fig. 8.1. Thus, when the osmotic pressure increases from a value outside the membrane of $2c_{\infty}$ (for a $z:z$ salt), to $c_{T,m}$ inside the membrane, the hydrostatic pressure changes by that same amount.

We can also use Eq. (8.3) to derive this result of the pressure changes across a Donnan layer. When considering transport over macroscopic distances of a few μm or more, all terms in Eq. (8.2) are roughly of the same order of magnitude, because why else consider them at all, but in the Donnan layer of only a few nm's thickness, the gradient-term in pressure on the left is now many orders of magnitude larger than all the other terms. Thus Eq. (8.3), when applied to the Donnan layer, simplifies to $\partial P^{\text{tot}}/\partial x = 0$, in which we can insert $P^{\text{tot}} = P^{\text{h}} - \Pi$ and thus derive after integration from one end of the Donnan layer to the other that across the Donnan layer any change in osmotic pressure is exactly the same as the change in hydrostatic pressure. Yet another derivation of this result is given [here](#). More details about the equivalence of concentration and osmotic pressure is given [here](#).

Together with these boundary conditions, Eq. (8.14) now explains how it can be that when between two reservoirs there is a small enough pressure difference, that water flows from a reservoir with low osmotic pressure (low concentration of solute) to a reservoir with high osmotic pressure. The explanation is that across the Donnan layers at the two membrane edges a hydrostatic pressure difference develops, and this hydrostatic pressure will be different on the two sides. When we have equal values of P^{h} outside the membrane, and when these two jumps in P^{h} on the membrane edges are different, a gradient in hydrostatic pressure develops in the membrane which pushes the water to one of the two sides, see Fig. 8.1.

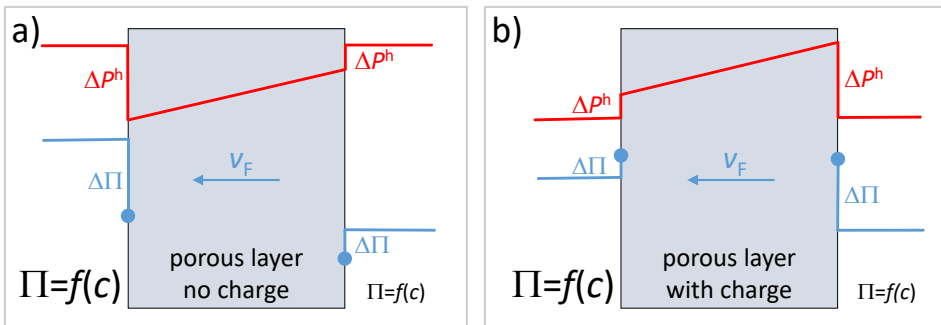


Fig. 8.1: Profiles of osmotic pressure Π and hydrostatic pressure P^h across a charged porous layer, such as a membrane, for the case of equal hydrostatic pressures on the two sides. At the edges of the layer, the change in Π determines the change in P^h (namely, they are the same). The osmotic pressure Π is a positive function of concentration. The direction of water flow is determined by the gradient in P^h across the layer (with the water flowing towards lower P^h). (a) The case of neutral solutes and a membrane with a partition (sieving) coefficient of the solutes of $\Phi_i < 1$. On the high concentration side the drop in Π is the steepest, and this ultimately leads to the hydrostatic pressure in the membrane decaying to this side and thus also water flowing to this side. (b) For a charged membrane in contact with two salt solutions with different concentration, the increase in osmotic pressure is the steepest on the low-salinity side, and just as for neutral solutes in panel a), the hydrostatic pressure in the membrane drops towards the high-salinity side, pushing the water in that direction.

Fig 8.1A discusses the case of neutral solutes, and a selective layer that has a partition (sieving) coefficient for the solutes that is less than unity, $\Phi_i < 1$. Thus the solute concentration in the membrane is lower than outside, and thus the osmotic pressure goes down when we enter the membrane, and the same is then the case for the hydrostatic pressure. This leads to a flow of water to the high-concentration reservoir. This effect is the highest on the high-concentration side of the membrane, see Fig. 8.1A.

We can analyze this situation in general based on Eq. (8.2), and we start first of all with a 1:1 salt solution and a charged porous medium (such as a membrane) with charge density X (which can be positive and negative). We assume that all ions have the same $K_{f,i}$ and D_i . We neglect ion volume effects, thus set $v_i = 0$ for all solutes, and thus $\eta = 0$ which leads to Eq. (8.3). We implement Eq. (7.71) in Eq. (8.2) and then obtain

$$-\frac{\partial P^h}{\partial x} = f_{F-m} v_F + \frac{1}{\varepsilon D_i} (1 - K_{f,i}) c_{T,m} v_F - (1 - K_{f,i}) \frac{\partial c_{T,m}}{\partial x} - X K_{f,i} \frac{\partial \phi}{\partial x} \quad (8.17)$$

where $c_{T,m}$ is a summation over all ion concentrations, i.e., the total concentration. Thus, Eq. (8.17) describes the pressure changes through a porous medium for a 1:1 salt solution when all properties of the ions are the same.

When we change to a dimensionless thickness, $\bar{x} = x/L_m$ we can rewrite Eq. (8.17) to

$$-\frac{\partial P^h}{\partial \bar{x}} = \left\{ \frac{1}{k_{F-m}} + \frac{1}{k_{m,i}} (1 - K_{f,i}) c_{T,m} \right\} v_F - (1 - K_{f,i}) \frac{\partial c_{T,m}}{\partial \bar{x}} - X K_{f,i} \frac{\partial \phi}{\partial \bar{x}}. \quad (8.18)$$

The current density, J_{ch} , can be calculated from the extended Nernst-Planck equation, Eq. (7.71). For a 1:1 salt, we have $J_{ch} = I/F = J_+ - J_-$, and with equal $K_{f,i}$ and D_i and a constant membrane charge density $X = c_{m,-} - c_{m,+}$, we arrive at

$$J_{ch} = -K_{f,i} \left(X v_F + k_{m,i} c_{T,m} \frac{\partial \phi}{\partial \bar{x}} \right). \quad (8.19)$$

For a process where $J_{ch} = 0$ (dialysis,ⁱⁱ reverse osmosis), Eq. (8.19) can be implemented in Eq. (8.18) to replace $\partial \phi / \partial \bar{x}$, and we then arrive at

$$-\frac{\partial P^h}{\partial \bar{x}} = \left\{ \frac{1}{k_{F-m}} + \frac{1}{k_{m,i}} (1 - K_{f,i}) c_{T,m} + \frac{X^2 K_{f,i}}{k_{m,i} c_{T,m}} \right\} v_F - (1 - K_{f,i}) \frac{\partial c_{T,m}}{\partial \bar{x}} \quad (8.20)$$

which for $K_{f,i} = 1$ simplifies to

$$v_F = - \left\{ \frac{1}{k_{F-m}} + \frac{X^2}{k_{m,i} c_{T,m}} \right\}^{-1} \cdot \frac{\partial P^h}{\partial \bar{x}}. \quad (8.21)$$

ⁱⁱDialysis is the process where a membrane is placed between two solutions with different composition and solutes (often salts) and water are allowed to flow through the membrane without an applied pressure difference or current. We also call this the osmosis experiment.

This equation is the same as Eq. (8.14), only that Eq. (8.21) also requires all diffusion coefficients to be the same, and a zero current density.

If instead we now consider that the porous medium is uncharged, $X=0$, then we replace $c_{T,m}$ by 2, and obtain from Eq. (8.20)ⁱⁱⁱ

$$\left\{ \frac{1}{k_{F-m}} + \frac{1}{k_{m,i}} (1 - K_{f,i}) c \right\} v_F = - \left\{ \frac{\partial P^h}{\partial \bar{x}} - (1 - K_{f,i}) \frac{\partial c}{\partial \bar{x}} \right\} \quad (8.22)$$

which we can integrate across the membrane to

$$\left\{ 1/k_{F-m} + (1 - K_{f,i}) \langle c \rangle / k_{m,i} \right\} v_F = - \left\{ P^{h,R} - P^{h,L} - (1 - K_{f,i}) (c^R - c^L) \right\} \quad (8.23)$$

where an average concentration, $\langle c \rangle$, is defined as $\langle c \rangle = \int_0^1 c \, d\bar{x}$.^{iv} In the present model for neutral solutes, $\langle c \rangle$ is given by $\langle c \rangle = \frac{1}{2} (c^L + c^R) + (c^L - c^R) \left(\frac{1}{2} (\tanh(\frac{1}{2} Pe_i))^{-1} - Pe_i^{-1} \right)$, where $Pe_i = v_F / k_{m,i}$ is a membrane-based Pe-number, see p. 296. We use notation L and R for positions just within the porous medium on the left and right side. Next we introduce an effective permeability k_{F-m}^\dagger given by $1/k_{F-m}^\dagger = 1/k_{F-m} + (1 - K_{f,i}) \langle c \rangle / k_{m,i}$. Only in the absence of solutes in the porous layer, or when they have no friction with the porous structure (then $K_{f,i} = 1$), do the two permeabilities (effective and ‘clean water’) coincide. With these changes, the left side of Eq. (8.23) becomes v_F / k_{F-m}^\dagger .

On the right side of Eq. (8.23) we can implement a partition function describing that the concentration just in the membrane (or, porous layer in general) c is given by $c = \Phi_i c_\infty$ where c_∞ is the concentration of neutral solutes, just on the outside of the membrane. The pressure just in the membrane, different on either side, P^h , relates to that on the outside, $P^{h,\infty}$, by $P^h = P^{h,\infty} + \Delta P^h$. This step change in hydrostatic pressure, as discussed before, equals the step change in osmotic pressure, $\Delta \Pi$, across the same solution-membrane interface. For ideal solutions this step change in osmotic pressure is simply the difference in solute concentration, which in case of a single solute is $\Delta \Pi = c - c_\infty$ where c without an index is that just in the membrane. We can implement the partition function, and we therefore arrive at $\Delta P^h = \Delta \Pi = (\Phi_i - 1) c_\infty$, and this result we can apply on both sides of the membrane. We then obtain

$$-v_F / k_{F-m}^\dagger = P^{h,R,\infty} + (\Phi_i - 1) c_{\infty,R} - P^{h,L,\infty} - (\Phi_i - 1) c_{\infty,L} - (1 - K_{f,i}) \Phi_i (c_{\infty,R} - c_{\infty,L}) \quad (8.24)$$

which we can simplify to

$$-v_F / k_{F-m}^\dagger = \Delta P^{h,\infty} + (\Phi_i - 1) \Delta c_\infty - (1 - K_{f,i}) \Phi_i \Delta c_\infty \quad (8.25)$$

ⁱⁱⁱThe total concentration of cations and anions, is now replaced by the concentration of neutral solutes.

^{iv}Further on, the same definition of an average is used for $c_{T,m}$ and also an inverted average $\langle c \rangle^\dagger$ is defined.

where we implemented $\Delta P^{h,\infty} = P^{h,R,\infty} - P^{h,L,\infty}$ and $\Delta c_\infty = c_{\infty,R} - c_{\infty,L}$. Eq. (8.25) can be rearranged to

$$v_F = -k_{F-m}^\dagger \left(\Delta P^{h,\infty} - (1 - K_{f,i} \Phi_i) \Delta c_\infty \right). \quad (8.26)$$

Eq. (8.26) shows how we can have flow of water (osmotic flow) when solutes are excluded from the membrane ($\Phi_i < 1$), as depicted in Fig. 8.1A, or when they have friction with the membrane matrix, thus $K_{f,i} < 1$. The osmotic driving force Δc_∞ is not as effective as the hydrodynamic driving force $\Delta P^{h,\infty}$ because it is reduced by a factor $1 - K_{f,i} \Phi_i$. The effective permeability k_{F-m}^\dagger is a function of the average concentration in the membrane, $\langle c \rangle$. This concentration is the average of concentrations just in the membrane on the left and right sides at low membrane Pe-numbers, and at high Pe-numbers is close to the concentration just in the membrane on the upstream side, which is the side from where water is pushed into the membrane.

We can replace Δc_∞ by $\Delta \Pi^\infty$ in Eq. (8.26) and replace $1 - K_{f,i} \Phi_i$ by σ_i , a factor called the reflection coefficient in the reverse osmosis (RO) literature. With these modifications we obtain a classical expression from the field of RO, which is

$$v_F = -k_{F-m}^\dagger \left(\Delta P^{h,\infty} - \sigma_i \Delta \Pi^\infty \right). \quad (8.27)$$

Osmotic Equilibrium. The phenomenon of osmosis is often discussed in terms of the hydrostatic pressure that develops between two containers with different solution concentration, between which is placed a membrane that allows passage for the solvent but not for the solutes. This hydrostatic pressure is then dubbed ‘the’ osmotic pressure that has developed. Often the situation is discussed where fluid flow through the membrane has become zero (mechanical equilibrium). We can use Eq. (8.26) to analyze this situation. We have $v_F = 0$ at equilibrium, we assume zero solute flow, for instance because $\Phi_i = 0$, and with $\Delta \Pi^\infty = \Delta c_\infty$ (because throughout this book all pressures are expressed in units of mol/m^3 , and can be multiplied by RT to obtain a pressure in Pa), we arrive at

$$\Delta P^{h,\infty} = \Delta \Pi^\infty \quad (8.28)$$

i.e., the hydrostatic pressure difference across the membrane equals the osmotic pressure difference. If one solution is pure solvent, not containing solutes, the osmotic pressure there is zero, and if we set the hydrostatic pressure there to zero as well, then in the other reservoir we have $P^h = \Pi$, i.e., ‘the’ hydrostatic pressure is equal to ‘the’ osmotic

pressure. So in this particular case indeed the two pressures 'are the same', but in general, with solutes also flowing across the membrane, this is not the case.

There are many papers that philosophically discuss why water flows to a high-concentration side of the membrane such that ultimately the osmotic and hydrostatic pressures become the same (Guell and Brenner, 1996). The mechanical, or microscopic, explanation of this why-question is discussed throughout this chapter, relating to a pressure gradient developing inside the membrane that pulls water to the side of high solute concentration.

The other approach to the why of water flow, is the thermodynamic fact that systems tend to minimize the total energy. We can make such an analysis here as well. When we have a vertical tube containing solutes and solvent (e.g., water), and at the bottom of the tube is a selective membrane that only allows passage of water (vertical position $h=0$). It is placed in a large container of water without solutes in which the hydrostatic pressure is constant. In the vertical tube we have an initial height h_{ini} and initial concentration of solutes c_{ini} . Analysis of the total energy in the system only requires us to consider the tube. (The pressure energy in the surrounding bath is constant and does not have to be considered.) In the tube, we have gravitational energy $\frac{1}{2}\rho_L g h^2$, while the entropy of the solutes contributes a term $RT h c \ln c$ to the energy. We leave out a multiplier A for cross-sectional area in both terms. Concentration c is given by $c \cdot h = c_{ini} \cdot h_{ini}$. We implement this, add together the two energy terms, take the derivative with height, and set this to zero. This is the criterion of mechanical equilibrium, when the energy is at a minimum. This calculation immediately leads to $\rho_L g h = c$, and with the left part equal to the hydrostatic pressure and the right part equal to the osmotic pressure, we just demonstrated that minimization of the total energy in a container connected to another container by a membrane not permeable to solutes, leads at mechanical equilibrium to $P^h = \Pi$, i.e., the hydrostatic pressure (difference across the membrane) equals the osmotic pressure (difference across the membrane).

Thus energy minimization leads to mechanical equilibrium, and thus solvent will flow until across the membrane mechanical equilibrium is reached, $\Delta P^{h,\infty} = \Delta \Pi^\infty$. So solvent flows to minimize the energy of a system.

Interestingly, this equality only holds right at the membrane (and other positions at that hydrostatic pressure); the higher up we go in the column, the osmotic pressure Π is still the same, but the hydrostatic pressure P^h drops steadily. Nevertheless, also at these positions $h > 0$ we have mechanical equilibrium.

When there is solute leakage across the membrane, and thus mechanical equilibrium is not established between the two sides of the membrane, then $P^h \neq \Pi$, so this simple analysis does not apply. Then the full set of equations from this chapter can be used to analyze these more realistic situations.

We just discussed the flow of neutral solutes through a neutral membrane, and water flowing to the high-concentration side. When instead of a neutral system we have two ionic solutions at different concentrations and a charged membrane, the result is the same, that again the water flows to the side with high concentration of solutes. But there is a very distinct difference with the neutral case, that now the solute concentration in the membrane is higher than outside, not lower, and pressures go up when moving from outside to inside the membrane, see Fig. 8.1B. But also in this case the changes in osmotic and hydrostatic pressures are such that we again have a gradient in P^h inside the membrane that pushes water to the high-salinity side, see Fig. 8.1B. For ionic solutions and a charged membrane, electrostatic effects, which is the second term in Eq. (8.14), can further modify the amount and direction of water flow, as we will discuss in detail in the next section.

Mechanical energy from osmosis. In Fig. 8.1 we considered the situation that the hydrostatic pressure, P^h , is the same on the two sides of the membrane. But Fig 8.1 also suggests that we can set P^h to a somewhat higher value on the high-concentration side, and still the water will flow to that side. We then have water flowing against a hydrostatic pressure difference between the two reservoirs. Thus the osmotic pressure difference between two solutions works as an engine that pumps water from low to high hydrostatic pressure. This interesting phenomenon is at the basis of a process called pressure retarded osmosis, by which energy in the form of a concentration difference (which can be called chemical energy, or osmotic energy) is converted into mechanical energy. A related process using charged membranes converts the same type of osmotic energy into electricity, and this process is called reverse electrodialysis.

The sign of pressure change on a membrane interface. Mechanical equilibrium at a solution-membrane interface leads to the osmotic pressure and hydrostatic pressure changing in the same direction, when going from outside to inside the membrane. If the membrane is charged, then a Donnan effect is operative, and then the total ions

concentration in the membrane is larger than outside, and thus the osmotic pressure goes up into the membrane, and thus hydrostatic pressure as well. But if the membrane is uncharged and there is only a non-electrostatic partition effect, Φ_i , then the osmotic and thus hydrostatic pressure go down going from outside to inside the membrane (Mauro, *Science* **149**, 867–869, 1965). When a charged membrane also has a non-electrostatic Φ_i -effect, an interesting consequence is that for a given membrane charge density, X , there is a critical salt concentration above which these two pressures decrease from outside to inside the membrane, while below this value, they go up. Thus, in reverse osmosis (RO), where on the upstream side of a membrane the salt concentration is quite high (for instance at the level of seawater, ~ 600 mM) but on the downstream side it can be 99% lower (e.g., 6 mM), we likely have the two external salt concentrations on either side of this critical value. As a consequence, on the upstream side of the membrane, the pressure goes down when we enter the membrane, and on the downstream side it again goes down, now when we *exit* the membrane. This sequence of downward steps in the flow direction is not related to the water flow directly: for other values of X or Φ_i , the pressure would change in the same way on both sides, for instance going down in both cases when we go from outside to inside the membrane. That these interfacial pressures only step downward in the direction of flow, may look like a logical consequence of the Darcy equation, with fluid flowing in the direction of decreasing pressure, but for the membrane surfaces this equation does not apply. On a membrane edge we can also have water flow in the direction of increasing pressure.

Thus, the hydrostatic pressure change upon entering the membrane, is the same as the osmotic pressure change, and for a 1:1 salt this change is given by

$$\Delta P^h = \Delta \Pi = c_{T,m} - 2c_\infty = \sqrt{X^2 + (2c_\infty \Phi_i)^2} - 2c_\infty \quad (8.29)$$

where $c_{T,m}$ is the total ions concentration just inside the membrane, at that interface, while c_∞ is the salt concentration outside the membrane. The non-electrostatic partition coefficient, Φ_i , is the geometric mean of the two coefficients for each ion individually, see Eq. (2.42), $\Phi_i = \sqrt{\Phi_+ \Phi_-}$, and includes all partition effects of affinity or ion volume, but we do not include the Donnan effect in here which relates to maintaining electroneutrality in the membrane. If we set the pressure change to zero, we obtain

$$\left(\frac{X}{2c_\infty} \right)^2 + \Phi_i^2 = 1 \quad (8.30)$$

which results for the critical salt concentration in

$$c_{\infty}^{\text{crit}} = \frac{1}{2} \cdot X / \sqrt{1 - \Phi_i^2}. \quad (8.31)$$

Thus for a membrane charge density of $X = 200$ mM, and a non-electrostatic partition coefficient of $\Phi_i = 0.2$, the critical salt concentration is $c_{\infty}^{\text{crit}} \sim 102$ mM. Thus for an external salt concentration larger than c_{∞}^{crit} the pressure goes down upon entering the membrane, and for $c < c_{\infty}^{\text{crit}}$ it goes down when we *leave* the membrane. Actually, for any value of $\Phi_i < 0.5$, the critical salt concentration is not much above $c_{\infty}^{\text{crit}} \sim \frac{1}{2}|X|$. Thus, indeed, for an RO membrane, with the aforementioned values of upstream and downstream salt concentration, for any moderate value of the membrane charge density, feed and permeate concentrations are on either side of the critical salt concentration calculated by Eq. (8.31). Thus the pressure goes down when we go into the membrane on the upstream side, and goes down again on the downstream side when we leave the membrane, resulting in a profile of pressure that in the direction of water flow each time ‘steps downward’.

Negative pressures inside a membrane lead to cavitation. Another consequence of the theory discussed in this section, i.e., mechanical equilibrium across a solution-membrane interface, is that negative hydrostatic pressures can develop in membranes. This means the liquid is under tension, and there likely is cavitation, i.e., vapour bubbles form. This occurs when the hydrostatic pressure outside the membrane is low (for instance atmospheric pressure), the osmotic pressure outside the material is high, and solute molecules are well excluded from the membrane ($\Phi_i \ll 1$, membrane charge low). Bubbles have indeed been observed to form in tight desalination membranes, such as on the side of the draw solution of forward osmosis membranes (refs. i, ii), while the same topic has also been addressed in the biophysical literature (iii, iv).

i) E.W. Tow, M.M. Rencken, and J.H. Lienhard, “In situ visualization of organic fouling and cleaning mechanisms in reverse osmosis and forward osmosis,” *Desalination* **399**, 138–147 (2016). (Fig. 14e,f)

ii) L. Song, M. Heiranian, and M. Elimelech, “True driving force and characteristics of water transport in osmotic membranes,” *Desalination* **520**, 115360 (2021).

iii) J.L. Anderson and D.M. Malone, “Mechanism of osmotic flow in porous membranes,” *Biophys. J.* **14**, 957–982 (1974).

iv) M.A. Zwieniecki, P.J. Melcher, N.M. Holbrook, *Science* 291, 1059–1062 (2001).
M.T. Tyree, J.S. Sperry, “Vulnerability of xylem to cavitation and embolism,” *Annu. Rev. Ecol. Syst.* **40**, 19–38 (1989).

8.3 Osmosis and electro-osmosis in charged membranes

8.3.1 Introduction

In the literature on ion transport through charged membranes, an intuitive understanding has developed of the concepts of osmosis and electro-osmosis, as two distinct mechanisms of water flow through membranes, based on two classical experiments. We discuss these experiments and their analysis. However, as we will explain, they are different, in that osmosis is a fundamental force acting on a fluid, as discussed in the previous sections, but electro-osmosis is not such a fundamental force. Instead, it is the phenomenon that electrolyte flows through a membrane when an electrical current is applied. In the next sections we first introduce both experiments/phenomena, and later on analyze both in more detail.

8.3.2 Osmosis

In a study of dialysis, the flow of salts and water across a membrane is measured as function of an osmotic pressure difference (with equal hydrostatic pressure).^v When the membrane has a high charge density, X , there is hardly any transport of ions through the membrane. This is because transport of the coion is rate-limiting, i.e., it has a very low flux through the membrane, and because of the zero current condition, the counterion has the same low flux. It is mainly water that flows through the membrane.

The water that flows is then the ‘free water’, i.e., the water around the hydrated ions, see Fig. 7.7.^{vi} In this experiment water flows because of only one driving force, which is the difference in osmotic pressure between the solutions outside the membrane. As we

^vThough for the separation of salts, generally the membrane is charged, for solutions of macromolecules such as proteins, the membrane does not have to be charged, but it only needs to be selective in blocking the protein.

The case of neutral solutes and an uncharged membrane was discussed in §8.2.

^{vi}From this point onward, we leave out ‘free’ again. By ‘water’ we mean the water flowing around the ions. Instead, the water molecules bound into the hydrated ion, they are part of the entity we call an ion.

explained in §8.2, water flows through the membrane due to an internal hydrostatic pressure gradient that builds up because of the external osmotic pressure difference, see Fig. 8.1.) The rate of water flow divided by the osmotic pressure difference ($\text{m}^3/\text{m}^2/\text{s}/\text{Pa}$) is the osmotic permeability of the membrane.

The osmosis experiment (dialysis) can be done accurately because there is only one membrane between two containers and we can measure volume changes and salt concentration changes. Together with an overall volume balance and an overall salt balance, these data can be checked against one another, and we can accurately determine the volumetric flow rate through the membrane as well as the flux of salt through the membrane. These data can be used to validate a membrane transport theory, as we will do in §8.3.5.

8.3.3 Electro-osmosis

In the electro-osmosis experiment the electrolyte flow through a membrane is measured (again based on volume changes) as function of the current density. The solutions on both sides have the same salt concentration, and thus the osmotic driving force is zero. Again, there is no hydrostatic pressure difference between the two solutions. To quantify electro-osmosis the volume flow through the membrane is divided by the current, and then an electro-osmotic flow parameter follows that has the unit $\text{m}^3/\text{s}/\text{A}$, thus m^3/C . If we implement the water molecular volume of 55.5 mol/L, we can convert this number to moles of water ‘per C’ transported (mol/C). And if we multiply by Faraday’s number we have the water transport over charge transport in mol/mol.

In the classical interpretation, electro-osmotic water flow is associated with the water molecules in the hydration shell of the counterions that go through the membrane to carry the current. However, in analysing this experiment, we must realize that besides the ions and their hydration water molecules, also water flows because it is being dragged along with the ions (repeating ourselves, this is the ‘free’ water around the hydrated ions). The drag on the free water is likely very significant. So even though this experiment provides an output that has the unit mol/mol/mol, this should not be taken to mean that only the flow of water tightly bound to the ions in the hydration shell is measured in this experiment. Because also the water in between the ions flows. Thus, although in this experiment there are no driving forces that pull the water through the membrane, there is friction of the water with the ions. These ions drag the water along when they are pulled through the membrane because of the applied current.

8.3.4 What is measured in the osmosis and electro-osmosis experiments?

We explain in this section in more detail what is exactly measured in an osmosis- and electro-osmosis experiment.

The osmosis experiment probes the permeability for water flow through a membrane under the influence of osmosis as a driving force. The water has friction with the membrane and with the many ions that are in the membrane. The concentration of counterions is high but they hardly move, while coions are at a much lower concentration. A driving force acts on the water and we can measure an osmotic permeability. This number can be compared with the hydraulic permeability measured by applying a pressure difference across the membrane and observing the flow of water. For a highly charged membrane, the two numbers should be the same, but when the membrane charge is not so high the osmotic permeability decreases and the concentration difference across the membrane becomes increasingly ineffective in generating a volume flow, because it no longer generates a significant internal pressure difference, see §8.3.5.

The electro-osmosis experiment is more complicated. In this experiment the resulting volume flow has two contributions. There is the flow of water, and besides that we have the volumetric flow of the hydrated ions. The water flows because it is dragged along by the ions that are pulled through the membrane because of the current. Thus in the electro-osmosis experiment the sum of the volume flow of water and of ions is measured. If we know the molar volume and flux of ions we can calculate the flow rate of water. For a further discussion on measuring volume changes in this experiment, see [here](#).

Thus, these two experiments demonstrate that osmotic pressure and current drive fluid flow. However, what is measured in these experiments is not necessarily one-to-one convertible to the fundamental driving forces that act on the water (the fluid), or the frictional forces of the water with ions and the membrane. This is because flow of water in the membrane results from the interplay of four contributions to the force balance acting on it, namely: hydrostatic pressure gradients; osmotic pressure gradients; friction with ions and other solutes; and friction with the membrane. The first three of these forces can negatively and positively contribute to the actually realized water velocity, while friction with the membrane matrix always slows down fluid flow. While osmosis is one of these four fundamental forces, electro-osmosis is not.

8.3.5 Mathematical analysis of osmosis and the osmotic permeability

In this section we explain how the membrane theory used throughout this book (e.g., in Chs. 11 and 12) also applies to dialysis (the osmosis experiment) and electro-osmosis. We first discuss dialysis (the osmosis-experiment). Unless noted otherwise, we assume in the next sections that *all ions are volumeless*, thus for all ions $v_i = 0$, thus the total volume fraction is zero, $\eta = 0$, and $\mu_{\text{exc},i} = 0$. Besides the Donnan equilibrium, also a partition function, Φ_i , is included for all non-Donnan (non-electrostatic effects). From this point onward, we assume that we have a 1:1 salt solution, with equal diffusion coefficients of the two ions in the membrane.

As a first element of the theory we describe the two membrane/solution interfaces where we have a change in osmotic pressure and hydrostatic pressure when going from outside to inside the membrane, as illustrated in Fig. 8.1, and described by Eq. (8.29). Without ion-membrane friction, i.e., for $K_{f,i} = 1$, the flow of water through the membrane is given by Eq. (8.14) integrated across the membrane, which results in

$$v_w = -k_{F-m} \left(\Delta P^{\text{h,m}} - X \Delta \phi^{\text{m}} \right) \quad (8.32)$$

where $\Delta P^{\text{h,m}}$ is the hydrostatic pressure difference between two positions just inside the membrane, right at the two membrane/solution interfaces (counting right minus left, see p. 507). The pressures in the membrane at the outer edges follow from Eq. (8.29), with the hydrostatic pressure outside the membrane the same on both sides. The second term in Eq. (8.32) is because of friction of water with ions in the membrane. The membrane charge density X can be both positive and negative. Starting with Eq. (8.32), we have changed from a more general fluid velocity, v_F , to the velocity of water, v_w , which mathematically has the same meaning.

Eq. (8.19) can be rewritten and then integrated across the thickness of the membrane, which results in a voltage across the inner region of the membrane of

$$\frac{\partial \phi^{\text{m}}}{\partial \bar{x}} = -\frac{1}{k_{m,i} c_{T,m}} \left(\frac{J_{\text{ch}}}{K_{f,i}} + X v_w \right) \rightarrow \Delta \phi^{\text{m}} = -\frac{1}{k_{m,i} \langle c_{T,m} \rangle^\dagger} \left(\frac{J_{\text{ch}}}{K_{f,i}} + X v_w \right) \quad (8.33)$$

where $1/\langle c_{T,m} \rangle^\dagger = \int_0^1 1/c_{T,m} d\bar{x}$.

For a zero current, the voltage difference $\Delta \phi^{\text{m}}$ that develops in the membrane speeds up the coions and slows down the counterions at the same time, to make sure they have equal fluxes at each position in the membrane, even though there are far more counterions in the membrane than coions.

We can combine Eqs. (8.32) and (8.33) and arrive at

$$v_w = -k_{F-m} \frac{k_{m,i} \langle c_{T,m} \rangle^\dagger \Delta P^{h,m} + X J_{ch} / K_{f,i}}{k_{m,i} \langle c_{T,m} \rangle^\dagger + k_{F-m} X^2} \quad (8.34)$$

which shows that for $J_{ch} = 0$ the water flux through the membrane does not depend of the sign of the membrane charge, X , but only on its magnitude. (This is different when cations and anions in the membrane have different diffusion coefficients.)

We continue this section for $J_{ch} = 0$ and $\Phi_i = 1$. We define a dimensionless osmotic permeability \mathcal{P}_{osm} as the flow of water v_w divided by the maximum flow of water, i.e., $\mathcal{P}_{osm} = v_w / v_{w,max}$, where $v_{w,max} = k_{F-m} \Delta \Pi^\infty$ where $\Delta \Pi^\infty = 2 (c_{salt-high} - c_{salt-low})$ (right minus left). In Fig. 8.2 we show results of \mathcal{P}_{osm} as predicted by Eq. (8.34), as function of membrane charge density, X , and of the ratio of the ion-fluid mass transfer coefficient, $k_{m,i}$, over fluid-membrane friction coefficient k_{F-m} (this ratio has unit mol/m^3), and we observe how \mathcal{P}_{osm} first increases with membrane charge and then decreases again. Fig. 8.2 shows that for $X = 0$ there is no osmosis at all: water does not move, and ions just diffuse from high to low concentration. Instead, for a hydrostatic pressure gradient to develop inside the membrane, we need the membrane to be charged (or we need $\Phi_i < 1$). This can be understood from analysing Eq. (8.29) in the low- X limit

$$\Delta P^{h,int} = \frac{X^2}{4c_\infty} + \mathcal{O}(X^4) \quad (8.35)$$

which shows that in this limit, there is no hydrostatic pressure building up. In dialysis, with equal $P^{h,\infty}$ on the left and right outside the membrane, we have $\Delta P^{h,m} = \Delta P^{h,int,R} - \Delta P^{h,int,L}$ and thus the water flow in this limit is now obtained from combining Eqs. (8.34) and (8.35), assuming that the denominator in Eq. (8.34) is close to 1 because X is small, resulting in

$$v_w = -1/4 k_{F-m} X^2 \left(c_{salt-high}^{-1} - c_{salt-low}^{-1} \right) \quad (8.36)$$

which is the dashed line on the left in Fig. 8.2.

At high X the build-up of hydrostatic pressure is at a maximum, across each interface given by

$$\Delta P^{h,int} = X - 2c_\infty \quad (8.37)$$

and thus the pressure between the leftmost and rightmost positions in the membrane is given by $\Delta P^{h,m} = \Delta \Pi^\infty$.

Despite this constant high value of the internal pressure difference, nevertheless at high X the osmotic permeability, \mathcal{P}_{osm} , goes down. This is because there is more and more friction

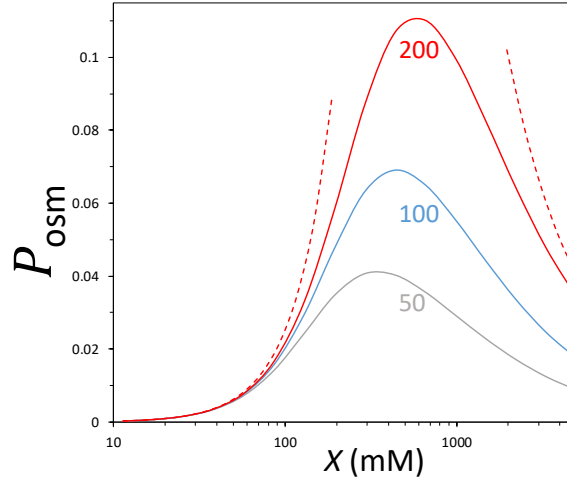


Fig. 8.2: The osmotic permeability \mathcal{P}_{osm} as function of membrane charge X ($c_{\text{salt-high}} = 0.5$ M, $c_{\text{salt-low}} = 0.1$ M, for several values of $k_{m,i}/k_{F-m}$, unit mM), based on Eq. (8.34).

of the water with the increasing number of (almost stagnant) counterions in the membrane. At high X we can simplify Eq. (8.34) to

$$v_w = -k_m |X|^{-1} \Delta\Pi^\infty \quad (8.38)$$

which shows the inverse dependence on the magnitude of the fixed charge density, $|X|$, as indicated by the red dashed line on the right in Fig. 8.2.

What we note is that the osmotic coefficient \mathcal{P}_{osm} is far below unity, even at the maximum: on the one hand the friction of water with the ions in the membrane reduces the flow of water while at low and moderate X the osmotic pressure difference between the two outer compartments does not translate fully to the same hydrostatic pressure difference inside the membrane, because the ratio X/c_∞ is not high enough. Note that for the data that we discuss in the next section, the factor $k_{m,i}/k_{F-m}$ is much larger ($>7,000$ mol/m³) and thus the osmotic coefficient is much larger as well, $\mathcal{P}_{\text{osm}} \sim 0.6$.

What would be the permeability when instead of an osmotic pressure difference, we apply a hydrostatic pressure difference? With the same salt concentration on both sides, the osmotic pressure increase across the Donnan layers is the same on both sides, and thus the jumps in hydrostatic pressure across the Donnan layers on the edges of the membrane are also the same on both sides. Thus the pressure difference across the inner region of the membrane is the same as the pressure difference between the two outer compartments, i.e.,

$\Delta P^{\text{h,m}} = \Delta P^{\text{h,\infty}}$. We have the same value of $c_{\text{T,m}}$ at the edges of the membrane, and we assume this value to be the same at each position inside the membrane. We can now again use Eq. (8.34) and at high X we also obtain Eq. (8.38) but with $\Delta\Pi^\infty$ replaced by $\Delta P^{\text{h,\infty}}$. However, at low X , Eq. (8.34) no longer has Eq. (8.36) as limit, but instead v_w goes to a maximum value given by $v_w = -k_{\text{F-m}}\Delta P^{\text{h,m}}$. Thus, the hydrostatic pressure is ‘fully used’, in contrast to the osmotic pressure which in the example above is only used to drive water across the membrane up to a maximum value of $\sim 11\%$.

8.3.6 Mathematical analysis of dialysis with charged membranes

Next we discuss actual dialysis experiments with osmosis of water across a charged cation-exchange membrane (CEM). Data are presented in Fig. 8.3A for the volume flow and salt flow across a membrane, at several values of the two reservoir concentrations. For technical details of the experimental program and data analysis, see [here](#).^{vii} In the experiment there is a volumetric flow from the diluate side to the concentrate side (squares), and at the same time a flow of salt *in the other direction*. We therefore know for sure that in the membrane there must be water flowing past the salt ions. If we multiply the salt flux by an estimate of the volume of hydrated ions, and if we assume a fairly large ion volume based on a size of a hydrated ion of 0.5 nm, the volume flow associated with the salt flux is only 2% of the measured volume flow. Thus in this experiment –and likely in many other similar experiments– the volume flow associated with the hydrated ions diffusing through the membrane is not very large, and as a good starting point we can assume in the transport theories that the ions are volumeless point charges. This significantly simplifies many equations. And a consequence, we can equate the measured J_{vol} to the theoretical property of the flow velocity of the water, v_w (neglecting a contribution of ions to the measured J_{vol}).

So, can we fit the equations derived in this chapter, based on the two-fluid model, to these data for the flow of water and of salt? To find out, we first derive an equation for the salt flux. This follows from the same extended Nernst-Planck equation that also gave us the expression for current, Eq. (8.19), but we now we add cation and anion fluxes to obtain the salt flux, J_{salt} , according to

$$2J_{\text{salt}} = J_+ + J_- = K_{\text{f},i}c_{\text{T,m}}v_w - K_{\text{f},i}k_{\text{m},i} \left\{ \frac{\partial c_{\text{T,m}}}{\partial \bar{x}} - X \frac{\partial \phi}{\partial x} \right\}. \quad (8.39)$$

^{vii}We are not aware of similar data published elsewhere on salt and water flow measured simultaneously in dialysis, and a fit with a transport theory.

We can implement Eq. (8.33) with $J_{\text{ch}} = 0$, and obtain

$$J_{\text{salt}} = \frac{K_{f,i}}{2} \left(c_{T,m} v_w \left(1 - X^2 / c_{T,m}^2 \right) - k_{m,i} \frac{\partial c_{T,m}}{\partial \bar{x}} \right). \quad (8.40)$$

The first term on the right is a combination of convection and electromigration, while the second term describes diffusion of salt to the diluate side. This entire first term approaches zero when the membrane is very highly charged. Then only the second term, diffusion, remains. For the theory fits that we obtain in Fig. 8.3 for a cation-exchange membrane (CEM), a membrane used in electrodialysis (ED), the first term is about 8% of the second, diffusion, term.

We can integrate Eq. (8.40) to

$$J_{\text{salt}} = \frac{K_{f,i}}{2} \left\{ v_w \left(\langle c_{T,m} \rangle - \frac{X^2}{\langle c_{T,m} \rangle^\dagger} \right) - k_{m,i} \Delta c_{T,m} \right\} \quad (8.41)$$

In this section we will solve Eq. (8.41) by assuming that the concentration $c_{T,m}$ changes linearly across the membrane, but an exact integration will be discussed in §11.7. We find that it is possible to fit the model to the data when we assume $K_{f,i} = 1$. We then use Eqs. (8.34) and (8.41) together with the solution/membrane boundary conditions, Eq. (8.29), by tuning the three parameters in the theory ($k_{m,i}$, k_{F-m} , and Φ_i ; $X = -5.1$ M). A very good fit is obtained for $\Phi_i = 0.53$. However, based on salt absorption data for ion-exchange membranes we know that Φ_i is likely somewhat larger, $\Phi_i \sim 0.82$ (Galama et al., 2013, p. 136, $\Phi_i = \exp(-\mu^*)$ with $\mu^* = 0.2$). We continue with this latter value of Φ_i and make the analysis once again.

To then fit the model to the data we must include in the transport equations the friction of ions with the membrane matrix, not just with the water, thus we now use a $K_{f,i}$ less than unity (for both ions we use the same value). Now Eq. (8.29) is still valid, but Eqs. (8.32) and (8.34) no longer apply. We start at the general fluid transport equation, Eq. (8.3)

$$-\frac{\partial P^h}{\partial \bar{x}} + \frac{\partial \Pi}{\partial \bar{x}} - \frac{1}{k_{F-m}} v_F = - \sum_i \frac{1}{k_{m,i}} \left(K_{f,i} c_i v_w - K_{f,i} k_{m,i} \left(\frac{\partial c_i}{\partial \bar{x}} + z_i c_i \frac{\partial \phi}{\partial \bar{x}} \right) - c_i v_F \right) \quad (8.42)$$

in which we inserted Eq. (7.71). Replacing $\sum_i c_i$ with $c_{T,m}$, we obtain

$$-\frac{\partial P^h}{\partial \bar{x}} + \frac{\partial \Pi}{\partial \bar{x}} - \frac{1}{f_{F-m}} v_F = \frac{1}{k_{m,i}} (1 - K_{f,i}) c_{T,m} v_w + K_{f,i} \frac{\partial c_{T,m}}{\partial \bar{x}} + K_{f,i} \sum_i z_i c_i \frac{\partial \phi}{\partial \bar{x}} \quad (8.43)$$

in which we can implement local electroneutrality, $\sum_i z_i c_i + X = 0$, and $\Pi = c_{T,m}$, resulting in

$$-\frac{\partial P^h}{\partial \bar{x}} - \frac{1}{k_{F-m}} v_F = \frac{1}{k_{m,i}} (1 - K_{f,i}) c_{T,m} v_w - (1 - K_{f,i}) \frac{\partial c_{T,m}}{\partial \bar{x}} - K_{f,i} X \frac{\partial \phi}{\partial \bar{x}} \quad (8.44)$$

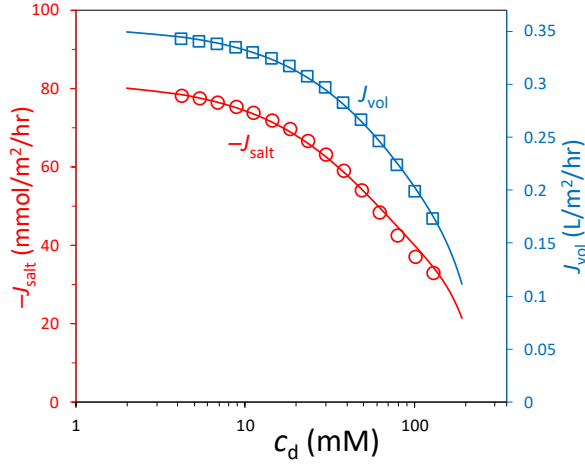


Fig. 8.3: Results of a dialysis experiment. Osmosis of water through a charged cation-exchange membrane placed between two solutions at different salt concentrations. Data and theory are presented for the volume flow through the membrane (blue squares), and the salt flux (red circles) *in the other direction*, as function of the salt concentration in the diluate solution, $c_{\infty,low}$. For parameter settings and values of $c_{\infty,high}$, see main text.

in which we can implement Eq. (8.33) to arrive at

$$\frac{\partial P^h}{\partial \bar{x}} + \frac{1}{k_{F-m}} v_F = -\frac{1}{k_{m,i}} (1 - K_{f,i}) c_{T,m} v_w + (1 - K_{f,i}) \frac{\partial c_{T,m}}{\partial \bar{x}} - \frac{K_{f,i} X^2 v_w}{k_{m,i} c_{T,m}} \quad (8.45)$$

which we can rearrange to

$$\frac{\partial P^h}{\partial \bar{x}} = -\left(\frac{1}{k_{F-m}} + \frac{1 - K_{f,i}}{k_{m,i}} c_{T,m} + \frac{K_{f,i} X^2}{k_{m,i} c_{T,m}} \right) v_w + (1 - K_{f,i}) \frac{\partial c_{T,m}}{\partial \bar{x}}. \quad (8.46)$$

We can integrate Eq. (8.46) across the membrane (between points at the edges, but just inside, the membrane), resulting in

$$\Delta P^{h,m} = -\left(\frac{1}{k_{F-m}} + \frac{(1 - K_{f,i}) \langle c_{T,m} \rangle}{k_{m,i}} + \frac{K_{f,i} X^2}{k_{m,i} \langle c_{T,m} \rangle^\dagger} \right) v_w + (1 - K_{f,i}) \Delta c_{T,m} \quad (8.47)$$

which we can rearrange to

$$v_w = -\frac{k_{m,i} k_{F-m} (\Delta P^{h,m} - (1 - K_{f,i}) \Delta c_{T,m})}{k_{m,i} + k_{F-m} \langle c_{T,m} \rangle (1 - K_{f,i}) + k_{F-m} K_{f,i} X^2 / \langle c_{T,m} \rangle^\dagger}. \quad (8.48)$$

Without ion-wall friction we have $K_{f,i} = 1$, and we return to Eq. (8.32). To calculate the salt flux, we again use Eq. (8.41).

Application to reverse osmosis. The above equations apply to a 1:1 salt that transfers across a membrane without current, such as in dialysis and reverse osmosis (RO). RO is a water desalination method where water is pushed through a membrane by applying a pressure difference across a membrane, as will be analysed in detail in Ch. 11. We can apply Eq. (8.48) to RO, and assuming that k_{F-m} is much smaller than $k_{m,i}/X$, we can replace the entire factor in front of the driving forces by the water permeability A , which leads to

$$v_w = -A \left(\Delta P^{h,m} - (1 - K_{f,i}) \Delta c_{T,m} \right) \quad (8.49)$$

and we now wish to express the driving forces as those between two positions just outside the membrane. Across each membrane edge the total pressure, $P^h - \Pi$, is invariant, and thus a total pressure difference between a point in the membrane on one side, and a point in the membrane on the other side, will also be the same as the total pressure difference between two points just on the two outsides (referred to with index ' ∞ '). Thus

$$\Delta P^{h,m} - \Delta c_{T,m} = \Delta P^{\text{tot}} = \Delta P^{h,\infty} - \Delta \Pi^\infty \quad (8.50)$$

where we use the fact that in the membrane Π equals $c_{T,m}$ and outside it is equal to $2c_j$ where c_j is a salt concentration just outside the membrane on either side. All of this we can implement in Eq. (8.49), and if we assume that on the right side 'R' of the membrane (to which the water flows), the salt concentration is much lower than on the left 'L'-side, thus the osmotic pressure there at 'R' is negligible to that at position 'L', then we arrive at

$$v_w = -A \left(\Delta P^{h,\infty} - \sigma' \Pi_L \right) \quad (8.51)$$

where a modified salt reflection coefficient, σ' , is defined as

$$\frac{1 - \sigma'_i}{1 - \sigma_i} = \sqrt{\left(\frac{C}{c_L} \right)^2 + 1} - \frac{C}{c_L} = 1 - C/c_L + \mathcal{O}\left((C/c_L)^2 \right) \quad (8.52)$$

where σ_i is the standard reflection coefficient for neutral solutes and neutral membranes, $\sigma_i = 1 - K_{f,i} \Phi_i$, and C is a charge factor given by $C = |X|/(2\Phi_i)$. The Taylor expansion at the end of Eq. (8.52) is only valid for low C relative to c_L .

A good fit to the data reported in Fig. 8.3 is obtained with $K_{f,i} = 0.51$, $k_{F-m} =$

87 (mm)⁴/mol/s, and $k_{m,i} = 0.62 \mu\text{m/s}$. The value of k_{F-m} together with a membrane thickness of $L_m = 120 \mu\text{m}$ recalculates to a value for the water-membrane friction coefficient of $f_{F-m} = 96 \text{Tmol.s/m}^5$, which is in between two values reported in Tedesco *et al.* (2017). The mass transfer coefficient $k_{m,i}$ recalculates to a $D_{m,i}$ which we can multiply by $K_{f,i}$ and that group is about 40 – 50× less than the free diffusion coefficient of ions in solution (which is $\sim 1.5\text{--}2.0 \cdot 10^{-9} \text{m}^2/\text{s}$), in line with results in Fig. 7.2.

In conclusion, we can exactly describe data for osmosis through a charged membrane by the theories explained in this book, with a realistic, non-unity, value of the partition coefficient Φ_i , and a realistic non-unity ion-membrane friction factor $K_{f,i}$.

8.3.7 Mathematical analysis of electro-osmosis in a nanoporous medium

Electro-osmosis generally refers to an experiment in the field of electrokinetics using a thin channel through which a current runs with the EDLs at the sides of the channel not overlapping (see, e.g., Kortüm (1965), p. 424). Instead, in this section we describe electro-osmosis for a charged microporous material such as an ion-exchange membrane. Compared to the description of the dialysis-experiment of the last section we now do not have an osmotic pressure difference, but instead we apply a current. Because the two external solutions have the same salt concentration, and are at the same hydrostatic pressure, the hydrostatic pressures just inside the membrane, $P^{h,m}$, are also the same on the two membrane/solution edges, and the same holds for $c_{T,m}$. Though not correct by definition, we now also assume these two properties do not vary across the membrane, though it is possible they go down, then up again, or vice-versa. See [here](#) for a technical remark about the notation of $c_{T,m}$.

We analyse this experiment allowing for the possibility that $K_{f,i} \neq 1$. Thus based on Eq. (8.18) together with Eq. (8.39) with $\partial c_{T,m}/\partial x = 0$ and $\partial P^{h,m}/\partial x = 0$, we obtain a perfect proportionality between v_w and J_{ions} (which is the total ions flux, equal to twice the salt flux J_{salt})

$$\frac{v_w}{J_{\text{ions}}} = \frac{1}{k_{m,i}/k_{F-m} + c_{T,m}} \quad (8.53)$$

which contains the same factors as discussed in the last section. There are several intriguing aspects to Eq. (8.53). First is that the result is completely independent of membrane thickness L_m and of the factor $K_{f,i}$. In retrospect the independence of $K_{f,i}$ makes sense because we describe here the water flow as function of the total flux of ions, and how much friction these ions have with the membrane matrix will not influence how strongly they drag on the water. Second, interestingly, Eq. (8.53) is valid irrespective of the membrane charge. Also

at very low charge, we find this proportionality, and because we know that in the limit of a very low charge (i.e., a non-selective membrane) the ratio of J_{ions} over current density J_{ch} goes to zero (zero current efficiency, see Eq. (12.8) in Ch. 12), we know that v_w goes to zero if X goes to zero: there is no electro-osmosis for an uncharged membrane.

For a highly charged membrane we know that $J_{\text{ions}} \sim |J_{\text{ch}}|$ while $c_{\text{T,m}} \sim |X|$, and then we can rewrite Eq. (8.53) to an expression for the aforementioned ratio of water molecules transported per charge, which unit ‘mole/mole’. This electro-osmotic coefficient, α , is given by

$$\alpha = \frac{v_w}{|J_{\text{ch}}| \nu_w} = \nu_w^{-1} \left(\frac{k_{\text{m},i}}{k_{\text{F-m}}} + |X| \right)^{-1} \quad (8.54)$$

where we introduce the water molar volume $\nu_w \sim 18 \text{ mL/mol}$. The electro-osmotic coefficient α is independent of current, and thus the water flow v_w is proportional to current, and this may then look experimentally as if a certain number of water molecules moves through the membrane tightly bound to the ions. But actually Eq. (8.54) describes the flow of water, dragged along because of ion-water friction. We derived that α is not some intrinsic property of water hydration, but depends on membrane charge and on ‘free’ transport parameters. Inserting the parameters derived in fitting the dialysis-data of the last section (for the $K_{\text{f},i} \neq 1$ -case), we obtain $\alpha = 4.5$, a very realistic number similar to what has been measured for electro-osmosis of charged membranes.

To this contribution by the flow of water, we can add the volume flow associated with the flux of the hydrated ions. This flow is an additional contribution to α of for instance $\alpha_{\text{hyd}} = 2-5$ (but only when $J_{\text{ions}} \sim |J_{\text{ch}}|$, otherwise the contribution is less), typical values for the hydration number of ions. Clearly, the contribution of water molecules in the hydration shell of ions cannot be distinguished easily from the free flow of water.

In summary, also in the electro-osmosis experiment there is a significant flow of ‘free’ water, in addition to the water molecules locked in the hydration shell of ions. The electro-osmosis experiment can be used to measure the ratio $k_{\text{m},i}/k_{\text{F-m}}$ of a membrane, if we have a means to exactly estimate the hydration number of ions in a charged membrane.^{viii}

^{viii}Note that the present analysis assumed equal ion diffusion coefficients, equal ion-membrane frictions, absence of partition effects, absence of diffusion boundary layers, full ion dissociation, ... Also experimentally, the measurement of volume flow through a single membrane in an experiment with current running between two electrodes, possibly with gas evolution, can introduce errors. So an accurate determination of frictional factors based on analysis of an electro-osmosis experiment is a task that is not to be taken lightly ...

8.3.8 Electrokinetic cross-functions

In the field of electrokinetics, many additional relations and experiments are in use, coupling applied pressures, currents, voltages, etc. In this section we discuss two such cross-effects.

First, we can run the electro-osmosis experiment described above, but now push the water back by a pressure difference such that there is no water flow. The relation that we want to find is the pressure difference as function of current and water flow. First we derive the extension to Eq. (8.53) including a pressure difference which results in

$$v_w = \frac{J_{\text{ions}} - k_{m,i} \Delta P^{\text{h},\infty}}{k_{m,i}/k_{\text{F-m}} + c_{\text{T,m}}}. \quad (8.55)$$

This is the flow of water. At the point that the total volume flow is zero, this water flow and the volumetric flow of the ions, add up to zero, thus we then have $v_w + v_{\text{ion}} J_{\text{ions}} = 0$, where v_{ion} is the volume of the hydrated ions (mL/mol). Inserting this information in Eq. (8.55) we arrive at

$$\frac{\Delta P^{\text{h},\infty}}{J_{\text{ions}}} = \frac{1}{k_{m,i}} + v_{\text{ion}} \left(\frac{1}{k_{\text{F-m}}} + \frac{c_{\text{T,m}}}{k_{m,i}} \right) \quad (8.56)$$

and when we assume $J_{\text{ions}} \sim |J_{\text{ch}}|$ and $c_{\text{T,m}} \sim |X|$, we obtain for the cross-function describing the pressure-current ratio at zero water flow

$$\frac{\Delta P^{\text{h},\infty}}{|J_{\text{ch}}|} = \frac{1}{k_{m,i}} + v_{\text{ion}} \left(\frac{1}{k_{\text{F-m}}} + \frac{|X|}{k_{m,i}} \right). \quad (8.57)$$

If we assume the ions to have no volume ($v_{\text{ion}}=0$), Eq. (8.57) simplifies significantly, to

$$\frac{\Delta P^{\text{h},\infty}}{|J_{\text{ch}}|} = \frac{1}{k_{m,i}}. \quad (8.58)$$

Eqs. (8.57) and (8.58) suggest that the pressure that must be generated as the consequence of a current to keep a zero water flow, is a direct measure of the ion-water friction coefficient (which also includes the membrane thickness), $k_{m,i}$, and the water-membrane friction, $k_{\text{F-m}}$, but just as in electro-osmosis, is independent of a possible ion-membrane friction as described by $K_{f,i}$. For $v_{\text{ion}}=0$, the result only depends on the ion-water friction, $k_{m,i}$. In this coupling experiment, the water and the membrane both have a zero velocity, and this must be why $K_{f,i}$ does not play a role.

—

The second cross-effect we consider is the electrical potential across the membrane when water is pushed through, at zero current. The two external solutions have the same salt

concentration. Thus inside the membrane we can again assume $\partial c_{T,m}/\partial x = 0$ and the changes in voltage across the Donnan layers are the same on each side, and the same for the changes in pressure. Thus we aim to establish the relationship between $\Delta\phi^m = \Delta\phi^\infty$ and $\Delta P^{h,m} = \Delta P^{h,\infty}$. This is called the streaming potential.

We again start with Eq. (8.18), and combine with Eq. (8.19). We assume $c_{T,m} \sim |X|$ and arrive at

$$\frac{\Delta\phi^\infty}{\Delta P^{h,\infty}} = \frac{1}{k_{m,i}/k_{F-m} + |X|} \quad (8.59)$$

and this ratio is independent of membrane thickness or $K_{f,i}$. For the parameters derived for dialysis in §8.3.5, this ratio is about 0.08 M^{-1} . This recalculates to a streaming potential of $\sim 0.08 \text{ mV/bar}$. This is a very low number which is because the water-membrane friction is high and the charge density is high. For a more open material with thus a higher k_{F-m} and a lower X , the streaming potential is much larger.

Water flow in the electro dialysis process. When we have a series of flow channels containing electrolyte with salt concentration c_∞ , separated by alternately positively and negatively charged membranes, called AEMs and CEMs, we can build a membrane stack for electro dialysis (ED), see Ch. 12. With current directed through this stack, the salt concentration will go up in the 1st, 3rd, 5th, ... channel (the c-channels), while every other channel is being desalinated (the d-channels). While ions move to the c-channels, also water moves there (both through the AEMs and CEMs). The water moves there because of the higher osmotic pressure in the c-channel relative to the d-channels, and that difference pulls the water there, and in addition because of the electro-osmotic effect, which is proportional to $X\Delta\phi_m$, see e.g. Eq. (8.32). Interestingly, as long as some current flows, this water flow will continue forever. One way to make it stop is when there is an increasing hydrostatic pressure pushing back from the c-channels, but otherwise all the water and salt will go to the c-channels.

8.4 Mechanical forces between colloidal particles and charged media

There are many pressures in electrochemical systems. In several chapters we discussed (and will discuss) hydrostatic pressures and osmotic pressures. In Chs. 1 and 5 we discussed the surface pressure. In the present section we first describe the pressures in ‘free solution’, in

relation to the structure of the EDL and the electrostatic forces between colloidal particles, and subsequently the mechanical pressures that develop between two charged porous layers across which an electrical current is directed.

8.4.1 The electrostatic contribution to the disjoining pressure

In this section we discuss the forces, or pressures, between colloidal particles. These forces are the hydrostatic and osmotic pressures, while we also discuss the Maxwell pressure. We explain how these pressures determine the electrostatic contribution to the disjoining pressure, which is the force or pressure acting on a charged particle when there are other charged particles nearby, interacting across an electrolyte solution. We consider mechanical equilibrium, which implies that all velocities, those of the fluid, surfaces, and ions, are all zero (relative to one another).

Analysis of these forces is of special importance for the interaction between two particles with overlapping EDLs, leading to an electrostatic repulsion or attraction between the two materials, see Ch. 6. Thus we focus on the analysis of the pressures inside the gap between two charged surfaces.

The force on a charged particle because of the presence of other charged particles^{ix} is given by the disjoining pressure, P^{dis} , integrated over any surface that encloses this particle, multiplied by the vector normal to that surface. Thus the total force is $\mathcal{F} = \oint_S (P^{\text{dis}} \cdot \mathbf{n}) \, dS$. The enclosed area can include some electrolyte phase around the particle, but can also directly track the particle's surface. For homo-interaction of two equally-sized spheres, integration over the symmetry plane between the two particles is the logical choice often made (and then the integration extends along this surface to infinitely far away).

The disjoining pressure is a sum of the hydrostatic pressure and the Maxwell pressure^x

$$P^{\text{dis}} = P^{\text{h}} - \frac{\varepsilon}{2RT} E^2 \quad (8.60)$$

where the hydrostatic pressure is always repulsive (or zero), and the Maxwell pressure always attractive (or zero). It is probably not surprising that a hydrostatic pressure acts as a force on a particle. The Maxwell pressure is also familiar because it equals the force acting across a dielectric region with non-zero field strength E , e.g., between any two oppositely charged plates, with charge density $\pm\Sigma$. [The electrical energy in a dielectric layer of thickness d

^{ix}Also a neutral particle exerts a pressure on a charged particle. This is because the neutral particle, when it enters the diffuse layer around a charged particle, excludes volume for counterions, i.e., for the ions less space is available. Thus the electrical potentials in the EDL go up to attract enough counterions to compensate the loss of volume. This increase in potential leads to a disjoining pressure (acting equally on both particles).

^xPressures P are in mol/m³, and can be multiplied by RT to a dimensional pressure \bar{P} in Pa.

that separates two regions of charge $\pm\Sigma$, resulting in a voltage difference V across the layer, has an electrical energy of $\frac{1}{2}\Sigma V$, as can be calculated from a charging process where Σ is increased from zero, at fixed d . Implementing Gauss' law ($\Sigma = \pm\varepsilon E$) with $E = \pm V/d$ (linear decrease in voltage), and for fixed Σ taking minus the derivative of this energy with d , results in an attractive force (a negative pressure) of $-\frac{1}{2}\Sigma^2/\varepsilon$, or $-\frac{1}{2}\varepsilon E^2$, just like the second term in Eq. (8.60).]

Now, interestingly, the Navier-Stokes equation, Eq. (8.16), predicts that at mechanical equilibrium we have (Verwey & Overbeek (1948), Eq. (42a) on p. 92)

$$RT\nabla P^h - \rho\mathbf{E} = 0 \quad (8.61)$$

which we can combine with Poisson's equation. We can integrate this result across a planar one-dimensional EDL, i.e., across the gap between two charged surfaces. The result is that there is a property, equal to the right side of Eq. (8.60), which has a constant value, i.e., is the same wherever we are in this planar gap.

This constant is the disjoining pressure. The invariance of the disjoining pressure with position in a gap between two parallel planar surfaces, is also the case for the center region between two curved surfaces that are very close (distance between the surfaces \ll than the radius of the spheres). This result, of a constant P^{dis} , does not generally follow from Eq. (8.61) when \mathbf{E} varies in more than one direction.

Based on Eq. (8.15) we also know that for mechanical equilibrium at each point in an EDL we have $\nabla P^h = \nabla\Pi$, i.e., if we set the hydrostatic pressure to zero far from the particles, then at any point in an EDL, $P^h = \Delta\Pi = \Pi - \Pi^\infty$. This is correct whatever is the geometry of the space that we analyse, i.e., valid between any two points inside and outside an EDL, and whatever is the exact function we use to describe the osmotic pressure. When we assume the ions to be ideal point charges, and for a 1:1 salt, we will have $P^h = 2c_\infty (\cosh\phi - 1)$.

We can combine this equality of P^h and Π with Eq. (8.60) that describes the disjoining pressure inside a planar gap between two surface, and arrive at

$$\frac{P^{\text{dis}}}{c_\infty} = 2 (\cosh\phi - 1) - \lambda_D^2 \left(\frac{\partial\phi}{\partial x} \right)^2 \quad (8.62)$$

for a 1:1 salt solution. At the centerpoint along this line between the two surfaces (i.e., halfway), it is the case that:

1. For homo-interaction, there is symmetry halfway, thus $E=0$ there, and thus the disjoining pressure is given by the first term on the right of Eq. (8.62). Thus only the hydrostatic/osmotic pressure plays a role. This is also the case for asymmetric salt solutions.
2. For hetero-interaction of two exactly oppositely charged surfaces, we have at this center-position $P^h = \Delta\Pi = 0$ (the salt concentration here is the same as outside the EDL, and $\phi=0$

at this centerpoint), and the disjoining pressure is only given by the attractive Maxwell pressure, $\bar{P}^{\text{dis}} = -1/2\epsilon E^2$. (This is only the case for a symmetric salt solution).

Though these two simplified cases are useful, in general we must consider both contributions to the disjoining pressure, both the osmotic pressure (equal to the hydrostatic pressure), and the Maxwell pressure. And we can then evaluate the sum of these two terms, using Eq. (8.62), at any position along a direct line between two planar parallel surfaces, and it will always give the same outcome, irrespective of what type of EDL model is used (Langmuir, 1938).

Based on the fact that the disjoining pressure, for instance evaluated by Eq. (8.62), is the same at any position in a one-dimensional planar EDL, we can calculate the potential profile using the Poisson-Boltzmann equation (or any modification) across a planar gap. We only have to solve a single ordinary differential equation (ODE), for instance Eq. (8.62), once we know the disjoining pressure. If P^{dis} is positive, the surfaces are repulsive. We then solve Eq. (8.62) from a position $x=0$ where $\partial\phi/\partial x$ is zero, and this ODE is then

$$\partial\phi/\partial x = \kappa\sqrt{2(\cosh\phi - 1) - P^{\text{dis}}/c_\infty} \quad (8.63)$$

with $\phi|_{x=0}$ chosen such that at $x=0$ the entire right side is zero. If instead $P^{\text{dis}} < 0$, then we solve Eq. (8.63) from a position $x=0$ where $\phi=0$ (and thus $\partial\phi/\partial x$ will not be zero there).

This finalizes our discussion of the various types of pressures of relevance for the study of the interaction forces between charged particles. The expressions in this section for the disjoining pressure can also be used to describe the expansive forces inside a porous charged medium, as briefly mentioned for the Donnan model on p. 41.

8.4.2 Forces between charged porous media when current flows

In the previous section we discussed pressures that develop at mechanical equilibrium. We next continue with a calculation of pressures that only develop off-equilibrium, i.e., when current flows. Extremely high (negative) pressures are predicted to develop in the junction of an anion-exchange layer (AEL) and a cation-exchange layer (CEL) inside a bipolar membrane (BPM) when a current flows through this BPM. The junction is the interface where AEL and CEL touch. The description of the junction structure is based on equilibrium, though the required flow of current running across the BPM makes this a non-equilibrium problem, because if this current would not be there, the pressures in the junction disappear, becoming the same as outside the membrane (on either side of the membrane we assume there is the same pressure).

For the cations and anions, say Na^+ and Cl^- , at steady state there is a certain flux across the BPM, in one direction for the cations, and for the anions in the opposite direction. For a symmetric system (equal diffusion coefficients, equal $|X|$ of the two layers, equal thickness, etc., these two fluxes have exactly the same magnitude. In that regard the BPM is symmetric. For the water, in this perfectly symmetric case, there is no preferred direction. Thus, there is no water transport across the BPM. This poses a question, because why does it stop flowing: each layer by itself is a membrane and current passes it between an outside solution and the junction region (which is also a kind of outside solution, even though its thickness can be vanishingly small). Such a membrane by itself would have water flow across it when there is current. To understand what now happens, we can analyze Eqs. (8.29)-(8.19). We evaluate the situation that the current I flows as counterions from the junction outward, so cations flow outward through the CEL, and likewise for the AEL anions flow from the junction outward. [As coions the same ions arrive via the other layer in the junction. This is a steady-state process, and thus there is one flux of cations across the BPM, and the same for the anions. There is no accumulation of salt in the junction.] With current directed in the way just described, and when current is sufficiently high, we know that the concentration in the junction goes to extremely low salt concentrations, in the μM or nM range. While the osmotic pressure in the membrane is around $|X|$ (times RT , to obtain a pressure with unit Pa), it is very close to zero in the junction, while in the outside solution it is $2c_\infty$.

If we combine Eq. (8.32) with the relation between $\Delta\phi^m$ and J_{ch} from Eq. (8.33) for $v_w=0$ and $K_{f,i}=1$, and include mechanical equilibrium at each membrane-solution interface (including that between a membrane layer and the very thin junction), Eq. (8.27), we arrive at

$$P^{\text{h,jct}} + c_{\text{T,m}} - \left(P^{\text{h},\infty} + c_{\text{T,m}} - 2c_\infty \right) + \frac{XJ_{\text{ch}}}{k_{\text{m},i}c_{\text{T,m}}} = 0 \quad (8.64)$$

and if we assume $c_{\text{T,m}} \sim |X|$ (constant across a layer), and make the replacement $I = -FJ_{\text{ch}}$ (current I now defined as directed from junction outward), and we evaluate the function for the CEL ($X < 0$) we obtain for the pressure in the junction

$$P^{\text{h,jct}} = P^{\text{h},\infty} - 2c_\infty - \frac{XI}{Fk_{\text{m},i}} \quad (8.65)$$

and thus when the current direction is such that cations flow through the CEL from junction outward (entering the BPM on the AEL-solution interface), and likewise the anions flow from junction outward through the AEL, then the hydrostatic pressure in the junction will be much lower than in the outside solution, and can even be negative. The hydrostatic pressure in the junction pressure, $P^{\text{h,jct}}$, becomes the more negative the larger the current or the thicker the membrane ($k_{\text{m},i}$ is inversely proportional to thickness). While the two layers strongly

push on each other with their polymer structures, this negative pressure that develops in the fluid in the junction creates a pressure gradient in the fluid inside the membrane layer, with the pressure decreasing toward the junction, and that is a force to hold back the fluid against the forces that try to pull the fluid out of the junction, which is the electro-osmotic effect, $X\Delta\phi^m$. The effect of the low salt concentration in the junction, which is depleted of salt already at quite low currents, in combination with mechanical equilibrium at each of the interfaces of each layer (with the osmotic pressure change equal to the hydrostatic pressure change), leads to the junction pressure $\bar{P}^{\text{h, jct}}$ being at least $2RTc_\infty$ lower than outside, thus for a 1 M salt solution, $P^{\text{h, jct}}$ can easily be beyond 50 bar less, and on top of that is the electro-osmotic effect.

We numerically analyse the junction pressure based on Eqs. (8.29)-(8.19) and compare with Eq. (8.65) in Fig. 8.4. We see that for sufficiently high currents, indeed Eq. (8.65) correctly describes the pressure in the junction (a negative value!) as function of the applied current. The full numerical model shows that at very low currents, when inside the junction c_∞ approaches the value in outside solution, the pressure approaches zero, but already at quite low currents, salt concentration here drops to values close to zero, and from that point onward Eq. (8.65) correctly predicts the negative hydrostatic pressure in the junction between the two layers in a BPM. In both types of calculations we consider a perfectly symmetric BPM with a cation and anion of equal diffusion coefficient. Detailed calculations (not reported here) where we also include the H^+ - and OH^- -ions show that beyond $I/I_{\text{ref}}=0.01$ these ions are the main carriers of the current when they flow from the junction outward, i.e., H^+ and OH^- are formed at the junction. The current carried by the cation and anion (e.g., Na^+ and Cl^-) levels off at $I/I_{\text{ref}}=0.01$, with the cation coming through the AEL and jointly with the H^+ -ion moving outward through the CEL, while the anion flows does the exact opposite. The prediction of very negative junction pressures remains the same.

What happens now when the direction of the current is reversed in this BPM? Then quickly the salt concentration in the junction goes from very low to very high, and the field strength in each layer reverses sign. The two membranes are no longer in intimate contact, but a high pressure develops in the junction, and as a consequence the two layers are pushed apart from the inside. This may lead to delamination that can be avoided by sandwiching the BPM between outside structures and assembled tightly.

This entire topic of the forces on a charged structure at mechanical equilibrium, or due to a flow of current, resulting in hydrostatic pressures, and tensions inside the material, is important besides the study of the forces on fluid and ions. Tensions in a material also influence the structure (porosity) and thus influence ion and fluid flow. Thus, the expansion or compression of a material, for instance at high currents, ‘feeds back’ in what are the rates

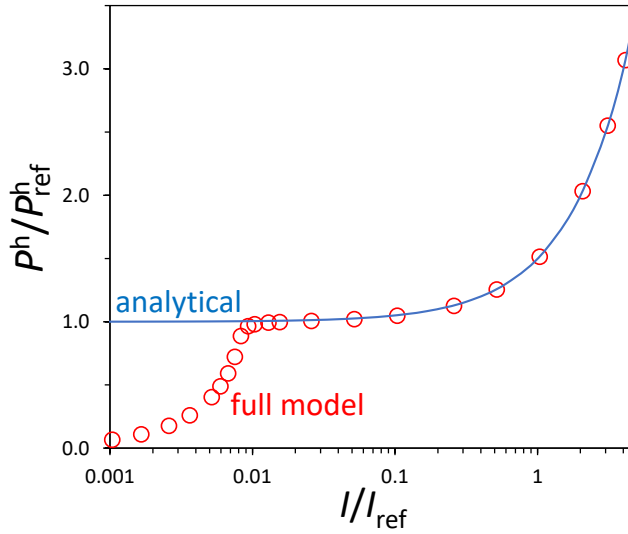


Fig. 8.4: The junction pressure P^h in a bipolar membrane (BPM) (relative to outside the membrane), a negative number, divided by a reference value $P_{\text{ref}}^h = -2c_{\infty}$ (1:1 salt), plotted against current density I . We analyze a 1:1 salt. The reference current is $I_{\text{ref}} = Fc_{\infty}D_{m,i}/\delta$ where δ is the thickness of each membrane layer. Analytical calculation based on Eq. (8.65) compared with numerical calculations based on Eqs. (8.19)-(8.29). Calculation for a BPM where for each layer $|X| = 4$ M, $c_{\infty} = 100$ mM, $k_{m,i} = 2.0 \mu\text{m/s}$, $I_{\text{ref}} = 19.3 \text{ A/m}^2$.

of fluid and ion transport across a porous material.

Heating and cooling in electrochemical systems

In electrochemical systems, electron-conducting and ion-conducting phases (metallic wires, and electrolyte) heat up when current passes, because of an electronic or ionic resistance. On top of that, electrical double layers (EDLs) strongly heat up or cool down dependent on the direction of the current through the EDL. This effect is well-known in solid state physics (Peltier effect) while the same phenomenon also takes place at the junction between aqueous phases generally encountered in electrochemical processes, such as on the outer surface of ion-exchange membranes.

9.1 Introduction

Heating and cooling are very important effects in electrochemical systems. These effects take place in bulk solution (electrolyte), in electron-conducting phases (metals), and at the interface between different phases, where EDLs form.

Heating will be ‘irreversible’ in a bulk electrolyte: whichever direction the current goes, there will be heating, often described by Ohm’s law and then called Joule Heating. In an EDL the situation is very different, and heating and cooling are ‘reversible’: for a certain EDL potential, ΔV_{EDL} , current I in one direction leads to heat production given by $I \cdot \Delta V_{\text{EDL}}$ (unit W/m^2), and when the current direction is reversed, we have cooling, with the same magnitude as the earlier heating, just with the sign reversed.

At the interface between two electron-conducting materials, this reversible cooling and heating in the EDL is called the Peltier effect, with the materials optimized in chemical composition to give both materials a fixed high charge, opposite in sign (one material having positive fixed charges, the other negative). In this way the EDL voltage is maximized and thus the heating and cooling during current flow is maximized as well.

This reversible heating and cooling in the EDL also takes place when two different metals are brought in contact with current passing across the junction between them. This is because in any pair of two metals electrons re-distribute because of differences in electron affinity of the metals. Thus an EDL is formed with two regions of opposite charge. In one region in the EDL there is an excess of electrons, while there is an excess of positive electronic charge in the other region of the EDL. These two charged regions create the EDL and a voltage difference develops across the interface. The EDL voltage at the junction between two randomly chosen metals will not be as pronounced as for designed materials with high fixed charges, but nevertheless there is reversible heating and cooling when current flows through this junction.

In the next sections we do not discuss metal junctions, but focus on cooling and heating in electrolyte phases. This can be an electrolyte in contact with a metal, thereby forming an electrode, or the interface between two electrolytes, one of which can be a charged porous medium such as an ion-exchange membrane or both are as in the bipolar membranes discussed in §8.4.2. At all interfaces where an EDL is formed reversible heating and cooling are possible.

9.2 The heat balance

Heating and cooling in an electrolyte is described by the heat balance given by

$$\rho_L c_p \frac{\partial T}{\partial t} = \lambda \frac{\partial^2 T}{\partial x^2} - v_{\text{tot}} \rho_L c_p \frac{\partial T}{\partial x} + \mathbf{I} \cdot \mathbf{E} - \sum_i R_i h_i + Q \quad (9.1)$$

which we set up for a one-dimensional planar geometry (see footnote on p. 198). In Eq. (9.1), we assume that irrespective of the ionic composition, the heat capacity per unit volume of electrolyte is $\rho_L c_p$ (unit of this entire term $\text{J}/(\text{m}^3 \cdot \text{K})$). We include a diffusive heat flow based on Fourier's law, $J_F = -\lambda \partial T / \partial x$, with λ the coefficient for heat conduction in $\text{W}/(\text{m} \cdot \text{K})$, and include convective heat transport, assuming a fixed value of the velocity of the electrolyte phase (solvent plus ions), v_{tot} . In Eq. (9.1), \mathbf{I} is the current density (here a vector with unit A/m^2) and \mathbf{E} is the field strength, i.e., minus the voltage gradient (also a vector, with unit V/m). The penultimate term describes heat production due to chemical reactions, as a sum over all components i of their formation rate, R_i (unit $\text{mol}/(\text{m}^3 \cdot \text{s})$), times their molar enthalpies, h_i . When reactions lead to products with a lower enthalpy than the reactants, this will result in the production of heat (i.e., it is an exothermic reaction). The last term, Q , describes heating or cooling by a Peltier element or other heating/cooling device or mechanism, and also includes the heating due to stirring of a solution (viscous dissipation). The electrical term $\mathbf{I} \cdot \mathbf{E}$ is the inner product of two vectors, and this quantity can be negative or positive, as we will analyze below.

Another term, just as $\mathbf{I} \cdot \mathbf{E}$ the inner product of two vectors, must also be added to Eq. (9.1) for fluid flow through a restrictive (porous) medium, and is given by $-\mathbf{v}_{\text{tot}} \cdot \nabla P^h$, which is minus the inner product of fluid flow velocity and hydrostatic pressure gradient. When this entire term (including the minus-sign) is positive, the fluid will heat up, a general effect in fluid flow, described as viscous dissipation, i.e., the heating of a fluid due to pumping. However, the reverse is also possible, i.e., flow-based cooling, which occurs when a fluid flows towards higher hydrostatic pressures, an effect that for instance occurs in the EDL at one of the edges of a membrane in the forward osmosis process.

The heat balance presented by Eq. (9.1) can be solved over part of a volume of solution phase. But it is also possible to apply this heat balance across an EDL, for instance on the outside of an ion-exchange membrane. To describe heating and cooling in a such an EDL, we integrate the heat balance over the EDL, thus integrate from one to the other side of the EDL. The EDL in this case is a very thin layer and thus the accumulation of heat, represented by the left side of Eq. (9.1), can be neglected. Across the EDL there is no

change in temperature, only a change in temperature gradient.ⁱ Because the temperature is continuous (i.e., does not change across the EDL), the convective term in the heat balance is zero. Integration of Eq. (9.1) following a coordinate x across the thickness of the EDL leads to

$$\lambda \cdot \left(\left. \frac{\partial T}{\partial x} \right|_{\text{R}} - \left. \frac{\partial T}{\partial x} \right|_{\text{L}} \right) - I \Delta V_{\text{EDL}} - \sum_i r_i h_i = 0 \quad (9.2)$$

where we use a surface-based reaction rate, r_i (in mol/(m².s)), and define the two sides of the EDL either by ‘L’ for left, or ‘R’ for right. The EDL voltage in Eq. (9.2) is defined ‘right minus left’, see p. 507. Heat production in the EDL is described by the product of I and ΔV_{EDL} , has unit W/m² and can be negative and positive. This expression for a reversible heat production –not the consequence of a resistance– was first put forward by Le Roux in 1866, see Langmuir in 1916, when discussing the case of current flow through a metal-metal junction.

9.3 The current density in an electrolyte bulk phase and membrane

One important element in Eqs. (9.1) and (9.2) is heat production due to a current. In bulk electrolyte this results in an Ohmic-like relationship based on a resistance to current, and then always heat is produced, while at interfaces (in the EDLs), heating and cooling are reversible, and both are possible.

In bulk solution, away from any interfaces, current I and field strength $E = -\partial V/\partial x$ (writing all properties now as function of only one coordinate x), generally are in the same direction (have the same sign), thus their inner product is positive which leads to heating (i.e., a positive contribution to the heat balance). In addition, they are often proportional as well, and then an ionic conductivity σ can be defined, such that

$$I = -\sigma \cdot \partial V/\partial x \quad (9.3)$$

where σ has the unit of S/m (S for Siemens) or ($\Omega \cdot \text{m}$)⁻¹, where $S = 1/\Omega = \text{A}/\text{V}$. Often Ω is called (and written as) ‘Ohm’, see also Eqs. (7.18) and (7.19). A volumetric resistance can be defined as $\rho = 1/\sigma$ of which the unit is $\Omega \cdot \text{m}$.

ⁱThis is analogous to the situation with Gauss’s law of electrostatics for a charged (infinitely thin) interface, which predicts that there is a difference in the gradient in potential between the two sides of the charged interface, while the potential itself stays the same when crossing the interface.

In §7.2 current density was described as function of ionic fluxes by Eq. (7.18). Based on this equation, we can quickly see that in two situations we arrive in bulk electrolyte at a proportionality between current and voltage gradient. The first situation is when concentration gradients can be neglected, for instance because (up to the moment of measurement) there has been enough mixing for concentration gradients to be small or absent, and for this reason the diffusion term on the right side of Eq. (7.18) disappears. The other option is that all ions have the same diffusion coefficient. Then, irrespective of the valencies of the ions, and also in the presence of concentration gradients, because of local electroneutrality, the diffusion term disappears. Thus, in both these situations we arrive at Eq. (9.3) for the relation between current density and voltage in bulk electrolyte. If we integrate over a certain layer of thickness L , and we introduce a voltage change, ΔV , defined ‘right minus left’ (with the x -coordinate pointing to the right), Eq. (9.3) can be rewritten to

$$I = -R^{-1}\Delta V \quad (9.4)$$

where $R = L/\sigma$ is an ionic resistance with unit $\Omega \cdot \text{m}^2$, dependent on layer thickness, but not on the perpendicular area through which the current runs.

If we now multiply each side of Eq. (9.4) by the area A through which the current runs, we obtain the current I_{sys} with unit A, and a resistance R_{sys} with unit Ω (Ohm),

$$I_{\text{sys}} = -R_{\text{sys}}^{-1}\Delta V. \quad (9.5)$$

Each of the last three equations can be called Ohm’s law, describing a proportionality between ionic current and gradients, or differences, in the voltage in an electrolyte phase. In many cases, Ohm’s law will be reasonably valid for current transport across an electrolyte phase. If there is a spacer mesh or other porous medium that blocks out part of the available volume for electrolyte, with porosity p remaining as open fraction, then conductivity σ is reduced because there is less cross-sectional area to flow through, and because of the tortuosity of the pathways for ion transport (and fluid flow) that are not straight across a material and that reduces the ion fluxes (thus current) along these pathways for a given driving force across the material. Thus the resistance will depend on a factor $\varepsilon = p/\tau$. Based on a measured σ or R , the factor ε can be derived. In a nanoporous medium, in addition we have $K_{f,i} \neq 1$, and thus the measured σ_m^* is $\sigma_m^* = K_{f,i}\varepsilon\sigma_\infty$, see a box on p. 166.

When Ohm’s law applies, we can easily calculate the heating in an electrolyte phase. Based on Eq. (9.1) we know that electrostatic heating, described by the heat production rate, HPR, is given by $\text{HPR} = I \cdot E$ (we assume that all transport is only along one coordinate). Combining with Eq. (9.4), we arrive at

$$\text{HPR} = \rho \cdot I^2 \quad (9.6)$$

which shows that HPR is always positive. This heating in a bulk phase, which is a quadratic function of current, is called ‘Joule heating’.

Inside a porous medium (such as an ion-exchange membrane), Eq. (7.18) can still be used, but now the convective contribution to current is no longer zero. From evaluation of $I = F \sum_i z_i J_i$ and Eq. (7.71), we can express current density in a membrane as

$$I = F v_w \sum_i K_{f,i} z_i c_i - F \sum_i \left\{ D_{m,i}^* z_i \frac{\partial c_i}{\partial x} \right\} - \sigma_m^* \frac{\partial V}{\partial x} \quad (9.7)$$

where $D_{m,i}^* = K_{f,i} \varepsilon D_i$, and where σ_m^* is the ionic conductivity in the membrane, $\sigma_m^* = K_{f,i} \varepsilon \sigma_\infty$, see p. 166, where conductivity in solution, σ_∞ , is defined by Eq. (7.19). When for all ions $K_{f,i}$ is the same and we implement local electroneutrality, $\sum_i z_i c_i + X = 0$, then the first term becomes $-F K_{f,i} X v_w$. Eq. (9.7) shows that in a membrane we generally have a complicated relationship between current, conductivity, and the voltage gradient. If the convection term can be neglected, and likewise the diffusion term (because all diffusion coefficients are the same or all concentration gradients small), then I and $\partial V / \partial x$ are proportional to one another. In that case Ohm’s law relates current and voltage across (the inner coordinate of) the membrane, such as Eq. (9.3), and we can measure a membrane conductivity or resistance experimentally. To do that, the measured voltage between the solution phases outside the membrane is corrected for the Donnan voltages at the membrane outer surfaces. Then a voltage gradient inside the membrane can be reliably estimated and a membrane resistance derived. Reliable methods to measure a membrane resistance are discussed in the box on p. 166.

In the inner structure of a membrane, generally current will flow in the direction of lower voltage, thus we can expect irreversible heating, perhaps not of the ‘Joule type’, Eq. (9.6), but heating nonetheless. However, Eq. (9.7) demonstrates that exceptions are possible.

9.4 Heat production due to current in a steady-state EDL

Heating and cooling in an EDL is relatively straightforward to model when this EDL is part of a steady state process. Then the EDL does not change in time while current flows across it. This will generally be the case for the EDLs on the outsides of a membrane structure in water, as in electrodialysis. Then there is an established Donnan potential, ΔV_{EDL} , and

dependent on the current direction there is either heating or cooling, with a magnitude linear in the rate of current.ⁱⁱ

As an example, with a negatively charged membrane (cation-exchange membrane) thus where cations easily move across the membrane, on the upfront side (where cations enter, thus where the current is positive into the membrane), the Donnan potential drop is negative, see Fig. 9.1. There the product of current and Donnan potential is negative and locally this membrane interface will heat up. On the other side of the membrane we have the same current, now leaving the membrane, but in this direction (out of the membrane) the voltage goes up when crossing the EDL, and thus this membrane interface cools down. In effect, such an ion exchange membrane combines two Peltier junctions at a short distance from one another, where at the same time one heats up and the other cools down. In an actual experiment, these two reversible effects are combined with Joule heating that goes on in the bulk electrolyte phases and in the membrane interior. Results of an experiment with a cation exchange membrane where the current direction is reversed every 60 s, are shown in Fig. 9.1B (Porada *et al.* (2019)). It must be noted that detailed comparison of theory and data was not quite satisfactory, with experimental changes in temperatures after a current reversal much slower than predicted by the full theory (Porada *et al.*, 2019). This discrepancy was unexpected because the model included a dynamic differential heat balance and included all details of ion transport towards and in the membrane. One possible cause for the difference is that also water flows through the membrane, in the direction of counterion flow, and upon current reversal, the water flow rate is also reversed. Water flow has an impact on temperatures because of convection of heat, because water flow leads to friction thus heating, and because at the edges of the membranes (EDLs) there is mechanical equilibrium, resulting in sudden changes in hydrostatic pressure, the value of which depends on the salt concentration just outside the membrane, see Ch. 8. The product of this pressure change and water flow rate in the EDLs is also a source term in the heat balance at the membrane interfaces, Eq. (9.2). These effects were not yet implemented.

9.5 Heat production in a capacitive electrode

The EDL at a flat, smooth electrode surface, or inside the pores of a porous electrode, will also be subject to electrostatic heating and cooling, with the EDL heating up when the electrode is charged (i.e., when the diffuse layer of ions is building up, thus with an

ⁱⁱBecause ion concentrations near the EDL depend on current, and ΔV_{EDL} therefore as well, a perfect proportionality between heat production and current will only be observed experimentally at low currents.

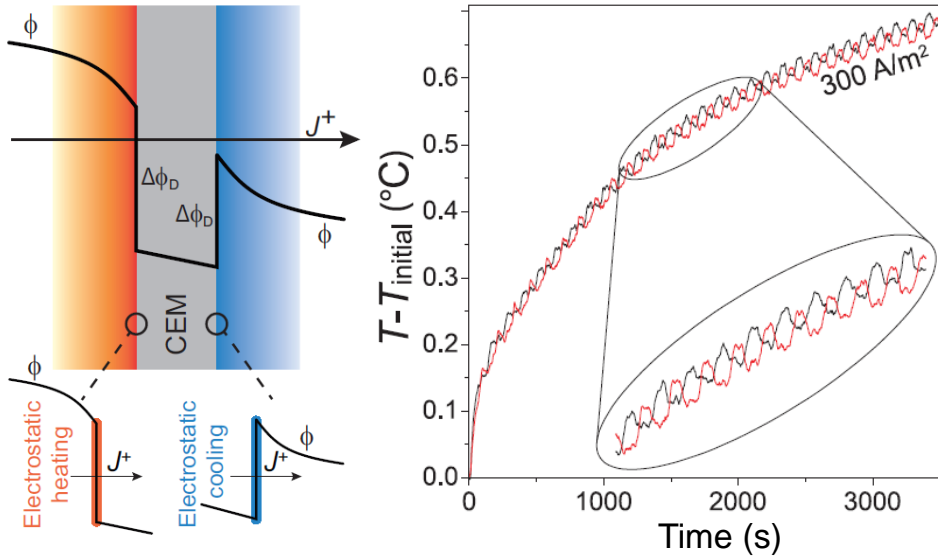


Fig. 9.1: Electrostatic heating and cooling when a current is directed through an ion-exchange membrane. In this case, with a cation exchange membrane, we have heating where current flows into the membrane, and cooling on the other side. In an experiment where the current direction is reversed every 60 s, the temperature difference between the two sides of the membrane flips sign after each current reversal. The two measured temperatures (either side of the membrane) are shown as black and red traces in panel on right. Because of Joule heating in the bulk phases, the temperature gradually increases over many cycles ($c_{\infty} = 0.5 \text{ M KCl}$).

increasing concentration of ions in the diffuse layer), and vice-versa, when the electrode discharges, the EDL cools down.

Also in this problem, the term $\mathbf{I} \cdot \mathbf{E}$ exactly describes the local heating. For the diffuse layer of a GCS model, it is important to realize that \mathbf{I} is the local ionic current, and is not the total current. The total current is the ionic current outside the EDL, which is also equal to the electronic current. However, in a capacitive electrode, *and without any electrode reaction*, then inside a diffuse layer the ionic current slowly drops from the bulk value to a value of zero at the Stern plane (where the diffuse layer ends). This decrease is compensated by the Maxwell current (which relates to the local change of the field strength in time), but Maxwell current is not part of the ionic current \mathbf{I} that enters the heat balance. Thus, with the ionic current decreasing towards the surface, the local heating rate also goes down. The heating rate is zero at locations without any ionic (or electronic) current. This implies that when neither ions nor electrons cross the Stern layer, it does not contribute to electrostatic heating or cooling of an EDL.

Next we discuss heating and cooling during EDL formation in more detail. We start with the ideal Donnan model that can be used for small (micro-)pores, e.g., in porous electrodes. In the Donnan model, all ions in the diffuse layer experience the same electrical potential. This potential is equal to the potential outside the pore plus the Donnan potential, ϕ_D . Thus, when ions move from outside the pore to inside, they all experience a potential change equal to the Donnan potential.ⁱⁱⁱ Thus the heat production rate is equal to the product of ionic current running from the outer-pore region into the pores, I_{ion} , times the Donnan potential ϕ_D , times the thermal voltage, V_T . This ionic current will be equal and opposite to the local electronic current going into the same micropores. If we know this current I_{el} per unit total electrode volume (e.g., per 1 mm^3 total electrode), the heat production rate, HPR, in W/m^3 electrode, will be

$$\text{HPR} = I_{\text{el}} V_T \phi_D . \quad (9.8)$$

The heat production rate, HPR, of Eq. (9.8) can replace the term $\mathbf{I} \cdot \mathbf{E}$ in the heat balance, Eq. (9.1), and must be supplemented with an expression for the Donnan potential, ϕ_D . Eq. (2.7) in Ch. 2 provides such an expression for a 1:1 salt, $\phi_D = \sinh^{-1} (\sigma_w / 2c_\infty)$, where σ_w is the electronic charge density located in the pore walls (charge expressed in moles per unit pore volume), and where c_∞ is the salt concentration just outside the pore. For a

ⁱⁱⁱThus, in the Donnan model there is (at each time) one value of the ionic current, independent of position in the EDL. This is different from a more detailed diffuse layer model as just discussed above, where the ionic current decays towards the Stern plane. Effectively in the Donnan model the Maxwell current is set to zero.

capacitive process, the stored charge σ_w depends on current I_{el} according to

$$p_{mi} \frac{\partial \sigma_w}{\partial t} = + \frac{I_{el}}{F} \quad (9.9)$$

where p_{mi} is the microporosity of the electrode (fraction of total electrode volume that contains micropores). If an electrode is charged with a constant current I_e , starting at zero charge, $\sigma_w = 0$, then $\sigma_w = I_{el}t/p_{mi}F$ which we combine with Eq. (2.7), and then Eq. (9.8) leads to

$$\text{HPR} = I_{el}V_T \sinh^{-1} \left(\frac{I_{el}t}{2Fp_{mi}c_\infty} \right) \quad (9.10)$$

which at early times simplifies to

$$\text{HPR}|_{\text{early time}} = I_{el}^2 t \frac{RT}{2F^2 p_{mi} c_\infty} \quad (9.11)$$

which shows that early on, after start of charging, the heat production in an EDL, HPR, increases linearly with time and depends quadratically on current. At longer times, the dependency of HPR on time t and current I_{el} is more convoluted, but in any case is (much) larger than at shorter times. Thus to continue to charge an already highly charged EDL requires more energy and will generate more heat than an electrode that was uncharged. The total heat production, HP (unit J/m^3) for charging from zero to a final value σ_w is

$$\text{HP} = \int_0^t \text{HPR} dt = \int_0^t I_{el} V_T \phi_D dt = p_{mi} RT \int_0^t \phi_D \frac{\partial \sigma_w}{\partial t} dt = p_{mi} RT \int_0^{\sigma_w} \phi_D d\sigma_w \quad (9.12)$$

in which we can insert Eq. (2.7) and derive

$$\text{HP} = p_{mi} RT \int_0^{\sigma_w} \sinh^{-1} \frac{\sigma_w}{2c_\infty} d\sigma_w = p_{mi} RT \left(\sigma_w \cdot \phi_D - (c_T - c_T^0) \right) \quad (9.13)$$

where the total ions concentration in the pores, c_T is given by

$$c_T = 2c_\infty \cosh \phi_D = \sqrt{\sigma_w^2 + (2c_\infty)^2}$$

and the initial total ions concentration is $c_T^0 = 2c_\infty$. Thus, the heat production, HP, by Eq. (9.13), can be completely written as a function of σ_w or ϕ_D .

In a micropore which is being positively charged, i.e., $I_{el} > 0$, then to keep electroneutrality and to attract the required anions, starting from zero the Donnan potential ϕ_D increases more and more. Thus the product of I_{el} and ϕ_D is positive at all times and this means that heat is produced, thus HPR and HP are positive, as indeed Eqs. (9.8)–(9.13) show.

But what during discharge? Then the current I_{el} changes sign and ϕ_D changes sign as well. Thus, we still have a positive HP(R), i.e., heating during discharge? However, this is not the case, and the statement just made contains one significant error: the current I_{el} may change sign, but the Donnan potential *does not*. During charging the Donnan potential ϕ_D was positive and was steadily increasing, and now that we start to discharge, ϕ_D will start to decrease but at first remains positive. It is only down to zero again when the electrode has discharged completely.^{iv} Indeed, to push out the stored anions it is not necessary to make the Donnan potential negative, but just make it a bit less positive, such that there are ‘too many’ anions for the (decreasing) Donnan potential.^v Thus, during discharge ϕ_D is still positive but now I_{el} is negative. The total ‘cooling power’ will be exactly the opposite of HP given by Eqs. (9.12) and (9.13), but Eqs. (9.10) and (9.11) no longer apply. Instead, during discharge Eq. (9.11) becomes

$$\text{HPR} = I_{el} V_T \sinh^{-1} \left(\frac{F\sigma_w^* + I_{el}(t - t^*)}{2F\rho_{mi}c_\infty} \right) \quad (9.14)$$

where I_{el} is now a negative quantity, and the electronic charge (a positive quantity) that is stored at the start of the discharge step is σ_w^* . The discharge step starts at time t^* . Initially the numerator of the fraction stays positive, and thus HPR is negative, we have cooling. After a time $t = t^* - F\sigma_w^*/I_{el}$ the numerator turns negative, and HPR turns positive. This is when the electronic charge in the micropores goes through zero to negative, and the micropore EDL is again charging up.^{vi}

As previously discussed, if a Stern layer is part of the EDL model, it does not participate in heating or cooling if no current runs across it. Thus also charging of a perfect dielectric capacitor does not lead to any heat effect: it can be charged and discharged, but it will not heat up or cool down in this process.

This finalizes the discussion of heating and cooling in a Donnan model, and we continue with a discussion of heating and cooling in the diffuse layer according to the Gouy-Chapman(-Stern) model, where the structure of the diffuse layer (we do not need to consider the Stern

^{iv}This is a general topic in the cyclic charging of (porous) electrodes, that a reversal of current direction does not imply a reversal of (electrode, or cell) voltage. This reversal of voltage only occurs for the bulk solution where a version of Ohm’s law may apply. But in a capacitive electrode, this is different. In such an EDL a change of current direction leads to a reversal in the *change of* EDL voltage in time, but does not imply an instantaneous change in the *sign* of the EDL voltage itself.

^vFor each Donnan potential at equilibrium there is one corresponding amount of anions in the micropores: if the Donnan potential (still positive) starts to decrease, the attraction to anions goes down, and the concentration of them in the micropores must decrease because there are now too many, i.e., some of them will flow out of the electrode, and thus there is a negative ionic current in the direction out of the micropores, which also implies a negative electronic current into the electrode, i.e., during this discharge step, I_{el} is negative.

^{vi}In this context, ‘charging’ means: to increase the magnitude of charge, whichever is the sign.

layer) is governed by the Poisson-Boltzmann equation. We consider a flat surface and a 1:1 salt, and neglect ion volume effects. In this case, the heat production of charging an electrode, HP, is (starting from zero charge)

$$HP = V_T \Sigma \phi_D - 24 c_\infty RT \lambda_D \sinh^2(\phi_D/2) = V_T \Sigma (3 - 3 \cosh(\phi_D/2) + \phi_D \sinh(\phi_D/2)) \quad (9.15)$$

where Σ is the surface charge in C/m^2 , and ϕ_D the diffuse layer potential (potential at the Stern plane, relative to a position outside the diffuse layer). The heat production rate, HPR, of the entire EDL, which is the term that enters a heat balance, is

$$HPR = V_T I \left(\frac{1}{\sinh \phi_D} + \phi_D - \frac{1}{\tanh \phi_D} \right) = V_T I \left(1/2 \phi_D + 1/24 \phi_D^3 + \dots \right) \quad (9.16)$$

where I is the electronic current density into the electrode (unit A/m^2). For a positive I , the electronic charge goes up, ϕ_D goes up (starting at zero), thus is positive, and thus we produce heat. If we would start at an uncharged electrode, and if the current I were negative, then the electrode would be charged negatively, thus ϕ_D would be negative, and again HPR according to Eq. (9.16) is positive, and also in this case there is heating. Thus for the electrode to be heating up (HPR to be positive), the sign of charging does not matter, only that we charge 'further', i.e., increase (or decrease) the *magnitude* of the charge.

Next we can consider what happens upon current reversal. When an electrode was charged positively to some degree (say positively charged electronically), then ϕ_D is positive. If we now switch the sign of the current I , then ϕ_D will initially stay positive, and then Eq. (9.16) shows that HPR is now negative, i.e., the EDL cools down. This is the same as in the previous discussion for the Donnan model.

How to include the expressions for HPR in a heat balance? For the Donnan model, with volumetric currents, and HP in W/m^3 , HPR can be directly included in a volumetric heat balance such as Eq. (9.1), replacing the term $\mathbf{I} \cdot \mathbf{E}$. Also the HPR for a flat surface, given by Eq. (9.16), can be included in such a volumetric heat balance when we multiply by an area-over-volume ratio of the electrode surface, i.e., multiply HPR by a specific area, a .

But let us at this point insert the Gouy-Chapman expression for the heat production rate into the surface-based heat balance of Eq. (9.2), and thus use HPR of Eq. (9.16) to replace the term $-I \Delta V_{EDL}$ in Eq. (9.2). We neglect chemical reactions and we assume heat can only flow away 'to the right' (on the left side of this electrode we assume an insulating material), resulting in the boundary condition

$$V_T I \left(\frac{1}{\sinh \phi_D} + \phi_D - \frac{1}{\tanh \phi_D} \right) = -\lambda \left. \frac{\partial T}{\partial x} \right|_{x=0} \quad (9.17)$$

that we can use in a dynamic calculation of temperature profiles in the region to the right of this (dis-)charging electrode, with temperature developments in this region described by Eq. (9.1).^{vii} For a constant current I , this boundary condition, Eq. (9.17), shows that heat production starts at zero (when ϕ_D is still zero) and in time steadily increases. As a consequence, the gradient in temperature at this interface ($x=0$), which started off at zero, becomes steeper and steeper over time. With the fluid heating up because of Joule heating, the surface temperature increases faster than the bulk fluid, and does so in a non-linear fashion.

When the current direction is reversed at some moment (which will lead to Σ and ϕ_D decreasing, but both staying positive for a while), the temperature gradient at the surface immediately changes sign, and this interface starts to cool relative to the region next to the electrode. The reversal of current does not influence the Joule heating in the bulk of the electrolyte which simply continues as before. The temperature gradient at the surface is at its steepest right after reversing the current direction and this slope decreases (in magnitude) over time, until the electrode is discharged again, at which point the slope $\partial T/\partial x$ becomes zero.

Did we now heat up the layer as a whole? Yes we did. The EDL heating and cooling process was reversible, so the HPR by the EDL, Eq. (9.16), averaged over the entire cycle, was zero and thus the charging and discharge of the EDL does not lead to overall heating or cooling,^{viii} but Joule heating in the electrolyte bulk is not reversible. On the contrary, in this layer heat is produced all the time, at all positions, irrespective of current direction. If here we assume Ohm's law and a conductivity σ , and if there was no heat flow out of this layer (the electrolyte layer is thermally insulated on all sides) then after one cycle the average temperature change is $\Delta T = \sigma^{-1} |I|^2 t_{\text{tot}} (\rho_L c_p)^{-1}$ where t_{tot} is the cycle time.^{ix}

^{vii}In Eq. (9.17), ϕ_D is the diffuse layer potential, thus the potential difference only over the nanoscopic diffuse layer.

It is calculated from the Gouy-Chapman equation, Eq. (3.15), where charge Σ is obtained from $\partial \Sigma / \partial t = I$.

^{viii}Note that this is only true when the composition of the solution just outside the EDL, for a 1:1 salt described by c_∞ , stays the same during the cycle. When it does change, for instance during charging c_∞ is on average lower, while higher during discharge (this would be an expected scenario), then there is a net effect, with in this example the heating during charging larger than the cooling during discharge.

^{ix}Here we assume that the magnitude of the current $|I|$ is the same during charge and discharge.

9.6 The relation between the heat production rate and the free energy of an EDL

There are multiple ways to subdivide the various contributions to the (free) energy of an EDL structure. In Ch. 5 a distinction was made between an electrical and chemical contribution, as well as a distinction between a surface and diffuse contribution. For an electrode that is externally charged, chemical effects are absent, and the total energy is electrical. This is the term F^{EDL} of Eq. (5.9) (to which a Stern layer energy $\frac{1}{2}C_{\text{St}}^{-1}\Sigma^2$ can be added). This electrical work can be further split out in a term related to the field energy, and one due to ideal entropy of the ions, and in models that include ion volume, a third term due to volume effects.

Now, it turns out that the heat production, HP, in charging an electrode, calculated from the term $\mathbf{I} \cdot \mathbf{E}$ integrated over the thickness of the ‘growing’ diffuse layer, and integrated over time, exactly corresponds to the ideal entropy term (and if volume effects are included, these also contribute), but the field energy term does not contribute. Instead this field energy relates exactly to the Maxwell current (integrated over time and place) and we already addressed that this current does not contribute to heating or cooling. For the GC(S) model these two contributions are

$$F^{\text{ion entropy}} = V_T \Sigma \phi_D - 24c_\infty RT \lambda_D \sinh^2(\phi_D/4), \quad (9.18)$$

$$F^{\text{field energy}} = 8c_\infty RT \lambda_D \sinh^2(\phi_D/4). \quad (9.19)$$

Together these two terms are exactly the total energy $F^{\text{EDL}} = F^{\text{D}} + F^{\text{S}}$ for an electrode as was described in Ch. 5. Note how the ion entropy contribution to the energy, Eq. (9.18), is identical to the heat production in the GC(S) model, Eq. (9.15). At low electrode charge (potential), field energy and ion entropy are exactly 50/50, but this ratio rapidly changes when charge goes up. For a salt concentration of 10 mM, at a charge of 1 C/m², the contribution to the energy by the field energy is around 10%, and the remainder, 90%, is then ion entropy. However, with volume effects included (e.g., in a calculation including ion volume using Carnahan-Starling with all ions having a radius of 0.33 nm), the contribution of field energy only decreases to ~30% of the total at 0.1 C/m² charge, to increase again to a contribution of 60% at 1 C/m² charge.

For the surface pressure that an EDL exerts in the direction along a surface, as was analyzed in Ch. 5, we can also split the total surface pressure, which was given by Eq. (5.13), into contributions of ion entropy and field energy. These two terms are

$$P^{\text{surf,ion entropy}} / (4c_\infty RT \lambda_D) = -\beta A + 3B \quad (9.20)$$

$$P^{\text{surf,field energy}} / (4c_{\infty}RT\lambda_D) = +\beta A - B \quad (9.21)$$

where $A = 1/\sqrt{1 + 1/\beta^2}$, $B = \sqrt{1 + \beta^2} - 1$, and $\beta = \Sigma/(4Fc_{\infty}\lambda_D)$.

Also these two pressures start off at 50/50 at low charge, but their relative contribution to the total surface pressure rapidly changes at higher charge. Without volume effects, the contribution of field energy rapidly disappears, to contribute only 1% at 1 C/m² charge, but when ions do have volume, the situation is again completely different, with the contribution of field energy decreasing to a minimum of approx. 20% at 60 mC/m², and after that it increases again to a 80% contribution of the total pressure at 1 C/m² charge.

Though volume effects (in this example calculated with Carnahan-Starling for spheres of 0.33 nm radius and $c_{\infty} = 10$ mM) make all the difference to the relative importance of each contribution to the energy, volume effects themselves never contribute more than ~25% to the total energy or pressure.

It is interesting to analyze the heating and cooling during EDL formation in an intercalation material, see Ch. 1, but we must leave that exercise for a later time.

The theory of heat effects in reactive systems is important. This can be in bulk, to describe for instance heating when acid and base react, or for any other protonation or deprotonation reaction. The effect of reactions on heat production is also important at surfaces, to describe the heat effects of adsorption, but also to understand the heat effects of electrode reactions. These important topics are left for another time.

Combined mass transport and chemical reactions

In electrochemical processes, while ions and other solutes are transported through electrolyte solutions and (charged) porous media, they can also react with one another forming other species. Examples are acid-base reactions, ion pair formation, and solution-based redox reactions. We summarize four methods of how to include chemical reactions during ion transport in electrochemical processes, and explain why the assumption of local equilibrium (instantaneous reactions) is such a useful approach that immensely simplifies the mathematical analysis. We illustrate the theory with an example calculation of CO_2 -adsorption in water and MEA solutions, and an example how protons are transported across an anion-exchange layer by a combination of two acid-base shuttles.

10.1 Introduction

In the previous chapters we discussed in detail the transport of ions through electrolyte solutions and through porous media, towards interfaces such as electrodes, and in all cases we made the assumption that the ions are inert, i.e., while they move through solution or through a porous layer they do not react with one another. Only when arriving in an electrode they can react away.

To describe ion transport in electrochemical processes we generally use the Nernst-Planck (NP) equation, or extensions thereof, see Ch. 7. The NP equation describes ion velocities as function of fluid flow rates, concentration gradients, and the electrical field strength. These flux equations are combined with differential mass balances for each ionic species, and are supplemented with a statement of local electroneutrality, or inside an EDL we use Poisson's equation. For inert ions, which do not undergo chemical reactions, this framework suffices to tackle many problems as laid out in many chapters in this book, including for water desalination in Chs. 11 and 12.

However, in many electrochemical processes, some or all of the ions present in the electrolyte phases also undergo chemical reactions with one another. An important type of reaction involves as one of the participating species the hydronium ion, H_3O^+ , or hydroxyl ion, OH^- , and they change the protonation degree of ions such as the bicarbonate ion.

There are three main types of such chemical reactions in water:

I. Acid-base reactions. Omnipresent in water are acid-base reactions that involve on the one hand H_3O^+ and OH^- , and on the other ions such as from the group of carbonic acid, which are H_2CO_3 , HCO_3^- and CO_3^{2-} . These ions are generally present in water equilibrated with air. Another example of a group of such reactive ions is the phosphate group, H_3PO_4 , H_2PO_4^- , HPO_4^{2-} , and PO_4^{3-} , which are found in many environmental systems. Also ammonia and ammonium are examples of ions participating in acid-base reactions.

II. Ion pair formation. A very common reactions is when at high salt concentrations for instance Na^+ reacts with Cl^- to a neutral ion pair NaCl . But we can also have Mg^{2+} reacting with one Cl^- -ion to the ion pair MgCl^+ . A next step is when these ion pairs combine into larger (nano-)particles and eventually form larger solid deposits, for instance leading to scale formation, but these latter situations are not considered in the theory of this chapter.

III. Redox reactions. This class of reactions involves at least four groups of species. An electron is taken away from group A, which therefore becomes a group B. The electrons is taken up by a group C which thereby reacts to group D. The reaction of A to B is an oxidation, of C to D a reduction. At equilibrium concentrations of (one component of) each group relate to those of the other groups by the Nernst equation. This reaction is likely best

modelled with a finite rate, not as infinitely fast.

As we discuss below, it is possible that locally these reactions are at chemical equilibrium (i.e., it is a 'very fast' or instantaneous reaction), or the reaction is slower. In a complex situation with many reactions, likely some are fast and others are slow.

In this chapter we focus on acid-base reactions, which is the first case discussed above. Acid-base reactions critically depend on local pH. When pH changes, the ratio of the concentrations of the species involved in the reaction also changes. For instance when pH changes, the distribution between the neutral ammonia ion and the positively charged ammonium ion changes.

Various types of transport models are possible that include these chemical reactions in more or less detail. Here we briefly summarize four different types of ion transport models that incorporate chemical reactions:

I. In the simplest approach all ion types that form a common group (e.g., NH_3 , NH_4^+) are taken together and described as one uncharged species, such as NH_3 . In these models Fick's law is used to model ion transport, only subject to diffusional forces. These models do not incorporate acid-base equilibria, and therefore do not describe for instance the effect of pH on adsorption and transport.

II. In a more detailed model all of the ions are separately considered, and acid-base reactions are included. But still Fick's law is used, describing diffusional transport of the ions, but neglecting the migration of ions due to the electrical field. However, such an electrical field always develops and influences ion transport. And importantly, this model is inconsistent, because when transport of all ions is described using Fick's law, the calculation outcome will not comply with local electroneutrality (EN). To avoid this, one can omit solving the transport equations for one of the ions (thus the diffusion coefficient of that ion does not participate in the mathematical model), and have the concentration of this ion determined by EN. But this is just not correct.

III. A better model is when electromigration is included as a transport mechanism for all charged species. Then the problems associated with the Type II model are resolved. In this approach acid-base reactions are described by rate equations similar to reaction modelling common in chemical engineering. For instance the acid-base reactions are described by a rate equation such as $r = k_f \cdot [\text{HCO}_3^-] - k_b \cdot [\text{CO}_3^{2-}] \cdot [\text{H}^+]$, for the example of the reaction between bicarbonate ions and carbonate ions. Here, k_f and k_b are forward and backward rate constants. Unfortunately, there are many problems with this approach. We identify five of these problems here. The first is that the acid-base reactions are often very fast compared to diffusion and migration, and thus, when this model is solved numerically as

function of time, the set of equations is ‘stiff’, which leads to a very slow calculation with potentially inaccurate results. Second, values for k_f and k_b must be known, and not just the equilibrium constant of the reaction. Related, as a third problem, we must assume the reaction has a certain structure, for instance the one described above where all reactions are linear in concentration. And that is an assumption. A very fundamental problem is the fourth one. These reactions involve the hydronium ion, such as in the example above with the bicarbonate ions. But they are also possible with the hydroxyl ion as reactant or product, and the involvement of water. This additional option implies that another two kinetic constants are required. And we then have these two reactions operating in parallel, one more important at high pH, the other at low pH, and in some intermediate pH region both are important. This is making things quite complicated; do we really know the values of all of these forward and backward reaction rates, that depend on H^+ or OH^- ? A fifth problem is encountered near reactive interfaces, and this relates to the question which ions participate in the electrode reactions there. For example, when acetate is converted into CO_2 in bio-electrochemical systems (Ch. 17), we need to know whether it is the acetate anion (Ac^-) that reacts away, or the acetic acid (HAc) molecule. And this is often not known (and probably both molecules are reactive). Thus here again a choice must be made, and again it must be decided whether H^+ is involved or OH^- . All in all, a long list of problems are associated with this approach.

IV. In the fourth approach, all of the problems outlined above, disappear as if by magic. We therefore strongly suggest to use this approach. Key to this approach is to assume that all acid-base reactions in solution are infinitely fast. This method is so advantageous that even when there is evidence that some reactions are not so fast, we advise to nevertheless first solve the model that makes this assumption. In this approach, mass balances of the individual species are combined in such a way that chemical reaction rates Γ_i disappear from these combined balances. Into these balances of ‘groups’ of ions we insert the acid-base equilibria. As a result, the model does not require assumptions on the structure of the rate equations, and neither requires values of the many rate constants, k_f and k_b , which are often unknown, but the only inputs are the pK-values of each of the acid-base equilibria, and these values are readily available. We do not need to provide as input in the calculation information of whether H^+ or OH^- is involved, or in what ratio. Instead, the calculation will tell us as *output* which ion was involved. The calculation is also numerically less challenging (we have less unknowns in the calculation) because per group (such as the group of the three carbonate species), only the concentration of one of the ions is ‘tracked’ throughout the calculation. [Properties of all other ions in a group are still part of the calculation scheme, such as diffusion coefficients.] After the calculation is finished, we can back-calculate all (place- and time-dependent) reaction rates and concentrations and fluxes of all ions that

constitute a group. They are not neglected, we just don't need to track all ions in the core calculation. The assumption of infinitely fast acid-base rates in solution, still allows for reaction rates at domain boundaries (such as electrodes) to have finite rates.

In the next section we further explain Method IV for the modelling of ion transport and acid-base reactions in electrolyte phases and charged porous media, and thereafter apply it in an example calculation for the absorption of CO_2 from air into water, with and without molecules that can bind CO_2 . In this last example we extend the model by including ion pair formation as well. Subsequently we present results of a calculation where two acid-base groups shuttle protons across an AEM, 'handing over' the proton half-way in the membrane.

10.2 Theory of ion transport and acid-base reactions

When we describe transport of ions and other solutes that participate in chemical reactions, then the models that we presented in earlier chapters must be extended slightly. Interestingly, this modification is not on the level of the ion fluxes, which remain unchanged in their mathematical formulation, but chemical reactions are included in solute mass balances. This clearly shows that chemical reactions are not a driving force acting on ions in the way that diffusion and electromigration are. Instead, chemical reactions are described in a completely different way.

Thus, the molar flux of reactive species is the same as for inert (non-reactive) solutes and ions, described by the Nernst-Planck equation, Eq. (7.2) in Ch. 7. For each type of ion, reactive and unreactive, we set up and solve mass balances. The balances for the reactive ions are the same as for inert ions, only extended with a reaction term, Γ_i , which describes the rate by which ions are formed or react away, and thus

$$\frac{\partial c_i}{\partial t} = -\frac{\partial J_i}{\partial x} + \Gamma_i \quad (10.1)$$

where Γ_i is the formation rate of species i ($\text{mol m}^{-3} \text{s}^{-1}$). For unreactive solutes, $\Gamma_i = 0$. These are volumetric mass balances and include reactions between ions in solution. A reaction at a surface, such as at an electrode, is not part of such a balance, but will enter the calculation as a boundary condition. [This is different in a macroscopic 'stirred tank' mass balance over an entire phase, then surface reactions and other fluxes at boundaries of a domain are part of a macroscopic balance. An example is Eq. (17.9) in Ch. 17.]

How do we incorporate acid-base reactions in these equations? Let us illustrate our approach using the group that consists of the ammonium and ammonia species. The

acid-base reaction that involves ammonia and ammonium can take place everywhere (in an electrolyte phase, charged membrane, porous electrode, etc.) and it can go in either direction. The key step is to use the fact that the production of the one ion, say ammonia, Γ_{NH_3} , equals the consumption of the other ion, in this case the ammonium ions, $\Gamma_{\text{NH}_4^+}$. And thus we have $\Gamma_{\text{NH}_3} + \Gamma_{\text{NH}_4^+} = 0$. We use this equality when we add together the mass balances of these two species, and then the Γ -terms disappear. Note that this addition also works in a dynamic situation, where $\partial c_i / \partial t$ is not zero. [Note also that this specific step does not yet assume anything about the kinetic equations, fast or slow.] The same approach works equally well for a group that consists of two ions, as for a group with more ions, such as the group consisting of the carbonate ion, bicarbonate ion, and carbonic acid. In this case we have $\Gamma_{\text{CO}_3^{2-}} + \Gamma_{\text{HCO}_3^-} + \Gamma_{\text{H}_2\text{CO}_3} = 0$. For the protons and hydroxyl ions, we do not set up such a mass balance for a group. This is unnecessary and it is not very intuitive how to do it. As will become evident in this chapter, no group needs to be established for these water ions, but nevertheless their concentrations and fluxes follow naturally from the overall model.

An interesting question is, what to do when a species is formed which is a member of various groups? An example of such a reaction between ions of different groups is the formation of the carbamate ion from the reaction $\text{HCO}_3^- + \text{NH}_3 \rightleftharpoons \text{NH}_2\text{CO}_2^- + \text{H}_2\text{O}$. The carbamate complex is part of the ammonia-group of ions, and of the carbonate ions. To deal with such complexes, or ion pairs, the first option is to describe this reaction by a rate equation with a finite rate, such as by method III. That works. But we can also use method IV with all reactions infinitely fast. We simply add this ‘combined’ species to all groups of which it is part. In this case, we add the carbamate ion to the group of carbonate species, and we add it to the group of ammonia species. Thus for instance the summation of the Γ_i ’s for the ammonia-group becomes $\Gamma_{\text{NH}_3} + \Gamma_{\text{NH}_4^+} + \Gamma_{\text{NH}_2\text{CO}_2^-} = 0$, and for the carbonate-species we go from three terms in the summation of Γ_i ’s, to four terms.

Thus we can readily include an ‘inter-group’ reaction when we use Method IV. The methodology that we used in the example above of how to include the carbamate ion, is the same as when we would include formation of ion pairs, such as NaCl or MgCl^+ . An ion pair NaCl becomes part of the ‘Na-group’ as well as of the ‘Cl-group’. Thus we add a Γ -term to the mass balance for Na^+ , and to the mass balance of NaCl, and then use $\Gamma_{\text{Na}^+} + \Gamma_{\text{NaCl}} = 0$ when we add up the two balances. We then have a combined balance for the group of $\text{Na}^+ + \text{NaCl}$. And by the same approach we will have an overall mass balance for $\text{Cl}^- + \text{NaCl}$. Thus, with or without ion pair formation or other inter-group reactions, we can sum Eq. (10.1) over the different ionic species in a group (where a group would for instance be the NH_3^- and NH_4^+ -ions in the ammonia-group, possibly extended with carbamate ions), and then the Γ_i -terms completely cancel out. The resulting group-level mass balance describes accumulation

and transport of the two species NH_3 and NH_4^+ together, as function of gradients in the concentrations of the individual components, in this case NH_3 and NH_4^+ , and as function of the gradient in potential ϕ .

In this method we arrive at one balance for each group (such as one for all carbonate species combined; or for all ammonia species, etc.), and in addition we have balances for each inert ion. We also set up a balance in charge density, $\partial\rho/\partial t = \dots$, and this balance is zero, i.e., the divergence of current is zero. This is generally correct at any position in a flow channel filled with electrolyte, or in membrane,ⁱ and the charge balance can then be written as

$$\frac{\partial}{\partial x} \sum_i z_i J_i = 0. \quad (10.2)$$

In this balance we sum over all species, including H^+ and OH^- . It is only in this balance that the diffusion coefficients and valencies of H^+ and OH^- show up. We advise for the use of this charge balance, and not one of several alternative balances, such as a balance in ‘water charge’ (based on the hydronium ions and hydroxyl ions), or a balance based on the vague concept of ‘alkalinity’. Those other balances are more complicated to set up and interpret and check. Note that Eq. (10.2) is not equivalent to the local electroneutrality (EN) condition. Instead, EN is a constraint, an equation, that is solved in addition to the aforementioned balances, at all positions x in the calculation domain.

We can solve all these balances jointly, together with acid-base equilibria, of which two examples areⁱⁱ

$$K_{\text{a,NH}} [\text{NH}_4^+] = [\text{NH}_3][\text{H}^+] \quad , \quad K_{\text{w}} = [\text{OH}^-][\text{H}^+] \quad (10.3)$$

and together with local electroneutrality, and this works fine. The various problems related to method III (based on kinetic rate equations with finite rates) are resolved when we use method IV. And as an additional advantage compared to method III, we can now reduce the total number of equations significantly, when we implement the acid-base equilibria into these balances, and not retain them as separate equations.

In some cases an analytical model can be derived but often the problem must be solved numerically. In setting up a robust numerical model, it is highly preferable to not insert the acid-base equilibria directly in the differential mass balances.ⁱⁱⁱ It is better to first discretize the balances (one balance for each group, one balance for each inert ion, and a charge

ⁱBut not in a porous electrode, see Ch. 15, or *inside* a changing EDL structure (overall, an EDL is nevertheless charge-neutral).

ⁱⁱAs shown here, we use in this book both the notation [...] and the symbol c to describe concentrations.

ⁱⁱⁱBecause if the acid-base reactions are inserted here, many partial differentiations must be worked through and implemented correctly which is bothersome and one easily makes an error.

balance) at a predefined number of gridpoints, or nodes, by employing the finite difference method, see Ch. 21. And only after this discretization do we implement the equilibrium relations, thereby ‘removing’ from the numerical code as free parameter the concentrations of all species in a group except for one –arbitrarily chosen– species per group, the ‘master species’. The EN equation can be solved jointly with all other equations, as an algebraic equation to be solved on each gridpoint, or we use EN to remove one more concentration from the calculation scheme, further reducing the number of unknowns per gridpoint.

Both in the analytical and numerical approaches, we then arrive at a situation that from each group of ions, only one ‘master species’ or ‘key species’ remains that is tracked in the calculation. In addition we must track the concentration of the hydroxide ion, OH^- , or hydronium ion, H_3O^+ . The latter is often simply called a proton, and written alternately as H_3O^+ or simply as H^+ . These notations have the same meaning. That we track the concentration of either of these ions, of which H^+ is the more common choice, does not mean we have to set up a balance in this species, the proton, or in the charge of water, or in something such as ‘alkalinity’. This is not the case, the number of balances (equations), already equals the number of unknowns. Our model is already complete and all internal variables are considered. We do not track the bulk flow or concentration of water, nor do we need to.

Until this point we described (acid-base) reactions in bulk solution. Next we address reactions and transport at interfaces, and why method IV is so advantageous. At interfaces, for instance the G/L interface, or at a reactive electrode, the advantages of assuming equilibrium in solution become apparent and are manifold. Note that at the interfaces, the (electrode) reactions occurring here can have a finite rate.

How to discuss transport and reactions at an interface? For instance, in transport across the G/L interface, we have evaporation or adsorption of some neutral gaseous molecule. We have physical equilibrium at the G/L interface, of a gas phase molecule with a neutral species from a group of ions, such as carbonic acid, or ammonia. Repeating this point, a physical equilibrium relation such as Henry’s equation relates the gas phase concentration to only the concentration of the same neutral entity in solution, for instance NH_3 , *not* to the concentration of the entire ammonia-group (NH_3 plus NH_4^+) as a whole.

Next we must consider the molecular fluxes at this interface. Thus, there will be an ‘incoming’ flux of for instance NH_3 from the gas phase, adsorbing at the G/L interface. Now one might intuitively think that this flux equals the flux in the aqueous phase of the same ammonia species, and then further away NH_3 reacts to NH_4^+ . However, the situation is more interesting than that. What was just suggested would be correct when the reaction in solution between NH_3 and NH_4^+ would have a finite reaction rate. But in our model with infinitely

fast reactions in solution, the gas phase flux of ammonia 'arriving at the G/L interface' is not equal to the flux of aqueous ammonia there, but is equal to *the sum of the* fluxes of ammonia and ammonium in the water. Thus it can be that a large part of the ammonia that arrives at the G/L interface from the gas phase, leaves the interface and enters the electrolyte phase in the form of an ammonium ion.

Thus at an interface we relate the flux of a group of ions as a whole one side to the same sum of fluxes on the other side of the interface. In the examples with carbonate and ammonia and a water/air interface, on one side (the gas phase) only one species from a group exists (ammonia, carbonic acid) and only that species needs to be considered on that side of the flux equation, but to evaluate the flux for the other side (water), all incoming fluxes of all species in a group must be added up. For a group of ions of which none of the species evaporates or reacts, the summed flux of the group is zero at such an interface. Thus for instance, for a group consisting of Na^+ and NaCl , it is the sum of fluxes of the two species together at the G/L interface that is zero. It is not the case that each separate species has a zero flux at the G/L interface. Or for ammonia that does not participate in an electrode reaction, at a planar electrode the sum of fluxes of NH_3 and NH_4^+ is zero, thus $J_{\text{NH}_3} + J_{\text{NH}_4^+} = 0$ in that case. There may be a flux of NH_3 into the electrode, that 'returns' from the surface as NH_4^+ . These two fluxes are then equal in magnitude, opposite in direction. And what to do here with the H^+ and OH^- -species? The answer is, just as for the mass balances in solution, away from interfaces, also at boundaries no relations need to be set up for H^+ and OH^- . This is a very interesting outcome and it dramatically simplifies the calculation. For instance in an electrode reaction involving H_2 or acetate, we do not need to decide upfront how many H^+ -ions or OH^- -ions are involved in the reaction. Nothing needs to be prescribed about H^+ - or OH^- -fluxes. This is a tremendous advantage because this knowledge is not available upfront anyway. It is actually the case that the calculation will tell us *afterwards* the fluxes of H^+ - and OH^- ions towards or away from the interface. The only relation we still need is a (boundary) condition in current density, such as zero current density at a G/L interface (and thus zero current everywhere in a 1D calculation). Or not a direct statement of a prescribed current, but of an applied voltage difference between for instance two electrodes. Indeed, in a typical calculation current is either prescribed as an input of the calculation, or it is a free parameter, and for instance the cell voltage (the voltage across an entire electrochemical cell) is set, which indirectly results in a certain current density.

If the interface is reactive, such as for certain electrodes, method IV is again advantageous. For instance we have the acetate molecule, which can be neutral or charged. Which of these two forms reacts away? In method III these questions must be answered before rate-based boundary conditions can be set up. However, in the approach of method IV we do not have

to know, but instead the model will tell us. It is even the case that if we would attempt to implement this kind of information, the model becomes over-specified, and thus unphysical. [The same for an attempt to decide how many H^+ -ions are involved in an electrode reaction or how many OH^- -ions. It will lead to an unphysical model if we used method IV to describe reactions in solution.] Instead of having to specify which species reacts (which we can't specify upfront), the model uses the two fluxes of the two acetate species added together in a flux expression. And what about the product of the reaction, which are carbonate ions, do we have to decide upfront which type of carbonate ions is formed? Again, we do not have to decide, but the model will decide. The calculation will tell us which types of species form and diffuse away, and this will depend on pH at the surface (which is also an output of the model). Thus, we do not have to provide information about which species reacts away or is formed. In contrast, the model will provide this information as output.

To describe the electrode reaction stoichiometry, we use available chemical information. In the example just discussed of a reaction between carbonate and acetate, we know that always two molecules from the carbonate group are formed for each acetate ion (whichever one it is) that reacts away (or vice-versa, one acetate ion forms from two carbonate ions). In addition, we also know that the formation of one acetate molecule involves eight electrons, and in this way the acetate flux and carbonate flux are coupled to the current density. Thus the theoretical model states that the sum of fluxes of the two acetate species, is to be multiplied by two, and then is equal (with a minus sign) to the flux of the three carbonate species combined (and with the carbamate ion also considered, this ion is also included in this addition-of-fluxes).

Then remains the question, at such a reactive electrode: how many protons are involved, and how many OH^- -ions? Are protons formed, or are OH^- -ions serving as reactant and is water formed? How do we know? Well, we are fortunate because the model does not ask for this information. Instead, it will *tell us* the answer after the calculation ran successfully. And the answer is likely a fractional number, such as that at the surface there was a net incoming flux of H^+ that was $2.3412\times$ the flux of the group of carbonate ions.

Another point of concern is whether or not we need a different model at low pH and at high pH. Don't we need to set up reaction equations that specifically depend on participation of H^+ at low pH, and similar equations for participation of OH^- for high pH? Because we know that at low pH the former reaction is important, and vice-versa at high pH. As you may have anticipated, the answer is: no, we do not have to do this. One and the same (simple) model suffices. Analysis afterwards will tell us that at high pH mainly OH^- -ions were involved, and mainly H^+ if the near-surface region was at low pH. Irrespective of pH, the model structure, including acid-base equilibria such as Eq. (17.6)A, can always be based

on H^+ , also at high pH.

So what about electrons in this reaction? Again, chemistry tells us that for each acetate molecule reacting away (irrespective of which species it is from the group; and irrespective of what ion from the carbonate group is the product), a number of 8 electrons are liberated. And in the electrode this electronic current is equal to the ionic current, one of the boundary conditions in the calculation. All of this is of course very elegant. It is so elegant that if we have an electrode reaction involving only 'water charges', for instance when H^+ -ions react to H_2 -gas, no boundary condition needs to be formulated at all about which ions react away. The model has no need for it, and would not even know how to incorporate it. The only boundary condition is that the electronic current equals the ionic current, and that the various inert ions, and groups of ions, have zero flux at this electrode.

Until now we discussed relations between different fluxes at interfaces, including the relation to the current (charge flux). But doesn't this need to be supplemented with information on the rate of the reaction, how fast it is? Actually, in many instances we do not need to do this. If we use a fixed current (in the calculation) then we can run the calculation as described above, and this is done for instance in Ch. 17. But doesn't the rate have any importance? For instance, when we use the Butler-Volmer (BV) equation for electrode kinetics, how does that equation, and the parameters in there, influence the calculation? The answer is that this equation, when we know the current density, provides us with information of the electrode potential, i.e., the voltage change between solution and metal. The resulting electrode potential does not feed back into the model in the calculation above, if the current is fixed. Thus the kinetic expression for the electrode, see also Ch. 14 for many details on electrode kinetics, is not required for us to make a calculation of all the fluxes and concentration profiles in the electrolyte, if current density is an input value. Instead, in an experiment with a certain applied cell voltage, then we have a different situation, and we do need to consider the BV-equation and the electrode potential as elements of the model. The same holds for a calculation where along the electrode there are changes in solution properties, and thus the total applied current is not necessarily equally distributed, and thus not known. Then we also need to evaluate the BV equation as function of position along the electrode.

In using such a BV-like equation, one can take this rate as infinitely fast, and we then end up with the Nernst equation, relating the electrode potential to the concentrations of the participating ions near the electrode, or we can use a rate equation with finite rate constants. The expression for the electrode reaction rate can have any shape or form, and can use the total concentration of reactants and products, or the concentration of just one member of a group of ions. Neither choice impacts the fact that they can be combined with the infinitely

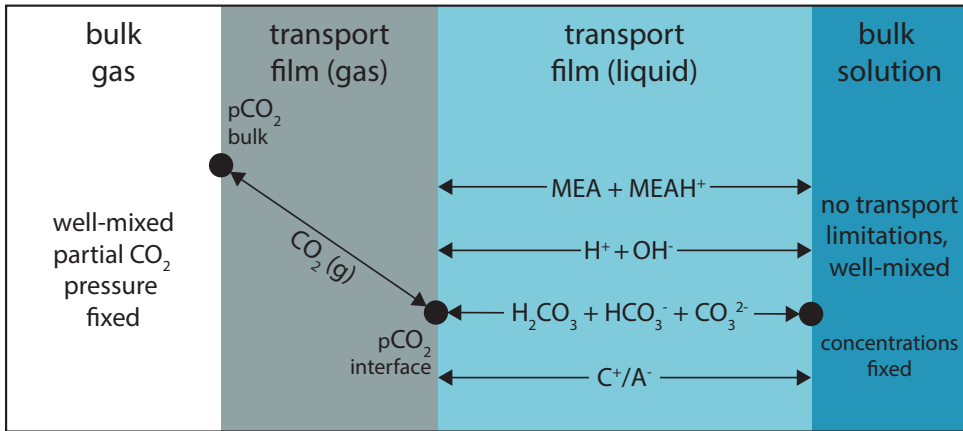


Fig. 10.1: Schematic picture of CO_2 adsorption in an aqueous solution containing MEA, an amine molecule that buffers the pH of water. At the gas-liquid interface, the CO_2 gas pressure relates to the concentration of H_2CO_3 in the water using Henry's law. Bicarbonate ions and MEA diffuse across the transport film and a pH profile is established.

fast reaction scheme that we use in bulk solution which we just discussed. Many elements of this general explanation are used in the example calculation that we present in the next section.

10.3 Example calculation: chemical adsorption of CO_2 in water with MEA

In this section, we make an example calculation for a very relevant electrochemical process, the absorption of CO_2 in water, water that can also contain MEA, a well-known amine-like molecule that buffers the pH of the water, and also binds CO_2 directly.

Next to the interface of air and water, we assume a film layer, see §7.1.1, through which all molecules must diffuse from the G/L interface to the bulk solution. In bulk solution pH, total carbonate content, and total MEA content are fixed. There is no added salt, but only some Na^+ or some Cl^- , as if some NaOH or HCl was added, to adjust bulk pH to a set value.

We use the equations explained in the previous section. Interestingly, in this calculation using a standard film layer the transport of the inert ion, Na^+ or Cl^- , is zero, because they cannot enter or leave through the G/L interface, and thus we can use the Boltzmann equation

for these ions to describe their concentration profile across the film. The summation of the fluxes of the two MEA-related species (one neutral, the other positively charged) is also zero. The adsorption rate of CO₂ from the gas phase equals the sum of fluxes of the three carbonate species. When also the CO₂-MEA complex (similar to the carbamate ion discussed in the last section) is considered, the group of CO₂-related molecules is extended with this carbamate ion, and also the MEA group incorporates this species. In steady-state, at each position in the film the sum of fluxes of all species in the carbonate group (including the carbamate ion) equals the adsorption flux of CO₂ from the gas phase. For the MEA group, now including carbamate as a third species, in steady-state, the sum of fluxes of the species in this group is zero at each position in the film. The concentration of the carbonic acid, H₂CO₃, in the water at the interface, relates to the gas phase CO₂ concentration according to the Henry equation, $[H_2CO_3] = K_H \cdot p_{CO_2}$, where the Henry's constant is $K_H \sim 33.5$ mM/bar at room temperature. Important to notice is how the gas phase CO₂-concentration relates to the concentration of the neutral H₂CO₃-species from the group of carbonate molecules, and is not directly related to the total concentration of the group as a whole.

—

We can simplify this problem significantly when we assume that all ions have the same diffusion coefficient. Because of the constraint of zero current in this problem, the consequence is that the potential gradient (field strength) is now zero throughout the film, see Eq. (9.4). This also implies that adding more or less NaCl will not influence the calculation outcome because all inert species just have flat concentration profiles in this case. We first neglect the possible formation of the carbamate ion. Thus in the carbonate group we have the three species H₂CO₃, HCO₃⁻, and CO₃²⁻. In the MEA-group, we have MEA and MEA⁺. The combined flux over the three species in the carbonate group is constant, and this flux expression can then be integrated to

$$J_c/k_L = \Delta[H_2CO_3] + \Delta[HCO_3^-] + \Delta[CO_3^{2-}] \quad (10.4)$$

and for the combined set of species in the MEA-group we have

$$J_m/k_L = 0 = \Delta[MEA] + \Delta[MEA^+] \quad (10.5)$$

In these equations, fluxes are defined in the direction from interface into bulk, and Δ 's are defined as concentrations at the interface minus bulk. A similar relation also holds for the current (where we can leave out Na⁺ and Cl⁻ because they do not flow anyway)

$$0 = -\Delta[HCO_3^-] - 2\Delta[CO_3^{2-}] - \Delta[OH^-] + \Delta[H^+] + \Delta[MEA^+] \quad (10.6)$$

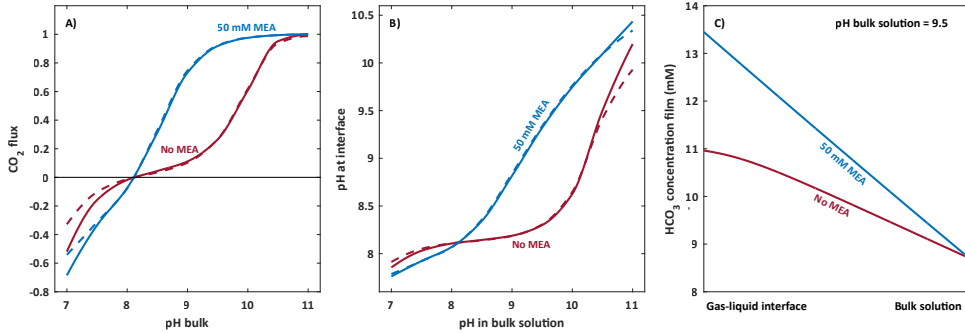


Fig. 10.2: The adsorption of CO_2 from air into an aqueous solution based on the theoretical approach of this chapter, as sketched in Fig. 10.1. A) CO_2 adsorption as function of bulk pH, both with and without MEA in solution. B) pH at the G/L interface as function of bulk pH. C) Concentration profiles of the HCO_3^- ion across the film layer. Solid lines are full numerical model and dashed lines are calculated with the semi-analytical model based on equal diffusion coefficients.

We relate the flux of the CO_2 -species to the gas-phase flux of CO_2 by

$$J_c = k_G \left(p_{\text{CO}_2, \infty} - K_H [\text{H}_2\text{CO}_3]_{\text{int}} \right) \quad (10.7)$$

in which we implemented the Henry equation. We can make a calculation where the bulk concentrations are known. After implementing the various equilibrium relations for the acid-base reactions, this results in four equations in the four unknowns $\Delta[\text{HCO}_3^-]$, $\Delta[\text{MEA}^+]$, $\Delta[\text{H}^+]$, and CO_2 adsorption rate J_c .

Thus, we have presented here an analytical model –which can be built into a larger scale engineering model for a CO_2 absorption tower– that relates the rate of CO_2 adsorption to bulk concentrations (incl. pH) and two mass transfer coefficients. The only assumption is that all diffusion coefficients are the same; and we made use of the standard film model. The ion pair binding between CO_2 and MEA is not yet included.

Ion pair binding between CO_2 and MEA. In the theory outlined above, we did not yet include the ion pair binding between CO_2 and MEA. This ion pair (or complex) can be included in the theory when we consider the chemical equilibrium between bicarbonate, uncharged MEA, and a negatively charged MEA- CO_2 complex, $\text{HCO}_3^- + \text{MEA} \rightleftharpoons \text{MEACO}_2^-$. We evaluate Eq. (10.1) for MEACO_2^- , which includes a production term, Γ_i , for this species, and we can remove this term when we set up the following two mass

balances, in the MEA-group of ions, and the carbonate group,

$$\frac{\partial}{\partial x} \left(J_{\text{MEA}^{\text{H}^+}} + J_{\text{MEA}} + J_{\text{MEACO}_2^-} \right) = 0 \quad (10.8)$$

$$\frac{\partial}{\partial x} \left(J_{\text{H}_2\text{CO}_3} + J_{\text{HCO}_3^-} + J_{\text{CO}_3^{2-}} + J_{\text{MEACO}_2^-} \right) = 0. \quad (10.9)$$

With these two balances evaluated at each position in the transport film, the CO₂-MEA complex is included in the theory. The flux of carbamate is also included in the expression for the rate of adsorption of CO₂, Eq. (10.4).

In Fig. 10.2 we present results for the rate of CO₂ adsorption vs. pH for the case without MEA in the system and with MEA. In this second case, we neglect the CO₂-MEA complex formation. We show results of a numerical calculation based on Eqs. (17.1), (10.1), (17.5), (10.2), and (17.6), and we compare with the simple model discussed above which is based on the assumption of equal diffusion coefficients of the carbonate ions and of the MEA ions. Details of parameter settings are provided «HERE». The calculation results show how pH and MEA concentration strongly influence the rate of CO₂ adsorption. For instance at pH 9.5 we can have a high CO₂ adsorption in the presence of MEA but CO₂ adsorption is close to zero without MEA. The semi-analytical model we present above makes predictions that are very close to the full numerical model. This simplified model can be useful for a larger scale calculation. We also find that calculations including the CO₂-MEA carbamate complex do not predict a much enhanced CO₂-adsorption rate for the concentrations of total MEA that we chose. Thus, these results suggest that regulation of pH is the most important effect of MEA addition, not a direct binding with CO₂.

In summary, this example calculation illustrates how the theory of this chapter can be used quite easily to describe CO₂ adsorption and the influence of MEA-addition and pH on the rate of CO₂ adsorption from air, while including all acid-base equilibria in a mass transport film layer. A model along these lines, which can also easily incorporate electrode reactions such as the example of acetate and carbonate that was discussed, can be quite easily set up and solved. It is really impressive how much information is obtained based on only very limited input.

10.4 Example calculation: ion transport with multiple pairs of ionizable ions

We next analyze a second example, which further highlights the many unexpected results that can be encountered when we have ions that can (de-)protonate, that is are part of acid-base reactions. In one highly intriguing example (Dykstra *et al.*, 2021) we analyze ion transport in an anion-exchange membrane (AEM) between two solutions at different pH (left pH 2.0; right pH 4.35) with different concentrations of sulphate ions and acetate ions. With also Na^+ and Cl^- present we have 8 ions in this system in total (we neglect H_2SO_4). Below we present one particular calculation result, based on the Nernst-Planck equation solved in the membrane together with the familiar equations for the Donnan equilibrium at the membrane edges, local electroneutrality in the membrane, etc.

The particular result that we present here uses values for reaction equilibria K_j and ion diffusion coefficients D_i given in Dykstra *et al.* (2021). The ionic current density is $I = 5 \text{ A/m}^2$, membrane thickness is $100 \mu\text{m}$, ‘free’ diffusion coefficients are divided by 100 to apply to membrane transport, and the membrane charge density is $X = 4 \text{ M}$. On the left we have in solution $[\text{Na}^+] = 52 \text{ mM}$, $[\text{HAc}] = 300 \text{ mM}$, $[\text{HSO}_4^-] = 12 \text{ mM}$, and on the right $[\text{Na}^+] = 62 \text{ mM}$, $[\text{HAc}] = 60 \text{ mM}$, $[\text{HSO}_4^-] = 0.04 \text{ mM}$. Concentrations of Cl^- follow from electroneutrality.

Calculation results are made for steady state transport. Across the membrane the profiles in concentrations and pH change monotonously (for instance, within the membrane pH changes from pH 3 on the left to pH 5.5 on the right), but nevertheless the profiles in ion flux and reaction rates are quite intriguing, see Fig. 10.3.

First of all, in this calculation, there is hardly any flux of the inert Na^+ or Cl^- , and neither of the sulphate ‘s’ group, or acetate ‘a’ group as a whole. The flux of the acetate group (HAc plus Ac^-) to the left is around 7% of the current (when we convert current in A/m^2 to $\text{mol/m}^2/\text{s}$), but all other fluxes are negligible, for instance the total sulphate flux (flux of the s-group) is less than 0.5% of the current. Nevertheless, when we calculate the fluxes of the species forming a group (e.g., HSO_4^- and SO_4^{2-}), we find that these individual fluxes are very high in some part of the membrane, with for instance HSO_4^- flowing right and SO_4^{2-} flowing left in the left half of the membrane, while these two fluxes are close to zero in the right half of the membrane. But it is hard to interpret these as ‘real’ fluxes. Because as a group, the sulphate molecule hardly moves. Each molecule switches infinitely fast between a protonated and a deprotonated state. And when in the one form, it has a tendency to move left, and in the other form, it has a tendency to move right. But once on the move, right away it already reacts to the other form and then moves in the other direction again, thus

effectively it is not moving much at all. And this is the averaged behavior. If we would follow a certain sulphate ion, it will just randomly diffuse left and right, sometimes in the protonated form, sometimes deprotonated.

Thus, it is hard to state there is a certain flux of HSO_4^- and of SO_4^{2-} . However, there is another type of flux, that more clearly 'flows' in a certain direction. This is the flux of protonic charge associated with the two sulphate ions. Protonic charge flows to the right as part of the HSO_4^- -ion. On its way it will hop from sulphate to sulphate ion and effectively diffuse to the right, due to the diffusion and electromigration of the sulphate ions. It is the small steps of HSO_4^- ions to the right that transport the proton in this direction, and then the proton might jump to another sulphate ion, making another move to the right. The ion it leaves behind (which becomes SO_4^{2-}) moves left again. Effectively we have the group of sulphate ions not moving much at all, and simultaneously a quite significant flux of protons moving to the right.

Is there also some transport of protonic charge 'on its own'? Yes, in the left half of the membrane, it also flows by itself. Here, it has a transport number up to $\sim 5\%$. However, once we reach the right half of the membrane, this mechanism disappears.

Indeed, from around halfway in the membrane, the acetate group 'takes over' the transport of protons. It accepts the proton from the sulphate shuttle system and continues to transport it to the right, out of the membrane. Now the proton is piggy-backing on the HAc molecule. Similar to the sulphate molecules in the left half, also in this half the net flux of the acetate group is very low (slightly moving as a whole to the left) while the flux of protonic charge enabled by the acetate group is about $15\times$ larger in magnitude than that.

Thus, which species carries the current? It is not correct to say that sulphate carries the current. As just pointed out, the sulphate ions hardly move as a group. And the same is the case for the acetate ions. Instead, the current is carried by protons, which move across a 'sea' of sulphate ions in the left half of the membrane, and move across the membrane together with the acetate ions in the right half of the membrane. Indeed, the total flux of protons, by the three routes, one, as free protons, two, with the sulphate, and three, with the acetate, is a constant flux, and it is 93% of the current. Thus, proton flow carries the current for 93%. We must admit, we find it difficult to say what then exactly is the other 7%.

To quantify how the proton is transported by the sulphate group and by the acetate group, we can define a 'proton shuttle number' (PSN) for each of these groups, which is its contribution to proton transport, presented in Fig. 10.3. Clearly, in the left half of the membrane, the proton is transported by the sulphate group, and in the right half by acetate. In the center region the proton is handed over from one group to the other. This does not mean that the sulphate group is not present in the right half of the membrane. On the contrary,

also there sulphate ions are the majority species, mainly SO_4^{2-} at a concentration of ~ 1.8 M (while Cl^- is at 0.2 M and Ac^- at 0.3 M). But both SO_4^{2-} and HSO_4^- now have an almost zero flux in this right half of the membrane. That sulphate is the majority route for proton transport in the left half, and acetate in the right half, relates to the pH profile, which starts at 3.0 on the left, and increases to 5.5 on the right side. On the left pH is closer to pK of sulphate (1.92) and on the right closer to pK of the acetate group (4.76). It seems that such a group (which we will call ‘acid-base couple’ from now on) will only transfer a protonic charge when it has buffer functionality, i.e., when the local pH is around the pK-value of the group. If that is the case, it is because pH increases to the right, that at some point the proton is transferred from one to the other acid-base couple, in this case from the sulphate transport system to the acetate system. Fig. 10.3B quantifies this ‘proton transfer rate’, PTR, which is the transfer rate of protons to go from the sulphate group to the acetate group, in moles per time per volume.

Thus we can conclude, the transport of charge across the AEM is mostly in the form of protons, which are by and large transported by the movement of individual species that are part of acid-base couples, which themselves, as a group, do not necessarily move at all, or only very slightly. Thus, these results describe an example with two acid-base couples, the sulphate-group and the acetate-group, where each functions as a shuttle, a carrier, for proton transport, and these two groups together transport most of the charge across the membrane in the form of protons, handing over the proton about half-way into the membrane. In Dykstra et al. (2021) another example is provided with not two but *three* groups of ions working together to shuttle protons across the membrane.

This analysis suggests that we need at least two acid-base couples, each active on one side of the membrane as a proton shuttle. Some calculations were attempted to find conditions that a single acid-base group transports protons across the membrane but as a whole would have a very low flux, but no conditions could be found were this was the case. Thus it may be that we indeed need at least two such couples. However, Dykstra et al. (2021) also discuss an transport in a bipolar membrane with an anion-exchange layer (AEL) that on one side is in contact with a cation-exchange layer (CEL), and through the CEL only free protons move. In that case a single acid-base couple suffices in the AEL to shuttle protons from solution to the CEL. Thus, also in this case protons are the main charge carrier in an AEL when an acid-base couple is present. Because of the CEL, a single acid-base couple seems to be enough for this mechanism to function.

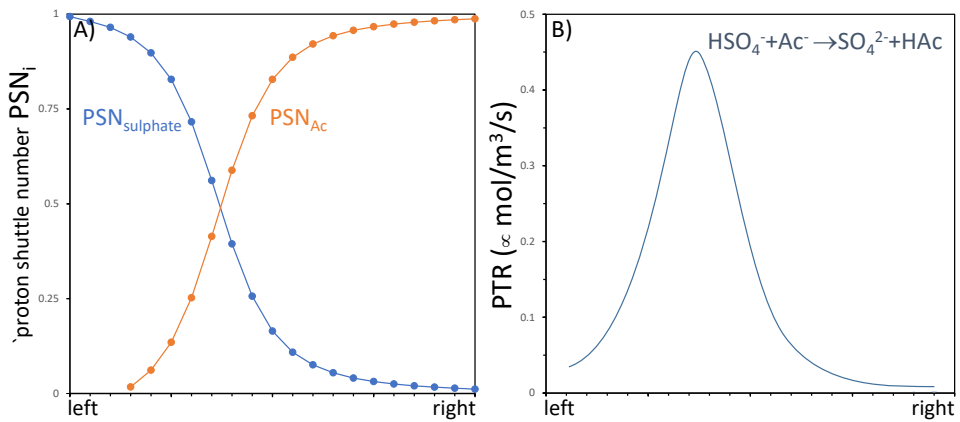


Fig. 10.3: Steady-state ion transport across an anion-exchange membrane with an imposed current between two solutions at different pH and composition, containing sulphate and acetate. A) Profiles of the proton shuttle number, which describes the contribution of a group of ions to the transfer of protons. B) The proton transfer rate, which is the rate by which protons are handed over from sulphate to acetate as the main carrier system. Parameter settings discussed in main text.

Part III

Membrane Processes for Water Desalination

One of the key topics in electrochemical engineering is the desalination of water. Sources of water that must be desalinated can have a salt concentration as high as in seawater (approx. 30 g/L of salts) but other water sources that are too salty for human consumption or agriculture must also be desalinated. This broad category is called brackish water, and ranges from water that is just above suitable for use, from approx. 20 mM salt concentration and higher, up to seawater. Other water sources are in principle potable or suitable for agriculture if it were not for a contamination with certain specific ions. These could be divalent cations that lead to scaling and system malfunction, though at certain levels these ions are also beneficial for water quality. Other ions may lead to undesired colour, taste or odour or excessive biological growth, for instance related to ions such as iron, ammonia and phosphate. Other ions are harmful or toxic such as arsenic (for human consumption) or boron (for agriculture). But metal ions can also be valuable and their harvesting from water an economically viable activity, such as potentially one day the recovery of lithium, gold, or uranium from seawater. Not only natural water sources can be treated but industrial effluent streams as well. Most notably, mining effluents are high in complex salt solutions and often contain toxic metals, for instance mercury, but also have high concentrations of valuable metal ions.

For all of these reasons, here summarized very briefly, water desalination is of key importance to protect the environment and important for modern day society. In this part of our book we address membrane-based water desalination by pressure-driven methods such as reverse osmosis (RO), and by electricity-driven processes such as electrodialysis (ED). We focus on the theoretical aspects of treating water streams for an ideal situation where we have fully dissociated, symmetric, and monovalent salt solutions. Other simplifying assumptions are to assume equal ion diffusion coefficients, equal non-electrostatic partitioning coefficients, and in ED an equal magnitude of the membrane charge density of the two membranes.

—

In general, water can be desalinated by one of five methods, see Fig. III-1:

- By using *ion exchange resin material*, we can exchange cations for protons, and anions for hydroxyl ions, and in this way desalinate water. The ion exchange material must be regenerated which makes this method different from the next four methods where salt is separated from one stream and concentrated in another, without the requirement of absorbent material to be regenerated somewhere else.

Water desalination method	Key component	Driving force	cyclic or steady state	Regeneration elsewhere?
Ion exchange	Ion-exchange (resin) particles	Ion affinity	cyclic	Yes
Capacitive Deionization	Capacitive electrodes	Electricity	cyclic	No
Reverse Osmosis and Nanofiltration	Charged nanoporous membranes	Pressure	steady state	No
Electrodialysis	Ion-exchange membranes	Electricity	steady state	No
Distillation	Heaters and condensers	Heat	steady state	No

Fig. III-1: Overview of the five main methods of water desalination.

- We can use *capacitive electrodes* to remove ions from water, with cations going into one electrode (to compensate negative electronic charge), and anions going into another electrode. This method is called Capacitive Deionization (CDI). It has similarities to the use of ion-exchange material in also being cyclic (after a salt adsorption step comes a salt release step) but is different because the electrode adsorbent is regenerated within the device. That makes CDI more similar to the next methods listed here.
- We can use *pressure and push water through a membrane* with very small pores. This method used to be called hyperfiltration but nowadays has the name reverse osmosis (RO). Nanofiltration (NF) is similar to RO but the pores are slightly larger, i.e., the membrane structure is more ‘loose.’ Both methods are discussed in Ch. 11. A general difference between RO and NF is that RO retains most of the ions in a stream, while NF removes divalent ions very well but monovalent ions have a low rejection. However, the distinction is not very strong: also in RO ions have different rejections (selectivity), while in NF all ions have at least some rejection. Thus there is not a fundamental difference between RO and NF.^{iv}
- We can use pairs of (oppositely charged) *ion-exchange membranes* and a constant electrical current to desalinate water. This method is called Electrodialysis (ED) and is explained in Ch. 12.^v
- Finally, by using heat, we can *distill the water*, condense the vapour, and in this way obtain highly deionized water as the distillate.

^{iv}Forward Osmosis is a related method using a ‘draw solution’ on the permeate side.

^vA related method only uses membranes of one charge sign and is called shock electrodialysis.

Despite the differences between these methods, one general topic goes beyond the specifics of any particular desalination method. This is the definition of setpoints, and the minimum energy cost of desalination and how that depends on these setpoints. The analysis of setpoints and energy uses the fact that in water desalination we always separate one feed stream into two exit streams. In reverse osmosis and nanofiltration (RO and NF) these two streams are called retentate and permeate, while in electrodialysis (ED) the terminology of diluate and concentrate is used. Other terminology is freshwater for the dilute stream, and brine or ‘reject’ for the concentrate stream. In the present section we use the terms diluate and concentrate (d and c).

Two setpoints define any water desalination process. These are the *water recovery*, WR (also often written as α , sometimes called ‘water recovery ratio’), and *desalination*, $\langle \Delta c_i \rangle$.

Water recovery, WR, is the volume flow of diluate (freshwater), $\phi_{v,\text{diluate}}$, relative to the volume flow of feedwater, $\phi_{v,\text{feed}}$, thus

$$\text{WR} = \alpha = \frac{\phi_{v,\text{diluate}}}{\phi_{v,\text{feed}}} . \quad (\text{III-1})$$

Even though this seems simple enough, there are practical issues that can complicate this definition. One topic is that we can define WR in different ways, either as all the water produced of a certain quality, for instance of a concentration less than a certain value, or we simply decide we will operate at a certain WR and if necessary do not treat part of the feed and send it directly to the freshwater collection tank (bypass). Then of course the salt concentration of the freshwater will increase. Especially for cyclic processes such as CDI these technical issues require attention. More discussion on this topic is [here](#).

The other setpoint is the desalination, $\langle \Delta c_i \rangle$, which is the absolute change in concentration of an ion i , or of the total salt content, between the feed stream and the diluate (permeate, or product water). The calculation of desalination, $\langle \Delta c_i \rangle$, must be based on concentrations in the same product stream that determines water recovery, WR. For a steady-state process such as ED, RO and NF, the desalination $\langle \Delta c_i \rangle$ will be relatively unvarying in time and can easily be established by comparing the unchanging concentration of an ion i in the feed and permeate. However, for a cyclic process such as CDI, we must find the ‘mixed cup’ salt concentration of all the freshwater produced, i.e., the concentration in the collection tank for freshwater (allowing for at least a few cycles, to make sure the concentration in here starts to average out).

Especially in RO and NF, instead of using ‘desalination’ as a setpoint as described above (as a change in salt concentration between feed and permeate), instead rejection (also called

retention) can be used as a setpoint, defined according to

$$R_i = 1 - \frac{c_{p,i}}{c_{f,i}}. \quad (\text{III-2})$$

A related setpoint is (salt) passage, P_i , or (salt) transmission, which relates to rejection according to $P_i = 1 - R_i$.

—

Having discussed these two setpoints, of water recovery, WR, and desalination, $\langle \Delta c_i \rangle$, we can continue with a thermodynamic analysis. The minimum energy input in water desalination can be easily calculated based on the entropy content of the three water streams (feed, diluate, concentrate). The first part of this calculation uses the assumption of ideal thermodynamics, because this is a very good approximation for most water streams, even seawater.^{vi} Note that in a determination of ion entropy, we simply count the concentrations of all ions, and do not have to consider the charge of each species. We do have to assume in the simplified calculation that all salts are fully dissociated (or when ion pairs are formed, their total number flowing into the system is the same as leaving the system, i.e., we do not consider acid-base reactions or ion pair formation, and all species in the system are considered to be inert (unreactive).^{vii}

In any desalination process we have the following balances relating feed (f), concentrate (c), and diluate (d) streams. These balances assume steady-state operation. First we have the volumetric flow balance

$$\phi_{v,f} = \phi_{v,d} + \phi_{v,c} \quad (\text{III-3})$$

and for each ion or other solute we have conservation of mass

$$c_{f,i} \phi_{v,f} = c_{d,i} \phi_{v,d} + c_{c,i} \phi_{v,c} \quad (\text{III-4})$$

in which we can implement the definition of water recovery, to arrive at

$$c_{f,i} = \text{WR} c_{d,i} + (1 - \text{WR}) c_{c,i}. \quad (\text{III-5})$$

To calculate the minimum energy consumption, we calculate for each of the three streams, j , the entropy, S_j ,

$$S_j = -\phi_{v,j} R \sum_i c_{i,j} \ln c_{i,j}. \quad (\text{III-6})$$

^{vi}In these thermodynamic calculations, neglecting effects beyond ideal entropy leads to errors in energy never much more than 15%, and often much less.

^{vii}If we do include these reactions, the analysis must be extended with reaction enthalpies.

The minimum energy (consumption), EC_{\min} , that we need to invest to run the desalination process, is equal to the increase in the free energy of the streams, from feed stream to exit streams, ΔG , which in turn is equal to minus the entropy change of the streams times temperature T

$$EC_{\min} = \Delta G = -T (S_d + S_c - S_f) \quad (\text{III-7})$$

an expression into which the above equations can be inserted. Eq. (III-7) can be used to calculate the minimum energy for a desalination process with unit $J/s=W$. Often, EC_{\min} is divided by the volume of freshwater produced, i.e., divided by $\phi_{v,d}$, and the resulting specific energy consumption, SEC_{\min} , then has unit J/m^3 . Often SEC_{\min} is expressed in kWh/m^3 by making use of the fact that $1 kWh = 3.6 MJ$. Note that both anions and cations must be considered in a calculation. For a symmetric salt solution both have the same concentration c in all streams. This leads to the factors '2' in the equations below where c is salt concentration.

A very elegant expression for SEC_{\min} , thus for the minimum energy input per volume of freshwater produced, for a symmetric salt solution, is

$$SEC_{\min} = 2RT \left(\frac{c_f}{WR} \ln \frac{c_c}{c_f} - c_d \ln \frac{c_c}{c_d} \right) \quad (\text{III-8})$$

where concentration c_j is the salt concentration (not total ions concentration).

For (close to) complete desalination, when (almost) all salts end up in the concentrate stream, Eq. (III-8) simplifies to

$$\frac{SEC_{\min}}{2RT c_f} = -WR^{-1} \cdot \ln(1 - WR) = 1 + \frac{1}{2} WR + \frac{1}{3} WR^2 + \dots \quad (\text{III-9})$$

which in the limit of low water recovery simplifies to

$$SEC_{\min} = \Pi_f = 2 RT c_f . \quad (\text{III-10})$$

Thus in this limit of producing a small amount of completely desalinated freshwater, the minimum energy that is required (per volume of freshwater) equals the osmotic pressure of the feedwater, Π_f . Note that when we are not in this limit (that both WR and c_d go to zero) the prediction of SEC_{\min} by Eq. (III-10) deviates strongly from the correct prediction given by Eq. (III-8), with both much higher and much lower predicted values for the energy possible.

The other limiting situation is that we go to $WR \rightarrow 0$, but the diluate, freshwater, concentration is not going to zero, thus $c_d > 0$. Then Eq. (III-10) does not apply, and cannot simply be modified to ' $c_f - c_d$ '! Instead, in this limit we have

$$SEC_{\min} = 2 RT (c_f - c_d (1 + \ln(c_f/c_d))) . \quad (\text{III-11})$$

A typical result of Eq. (III-8) is that complete desalination of artificial seawater of $c_f = 525$ mM salt concentration (thus 1050 mM total ions concentration), at a water recovery of $WR = 50\%$, results in a minimum specific energy consumption of $SEC_{\min} = 1.0$ kWh/m³ ($T = 298$ K).

The minimum energy consumption can always be easily calculated for a certain desalination performance, and when we know the energy input that was required in an actual process, SEC_{act} , which in RO and NF relates to pressures applied times volume flow rates, and in ED and CDI mainly relates to the product of electrical current and cell voltage, then we can calculate an efficiency of the desalination process by

$$\eta = \frac{SEC_{\min}}{SEC_{\text{act}}} . \quad (\text{III-12})$$

The energy efficiency, η , describes how efficient energy is used to desalinate water in a particular process. When different processes are compared in terms of η , it is essential that all relevant metrics such as water recovery and desalination $\langle \Delta c_i \rangle$ are the same, to compare in an appropriate way. If we invert Eq. (III-12), the result is a metric that will have a value > 1 that describes how many times an actual process is beyond operation at the thermodynamic minimum.

—

We can extend this analysis of the minimum energy for desalination by including in Eq. (III-6) ion volume effects, for instance described by Eq. (4.4) (when all ions have the same hydrated size and can be approximated as spheres), and an effect of ion-ion Coulombic interactions, described by Eq. (4.26) for a salt solution where all ions are monovalent. We now obtain for the free energy of each stream, G_j , for a monovalent salt solution, with c_i the concentration of an individual ion in mol/m³, and $c_\infty = 1/2 \sum_i c_i$ the total salt concentration,

$$G_j = \phi_{v,j} \cdot RT \cdot \left(\sum_i c_{i,j} \ln c_{i,j} + \frac{\eta_j^2}{v_{\text{ion}}} \frac{4 - 3\eta_j}{(1 - \eta_j)^2} - 3/2 \alpha \lambda_B \sqrt[3]{N_{\text{av}} c_{\infty,j}} c_\infty \right) \quad (\text{III-13})$$

where $\alpha = 1$, and η_j is the volume fraction of all ions together, given by $\eta_j = 2v_{\text{ion}}c_\infty$ where v_{ion} is the hydrated molar volume of the ions in m³/mole (we assume the same v_{ion} for all ions).^{viii}

^{viii}Formally, in Eq. (III-13), the first entropy term is not just $c_{i,j} \ln c_{i,j}$ but it is $c_{i,j} (\ln (c_{i,j}/c_{\text{ref}}) - 1)$, but these additional terms cancel when the total inflow of ions is the same as the total outflow (conservation of moles of salt).

Contribution to energy by volume effects and Coulombic interaction. How did we arrive at the second and third term in Eq. (III-13)? They are free energy contributions due to a volume (excess) term, and due to an ion-ion Coulombic interaction, of which the expressions for their contribution to an ion's chemical potential are given in Ch. 4 respectively as Eq. (4.4) when all ions are of the same size and spherical, according to the Carnahan-Starling (CS) equation of state, and as Eq. (4.26), in case of a monovalent salt solution. The related free energy densities, i.e., per unit volume, are given by

$$f_{\text{exc},i} = 2 RT \int \mu_{\text{exc}} d c_{\infty} = RT \frac{\eta_j^2}{v_{\text{ion}}} \frac{4 - 3\eta_j}{(1 - \eta_j)^2} \quad (\text{III-14})$$

$$f_{\text{i.i.c.i.},i} = 2 RT \int \mu_e d c_{\infty} = -3/2 \alpha RT \lambda_B \sqrt[3]{N_{\text{av}} c_{\infty,j}} c_{\infty}$$

where the factors '2' in both integrations are because there are equal numbers of cations and anions in a salt solution.

Making now the same calculation as just before, with feedwater of 525 mM salt concentration from which we produce fully desalinated water at a water recovery of 50%, we now calculate an energy consumption of 0.864 kWh/m³ if we only include the ion-ion Coulombic interaction, i.e., it now becomes less energy-consuming, and when we additionally include ion volume effects, then when we assume hydrated ions of a size of 0.41 nm, we are back at 1.0 kWh/m³, while with ions that have a size of 0.50 nm, EC_{min} increases to approx. 1.14 kWh/m³. Thus ion-ion Coulombic interaction, and ion volume exclusion, both have a marked effect on the calculated minimum energy for desalination. Effects of (de-)protonation reactions, the formation of ion pairs, or neutral salt aggregates, related to the chemical energy of their associations, can also play a significant role in further modifying these numbers.

Reverse Osmosis and Nanofiltration

Pressure-driven membrane separation is one of the most relevant processes in electrochemical technology. It is used for water desalination and the removal of micropollutants from water, with reverse osmosis (RO) and nanofiltration (NF) the two main technologies. They are very similar, only with NF membranes having slightly larger pores which leads to lower required pressures, but certain solutes such as monovalent ions are now retained less. For RO and NF we discuss theories for ion and water transport in the direction across the membrane, i.e., the transmembrane direction, and also extend to theory for a full module, which also includes modeling transport along the membrane. Because of the larger pores, theories for NF sometimes also include a detailed description of concentration profiles across the cross-section of a pore (space charge theory) but that extension is unnecessary for membranes for water desalination and will not be discussed. Instead, we discuss in detail the effects of ion-matrix and ion-ion friction on transport and salt rejection.

11.1 Introduction

In this chapter we describe desalination of water by applying pressure to push water through the pores in polymer or ceramic membranes. Solutes, such as salt ions and organic micropollutants (OMPs), are retained by these membranes to a very large degree by a combination of mechanisms such as an energy penalty for ions to enter, which can be due to the small pore size or low solubility, and they are retained because membranes are charged, and because they have friction with the membrane structure while they flow through the membrane. In this chapter we do not distinguish between reverse osmosis (RO) and nanofiltration (NF). These are the two main methods of water treatment with membranes where water is pushed through the membrane by applying a pressure. In NF the pore structure is more open and thus rejection is lower (especially of monovalent ions) and because of the lower rejection, and the more open membrane structure, the necessary pressure is less, or for the same pressure, the water flow through the membrane is higher. In practical RO and NF membranes, the selective layer is often a very thin 'toplayer' (less than 1 μm thickness) with pores less than 1 or 2 nm in size, which is positioned on top of a support structure that has much larger pores and these pores do not have selective properties. This support layer is important because it provides mechanical strength to the entire structure. This layout is called a 'thin film composite' (TFC) membrane. When we write 'membrane' in this chapter, we refer to the sub-micron selective toplayer only.

In practice, in RO and NF water flows into a module containing a large membrane sheet that is rolled up in a 'spiral wound' geometry and fitted inside a cylindrical housing. Feed water flows into this module on one side of the membrane, the upstream side. Water and solutes that do not pass the membrane, leave the module again on the same side of the membrane. This is the concentrate or retentate stream. Water and solutes that do pass the membrane, i.e., water and solutes that travel across the membrane (*trans*-membrane transport) go to the permeate side. This is the downstream side. On this side, after having passed the membrane, salt and water will also flow for some distance along the membrane and then leave the module as the permeate or product water. [Of course dependent on application, it may be that the retentate is the 'real product' but in this chapter we assume that the permeate, of low solute concentration, is the desired stream, i.e., is the product stream.]

In this chapter we first explain theory for an experiment where on the feed side the concentration c_f is the same at each position along the membrane surface. This theory applies to an experiment with a full module if the experiment is performed at low water recovery. And it also applies to a batch experiment where a certain volume of feedwater has

an equalized concentration (because of stirring) and is pressurized in a closed-off container and flows through a piece of (often flat) membrane, sometimes called a ‘coupon’. This is then an experiment that only requires a one-dimensional (1D) model. The permeate (the water flowing through the membrane) is collected and its solute composition measured. In a batchwise experiment, because the membrane retains solutes, solute concentrations on the high-pressure side increase in time, and the permeate composition will then also change over time. Nevertheless, at each moment in time, we can model the process as if in steady state (the changes of concentration in the batch volume are gradual). In § 11.3 we discuss a complete 2D module calculation. In that case differential mass balances for solutes and water are solved on both sides of the membrane as function of position z along the membrane.

11.2 One-dimensional model of pressure-driven membrane separation for neutral solutes

We start this chapter with theory for pressure-driven membrane separation for the transport of solutes (molecules, ions) through a membrane, often in combination with a diffusion boundary layer (DBL) located on the upstream side of the membrane. The upstream side, or feed side, is where the membrane module is fed with the water to be treated, see Fig. 11.1. Other terminologies used for the DBL are: (mass) transport film, stagnant diffusion layer (SDL), and concentration polarization (CP) layer. A DBL is typically neglected on the downstream side of the membrane. In this chapter the fluid or solvent is water, but for other solvents the theory is the same. Solutes are the dispersed or dissolved species, thus ions or other charged or uncharged molecules; all of these terms are used.

Inside the membrane, we assume solutes diffuse while they have friction with solvent and the membrane structure. In this initial part of the chapter we leave out electromigration and volume effects, and thus we can use Eq. (7.71) to arrive at

$$J_i = K_{f,i}c_{m,i}v_w - K_{f,i}D_{m,i} \frac{\partial c_{m,i}}{\partial x} \quad (11.1)$$

where we use the membrane diffusion coefficient $D_{m,i} = \varepsilon D_i$, with index ‘m’ referring to inside the membrane. Diffusion in the membrane, described by $D_{m,i}^* = K_{f,i}D_{m,i}$, is much slower than in solution due to the porosity p_m and tortuosity τ_m of a membrane that enter the parameter ε , as well as ion-matrix friction which leads to a low $K_{f,i}$. Eq. (11.1) explains how transport is driven simultaneously by diffusion and by convection. If we include charge and volume effects, we start the analysis with Eq. (7.70).

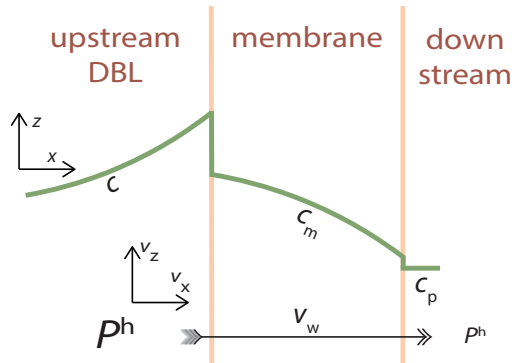


Fig. 11.1: Basic layout of a separation process where water is pushed through a membrane that retains ions and other molecules. Water flows across the membrane from the upstream high pressure feed side (left) to the downstream low pressure permeate side (right). The transmembrane water velocity is v_w . A diffusion boundary layer (DBL) can be included in the theory, and because solutes cannot pass the membrane freely, in the DBL their concentration increases. At the two edges of the membrane, the ratio between the solute concentration inside the membrane relative to that on the outside, $c_{m,i}/c_{o,i}$, has electrostatic and non-electrostatic contributions. Here is depicted one cross-section or ‘slice’ out of a full 2D module. In a full module there is also solution flow along the membrane in the z -direction.

Solute partitioning and the permeate equation. As discussed before, at membrane-solution boundaries (the two outsides of the membrane), the solute concentration just in the membrane is related to that just outside by a partition function that follows from chemical equilibrium of a species i between locations just within and just outside the membrane (i.e., across the interface), resulting for neutral solutes in

$$\Phi_i = S_i = \frac{c_{m,i,j}}{c_{o,i,j}} \quad (11.2)$$

where concentrations with subscript ‘o’ refer to a position just outside the membrane, and where j refers to either of the two sides of the membrane. For ions, an additional Donnan effect arises to retain electroneutrality in the membrane, which in this book we treat separately, i.e., do not include in S_i or Φ_i . The non-electrostatic partition coefficient, Φ_i , describes the solubility of a species in a material, S_i , and can be due to all kinds of energy barriers for entry in the membrane. This term is for instance due to the chemical affinity of a solute with a certain phase (medium) relative to its affinity with another phase, but also other effects of solute-membrane interaction can

be absorbed in Φ_i such as a volume exclusion effect. In RO with neutral solutes, we always have $\Phi_i < 1$ or $K_{f,i} < 1$, and ideally both are significantly less than unity.

A further element in RO modeling is the ‘permeate equation’, an equation essential to describe RO in a one-dimensional (1D) geometry, valid when there is no flow along the membrane on the permeate side. This equation is

$$c_{p,i} = \frac{J_i}{v_w} \quad (11.3)$$

which looks simple but is an intriguing result. It states that the concentration of solutes on the permeate side is a direct function of the ratio of solute flux through the membrane over the permeate water flux, v_w (this is a volumetric flow rate expressed in $\text{m}^3/\text{m}^2/\text{s} = \text{m}/\text{s}$). This condition holds for steady state, thus when conditions on the upstream side do not vary too much over time. The equation is also valid when on the upstream side conditions do change in time, but the permeate is regularly removed. Then the water that permeated the membrane at earlier moments does not mix up with fresh permeate. It is also valid in a calculation where along the membrane, in z -direction, conditions change in the feed channel, as long as the permeate flows through the membrane at each position z are assumed to not mix up with flows that pass the membrane at other z -positions. In a full module, Eq. (11.3) also applies for the exit permeate concentration when J_i is the average solute flux in the entire module, and v_w likewise the average water flux.

If we assume steady state, and one-dimensional flow, solute flux J_i is the same at each x -position in the membrane, and we can integrate Eq. (11.1) across the membrane, noting that the volumetric water flux, v_w , is always the same at each x -position (this is also the case if we do not have steady state). We introduce a dimensionless position in the membrane, $\bar{x} = x/L_m$, with L_m the membrane thickness. We furthermore use a membrane Péclet-number given by $\text{Pe}_i = v_w/k_{m,i}$ with $k_{m,i}$ a mass transfer coefficient given by $k_{m,i} = \varepsilon D_i/L_m$, and finally a characteristic concentration c^* given by $c^* = J_i/(K_{f,i}v_w)$. In the integration, this concentration c^* is a constant factor. The first step is to rewrite Eq. (11.1) to

$$\frac{1}{c_{m,i} - c^*} \frac{\partial c_{m,i}}{\partial \bar{x}} = \text{Pe}_i \quad (11.4)$$

which can be integrated to an explicit expression for the concentration of solutes in the

membrane as function of position \bar{x}

$$c_{m,i}(\bar{x}) = c_{m,i,L} - (c^* - c_{m,i,L}) \left(e^{\text{Pe}_i \bar{x}} - 1 \right) \quad (11.5)$$

where subscript L is introduced which refers to the left side of the membrane, at a position just inside the membrane. Below we will also use R for the right side of the membrane, also just inside the membrane. We associate 'left' with the upstream, high-pressure, feed/retentate side, for which we use the symbol 'f' in this section, and we associate 'right' with the downstream, low-pressure, permeate side (freshwater, diluate), for which we use subscript 'p'. Eq. (11.5) shows that the concentration in the membrane first decreases slowly and then faster and faster.

We can evaluate Eq. (11.5) across the complete membrane layer from position L to R, which then leads to the Hertz equation (Bresler, 1981)

$$\frac{J_i}{K_{i,i} v_w} = c^* = \frac{c_{m,i,L} - c_{m,i,R} F}{1 - F} \quad (11.6)$$

where we introduce $F = \exp(-\text{Pe}_i)$.

Average concentration in the membrane. We can integrate Eq. (11.5) across the membrane and implement Eq. (11.6), to arrive at an expression for the average concentration in the membrane that is

$$\langle c \rangle = \frac{1}{2} (c^L + c^R) + (c^L - c^R) \left(\frac{1}{2 \tanh(\frac{1}{2} \text{Pe}_i)} - \frac{1}{\text{Pe}_i} \right) \quad (11.7)$$

which predicts that at low Pe_i the average concentration is the average of the two concentrations on the two sides, but with increasing Pe -number, it approaches the concentration on the upstream side. The exact expression above, can be simplified to

$$\langle c \rangle \sim \frac{1}{2} (c^L + c^R) + \frac{1}{2} (c^L - c^R) \tanh(\text{Pe}_i/6) \quad (11.8)$$

which has the correct limits for $\text{Pe}_i \rightarrow 0$ and $\text{Pe}_i \rightarrow \infty$, and in a Taylor expansion is correct in the term linear in Pe_i , as well as that in Pe_i^2 (namely that the quadratic term is absent), and only starts to deviate in Pe_i^3 . These expressions for average concentration are required in a calculation of the friction between a fluid and solutes in a porous medium, see p. 218.

The theory just outlined for RO is the solution-friction (SF) model and combines two causes of solute rejection, namely a non-unity partition coefficient (or, solubility), $\Phi_i < 1$,

and a non-unity solute-membrane friction coefficient, $K_{f,i} < 1$. This model is similar to the friction models by Spiegler and Kedem from the 1950s and 1960s, though there are differences in the derivation. Next we implement in Eq. (11.6) the partition function, Eq. (11.2), and rewrite to

$$J_i = v_w (1 - \sigma_i) \frac{c_{\text{int},i} - c_{p,i} F}{1 - F} \quad (11.9)$$

where we introduce the concentration $c_{\text{int},i}$ which is directly on the outside of the membrane, on the upstream side (between DBL and membrane), i.e., at the membrane/solution interface. In the absence of a DBL, $c_{\text{int},i}$ equals the concentration further away in the channel, and if this upstream side is well-stirred, with low water recovery, we can replace it by $c_{f,i}$. We also introduce the sieving coefficient, σ_i , given by

$$\sigma_i = 1 - K_{f,i} \Phi_i. \quad (11.10)$$

Eq. (11.9) can also be written as (Perl, 1973)

$$J_i = v_w (1 - \sigma_i) (\Delta c / (2 \cdot \tanh(\text{Pe}_i/2)) + \langle c \rangle) \quad (11.11)$$

where $\Delta c = c_{\text{int},i} - c_{p,i}$ and $\langle c \rangle = \frac{1}{2} (c_{\text{int},i} + c_{p,i})$. For low water velocities v_w (low Pe-number), Eq. (11.11) simplifies to

$$J_i = (1 - \sigma_i) (k_{m,i} \Delta c + \langle c \rangle v_w) \quad (11.12)$$

which is called the arithmetic mean expression (Bresler, 1981). In the RO literature Eq. (11.12) is often presented as the general solution but with $\langle c \rangle$ replaced by \bar{c} given by $\bar{c} = \Delta c / \ln(c_{\text{int},i}/c_{p,i})$, but this is not exact at all.

And if $\text{Pe}_i = v_w/k_{m,i}$ is really low, solute flux is just related to the concentration difference across the membrane

$$J_i = B (c_{\text{int},i} - c_{p,i}) \quad (11.13)$$

where the salt permeability is $B = k_{m,i} K_{f,i} \Phi_i$. Eq. (11.13) is also used in the solution-diffusion (SD) model (but based on a very different derivation), a model that will be discussed further on.

In the other limit, of a high transmembrane water flux, v_w , Eq. (11.11) simplifies to

$$J_i = (1 - \sigma_i) c_{\text{int},i} v_w \quad (11.14)$$

and thus in this limit solute flux is only due to convection, and the only concentration that enters the expression is that on the upstream side.

Next we combine Eq. (11.9) with the expression for rejection, R_i , Eq. (III-2), which results in

$$R_i = \frac{(1 - F) \sigma_i}{1 - \sigma_i F} \quad (11.15)$$

which shows that for $\sigma \rightarrow 1$ (perfect reflection) we have perfect rejection irrespective of the water transmembrane flux v_w , and likewise, for $\sigma_i \rightarrow 0$ (zero reflection) we have no rejection. In the limit that water flux goes to zero, irrespective of σ_i , we approach zero rejection, i.e., $R_i = 0$. All these predictions make much sense.

In the high Pe-limit, rejection is described by

$$R_i = \sigma_i = 1 - K_{f,i} \Phi_i \quad (11.16)$$

and this expression clearly shows how any RO membrane has a natural limit in what rejection it can achieve, determined by the extent to which solutes are excluded from the membrane (which implies a value of $\Phi_i < 1$), and by the extent of solute-membrane friction (the more the better, which leads to lower and lower values of $K_{f,i}$). If a membrane does not do either, i.e., it does not exclude solutes, i.e., $\Phi_i = 1$, and it does not impose a frictional force on solutes at all, i.e., $K_{f,i} = 1$, then the three equations above correctly predict that rejection will be zero at all values of v_w . So, for a neutral membrane to block neutral solutes, either there must be some solute-membrane friction leading to $K_{f,i} < 1$, or a degree of partitioning ($\Phi_i, S_i < 1$).

Next we include the effect of mass transfer in the diffusion boundary layer (DBL, or CP layer) that is on the upstream side of the membrane, and which can play a role in the transport process. We use the standard film model of a certain thickness. Solute are convected across the DBL by the flow of water, but a large part of the solutes is retained, and thus must diffuse back, resulting in the solute concentration going up towards the membrane (as depicted on the left in Fig. 11.1).¹ Solute flux through the DBL towards the membrane is described by Eq. (11.1) where we remove index m and set $K_{f,i} = 1$. We then have

$$J_i = c_i v_w - \varepsilon D_i \frac{\partial c_i}{\partial x} \quad (11.17)$$

where v_w is the same water velocity as in the membrane, and ε is now a property of the spacer mesh in front of the membrane. In the absence thereof, $\varepsilon = 1$. Just as we did in the

¹It is actually not correct to state that solutes 'diffuse back'. Correct is that solutes are convected towards the membrane, and because solutes are retained concentrations go up at the surface and a diffusional term develops that slows down the further movement of solutes towards the surface. The velocity of solutes towards the surface remains positive.

membrane calculation, because of steady state we can integrate Eq. (11.17) across the DBL, to arrive at

$$\frac{J_i}{v_w} = \frac{c_{f,i} - c_{int,i} \exp(-\text{Pe}_{dbl,i})}{1 - \exp(-\text{Pe}_{dbl,i})} = \alpha \cdot \Delta c_{dbl,i} + \langle c_{dbl,i} \rangle \quad (11.18)$$

where $\alpha = 1/(2 \cdot \tanh(\text{Pe}_{dbl,i}/2))$, $\Delta c_{dbl,i} = c_{f,i} - c_{int,i}$ and $\langle c_{dbl,i} \rangle = 1/2 (c_{f,i} + c_{int,i})$, and where the DBL Péclet-number for species i is given by $\text{Pe}_{dbl,i} = v_w/k_{dbl,i}$ where the mass transfer coefficient in the DBL, $k_{dbl,i}$, is the diffusion coefficient in free solution, D_i , times ε , divided by the DBL thickness. Eq. (11.18) can be rewritten to an explicit expression for the interfacial concentration $c_{int,i}$ given by

$$c_{int,i} = c_{f,i} \exp(\text{Pe}_{dbl,i}) - (\exp(\text{Pe}_{dbl,i}) - 1) \frac{J_i}{v_w} \quad (11.19)$$

which correctly predicts that 'in the absence of a DBL,' i.e., when $k_{dbl,i} \rightarrow \infty$, that there are no concentration changes across the DBL: $c_{int,i} = c_{f,i}$. In the other limit, when $J_i \ll v_w c_f$ (and thus automatically also $J_i \ll v_w c_{int}$ because $c_f < c_{int}$), then Eq. (11.19) simplifies to

$$c_{int,i} = c_{f,i} \exp(\text{Pe}_{dbl,i}) . \quad (11.20)$$

In a dead-end experiment we can use Eq. (11.3), and then Eq. (11.19) simplifies to

$$c_{int,i} = c_{f,i} e^{v_w/k_{dbl,i}} - c_{p,i} \left(e^{v_w/k_{dbl,i}} - 1 \right) e^{v_w/k_{dbl,i}} = c_{p,i} + (c_{f,i} - c_{p,i}) e^{v_w/k_{dbl,i}} . \quad (11.21)$$

Interestingly, this equation not only applies to neutral solutes but also to any binary salt solution, by replacing D_i with the harmonic diffusion coefficient, D_{hm} , given by Eq. (7.30), which then changes $k_{dbl,i}$ and thus $\text{Pe}_{dbl,i}$.

When the total concentration, c_{tot} , is (assumed to be) proportional to osmotic pressure, i.e., $\Pi = c_{tot}RT$, and $k_{dbl,i}$ is the same for all solutes, then Eq. (11.21) can be rewritten to the elegant

$$\frac{\Pi_{int} - \Pi_p}{\Pi_f - \Pi_p} = \exp\left(\frac{v_w}{k_{dbl}}\right) . \quad (11.22)$$

If we combine Eq. (11.13) with Eq. (11.21), and implement the definition equation for rejection, we obtain

$$J_i = B c_{f,i} R_i e^{v_w/k_{dbl,i}} . \quad (11.23)$$

We can combine Eq. (11.9) (where we replace $c_{f,i}$ with $c_{int,i}$) with the flux expression for the DBL, Eq. (11.18), and obtain the generalized RO solute flux equation that includes the effect of the DBL, thus including concentration polarization

$$J_i = \frac{c_{f,i} v_w}{1 + \gamma} , \quad \gamma = \frac{1 - F}{\exp(\text{Pe}_{dbl,i})} \cdot \frac{\sigma_i}{1 - \sigma_i} \quad (11.24)$$

where γ is a parameter that we use to simplify notation. It must be stressed that Eq. (11.24) is valid also in a 2D model where Eq. (11.3) does not apply. If we do include Eq. (11.3), valid for a 1D experiment, as well as (III-2), then Eq. (11.24) results for rejection in

$$R_i = \gamma / (1 + \gamma) . \quad (11.25)$$

This expression is equivalent to Eq. (13) in Starov and Churaev (1993) and Eq. (32) in Biesheuvel *et al.* (2022). When the mass transfer coefficient of the DBL, $k_{dbl,i}$, is large enough, for instance because of sufficient stirring, then Eq. (11.25) simplifies to Eq. (11.15). But the general case based on Eq. (11.25) can also be easily solved in commercial spreadsheet software. In this procedure we take the permeate water flux, v_w , as input, then calculate rejection with Eq. (11.25), and from that we can easily calculate $c_{p,i}$ and solute flux J_i . Then, Eq. (11.21) can be used to calculate the solute concentration at position ‘int’, i.e., just outside the membrane. Concentrations on either side just in the membrane follow from $c_{int,i}$ and $c_{p,i}$ by multiplying with Φ_i . Some calculation results are presented in Fig. 11.2.

A different approach used in RO is the solution-diffusion (SD) model which neglects convection of solutes (and only considers neutral solutes), and thus solute flux is based on Eq. (11.13). According to the SD model rejection is given by

$$R_i = \frac{v_w}{v_w + B \exp(v_w/k_{dbl,i})} \quad (11.26)$$

which predicts that without a DBL there can be 100% rejection at high enough water flux, even when the product of $K_{f,i}$ and Φ_i is unity (thus $\sigma_i = 0$). It does not predict the limiting rejection of Eq. (11.16).

Sometimes in RO, an *intrinsic* membrane rejection, R_{int} is calculated on the basis of the *observed* rejection, R_{obs} with R_{obs} the rejection as defined in all of the above text, namely $R_{obs} = 1 - c_p/c_f$, and the intrinsic rejection being more representative of the actual performance of the membrane because the DBL is corrected for. If we define R_{int} as $R_{int} = 1 - c_p/c_{int}$, then we can combine these definitions with Eq. (11.21) and arrive at

$$R_{int} = \frac{R_{obs} \exp(v_w/k_{dbl,i})}{1 + R_{obs} (\exp(v_w/k_{dbl,i}) - 1)} \quad (11.27)$$

which predicts that in all cases $R_{int} > R_{obs}$. This equation can only be used if we know $k_{dbl,i}$, and for conditions that the dead-end equation can be used (for a stirred cell, or a module at low water recovery). It is also based on the assumption that the convection-plus-diffusion approach for the DBL, on which Eq. (11.21) is based, is valid.

Alternative CP model. We set up an alternative model for the DBL that includes convection and diffusion, but does not assume a DBL of fixed thickness. Instead, similar to Eq. (7.15) in §7.1.4 we include solute refreshment, with the refreshment rate proportional to the distance from the membrane. The water velocity, which is directed to the membrane, v_w , is constant, an assumption that in more accurate 2D calculations can be relaxed, see Elimelech and Bhattacharjee, *J. Membr. Sci.* **145** 223–241 (1998). This model is described by the one-dimensional differential equation

$$y'' - \xi y + \alpha \text{Pe}_{\text{dbl}} y' = 0 \quad (11.28)$$

where derivatives make use of a dimensionless coordinate ξ that points from the membrane into solution. Explanation of this coordinate ξ , concentration y , the constant α , and the definition of k_{dbl} as function of diffusion coefficient and refreshment rate are all provided in §7.1.4. We make numerical calculations where we evaluate y' at the membrane surface where $\xi = 0$, while $y' = y = 0$ for $\xi \rightarrow \infty$. Even up to $\text{Pe}_{\text{dbl}} = 2.5$, which implies an upconcentration at the membrane by a factor of ~ 12 , we do not find a difference between the outcome of this new approach and the standard DBL model, Eq. (11.18). Most probably they are mathematically equivalent also at higher Pe-numbers, but in any case we can conclude that for all practical purposes, Eq. (11.18) is an accurate 1D steady state model for the CP layer.

Next we discuss the water flow through the membrane as function of pressure, or vice-versa, we discuss the question what pressure is required to arrive at a certain transmembrane water flux, v_w . We assume there is only one type of solute (or more types but their properties are all the same) so we can use Eq. (8.27) from Ch. 8 that we modify slightly

$$v_w = -k_{\text{F-m}}^\dagger \left(\Delta P^{\text{h},\infty} - \sigma_i \Delta \Pi^\infty \right)$$

where $k_{\text{F-m}}^\dagger$ is a effective permeability for water flow through the membrane, influenced by solute-membrane frictions, i.e., it describes the permeability for water to flow through a porous membrane that also contains solutes that partly flow along with the water but are also obstacles that generate more resistance for flow of water. This factor is given by $1/k_{\text{F-m}}^\dagger = 1/k_{\text{F-m}} + (1 - K_{\text{f},i}) \cdot \langle c \rangle / k_{\text{m},i}$ where $\langle c \rangle$ is the average solute concentration in the membrane for which an analytical solution was provided in Ch. 8. The two pressure differences, $\Delta P^{\text{h},\infty}$ and $\Delta \Pi^\infty$, are those across the full membrane (between locations just outside the membrane). When there is a DBL, this pressure counts from a position on the

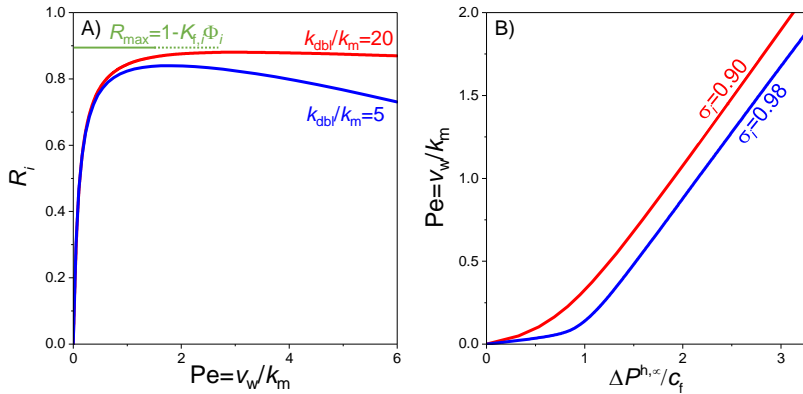


Fig. 11.2: Theory for the removal of neutral solutes by RO membranes based on the solution-friction model including concentration polarization, i.e., a diffusion boundary layer on the upstream side, and solute partitioning. A) Solute rejection, R_i , as function of trans-membrane water velocity, v_w , for various values of $k_{dbl}/(k_m)$ ($\sigma_i = 0.9$). B) Water velocity, v_w , as function of applied hydrostatic pressure for two values of σ_i ($k_{dbl}/k_m = 5$, $k_{F-m}^\dagger = k_{m,i}/c_f$).

upstream side between DBL and membrane (called ‘int’), to the permeate. The hydrostatic pressure at position ‘int’ is the same pressure as further away from the membrane, on the bulk side of the DBL, because across the DBL the hydrostatic pressure does not change. However, the osmotic pressure certainly changes through the DBL, in the same way that concentration changes. If solutes have no friction with the membrane, then $K_{f,i} = 1$, and the effective permeability k_{F-m}^\dagger simplifies to k_{F-m} which is the membrane clean water permeability.

Fig. 11.2 illustrates the theory explained above, for solute rejection as function of water flux (expressed as a membrane Pe-number), and as function of the mass transfer coefficient of the DBL, k_{dbl} . For each value of k_{dbl} there is a maximum rejection at a certain membrane Pe-number (which is a measure of transmembrane water flux). Beyond that point rejection drops again because of the increasing solute concentration directly near the membrane (at position ‘int’), leading to more leakage of solutes through the membrane. In the limiting situation that the DBL plays no role, then for sufficiently high water fluxes we arrive at the maximum rejection given by Eq. (11.16). The relation between pressure and water flux is also illustrated in Fig. 11.2. The calculation shows that also at very low pressures there is some flow of water through the membrane. It is not the case that there is some minimum pressure below which there is no water flow at all. However, for low enough Φ_i (or for low enough $K_{c,i}$) there is a clear transition at a pressure equal to the osmotic pressure of the feed. Below that pressure, water fluxes are very low, and above, they quickly increase. Not shown

is a graph of solute flux versus pressure. Results are that solute flux increase quite linearly with pressure (starting at zero, at zero pressure).

11.3 RO module calculation for neutral solutes

In the previous section we considered RO for a mixture of neutral solutes from a large batch of water of constant composition, as if it is a module that is operated in the limit of a very low water recovery. The upstream concentration is at a constant value, c_f . We now continue and describe a more realistic RO module where on the upstream side between inlet (feed) and exit (retentate) the composition gradually changes along the membrane (z -direction). We first describe general balances, where transport along the membrane is in plug flow, i.e., there is one water velocity in z -direction and one z -dependent solution concentration. The CP layer is included as part of the membrane flux equations, i.e., it is included as a boundary condition. Thus, we extend the one-dimensional model for RO to a more realistic two-dimensional (2D) model for an RO module. Previous models were one-dimensional, only considering the x -direction straight towards and through the membrane. We now also include the z -direction along the membrane, from module inlet (feed) to outlet (retentate). Thus we now also consider transport along the membrane, which is transport through flow channels (also called spacer channels), which are the thin and long channels placed next to the membranes. Transport through these channels (i.e., in the direction from entrance to exit) is modelled by convection: solute is taken with the water that passes along the membrane. Thus, in this direction diffusion is neglected.

In these flow channels there is typically a spacer material material, or ‘mesh’, such that only an open fraction p_s remains through which the water flows. This spacer material enhances mixing and provides structural integrity to the module. The channel has a thickness between 200 μm and 1 mm (this is the height, h_{ch} , in x -direction in Fig. 11.1). The channel can have a path length between inlet and outlet of the module (i.e., in the z -direction along the membrane) of typically between 10 and 100 cm.

Next we first analyze a model based on the plug flow-assumption, which implies that water velocity v_z and solute concentration c_i change with z -coordinate, but not with x -coordinate (i.e., at any z -position, across the channel we have the same values of v_z and c_i . (In other models, ‘plug flow’ refers to a flat velocity profile, with concentration profiles allowed to develop.) We first describe how to set up a model that uses the most detailed models for v_z and J_i from the last section (e.g., including the DBL), while adding transport in z -direction along the membrane. The equations of the previous section for the flux of water and solutes through DBL and membrane, which are Eqs. (8.27) and (11.24) respectively, are used in

this calculation. In Eq. (11.24) we must replace concentration $c_{f,i}$ by c_i , the z -dependent concentration in the upstream channel. To evaluate $\Delta\Pi^\infty$ in Eq. (8.27) we use Eq. (11.18) to find $c_{\text{int},i}$ (not Eq. (11.21)!), and after multiplying $c_{\text{int},i}$ and $c_{p,i}$ with Φ_i we have the concentrations c^L and c^R in the membrane which we need in Eq. (11.7) to calculate $\langle c \rangle$ which we need in the calculation of $k_{\text{F-m}}^\dagger$, see an in-line equation on p. 218.

To solve the model we set up differential balances in the upstream channel. A differential volume balance (to be solved at each z -position) is

$$\frac{\partial v_z}{\partial z} = -\frac{v_w}{h_{\text{ch}}} \quad (11.29)$$

where v_w is the transmembrane water velocity directed from the upstream side to the permeate side.ⁱⁱ There is no accumulation term in Eq. (11.29) because volume cannot accumulate. In Eq. (11.29) both v_z and v_w depend on position z .

Next we set up a mass balance for each of the solute components in the upstream channel

$$p_s \frac{\partial c_i}{\partial t} = -\frac{\partial}{\partial z} c_i v_z - \frac{J_i}{h_{\text{ch}}} \quad (11.30)$$

where in the z -direction we assume that the solutes are only convected with the water, and thus we neglect diffusion and electromigration in this direction. This is valid because compared to the width (height) of the channel, the channel is very long, and therefore in that direction convection is by far the most important transport mechanism.

On the permeate side we can also solve the above volume and mass balances as well, with a flipped sign for v_w and J_i . However, because of overall volume and mass balance, we do not have to solve these differential balances on the permeate side, but can add up each type of balance, and arrive at

$$\sum_k \left\{ h_k \cdot \left(v_{z,k}(z) - v_{z,k}|_{z=0} \right) \right\} = 0 \quad (11.31)$$

and (for steady state, no accumulation)

$$\sum_k \left\{ h_k \cdot \left(c_{k,i}(z) v_{z,k}(z) - c_{k,i} v_{z,k}|_{z=0} \right) \right\} = 0 \quad (11.32)$$

where counter k refers either to the upstream channel, or to the downstream, permeate, channel. At $z=0$, the velocity v_z in the permeate channel is zero.

ⁱⁱNote that water velocities in the channel, v_z , is a superficial velocity, or ‘empty tube’, velocity, i.e., it is a volume flow rate in m^3/s , divided by a total cross-sectional area. The same holds for v_x that will be discussed in the next section. Concentrations are defined per open volume.

Now we only need to find the difference in hydrostatic pressure across the membrane at each z -position. This is the most intricate part, because on the upstream side the pressure goes down with z , because water must be pushed through the flow channel (Darcy's law), but the rate of decrease slows down towards the end of the channel because v_z goes down (more and more water has already passed the membrane to the other side), while on the permeate side the pressure decrease 'starts off slowly' but then increases faster and faster with z , because the accumulated flow of water through the membrane increases.

A typical calculation input is the pressure at the feed inlet minus in the permeate exit. This means that the calculation cannot simply run 'from start to finish' but either the entire module is 'discretized' and solved all at once, see Ch. 21, or we start at position $z = 0$ with an estimated pressure on the permeate side, run the calculation to $z = \ell$ and repeat this calculation until the exit permeate pressure is as required. Thus we need an iterative calculation.

Therefore, to simplify this calculation, one can assume on the permeate side a constant pressure (independent of z -position), which is a valid assumption when pressure changes in the permeate channel remain much less than on the upstream side. Thus only on the upstream side we need to calculate the profile of hydrostatic pressure in z -direction, and this will decrease with z , starting from a certain inlet value, according to Darcy's law

$$\frac{\partial P^h}{\partial z} = -\frac{1}{\mathbb{k}_s} v_z \quad (11.33)$$

where \mathbb{k}_s is the spacer permeability, a function of viscosity (thus temperature), spacer porosity, tortuosity and mesh size. There is no influence of thickness of the channel, h_f , here, but note that for a given fluid flow $\phi_{v,f}$ (in m^3/s), the velocity v_z is higher when the channels are thinner, and as a result the pressure gradient in z -direction will be higher.

This completes the outline of a general plugflow model for a full module. With a feed concentration, c_f , and upstream hydraulic pressure, $P^{h,\infty}$, set to certain values at $z = 0$ (relative to the pressure on the permeate side), we can run the calculation for a membrane module with transport across the membrane described by expressions for v_w and J_i described above (but not implementing Eq. (11.3) because this equation only applies to the earlier 1D models). Thus in this general model the DBL is included as well as the gradual decrease in pressure in z -direction through the upstream channel. This calculation predicts the total amount of water flow through the membrane, thus water recovery, and calculates the retentate and permeate concentrations and thus the solute rejection in the module.

11.4 1D RO module calculation in convection-only limit

The general plug flow model of the previous section for RO with neutral solutes, can be solved numerically without too much trouble. But nevertheless, it is interesting and relevant to develop some simplifications. We first discuss a simplification that leads to a very elegant result. We analyze Eqs. (11.29) and (11.30) in the steady state for the upstream channel and combine the two, resulting in

$$-h_{\text{ch}} v_z \frac{\partial c}{\partial z} = J_i - c v_w . \quad (11.34)$$

leaving out index i for the concentration of a certain solute. Now, an elegant result is obtained when we use the high Pe-limit of the membrane model, i.e., the ‘convection-only’ limit, and when also the DBL is neglected. This is Eq. (11.14), and when we implement it we obtain

$$h_{\text{ch}} v_z \frac{\partial \ln c}{\partial z} = \sigma_i v_w \quad (11.35)$$

and when we insert Eq. (11.29) we have

$$\frac{\partial \ln c}{\partial z} = -\sigma_i \frac{\partial \ln v_z}{\partial z} \quad (11.36)$$

which we can rewrite to

$$\partial \ln c = -\sigma_i \partial \ln v_z . \quad (11.37)$$

We integrate Eq. (11.37) from the inlet of the upstream channel to any position further on, which leads to

$$\ln \frac{c}{c_f} = -\sigma_i \ln \frac{v_z}{v_{z,f}} . \quad (11.38)$$

Now we introduce a factor f which is the flowrate, ϕ_v , at some position in the upstream channel, relative to the inlet value, $\phi_{v,f}$. The ratio of flowrates is the same as the ratio of velocities v_z , thus $f = v_z/v_{z,f}$. This factor f starts off at $f = 1$ at the inlet, and decreases to a value $f = 1 - \text{WR}$ at the retentate side (outlet of upstream channel). We implement this factor and arrive at

$$\ln \frac{c}{c_f} = \ln f^{-\sigma_i} \quad (11.39)$$

which can be rewritten to

$$\frac{c}{c_f} = \left(\frac{1}{f} \right)^{\sigma_i} . \quad (11.40)$$

In Eq. (11.40) we can implement that at the outlet of the upstream channel we have $f = 1 - \text{WR}$, and the resulting c is now the retentate concentration, c_r . Then an overall mass balance

results in the permeate exit concentration and thus solute rejection of this module. Indeed, combining Eqs. (III-2), (III-5), and (11.40), results in

$$R_i = 1 - \frac{1 - (1 - \text{WR})^{1-\sigma_i}}{\text{WR}} \quad (11.41)$$

which shows how rejection depends solely on the reflection coefficient, σ_i , and water recovery, WR. It is interesting to compare this equation for rejection in a module in the convection-only limit, with a similar expression for the batch experiment, which is equivalent to a module operating at very low WR, Eq. (11.16). To this end, we expand Eq. (11.41) around low WR, resulting in

$$R_i = \sigma_i - \frac{1}{2} \cdot \sigma_i \cdot (1 - \sigma_i) \cdot \text{WR} + \dots \quad (11.42)$$

which shows again that in the limit of $\text{WR} \rightarrow 0$ in the convection-only limit we have a rejection of $R_i = \sigma_i$, see also Eq. (11.16). But Eq. (11.42) also shows that when WR increases, rejection drops. So a high water recovery, which in general will be relevant to produce more freshwater, always goes at the expense of rejection (i.e., rejection goes down). This is because of the increasing concentration on the upstream side towards the retentate exit, and thus the solute concentration of the water that flows through the membrane further down the module is higher than earlier on, which reduces rejection in a module.

—

Next we calculate the pressure as function of z -coordinate in the module which we need to find out the energy input to push the water into the module, and to evaluate the potential for energy recovery from the retentate stream. We derive a single ordinary differential equation that describes the hydrostatic pressure on the upstream side, P^h (relative to the constant value in the permeate). We use Eq. (11.29), in which we implement that $\phi_v = v_z h_{\text{ch}} A / \ell$, where A is membrane area and ℓ is the length of the flowpath between feed and retentate (i.e., between inlet and exit), resulting in

$$\frac{\ell}{A} \frac{\partial \phi_v}{\partial z} = -v_w. \quad (11.43)$$

We introduce a non-dimensional coordinate in the flow direction, ξ , from $\xi = 0$ at the inlet, to $\xi = 1$ at the outlet, and we then have $\partial z = \ell \partial \xi$. We also make use again of the factor f . We then arrive at

$$\frac{\phi_{v,f}}{A} \frac{\partial f}{\partial \xi} = -v_w. \quad (11.44)$$

Next we implement an expression for v_w . We implement Eq. (8.27) in Eq. (11.44) and arrive at

$$\frac{\phi_{v,f}}{A} \frac{\partial f}{\partial \xi} = -k_{F-m}^{\dagger} \left(P^h - \sigma_i \Delta \Pi \right) \quad (11.45)$$

with both P^h and $\Delta \Pi$ dependent on position ξ . From this point onward we use one constant value for $k_{F-m}^{\dagger} \rightarrow k_{F-m}^{\text{eff}}$. The osmotic pressure difference across the membrane is $\Delta \Pi = c(z) - c_p(z)$, where c without subscript is that on the upstream side. (We neglect the DBL in the present approach, so we can use here $c(z)$ which is the concentration in the bulk of the channel.) Using the mass balance Eq. (III-5) we obtain $c(z) - c_p(z) = (c(z) - c_f) / (1 - f)$, and now we can use Eq. (11.40) and arrive at

$$-\frac{\text{SP}}{\text{WR}} \cdot \frac{\partial f}{\partial \xi} = p^* - \frac{\sigma_i}{f^{\sigma_i}} \frac{1 - f^{\sigma_i}}{1 - f} \quad (11.46)$$

where we introduce a specific productivity, $\text{SP} = \phi_{v,\text{prod}} / A k_{F-m}^{\text{eff}} c_f$, where the produced water flowrate is $\phi_{v,\text{prod}} = \text{WR} \phi_{v,f}$, and we use a dimensionless pressure given by $p^* = P^h / c_f$. This differential equation can be solved from $\xi = 0$ to $\xi = 1$ for given values of SP and σ_i and an estimate of p^* , resulting in a certain final value of f at $\xi = 1$ (starting at $f = 1$ at $\xi = 0$). We adjust the estimate for p^* until we arrive at the required value of f , which is $f_{\xi=1} = 1 - \text{WR}$. This is now a complete model that can be numerically solved.

We can arrive at a semi-analytical expression in case of a membrane that perfectly retains the solutes, in which case $K_{f,i}$ or Φ_i must be zero, and we obtain

$$\frac{f}{p^* f - 1} df = -\frac{\text{WR}}{\text{SP}} d\xi \quad (11.47)$$

which we integrate from $\xi = 0$ to $\xi = 1$, to

$$\frac{1}{\text{WR}} \ln \frac{(1 - \text{WR}) p^* - 1}{p^* - 1} + \frac{p^{*2}}{\text{SP}} - p^* = 0 \quad (11.48)$$

based on which we can semi-analytically derive p^* for any value of WR and SP. This dimensionless pressure p^* increases with WR and SP. At low SP, p^* approaches 'from above' a value of $1/(1 - \text{WR})$.

With pressure $P^h = p^* c_f$ now obtained, we can calculate the total energy input and energy recovery. The energy input is the feed pressure P^h times $\phi_{v,f}$. Energy recovery is the retentate pressure times retentate volume flow rate (which is inlet volume flow rate times $1 - \text{WR}$), times the efficiency of an energy recovery device, η_{ERD} , if that is installed. The energy input minus energy recovery can be compared to the thermodynamic energy of separation, and we can in this way derive the energy efficiency of module operation, see Eq. (III-12).

11.5 2D module calculation for RO and NF

Next we extend the plugflow model by describing concentration profiles in the upstream channel in more detail in x - and z -direction. Now the DBL is naturally included in the model. This is an important improvement because it is an interesting question whether the use of the analytical film layer approach is a good way to model flow in the very thin channels of a membrane separation unit. This is a reasonable doubt because the DBL concept assumes a layer of a certain thickness in front of the membrane through which all solutes and water must flow in x -direction to the membrane, without any flow coming ‘sideways’ (entering the DBL by flow in the z -direction). The DBL concept also assumes that flow is ‘fully developed’, i.e., inside the DBL we have steady state transport in x -direction across a layer of fixed thickness. In reality, early on in the module, the DBL may not yet be ‘formed’, with the fresh inflow arriving in the flow channel at all distances from the membrane, entering the layer ‘sideways’. Thus, though the DBL is a useful concept to explain many phenomena, it may not be optimal when the aim is a precise module calculation.

Thus the DBL concept is no longer used in the more advanced model that we discuss next. Expressions for membrane fluxes J_i and v_w now use a z -dependent interfacial concentration c_{int} replacing c_f . In the feed channel, we now consider concentration profiles not only in the z -direction, but also in the x -direction. The water velocity in z -direction is in good approximation still assumed to be invariant with x (we still have plug flow of the water in z -direction), but just like before, the velocity in z -direction will decrease with z . This implies we now use a differential volume balance

$$\frac{\partial v_z(z)}{\partial z} = -\frac{\partial v_x(x, z)}{\partial x} = -\frac{v_w}{h_{\text{ch}}} \quad (11.49)$$

where x is a coordinate towards the membrane and z along the membrane. For a flat channel, the plug flow profile for the water velocity in z -direction, implies that the water velocity in the x -direction, v_x , increases from zero at the backside of the flow channel (the position the furthest away from the membrane), to a value equal to v_w at the membrane interface. Thus with x starting at zero at the backside, and with h_{ch} the thickness of the channel, we have $v_x = v_w \cdot x/h_{\text{ch}}$. The solute mass balance, Eq. (11.30) now changes to

$$p_s \frac{\partial c_i(x, z)}{\partial t} = -\frac{\partial}{\partial z} c_i(x, z) v_z(z) - \frac{\partial}{\partial x} J_{x,i}(x, z) \quad (11.50)$$

where we include convection along the membrane (in z -direction), and a flux of solutes in x -direction that has many contributions. In x -direction the solute (ion) flux is described by the extended Nernst-Planck equation, Eq. (7.2), where we use v_x instead of v_F . Furthermore,

there is a factor ε accounting for porosity and tortuosity. There is no factor $K_{f,i}$ here because in a spacer channel there is no relevant friction of solutes with the mesh matrix (this is different from flow of solutes through a membrane, where pores are smaller by many orders of magnitude). Implementing Eq. (7.2) as well as $v_x = v_w \cdot x/h_{ch}$ in Eq. (11.50), we arrive for steady state at

$$v_z \frac{\partial c_i}{\partial z} + v_x \frac{\partial c_i}{\partial x} = \varepsilon D_i \frac{\partial}{\partial x} \left(\frac{\partial c_i}{\partial x} + z_i c_i \frac{\partial \phi}{\partial x} \right) \quad (11.51)$$

where we also implemented Eq. (11.49). Note that v_x depends on x by increasing linearly from zero at $x = 0$ to a value of v_w at the channel/membrane interface. The velocity in z -direction is independent of x but decreases with z according to Eq. (11.49).

For a single neutral solute, as well as for any binary salt solution, we can simplify Eq. (11.51) to

$$v_z \frac{\partial c}{\partial z} + v_x \frac{\partial c}{\partial x} = \varepsilon D \frac{\partial^2 c}{\partial x^2} \quad (11.52)$$

independent of a gradient in electrostatic potential, ϕ , similar to results developed in §7.3. For a binary salt, c is the monovalent equivalent salt concentration, see p. 173, and the diffusion coefficient D in Eq. (11.52) is the harmonic mean diffusion coefficient, D_{hm} , see Eq. (7.30).

Next we solve for the pressure gradient in z -direction for which we use Eq. (11.33) (for some details see [here](#)). For the downstream compartment (permeate side), the same set of equations can be used as for the feed channel, though we can also use the approach of the previous model for the permeate side. Then we set the pressure on the permeate side to one value, independent of z -position, while we neglect concentration gradients in x -direction in the permeate channel, gradients that most likely are small. The relevant volume and mass balances to be solved on the permeate side are then Eqs. (11.29) and (11.30). The final element is boundary conditions in solute flux in the upstream channel at $x = 0$ and $x = h_{ch}$. At $x = 0$ (the backside of the channel; which is the very left in Fig. 11.1), the derivative in x -direction in concentration is set to zero. At $x = h_{ch}$, which is the channel/membrane interface, the flux of a neutral solute is given by $J_i = v_w c_{int,i} - \varepsilon D_i \partial c_i / \partial x \big|_{x=h_{ch}}$ which at each z -position is then equal to the solute flux in the membrane, given by Eq. (11.9) (with $c_{f,i}$ replaced by $c_{int,i}$). For a binary salt this boundary condition is also valid, with J_i now the monovalent equivalent flux, c_i the monovalent equivalent salt concentration, and D_i the harmonic mean diffusion coefficient. This finalizes the overview of required equations for an RO module calculation for neutral solutes or a binary salt. For solutions with more than two ions, then Eq. (11.52) can no longer be used, and we must set up full mass balances in at least two of the ions, a statement that the divergence of current is zero, and combined with local

electroneutrality. These equations are discussed in §11.6 followed by simplified models for binary symmetric salts. Relevant is chemical equilibrium for ions at the channel/membrane interfaces, i.e., Donnan equilibrium, which was discussed in §2.8.

Important is the charge of ions because most solutions to be treated by RO or NF are electrolytes. Also many organic molecules, proteins and nanoparticles, are charged, with the charge often dependent on pH. Also the membrane is more likely charged than not. One consequence of the charge of ions and membrane, is that the transport of each species becomes strongly coupled to the transport of all other species. This is due to two effects. First of all, the net current through an RO membrane is zero.ⁱⁱⁱ This constraint leads to a coupling of the fluxes of the ions through the membrane such that the flux of positive charges becomes equal to that of the negative charges. It is the electric field that develops in the membrane that leads to these two fluxes to be exactly the same: if –as an example– the anions on average are slower, or have a lower concentration in the membrane, the electric field will develop in such a way that these anions go faster, while that same electric field will slow down the cations. The second effect of the charge of solutes and membrane, is that at each position in the membrane there must be local electroneutrality, which implies that the membrane charge together with all the charges of all the ions residing nearby, add up to zero. This constraint of local electroneutrality (EN) holds at each position in the membrane. At the outer surfaces of a membrane, i.e., at the solution/membrane edges, there is local charge separation in the Donnan EDLs formed there (but overall the Donnan layer is also electroneutral). For more discussion on this topic, see [here](#). These EDLs likely do not extend more than a few nm into the membrane, so the in the largest part of the membrane there is local EN. Donnan equilibrium was discussed in §11.6.

11.6 RO and NF with charged membranes - Ion transport inside the membrane

Having all equations established for the flow channel and for the interface between solution and membrane, we can now discuss the transport phenomena of ions inside a charged membrane. Ions and solutes are not only convected by the water which is pushed through the membrane, there are also diffusional and migrational forces acting on them. With ‘migration’ or ‘electromigration’ we refer to the forces on the ions because of their charge and the electric field. The electric field is the negative of the gradient in electrical potential,

ⁱⁱⁱIn an RO module there is the theoretical possibility of a net current through the membrane at one position, compensated by current in the other direction at another position, but this effect is likely very small.

$\mathbf{E} = -\nabla V$, or if only one coordinate x is considered, $E = -V_T \cdot \partial\phi/\partial x$ where we use the dimensionless electrical potential, ϕ , a number which can always be multiplied by $V_T = RT/F$ which is around 25.6 mV at room temperature, to return to the electrical potential, or voltage, V , with unit (m)V.

To describe the ionic flux J_i we use Eq. (7.71) which describes transport by convection, diffusion and migration, including also ion friction with the membrane structure, leading to $K_{f,i} < 1$. Note that all concentrations are defined per unit pore volume, while all ion fluxes and water velocities are defined per total ‘projected’, or geometrical, membrane area, i.e., these are superficial velocities, not interstitial. In a steady state process, ion flux J_i is constant across the membrane (except for reactive ions, see below), and this simplifies the (numerical) solution, but in general we must solve a differential mass balance for a volume element of total membrane phase,

$$p_m \frac{\partial c_i}{\partial t} = -\frac{\partial}{\partial x} J_i + R_i \quad (11.53)$$

where we assume a Cartesian (planar) geometry with ions flowing in only a single x -direction. It is known that in certain unsteady, dynamic, membrane processes (e.g., for membrane capacitive deionization with mixtures of ions), the accumulation of ions in the membrane significantly affects the separation process, and in those cases this mass balance, Eq. (11.53), must be solved.

Both in steady state and in a dynamic problem, in RO and NF the ionic current (or, ‘charge flux’, J_{ch}) through the membrane will be zero, and thus

$$J_{\text{ch}} = \sum_i z_i J_i = 0 \quad (11.54)$$

is one constraint, while local charge neutrality, Eq. (2.35), will also hold at each position in the membrane. The constraint of a zero ionic current must be considered at each position in the membrane, and can also be phrased as the divergence of ionic current being zero

$$\frac{\partial J_{\text{ch}}}{\partial x} = \frac{\partial}{\partial x} \sum_i (z_i J_i) = 0 \quad (11.55)$$

which, interestingly, must also hold in a dynamic calculation, and also when ions are adsorbing at/reacting with the membrane.

The reaction term R_i in Eq. (11.53) above relates to ion-pair formation, or acid-base reactions between different ions in a group of correlated species (like the three species in the group of carbonate ions), and relates to reactions of the ions with the membrane charges. As explained in Ch. 10 of this book, to account for the acid-base reactions between ions, we

set up groups of ions (for instance the three types of carbonate ions form a group) and add up both sides of Eq. (11.53) for all members of a group after which the R_i -terms vanish. Mathematically, this is very advantageous when subsequently we assume the acid-base reactions to be much faster than ion transport, such that locally there is chemical equilibrium between the reactive species (see [here](#) for more discussion).

The description of the flux of water across the membrane as function of pressure is discussed in §8.1 and when for all ions we can assume $K_{f,i} = 1$, water flux can be based on Eq. (8.14) or (8.20) (which for RO are the same except that Eq. (8.20) assumes equal diffusion coefficients, and Eq. (8.14) does not), or, when $K_{f,i} \neq 1$ but all $K_{f,i}$'s and D_i 's are the same for all ions, we can use Eq. (8.20). Otherwise we have to return to the general equations (8.2) and (8.8).

11.7 RO and NF with charged membranes - analytical solutions

In this section we present (semi-)analytical solutions of the transport rate of ions through charged membranes. Here we only discuss a 1:1 salt with cations and anions having the same diffusion coefficient and the same $K_{f,i}$ and Φ_i . For these assumptions, the extended Nernst-Planck equation can be set up for both ions, combined with electroneutrality and the zero-current constraint, and then we arrive for salt flux through the membrane at Eq. (8.40), which we reproduce here replacing J_{salt} by J ,

$$J = \frac{K_{f,i}}{2} \left\{ v_w \left(c_{T,m} - \frac{X^2}{c_{T,m}} \right) - k_{m,i} \frac{\partial c_{T,m}}{\partial \bar{x}} \right\}. \quad (8.40)$$

It is possible to solve Eq. (8.40) analytically, with J implicitly related to the $c_{T,m}$'s on either side, to v_w , etc., but the result is rather cumbersome. Thus we follow a different approach. We first integrate Eq. (8.40) to

$$J = \frac{K_{f,i}}{2} \left\{ v_w \left(\langle c_{T,m} \rangle - \frac{X^2}{\langle c_{T,m} \rangle^\dagger} \right) - k_{m,i} \Delta c_{T,m} \right\}. \quad (8.41)$$

which is Eq. (8.41) in Ch. 7. Now we only must find the two averages $\langle c_{T,m} \rangle$ and $\langle c_{T,m} \rangle^\dagger$. The first average, $\langle c_{T,m} \rangle$, is the average value of $c_{T,m}$ in the membrane, which has a value between a. the average of the $c_{T,m}$'s at the two sides of the membrane, which will be the case at low water flow rate, and b. a value close to the upstream-side value of $c_{T,m}$, which happens

at high water flow rates. The average with index \dagger is given by $1/\langle c_{T,m} \rangle^\dagger = \int_0^1 1/c_{T,m} d\bar{x}$. To find these two averages, we make use of $\partial J/\partial \bar{x} = 0$ after which Eq. (8.40) leads to

$$\frac{\partial^2 c_{T,m}}{\partial \bar{x}^2} = \text{Pe}_m \left(1 + \frac{X^2}{c_{T,m}^2} \right) \frac{\partial c_{T,m}}{\partial \bar{x}}. \quad (11.56)$$

Interestingly, Eq. (11.56) immediately shows that with positive water flow rate, and with $c_{T,m}$ decreasing through the membrane, thus a negative gradient, that the second derivative of $c_{T,m}$ is also negative, i.e., the decrease in concentration always goes faster and faster towards the downstream side of the membrane. We numerically solve Eq. (11.56) at gridpoints $1 \dots N$ and then easily calculate the two averages that we need in Eq. (8.41) by summation (trapezoid rule), see Ch. 21. We combine this result with Donnan equilibria on the two boundaries, an expression for the DBL layer, and the dead end condition, and in this way calculate J for any given v_w , X , c_f , etc. The relationship between v_w and hydrostatic pressure across the membrane, $\Delta P^{h,\infty}$, we discuss below.

First we discuss two approaches, a semi-analytical approach, and a fully analytical solution for rejection as function of c_f and v_w . These approaches used the result that full numerical calculations that could fit real RO data, see Fig. 11.3, showed linearly decaying profiles for $c_{T,m}$ across the membrane. Then the average $\langle c \rangle$ is the average of the two c 's at the two membrane edges, c_1 and c_2 , while for the 'inverted average' we then obtain $\langle c \rangle^\dagger = (c_1 - c_2) / \ln(c_1/c_2)$. This model gives results that are very close to the full model that uses Eq. (11.56). Replacing the average $\langle c \rangle^\dagger$ by the regular average $\langle c \rangle$ only leads to a small change, and can also be implemented. For experiments where c_p is much lower than c_{int} , the DBL equation can be simplified to Eq. (11.20). To obtain a simple analytical equation we leave out the convection and migration terms in Eq. (8.41), which we find leads to an error of around 5 to 10%, but then we have the compact result that salt flux is

$$J = -1/2 k_{m,i} K_{f,i} \Delta c_{T,m} \quad (11.57)$$

which we can combine with Eq. (12.29) and rewrite to

$$J = P \left(\sqrt{C^2 + c_{\text{int}}^2} - \sqrt{C^2 + c_p^2} \right) \quad (11.58)$$

where $P = k_{m,i} K_{f,i} \Phi_i$ is a salt transfer coefficient with unit $\text{L}\cdot\text{m}^{-2}\cdot\text{h}^{-1}$ (from now on abbreviated as LMH), and where we also introduce a charge parameter, $C = |X|/2\Phi_i$, that has unit mM. Expansion of Eq. (11.58) for low C is tricky except for the first term which is

$$J = P (c_{\text{int}} - c_p). \quad (11.59)$$

For the ‘dead end’ experiment (low water recovery), based on Eq. (11.58), and if we use $c_p \ll c_f$ and $\Phi_i c_p \ll |X|$, we arrive at

$$R_i = 1 - \frac{P}{v_w} \left(\sqrt{\alpha^2 + \exp(2v_w/k_{dbl})} - \alpha \right), \quad \alpha = \frac{C}{c_f}. \quad (11.60)$$

At high c_f , Eq. (11.60) predicts a limiting rejection independent of c_f and independent of C

$$R_i = 1 - \frac{B}{v_w} \exp(v_w/k_{dbl}) \quad (11.61)$$

where B is a traditional salt permeability, which in this limit is the same as P . However, below a certain c_f , according to Eq. (11.60) rejection is no longer independent of c_f . Even though Eq. (11.61) uses the same parameters as Eq. (11.26), they have a very different derivation. As long as rejection is better than 90%, the difference between the two equations is small, less than 10% difference in passage; and much less at the point where rejection is at a maximum. Series expansion of Eq. (11.60) leads to

$$R_i = 1 - \frac{P}{v_w} \cdot \alpha \cdot \sum_{n=1, \dots, \infty} \frac{Q_n}{n! \cdot \alpha^{2n}} \cdot e^{\frac{2n v_w}{k_{dbl}}} \quad (11.62)$$

where the prefactor is $Q_n = \prod_{j=1 \dots n} q_j$, where $q_j = q_{j-1} - 1$ and $q_1 = 1/2$. If we only take the first element in this series we arrive at

$$R_i = 1 - \frac{P \Phi_i c_f}{2 v_w C} e^{\frac{2 v_w}{k_{dbl}}} \quad (11.63)$$

which is the ‘good co-ion exclusion limit’ that we obtain at high charge or low c_f . This limit will also be discussed further on.

As we show in Fig. 11.3A, this model accurately describes a large dataset of RO with a commercial seawater desalination membrane (Dupont SW30-HRLE), with feed salt concentration from 50 to 600 mM, reproducing that in the higher salinity range data of rejection overlap, while rejection increases with further lowering c_f when c_f is less than 200 mM. Data are presented as passage, P_i , which is 100% minus rejection, R_i . Data are very well described when we use $k_{dbl} = 110$ LMH, $P = 0.39$ LMH, and $C = |X|/2\Phi_i = 58$ mM. If we use an estimate of membrane charge X of a few mM, say $X = 3$ mM (based on results in Kimani *et al.*, 2022), the non-electrostatic partition coefficient is $\Phi_i \sim 0.03$. If we then assume a membrane thickness of $L_m = 100$ nm, and take a salt diffusion coefficient of $D_i = 1.6 \cdot 10^{-9}$ m²/s, we derive for $K_{f,i}\epsilon$ a value around $2.5 \cdot 10^{-4}$, i.e., a membrane reduction factor (mrf) of the order of 4,000, definitely a very high number compared to values earlier derived for electrodialysis membranes, see p. 166. These results underpin that

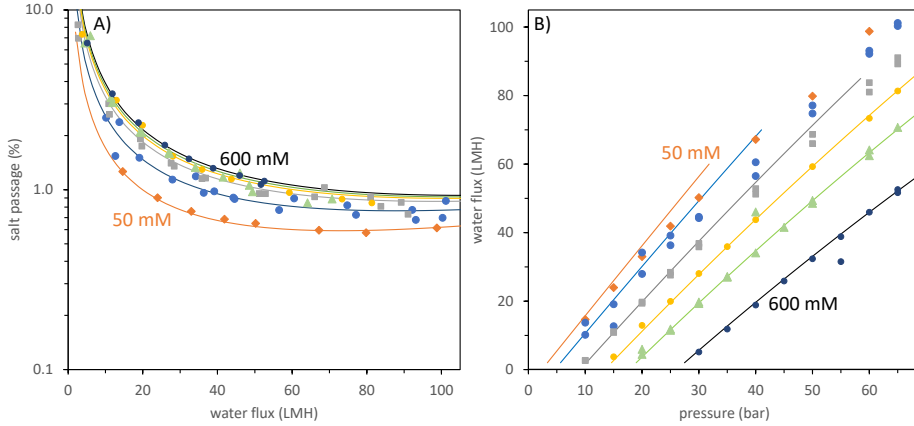


Fig. 11.3: Data and theory for desalination of water containing NaCl at various concentrations, for different transmembrane water fluxes. Theory based on Eq. (11.60). A) Results for passage, P , which is 100% minus rejection. B) Water flux versus applied pressure.

the membrane is charged, and that charge must be included in the theory, because theories based on neutral solutes do not show any dependency of rejection of feed concentration. To recalculate from membrane parameters P and C to the classical salt permeability B , we must match Eq. (11.60) and Eq. (11.61) with one another for one reference salt concentration and water flowrate for which we choose $c_f = 500$ mM and $v_w = 40$ LMH. We then obtain $B = 0.36$ LMH.

To find the associated relationship between applied pressure and water flux, we use Eq. (8.3) and insert the simplified salt flux equation of the present section, Eq. (11.57) (thus we assume in the membrane c changes linearly, and $\langle c \rangle = \frac{1}{2}(c_1 + c_2)$). This will lead to a modification of Eq. (8.47) where the term within (...) -brackets becomes $1/k_{F-m} + \langle c_{T,m} \rangle / k_{m,i}$. Eq. (8.47) only describes the pressure change within the membrane, so we must implement mechanical equilibrium at both membrane-solution edges which leads to $\Delta P^{h,m} = \Delta P^{h,\infty} + c_{T,m}^R - \Pi_p - (c_{T,m}^L - \Pi_{int})$, and we then arrive at^{iv}

$$\Delta P^{h,\infty} + \Delta c_{T,m} - \Pi_p + \Pi_{int} = - \left(\frac{1}{k_{F-m}} + \frac{\langle c_{T,m} \rangle}{k_{m,i}} \right) v_w + (1 - K_{f,i}) \Delta c_{T,m} \quad (11.64)$$

^{iv}Note: $\Delta P^{h,\infty} < 0$. Indices L and R refer to the left and right side of the membrane. The left side, L, is the upstream side, where on the outside of the membrane we have salt concentration c_{int} , while the right side, R, refers to the permeate, where we have Π_p . We use here osmotic pressure Π which for an ideal symmetric salt solution equals $2c_{\infty}$.

which becomes

$$\Delta P^{h,\infty} + K_{f,i} \Delta c_{T,m} - \Pi_p + \Pi_{int} = - \left(\frac{1}{k_{F-m}} + \frac{\langle c_{T,m} \rangle}{k_{m,i}} \right) v_w . \quad (11.65)$$

Because we can reasonably assume that $K_{f,i} \Delta c_{T,m}$ is much smaller than the other terms combined, we can leave out this term and arrive at

$$v_w = \left(\frac{1}{k_{F-m}} + \frac{\langle c_{T,m} \rangle}{k_{m,i}} \right)^{-1} \left(|\Delta P^{h,\infty}| - |\Delta \Pi_m| \right) \quad (11.66)$$

where $\Delta \Pi_m$ is the osmotic pressure difference directly across the membrane, between ‘int’ and ‘p’. Comparison with experiments, see Fig. 11.3B, showed that the entire second part within $(\dots)^{-1}$ is small compared to the constant factor $1/k_{F-m}$ which simplifies Eq. (11.66) to the classical result

$$v_w = A \cdot \left(|\Delta \bar{P}^{h,\infty}| - |\Delta \bar{\Pi}_m| \right) \quad (11.67)$$

where dimensional pressures, \bar{P} and $\bar{\Pi}$, expressed in Pa or bar, are pressures P and Π multiplied by RT . In Eq. (11.66), A is water permeability, in the theory the same as k_{F-m}/RT .

Eq. (11.67) can be combined with Eq. (11.21) if we make the assumption that the osmotic pressure only has an ideal contribution, i.e., that $\Pi \sim \Pi_{id}$, where $\Pi_{id} = 2c$ in case of a symmetric salt solution. We then obtain

$$v_w = A \cdot \left(|\Delta \bar{P}^{h,\infty}| - \bar{\Pi}_f R_i e^{v_w/k_{dbl,i}} \right) \quad (11.68)$$

which is an equation only valid when the dead-end condition, Eq. (11.3), also applies, and when osmotic pressure does not have other than ideal contributions.

If we use Eq. (11.68) to describe the data as presented in Fig. 11.3 the osmotic pressure that ‘pushes back’ is overestimated, and thus the pressure at which v_w starts to increase (intersection point with x -axis) is overestimated, for instance at $c_f = 600$ mM by about 4 bar. We therefore implement the correction discussed in Ch. 4 due to electrostatic ion-ion interaction, and write Π at the membrane upstream surface (‘int’) as a summation of an ideal term, $\Pi_{id} = 2c_{int}$, and a contribution due to electrostatic interactions. This correction can be implemented by multiplying the ideal osmotic pressure, $2RTc_{int}$, with the correction $1 - 0.015 \sqrt[3]{c_{int}}$ (c_{int} in mM). At room temperature and $c_f = 600$ mM this correction leads to a reduction in osmotic pressure of 4 bar. Furthermore, because rejections are very high, we can assume $c_p = 0$. We then arrive at the equation we use for pressure versus water flow rate in the dead-end experiment (limit of low water recovery)

$$v_w = A \cdot \left(|\Delta \bar{P}^{h,\infty}| - 2RTc_{int} \left(1 - 0.015 \sqrt[3]{c_{int}^{mM}} \right) \right) , \quad c_{int} = c_f \exp(v_w/k_{dbl}) . \quad (11.69)$$

As Fig. 11.3B shows, a very good fit of theory to the data is obtained, certainly for $c_f = 200$ mM and higher. For water permeability we derive $A = 2.2$ LMH/bar.

In the limit that the charge factor C is high, much larger than the salt concentration on both sides of the membrane, then we will be operating in the good coion exclusion limit. Then the concentration of counterions in the membrane ('ct') is close to the fixed membrane charge, $|X|$, and the coion ('co') concentration in the membrane is much smaller. We can then derive for salt flux^v

$$J = \frac{2v_w}{|X|} K_{f,i} c_{\text{int}} c_p \Phi_i^2 \frac{\sinh(v_w/k_{m,i} + \ln(c_{\text{int}}/c_p))}{\sinh(v_w/k_{m,i})}. \quad (11.70)$$

In the derivation of Eq. (11.70) use is made of the assumption $c_{m,\text{co}} \ll c_{m,\text{ct}}$ and thus $c_{m,\text{ct}} \sim |X|$. Eq. (2.46) then leads to $c_{m,\text{co}} = \Phi_i^2 c_{\infty,j}^2 / |X|$ at each side of the membrane. The derivation of Eq. (11.70) assumes equal diffusion coefficients in the membrane and an equal partition function, Φ_i . Eq. (11.70) does not make an assumption on the value of c_p relative to c_f . The equation can be combined with an expression for the DBL, Eq. (11.18), and with the dead-end condition, Eq. (11.3), which is only valid in case of a low water recovery. If we assume $c_p \ll c_f$, we then arrive at Eq. (11.63).

Finally, an interesting semi-analytical approach for RO is the convection-only limit by Dresner (1972) who shows that in a membrane concentrations are constant in the first part of the membrane and only drop off near the permeate side. The field strength, $E = -\partial\phi/\partial x$, is constant in this first region. This constant- c/E region is located near the upstream side, progressing until a position about a distance $D_{m,i}^*/v_w$ away from the downstream edge of the membrane. It is for thick membranes that this model can be relevant. In that case it is possible that most of the membrane is in the constant-concentration regime, and then all fluxes in the membrane can be calculated based on the composition of the upstream side of the membrane, making use of an extended Nernst-Planck equation *where concentration gradients are neglected*, which based on Eq. (7.71) is

$$J_{i,\text{Dresner}} = K_{f,i} \left(c_i v_w - k_{m,i} z_i c_i \frac{\partial\phi}{\partial x} \right). \quad (11.71)$$

^vBiesheuvel *et al.*, *J. Membr. Sci. Lett.* **2**, 100010, 2022.

In this model by Dresner, many physical-chemical details can be easily included, also including all of the acid-base reactions and ion-pair formations between all the ions. All partition effects (different between ions) can be included, as well as the various constraints of local electroneutrality and zero current, and the adsorption of ions to the membrane structure as described by a Langmuir isotherm or similar approaches. The Dresner-model leads to a set of algebraic equations without having to consider any concentration gradients across the membrane and the numerical solution thereof. In our view this is a very interesting modelling framework to further develop and test.

Electrodialysis

Membranes can desalinate water in two ways: by applying a pressure difference and thereby pushing the water through the membrane, as discussed in the previous chapter, and by applying a current across a charged membrane. In this second method, called electrodialysis (ED), counterions are the main species travelling across a membrane and they carry most of the ionic current. In ED, cells are assembled with one membrane that transfers cations and one membrane that transfers anions, and thereby it is possible to remove both anions and cations from a flow channel and thus desalinate water. This process of electrodialysis is discussed in this chapter.

12.1 General introduction to electrodialysis

In electrodialysis (ED), cell pairs are constructed with one anion-exchange membrane (AEM), one cation-exchange membrane (CEM), and two flow channels (spacer channels), and many of these cell pairs are combined into an ED stack, see Fig. 12.1. Electrical current is supplied to one of the end-electrodes, and this current runs through all of the membranes and channels and exits the stack on the other end-electrode. Faradaic reactions take place at the end-electrodes to convert the electronic current into an ionic current. Averaged over a cell cross section, the ionic current is the same at each position between the end-electrodes. All cell pairs behave in the same way. Just like NF and RO, ED operates in steady-state, i.e., if nothing goes wrong, the process can in principle continue forever.

In ED, in a cell pair, one channel is for water that will be desalinated, thus upon flowing out of the cell the water has become the freshwater or ‘diluate’. This channel is called the diluate channel or diluate compartment. The other channel is for the water that becomes increasingly concentrated; here ‘concentrate’ is produced and this is the concentrate compartment. The vocabulary used in RO and NF –of feed, retentate and permeate– is not used in ED, because in ED the water remains in the channel, and freshwater is produced by removing salt ions from the water.

In ED, if each channel is fed with the same water flow rate, then the water recovery, WR, will be 50%, i.e., of all the incoming water, 50% becomes freshwater (diluate) and 50% concentrate.¹ To increase WR, we can increase the water flow rate in the diluate channels (the channels that produce freshwater) relative to that in the concentrate channels. Note that there is always some water flow through the membranes (to the concentrate side), and thus water recovery based on exit streams is slightly less than water recovery based on the inflow.

Membrane transport in ED is described by the exact same physical laws and equations as presented in Ch. 11 to describe RO and NF. The same equations are used for the transport of ions and other molecules, as well as for the flow of the fluid, the water. The same equations are used both in the membranes and in the spacer channel, and also in the Donnan interfacial layers the equations are the same for these different membrane processes.

A sole difference is that in ED the ionic current is no longer zero, but is now equal to the current applied to the ED stack. The divergence of current is still zero, i.e., if we only have one direction in a planar (Cartesian) geometry, the ionic current does not change with position. In ED, the pressure difference across a membrane is now close to zero. Therefore, in an ideal situation the transmembrane water flow v_w can be low, and then in a

¹Water recovery, WR, is defined as the volume flow of freshwater produced, over total flow rate fed to a desalination device. See p. ?? for a detailed discussion of definitions of water recovery.

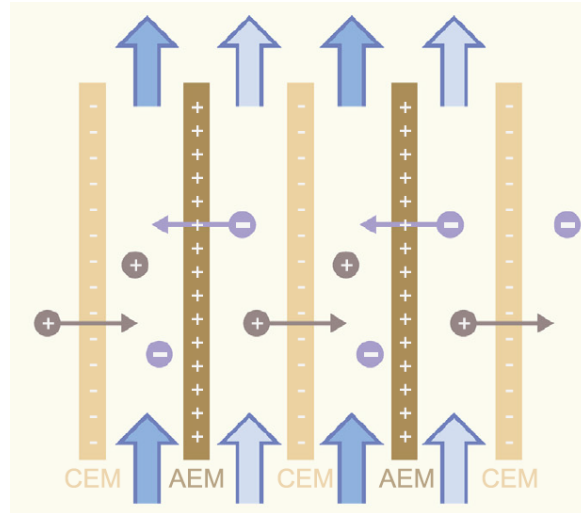


Fig. 12.1: Schematic view of an electrodialysis stack showing multiple cell pairs, each consisting of two flow channels, one where diluate (freshwater) is produced, the other producing concentrate. Here two cell pairs are drawn, but a practical stack contains hundreds of cell pairs.

first approximation set to zero. Thus, the x -component to the velocity in the spacer channel is then zero, and therefore the z -component to the velocity is unchanging, in both x - and z -direction; see Fig. 12.2 for a description of the x -coordinate (towards the membrane) and the z -direction (along the membrane).

Water flow through the membranes in ED. It must be noted that the assumption of no water flow through ED membranes is only an ideal case. In reality there are two driving forces for water to flow to the high-concentration side, first of all because the flow of counterions through the ion-exchange membranes drags water along, and secondly when a concentration difference develops between the two sides of the membrane, the hydrostatic pressure gradient in the membrane will be downward towards the concentrate side, thereby also pushing the water to the concentrate side, see §8.2 and §8.3. Thus there certainly is transmembrane water flow in ED. Also the water that is in the hydration shell of the ions is –as part of the hydrated ion– transported to the high-concentration side. Of these causes for water flow to the concentrate side, the osmotic effect is not related to current but is due to a concentration difference that develops across

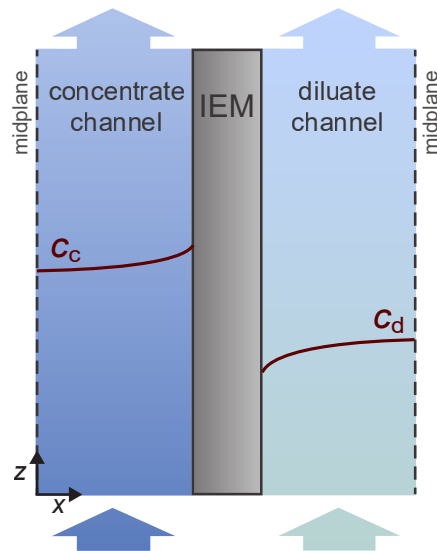


Fig. 12.2: Schematic view of an ED cell pair with typical concentration profiles across the channel from channel midplane to membrane. The simplified geometry depicted here, where only half of each channel needs to be considered, is applicable in case of a binary symmetric salt solution with ions of equal diffusion coefficients, and membranes that are equal in all regards except for the sign of membrane charge.

the membrane. This effect can be reduced by making the membrane thicker, but the other effects are still directly proportional to the counterion flux and thus independent of thickness. We can aim for a design where on the concentrate side the hydrostatic pressure is higher than on the diluate side, and this will push back the flow of water. (For ultrathin membranes (less than $1\ \mu\text{m}$ thickness) placed between two solutions with different salinities, water flow by osmosis will be very significant even when there is no current. See §8.3 for a related discussion on osmosis and electro-osmosis.)

Practical differences of ED in comparison to RO are that membranes in ED tend to be much thicker than in RO; instead of 100–200 nm in RO, the membrane thickness in ED is now 10s of microns, up to $\sim 200\ \mu\text{m}$. This thickness is necessary to avoid coion diffusion (which is always in the wrong direction, opposing salt removal from freshwater to concentrate). Thick membranes help because coions flow through the membrane to a large extent because of diffusion, and the gradient in concentration across the membrane that determines this diffusional flux will be lower for thicker membranes. This gradient and thus the flux of coions will go down by a factor of 10 when a membrane becomes 10 \times thicker. Thus, in ED and related current-driven membrane processes, one cannot make the membranes too thin.

The fixed membrane charge density in commercial ED membranes is as large as $|X|=5\ \text{M}$ and higher (X defined per unit open pore volume). To compare, in RO the membrane charge X is more typically a few mM. The proton-conducting material Nafion[®] used for fuel cells is an ion-exchange material with a moderately high charge density of $|X|\sim 2.7\ \text{M}$.

Geometrically, whereas in RO the flow channel only has a membrane on one side, in ED the channel has membranes on both sides, where one membrane is an AEM, the other a CEM.ⁱⁱ Whereas in RO there is a zero flux of solutes and water on one side of the flow channel, now in ED such mathematical simplifications are not possible, and in general any theoretical model for an ED cell pair must include two flow channels and two membranes. Only in a simplified calculation can we use the midplane in each channel as a symmetry plane. This is possible for a symmetric salt solution and when the two membranes have exactly equal properties (except that one is negatively charged and the other positive) and the two ions have the same diffusion coefficients.

In RO modelling, significant attention is given to the spacer channel on the feed side because concentration polarization (CP) in the diffusion boundary layer (DBL) leads to an increased concentration of solutes on the channel/membrane interface, which increases passage of solutes, and increases the osmotic pressure and thus reduces the

ⁱⁱIn a process called ‘shock electrodialysis’ both membranes are CEMs or both are AEMs.

transmembrane water flow. In ED there is also much interest in concentration polarization, i.e., the concentration of ions at the channel/membrane interface compared to an average concentration in a channel. In ED, however, different from RO, in the channel that is the most critical, which is the diluate channel, the concentrations do not increase towards the membrane, but instead go down, while in the concentrate channel, concentrations are higher at the membrane interface than in the center of the channel, see Fig. 12.2.

The decreasing salt concentration towards the membrane in ED is important because in the diluate channel concentrations are low, the more so the further we are away from the entrance, and decrease further towards the membrane. Thus the resistance across the diluate channel will be larger than in the concentrate channel (i.e., the voltage drop over the channel for a given current) and this resistance becomes even larger when the salt concentration drops to very lower values near the membrane. Furthermore, when for one of the ions the concentration at the solution/membrane interface decreases so much that it hits zero, the *limiting current*, LC, is reached, at least for this ion.ⁱⁱⁱ When this point is reached, theory based on an equilibrium Donnan model for the EDL structure at the solution/membrane interface is predicted to break down and we must revert to a theory based on the Poisson equation including ion transport in a region of several μm 's beyond the solution/membrane interface. This wider region is called the extended space-charge (SC) region. Theory that includes the extended SC region allows the current I to go beyond the LC.

Other mechanisms also enable operation for $I > LC$ without the concept of the extended SC region. The first mechanism is the reaction of water to H^+ and OH^- , i.e., water self-dissociation, which generates additional ions that carry the current. The second mechanism is when $I \rightarrow LC$ that the pH in the membrane changes to very high/very low values in such a way that the membrane charge is neutralized. For instance, for a negative membrane pH in the membrane becomes very low and a protonation reaction leads to a reduction of the charge of the membrane. As a consequence, the membrane becomes more leaky for coions which enables a higher current, and the extended SC region does not develop. Thus the equilibrium Donnan model remains valid. This might sound as a positive effect, but it is not, because the extra current is ineffective because it is carried by coions which go in the wrong direction (to the diluate channel). Thus these extreme pH values lead to 'current induced membrane discharge' as a mechanism that makes $I > LC$ possible in ED, while the equilibrium Donnan model remains applicable (Andersen *et al.*, *Phys. Rev. Lett.* **109** 108301, 2012).

ⁱⁱⁱBecause of various effects, as discussed in this and the next paragraph, the concentration will in the end never reach zero. Thus, with LC is implied the calculated final current when the concentration at the membrane is predicted to drop to zero, based on a theory that does not include these extra effects.

In bipolar membranes, which are membranes consisting of an anion-exchange layer in direct contact with a cation-exchange layer, similar (over-)limiting currents are observed with the concentration of one of the participating ions going to zero at one of the interfaces. Interestingly, now this limit is due to the concentration of one of the ions going to zero not outside the membranes, but at a point *inside* one of the membrane layers near the junction where the two layers are in contact (Tedesco *et al.*, pers. comm., 2020).

In this chapter we discuss the classical ED geometry with two channels, and one AEM and one CEM, and use the equilibrium Donnan model at the channel/membrane interfaces. We first consider the case without water flow through the membrane and later on present theoretical calculations that do include this effect.

12.2 The Sonin-Probstein approach for electro dialysis

Very similar to the module design for RO and NF, also in ED we have thin flow channels, or spacer channels, placed adjacent to a membrane. Through these layers the water flows along the membrane. In ED, there are actually two different membranes, CEMs and AEMs, placed in an alternating manner in an ED stack. Thus each channel is sandwiched between one AEM and one CEM.

In ED, while water flows in the z -direction through these channels along the membranes, by various transport mechanisms ions are moving sideways, across the narrow channel in x -direction and through the membranes. In z -direction we only consider convection, and because of that we can numerically solve the transport equations in such a way that we sequentially step through the z -domain where we solve all equations (relating to transport in the x -direction) at a certain z -coordinate, and then we move to the next z -coordinate.

In the Sonin-Probstein (SP) approach (Sonin and Probstein, 1968; Tedesco *et al.*, 2016–18) we solve the entire x -directional domain of a spacer channel by the same physical description, without making the assumption of a bulk phase that is adjacent to a diffusion boundary layer. Instead, in the SP-approach, we solve the same equations at each position in the channel, and we include how at each x -position there is flow of water and ions in z -direction, not only ‘outside the DBL’ but at each x -coordinate, right up to the membrane. Any flow pattern for the z -component of the fluid velocity can be considered, such as a parabolic dependence of v_z on position x , where velocity v_z is zero at the membrane edge, and it increases to a maximum in the center of the channel. However, in ED the flow channels are filled with spacer mesh material that promotes mixing and this leads to a situation where a flat velocity profile may be more realistic. We also find that calculations with parabolic or flat velocity profiles by and large give the same result. Thus, we suggest to assume ‘plug flow’, i.e., we

assume that the z -component of the velocity, v_z , is independent of x , just as we assumed for the feed channel in an RO module, see Ch. 11. Note, that now v_z is independent of x , does not imply that concentrations are also invariant with x ! Instead, the profiles of $c(x)$ is the topic of much to follow in this chapter.

At each (x,z) -coordinate we can solve the component mass balance, Eq. (11.51) from Ch. 11. Note that this equation includes the flow of water through the membrane (water velocity v_w at the membrane surface) and thus includes how v_x gradually changes with x towards the value v_w at the channel/membrane interface, while v_z decreases with z when water flows out through the membrane. Let us simplify this model and neglect membrane water flow from this point onward. This implies that v_x is zero at each x -position, and based on Eq. (11.29) we can also conclude that v_z is now invariant both with x and z . We now obtain the ion mass balance that we solve at each (x,z) -coordinate, Eq. (11.51) with $v_x=0$,

$$v_z \frac{\partial c_i}{\partial z} = \varepsilon D_i \frac{\partial}{\partial x} \left(\frac{\partial c_i}{\partial x} + z_i c_i \frac{\partial \phi}{\partial x} \right) \quad (12.1)$$

which we can further simplify when we have a binary salt solution (i.e., only one anion and one cation), see §7.7,

$$v_z \frac{\partial c}{\partial z} = \varepsilon D_{\text{hm}} \frac{\partial^2 c}{\partial x^2} \quad (12.2)$$

where c is the monovalent equivalent (m.e.) salt concentration, $c = c_+/z_+ = c_-/|z_-|$, see Eq. (7.29), and D_{hm} is the harmonic mean diffusion coefficient, see Eq. (7.30). From this point onward we often leave out index 'hm', and often leave out the factor ε as well; it should be straightforward to see where this index and factor can always be included again.

We solve Eq. (12.2) using the method of sequential steps, i.e., we use the implicit Euler method to discretize in the z -direction, from a coordinate z_{j-1} to z_j , after which we arrive at

$$\frac{c_j(x) - c_{j-1}(x)}{\tau} = D \frac{\partial^2 c_j(x)}{\partial x^2} \quad (12.3)$$

where time τ is the length of the step in z -direction, divided by the water velocity in z -direction, v_z . For a sequence of such steps in z -direction, we can numerically solve Eq. (12.3), where we discretize the right side of Eq. (12.3) using the central difference approximation. We can now completely solve at each z -position for all x -positions simultaneously where the problem is formulated as a set of algebraic equations, and then we move to the next z -position.

An important point we address further on is how the current is distributed over the channel length. Typically more current flows early on in a channel and less further down towards the exit. The easiest is when we can assume the cell pair voltage, V_{cp} , is the a certain preset

value, thus the same at each z -position. We run the calculation finding the profile of current I with position z , average, and in this way find the total stack current density for the imposed value of V_{cp} .

Interesting analytical expressions are obtained when we now assume there is one single step in z -direction, as if we immediately step from the entrance to the exit of the cell. This will be a valid approximation for a relatively short cell, or when the degree of desalination is low. Then c_{j-1} equals the inlet concentration c_{in} , and τ is the channel residence time, given by $\tau = V_c/\phi_v$ where V_c is the channel volume and ϕ_v the volumetric flow rate.^{iv} Concentration c_j is now the effluent concentration (at position x), which we will denote by $c(x)$ from this point onward.

For this 'single step' case, Eq. (12.3) has the analytical solution

$$c(x) = c^* + (c_{in} - c^*) \left(1 - \frac{\cosh(\varphi \cdot x/h)}{\cosh \varphi} \right) \tag{12.4}$$

where c^* is the salt concentration at the channel/membrane edge (at $x = h$), and where $\varphi^2 = h^2/(\tau D)$.^v To derive Eq. (12.4), we assumed that at the midplane we have $\partial c/\partial x|_{x=0}$. In Eq. (12.4), x runs from the midplane of the channel towards the membrane (where $x = h$). Note that h is the half-thickness of the channel, thus the width of the channel is $\delta = 2h$. The concentration at the midplane follows from Eq. (12.4) when we implement $x = 0$.

At the edge of the channel we can evaluate the flux J , defined as

$$J = -D \cdot \partial c/\partial x|_{x=h} \tag{12.5}$$

and combination with Eq. (12.4) results in

$$J = \sqrt{\frac{D}{\tau}} (c_{in} - c^*) \tanh \varphi \tag{12.6}$$

which for a wide enough channel, i.e., for $\varphi \gtrsim 2$, simplifies to Eq. (7.13),

$$J = \sqrt{D/\tau} (c_{in} - c^*) .$$

In general, for symmetric and asymmetric salts, this flux at the boundary of the channel can be recalculated to a current J_{ch} and transport numbers T_+ and T_- by Eq. (7.41).

^{iv}All fluxes and velocities are superficial velocities, i.e., the velocity and flux as if the spacer material were not there. Thus, the volume V_c is the empty volume of a channel, i.e., the product of cross-sectional area and channel width.

^vNote that φ is not the same as ϕ , the electrostatic potential.

From this point onward we consider a 1:1 salt with both ions having the same diffusion coefficient. There can be more types of ions, but we must assume they all have the same diffusion coefficient. Then we can use Eq. (7.44) (with $z=1$) and arrive at

$$J_{\text{ch}} = I/F = 2/\lambda \cdot J \quad (12.7)$$

and in this way connect the above equations to the current I . In Eq. (12.7) the current efficiency, λ , arises, a parameter that quantifies ion transport in a 1:1 salt solution, and which relates to ion transport numbers according to $\lambda = T_+ - T_-$, see §7.2. (All of this assumes there is one cation and one anion). For a 1:1 salt, this current efficiency is also the ratio of total ions flux through a membrane, $J_{\text{m,ions}} = J_{\text{m,+}} + J_{\text{m,-}}$, over current density, J_{ch} , because

$$\lambda = T_+ - T_- = \frac{J_+}{J_{\text{ch}}} + \frac{J_-}{J_{\text{ch}}} = \frac{J_{\text{m,ions}}}{J_{\text{ch}}} . \quad (12.8)$$

In ED the current efficiency of membrane transport is between -1 and +1.^{vi} Combination of Eqs. (12.6) and (12.7) leads to

$$I = \frac{2F}{\lambda} \sqrt{\frac{D}{\tau}} (c_{\text{in}} - c^*) \tanh \varphi = \frac{F\delta}{\lambda\tau} (c_{\text{in}} - c^*) \eta \quad (12.9)$$

where $\eta = 1/\varphi! \cdot \tanh \varphi$ is the effectiveness factor for desalination. This factor has the limits $\eta \rightarrow 1$ for $\varphi \rightarrow 0$, and $\eta \rightarrow 1/\varphi$ for $\varphi \rightarrow \infty$ (in practice $\varphi > 2$ suffices to be in this second limit). Eq. (12.9) shows a relationship for current density across a channel in ED as function of inflow salt concentration, the salt concentration at the channel/membrane interface, c^* , and factors relating to channel size and water flow rate. This equation, based on the Sonin-Probstein approach, is analytical and does not include the concept of a DBL of a certain thickness with a certain transfer coefficient of which it is assumed that ions only move across it from a core bulk phase to the membrane. Instead, this SP model equation includes convective flow of salt along the membrane at all x -positions, and thus the concentration profiles depend on fluid residence time and channel volume, which are key properties of design and operation of an ED process.

For $\varphi > 2$, i.e., for a wide enough channel relative to the product of residence time and diffusion coefficient, Eq. (12.9) simplifies to

$$I = 2F/\lambda \sqrt{D/\tau} (c_{\text{in}} - c^*) . \quad (12.10)$$

^{vi}As long as there is no water flow across the membrane. When there is water flow across the membrane, current efficiency can be outside this range, see Fig. 12.6

Eqs. (12.9) and (12.10) also give a prediction for the limiting current, which is reached when $c^* = 0$. Based on the general result, Eq. (12.9), we obtain

$$I_{\text{lim}} = \frac{2Fc_{\text{in}}}{\lambda} \sqrt{\frac{D}{\tau}} \tanh \varphi = \frac{Fc_{\text{in}}\delta}{\lambda\tau} \eta \quad (12.11)$$

which for a low desalination effectiveness, $\eta \rightarrow 0$, e.g., because of a sufficiently wide channel, simplifies to

$$I_{\text{lim}} = \frac{2F}{\lambda} \sqrt{\frac{D}{\tau}} c_{\text{in}} \quad (12.12)$$

a result quite different from a DBL-based approach where $\sqrt{D/\tau}$ would be replaced by D/δ , with δ a hypothetical thickness of the DBL. The new analytical result for the limiting current, I_{lim} , does not contain this thickness δ but includes the residence time, a measure of the rate by which fluid is refreshed because of convection along the membrane.

The next step is to obtain a second expression for the ionic current, I , which we obtain from $I = FJ_{\text{ch}}$ and Eq. (7.41)b in case $D_+ = D_-$ and a 1:1 salt, resulting in

$$I = -2FDc \frac{\partial \phi}{\partial x}. \quad (12.13)$$

To obtain the current-voltage relationship for the entire spacer channel of width $\delta = 2h$, we integrate Eq. (12.13) based on the fact that I is invariant across the width of the channel, which leads to

$$\left| \frac{\Delta V_s}{I} \right| \frac{DF}{V_T} = \int_0^h \frac{1}{c(x)} dx \quad (12.14)$$

where ΔV_s is the full voltage drop over the spacer channel, with $V_T = RT/F \sim 25.6$ mV at room temperature. We insert Eq. (12.4) in Eq. (12.14) and obtain

$$\left| \frac{\Delta V_s}{I} \right| \frac{DF}{V_T} = \frac{\delta}{\sqrt{AB}} \frac{\cosh \varphi}{\varphi} \tanh^{-1} \left\{ \sqrt{\frac{A}{B}} \tanh \frac{\varphi}{2} \right\} \quad (12.15)$$

where $A = c_{\text{in}} \cosh \varphi + (c_{\text{in}} - c^*)$ and $B = c_{\text{in}} \cosh \varphi - (c_{\text{in}} - c^*)$. We analyze Eq. (12.15) together with Eq. (12.9) in Fig. 12.3. Interestingly, when the limiting current is reached, $c^* \rightarrow 0$, then the argument in the \tanh^{-1} -function approaches unity (one) (for $c^* = 0$ the square root of the ratio of A over B is exactly opposite to $\tanh \varphi/2$), and because the terms in front always stay bounded, also when $\varphi \rightarrow \infty$, Eq. (12.15) predicts that when the limiting current is reached, ΔV_s will diverge, whatever is the value of δ , τ , or D .

When we assume that across the channel concentration gradients are small, e.g., because we set τ to a very low value, then Eq. (12.15) simplifies to Ohm's law for this case of an

ideal 1:1 salt with equal ion diffusion coefficients, the same as Eq. (7.56)

$$\left| \frac{\Delta V_s}{I} \right| \frac{DF}{V_T} = \frac{\delta}{2c}. \quad (12.16)$$

The above model can be solved if we know the current efficiency, λ , and then we can establish the current-voltage, I - V , curve, when we combine Eq. (12.9) and Eq. (12.15). The calculation of λ requires evaluation of a membrane model, and this is what we will do in the next section. But for now we simply assume a membrane that is perfectly selective and thus only allows counterions to go through, thus we set $\lambda = 1$.

Calculation results for the voltage across the diluate channel based on Eq. (12.15) are presented in Fig. 12.3 as function of current density. We use a reference value of $\varphi = 1$ which is realistic, based on $D = 1 \cdot 10^{-9} \text{ m}^2/\text{s}$, residence time $\tau = 10 \text{ s}$, inflow concentration $c_{\text{in}} = 100 \text{ mM}$, and channel width $\delta = 200 \mu\text{m}$. Results are presented as function of current divided by the limiting current at $\varphi = 1$, which based on Eq. (12.10) is $I = 147 \text{ A/m}^2$. Calculations at higher and lower φ represent respectively a lower and higher residence time τ (with D and δ unchanged). Fig. 12.3 shows that when we approach the limiting current, the voltage across the diluate channel diverges, as expected.^{vii} For a higher residence time (slower flow of water), thus for a lower value of φ , the limiting current is lower, and the reverse is the case when we flow faster (lower τ and higher φ).

An overall salt balance for the diluate channel relates current density I and membrane area to the product of volume flow rate, $\phi_{v,d}$, and the change in salt concentration between inlet and outlet of the channel, $c_{\text{in}} - \langle c_{\text{out}} \rangle$, by

$$\lambda I A = F \phi_{v,d} (c_{\text{in}} - \langle c_{\text{out}} \rangle) \quad (12.17)$$

and the average outflow concentration is given by integration of Eq. (12.4), resulting in

$$\langle c_{\text{out}} \rangle = c_{\text{in}} - (c_{\text{in}} - c^*) \eta \quad (12.18)$$

which also follows from combining Eqs. (12.9) and (12.17).

How far can we desalinate water according to Eq. (12.18)? If we work at the limiting current, then $c^* = 0$, and we obtain

$$1 - \frac{\langle c_{\text{out}} \rangle}{c_{\text{in}}} = \eta = \frac{\tanh \varphi}{\varphi} \quad (12.19)$$

which shows that when $\varphi \rightarrow \infty$ and thus $\eta \rightarrow 0$ (wide channel, fast flow of water) we do not desalinate much, i.e., $\langle c_{\text{out}} \rangle \sim c_{\text{in}}$, but in the opposite limit of a thin channel or long residence

^{vii}For $\varphi = 1$, when the limiting current is reached, the concentration at the center line of the channel is 35.2 mM, and the average concentration is 23.8 mM.

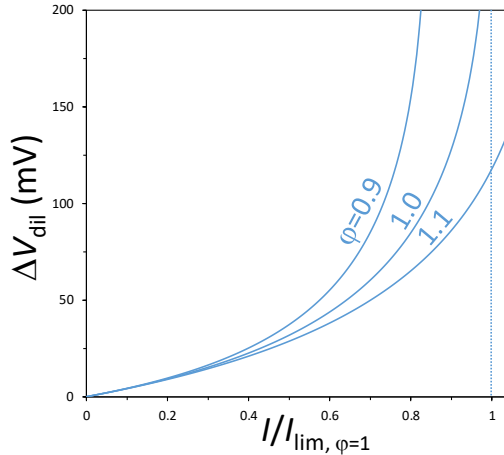


Fig. 12.3: The voltage across a diluate channel in electrodialysis as function of current I and the flow parameter ϕ . Higher values of ϕ are because of a lower residence time τ and thus a faster flow of water through the channel ($D/h=10 \mu\text{m/s}$, $c_{\text{in}}=100 \text{ mM}$, $\lambda=1$).

time, and thus $\phi \rightarrow 0$ and $\eta \rightarrow 1$, we can reach full desalination. The assumptions underlying Eq. (12.19) include that we work at the limiting current at the exit of the channel, thus have $c^*=0$ at the exit. If that is indeed the case (which in reality will not be so), the above result is obtained independent of the value of current efficiency, λ . A comprehensive ED-model which does not use this assumption of $c^*=0$ at the outlet is discussed in the next section.

12.3 1D model for an ED cell for non-unity current efficiency

How would a more realistic ED model for a full cell pair look like? Such a model can be based on the elements outlined above, for transport in flow channels and in membranes, with Donnan layers at the edges between these domains. Water flow through the membrane can be included by methods outlined in Ch. 11. Both across the channel and the membrane we discretize in x -direction and solve the resulting set of algebraic equations, while we ‘step through’ the z -coordinate by sequential calculations at z -coordinate j , then $j+1$, etc.

In this section, however, we first discuss a more simple approach, in continuation of the model for the diluate channel of the last section. We also include the Donnan layers at the membrane/solution edges, and the membranes themselves. We again consider an ideal 1:1

salt solution with ions having equal diffusion coefficients in the channel (and also in the membrane we assume the same mobilities: $D_m = D_{m,\text{anion}} = D_{m,\text{cation}}$). The two membranes have an equal magnitude of the membrane charge, $|X|$, equal thickness, and we use the Nernst-Planck equation for ion transport. In the first part we assume no water flow through the membrane.

We are also going to address changes in z -direction in more detail. Whereas in the previous section, in z -direction only a single ‘position line’ was considered, we are now going to solve a model with a sequence of such z -lines. In this way we describe more precisely the plug flow character of flow in each channel. With plug flow we mean that in z -direction ions are mostly transported by convection, and there is not much transport by diffusion and dispersion in z -direction. Instead, in the approach of the last section with only a single z -line, the mixing in z -direction was at a maximum, because the concentration at a certain x -coordinate was assumed to be the same from entrance to exit of the channel.

In the present section we combine a plug flow model for flow in the z -direction, with a result from the previous section for ions flux, which we base on Eq. (12.6), and is then

$$J_{m,\text{ions}} = k_s (c - c^*) \quad (12.20)$$

where c is now the z -dependent average salt concentration in the channel, and as before, c^* is the salt concentration at the channel/membrane interface. (Thus we replaced c_{in} by c .)^{viii} We introduce the channel transfer coefficient $k_s = \sqrt{D/\tau} \tanh \varphi$, which is a function of channel width, ion diffusion coefficient, and a surface refreshment time, τ , similar to the concept of surface renewal in the Danckwerts theory of mass transfer from chemical reactor engineering. The parameter τ , which in the last section was the residence time in the entire channel, now becomes a characteristic time required for ions to be mixed up along the z -coordinate. Using Eq. (12.20) we calculate a surface salt concentration c^* which is required in equations for the Donnan layer at the channel/membrane interface. For a very high surface renewal rate, thus τ very small, Eq. (12.20) simplifies to the statement that $c^* = c$, i.e., absence of concentration gradients across the channel.

Assuming transport only by convection in z -direction, then for steady state a salt balance for an ED channel (without water flow through the membranes) will be

$$-2 v_z \delta \frac{\partial c}{\partial z} = J_{m,\text{cem},+} + J_{m,\text{cem},-} - J_{m,\text{aem},+} - J_{m,\text{aem},-} \quad (12.21)$$

^{viii}For wide channels this result is unproblematic, it functions as an analytical equation for the DBL, but for a thinner channel we must realize c is an average concentration, not the concentration on one side of the DBL and c^* that on the other side. Problematic is that Eq. (12.20) is based on an ‘Euler backward’ discretization, with flux $J_{m,\text{ions}}$ and concentration c^* evaluated at the end of a discrete step in z -direction, while c is the average concentration at the start of this step.

where on the left we have transport by convection of *all ions*, therefore the factor 2, while on the right we have four fluxes through the membrane, of cations and anions, through CEM and AEM. In the coordinate system defined as ‘to the right’, the CEM is assumed here to be to the right of the channel, the AEM left. We assume that counterion fluxes are the same in magnitude; thus the magnitude of cation flux through the CEM is equal to anion flux through the AEM, and the same holds for the coions, thus $J_{m, \text{cem}, +} + J_{m, \text{aem}, -} = 0$ and $J_{m, \text{cem}, -} + J_{m, \text{aem}, +} = 0$. And we introduce the total ions flux through one membrane as $J_{m, \text{ions}} = J_{m, +} + J_{m, -}$. In balances such as the next one, we make sure $J_{m, \text{ions}}$ is a positive number when indeed there is an ions flux leaving a channel (and negative when there is a flux of ions entering a channel). We then arrive at

$$v_z \frac{\partial c}{\partial z} = -\frac{J_{m, \text{ions}}}{\delta} \quad (12.22)$$

which we will use in both the diluate and the concentrate channel, and we can in this way analyze co-current flow as well as counter-current flow. In both cases there is only the z -direction to consider in the mathematical code.^{ix}

We now first describe the model for the ion-exchange membrane. Just as for RO and NF in Ch. 11, also in ED, the fluxes of all ionic species through the membrane are given by the Nernst-Planck equation in combination with local electroneutrality (which involves the membrane charge, X). Furthermore, we know that the ionic current is unvarying across the membrane. We analyze the situation of no transport of water across the membrane. In steady state and for unreactive ions, also the flux of each ion is unvarying across the membrane. We use Eq. (7.71) and combine the factor $K_{f,i}$, ε , D_i and thickness δ into the membrane transfer coefficient $k_{m,i}^* = K_{f,i} \varepsilon D_i / \delta$. When we have a 1:1 salt with D_i and $K_{f,i}$ the same for anion and cation, then we obtain for the ionic current density, $J_{\text{ch}} = J_+ - J_-$,

$$J_{\text{ch}} = I/F = -k_{m,i}^* c_{T,m} \frac{\partial \phi_m}{\partial \bar{x}} \quad (12.23)$$

where $\bar{x} = x/\delta$. We can integrate Eq. (12.23), resulting in

$$\int_0^1 \frac{1}{c_{T,m}} d\bar{x} = \frac{1}{\langle c \rangle^\dagger} = -\frac{k_{m,i}^*}{J_{\text{ch}}} \int_0^{\Delta \phi_m} d\phi_m \quad (12.24)$$

where to solve the left side we need to know how the total ions concentration, $c_{T,m}$, changes across the membrane. Because this concentration does not change much for a good ion-exchange membrane, we can replace the left side by $1/\langle c_{T,m} \rangle$ where $\langle c_{T,m} \rangle$ is the regular

^{ix}In Biesheuvel *et al.*, *J. Membrane Sci.* **647** 120221 (2022), cross-current flow in ED is considered as well.

average, which for a linear profile is the average of $c_{T,m}$ evaluated at the two outer edges of the membrane (just in the membrane). The error made in replacing $\langle c \rangle^\dagger$ by $\langle c \rangle$ can be estimated as $1/12\Delta c^2/\langle c \rangle$ in case of a linear profile in $c(x)$.^x Even for a moderately charged membrane with $X=2\text{ M}$ ($c_{T,m}$ is always slightly above X), and a rather extreme difference in $c_{T,m}$ across the membrane of $\Delta c_{T,m}=0.2\text{ M}$, the error made in taking the average is only as small as 0.1%. For a lower concentration difference, and membranes with a higher charge, the error will be even less. Thus, we can safely use the average concentration $\langle c_{T,m} \rangle$ and obtain after integration

$$J_{\text{ch}} = -k_{m,i}^* \langle c_{T,m} \rangle \Delta\phi_m. \quad (12.25)$$

Note that Δ 's denote a value at a position 'right' minus 'left', in both cases just inside the membrane on either side. For the total ions flux in a membrane, $J_{m,\text{ions}} = J_+ + J_-$, we obtain

$$J_{m,\text{ions}} = -k_{m,i}^* \left(\frac{\partial c_{T,m}}{\partial \bar{x}} - X \frac{\partial \phi_m}{\partial \bar{x}} \right) \quad (12.26)$$

where X is either negative (CEM) or positive (AEM). This equation can be integrated without making any assumption (as long as X is not a function of position) to

$$J_{m,\text{ions}} = -k_{m,i}^* (\Delta c_{T,m} - X\Delta\phi_m). \quad (12.27)$$

Eq. (12.25) and Eq. (12.27) can be combined with equations for the two flow channels, and the Donnan layers at the channel/membrane edges, and with an overall condition which can be a cell pair voltage or current.^{xi} We can calculate for each z -coordinate the current efficiency, λ , by Eq. (12.8).

Current efficiency. As an intermezzo, let us evaluate the parameters that determine the current efficiency. If we implement the equations for $J_{\text{ch}} = I/F$, Eq. (12.25), and for $J_{m,\text{ions}}$, Eq. (12.27), in the expression for current efficiency, Eq. (12.8), we obtain

$$\lambda = \frac{J_{m,\text{ions}}}{J_{\text{ch}}} = \frac{X}{\langle c_{T,m} \rangle} - \frac{k_{m,i}^* \Delta c_{T,m}}{J_{\text{ch}}} \quad (12.28)$$

^xThis expression is based on comparing the approximation with a more rigorous approach where we assume a linear decay of c across a layer, and implement that x -dependence on the left side of Eq. (12.24) and make the integration.

^{xi}Typically we apply a certain total current to the total cell. But the current density will vary with z -position. The only property not varying with z -coordinate, is the cell pair voltage. This will be the same at each z -coordinate, while for co-current flow the current density typically decreases with z . This is further analyzed in the next section.

where we evaluate λ , X , J_{ch} , and $J_{\text{m,ions}}$ all as positive quantities (further on in this box we again use the $|\dots|$ -notation to indicate that we use positive quantities). We can simplify Eq. (12.28) when on both sides the salt concentration just outside the membrane, c^* , is much lower than X . In that case $c_{\text{T,m}}$ will be close to X and thus the first term on the right will be close to unity. In this limit, the expression for total ions concentration in the membrane is (for a fully dissociated 1:1 salt, with Φ_i the geometric mean partition coefficient for non-electrostatic effects, see §2.8)

$$c_{\text{T,m},j} = \sqrt{X^2 + \left(2 \Phi_i c_j^*\right)^2} \quad (12.29)$$

which can be linearized for small values of c^*/X , and the difference in $c_{\text{T,m}}$ is then

$$\Delta c_{\text{T,m}} = \frac{2}{|X|} \left(c_c^{*2} - c_d^{*2} \right) \quad (12.30)$$

where ‘c’ and ‘d’ refer to concentrate and diluate channel, with index * referring to a salt concentration right next to the membrane. This expression can be inserted in Eq. (12.28), and we then arrive at

$$\lambda = 1 - \frac{2 k_{\text{m},i}^* F}{|X| |I|} \left(c_c^{*2} - c_d^{*2} \right) \quad (12.31)$$

which shows that λ drops when a membrane becomes thinner or for other reasons has easier mass transport (higher $k_{\text{m},i}^*$). It then loses its functionality in ED to retain coions from moving across a membrane and charge efficiency drops. This is because coions mainly move across an ED membrane by diffusion, the rate of which is directly proportional to $k_{\text{m},i}^*$. The dependence on the flow channel salt concentrations is also very interesting: a membrane that may seem to be very selective and only allow counterions to pass through when salt concentrations are low on both sides, say $c_{\text{in}} = 10$ mM, may no longer be that selective at 500 mM. And the membrane becomes especially leaky when a concentration difference develops across the membrane. When the salt concentration in the concentrate channel goes up and in the diluate channel goes down, Eq. (12.31) shows that current efficiency drops. Also at low currents the membrane becomes more leaky. For all these reasons the theory predicts that the further one progresses into an EDL channel, the lower is current efficiency, i.e., the larger is coion leakage as indicated as well in Fig. 12.4.

The influence of membrane thickness on $k_{\text{m},i}^*$ and thus on efficiency, is also why processes to harvest energy from saltwater and fresh water, which is the reverse of ED

(called ‘reverse electrodialysis’ (RED), ‘blue energy’, ‘osmotic power’, or ‘nanopore power generation’) when ultrathin membranes are used, will never be viable. Even though power densities can be very high in certain laboratory experiments where the solutions on the two sides of the membrane are kept at a high concentration difference, nevertheless, in a real (R)ED membrane system, the massive coion leakage (because of a very low value of λ and a high value of $k_{m,i}^*$) leads to very rapid mixing of the freshwater and concentrated water, and the power production in this device will be orders of magnitude less than in an optimized RED stack with membranes of an optimized thickness of for instance $\delta = 20 \mu\text{m}$, see Tedesco *et al.* (2018). In reality the situation is even worse because the present analysis neglects the significant, and adverse, water flow that would also run through an ultrathin membrane, quickly diluting the concentrate water stream.

We continue with our ED calculation where we only have ion transport by convection in z -direction (plug flow) with no transmembrane water flow. The above equations can all be combined, including also Eq. (12.29) at both membrane edges, and this set of equations can be solved for a given current density $I (=F \cdot J_{\text{ch}})$. However, with λ a varying parameter, given by Eq. (12.8), we obtain a quite convoluted set of equations. It is much better to solve the entire set of equations numerically. In addition, the condition of a constant current density is not realistic for ED. Instead, in ED it is not the current density that is unvarying with z -coordinate, but the cell pair voltage, V_{cp} , is constant from entrance to exit of the cell.^{xii} The cell pair voltage is a summation of various terms which all change as function of the z -coordinate in the channel, while the summation, V_{cp} , remains constant. The cell pair voltage is given by

$$\frac{V_{\text{cp}}}{2V_{\text{T}}} = \sinh^{-1} \frac{|X|}{2\Phi_i c_{\text{d}}^*} - \sinh^{-1} \frac{|X|}{2\Phi_i c_{\text{c}}^*} - \Delta\phi_{\text{m}} + \Delta\phi_{\text{s, sr, d}} + \Delta\phi_{\text{s, sr, c}} \quad (12.32)$$

in which the inner membrane potential, $\Delta\phi_{\text{m}}$, follows from Eq. (12.25), and the last two terms are the voltage drops over the d- and c- half-channels based on Eq. (12.15), which as an example for the d-channel is given by

$$\Delta\phi_{\text{s, sr, d}} = \frac{J_{\text{ch}}}{D} \frac{h_{\text{d}}}{\sqrt{A_{\text{d}} B_{\text{d}}}} \frac{\cosh \varphi_{\text{d}}}{\varphi_{\text{d}}} \tanh^{-1} \left\{ \sqrt{\frac{A_{\text{d}}}{B_{\text{d}}}} \tanh \frac{\varphi_{\text{d}}}{2} \right\} \quad (12.33)$$

^{xii}Unless we work with a cell with ‘segmented electrodes’. In that case the current can be more evenly distributed and V_{cp} is no longer the same at each z -position.

with the definition of A and B provided below Eq. (12.15), in which we replace c_{in} by c . Note that one parameter in this equation is τ (an element of A , B and φ) which is the surface renewal time, a tunable parameter that can be interpreted as the extent of mixing of ions across the channel, i.e., the dispersion across the channel. (The same parameter τ is also included in the channel transfer coefficient k_s used in Eq. (12.20)). The first two terms in Eq. (12.32) are the Donnan potentials at the channel/solution interfaces for which we use Eq. (2.43). The factor 2 in Eq. (12.32) is because we have two channels and two membranes in a cell pair.

We solve this model for co-current flow of electrolyte in the d- and c-channels. In co-current flow the flow through the channels (along the membranes) has the same direction. We assume that the two channels are fed with the same water flow rate and the same inlet salt concentration, c_{in} , and we set all other properties of the two channels to the same values. In this section water flow through the membrane is set to zero, thus at all z -positions $v_w = 0$. (This is also assumed in Eqs. (12.20), (12.27), and (12.33).) As a consequence of these assumption, in this calculation the (average) concentrations in the two channels at each z -coordinate are related by $c_d + c_c = 2 c_{\text{in}}$. (The same relation also holds for the interfacial concentrations c_j^* when we use the same k_s -value in the two channels.). We present in Figure 12.4 the concentration in the diluate channel c_d , current density I , and current efficiency λ , all versus position z . Parameter settings are: $c_{\text{in}} = 500$ mM, $|X| = 4$ M, channel width $\delta = 200$ μm , water velocity through channel $v_z = 1$ mm/s, diffusion coefficient in channel $D = 1 \cdot 10^{-9}$ m²/s, $k_{m,i}^* = 1$ $\mu\text{m/s}$, renewal time $\tau = 2$ s, and $V_{\text{cp}} = 0.2$ V.

Fig. 12.4 shows how from the entrance onward all parameters change gradually: the concentration in the diluate channel gradually decreases, first fast, then slower, and the channel/membrane concentration is always lower, but the difference decreases with z . The further we move through the cell, the lower is the current efficiency, λ , dropping all the way to zero. At that point we have the situation that we are still directing current through the membrane but there is no further desalination. In this steady state which in this calculation is reached after about 6 cm into the channel, current (electrical field) drives counterion transport out of the diluate channels (leading to desalination), but this is completely offset by coion transport by diffusion. It is not the case that a certain ion now moves back from c- to d-channel through the same membrane it came from, but it leaks out of the c-channel on to the next d-channel, i.e., any type of ion only moves in one direction in a stack, there is no ‘back’-diffusion. In this steady state reached after (in this case) 6 cm into the channel, ions moving as counterions from d- to the c-channels has become equal to the same ions moving as coions from c-channels to d-channels. Clearly, in this latter part of the cell we only transport current but do not further desalinate, i.e., we are wasting energy without any

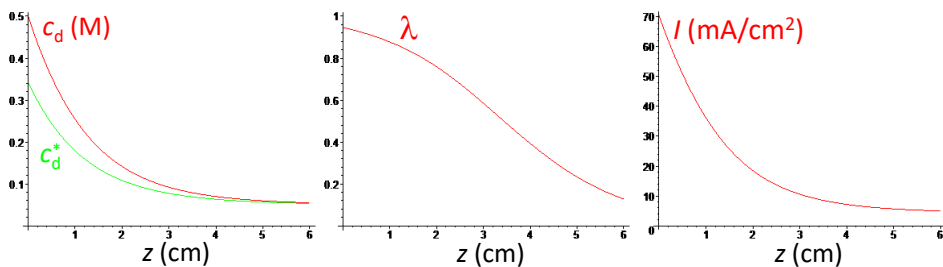


Fig. 12.4: Results of semi-analytical 1D transport model for co-current flow in electrodialysis, presented as function of distance z from inlet. (a). Average concentration in diluate channel, c_d , and channel/membrane salt concentration, c^* . Concentrations in concentrate channel are given by twice the inflow concentration minus the corresponding concentration in diluate channel. (b). Current efficiency, λ . (c). Current density, I (See main text for parameter settings).

advantage. The energy efficiency of this ED stack would improve if we make the cell shorter. We can also flow faster and desalinate more water in the same stack. These results clearly highlight that proper design of an ED cell pair (the key element of the ED stack) requires careful analysis.

12.4 2D model for an ED cell for non-unity current efficiency

The previous calculation made use of the surface renewal concept which used equations from earlier sections to obtain values for c^* and the voltage drop over each channel, $\Delta\phi_s$. This model was advantageous because we had a one-dimensional model that included most relevant elements. However, the derivation has an unphysical assumption which in the context of a 2D model leads to the poorly defined factor τ . If we want to include water flow through the membranes, then the equation for $J_{m,ions}$ can be corrected for this, as we will do below, but relations for c^* and $\Delta\phi_{s, sr, d}$, such as now Eqs. (12.20) and (12.33), no longer follow from Eq. (12.1). If we nevertheless apply these equations, the model becomes less accurate.

These objections can be resolved in a model that in many regards is more simple, and has one parameter less as well. Namely, we can construct a model based on the general ion balance, Eq. (12.2), discretize this equation in x -direction, and solve the set of equations using a numerical method called the ‘method of lines’. For the voltage drops over the

channels we use Eq. (12.14) which we solve numerically by the trapezoidal rule. Results of this full 2D approach are presented in Fig. 12.5, for the same parameters (not requiring a value for τ). Fig. 12.5 shows that we obtain quite similar results. In the new ‘methods of lines’-model the surface concentration starts at the inlet concentration, and in general is a bit closer to the average concentration than in the prior ‘surface renewal’ model. The initial current density is lower in the new model, but the two lines quickly converge. Thus, the full ‘method of lines’-model has one parameter less, does not include the somewhat unphysical factor τ , and in general is more transparent. This 2D calculation based on the method-of-lines is therefore preferred. We also need this more accurate modelling framework to be able to go to mixtures with three or more ions, with reactions between ions, etc.

Effect of membrane thickness on ED performance. An interesting calculation is to reduce the thickness of the membrane, thereby increasing the membrane transfer coefficient, k_m . The reduction of membrane thickness sounds like that is always a good idea, less resistance etc., but for thinner membranes current efficiency λ drops more rapidly, and there is much less desalination in the diluate channel. For the calculation in Fig. 12.5 desalination, defined as $(c_{d,in} - c_{d,out}) / c_{in}$, is almost 90% but when we reduce membrane thickness by a factor 100, desalination is less than 20%. At the same time current density remains at a high value along the entire channel, beyond 80 mA/cm², much higher than in Fig. 12.5. Thus, as also argued in the previous box, below a certain thickness, reducing the thickness of membranes will deteriorate operation of current-driven membrane processes.

One important feature stands out in the calculations just made, reported in Figs. 12.4 and 12.5, namely that salt concentration at the channel/membrane interface is not very much different from the average value. This suggests that a calculation neglecting these gradients in x -direction altogether would not be off by too much.^{xiii}

If we neglect concentration gradients in x -direction, the numerical model is much simplified. Including water flow across the membrane can now be done without too much difficulty. To do this, we must implement Eqs. (7.71), and (8.7). To calculate the hydrostatic pressure difference across (the inner coordinates of) the membrane, we follow the approach explained in Ch. 11 that the hydrostatic pressure change across a solution/membrane interface equals the osmotic pressure increase at that same interface. We neglect axial pressure

^{xiii}This is a result for a symmetric salt solution with only two ions. However, for three or more ions, with different mobilities and valencies, a detailed description of concentration profiles across the channel is of key importance to predict differences in transport rates, as we describe in §12.5.

gradients through the two channels, thus set the hydrostatic pressures there equal to one another, unvarying with z -coordinate.

How does transmembrane water flow influence the transport of ions and charge? In the general NP-equation we can also have a convection term, $K_{f,i}v_w c_i$. We can subtract anion flux from cation flux to arrive at an expression for J_{ch} just as Eq. (12.25), now with an additional term $-K_{f,i}v_w X$ (if $K_{f,i}$ the same for both ions). Similarly, for the expression for total ions flux through the membrane, given by Eq. (12.27), we add a term $K_{f,i}v_w \langle c_{T,m} \rangle$. We supplement this calculation with two overall balances. Because of the changing flow rates in the two channels, we have $\Phi_{v,d} + \Phi_{v,c} = 2\Phi_{v,in}$, and $c_d \Phi_{v,d} + c_c \Phi_{v,c} = 2c_{in} \Phi_{v,in}$ (assuming that the channels had the same inlet concentration and inlet flow rate).

With $k_{F-m} = 1 \cdot 10^{-8} \text{ m}^4/\text{mol/s}$ (this is an inverse water-membrane friction), and other parameters the same as in Fig. 12.5 (for both channels, $c_{in} = 0.5 \text{ M}$, inlet flow velocity through channel $v_{z,in} = 1 \text{ mm/s}$) we obtain the results reported in Fig. 12.6. We observe very intriguing predictions such as that the concentration in the diluate channel now drops more rapidly to zero (which is good), while the concentration in the concentrate channel, c_c , increases, but not in a mirror-like fashion compared to the drop in c_d . The water velocity across the membrane, v_w , starts high before dropping off to a low, but not negligible, value. This ongoing water leakage to the c-channel is why c_c decreases again after a few cm into the channel, while the water flow in the diluate channel goes down, which reduces water recovery. An optimal point to stop this process would be after 2 cm when a very much desalinated diluate stream is obtained. Thus now we reach a much lower salt concentration in the diluate channel, and we also reach it sooner, than without water flow. This is indeed the –counterintuitive– advantage of transmembrane water flow. However, this positive effect goes at the cost of a reduction in water recovery. As analyzed in Tedesco *et al.* (2017), if the aim is a water recovery of 50%, and to that end we must flow more water into the diluate channel (because part is lost by flow through the membrane), and if we then adjust the cell pair voltage to obtain a certain required desalination (a certain value of $c_{d,out} - c_{d,in}$), then the total energy cost (current times voltage) is higher for a system with water leakage than without. Thus, when we have water leakage through the membrane, the advantage of the resulting low diluate concentration as depicted in Fig. 12.6, is somewhat deceptive if taken as evidence of better performance, because the water recovery also drops steeply.

Finally, we briefly mention the possibility to consider not just co-current or counter-current operation of ED, which can both be described using the above 1D and 2D models. But with the modelling framework discussed in this chapter, we can also resolve the cross-current geometry that is generally used in a practical ED unit. Indeed, in many layouts of an ED cell a cross-current flow geometry is used, where the flow in the c-channels, when projected

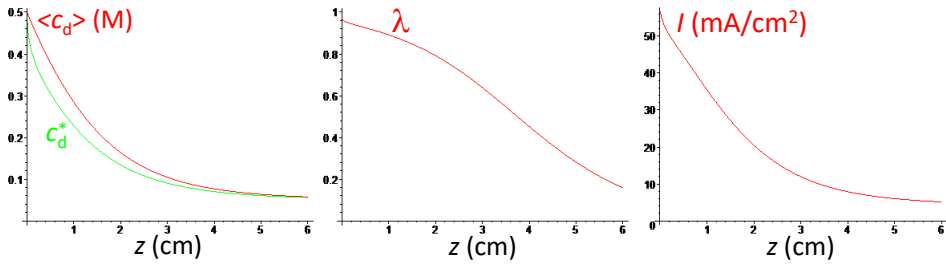


Fig. 12.5: Results of 2D transport model for co-current flow in electrodialysis, presented as function of position in the cell, z , based on discretization of Eq. (12.2) in x -direction and solution in z -direction by the method of lines (transmembrane water velocity $v_w = 0$). (a). Average concentration in diluate channel, $\langle c_d \rangle$, and channel/membrane salt concentration, c_d^* . Concentrations in concentrate channel are twice the inflow concentration minus the corresponding concentration in diluate channel. (b). Current efficiency, λ . (c). Current density, I (See main text for parameter settings).

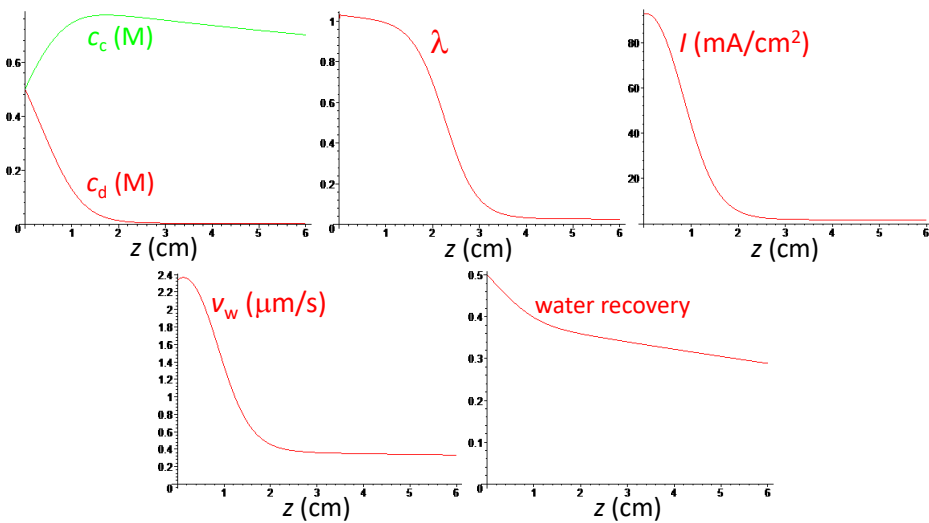


Fig. 12.6: Results of 1D transport model for co-current flow in electrodialysis including transmembrane water flow. (a). Concentrations in diluate and concentrate channels. (b). Current efficiency, λ . (c). Current density, I . (d). Transmembrane water velocity, v_w . (e). Water recovery (See main text for parameter settings).

onto the flow in the d-channels, is roughly at a ‘90 degree angle’. To solve this geometry we can set up a (quasi-)3D model, where, if flow in one channel is ‘north to south’, in the other channel it is ‘left to right’. To describe this practical module, we can set up an $N \times N$ grid of positions (nodes) and at each of these nodes (which describe a position in the d-channel, the aligned position in the c-channel, and the membranes in between) we solve the equations related to any of the approaches outlined in the present and the previous sections, with or without including transmembrane water flow, with or without concentration gradients in the x -direction (Biesheuvel *et al.*, *J. Membrane Sci.* **647** 120221, 2022).

12.5 Selectivity in electrodialysis with a three-ion mixture

In all previous sections we discussed ED for a perfectly ideal 1:1 salt. In practice, however, water that is treated is a multi-ionic solution, where the ions have different valencies and diffusion coefficients (in solution, and in the membrane). Ions also have different partition coefficients (at the solution/membrane interface), and they may react with one another and react with membrane groups (absorb in the membrane). All of these aspects require more advanced modelling than discussed until now. As one example, we describe in this section theory for ion transport in front of and inside an ED membrane for a salt mixture. We will discuss the case of two different cations, and one anion, all monovalent, with the only difference between the two cations that one has a twice higher mobility in solution and in the membrane than the other (the anion has the same mobility as the slow cation). We describe a single cation-exchange membrane ($X = -4$ M) with film layers on both sides. On both sides of the membrane is a bulk phase at fixed composition (25 mM of each cation). This simplified model illustrates several features of ED with an ionic mixture, and this model can always be extended to a calculation for a realistic ED cell.

Inside the membrane we use the NP-equation (without transmembrane water flow) with $\text{mrf} = 1/(K_{f,i}\varepsilon)$ set to $\text{mrf} = 50$ for each ion, see p. 166. For all ions we set the non-electrostatic partition coefficient to unity, i.e., $\Phi_i = 1$. All three ions participate in a local charge balance with a fixed membrane charge, X . Outside the membrane on both sides, we either use a standard film model of fixed thickness, see §7.1.1 (the DBL has then the same thickness as the membrane), or a DBL model with convective flow along the membrane, with fixed τ , described in §7.1.3. In the latter case we must then evaluate a modification of Eq. (7.11) because we also include electromigration as an extra contribution to transport, $z_i \partial / \partial x (c_i \partial \phi / \partial x)$.

These calculations show that the membrane hardly plays any role in determining the cation-cation selectivity, but only a difference in mobility in the solution phase matters. In the standard film model, irrespective of current, the selectivity S (ratio of fluxes of cations across the membrane) is the same as the ratio of mobility of the cations in solution, which in this case was a factor of two. The concentration profiles of both cations are the same, only their fluxes are a factor of two different. For the DBL model with convective flow we use a value of τ such that at an intermediate current the salt concentration on the upstream side of the membrane is the same as for the simple film layer model. Now, when we have a mobility ratio of 2, the ion profiles of the two cations become somewhat different, and selectivity is no longer $S=2$, but less, and somewhat dependent on current, from $S \sim 1.79$ at low current to $S \sim 1.72$ at high current. Thus, calculations indicate that for a typical ED membrane, the cation-cation selectivity depends on cation mobilities in solution, and on the chosen DBL model, but not on cation mobilities inside the membrane.

The above calculations were for the same bulk concentration on both sides of the membrane. A calculation with the standard DBL model where on the concentrate side concentration of the fast cation was increased 4 times, and of the slow cation 2 times (to 100 and 50 mM, resp.), resulted in the same outcome as before: mobilities in the membrane play no role, and fluxes solely depend on the ratio of mobilities in solution. However, the use of the improved DBL model with convective flow (fixed τ), has a significant effect. The selectivity at high current, which was $S \sim 1.72$, now drops to $S \sim 1.56$. Increasing the concentration of the fast cation again by 4 and of the slow cation again by 2 (to 400 and 100 mM, resp.), we now have selectivity going slightly up again, but coion leakage starts to play a more important role and the flux of both cations is now lower than for the '100/50' case.

In this last case, with concentrations on the concentrate side at 400 mM and 100 mM for the fast and slow cation resp., using the DBL model with convective flow, if we now reduce the current, selectivity now steadily drops to unity and below (the fast cation is even removed less than the slower cation) and at even lower currents we arrive at a situation that the fast cation is not removed any more, but moves in the reverse direction back to the diluate side, with the slow cation still moving in the right direction. Clearly we are not removing the fast ion preferentially any more when on the receiving side the concentration of the fast ion has increased to values much higher than of the slower ion. This calculation shows that a composition on the concentrate side of for instance 400 mM/100 mM of fast/slow cations, resp., cannot be maintained at arbitrary low currents; at least a moderate current is needed to keep these cations in the concentrate stream. But also then we have significant fluxes of the slow cation and of the anion, thereby lowering selectivity. For these conditions with different compositions of the two bulk phases on either side of the membrane, concentration

profiles of ions across the membrane are more interesting than when the two bulk phases are the same (in that case for both cations concentration profiles are almost unvarying across the membrane with a maximum change of ~ 1 mM). In the new situation the concentrations of the cations change across the membrane by 100's of mM, with one going up, the other going down by these significant numbers. Also outside the membrane, concentration profiles can be very different between the two ions, for instance on the concentrate side an almost invariant concentration for the fast ion at high concentration (transported by migration), and the standard decaying profile (in direction away from membrane) for the slower cation.

Part IV

Electrode Processes

In Part I of this book we discussed the electrical double layer, mainly in the context of equilibrium studies, thus in the absence of reactions or ion transport. In Part II of this book, we developed various elements of transport theory in electrochemical systems. Now in Part III we can address electrode processes where transport and electrode reactions are combined with EDL effects.

An electrode is an EDL structure where a metallic (electron-conducting) phase is in contact with electrolyte, which can be liquid (solvent plus ions), solid (a solid salt like AgCl), or gaseous (a plasma). In an electrode, electronic charge from a conducting phase (like a metal) meets with ions and other molecules from the electrolyte (and possibly from other non-electrolyte phases). For Faradaic electrode processes, there is transfer of electronic or ionic charge *across the full EDL*, thus both reactants and products of the Faradaic process come from, and leave to, a bulk phase adjacent to (thus separate from) the electrode (the EDL).

Two types of processes can occur at an electrode, Faradaic and capacitive (non-Faradaic). In a Faradaic process there is transfer of ionic or electronic charge across the EDL, because a reacting ion or molecule arrives in the EDL from a bulk phase, picks up, or releases, electronic charge, and moves out of the electrode (EDL) again, back to the same bulk phase, or to another one.

This is easy to visualize for an ion from the bulk electrolyte phase being reduced or oxidized and moving back to the electrolyte phase. Also molecules such as H₂ can come from, or go to, a gas phase. Metal plating, where for instance a Cu²⁺ cation picks up electrons and plates out as solid metal, is likewise a Faradaic electrode process: the ion comes in from bulk electrolyte, picks up electrons and moves out of the EDL, in this case to the bulk metal phase. This metal phase is a bulk phase outside the electrode (the EDL). The EDL is only the very interfacial region between bulk metal and bulk electrolyte.

It is interesting to compare metal plating with other Faradaic processes. In most cases, it is electron(-ic) charge that crosses the EDL, such as in a fuel cell where H₂ molecules arrive from a bulk gas phase, react with electronic charge and move out as H⁺ ions into the electrolyte phase. This can be envisioned as the electronic charge transferring across the EDL. For metal plating, instead, it is now the ion that transfers across the EDL, because the electron came from the metallic structure, ‘waits for the ion to come in’ and after reacting with the ion to a metallic atom, they together become part of the metal bulk phase.

In both of these examples, the key point remains that ions and molecules as reactants in the Faradaic process come from a bulk phase outside the EDL, and end up in a bulk phase as

well (either the same bulk phase, or another one). Such a Faradaic process can run forever, without the electrode changing in composition, as long as external conditions, such as the supply of reactants, do not change.

Instead, in a capacitive, on non-Faradaic, process, ions or molecules move into the EDL structure (the electrode), perhaps associate or react with electronic charge, but the key point is, they stay there. There is not a product molecule that moves out of the EDL to a charge-neutral bulk phase. Thus there is storage of charge and ions. If current is continuously supplied, the composition of the electrode changes in time, and unless for a notable exception, the electrode potential changes as well.^{xiv} Interestingly, there is no accumulation of charge in an electrode. Instead, all sources of current into the electrode, add up to zero. For instance, an electronic current arriving from a metallic phase, leaves as ionic current. The current moves across the electrode unchanged in 'intensity' (in 'numerical value'). Nevertheless, its 'nature' did change, from electronic to ionic. So in some sense the current is unchanged while travelling across the electrode, it is the same current, in another sense it most definitely changed.

Both for Faradaic and capacitive electrode processes, the current that runs into an electrode influences the EDL structure, because it has an impact on the concentrations of ions and other molecules in the adjacent electrolyte phase. Nevertheless, with current flowing across an EDL, the EDL remains locally at chemical equilibrium, and thus the distribution of ions in the diffuse layer remains the same (i.e., described by the same EDL structure). This is because the ions distribute across the diffuse layer much faster than the rate of changes in the overall process outside the EDL. So, the EDL is modified (indirectly, via outside concentrations) by bulk transport processes, but the EDL can be described as if there is no transport (quasi-equilibrium), and thus typically the Boltzmann equation (and modifications thereof) can be used to describe the diffuse layer. Inside the EDL there are often (heterogeneous) chemical reactions, and other surface ad-/desorption steps, or (acid-base) reactions between ions inside the EDL, and these steps can be slow, and thus ion concentrations inside the EDL that relate to these reactions depend on current. But despite the involvement of these (possibly slow) heterogeneous or acid-base reactions, solutes and ions remain at equilibrium with an outside bulk and thus the EDL is at equilibrium, because changes around the electrode in the adjacent bulk phases have a slow rate, to which the EDL can quickly adjust to retain an equilibrium structure.

As discussed in in the preamble to Part I, on p. 15, this is different for flow across a nanoporous medium, such as an ion-exchange membrane. With global equilibrium, no flows

^{xiv}The notable exception is an electrode with local phase separation inside the EDL, and for low enough currents.

Then the potential can be more or less stable for a limited period of time.

at all, then the entire material is (described by) an EDL. However, when there is a current, this entire layer goes out of 'global' equilibrium, i.e., its structure is no longer at chemical equilibrium with one of the external bulk phases, but instead there are transport processes, from one side of the porous structure to the other. Then this layer is no longer (described as) an EDL. Exceptions are the 'Donnan layers' at the two edges (outside surfaces) of such a layer, and they are in equilibrium with the outside electrolyte (i.e., in equilibrium with the ion concentrations in the electrolyte phase just outside the EDL).

—

When ions inside the EDL have interactions with the metal surface, there is often a chain of reaction and transport steps. This sequence includes ion transport to the surface, ion adsorption and surface reactions, and ultimately one of the reactions at the electrode surface is the electrode reaction where atoms react with electronic charge. The rate and direction of this electrode reaction depend not only on ion concentrations near the reaction site, but also on the charge density of the metal phase. When this reaction step is very fast, it can be described by the Nernst equation. If this is the case, the rate of the overall process can still be limited by the rate of adsorption to the surface of reactants, or association and dissociation reactions on the surface, or surface diffusion. But because the electrode reaction is very fast we can simply use the Nernst equation for the electrode reaction. Note that all of this does not relate to the electrode process being Faradaic or capacitive. In both cases there can be an electrode reaction. To distinguish these two types of processes, the key point remains that in a capacitive process this sequence of reaction and transport steps is truncated somewhere and the product ion or molecule cannot leave the EDL, i.e., the chain of reaction and transport steps has an 'end-point' with one of the product species locked inside the EDL.^{xv}

—

Interestingly, in all of these processes, steady state or dynamic, capacitive or Faradaic, the electronic current arriving in an electrode (the EDL structure at the interface of bulk metal and bulk electrolyte) is equal to the ionic current leaving the electrode (the EDL). This is the case because taken as a whole the EDL is charge-neutral, and remains so, and thus all currents entering and leaving the EDL (ionic and electronic) together must add up to zero, see Fig. 13.3 in Ch. 13. Thus there is continuity of electronic and ionic current across the electrode.

^{xv}Or of course the reverse situation, that previously stored ions are now coming out of the electrode.

At an electrode, or other charged interface, in contact with (solid) electrolyte, there is always an EDL being formed, i.e., charge separation between different regions in the EDL.^{xvi} Two main types of EDL structures can be identified, and below we sub-divide them into five types in total. The sequence here is based on ‘increasing degrees of freedom’ in how the EDL structure can change while remaining at equilibrium.

Type I EDLs are formed when there is contact of two electroneutral *bulk* phases that via an electrode reaction or ion exchange are in chemical equilibrium (for the electron or at least one of the ions). The bulk phases must in principle be able to keep a constant chemical potential for the species that are exchanged, for instance because the bulk phases are continuously refreshed. These EDLs can be called ‘reversible’ or ‘non-polarizable’. Instead, Type II EDLs relate to processes without such a transfer of an ion or electron across the EDL, between different bulk phases. These processes can be called ‘(ideally) polarizable.’ For Type II EDLs there can be two bulk phases but there is no transfer of ions or electrons between them. The other option is that there is one bulk phase, in most cases a liquid electrolyte, and in addition there is a charged material that is entirely part of the EDL.

We next provide a sub-division of types of EDLs into five categories, where Type I relates to processes with chemical equilibrium of ions or electrons between two bulk phases. When the interface is an electrode, i.e., the interface between metal and electrolyte, and we have a Type I EDL, then a Faradaic electrode process can take place. Instead, an electrode of Type II is a capacitive electrode.

- **Type Ia EDL.** For certain interfaces, there is not much we can ‘change’ about the EDL structure. This is for instance the case for the metal-metal interface (the metal-metal ‘junction’), and for the interface between a metal and a solid salt (e.g., the interface between an Ag metallic wire, and the AgCl salt layer that covers it). At such an interface, an EDL forms, with regions of positive and negative charge within the EDL, and a resulting voltage difference across the EDL, but there is not much we can change about this equilibrium EDL structure. There is just ‘one single operational point’ of EDL charge^{xvii} and voltage. For the example of Ag metal covered with AgCl, we can try to push in some extra charge in the metal (by applying a certain current for a certain duration), but after that period, the EDL returns to the structure it had before the current injection. It does not ‘remember’ this flow of charge.

^{xvi}Of course along the ‘line’ from very negative to very positive charge in these regions, there are obviously situations with exactly zero charge separation, thus a zero EDL voltage.

^{xvii}‘EDL charge’ refers colloquially to the charge of one of the regions in an EDL, see p. 495, and see Fig. 13.3 in Ch. 13.

- **Type Ib EDL.** For this type of EDL, we have one extra degree of freedom compared to Type Ia because the EDL/interface is in contact with electrolyte of which the ion concentrations can be changed. This is for instance the case for the outside of an AgCl layer (which covers an Ag-metal wire), where the AgCl-layer is in contact with electrolyte. In colloid science AgI particles dispersed in water are a well known system. Also the interface between a Cu^{2+} -solution and a metal falls in this group, where the Cu^{2+} ion can transfer from solution to a bulk metal phase. For such interfaces, the EDL voltage follows the Nernst equation, and the EDL voltage has a logarithmic dependency on the electrolyte concentration of the ion (Cl^- , I^- , Cu^{2+}) that exchange between the two phases (irrespective of how other ions can modify the diffuse layer structure).

Similarly, for a Faradaic electrode process with either the reactant or product (or both) coming from, or going to, an electrolyte phase, the Nernst equation describes the dependence of EDL voltage on the concentrations of the ions *that participate in the overall electrode reaction* (concentrations taken at a location near the interface, just outside the EDL). Though an EDL forms, we cannot speak of charge storage (or storage of ions) at the interface. By this we mean, if we charge an electrode for some time, then after we cease current supply, charge will leak away again, and the electrode returns to the prior state. Thus, unless we change ion concentrations in the electrolyte phase near the surface, the EDL voltage cannot be changed.^{xviii}

- **Type IIa EDL.** Type IIa EDLs are formed at the interface of electrolyte and a charged material, not a metal; so it is not an electrode. Of the charged material we cannot change the surface charge density by external means, and in this respect it is like a Type Ib EDL in that there is only one equilibrium EDL structure based on the external composition of the solution just outside the EDL. However, except for that similarity, everything else is different. To describe the EDL structure, the ions that we need to consider are ALL ions. All of them participate in formation of the EDL, i.e., all of them influence the EDL voltage. The EDL depends on the concentration of charged groups of the material. Examples are the EDL theories discussed in Ch. 2 for the Donnan structure inside ion-exchange membranes, and Ch. 3 where we discuss the GCS theory.^{xix}

^{xviii}Or we can change EDL voltages if one of the reactants comes from a gas phase, or goes to a gas phase, and we change the gas phase pressure.

^{xix}Also the case of an ionizable surface falls in this group, where there is a surface with chemical charge that can change as function of pH and other concentrations, i.e., the surface is ionizable. So also here an ion such as a proton is at equilibrium between electrolyte and this charged region. However, it is an equilibrium of an ion between one bulk phase and the EDL, and not an equilibrium (of a proton) between two bulk phases, as is the case for instance for the I^- -ions in an AgI particle.

- **Type IIb EDL.** This is an EDL structure such as type IIa, again not an electrode, but now we can change the density of 'fixed groups' (for instance the adsorbed charged molecules in an interface, or the charged polymer of a polymer gel), and thus a capacitance can be defined as the change of a concentration with pressure. The EDL model not only relates ion adsorption to the charge of the fixed groups, but also includes a relation between external pressure and the density of these fixed groups. There being a capacitance implies that we can change the charge and ion concentration in the EDL by external means, a pressure in this case, and thus can 'store' charge and ions, to release them again at another pressure.
- **Type IIc EDL.** This EDL structure is the electrode where, like type IIb, capacitance plays a role, and we can store and release salt and charge by changing an external force. In this case capacitance relates to the result of a change in voltage applied to the electrode, the result being a change in charge or a change in ion adsorption. These are capacitive electrodes. The EDL model describes the relationship between charge, ion adsorption, and EDL voltage. The EDL voltage can be changed externally, leading to a different charge (and ion adsorption). Or for instance at a fixed charge, when the external salt concentration changes, the EDL voltage changes. These ways to modify the EDL structure are not possible in any of the other types of EDLs. The related EDL theory can be extended to describe the pressure that such an electrode exerts on its surroundings, for instance a volumetric expansive force exerted by a carbon electrode on the porous structure, or the surface pressure exerted on the L/G interface in electrowetting.

It is possible to have a combined capacitive-Faradaic electrode process as we will discuss in Ch. 14, i.e., Type Ib and IIc combined, and then the Faradaic process will 'depolarize' the electrode and if that goes on for long we end up in the Type Ib case. In an electrochemical cell with two or more electrodes we can have some electrodes being capacitive, and some electrodes are Faradaic.

—

As discussed earlier on, we define the EDL as the complete zone between two charge-neutral bulk phases, or between one such phase and one charged material that is completely inside the EDL. Thus a porous ion-exchange membrane, or a porous electrode (which is a porous structure of 100s of μm 's thickness with relatively large transport channels lined with particles that themselves are nanoporous), as a whole is an EDL when not externally perturbed much by flow across it. However, generally it will be perturbed a lot and then for nanoporous materials (ion-exchange membranes), the interior of the membrane is no longer

an EDL, though for a porous electrode, the individual particles that form the electrode can still be (described as) an EDL if inside them there are no strong transport limitations.

The difference between Faradaic and non-Faradaic electrode processes

Both Faradaic and non-Faradaic processes can take place at an electrode. In a Faradaic process both reactant and product species transfer between bulk phases outside the electrode. In a Faradaic process, after applying a constant current, the electrode charge, voltage and composition will go to constant values. Thus, a current-voltage curve, or polarization curve, can be constructed based on data from steady-state experiments. For a non-Faradaic process, however, one cannot obtain a polarization curve, because upon applying an external current, electronic charge is progressively stored. Instead, to characterize a non-Faradaic process, one can inject a discrete amount of electronic charge into the electrode, after which the voltage makes a change to a new value. By repeating this procedure a charge-voltage curve can be constructed based on equilibrium data.

“How is one to differentiate between a faradaic and a nonfaradaic current? The answer is that any process which allows a continuous current to flow will be regarded as faradaic, whereas one which does not will be regarded as nonfaradaic. [...] The question of whether or not a continuous current flows hinges upon the question of whether or not the [reaction] products [...] can build up in concentration (or more strictly in chemical potential) [in the electrode] in such a manner as to stop the flow of current. If one or more of the products [...] can diffuse away, this will never happen, since more current will be needed to replace the substance which has diffused away.”ⁱ – David C. Grahame (1952) –

ⁱD.C. Grahame, J. Electrochem. Soc. **52**, 370C–385C (1952).

In electrochemistry and electrochemical engineering, there is a neat distinction between two types of processes that can take place at an electrode. These are called Faradaic and non-Faradaic (capacitive) processes. This difference is important because the two processes represent two fundamentally different modes of how an electrode behaves and how to characterize the electrode (process). Experimentally, for a Faradaic process we can construct a steady state current-voltage (i - V) curve, or polarization curve, and this makes it categorically different from a non-Faradaic process, which can be described by an (equilibrium) charge-voltage (σ - V) curve. Thus, the proper class of an electrode process can (with some restrictions) be established on the basis of experiments using an electrometer without knowledge of microscopic details of the electrode process. Let us explain the two types of electrode processes in more detail below.

To have a Faradaic process, there must be an electrode reaction where an ion or atom is reduced or oxidized to another species, and in addition the reactant must come from a bulk phase, and the product of the reaction must leave the EDL and go to a bulk phase, see Figure 13.1. This can be the same bulk phase (where the reactant came from) or another one. Bulk phases are the phases outside the metal/electrolyte interface, i.e., outside the EDL, outside the electrode. Thus, in a Faradaic process, reactants and products of the electrode reaction enter and leave the electrode (i.e., enter and leave the interface, the EDL).

In Faradaic processes, in most cases there is the transfer of electrons across the EDL, from a conductor (metallic) bulk phase, to the ionic bulk phase (or vice-versa). If electrons move to the ionic phase, the ions (or other molecules) that enter the EDL in oxidized form leave as reduced species and go back to an electrolyte phase (or alternatively to another phase, such as a gas phase). In the other case of Faradaic processes, it is the ion that crosses the EDL, coming from a bulk solution and ending up in a bulk metal phase (or vice-versa). This is what happens in metal plating.

In both these types of Faradaic processes, electrons or ions transfer across the EDL. In neither case is charge progressively stored in the EDL.ⁱⁱ The bulk phases serve as a reservoir for reactants and products that are involved in the electrode reaction. These are reservoirs where we can in principle establish a constant chemical potential (activity, concentration) of the relevant molecules, for instance by constantly refreshing the reservoir, or by making it large.

ⁱⁱSee p. 495 for a discussion of how the EDL is always charge neutral overall, but there are multiple regions of charge, σ_i , that together are charge-neutral. In case there are only two such regions, then $\sigma_1 + \sigma_2 = 0$, i.e., the two charges are the same in magnitude but opposite in sign. The charge in one arbitrary region is colloquially referred to as the EDL charge, and typically this region is the metallic phase if there is one, or else it is the more 'solid' phase.

For at least one component this bulk phase will be an electrolyte phase (either liquid or solid), in which ions or uncharged molecules are dissolved (or are a constituent of the solvent), but the other reservoir can also be something else, such as a bulk metal phase, as is the case for a plating reaction. Alternatively, an oxidic layer formed on a metal can serve as reservoir, or a solid salt, as is the case for a corrosion process, for the lead acid battery, or for the Ag/AgCl electrode. Finally, one of the bulk phases can also be a gas phase, as for hydrogen fuel cells.

With ionic (atomic, molecular) reactants coming from such a bulk phase, and products eventually going there, we have a Faradaic process. In that case we can characterize the electrode process by construction of a polarization curve (i - V curve). This is the same when the electrode reaction is part of a chain of reaction steps where prior to and after the electrode reaction the ions (atoms, molecules, adsorbed species) are involved in transport and reaction steps without an electron (not an electrode reaction), such as adsorption/desorption to/from the surface and association/dissociation reactions on the metal surface. Also in this more complex reaction scheme, the key requirement for a process to be Faradaic or not is still whether or not the electrons and ions that enter the EDL and participate in an electrode reaction, also leave the EDL again in the form of a different molecule, and go to an external bulk phase. For such a Faradaic process, as long as the external bulk phases do not change their composition (and do not disappear altogether), steady-state operation is possible, where each value of current corresponds to one value of electrode potential and vice-versa. So these are Faradaic processes.

—

In contrast, in a capacitive electrode process, i.e., a non-Faradaic electrode process, with current flowing across the electrode, charge is progressively stored. But what does charge storage mean, because isn't the EDL always charge neutral overall? The answer is that in an EDL there are regions of positive and negative charge. And indeed, the charges in all these regions together always add up to zero. But in a capacitive process, with current flowing, the charge in each of these regions continuously changes, and in one region the charge will go up, in the other go down.ⁱⁱⁱ

Interestingly, in a capacitive process there can also be an electrode reaction involving electrons and ions (atoms, groups, etc). But the ions (atoms, etc) that enter the EDL are not

ⁱⁱⁱColloquially this is expressed as that 'the EDL charge goes up/down.'

able to leave the EDL.^{iv} Examples of a capacitive process in which there are certain atoms located inside the EDL that undergo an electrode reaction, is the storage of charge (and ions) in intercalation materials such as Prussian Blue Analogues (PBA), which are materials of importance for capacitive deionization (CDI), see Ch. 1. During cation adsorption in the pores of these materials the Fe^{3+} lattice atoms (atoms which are part of the solid crystal structure of the PBA) are reduced when they take up an electron. Then, the PBA lattice (one region in the EDL) decreases in charge, while the pore solution (another region of the EDL) increases in charge. In these cases we have a non-Faradaic process, for which a σ - V curve can be constructed, and not an i - V curve. The σ - V curve of these electrode materials can be analyzed to derive values for capacity (a number typically with unit C/g) or capacitance (F/g), see p. 495.

The distinction between Faradaic and non-Faradaic electrode processes has in literature sometimes led to some confusion. In some cases a Faradaic process was associated with transfer of an ion or electron across some *surface* inside the EDL structure, where surface then is a dividing plane theoretically presumed to exist in the EDL.^{vi} The notion of a such a theoretical surface, however, is problematic because many surfaces can be defined in a microscopic model of an EDL.

Other literature sources assume that the simply presumption of there being an electrode reaction is sufficient to qualify the process as Faradaic. However, these two criteria depend strongly on a microscopic perspective of the EDL, i.e., on the theoretical picture proposed of the atomistic details of what occurs in the electrode (see p. 15). But this picture may be up for discussion. And this perspective neglects the experimental side of the EDL concept, which relates to (the identification of relevant) metrics and characterization methods. This strong focus on the microscopic perspective may have been why these two criteria led to a blurring of the clear distinction between these two basic types of electrode processes, and why as a consequence much additional vocabulary was generated over the past decades to describe purported intermediate cases.

The confusion is absent when the definition of a Faradaic electrode process includes the specification that both reactants and products move in and out of the interface (the EDL, the electrode), to and from adjacent bulk phases, and neither of them accumulates in the EDL,

^{iv}When such a capacitive process is run in reverse, the ions do leave the electrode, but they came at that moment from the EDL, where they had been stored for a (potentially long) time; i.e., they didn't come in from a bulk phase 'a second ago'. Also in this case the charge and ionic composition of the EDL changes in time, which shows this is a capacitive process.

^vIn contrast to this notion, we argue that a Faradaic process requires the transfer of an electron or ion across the complete *interface*, i.e., across the EDL, or electrode.

^{vi}See p. 495 for a further definition of interface vs. surface.

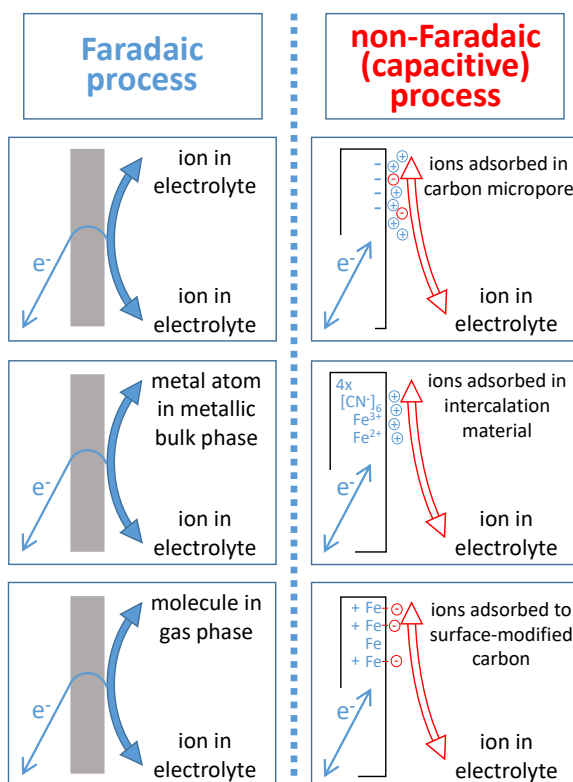


Fig. 13.1: The storage of ions and charge as the key difference between Faradaic and non-Faradaic (capacitive) electrode processes, using six examples.

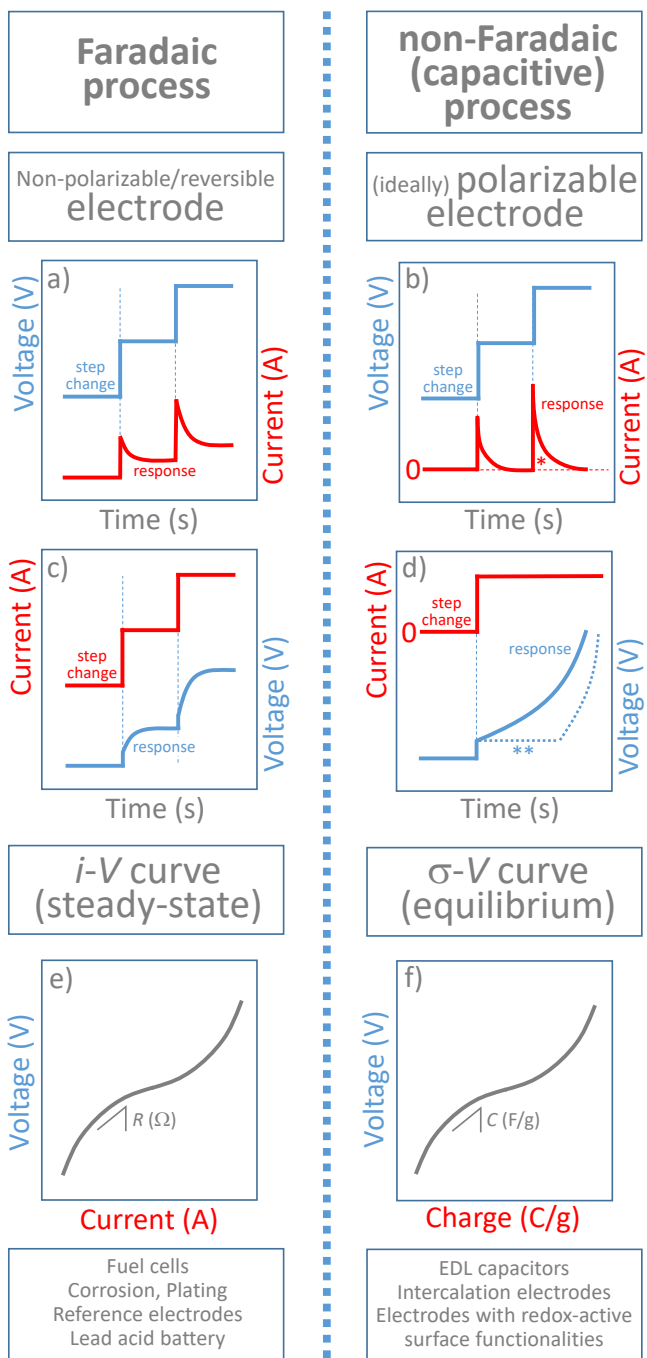


Fig. 13.2: Operational differences between Faradaic and non-Faradaic (capacitive) electrode processes.

as already explained by Grahame in 1952, see p. 357. In this case a steady state process is possible for a Faradaic process, with a constant current and an ongoing electrode reaction, while the charge in the various regions in the interface stays the same. This does not happen in a capacitive process.

Thus, the distinction between capacitive and Faradaic electrode processes depends on whether during current flow there is accumulation of some species (and thus charge) in the interface between a metal and electrolyte bulk phase (this interface is the electrode, the EDL).^{vii} There is no need to search for or define a mathematical dividing plane (*surface*) inside a microscopic (theoretical) EDL model, and there is no need to decide whether inside the EDL electrons or ions hop across this surface. Instead, one can focus on finding (by experiment) an answer to the question whether the electrode changes its composition over time upon ongoing current supply. If there are no changes, the electrode process is Faradaic but if the question is answered in the affirmative, we have a capacitive (i.e., non-Faradaic) process.

Faradaic and non-Faradaic processes are easily distinguished, but two additional remarks are relevant. First, in an electrode both processes can occur at the same time. Thus there can be a capacitive process going on with increasing storage of charge and ions, while at the same a Faradaic current leads to charge leaking away. The opposite situation is when in a perfect Faradaic process, we change one of the external conditions, such as current, voltage, or electrolyte composition. Then for a (very brief) period some capacitive (non-Faradaic) current will flow to adjust the EDL interfacial structure to the new situation. But after that brief period of time, this extra current ceases and the electrode process continues in a steady-state Faradaic manner.

Faradaic and non-Faradaic processes can be distinguished on the basis of how they respond to a step change in voltage (see Fig. 13.2, panel a and b) or current (panel c and d). Upon a step change in electrode potential (panel a and b), the Faradaic process quickly levels out to a new value of the current (different from before). Instead, in the non-Faradaic process, after a voltage step change, after some time the current will return to zero, and it will do so after each step in voltage. The integral of current with time (denoted by * in panel b), is the additionally stored charge (see panel f). When instead of stepping up the voltage, we step up the current (panel c and d), the Faradaic process responds by going to a new electrode potential, while in the non-Faradaic process, any ongoing nonzero current will either result in the voltage increasing without limit, or the voltage is constant for a limited period of time before it also starts to increase. This second scenario is possible when there is internal phase separation in the electrode, related to strong interactions between ions in the EDL, see Chs. 1

^{vii} Accumulation refers to the change in time of a concentration or amount.

and 15.

Based on data from such experiments, we can construct two types of defining characteristic curves. For the Faradaic process, we can construct a current-voltage curve based on steady-state data, the i - V curve, or polarization curve, see Figure 13.1e. For the non-Faradaic, capacitive, process, the defining curve is very different, and it is a curve of charge, often defined per amount of electrode material, as function of electrode potential. The slope of the curve is the capacitance (also called differential capacity), an electrode property with dimension F/g, and a function of where we are on the curve, i.e., a function of EDL charge.

Let us analyze what happens when the current approaches zero and the system goes to equilibrium. For the Faradaic process the electrode potential goes to a value given by the Nernst equation, see Ch. 14. What does the Nernst potential depend on? It does not depend on all ions in the electrolyte. Instead, it only depends on the activity of those ions in the bulk phases that are reactive in the electrode, i.e., the activities of the reactant and product species involved in the electrode reaction. With the activities (chemical potentials) of these species fixed (in their bulk phases), there is no way to modify the EDL structure and the equilibrium Nernst potential, for instance by pushing in charge.^{viii} After pushing in charge for some time, and then turning off the current again, the charge just leaks away again because of the Faradaic process, and the system returns to the prior equilibrium EDL structure and the prior value of the Nernst potential. This is in stark contrast to what happens in a non-Faradaic, capacitive, process. Here, the equilibrium electrode potential and composition can be controlled by injecting extra charge, which does not leak away, but is stored. Examples of Faradaic and non-Faradaic electrode processes are discussed in Chs. 14 and 15.

—

Perhaps it was noticed that in the above discussion the term ‘charge transfer electrode’ was absent. This is a term often used to define a Faradaic process. The reason for its absence in this book is that all electrodes are charge-transfer electrodes, in the sense that in all electrodes there is continuity of electronic and ionic current, i.e., the electronic and ionic currents are the same ‘numerically’, though not in what are the charge-carrying entities. Thus, the EDL as a whole always remains charge neutral, see Fig. 13.3, so all electrode processes transfer charge across the electrode.

But it is possible to state whether in a certain Faradaic electrode process there is electron transfer or ion transfer across the interface, i.e., across the EDL, from one bulk phase to another. E.g., in case of ion transfer, a Cu^{2+} -ion transfers across the interface (the electrode) from the electrolyte bulk to the metal bulk. often it is an electron that transfers from the

^{viii}This is *at* equilibrium. When we are off-equilibrium, the EDL structure changes.

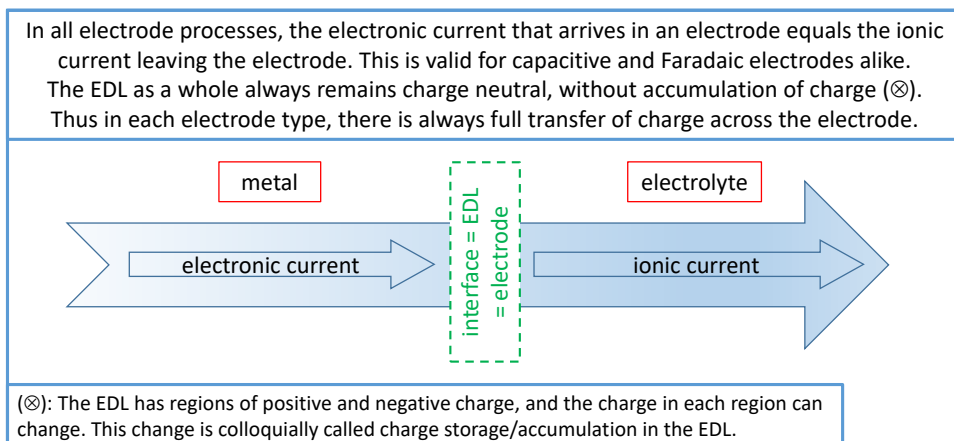


Fig. 13.3: In any electrode process there is complete transfer of charge across the interface, because the interface, the EDL, as a whole does not store charge. This is the case for capacitive (non-Faradaic) and Faradaic electrode processes alike.

metal phase to the electrolyte, recombining with an incoming ion and leaving as another ion. Thus we can use the term ‘charge transfer electrode’ to define a Faradaic process, if we realize it must mean the transfer of an ion or electron completely across the electrode, from one bulk phase to another. So the term ‘charged *species* transfer electrode’ would be more correct.

Electrode Kinetics

Ions and other species can adsorb at an electrode, diffuse over the surface, react with other species, and when the conditions are right, possibly combine with electronic charge to react to another species in an electrode reaction. This can happen both in capacitive and Faradaic processes.^a This electrode reaction—the reduction/oxidation reaction of an adsorbed (atomic, ionic) species with electronic charge—will often be fast relative to the other steps, which include: transport of ions from bulk electrolyte to the electrode, association/dissociation reactions at the electrode, and surface diffusion over the electrode. When the electrode reaction is fast, the Nernst equation can be used. In cases where the electrode reaction is (partially) rate-limiting, an expression where the rate depends on kinetic constants and the electronic and ionic charge must be used. In this case (where we have a limited rate of the electrode reaction) a detailed model of the EDL structure becomes important. This is also the case when there are multiple competing reactions on the same electrode.

^aIn a Faradaic process the reactants at the start of the entire sequence of adsorption and reaction come from an adjacent bulk phase, and the product of the reaction chain (after the electrode reaction) leave again to go to a bulk phase. This can be the same bulk phase as where the reactants came from, or it can be another bulk phase. In a capacitive process at some stage the reaction sequence is truncated and the intermediate species remains locked in the electrode.

14.1 Introduction

In 1965 it was Paul Delahay who wrote in his book ‘Double Layer and Electrode Kinetics’ that ‘mastery of electrode kinetics requires adequate understanding of double layer phenomena’, and we completely agree (of course). Thus, after many chapters in this book devoted to the EDL without considering electrode reactions, we can now take up the topic of electrode reaction kinetics and the influence of the EDL structure. We will consider Faradaic processes, thus after a step change in voltage or current, after some time a new steady state will be reached where an ion, metal atom, or gas molecule, is reacting away, and a product molecule formed, at a constant rate.

Electrode Kinetics, or *electrocatalysis*, is the scientific field in which the chemical steps occurring in an electrode are studied in detail.ⁱ These reaction and transport steps mainly occur inside the EDL, i.e., inside the electrode, which is the interface between a metal and an electrolyte phase. One of the reaction steps is an electrode reaction, which is the step where an atom or other adsorbed entity reacts with electronic charge. An electrode reaction can either be in the direction of oxidation, where an ion releases one or more electrons, and in the direction of reduction, where an ion picks up electrons, i.e., it is reduced. An example of reduction is when a cation picks up an electron and becomes a neutral atom.

Do we always have two (or more) electrode reactions? A very important question is, if we have a Faradaic reaction in one electrode, do we then also need to have a second Faradaic reaction in a second electrode?ⁱⁱ Such that the two Faradaic reactions together ensure that the electrons liberated in the anode, are taken up by the cathode. This is often implied in many texts, and for instance is the basic principle underlying the classroom exercise to combine two ‘half reactions’ into one full redox reaction. However, to have (at least) two electrodes, where in each a Faradaic reaction takes place, is only required for a steady-state process. But not in a dynamic process, which is a process where electrode properties are allowed to change in time. We will next discuss three situations where the requirement of two simultaneous Faradaic reactions is not met.

First, we can have an electrode reaction in a single electrode that is disconnected from any other electrode. When this electrode (one that allows an electrode reaction) is inserted in an electrolyte, or the conditions in the electrolyte are changed, then an

ⁱElectrode Kinetics is different from the field of Electrokinetics, which is the study of transport processes around, and in, charged materials and particles, often related to solving the Navier-Stokes equation including the electrostatic body force term, see Ch. 8.

electrode reaction will briefly take place. When on a piece of metal several half-reactions take place near each other (two Faradaic reactions), anodic and cathodic, even though this may be one and the same piece of metal, we nevertheless have different electrode structures, i.e., different *electrodes*, on its surface. These different electrodes form regions that may be very nearby one another, short-circuited through the metal, but different electrode reactions take place in the two regions. Such a two-electrode system on the same piece of metal, this can run for a very long time.

Second, in a cell with two electrodes, where one electrode is capacitive, and the other Faradaic, we can have electrode reactions in both (or only in the Faradaic electrode), but there is no equivalence between the rate of oxidation in the anode and the rate of reduction in the cathode.

Third, we can have two Faradaic electrodes, and even here the two Faradaic reactions do not always have to add up perfectly. Because after we change the cell voltage, or current, for a brief time the two electrode reactions in the two electrodes are not exactly equal, and the EDL structures (charge) in the two electrodes change. Only when steady-state is reached, do we end up in the situation that the two electrode reaction rates are the same again.

All of these situations are discussed in Ch. 16.

The electrode reaction will often be fast compared to all the other reactions and transport processes that occur in the electrode prior to, and after, the electrode reaction. By ‘prior’ and ‘after’, we refer to the sequence of reaction steps that takes a reactant from a bulk phase to a product in the same, or another, bulk phase. Then to describe the electrode reaction the Nernst equation can be used which assumes local chemical equilibrium between the species involved in the electrode reaction. The Nernst equation relates local concentrations of (adsorbed) species with a potential drop across an inner layer, a layer between the location of these species and a position in the metallic phase. In this way the chemical potential of the electron plays a role in the reaction rate. We can use the Stern layer concept from Chs. 2 and 3 and equate it with the inner layer across which the electron transfers. The EDL structure will now influence the electrode reaction equilibrium, because of the Stern layer potential and the ion concentrations inside the EDL. Also other non-reactive ions influence the EDL structure and in this way influence reaction rates and electrode selectivity.

Initial studies on the influence of the EDL on the electrode reaction (rate, direction) were by Frumkin (1933) who described how the rate of an electrode reaction depends on the Stern potential, and by Grahame (1952) who wrote how the rate of the electrode reaction is

a function of a local voltage drop across (part of) the EDL, and not dependent directly on the measured potential in the connecting wire relative to a reference electrode.

We will focus in this chapter of Faradaic processes, which are processes that can run in steady state (see p. 495) without the electrode structure changing. This implies there must be an electrode reaction taking place. There is an EDL formed, with a diffuse layer and other elements to the EDL structure, and the structure of the EDL strongly influences the current. For mixtures with various ions and other species, the EDL structure and the electrode potential not only influence the rate of conversion, but when there are multiple electrode reactions, these factors also influence the selectivity of the electrode process, i.e., they play a role in what are the main products of the electrode process.

We can study an electrode process by focusing on one electrode (which is then the 'working electrode' in a setup with also a counter electrode and a reference electrode), or we can study a full electrochemical cell with two electrodes, and run an entire electrochemical process. It is possible to place this primary electrochemical cell inside a larger, secondary, electrical circuit (which is then also an electrochemical cell as a whole) that pushes electronic charge into both electrodes of the primary cell, which influences rates and selectivities in the primary cell. This works best when the primary cell has very low electrode reaction rates. The best example of this method, of unfathomable importance to society, is the cathodic protection of steel and other metal structures. Metal must be protected from corrosion, which is the oxidation of metal atoms at the anode of the primary electrochemical cell. When the secondary cell pushes electrons into the primary cell, the electrode potentials in the primary cell go down, both in the anode and in the cathode, and thus the Nernst reaction in the anode is shifted away from oxidation, and pushed towards reduction, i.e., towards formation of the metal. At sufficiently low potentials, electrons and metal cations (in the oxidic corrosion products around the damaged metal piece) may even recombine to form metal again.

Even though two-electrode and multiple-electrode cells are of great interest, as indicated above, in the next sections we focus on the study of a single electrode. The theory of electrode kinetics in a single electrode is at the basis of the study of systems with multiple electrodes.

14.2 The Nernst equation, role of EDL structure, and surface transport

To explain how a model can be set up for transport of molecules to an electrode and subsequently an electrode reaction there, we make an example calculation for a very

important electrochemical reaction, namely the oxidation of CO on a platinum electrode to CO₂. The model we describe below illustrates the general structure of the theory and identifies the various factors that can influence the reaction rate. These can include transport of species towards and over the electrode surface, the structure of the EDL around the reaction site, and, via the Nernst equation, the electrode potential.ⁱⁱⁱ

The reaction of CO to CO₂ on a Pt-electrode in water follows an intricate set of reaction steps, and in the theory below we only include a limited number of these steps. The steps we include are as follows. First of all, we consider the diffusion of CO through the water to the platinum surface, and subsequently the diffusion of adsorbed CO over the electrode surface towards the reaction sites, which are terrace steps in the Pt-surface. At these locations, which can be envisioned as ‘lines’ running across the electrode surface, OH is adsorbed, the product of a reaction of water that releases an electron and a proton. When the diffusing CO_{ads} arrives, it reacts with OH_{ads} and CO₂ is formed, together with a proton and an electron. We assume that the reaction product, CO₂, immediately dissolves into the water, which has a constant CO₂ partial pressure. In the first calculation we neglect how this CO₂ can convert into bicarbonate ions. We also neglect how bicarbonate ions have a tendency to (re-)adsorb to the surface, slowing down electrode reactions.

Thus in this problem we envision lines criss-crossing the surface, with OH-species adsorbed at these lines (the terrace steps). The lines have all kinds of patterns, which we will not consider, but from optical images we can observe and measure the *line density* which is the length of line per unit electrode area, ℓ . The line density ℓ recalculates to an average distance between the reaction lines as $\delta = 1/\ell$. The CO dissolved in water at a certain bulk concentration first diffuses through the water to the surface, and adsorbs everywhere on the Pt. After being adsorbed, it diffuses over the surface to the reaction lines. We describe surface diffusion along a line described by a coordinate x that runs between two (assumed to be parallel) reaction lines. The CO_{ads} adsorbs anywhere between the reaction lines and then diffuses in this x -direction to the reaction lines.

The reactions at the OH-adsorption lines we consider later, but let us first describe the diffusion of CO through the water to the electrode surface and then across the surface. For the adsorbed CO-species, we can set up the mass balance on the electrode surface

$$\frac{\partial c_{\text{ads}}}{\partial t} = D_s \frac{\partial^2 c_{\text{ads}}}{\partial x^2} + J \quad (14.1)$$

where c_{ads} is the concentration of adsorbed CO and J is the x -dependent ‘incoming’ CO-flux (from solution). For this we can use any equation from Ch. 7, which all show that in

ⁱⁱⁱFor a more detailed model, see Koper *et al.*, 2002.

steady-state the flux towards a reactive interface is linearly dependent on the difference of bulk concentration, c_∞ , and surface concentration, c^* ,

$$J = k_L (c_\infty - c^*) \quad (14.2)$$

where the transfer coefficient k_L can have different dependencies on diffusion coefficients, stirring intensities, etc., dependent on the chosen dispersion model, see Section 7.1.

We assume that there is an instantaneous adsorption equilibrium $c_{\text{ads}} = K c^*$ at each position x . We will assume steady-state and thus set $\partial c_{\text{ads}}/\partial t$ to zero. Eq. (14.1) is then a second order ODE mathematically similar to Eq. (12.3) in Ch. 12. The solution is also given there as Eq. (12.4) and based on that result we can derive an expression for the flux along the surface of CO 'into the reaction lines' (from one side) J . Thus per unit electrode surface the CO conversion rate is $r_{\text{CO}} = 2 \ell J$, which is given by

$$r_{\text{CO}} = 2 \ell J = 2 \ell \sqrt{D_s k_L / K} \left(K c_\infty - c_{\text{ads}}^{\text{RL}} \right) \quad (14.3)$$

when the group $k_L/(\ell D_s K)$ is larger than around 10, which is the case when the reaction lines are sufficiently far apart (low ℓ). In Eq. (14.3) $c_{\text{ads}}^{\text{RL}}$ is the concentration of adsorbed CO at the reaction sites where CO will react with adsorbed hydroxyl ions.

Eq. (14.3) shows that transport limitations already are able to limit the rate of this process, whatever we do to enhance reaction kinetics, namely r_{CO} cannot be larger than the value given by Eq. (14.3) when we insert $c_{\text{ads}}^{\text{RL}} = 0$.

But let us continue for conditions that the supply of CO by transport is not rate limiting. Then we require further information on the rate of the electrode reaction.

Porous electrodes

Porous electrodes are important in electrochemical processes, for various purposes. They store energy in batteries, and they can be used for water desalination, as well as for enhanced Faradaic conversions. We present calculation results for these three examples based on porous electrode theory. This is a theory for transport, reactions and storage of ions and charge across a porous electrode, taking into account that a porous electrode is a multi-phase system with separate phases for ion transport, storage of ions and charge, and electron transport.

15.1 Introduction

Porous electrodes are encountered in many applications in electrochemical processes. An important application is water desalination by capacitive deionization, where ions are stored throughout the electrode in EDL structures formed in porous materials that can be electrified (electronically addressed, i.e., connected electronically to an external electric circuit). This porous material (often based on a finely dispersed powder that is compacted and solidified with a binder) is accessible for ions because of transport pathways that cross the full thickness of the electrode. In secondary batteries, such as Li-ion batteries, in the same way ions transport across the electrode and are stored in materials with a high capacitance. A notable difference is that the electrolyte salt concentration is many times larger than in water desalination, to avoid salt depletion and to minimize ionic resistances; also the solvent is generally not water. Hydrogen fuel cells also use a thin layer of porous electrode that is on top of a solid electrolyte phase and in contact with H₂-gas. In fuel cell electrodes catalytic nanoparticles are deposited on the porous electrodes to facilitate the conversion of H₂ to protons that go into the aqueous electrolyte phase and diffuse into the proton conducting membrane. In certain types of solid electrolyte fuel cell, instead of protons, O²⁻-ions travel across the membrane and on the other side react with H₂-gas to water. Porous electrodes can also be used in reactor systems to enable enhanced rates of electrode reactions because of the larger accessible area than for non-porous electrodes.

In all of these porous electrodes, not just contact with ions is important (and with gaseous fuels in fuel cells), but electronic charge must also be able to be transported throughout the electrode and reach the sites where electrode reactions take place and/or sites in the material where EDLs are formed. Thus not only the ionic conductivity inside the porous electrode is of importance, but the electronic conductivity as well.

The electronic conductivity is the key challenge when porous electrodes are applied as slurries or in fluidized beds. In such a system ionic contact is optimal, but electronic contact certainly problematic. Metallic mesh structures, thin channels, conductive additives, are all options that can be helpful and all are investigated to optimize these 'fluid electrode' systems. In this chapter, however, we focus on film electrodes, which are electrodes that are constructed as a permanent structure fixed in place.

A porous electrode consists of many phases. First of all there is a part that keeps the entire structure together, a 'glue', often a fibrous structure able to cast a web across all particles that binds all elements together. In a tight-packed and closed-off battery cell, this component might not be necessary but when there is a flow of water and/or gas through or along a porous electrode, a glue is necessary to keep the structure together.

Then we need a material that conducts electronic charge across the electrode with only a small loss of energy (low voltage drop). Thus we need a very conductive matrix, for instance made of graphite or carbon black or electron-conducting polymer. And then we need pathways for ion transport as well. These pores are often called ‘macropores’ as they are long (traverse the entire electrode) and relatively wide (order of a few microns). The electron-conducting phase and these macropores must form uninterrupted, i.e., continuous pathways. If there is a disconnect or bottleneck, transport beyond that point is hampered. What is required is a percolating network, both for electronic charge, and for ionic transport. In contrast, what does not need to be continuous are the locations where electronic charge and ionic charge ‘meet’ in EDL structures, either to be stored there (capacitive electrode) or to react to products that subsequently diffuse out of the electrode again (Faradaic electrode). These sites can be positioned to directly ‘line’ the macropores, which speeds up rates when the electrode is used for a Faradaic (conversion) reaction. Alternatively, when the aim is to store ions and charge in EDL structures, these EDLs are inside microporous materials, finely distributed across the electrode. These microporous materials can be porous ‘activated’ carbons, ‘intercalation host compounds’, or ‘insertion materials’, and the pores inside them simply called ‘micropores’. These EDL structures and reaction sites must be accessible both for ions (arriving from the macropores) and for electronic charge (from the conducting pathways). After constructing a porous electrode from various solid materials, the electrolyte-filled macropores are automatically formed as the remaining open phase in between these solid phases. that is

Of course any electrochemical cell has at least two electrodes, and this is also the case for porous electrodes. Nevertheless, on shorter time-scales, processes are possible in a single stand-alone electrode. A porous particle, disconnected from an electrical circuit, for a brief period can absorb some ions with a simultaneous electrode reaction that produces the electronic charge that is then charge-compensated by counterions in the EDL. But such a process ceases quickly, and to then make the process continue, the particle must be connected to an electrical circuit and thus to another electrode. This other electrode does not have to be another porous electrode. In fact, there are no fundamental restrictions on what the other electrode(s) should be. In this chapter we only discuss a single electrode.

We will discuss three relevant examples of porous electrodes in electrochemical processes, and in the context of each example illustrate the theory of porous electrode transport and storage.

15.2 Faradaic reactions in a porous electrode

To enhance the rate of electrode reactions, porous electrodes are useful because they provide more surface area. The carrier liquid then often flows through the electrode, through the (macro-)pores. These pores are the electrolyte-filled phase of a porous electrode. In direct contact with these pores is a fine dispersion of catalytic sites where we have the electrode reaction. The higher the number of these sites, the higher the electrocatalytic activity of the electrode.

A differential mass balance inside the porous electrode for a component i , which can either be a reactant or product of the reaction, isⁱ

$$p \frac{\partial c_i}{\partial t} = - \frac{\partial}{\partial x} J_i + R_i \quad (15.1)$$

where p is porosity, and concentrations c are defined per unit pore volume. The flux J_i is per geometrical ('total') cross-sectional area, and formation rates R_i are defined per total electrode volume.

For the molar flux J_i we can use the extended Nernst-Planck equation. Because the pores are generally relatively wide, we do not need to consider an ion-matrix friction, and like in prior chapters we can use

$$J_i = v_F c_i - \varepsilon D_{i,\infty} \left(\frac{\partial c_i}{\partial x} + z_i c_i \frac{\partial \phi}{\partial x} \right) \quad (15.2)$$

where the fluid flow rate v_F is per geometrical area. The factor $\varepsilon = p/\tau$ is included because porosity p is not 100% and because the pores are tortuous, i.e., longer than a straight pore. Often for porous structures, τ is related to p by the Bruggeman equation, $\tau = p^{-1/2}$. In these equations, concentrations and fluxes are in general time- and position-dependent. The electric potential here, ϕ , is that in the electrolyte-filled pores. Further on we also discuss the potential in the electron-conducting phase, ϕ_{ec} . At the edges of this electrode, this pore potential ϕ 'continues' into adjacent electrolyte phases without a potential jump, and the same for ion concentrations, c_i . So this is different from a charged membrane, where there is a Donnan layer at the membrane/solution edge that leads to a jump in potential and concentrations across this interface. Even though ϕ and c_i are continuous at these outer interfaces of the porous electrode, where they are in contact with solution/free electrolyte, the gradients $\partial c_i/\partial x$ and $\partial \phi/\partial x$ do make a jump because of the ε -factor (which is unity in

ⁱJust as in other chapters, we prefer here the use of the notation $\partial/\partial x$ to describe gradients. The extension to flow in many directions is unproblematic.

an open electrolyte phase, and less than unity in a porous electrode), because for each ion the fluxes are continuous across the interface, $J_{i,\text{just inside electrode}} = J_{i,\text{just outside electrode}}$.

If a reaction takes place on the catalytic sites that are dispersed throughout the porous electrode, then we can relate the surface concentration right next to these sites, $c_{s,i}$, to the average concentration in the pores, c_i , by a relation where $c_{s,i} - c_i$ is proportional to the reaction rate R_i . For a reactant, we will have $c_{s,i} < c_i$, and for a product of the electrode reaction it will be the other way around. For such correlations between a flux to the surface and this concentration difference, see Section 7.1. Thus within the electrode we can run into a ‘limiting current’ when the surface concentration of reactants hits zero. When this happens, locally the electrode potential will strongly increase, and the current that was flowing to this position will be redirected to other parts in the electrode.

In the transport pores there will be local electroneutrality based on the ions present in the pores. For instance, when we only have Na^+ and Cl^- as ions, then in the pores their concentrations are the same. This is because the charge in the EDLs is electroneutral by itself, decoupled from the pore charge balance, which is because the pores are generally quite wide (order of microns in the cross-section). This is very different from the electroneutrality condition in charged membranes for RO or ED, where pores are one or a few nm across and then the charge density of the membrane structure ‘on the surfaces of the pore’ interacts with the charge balance of ions inside the pores. So for the porous electrode, for all ions the mass balance, Eq. (15.1), is solved. For reactive ions, see Ch. 10, R_i also contains reactions between ions in solution, but these reactions are not considered in this chapter, and R_i only refers here to the electrode reactions throughout the porous electrode (taking place on electrocatalytic sites).

We inject per unit time a certain total current I_{tot} (in A) into a volume V of electrode, but this total current will not flow to all parts of the electrode in equal measure, i.e., more can go to one region and less to another. If the electrode reaction involves n electronic charges per atom converted, then a volume integration over the entire porous electrode leads to

$$I_{\text{tot}} = \pm n F \int_V R_i dV \quad (15.3)$$

where the reaction rate R_i can be position- and time-dependent.

The current I_{tot} is an electronic current arriving from the electronic circuit, and then distributing across the complete porous electrode, and is equal to the ionic current coming from the electrolyte phases around the electrode. More precisely, with these currents defined as positive when directed from outside into the porous electrode, then the summation over all these currents is zero. The porous electrode as a whole is always charge-neutral. This is not just the case in steady state, but also in a dynamic situation, when the electrode structure

changes. (As we see later, the same condition holds microscopically, at the scale of an EDL or catalytic site.) This ionic current typically enters the porous electrode on one side, namely where it is closest to the other electrode. At this interface we then have a certain ionic current density I_{ionic} . And on other sides of the electrode there is no ionic current going in or out, i.e., we have a zero-current condition, for instance where a dense layer serves as the current collector. Electronic current for instance enters the electrode at this current collector that was blocking for ionic current.

So how to describe the reaction rate R_i ? We already pointed out that the reaction rate increases with a higher density of reactive catalytic sites. Though of course when the catalytic reaction is fast enough, the mass transfer processes inside the electrode become rate-limiting, and more catalyst will not make the process faster.ⁱⁱ It also depends on the surface concentrations $c_{s,i}$ which depend on the average pore concentration (at that position) c_i and on a mass transfer coefficient k_L and on the intrinsic kinetics of the reaction itself.

To describe the rate of the electrode reaction, there are many options. The most common is the Butler-Volmer framework which relates the rate R_i to the concentrations of reactive ions in the electrolyte near the reaction site, and to the electrode potential, ϕ_e , which is the difference in potential between the electron-conducting (metallic) phase, and the electrolyte phase (inside the pores), i.e., $\phi_e = \phi_{\text{ec}} - \phi$. Thus, the electrode potential can enhance the rate of reaction, even making it reverse its direction. Thus, the electrode potential works as an extremely powerful ‘catalytic engine’, able to make a reaction go faster or slower, making it come to a standstill, and even make it go in reverse, switching around what is reactant and product!

According to the BV-equation, and for a one-electron reaction, $n = 1$, the reaction rate is given by

$$R_R = -R_O = \varrho_R - \varrho_O = k_{RCO}e^{-\alpha_R\phi_e} - k_{OCR}e^{+\alpha_O\phi_e} \quad (15.4)$$

where R_R is the formation rate of species R , i.e., the reaction rate in the direction of reduction, equal to $-R_O$, which is the formation rate of species O , i.e., the reaction rate defined in the oxidation direction. They are to be distinguished from the reduction reaction, i.e., only the reaction in the reduction direction, ϱ_R , and the oxidation reaction, ϱ_O . Instead, R_R (and similarly R_O) is always a combination of a reduction reaction and an oxidation reaction. The

ⁱⁱThis is a general ambivalence in the language of reaction modelling. It is often asserted for instance that enhancing the catalytic activity will enhance the reaction rate, making the reaction faster. Or the statement that larger pores or more stirring enhances the transport and reaction rate, etc. But of course these statements are only correct when that particular step is rate-limiting. This language is used to mean that the rate ‘prefactor’ of that particular step is improved, *potentially* making that step faster, irrespective of whether the reaction rate R_i will actually go up or not.

reactive species are the O - and R -species, and the reaction rate depends on the concentrations of the O - and R -species in the electrolyte phase just outside the EDL region (electrode), i.e., in the macropores at that particular position in the porous electrode. Species O is the *oxidant* (the species in the oxidized state, that will be reduced in the reaction, i.e., it will take up electrons to become species R , i.e., it becomes more negatively charged), while R is the *reductant* (the species in the reduced state, that will be oxidized in the reaction, i.e., give off electrons to become O , i.e., it becomes more positively charged). The transfer coefficients α_i add up to unity, $\alpha_O + \alpha_R = 1$, and typically are taken as $\alpha_O = \alpha_R = 1/2$. Because this is a reversible reaction, a concentration increase of the one species leads to an increase in the formation rate of the other species, for instance, a larger c_R leads to a higher ϱ_O and thus also to a higher R_O , and vice-versa. This is the same as in general descriptions of reversible reactions in chemical engineering. But different is the effect of the electrode potential. The reduction reaction, ϱ_O , which has as reactant the species in the oxidized state, the oxidant, also requires electrons as reactants. Thus we need to pull the electrons to where the ions are. We must pull them from the metal to the position just in the electrolyte, or in the electrode (the EDL structure), such that the ion and electron can react. If the drop in potential that the electron must make is negative, they do not like that, that is a penalty (electrons are negative species, they do not like to go to positions with a lower (more negative) potential). Thus to make this reaction go faster, this drop must be made less negative, or in other words, made more positive. Thus we must make the potential in the metal go down, relative to that in the electrolyte, thus ϕ_{ec} must be lowered, or put more simply, to enhance the reduction reaction, ϱ_R , the electrode potential ϕ_e must be lowered. This is exactly how the dependence of the reduction reaction on ϕ_e is formulated in Eq. (15.4) by a term $\exp(-\alpha_R\phi_e)$. For the oxidation reaction, ϱ_O , where electrons are the product, it is all the exact opposite, and thus we have a dependence on ϕ_e according to $\exp(+\alpha_O\phi_e)$. Thus by tuning the electrode potential, we can make the reaction go in any direction, which underscores the power of electrochemical catalysis as a method to achieve optimized reaction selectivity and kinetics.

When the reaction rate R_i is very low, relative to the forward and backward reactions, i.e., relative to ϱ_R and ϱ_O , the BV equation simplifies to the Nernst equation

$$\phi_e = \ln K + \ln(c_O/c_R) \quad (15.5)$$

where the equilibrium constant K relates to the kinetic rate constants k_i according to $K = k_R/k_O$. As Eq. (15.5) shows, when we increase ϕ_e , i.e., make the metallic phase more positive (relative to the pore solution), it becomes more favourable for electrons, and thus they are more reluctant to go out of this phase, and participate in a reduction reaction, and this will lead to a new equilibrium situation where in the pore we have an increased ratio of

the concentration of oxidant over that of the reductant.

A final expression is required, which describes the Ohmic transport of electronic charge across the porous electrode

$$I_{ec} = -\kappa_{ec} V_T \frac{\partial \phi_{ec}}{\partial x} \quad (15.6)$$

where the electronic conductance κ_{ec} in S/m depends on how much electron-conducting material is in the electrode, how well these particles are in contact, and their intrinsic conductivity (from very high for carbon nanotube fibers to much lower for inorganic intercalation materials). The higher is κ_{ec} , the more ϕ_{ec} is constant across the electrode even with current flowing. The potential ϕ_{ec} is known at the position where the conducting phase is in contact with wires that go to the external circuit. At outer areas of the porous electrode (blocking for electronic current), we know that in the direction normal to the outer surface we have $\partial \phi_{ec} / \partial x = 0$.

We must also describe how the divergence of the electronic current density, I_{ec} , and that of the ionic current, I_{ionic} , relate to the electrode reaction rate, which is according to

$$\frac{\partial I_{ec}}{\partial x} = -\frac{\partial I_{ionic}}{\partial x} = nFR_R \quad (15.7)$$

where as always, the current densities, here I_{ec} and I_{ionic} , are defined per geometric area (i.e., total area), and R_R is defined per total electrode volume.

This equation can be rewritten to a well-known second order partial differential equation in potential ϕ_{ec} ,

$$\kappa_{ec} \frac{\partial^2 \phi_{ec}}{\partial x^2} = nFR_O \quad (15.8)$$

where $V_{ec} = V_T \phi_{ec}$. This entire set of equations suffices to describe ion transport across a porous electrode with a simultaneously ongoing electrode reaction which convert one ion in the pores into another one.

Generalized Frumkin Butler Volmer equation. A more advanced model identifies how the reduction and oxidation reactions depend on the local charge stored in the metallic phase, i.e., the density of electronic charge. This charge density σ then determines a voltage drop over an inner layer (which can be called a Stern layer), ϕ_S , and this is one element of the EDL structure at the reaction sites, see Ch. 14. The other element is a diffuse layer with voltage ϕ_D , and together they add up to the electrode potential: $\phi_e = \phi_D + \phi_S$. We then have a porous electrode version of the generalized Frumkin-Butler-Volmer (gFBV) equation. For electrodes with micropores (see next

section), this gFBV equation including a full EDL model has been implemented to describe leakage currents in capacitive deionization in Dykstra *et al.* (Water Research, 2017).

An infinite range of possible calculations can now be made, transient and steady-state, with and without convection, background salt, etc. A calculation with a zero current to the electrode is even possible, which will then result in an internal current, with the electrode reaction going in one direction at one point in the porous electrode, and go in the other direction at another position in the layer.

We make here one example calculation, for transport across a porous electrode in x -direction only, for steady state. We include convection, thus use the full Eq. (15.2), with fluid flowing from left to right through the porous electrode. Negative charge is continuously injected in the electrode and in this way a cationic species in the oxidized state (the oxidant) is reduced to a neutral species (the reductant). Thus the electrode is a cathode. Besides this species that arrives in the oxidized state on the left and will leave as a reduced species on the right, we have inert monovalent anions. What flows out of the electrode on the right is collected in a beaker and the content thereof is (of course) electroneutral. Thus the ionic current leaving the electrode on the right, is zero. Because the electronic current entering the electrode is negative, we need to have a net positive ionic current entering the electrode on the left. These two currents, integrated over the entire electrode, add up to zero because there is no charge accumulation in the electrode and the current leaving the electrode on the right is zero. Because of steady-state, the flow of anions is constant across the electrode. Thus the flow of the oxidant exiting the electrode is the same as the anion flow (because the oxidant is a monovalent cation, the reductant is neutral). At each position in the pores of the porous electrode the concentration of oxidant equals that of the anion, to have local electroneutrality in these transport pores. All diffusion coefficients are the same. At the downstream, right, side, we use the ‘dead end’ condition, thus relate the salt concentration outside the electrode to the ionic flux and fluid flow. This results in the fact that at the downstream side we only have convection as driving force, and thus all concentration gradients here are zero.ⁱⁱⁱ No current flows out of the electrode here so for any binary salt also the potential gradient is automatically zero, see §7.3 and §7.4. On the upstream side we consider a transport film that includes all driving forces on solutes, which are diffusion, convection and migration.

We can set up a balance in the total species concentration, $c_O + c_R + c_-$, and we then find

ⁱⁱⁱThis is different in the theory of RO at the downstream side, where we do not have these zero concentration gradients. That is because in that problem we have a partitioning and Donnan effect at the edges of the layer.

that because of the ‘dead end’ boundary condition, and because of the equal values of D , that this total concentration is invariant across the upfront film layer and across the electrode. At any point in the electrode it has the same value as in the bulk phase on the left (upstream side), $c_{\text{tot}}^{\text{ups}}$. Because also everywhere $c_O = c_-$ because of local electroneutrality, we have $c_R = c_{\text{tot}}^{\text{ups}} - 2c_O$. In the upstream bulk we set all three concentrations equal to one another, to c_{ref} , and thus $c_{\text{tot}}^{\text{ups}} / c_{\text{ref}} = 3$. All dimensionless concentrations are $\bar{c} = c / c_{\text{ref}}$. Molar fluxes are nondimensionalized by dividing by $c_{\text{ref}} L / D$ where L is the electrode thickness and D the diffusion coefficient in the electrode including the ε -term. Fluid velocity is divided by D / L to arrive at the Pe-number. The formation rate R_O is divided by $c_{\text{ref}} D / L^2$ to arrive at a dimensionless \bar{R}_O . The kinetic constants k_i are divided by D / L^2 to also become dimensionless quantities, \bar{k}_i .

The differential mass balance that we now must solve in the electrode for the oxidant is

$$0 = -\text{Pe} \frac{\partial \bar{c}_O}{\partial \bar{x}} + \frac{\partial^2 \bar{c}_O}{\partial \bar{x}^2} + \frac{\partial}{\partial \bar{x}} \left(c_O \frac{\partial \phi}{\partial \bar{x}} \right) + \bar{R}_O \quad (15.9)$$

in combination with Eq. (15.4) and a charge balance (based on subtracting the balance in the anion, from the balance in the cation, i.e., the oxidant), which is

$$0 = 2 \frac{\partial}{\partial \bar{x}} \left(c_O \frac{\partial \phi}{\partial \bar{x}} \right) + \bar{R}_O. \quad (15.10)$$

On the upstream side we have a DBL, which implies a relation between concentrations in the upstream bulk, and at the electrode, related to current and to a mass transfer coefficient. To derive this equation, we must evaluate fluxes at the very left of this layer, and at the electrode surface. The latter is easily established, described by evaluation of Eq. (15.2) just inside the electrode, for instance dependent on the potential gradient there. However, the flux at the left side of the DBL (where it is in contact with the bulk) includes a contribution because of the current.^{iv} This current (divided by 2, with a \pm -sign) ends up in the boundary condition at this position for anions and cations. But how do we know the current when we actually make a calculation for a certain value of the potential of the metallic phase of the electrode, ϕ_{ec} ? (We also assume a highly electron-conductive electrode, thus no gradients in ϕ_{ec} .) The additional equation is that $\bar{J}_{\text{ch,ups}} = - \int_0^1 R_O d\bar{x}$. Here, the electronic current, which converts into a negative formation rate of the oxidant, leads to a positive current into the electrode on the upstream side. This equation works because there is no current flowing out of the electrode on the other side.

^{iv}This is different from similar modeling in Guyes *et al.* (Desalination, 2017) with porous capacitive electrodes, because in their DBL approach there was no current.

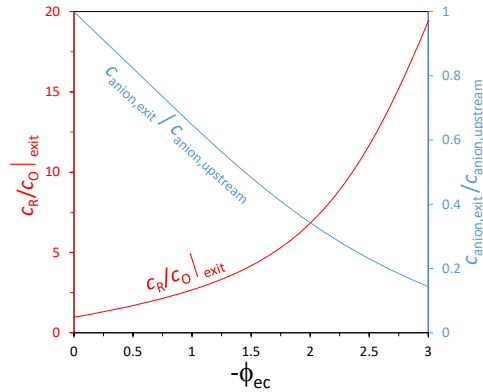


Fig. 15.1: Results of porous electrode theory for steady state reduction of a cation in a porous electrode with convection, as function of potential in the electron-conducting, i.e., metallic phase, ϕ_{ec} . With further lowering of ϕ_{ec} , the rate of reduction increases, and in the downstream effluent the concentration ratio of the species in the reduced state over that in oxidized state strongly increased, while the electrode also increasingly rejects the anion ($Pe = 5$, $\bar{k}_R = \bar{k}_O = 1$, $\bar{c}_R|_{ups} = \bar{c}_O|_{ups} = 1$).

We can make these calculations, and results are presented in Fig. 15.1, and these results are of quite some interest. By lowering ϕ_{ec} , the potential of the electron-conducting phase, we enhance the reaction towards the reductant species, i.e., we reduce the cation, to become a neutral species. At a potential $\phi_{ec} = 0$, nothing happens, and the water and ions will go through the electrode unchanged. But when we now apply a slightly lower potential of only -3 points (-77 mV) we can change this ratio in the effluent by a factor of 20. This is a dramatic change and thus this electrochemical conversion can be very effective. Also of interest is that the anion is rejected by this porous electrode. So even though there is no membrane ‘sieving’ effect at all, just the redox reactions involving a reductant/oxidant, this significantly blocks the inert anion from passing the electrode; at the most negative value of ϕ_{ec} , its concentration on the permeate side is down by a factor of 6, relative to the upstream side.

Thus, in conclusion, even this simple example of faradaic reactions in a porous electrode with convection leads to some quite ingenious mathematics, and some unexpected calculation outcomes.

15.2.1 The porous battery electrode

Secondary battery electrodes are based on charge storage in the electrode, i.e., in the EDL structure formed at the interface between electrolyte and electron-conducting phases. The primary example is the Li^+ -ion battery, where Li^+ -ions are stored in one of several possible ion insertion materials. The solvent is organic, not aqueous. There is likely phase separation inside the electrode, and in that case it is possible that there is a horizontal plateau in the equilibrium curve of electrode potential versus stored charge, equivalent to the constant pressure when a gas is slowly compressed, while liquid droplets are already formed. Thus when there is such a plateau, there is co-existence between a gas-like ('G'), or dilute, phase, where the intercalation degree is low, and a liquid-like ('L'), or dense, phase. While on average the concentration in the material increases with charging ('upon compression'), these two densities of the two phases are constant, and represent the edges of the plateau depicted in Fig. 15.2. This horizontal plateau makes it possible for the battery to operate with the electrode potential in principle independent of charge, if we discharge slowly enough.

The horizontal plateau encountered in an electrode with internal phase separation, see Fig. 15.2, arises in an EDL structure when the ions inside the EDL attract one another with sufficient strength, and then for intermediate values of the overall concentration, they phase separate. In Section 1.4 it was derived that using the extended Frumkin equation there is a critical attraction parameter of $g' = -4$, and for g' -values more negative than this value, phase separation can occur. In that case, the equilibrium curve for electrode potential vs. charge no longer steadily increases or decreases, but has a local minimum and maximum, and that non-monotonic curve is unstable. Instead, experimentally one likely finds a constant potential, i.e., the horizontal plateau in Fig. 15.2. Based on a 'Van der Waals-construction', one can find the potential of the plateau (or for a gas that condenses, the pressure). For a symmetric curve, as in Fig. 15.2, it is simply 'half-way', intersecting the 'full curve' at $\vartheta = 0.5$. Knowing the potential in the plateau region, we can find the density of the two co-existing phases (the 'edges' of the plateau, where it intersects the 'full curve'). The electrode potential in the plateau region is calculated from inserting $\vartheta = 1/2$ in Eq. (1.23), resulting in

$$V_{e,\text{plateau}} = V_{\text{ref}} + V_T \ln \frac{c_\infty}{c_{\text{ref}}} \quad (15.11)$$

and the densities of the two co-existing phases, ϑ , follow from

$$\ln \frac{\vartheta}{1-\vartheta} + g'(\vartheta - 1/2) = 0. \quad (15.12)$$

The more negative the value of g' , the wider the region of the horizontal plateau. With $g' = -4.5$ (just below the critical value), the two ϑ -values are at $\vartheta = \{0.22, 0.78\}$, thus

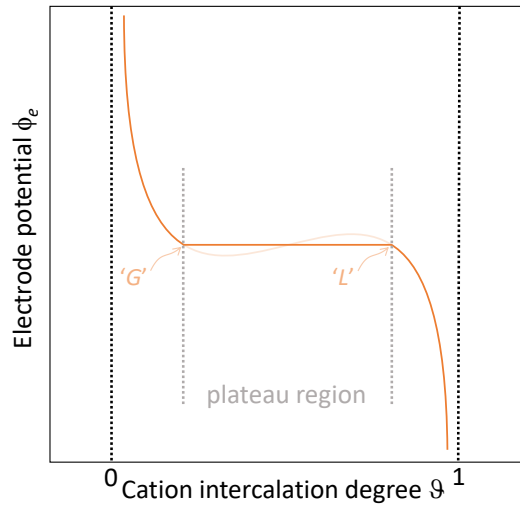


Fig. 15.2: Example of an equilibrium curve for electrode potential vs. charge for a porous electrode for which there is an attraction between ions inside the electrode that leads to a local phase separation between a gas-like ('G') dilute phase, and a liquid-like ('L') dense state. This results in a region where in theory we have a constant electrode potential, independent of charge. The entire curve depends on the ion concentration outside the EDL: for cations as absorbing species in the electrode, then with a lowering of the bulk cation concentration, the entire curve moves downward.

$\Delta\vartheta \sim 0.55$ apart, but when we reduce g' further, to $g' = -5.5$, the two end-values of ϑ are at $\{0.10, 0.90\}$, and thus $\Delta\vartheta \sim 0.8$, thus already for 80% of the complete charging curve, we can have operation with a 'horizontal plateau.' To reach a 90% usage, we need $g' = -6.5$.

If we operate the entire porous electrode in this 'plateau'-mode, we can potentially charge and discharge the electrode all the time at the same voltage. This will then appear as if a Faradaic reaction is going on in a steady-state process, but of course this is just appearances. Also the generated voltage, given by Eq. (15.11), has a dependence on ion concentration that seems to be similar to the Nernst-equation, Eq. (15.5). However, the crucial difference is that in the present case *only one ion is involved*. In any case, this kind of battery electrode does not operate by a Faradaic principle, because it is not the case that reactants and products freely flow in and out of the EDL structure (the electrode). Instead, this process is based on capacitive electrode charging, with the pseudo-Faradaic behavior only a consequence of counterions inside the electrode being mutually attracted to one another.

Porous electrode theory for these capacitive battery electrodes with internal phase separation is a challenging topic (Dreyer *et al.*, 2010): one option is to assume that at each macroscopic position in the electrode part of the active particles, or host particles, are for 100% in the L-state, while other particles are completely in the G-phase; the other option is that within a certain particle there is a co-existence of these two states. In that case, inside such a particle the two phases can be fully segregated, or there is a pattern in how they are distributed, for instance each phase forms stripes (and thus both phases are locally continuous), or one phase is dispersed in the other phase, so only the latter phase is continuous... While the electrode discharges, dependent on kinetic limitations, the material either is able to follow the horizontal plateau, or it tracks partially the meta-stable curve (the curve that has a minimum and maximum), see Dreyer *et al.* (2010).

Despite the high level of complexity, we can illustrate this problem by presenting a simplified model for ion transport and charge storage in such a battery electrode, focusing on the theory related to transport across the electrode. We use a function for the local charge-voltage curve that empirically includes the plateau as well as the steep parts outside the plateau. This model extends the model of the previous section because instead of a Faradaic reaction we now have capacitive storage of ions in the active or host particles. These particles are in contact with the transport pores through which ions flow. The two phases have porosity p_{tr} and p_{hp} , and we can set up a mass balance in the cation (the ion that can also go into the host particles) given by

$$\frac{\partial}{\partial t} (p_{tr}c_i + p_{hp}c_{\max}\vartheta) = D_i \left(\frac{\partial^2 c_i}{\partial x^2} + \frac{\partial}{\partial x} \left(c_i \frac{\partial \phi}{\partial x} \right) \right) \quad (15.13)$$

where c_i is a concentration inside the transport pores, and ϕ the potential in these same

pores. We included here the NP-equation, without convection. The diffusion coefficient D_i includes an effect of porosity and tortuosity, i.e., $D_i = p_{tr}/\tau_{tr} \cdot D_{i,\infty}$. We use variables similar to those in Ch. 1, thus again ϑ times c_{\max} is the concentration of cations in the host particles, i.e., the cation intercalation degree, or cation occupancy, and is also the charge of cations per volume of these particles (after multiplying with F). A decrease of ϑ means that cations flow out, and thus electronic charge flows into the electrode (electrons flow out). Note that at a given ‘macroscopic’ x -position, ϑ averages over the mixture of dilute (G) and dense (L) phases inside the host particles at that x -coordinate. [Below we discuss $\langle\vartheta\rangle$ which is an average over the entire electrode (over the complete x -coordinate).] For the anion, which cannot enter the host particles, we also use Eq. (15.13) but without the term $p_{hp}c_{\max}\vartheta$, and with an additional factor -1 before the electromigration term. It is useful to subtract the anion balance from the cation balance, to arrive at the charge balance

$$p_{hp}c_{\max} \frac{\partial \vartheta}{\partial t} = 2D \frac{\partial}{\partial x} \left(c \frac{\partial \phi}{\partial x} \right) \quad (15.14)$$

where we used charge neutrality in the transport pores, that at each position $c = c_- = c_+$. We also implemented here the assumption that both ions have the same diffusion coefficient.

We consider constant current charging, with a dimensionless current \bar{I} , which can be multiplied by F , the diffusion coefficient D , and a reference concentration c_{ref} , and divided by electrode thickness L , to obtain a current density in A/m². The current density \bar{I} relates to the average cation intercalation degree by

$$p_{hp}c_{\max} \frac{\partial \langle\vartheta\rangle}{\partial \bar{t}} = -\bar{I} \quad (15.15)$$

where dimensionless time \bar{t} can be multiplied by L^2/D to obtain a dimensional time. $\langle\vartheta\rangle$ averages the intercalation degree, ϑ , across the entire electrode, while ϑ is already an average of the local G- and L-phases.

We can integrate Eq. (15.14) across the electrode to obtain

$$p_{hp}c_{\max} \frac{\partial \langle\vartheta\rangle}{\partial \bar{t}} = 2 \left(c \frac{\partial \phi}{\partial \bar{x}} \Big|_{\text{back}} - c \frac{\partial \phi}{\partial \bar{x}} \Big|_{\text{front}} \right) \quad (15.16)$$

and knowing that $\partial\phi/\partial\bar{x} = 0$ at the backside of the electrode, for symmetry reasons, and implementing Eq. (15.15), we arrive at

$$c \frac{\partial \phi}{\partial \bar{x}} \Big|_{\text{front}} = \frac{1}{2} \bar{I} \quad (15.17)$$

as boundary condition at the front side of the electrode.

To describe the dependence of electrode potential on electrode charge, including the plateau, we use several approaches that all assume local equilibrium at each macroscopic coordinate x , i.e., equilibrium between the cations (e.g., Li^+ -ions) in the transport pores, and those in the host particles. In reality, transport limitations between the transport pores and the host particles are certainly possible. Also conversion of the dilute into the dense phase and vice-versa (the co-existing compositions) will have a finite rate. The first approach is the extended Frumkin equation, Eq. (1.22), with the electrode potential, ϕ_e , equal to the potential in the electron-conducting phase, ϕ_{ec} minus the potential in the transport pores, ϕ .^v We use this equation for the critical condition that $g' = -4$ which implies that around $\vartheta = 0.5$ the slope of potential vs. charge is zero. As a second option, instead of this isotherm we use the empirical expression

$$\phi_e = \phi_{ec} - \phi = \phi_{\text{ref}} + \ln \frac{c_i}{c_{\text{ref}}} - m \cdot (\vartheta - 1/2)^n \quad (15.18)$$

where m is an adjustable pre-factor (we use $m = 10^4$), and the power n is an odd integer, for which we use $n = 9$. With this curve, between $\vartheta = 0.2$ and $\vartheta = 0.8$ the electrode potential only varies by 0.4 dimensionless points (~ 10 mV), and between $0.3 < \vartheta < 0.7$ only 0.01 potential points. Outside this range the electrode potential quickly increases at low ϑ and decreases at high ϑ . For instance, at $\vartheta = 0.036$, the potential is 10 dimensionless points (~ 260 mV) above the plateau region. A third option is to explicitly model the phase separation and the horizontal plateau, but a model along these lines is difficult.

Just as in the previous section, we assume that in the electron-conducting phase we have no electronic resistance, thus across the electrode the potential in the electron-conducting phase ϕ_{ec} is the same at each position (though it will change in time). We model an electrode that is full of cations at a starting value of $\vartheta = 0.9$, and while we discharge this electrode at $\bar{I} = 0.2$, we track $\phi_{e,\text{overall}} - \phi_{\text{ref}}$ which is the relevant voltage of the electrode. We model an electrode with ionic current able to leave on the front side, while the backside is blocking for all ions, thus also for ionic current. We use a constant value of the salt concentration at the front side, c_∞ , and use $p_{\text{hp}}c_{\text{max}}/c_\infty = 2$ ($c_{\text{ref}} = c_\infty$).

It is interesting to notice from evaluating the model, that it is the front side which determines the entire electrode potential. The electrode potential here, thus the overall electrode potential, is a direct function of the intercalation degree ϑ at the front side of the electrode. Thus, when ϑ drops here, the voltage generated by the entire electrode drops, and

^vNote that in any porous electrode there is a local electrode potential, $\phi_e = \phi_{ec} - \phi$, as well as a ‘measurable’ electrode potential, which is the difference in potential between where the electrode connects to an electronically conducting surface or wire, and the potential in the electrolyte solution just outside the electrode, ϕ_∞ . If there are no electronic resistances across the electrode, we have $\phi_{e,\text{meas.}} = \phi_{ec} - \phi_\infty$.

vice-versa upon current reversal. Thus the aim of proper electrode design is also to have high enough mass transport rates across an electrode such that ϑ at the front side does not change much faster than at other points in the electrode.

Results of this calculation using the empirical function, Eq. (15.18), are presented in Fig. 15.3, where we show profiles in ϑ across the electrode when there is a positive electronic charge into the electrode and cations are going out, i.e., $\langle \vartheta \rangle$ is decreasing linearly in time. Starting at $\vartheta = 0.9$ at time zero, first $\vartheta(x)$ drops equally fast everywhere, and then –as shown in Fig. 15.3A– it starts to drop faster at the front side of the electrode (on the left in the panel). A sharp ‘wave’ travels through the electrode until it hits the back end, after which the entire electrode has a composition of $\vartheta \sim 0.2$, and continuing the charging process leads to a sharp further drop in potential. The voltage of this electrode (expressed as negative of the electrode potential), as shown in panel B, first quickly increases, but then from $\vartheta = 0.75$ onward (towards lower ϑ), the rate of voltage increase is much slower, only 0.15 points (4 mV) over the entire range until we reach $\vartheta = 0.25$. When we reverse the current, the voltage immediately drops by about that amount, and then steadily decreases until we are again at $\vartheta \sim 0.75$. This same slope $d\phi_e/d\vartheta$ is also found in the *equilibrium* curve, Eq. (15.18), at values of ϑ around $\{0.3, 0.7\}$. Outside this range of ϑ , the equilibrium curve is steeper, while it becomes very small and even zero when we approach $\vartheta = 0.5$. Thus, the voltage-charge curve as depicted in Fig. 15.3, derived from a dynamic transport model, shows in most of the $\langle \vartheta \rangle$ -range an ‘apparent capacitance’ (change of electrode charge with electrode potential) than the (empirical) equilibrium curve predicts. The steadily changing electrode potential shown in Figs. 15.3B,D is reminiscent of results of other models and experiments, and the same holds for the hysteresis loops in these figures, where we see that the voltage level depends on the direction of current (Dreyer *et al.*, 2010).

We can make a calculation for a fixed salt concentration which gives similar results (because c doesn’t change much across the electrode). With this assumption, we only have to solve Eq. (15.14), with ϕ a function of ϑ using Eq. (15.18). Results are practically similar to those of the full model as were presented in Fig. 15.3.

Porous electrode battery model with explicit consideration of phase separation. – in preparation –

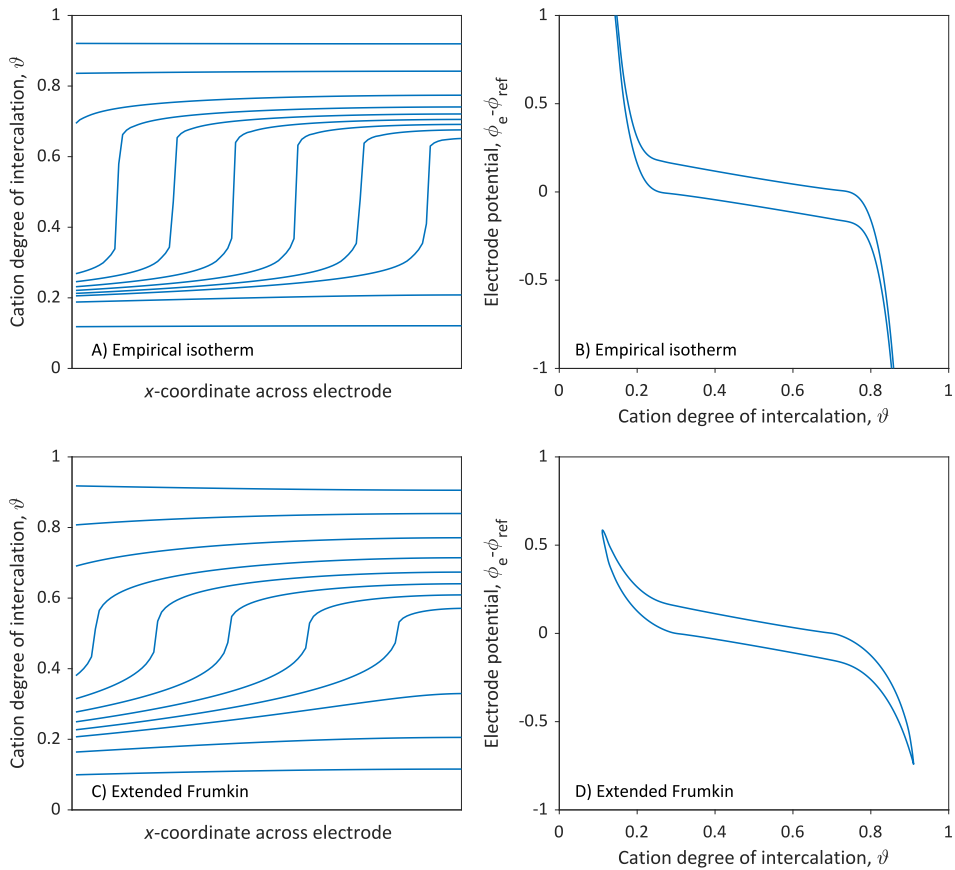


Fig. 15.3: Calculation results for profiles of intercalation degree ϑ across the thickness of one battery electrode, as well as the change in the overall electrode potential vs. average intercalation degree, $\langle \vartheta \rangle$, which first goes down linearly with time (constant current) and after current reversal increases again. Results presented using the empirical isotherm (A and B), Eq. (15.18), and the Extended Frumkin isotherm (C and D), Eq. (1.22).

15.3 Porous electrodes for water desalination

In the battery model discussed in the last section, we were interested in the relation between electrode potential and (dis-)charge rates (current). In the present section we discuss another example of porous electrode modelling, and now we are also interested in the resulting flows of ions into and out of the electrode as function of current. With two electrodes that can take up ions, we can construct a desalination cell. In such a cell, the ions flow into/out of the electrodes which leads to changes in salt concentration in the space between the two electrodes. The related technology is called Capacitive Deionization, abbreviated as CDI. Many options are possible for the chemistry and design of the porous electrodes in such a desalination cell, see §20.2 and §20.4. One option is that the two electrodes of a cell behave in a symmetric manner, with only the role of anions (anode) and cations (cathode) flipped. Another option is that the electrodes only allow one type of ion into the EDL structure, or that a cell asymmetry is established by placing ion-exchange membranes in between the two electrodes. Or the two electrodes are just very different. All options are open...

The degree of desalination in the channel depends on the total flow of anions and cations into the two porous electrodes. The total removal rate for anions and cations ('total' referring to a summation over the two electrodes) will be the same in case of a symmetric salt. Still, each electrode can have a different ratio between how many counterions it absorbs, versus how many coions it releases. Thus for a 1:1 salt, for each individual electrode we can measure the current efficiency, λ , which is the total molar flow rate of ions flowing in (or out) of the electrode, divided by the current. This current efficiency is not a material property of the electrode but depends also on salt concentration, current, etc. It can also change in time. At each moment, the average of the two current efficiencies is the total salt removal rate from the channel divided by the current. Thus for each individual electrode we need to establish (measure, or calculate by a model), the current efficiency as function of time. A full CDI model will combine a description of the electrodes with a description for the changing salt concentrations in the transport channel (the space between the porous electrodes). Transport and changing concentrations here, have an impact on the behaviour in the electrodes.

We now discuss a simple calculation where, just as in the last section, we neglect salt concentration changes in the channel. We again use the extended Frumkin equation for an intercalation material that only absorbs cations (such as a Prussian Blue Analogue). We now use a much lower salt concentration, 50× lower than in the prior calculation (corresponding to 20 mM salt concentration now, vs. 1 M in the battery calculation, while in both calculations $c_{\max} = 4 \text{ M}$). We start with an electrode where the concentration of cations is very low inside the host particles, $\vartheta = 0.1$, and we study the salt concentration profiles in the electrode, and

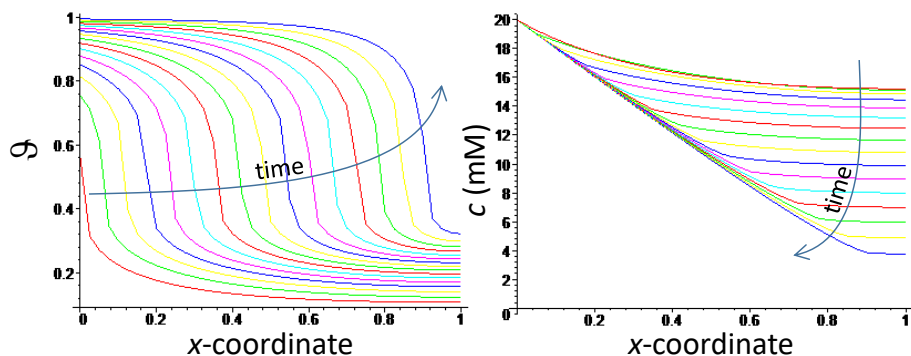


Fig. 15.4: Calculation results for water desalination with porous intercalation electrodes, showing time-dependent profiles of a) intercalation degree ϑ (cation adsorption in host particles), and b) salt concentration inside transport pores, across the thickness of one electrode. Results based on the Frumkin isotherm, Eq. (1.22), with $g' = -4$, for constant current $\bar{I} = -2$, and $p_{\text{hp}}c_{\text{max}}/c_{\infty} = 100$. The profiles are a time $\Delta \bar{t} = 2.5$ apart.

the current efficiency of this electrode, λ , vs. time. The theory of the last section can be used without further adjustments.

Results are presented in Fig. 15.4 for the cation adsorption in the host particles, ϑ , and for the profiles of salt concentration in the transport pores. While the host particles absorb more and more cations, going from almost empty to almost full, the transport pores in the electrode see a decay in salt concentration over time. During this process is a strong influx of cations, cations which all move into the host particles, and a very tiny flux of anions out of the electrode, with the current efficiency, starting at 0, quickly reaching a constant plateau of $\lambda \sim 0.998$. Thus, this electrode is highly selective because only cations can go into the host particles. For CDI, this high selectivity is an optimal situation. However, many types of materials for CDI absorb both anions and cations and then the current efficiency can be much lower.

This is for instance the case for many microporous carbon materials. For electrodes made of carbon, nomenclature for pores is that of macropores through which ions move (called transport pores until now), and micropores, in which the ions are stored in EDL structures. Ion storage in these micropores is described by a Donnan model.

The Donnan model is both a simplification and an extension of the extended Frumkin isotherm. It is a simplification because two terms are omitted: the term relating to the limited occupancy, $\ln(1 - \vartheta)$, and the ion-ion attraction term $g'(\vartheta - 1/2)$. It is an extension

because not only cations can now enter the micropores (where the EDLs are formed) but anions as well. And we include a Stern layer, describing a voltage drop between the electron-conducting phase and the aqueous micropore region where ions reside.

To accurately describe data both of charge and of salt adsorption (vs. cell voltage), the Donnan model for microporous carbon electrodes is often further extended with two features. First, the local charge balance not only includes the electronic charge in the carbon matrix and the ionic charge in the electrolyte-filled micropores, but also includes ‘chemical’ fixed charge, for instance due to carboxylic acid groups attached to the carbon material, thus attached to the ‘walls’ of the micropores. A second important modification is to consider that there are two types of micropore regions inside a typical microporous carbon: regions with negative wall charge, due for instance to carboxylic groups, as well as regions with positively charged groups on the pore walls. This amphoteric Donnan model is required to describe data for charge and desalination with CDI accurately (Mubita *et al.*, 2018, 2019). In a further extension, both types of these charged groups can be ionizable, i.e., we can include how this chemical charge in each region responds to local pH.

In this section we do not use this full model but make a calculation using the most simple Donnan model, where Boltzmann’s law describes the distribution of ions between the transport pores (macropores, mA) and micropores (mi). We include a Stern layer. We consider a 1:1 salt with equal diffusion coefficients. We again make a calculation with fixed current, and with salt concentration at the front side of the electrode fixed. Compared to the intercalation materials discussed above, we can now start with a negatively charged material (the electronic charge in the carbon is negative), and with a constant electronic current into the electrode we can increase this charge to zero, and then reverse the charge to positive, which leads to the electrode changing from cation desorbing to anion adsorbing, see Fig. 15.5. This reversal of charge sign is not possible with the intercalation materials discussed above.

The model is very similar to that of the previous sections. The ion balance is slightly different, and is now

$$\frac{\partial}{\partial t} (p_{\text{mA}}c_i + p_{\text{mi}}c_{\text{mi},i}) = D_i \left(\frac{\partial^2 c_i}{\partial x^2} + z_i \frac{\partial}{\partial x} \left(c_i \frac{\partial \phi}{\partial x} \right) \right) \quad (15.19)$$

both for anions and cations. We can assume local equilibrium between the ions in the micro-pores and in the macropores, and thus use the Boltzmann relation for each ion type, $c_{\text{mi},i} = c_i \cdot \exp(-z_i \phi_{\text{D}})$, where c_i without any further subscript is the concentration of an ion in the charge-neutral macropores. The Donnan potential ϕ_{D} is the potential in the micropores, relative to in the nearby macropores, and relates to the ionic charge in the

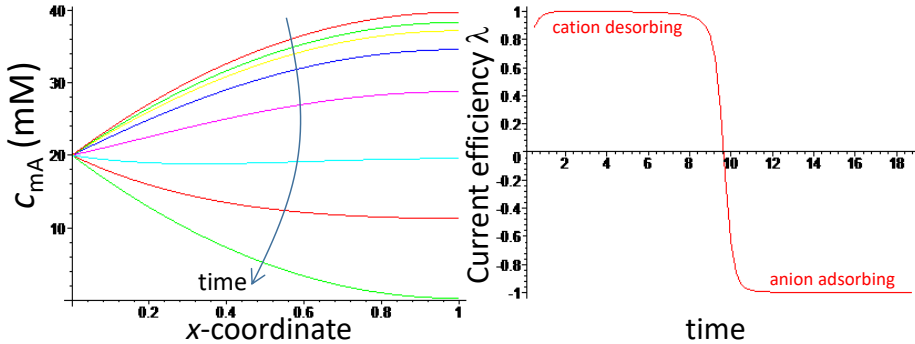


Fig. 15.5: Calculation results for water desalination with microporous carbon electrodes, showing the time-dependence of a) profiles of the salt concentration in the macropores, across the thickness of one electrode, and b) current efficiency, $\lambda = t_+ - t_-$. Results based on the modified Donnan model, for constant current $\bar{I} = 80$, $C_{St} = 0.2 \text{ GF/m}^3$, $\sigma_{\text{mi,ions,initial}} = 1.5 \text{ M}$ ($c_{\text{ref}} = 1 \text{ mM}$).

micropores: $\phi_{\text{mi}} - \phi = \phi_{\text{D}} = -\sinh^{-1}(\sigma_{\text{mi,ions}}/(2c))$, with the latter equality only valid for a 1:1 salt. Based on the Boltzmann equation, we can derive an additional relationship between total ions adsorption, $c_{\text{ions,mi}} = c_{\text{mi,+}} + c_{\text{mi,-}}$, and charge $\sigma_{\text{mi,ions}} = c_{\text{mi,+}} - c_{\text{mi,-}}$ in the micropores

$$c_{\text{ions,mi}}^2 = \sigma_{\text{mi,ions}}^2 + 4c^2 \quad (15.20)$$

valid for a 1:1 salt. The ionic charge in the micropores, $\sigma_{\text{mi,ions}}$, is simply opposite to the electronic charge density in the carbon matrix (all charge densities are defined in amounts per unit micropore volume), if we neglect the chemical ‘wall’ charge. Eq. (15.20) is similar to Eq. (2.11). In Eq. (15.20), c is the local (time-dependent) salt concentration in the macropores. The average charge in the electrode relates to current according to $p_{\text{mi}} \partial \langle \sigma_{\text{mi,ions}} \rangle / \partial \bar{t} = -\bar{I}$. The Stern voltage (drop) is given by Eq. (2.18) with σ_{w} in this equation the charge density in the carbon matrix (per unit micropore volume), which is minus the charge density of the ions in the electrolyte phase inside the pores, $\sigma_{\text{mi,ions}}$, which is given by the summation term of Eq. (2.5).

Calculation results for this charging and discharging process of a microporous carbon electrode are presented in Fig. 15.5. We start with an electrode where the micropores are full of cations. Upon discharging the electrode, these ions come out (while anions temporarily move from outside into the macropores), leading to a quick increase of salt concentration in the macropores (at time zero it was 20 mM everywhere) to a maximum of around 40 mM. Upon discharging the electrode, at some moment all cations are removed from the micropores

and then the situation quickly changes, and the entire salt concentration profile drops to a salt concentration deep in the electrode close to zero, while now the electrode absorbs anions into the micropores. Before this moment, the electrode was expelling around one cation from the electrode for each electronic charge injected ($t_+ \sim 1$), while after this moment, the same injection of one electronic charge leads to an anion being absorbed ($t_- \sim 1$) from solution. When we have two electrodes of which one is absorbing anions, and the other absorbs cations, water is desalinated, and upon current reversal both electrodes will desorb ions, until the reversal point where they will absorb ions again. In this operational mode, in one charge-discharge cycle, we have two periods of desalination and two periods of salt release (Fig. 7C in Porada *et al.*, 2013). We can also have in one charge-discharge cycle a single period of desalination and a single period of salt release if we switch from charging to discharge before the reversal point or implement elements such as an ion-exchange membrane that limits this reversal.

This concludes the discussion of one example calculation of water desalination using porous electrode based on the technology of capacitive deionization (CDI). Many options can be used in the design of a CDI technology, including ion-exchange membranes, movable electrodes, fluidized bed electrode slurries, water not flowing along but through the electrode; two electrodes that are similar to one another, or are very different in chemistry; the use of a third auxiliary electrode to change the total charge in the primary CDI cell pair, etc. Indeed, the list of intriguing ways to construct a CDI desalination device is very long.

Combined Faradaic and non-Faradaic (capacitive) processes

In many processes, Faradaic and non-Faradaic (capacitive) processes occur simultaneously, in either one and the same electrode, or in a cell with two or more electrodes. The two processes can operate jointly, and this can lead to various unexpected results. For instance, we can have a single electrode that sustains a Faradaic reaction while completely disconnected from any other electrode. We can also have two capacitive electrodes that store charge in a cyclic manner, with in addition in one of the electrodes a Faradaic reaction, which leads to a loss of charge in one electrode. This seems to be impossible, how can we have a Faradaic reaction in only one electrode? Shouldn't there then also be a Faradaic reaction in the other electrode, to compensate for the leakage of charge in the first electrode? In this chapter we show that this second reaction is not necessary, and we can have two capacitive electrodes operating in a cycle of charge and discharge, with an additional Faradaic reaction operating in only one electrode for some time.

16.1 Introduction

Every textbook on electrochemistry will teach the following two basic facts. First that we always need at least two electrodes for an electrochemical process to occur; electrochemistry with a single electrode is impossible. Second, when a Faradaic process occurs in one electrode, we also need a second electrode with a Faradaic reaction, because for every anodic reaction that liberates an electron, we need a cathodic reaction that consumes the electron.

These two facts must be true, right? Well, perhaps not. In this chapter we discuss examples that show that it can also be otherwise. The two statements above are correct, but only in a steady state process, i.e., when all time-dependencies have vanished. But until steady state is reached, or in a cyclical process, things can be different, as we already alluded to on p. 368, and as we will illustrate in the next sections, where we discuss in detail the interesting class of combined capacitive-Faradaic processes.

16.2 A single electrode

When we have a porous (carbon) capacitive particle in water with inert salt ions, and the particle is uncharged to start with, and if we now add additional ions that can participate in an electrode reaction in the carbon particle, then the particle will charge up, with a rate determined by the rate of the electrode reaction and/or by the rate of diffusion of the redox-active ions and the other ions towards/away from the particle.

With a typical redox reaction involving a reductant and oxidant, and with two other monovalent ions, such as Na^+ , Cl^- and the water ions, H^+ and OH^- , then we potentially already have to consider diffusion and migration of six ions around and inside (the macropores of) the porous particle. For the moment, let us neglect transport limitations of these ions, and assume that the ion distributions around the particle are at equilibrium, and thus, that the rate of the process of charging this electrode is determined solely by the rate of the electrode reaction, as described in Ch. 15 as Eq. (15.4), where the concentrations c_O and c_R are those near the reaction sites, for which we can use the concentrations in the micropores, described by the Donnan model for porous electrodes, see the explanation below Eq. (15.19). Thus we arrive at the rate of the redox reaction as

$$R_R = k_R c_{\text{mi},O} e^{-1/2\phi_s} - k_O c_{\text{mi},R} e^{+1/2\phi_s} \quad (16.1)$$

where we included that we evaluate concentrations in the micropores, and we include that the potential difference that drives the reaction is that between the micropore and the electron-

conducting phase, which is the Stern layer potential, ϕ_S . The concentrations of oxidant and reductant in the micropores relate to those in the macropores (and in the absence of mass transport limitations, these are the same as those in the bulk solution outside the particles), by

$$c_{\text{mi},i} = c_{\infty,i} e^{-z_i \phi_D} \quad (16.2)$$

where for the oxidant we have z_O and for the reductant we have z_R (with $z_O = z_R + 1$). Let us assume that both these ions are at low concentration, compared to the concentration of the inert ions, i.e., the salt concentration $c_{\infty,\text{salt}}$. Thus the ionic charge in the micropores is given by the well-known Donnan equation, $\sigma_{\text{mi,ions}} = -2c_{\infty,\text{salt}} \sinh \phi_D$ (for a 1:1 salt), and this ionic charge equals minus the electronic charge, $\sigma_{\text{mi,ions}} = -\sigma_{\text{elec}}$, and this electronic charge relates to the Faradaic reaction rate by $\partial \sigma_{\text{elec}} / \partial t = +R_R$, where t is time. We finally must relate the electronic charge to the Stern potential by $\sigma_{\text{elec}} = C_S^* \phi_S$ where $C_S^* = C_S V_T / F$, with C_S the Stern capacitance in F/mL.

When the oxidant and reductant are supplied, the electrode reaction will start, and it will continue until the moment that the EDL that forms in the carbon micropores has such a structure that R_R is reduced to zero, and then equilibrium is reached. When after that either $c_{\infty,O}$ or $c_{\infty,R}$ is changed, the reaction takes off again and the EDL structure again changes.

We can combine all equations to obtain

$$\frac{\partial \sigma_{\text{elec}}^*}{\partial t^*} = \beta e^{-z_O \phi_D - 1/2 \phi_S} - e^{-z_R \phi_D + 1/2 \phi_S} \quad (16.3)$$

where $t^* = t k_O$, $\sigma_{\text{elec}}^* = \sigma_{\text{elec}} / c_{\infty,R}$ and $\beta = k_R c_{\infty,O} / k_O c_{\infty,R}$. We provide some numerical calculation results of the development of the charge of the particle, σ_{elec}^* as function of dimensionless time t^* in Fig. 16.1, from an initial charge of zero. When charge levels off, the Faradaic reaction rate goes to zero, and ion absorption also goes to zero, and we arrive at a final equilibrium state that persists until one changes the concentration of the redox ions in solution, or we change the salt concentration of the inert ions. In this second case, the equilibrium potential is unchanged, but electrode charge and salt absorption will change. Indeed, as Eq. (15.20) illustrates, the charging of this particle will lead to absorption of ions, and thus we can even use this process to desalinate water (in an extremely impractical way, for sure).

When equilibrium is reached, the electrode potential is given by the Nernst equation

$$\ln \beta = \phi_{\text{EDL}}|_{\text{eq}} = \phi_D|_{\text{eq}} + \phi_S|_{\text{eq}} \quad (16.4)$$

and we must solve the Donnan EDL model (combination of diffuse layer and Stern layer) to calculate the electrode charge σ_{elec} as function of $c_{\infty,\text{salt}}$ and C_S . This shows that the

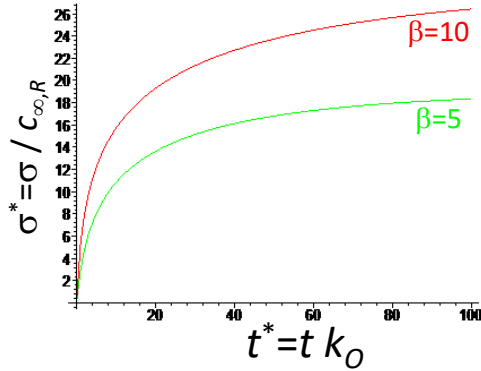


Fig. 16.1: Calculation results of the capacitive charging of a single porous particle, driven by a Faradaic reaction that starts after addition of a small amount of redox-active ions, as function of dimensionless time, t^* , and parameter β explained in the text ($C_S^*/c_{\infty,R} = 25$, $c_{\infty,\text{salt}}/c_{\infty,R} = 10$, $z_O = z_R + 1 = 3$).

equilibrium potential, $\phi_{\text{EDL}}|_{\text{eq}}$, does not depend on $c_{\infty,\text{salt}}$ but the equilibrium charge σ_{elec} does. Thus, a change in salt concentration (while keeping the ratio of $c_{\infty,O}$ over $c_{\infty,R}$ the same), will result in charging of the electrode particle, but the electrode potential will not change.ⁱ

16.3 A Faradaic electrode going to steady-state

The calculation in the previous section was about an isolated particle where Faradaic reactions take place upon a change in the concentration of redox-active ions, as well as of inert ions (via their influence on the structure of the EDL). In the present section we discuss an electrode that is electrically connected to another electrode, and thus we can also inject current. In this case the steady-state is not arrived at when the Faradaic reaction rate is zero, as in the prior example, but we have steady state when the Faradaic reaction rate is the same as the current injected into the electrode. Between start-up and reaching steady state, charge and potential in the electrode change.

Thus in this case the charge balance of the electrode is

$$\frac{\partial \sigma_{\text{elec}}}{\partial t} = R_R + I \quad (16.5)$$

where electrical current I is defined as being directed from the external circuit into the electrode, and it has the same unit as R_R (which is moles per volume per time). It can be

ⁱAt least, before and well after the addition, it is the same. It can be different while the system readjusts.

multiplied by the total electrode (micropore) volume, and by Faraday's number F , to arrive at a current with unit A.

In the steady state, Eq. (16.5) shows that $R_R + I = 0$, thus if electrical charge is injected in the electrode (i.e., electrons are extracted), then R_R is negative, i.e., the reaction goes in the direction of ions being oxidized (for instance, Fe^{2+} converting to Fe^{3+}).

We can make a calculation where starting at a certain charge, we apply a negative current and thus a reduction reaction will take place in the electrode. A first calculation is to find the current at which the equilibrium electrode charge is zero. In that case both ϕ_D and ϕ_S are zero, and based on $R_R + I = 0$ for steady state, from Eq. (16.1) we arrive at: $-I = k_R c_{\infty, O} - k_O c_{\infty, R}$, or in dimensionless notation: $I^* = I/k_O c_{\infty, R} = 1 - \beta$. Indeed, in the calculation shown in Fig. 16.2 for $\beta = 5$, the electrode remains uncharged for a current $I^* = -4$. For currents more positive, the electrode charge (at steady state) is positive, while it is negative for more negative currents. Thus, interestingly, there is a range of currents, $-4 < I^* < 0$, where current and electrode charge have different signs. Only for $\beta = 1$ do electrode charge and current always have the same sign (at least at steady state).

Fig. 16.2A shows the approach to steady state for an electrode to which we apply a certain current, starting at the situation that the electrode was uncharged. In this particular calculation with $\beta = 5$, this implies that until $t = 0$ the current was $I^* = -4$. Thus when we change the current I^* to zero, the charge increases to $\sigma^* = 18$, while for negative currents, $I^* = -1, -2, -3$, the final electrode charge is lower, and reached sooner. For currents more negative than $I^* = -4$ the electrode charge goes to negative values, and reaches the steady state quickly, e.g., for $I^* = -10$ we reach the steady state electrode charge of $\sigma^* = -5$ after a time $t^* = 2$.

In Fig. 16.2B, we analyze in more detail the steady state, or 'final', charge as function of the parameter β , and the applied current, I^* . The results are highly intriguing and not very intuitive, even while we have such a simple model. We notice that negative currents can be achieved without problem, but on the positive I^* -branch, the behavior is quite unexpected, with a local maximum in current, the more pronounced for low β , and then a limiting value of current when $\sigma_{SS}^* \rightarrow \infty$. The asymmetry between $+I^*$ and $-I^*$ relates to the valencies of the redox couple being in this case $z_R = 2$ and $z_O = 3$, and the asymmetry would be gone for the hypothetical cases of $z_R = -1/2$ and $z_O = 1/2$, but other than that there are no quick and easy interpretations of these results. They do point out how a simple Faradaic reaction, in combination with an EDL structure model, can result in unexpected behavior, with the current non-linearly related to charge; the same steady state current I^* can even be achieved at two different values of charge. In many physical problems, having multiple (physically valid) solutions often leads to intriguing behavior, including the possibility of bifurcation,

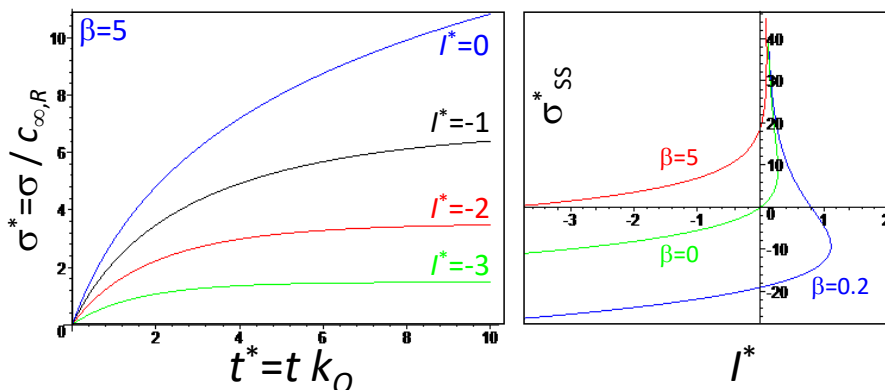


Fig. 16.2: A). Response of the electrode charge to a step change in current (starting at zero charge) for a Faradaic electrode, in solution with inert salt and a small amount of redox-active ions, as function of dimensionless time t^* and current I^* . B). Steady state relationship between current and electrode charge for different values of β . For parameter settings, see main text and Fig. 16.1.

etc.

Cyclic Voltammetry for a capacitive-Faradaic system. It is interesting to study what is the outcome of a simple cyclic voltammetry experiment for an electrode with this Faradaic reaction and EDL model. CV experiments are dynamic and thus the peculiar behaviour reported in Fig. 16.2B might play a significant role. However, CV diagrams we theoretically arrived at do not show very elucidating features, see Fig. 16.3. Here we show at the very left a diagram *without* Faradaic reactions, only the capacitive charging of the electrode based on the Donnan EDL model. Going right, the Faradaic reaction rate steadily increases (k_O and k_R are both increased by a factor 10 going from panel B to C to D). Consequently, the symmetric ‘capacitive’ profile in panel A gradually fades away to become a rather indistinct profile in panel D. Based on this calculation we like to advise that diagrams obtained in a CV experiment, for this (and other?) capacitive-Faradaic processes, are not a very useful starting point to study the underlying capacitive or Faradaic behavior. While the actual electrode kinetics can be very spectacular –see Fig. 16.2 for $\beta = 1/5$ – not much of particular interest can be read off from the CV diagrams. Thus, this example suggests that the use of CV diagrams as a means of obtaining useful information on an electrode process, may not be very easy for a combined capacitive-Faradaic process. Other methods ($i - V$

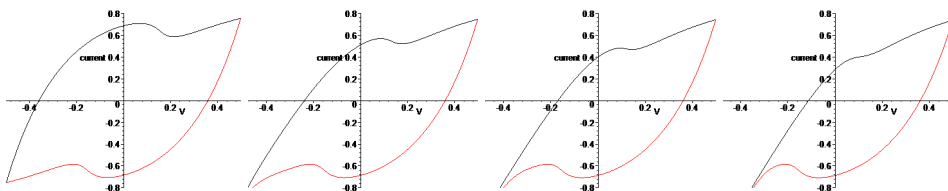


Fig. 16.3: Theoretical CV diagrams of an example of a capacitive-Faradaic process, with only capacitive EDL charging on the left, and increasing participation of Faradaic charging moving right (Parameter settings in main text, and box).

curve, charge titration, fixed current, see Ch. 22) may be useful to consider. [The CV calculation is made with parameter settings as before, including cycling of the applied potential V_{applied} between -0.5 V and $+0.5$ V, the same Faradaic reaction as before, the same Stern and diffuse layer capacitances, and a scan rate of the applied voltage of $dV_{\text{applied}}/dt^* = \pm 1$ mV (per dimensionless second). Part of this voltage drops over an external resistance, $V_{\text{Ohmic}} = V_T I^* R_{\text{Ohmic}}$ with $R_{\text{Ohmic}} = 10$.]

16.4 Two capacitive electrodes with Faradaic charge loss

Now we turn our attention to an electrochemical cell with two electrodes that both are primarily capacitive: they store charge without any loss, and thus when we transfer current for some time from one electrode to the other, and then we reverse the current direction, then when the same total current is transferred back, the electrodes have again the same charge as before. Thus, for such purely capacitive electrodes, the charge at the end of the cycle is the same as at the start.

If both electrodes are purely capacitive, this situation is not very spectacular. With a constant capacitance C (let's assume the same in both electrodes, and independent of charge), and with a certain charge Σ transferred, the electrode potential in each of the electrodes becomes Σ/C , and these two potentials can be added up to give the final charging cell voltage (if the electrodes were uncharged before the current was applied). When we reverse the current we go back to a zero cell voltage at the end of the cycle, and this will continue unchanged cycle after cycle.

But what now if one of the two electrodes ‘loses charge’ by an undesired Faradaic reaction. The first question then is, don’t we automatically have a Faradaic reaction in the other electrode as well? Or more generally, can we have one Faradaic electrode, and one capacitive electrode? The answer to the first question is ‘no’ (no need for a Faradaic reaction in both electrodes at the same time) and to the second, ‘yes’ (yes, we can have a working electrochemical cell with one Faradaic electrode and one capacitive). These asymmetric situations are possible, but not forever. At one point, when the limit cycle is reached, the cycle-averaged Faradaic reaction rate becomes the same in each electrode. But a lot of time can proceed before we arrive in that final situation.

One conclusion we arrive at is, that for galvanostatic operation, where equal charge is pushed back and forth in a cycle, or when at least one electrode is purely capacitive, in both electrodes the cycle-averaged Faradaic reaction rate must become zero.

To illustrate this statement, we make a calculation with two capacitive electrodes with one also subjected to a Faradaic reaction. We use the same equations as in the prior section, which assume a Faradaic reaction based on an oxidant and reductant molecule (redox couple). We will assume this reaction to only take place in one electrode, the cathode. At the same time the anode is purely capacitive, thus the charge we push into the anode, Σ , during charging, is simply returned in full during discharge. Thus we do not have to consider this electrode further. But in the cathode, part of Σ ‘leaks away’. But how does that work, how is that possible, isn’t there some law of charge balance that is violated? The answer is that no laws are violated, and we can have a situation with a nonzero Faradaic rate in one electrode and not the other. However, this can only continue for finite periods of time, not forever.

In such a calculation, if we would model an electrode pair where in the cathode we have a Faradaic reaction with a reaction rate that continues unchanged, then indeed we arrive at situations that are impossible. However, the Faradaic rate depends on the charge of the electrode, and thus can go down, reach zero, and reverse sign. If it would always be positive, even though small, theoretically the system will ultimately ‘diverge.’ Thus, in reality this is also not the case. The first possible option is that that beyond a certain electrode charge the Faradaic reaction becomes zero, and then the system will take the electrode charge into that ‘inert’ region. But more likely, during a cycle the electrode charge will go up and down in such a way that the Faradaic reaction rate is positive during one part of the cycle and negative in another part of the cycle. Either this is the same reaction going in reverse, or it is another reaction. In any case, after many cycles of charge and discharge, the cathode has leaked so much charge that now, averaged over a full cycle, the total Faradaic current of that electrode becomes zero. The entire operation is a very interesting –self-stabilizing– system, with any perturbation quickly damped out. Both in reality and in a correct theory,

a difference between anode and cathode in the cycle-averaged Faradaic current will lead to charge loss in one or both of the electrodes until the two cycle-averaged Faradaic currents are the same again.

So what does it mean to say the system has ‘lost charge’ until we reach this stable end-situation? It means that a certain amount of charge (number of Coulombs) has been taken from the electronic side of the electrodes, and made to react with ions to other ions. In some way this is similar to the calculation in the first section above, where a single electrode particle takes up charge and converts ions to other ions. The only difference is that now it is a two-electrode system that does this. If the two electrodes would be short-circuited, there is now one overall non-zero electronic charge, as if they together had been charged up by a third electrode. That value of the total electronic charge in the two electrodes together, is the one that results in a ‘stable cycle’ where the cycle-averaged Faradaic current in one electrode is equal to that in the other.

In Fig. 16.4 we show a calculation example of two capacitive electrodes where the cathode is also subjected to a Faradaic reaction, and we show here the cell voltage between the two electrodes vs. time, and the cathode electronic charge. For the chosen parameter settings (available from the authors), we can see how the cell voltage changes from cycle to cycle, but the changes dampen out later on, and the same holds for the cathodic charge, σ_C , which started off to be negative only, but in later cycles switches between positive to negative within a cycle.

Interestingly, a separate calculation gave the following result. In this calculation we allow the same electrode reaction to happen not only in the cathode but also in the anode, i.e., mathematically the two electrodes are now treated the same. Nevertheless, they behave very differently for many cycles from the start, just because of the way we start the charge/discharge cycle. Because we start the very first half-cycle by charging the cathode negatively (which attracts cations) and the anode positively (attracting anions), the electrode reaction (that in our example involves divalent and trivalent cations) is not occurring in any measure in the anode, even though mathematically it would be allowed. In the calculation related to Fig. 16.4 the Faradaic reaction is not taking off in the anode even after 100 cycles.

What happens thereafter, we cannot give a definite answer, but it seems that a symmetric situation does arise after many cycles, where ultimately the two electrodes behave the same, and with the charge and discharge steps becoming indistinguishable. The cell voltage now cycles between two values that (in magnitude) are the same. But in this particular calculation thousands of cycles were necessary to arrive in this situation. Thus, we can again conclude that capacitive-Faradaic processes demonstrate many peculiar features, some quite resistant to being readily understood.

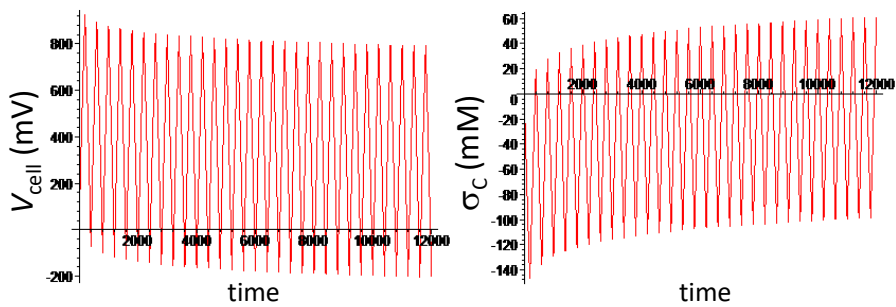


Fig. 16.4: Cell voltage and cathode charge for a capacitive cell pair that is cyclically charged and discharged at constant current for fixed periods of time. A Faradaic reaction takes place in the cathode. The cycle gradually levels out to a situation where the average Faradaic rate in the cathode approaches zero. In the meantime, the cathode has 'lost' charge.

Part V

Bio-electrochemical processes

Bioelectrochemical systems (BES) are electrochemical cells that use micro-organisms as the catalyst of reactions at one of the electrodes. A BES provides routes for

- the conversion of chemical energy stored in organic material into electricity in the microbial fuel cell (MFC),
- the production of valuable chemicals, such as H₂, using electricity in the microbial electrolysis cell (MEC), and
- the conversion of CO₂ into acetate, using electricity (the microbial electrosynthesis cell (MES)).

In the MFC and MEC, a biofilm is formed at the anode and there micro-organisms oxidize organic matter (the 'substrate'). Electrons are produced and are transported via an electrical circuit to the cathode, where they are used for the reduction of oxygen gas to OH⁻ ions (MFC) or for the reduction of protons to hydrogen gas (MEC). In an MFC, overall the reaction is thermodynamically favorable, and therefore electrical energy can be recovered. However, in an MEC or MES cell, electrical energy is required to drive the reaction, and the energy from the aqueous organic streams together with the electrical energy input is (partially) recovered as chemical energy in the form of hydrogen gas (H₂). In another type of bioelectrochemical system, the MEC, a biofilm grows at the cathode. These cells provide a sustainable route for the conversion of, for example, CO₂ into valuable chemicals, such as acetate, using electricity.

Fig. V-1 presents typical examples of the polarization curve for a microbial fuel cell (MFC), a microbial electrolysis cell (MEC) and a microbial electrosynthesis (MES) cell. The overall reaction occurring in an MFC, which is the conversion of organic matter such as acetate with oxygen to bicarbonate and water, is exactly opposite to the reaction occurring in a microbial electrosynthesis (MES) system. Currents produced in an MFC are up to ~ 10 A/m² for anode potentials between -0.3 and -0.5 V (vs. Ag/AgCl). The maximum current, *I*_{SC}, is reached when the system is short-circuited, when anode and cathode potential are equal, both in magnitude and sign. When we work with an anaerobic cathode, oxygen reduction is not possible, and with an input of electrical energy, hydrogen evolves at the cathode, which makes the system operate as an MEC (lower left side of the diagram). On the right-hand side of the diagram, we can reverse operation of the MFC and operate the system as a cell for MES. In this case, the production of acetate or other organic molecules requires a more negative cathode potential of at least -0.8 V vs. Ag/AgCl, while the overpotential at the anode is even higher, with typical anode operating potentials above +1.3 V vs. Ag/AgCl. While MFCs cannot reach a current higher than the short circuit current, when anode and

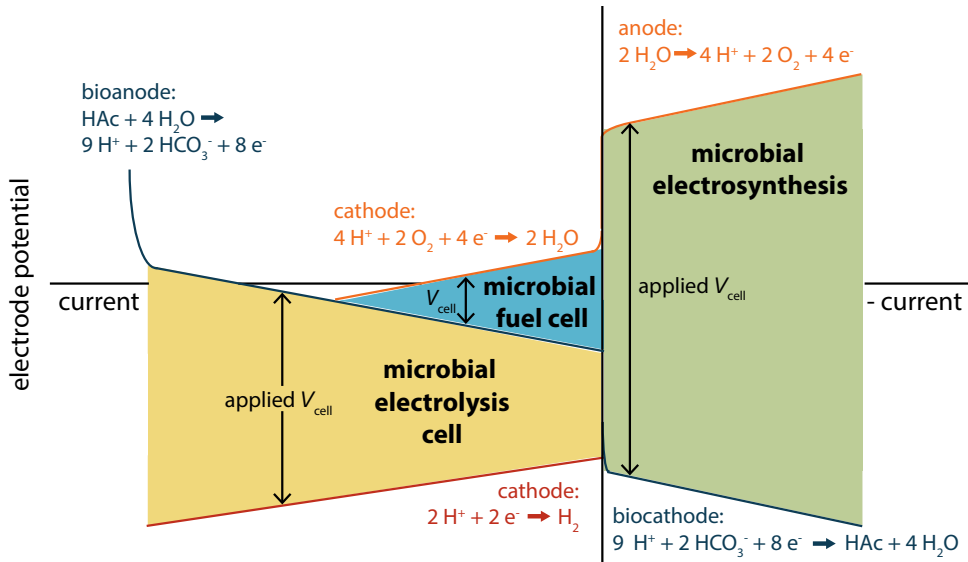


Fig. V-1: Representation of the polarization curve, i.e., the relation between voltage and current, for steady state conditions, for three bioelectrochemical systems: the microbial fuel cell (MFC), the microbial electrolysis cell (MEC), and cells for microbial electrosynthesis (MES).

cathode potential are equal, an MES cell can, in principle, be driven to increasingly higher rates, as long as sufficient energy (applied voltage) is invested in the reaction.

Ion transport in bioelectrochemical systems

Bioelectrochemical systems are electrochemical cells that use micro-organisms as the catalyst of reactions at one of the electrodes. Bioelectrochemical systems provide routes for the conversion of chemical energy stored in organic material, into electricity, or for the production of valuable chemicals, such as hydrogen and acetate, using electricity. A biofilm grows at the anode where micro-organisms oxidize organic matter, or it grows at the cathode where micro-organisms produce organic chemicals. In this chapter, we present a general approach to describe ion transport, amongst others across ion-exchange membranes, in a bioelectrochemical system. We include electrochemical reactions at the electrodes, as well as the acid-base reactions that take place in solution and in the membranes.

17.1 Ion transport in bioelectrochemical systems

In this chapter, we present a system-level model to study transport of a mixture of ions in bioelectrochemical systems, in combination with acid-base reactions at the electrodes and in solution, as well as ion transport across membranes that are placed in the cell, see Fig. 17.1.

In an electrochemical cell, the electrical current directly relates to the reaction rates both on the anode and on the cathode, and relates to the ionic current in the system. The reaction stoichiometry of the electrode reactions, together with the selectivities imposed by the membranes, determines the ionic fluxes, protonation degrees of all acid-base species, and changes in pH. An example geometry is shown in Fig. 17.1. This design includes two ion exchange membranes in a cell where acetate is produced at the (bio)cathode and transported to the extraction compartment where it is extracted from solution. Other designs use only one ion-exchange membrane.

In many bioelectrochemical systems the following (groups of) ionic species play an important role:

- organic material, which is either converted or produced at one of the electrodes, in this chapter represented by the model component acetate, which can be in an ionized form, Ac^- , or neutral (protonated) as HAc ;
- carbonic acid ions (H_2CO_3 , HCO_3^- , and CO_3^{2-});
- buffer ions, added to adjust the pH, here represented by HB and B^- . In Fig. 17.1 HSO_4^- and SO_4^{2-} are buffer ions;
- inert cations, such as Na^+ ;
- inert anions, such as Cl^- ;
- the hydronium ionsⁱ and hydroxyl ions (H_3O^+ and OH^-).

For many reasons as explained in Fig. 10, it is of significant utility and elegance to assume that all acid-base reactions are at local equilibrium, i.e., the acid-base reactions are much faster than the rates of transport of ions. This assumption can be made for all groups of ions, which are for instance $\text{HAc} \rightleftharpoons \text{Ac}^-$, $\text{H}_2\text{O} \rightleftharpoons \text{OH}^- + \text{H}^+$, for $\text{H}_2\text{CO}_3 \rightleftharpoons \text{HCO}_3^- \rightleftharpoons \text{CO}_3^{2-}$, and for $\text{B}^- \rightleftharpoons \text{HB}$.

A key element in many bioelectrochemical systems are ion-exchange membranes (IEMs) placed in the system, and transport of all these ions through the IEMs must be described by the theory. In this chapter we discuss ion transport theory for a membrane with a single

ⁱWe use the terminology of protons (H^+) and hydronium ions (H_3O^+) interchangeably.

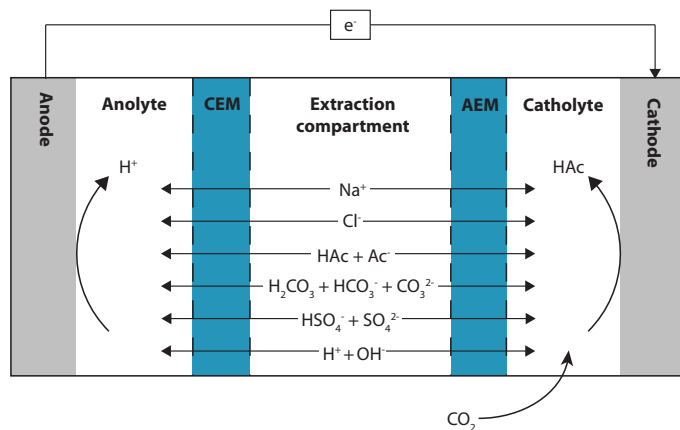


Fig. 17.1: Schematic view of ion transport and electrode reactions in one example geometry of a microbial electrosynthesis (MES) cell where acetate is produced from CO_2 and transported through an anion-exchange membrane (AEM) to the extraction compartment that it is in the middle of the cell.

charge sign (either an AEM or CEM). As we will explain later on, a bipolar membrane (BPM) can be modelled as a combination of an AEM and a CEM, in direct contact, with a layer of vanishingly small thickness in between. IEMs are characterized by their fixed membrane charge density which leads to selective transport, with counterion transport enhanced, and transport of co-ions hindered. Counterions are ions with a charge sign opposite to that of the membrane fixed charge groups, while co-ions have the same charge sign as the membrane. We can distinguish between an anion-exchange membrane (AEM), where anions are the counterions, and a cation-exchange membrane (CEM), where cations are the counterions. The transport of uncharged species is not directly influenced by the charge of the membrane, and they are transported through the membrane by diffusional forces only, neither accelerated nor retarded by the electrical field.

In this theoretical approach all fluxes are self-consistently calculated without the need to prescribe any of them. We do not need to set up ion mass balances in the ions H^+ or OH^- , which is one of the elegant aspects of the present modelling approach. We also do not need to know whether it is the H^+ -ion or the OH^- -ion that takes part in a certain electrode reaction, and this certainly makes the calculation of the electrode reactions much more straightforward. Instead, the theory will *predict* what are the fluxes of H^+ and OH^- at the electrodes and what will be pH there.

17.2 Ion transport in ion-exchange membranes

Diffusion and electromigration of ions through an IEM are described by the Nernst-Planck equation

$$J_i = -D_{m,i} \cdot \left(\frac{\partial c_{m,i}}{\partial x} + z_i c_{m,i} \frac{\partial \phi}{\partial x} \right) \quad (17.1)$$

where subscript i refers to ion type i , J is the ionic flux (mol/m²/s), D_m the diffusion coefficient in the membrane (m²/s), c_m is the ion concentration per volume aqueous phase in the membrane (mol/m³), x is the position in the membrane, z is the ion valency (e.g., +1 for Na⁺), and ϕ is the dimensionless electrical potential, which can be multiplied by the thermal voltage, $V_T = RT/F$, with R the gas constant (J/mol/K), T temperature (K), and F Faraday's constant (C/mol), to obtain the voltage with dimension V. The diffusion coefficient in the membrane is a certain fraction d_f of the value in free (dilute) solution, $D_{aq,i}$. We neglect in Eq. (17.1) advection of ions due to volumetric (water) flow through the IEMs, as discussed in the preceding chapters.

At each position in the membrane, mass conservation of every species is given by

$$\frac{\partial c_{m,i}}{\partial t} = -\frac{\partial J_i}{\partial x} + \Gamma_i \quad (17.2)$$

with t time (s) and Γ_i the chemical formation rate of species i (mol/m³/s) because of acid-base reactions. Note that in our model Γ_i does not need to be explicitly evaluated, and below we discuss how this is achieved.

The reaction-terms, Γ , are dealt with as follows. For the inert anions and cations, Eq. (17.2) is used with Γ_i set to zero. For all ions that undergo acid-base reactions, Eq. (17.2) is analysed per group of ions, in such a way that Γ_i disappears. (Note that this part of the analysis is valid irrespective of the kinetic rate of the reaction, fast or slow.) In many bioelectrochemical systems, at least the following groups of acid-base reactive ions must be considered: the organic material (group a), and carbonic acid species (group c). Taking acetate as a model species for group a, then we have the species HAc and Ac⁻, which react according to $\text{HAc} \rightleftharpoons \text{Ac}^-$. Group c consists of H₂CO₃, HCO₃⁻ and CO₃²⁻ which react according to $\text{H}_2\text{CO}_3 \rightleftharpoons \text{HCO}_3^- + \text{H}^+$ and $\text{HCO}_3^- \rightleftharpoons \text{CO}_3^{2-} + \text{H}^+$. As we discuss below, for the 'water ions', H⁺ and OH⁻, a balance such as Eq. (17.2) does not need to be set up but instead the more intuitive charge balance is used, which is Eq. (17.4) below.

How does Γ_i cancel out for each group of ions? Let us illustrate this by deriving a mass balance for group a. Independent of kinetics, at every moment and at every position, the formation of HAc is equal to the consumption of Ac⁻, i.e., $\Gamma_{\text{HAc}} + \Gamma_{\text{Ac}^-} = 0$, and we can sum

Eq. (17.2) over HAc and Ac^- , to derive a mass balance for group a where the production terms, Γ_i , cancel out. The combined mass balance becomesⁱⁱ

$$\frac{\partial}{\partial t} ([\text{HAc}]_m + [\text{HAc}^-]_m) = -\frac{\partial}{\partial x} (J_{\text{HAc}} + J_{\text{Ac}^-}) . \quad (17.3)$$

Note that Eq. (17.3) is valid irrespective of the reaction rates, fast or slow. For group C, we use a similar approach, but with three ionic species, and thus we consider two chemical reactions. In this case, the three formation rates sum up to zero: $\Gamma_{\text{H}_2\text{CO}_3} + \Gamma_{\text{HCO}_3^-} + \Gamma_{\text{CO}_3^{2-}} = 0$, and we derive a mass balance for group c, similar to that of a, where the production terms, Γ_i , cancel out.

A similar balance describes how the local ionic charge density does not change in time,

$$\frac{\partial}{\partial t} \sum_i z_i c_{m,i} = -\frac{\partial}{\partial x} \sum_i z_i J_i \quad (17.4)$$

where the summation runs over all ions, including H^+ and OH^- . Because charge cannot accumulate, the lhs in this equation is always zero, not just in steady state, but also for a dynamic problem.

Related, at each position in the membrane, local electroneutrality holds,

$$\sum_i z_i c_{m,i} + \omega |X| = 0 \quad (17.5)$$

where ω is the sign of the membrane charge (+1 for an AEM and -1 for a CEM) and X is the membrane charge expressed in moles per unit aqueous phase in the membrane. Again, the summation over i includes all ions present in the system.

The above mass balances are valid for fast and slow acid-base reactions alike. When we assume the acid-base reactions to be fast, we can make use of equilibria such as

$$K_a = \frac{[\text{Ac}^-][\text{H}^+]}{[\text{HAc}]}, K_{c1} = \frac{[\text{HCO}_3^-][\text{H}^+]}{[\text{H}_2\text{CO}_3]}, K_{c2} = \frac{[\text{CO}_3^{2-}][\text{H}^+]}{[\text{HCO}_3^-]}, \quad (17.6)$$

$$K_w = [\text{OH}^-][\text{H}^+]$$

which we can solve jointly with the mass balances per group at each position in the membrane.

This membrane model must be solved together with Donnan equilibria at the two membrane outer surfaces

$$c_{m,i} = c_{\infty,i} \cdot \exp(-z_i \cdot \Delta\phi_D) \quad (17.7)$$

ⁱⁱNote that in this book we use both the notation $[..]$ and the symbol c to describe concentrations.

where subscript ∞ refers to the concentration in solution, i.e., outside the membrane, and where $\Delta\phi_D$ is the Donnan potential, i.e. the potential just inside the membrane, minus that in solution. Finally, fluxes across the membrane in groups of ions must be evaluated, and must be related to the ionic current density, as discussed in Dykstra *et al*, Water Research (2021). A bipolar membrane (BPM) placed in a bioelectrochemical cell can be modelled as a combination of an AEM and a CEM placed in direct contact. Thus, the theoretical framework presented above for transport in an AEM or CEM can also be used to evaluate ion transport in a BPM.

Steady-state membrane transport. Often the changes in the compartments next to a membrane are much slower than the timescale of ion transport across an ion-exchange membrane. Then one can make the assumption of local steady-state in the membrane, and set the accumulation term, $\partial c_{m,i}/\partial t$, in mass balances to zero. In that case ion transport is constant across the membrane for unreactive ions such as Na^+ and Cl^- . For these species, to calculate the flux across the membrane, we combine Eqs. (17.1) and (17.2), integrate across the membrane, and arrive at

$$J_i = -\frac{D_{m,i}}{L_m} \cdot \left(c_{m,1,i} - c_{m,0,i} + z_i \int_{\phi_0}^{\phi_1} c_{m,i} \, d\phi \right) \quad (17.8)$$

which can be implemented in the overall ‘stirred tank’ mass balances for the flow compartments. In Eq. (17.8) subscripts ‘0’ and ‘1’ refer to the very left and very right sides, just in the membrane, and L_m is the membrane thickness. For the flux of a group of species (e.g., the HAc and Ac^- ions that together form the acetate group), we can evaluate Eq. (17.8) for each ion and add up. This summation is then the total flux of that group. Note, for such acid-base reactive species, the individual integrated expression, like J_{Ac^-} , calculated on the basis of Eq. (17.8), has no physical meaning, but only the summation of J_{Ac^-} and J_{HAc} has a physical meaning, as the total flux of the group of these two ions together. Similarly, we can evaluate for each ion J_i according to Eq. (17.8), multiply by the ion valency, z_i , to obtain the ionic current, J_{ch} , which is invariant across the membrane, i.e., $J_{\text{ch}} = \sum_i z_i J_i$, with J_i from Eq. (17.8). This ionic current is the same in each membrane (when area A is the same) and directly relates to the applied current density.

17.3 Mass balances for the anolyte and catholyte compartments

To evaluate ion concentrations in the separate compartments in a bioelectrochemical cell, we can again use the various detailed models including diffusion and dispersion as explained for instance in Chs. 7 and 12. However, because of the relatively low transport rates through the membranes in bioelectrochemical systems, concentration gradients in the flow compartments are small, and we can often model each of these compartments as a single ideally stirred tank reactor, and then following balances can be used for each ion

$$V_k \cdot \frac{\partial c_{k,i}}{\partial t} = A \cdot \sum_j J_{k,j,i} + V_k \cdot \Gamma_{k,i} \quad (17.9)$$

where \sum_j refers to the fluxes through the sides of the compartment, which are either membranes or electrodes, to be discussed below. In Eq. (17.9) A is the area of one membrane (i.e., the cross-area of the compartment, or cell) and V_k is the volume of aqueous phase in each compartment. Often the flow channel is fed from a larger exterior volume and its outflow is fed back there; V_k then refers to the volume of this complete cycle (exterior container, tubing, flow compartment).

For each inert cation and anion, Eq. (17.9) is evaluated with $\Gamma_{k,i} = 0$, while for the ions in the a, b and c-groups the balance is summed over all ionic species in a group, such that the $\Gamma_{k,i}$ terms cancel out, as described in Section 17.2. We can also sum over all species multiplied with their valency, z_i , to obtain the condition of electroneutrality to be evaluated in each compartment,

$$\sum_i z_i c_{k,i} = 0. \quad (17.10)$$

In each compartment mass balance, Eq. (17.9), two boundary fluxes J_i must be implemented. First of all there are the fluxes through the membranes. Note that each membrane flux will show up in two compartment balances, once as a positive contribution, once negative. Making use of the coordinate system as in Fig. 17.1, where the coordinate x -axis runs from left to right (and thus the fluxes J_i are defined positive towards the right), then a (membrane) flux entering the compartment on the lhs is taken as a positive contribution ('with a plus-sign') and a flux leaving on the rhs is implemented as a negative contribution ('with minus sign'). Secondly, there are contributions due to the electrode reactions, and these will be explained in the next section.

Electrolytes in compartments can be in equilibrium with air that can contain an absorbing species such as ammonia or CO_2 . Taking CO_2 as an example, we can then relate the partial

pressure of that component, in this case p_{CO_2} , to the concentration in solution of carbonic acid, H_2CO_3 , according to Henry's law

$$[\text{H}_2\text{CO}_3] = K_{\text{H},c} \cdot p_{\text{CO}_2} \quad (17.11)$$

with $K_{\text{H},c}$ Henry's coefficient for CO_2 -adsorption ($K_{\text{H},c} = 33.46 \text{ mM/bar}$). For H_2CO_3 , we assume that the equilibration between unhydrated CO_2 and hydrated H_2CO_3 in water is fast. When for a certain group, such as here the carbonate group, an equation such as Eq. (17.11) is used, then an overall mass balance, such as Eq. (17.9), no longer needs to be evaluated.

17.4 Electrode reactions

We can now proceed to explain how electrode reactions can be included in this theoretical framework. First of all, for the inert anions and cations, we simply have a zero reaction flux at each electrode. And the same holds for a group such as $\text{HB} + \text{B}^-$ that does not participate in an electrode reaction. Thus the flux at the electrode of this group as a whole is zero, i.e., at the electrode we have $J_{\text{HB}} + J_{\text{B}^-} = 0$. This does not imply that the flux of individual species, such as B^- , is zero there! Far from it. Instead, typically both fluxes have significant values, and because they are in opposite directions, effectively this b-group as a whole can 'deliver protons' to the surface. Thus, in the mass balances for the anolyte and catholyte compartments for inert ions, and for a group that is not reactive, such as the b-group, the electrode flux is zero and only a flux of ions through the membrane must be included.

This only leaves us to discuss how the electrode reactions impact the balances for the c- and a-groups. Note first of all, we do not need to consider which ion is involved in the electrode reaction. Thus, whether it is HAc or Ac^- that is formed at the electrode does not need to be pre-specified. Instead, the model will tell us the outcome, it will self-consistently calculate (i.e., predict) in which form the species will form at the surface. Note again that OH^- and H^+ do not need to be explicitly considered in relating electrode reaction rates to the current, as illustrated next.

Here we describe the electrode reactions as considered in Fig. 17.1. First, let us consider the anode. Here, we assume that the only reaction that takes place is water reacting to protons and oxygen (gas). Or, equivalently, OH^- -ions react to O_2 and water. From the point of reaction stoichiometry, these two reactions are equivalent. In any case, with this reaction on the anode, there is no involvement of either the c- or a-groups in the electrode reaction. So for these two groups, the electrode reaction flux J_i is zero in the anolyte. Because these two were the only balances remaining that possibly were influenced by the electrode reactions,

we can conclude that oxygen evolution at an electrode does not explicitly show up in any of the mass balances. Nevertheless, the calculations certainly predict what are the related properties of interest, such as pH changes in the anolyte.

Second, we consider the cathode. Let us discuss how the various fluxes are linked to one another here, and are linked to the electrical current. If we first assume that the reaction of acetate from carbonate is the only reaction taking place, we can relate the consumption/production flux of ions in the a- and c-groups to the electronic current, I (in A/m^2). This is because we know that for each carbonate ion that reacts away (irrespective of whether it is H_2CO_3 , HCO_3^- or CO_3^{2-}), four electrons enter into solution (from the electrode), while for each two carbonate ions that disappear one acetate ion is formed (again, irrespective of which ion from the a-group). This is quantified as

$$I/F \cdot CE = 4 \cdot J_{H_2CO_3+HCO_3^-+CO_3^{2-}}^e = -8 \cdot J_{HAc+Ac^-}^e \quad (17.12)$$

where superscripts e are implemented to distinguish this electrode flux from the membrane fluxes. In the ideal case just discussed, all electronic current is used to convert carbonate into acetate, and thus the Coulombic efficiency, CE, is unity ($CE = 1$). However, often also other reactions take place, involving water and the H^+ and OH^- ions, or other ions, which implies the Coulombic efficiency is less than unity. If no other reactions are considered but the carbonate to acetate reaction discussed above, and if CE is measured to be a number less than unity, this implies that the remainder of the electronic current is involved in a reaction with water, H^+ and/or OH^- . That part of the current does not show up in any of the mass balances. Instead, it is automatically accounted for because of the assumption of electroneutrality in each compartment.

17.5 Example of a membrane-electrode assembly with gas evolution

In this section we provide example results of a calculation of the transport and reaction in a system with many ions, of which many are an element of an acid-base reactive group, such as the group of ammonium/ammonia ions. The ions diffuse through an ion-exchange membrane towards an electrode that does two things at the same time: it is a cathode where H_2 is produced and thus a cationic current is set up directed towards this electrode, and it allows for evaporation of H_2 , NH_3 , CO_2 and H_2O , i.e., we have a G/L interface and physical exchange between dissolved molecules and gas phase molecules.

One prediction of the calculation is that even though the ionic current through the membrane is fully carried by the ammonium cation moving towards the cathode, where it fully converts to ammonia, it is not the case that the ammonia evaporation rate is the same as the current, but instead it is much less. This is because a lot of ammonia formed at the cathode stays in the aqueous phase and diffuses back through the membrane to the anode chamber, see Fig. 17.2. This complex example with multiple ions and reactive groups, a cathode and an evaporating interface, is solved quite easily using the theory outlined in the present chapter. These calculations are relevant because they clarify the relevance of membrane charge density, current rates, gas flow rates, etc., for this system, and are helpful in optimization and design of this and similar (bioelectrochemical) systems.

Similar calculations are possible for many other electrode reactions involving ions that can undergo acid-base reactions and have an equilibrium with an adjoining gas phase, e.g., for (microbial) electrosynthesis, CO₂ capture, etc.

Thus, we describe next the theory and illustrate with some calculation results of a particular example of a bioelectrochemical system, one where hydrogen gas is produced at a cathode in front of which a cation-exchange membrane is placed. In the system are not only inert ions and ‘water ions’, but also bicarbonate ions, acetate ions, and ammonia ions. Thus we must describe ion transport through a membrane of all of these species, and reaction at the cathode towards H₂-gas, as well as the evaporation of H₂, CO₂, NH₃ and H₂O; here, see Fig. 17.2.

In the cathode, we link the various fluxes (production of H₂, evaporation of NH₃ and CO₂) to one another, and to the electrical current. Assuming that hydrogen gas formation is the only electrode reaction, and that the absorption of H₂ in the liquid phase is zero, we can relate the hydrogen gas production flux $J_{\text{H}_2}^{\text{evap}}$ (flow rate per unit membrane area, in mol m⁻² s⁻¹) to the current, I (A m⁻²), by

$$I = 2 \cdot F \cdot J_{\text{H}_2}^{\text{evap}} \quad (17.13)$$

where the factor ‘2’ is due to the fact that always two electrons are required to form one hydrogen gas molecule.

The sum of the ionic fluxes (mol m⁻² s⁻¹) of NH₃, $J_{\text{NH}_3}^{\text{C}}$, and NH₄⁺, $J_{\text{NH}_4^+}^{\text{C}}$, through the membrane, evaluated at the edge with the cathode (denoted by superscript ‘C’ from this point onward), equals the evaporation flux of NH₃, $J_{\text{NH}_3}^{\text{evap}}$ (mol m⁻² s⁻¹)

$$J_{\text{NH}_3}^{\text{evap}} = J_{\text{NH}_4^+}^{\text{C}} + J_{\text{NH}_3}^{\text{C}} \quad (17.14)$$

This is quite interesting, that it is the sum of the fluxes of ammonia and ammonium in the membrane that together are equal to the ammonia gaseous evaporative flux. This relates to

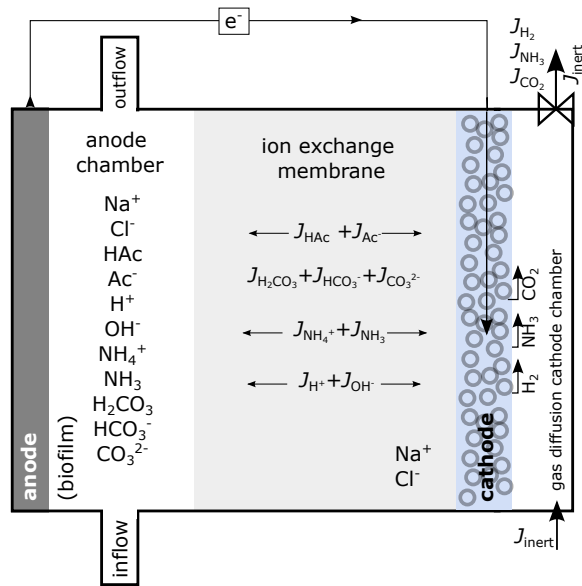


Fig. 17.2: Schematic view of ion transport through an ion-exchange membrane from a solution containing many types of ions that are inert or are part of an acid-base reactive group such as $\text{NH}_4^+/\text{NH}_3$. In the cathode H_2 forms and H_2 , CO_2 , NH_3 and water evaporate..

the use of a model with infinitely fast $\text{NH}_3 \leftrightarrow \text{NH}_4^+$ equilibration, leading to the use of mass balances in the concentration of the total ammonia group. If instead, we would use a model with finite rates of the reaction of NH_3 to NH_4^+ , then the flux of NH_3 in the water at the G/L interface must be set equal to the evaporation flux of gaseous NH_3 , while the flux of NH_4^+ at the interface must be set to zero. Thus, the choice between a finite rate equation for $\text{NH}_3/\text{NH}_4^+$ vs. the use of an equilibrium, leads to the necessity to have two separate mass balances (in NH_3 and NH_4^+) in the first case, and setting the evaporation flux equal to the flux in solution of NH_3 only, while when we assume equilibrium between NH_3 and NH_4^+ , the evaporation flux of ammonia is set equal to the combined flux of ammonia and ammonium.

Similarly, the evaporation flux of gaseous CO_2 , $J_{\text{CO}_2}^{\text{evap}}$, relates to the membrane fluxes of H_2CO_3 , $J_{\text{H}_2\text{CO}_3}^{\text{C}}$, HCO_3^- , $J_{\text{HCO}_3^-}^{\text{C}}$, and CO_3^{2-} , $J_{\text{CO}_3^{2-}}^{\text{C}}$, in the cathode

$$J_{\text{CO}_2}^{\text{evap}} = J_{\text{H}_2\text{CO}_3}^{\text{C}} + J_{\text{HCO}_3^-}^{\text{C}} + J_{\text{CO}_3^{2-}}^{\text{C}} \quad (17.15)$$

Since HAc and Ac^- neither react in the cathode, nor evaporate, the sum of their fluxes equals zero at this interface,

$$J_{\text{HAc}}^{\text{C}} + J_{\text{Ac}^-}^{\text{C}} = 0 \quad (17.16)$$

Note that Eq. (17.16) does not imply that the individual fluxes of the ionic species HAc and Ac^- are zero at the cathode (G/L interface) nor anywhere in the membrane. Due to the acid-base reactions it is possible that one ion diffuses in one direction through the membrane, gradually converts to the other ion, which diffuses back (see however the box at p. 424). The only constraint is that at each position in the membrane the sum of the two fluxes is zero (at least, in steady-state).

Finally, the total ionic current is related to the electrical current, I , according to

$$I = F \cdot \sum_i z_i \cdot J_i^{\text{C}} \quad (17.17)$$

where we sum over all ions, including H^+ and OH^- . At the cathode, the flux of inert ions is zero and they can be excluded here (and at steady state also at all positions in the membrane), but this is not the case for ions within a group, even if the group as a whole has a zero flux. Thus, for instance Ac^- must be included in this ionic current statement.

By relating both the hydrogen gas production and the total ionic current to the electrical current via Eqs. (17.13) and (17.17), we establish the essential relationships between electronic flow and hydrogen flow, without making any statements about which ions in solution ‘carry’ the protons through the membrane, the protons which in the cathode are

converted to hydrogen gas. Thus, a reaction such as $2\text{H}^+ + 2\text{e}^- \longleftrightarrow \text{H}_2(\text{g})$ is not explicitly used in any of the equations. Instead, all ions in solution that can protonate or deprotonate, potentially participate in carrying the protons to the electrode and G/L-interface where they are converted to hydrogen gas.

In the cathode, three-phase contact between the electron-conductive matrix, the gas phase, and the liquid phase is established. We assume that the ionic transport in the electrolyte-filled porous cathode is much faster than in the membrane. Thus, we do not need to model ionic transport from the membrane through the cathode to the G/L interface. We relate the partial gas pressure of the gases CO_2 and NH_3 to the evaporative fluxes as described by Eqs. (17.14) and (17.15) according to

$$p_i = p_{\text{tot}} \cdot \frac{J_i^{\text{evap}}}{\sum_n J_n^{\text{evap}} + J_G^{\text{inert}}} \quad (17.18)$$

where p_i is the partial pressure of gas i , p_{tot} the total pressure in the cathode chamber, J_G^{inert} an inert gas flow along the cathode, and where n runs over all gases (NH_3 , H_2 and CO_2). The inert gas flow rate J_G^{inert} has dimension $\text{mol m}^{-2} \text{s}^{-1}$ by dividing its molar flow rate (mol/s), by the membrane area (m^2). The relation between the concentration of the soluble gases, in this case CO_2 and NH_3 , in the cathode, and the partial pressure of these gases, is given by Henry's law

$$c_{C,i} = K_{H,i} \cdot p_i \quad (17.19)$$

with $K_{H,i}$ Henry's coefficient and $c_{C,i}$ the ion concentration in the electrolyte within the cathode. The concentration of the ions in the cathode follows from the concentration just in the membrane according to the Donnan equilibrium, as given by Eq. (17.7). Furthermore, for the electrolyte in this electroneutral cathode layer, we use the charge neutrality equation, Eq. (17.5). This model for the cathode layer as a charge-neutral 'virtual' layer, located between the charged membrane and the G/L interface, is also used for the virtual layer at the junction between an anion-exchange and cation-exchange layer in a bipolar membrane (BPM). Note that we have not considered the evaporation of water in our model, which leads to about 3 vol% water molecules in the gas phase at ambient conditions.

Many calculations with this model are described in Dykstra *et al.* (*Phys. Rev. E* **90** 013302, 2014) and compared with data from literature. A typical result is that when a CEM is used, the ionic current is carried through the membrane completely in the form of the ammonium ion, which at the cathode 'releases' the proton, which reacts to H_2 gas. [As mentioned before, this proton release is not explicitly part of the set of equations; there is no equation for this release. It is an 'emergent' output of the model, a model that only includes the transport equation described above.] However, the evaporation flux of ammonia, NH_3 ,

is much less than this flux of NH_4^+ , for instance 30%. This implies that about 30% of the ammonia formed at the cathode (G/L interface) evaporates, and the remainder diffuses back through the membrane. The same calculation with an AEM gives very different results, with the flow of OH^- and CO_3^{2-} leftward, i.e., ‘against’ the current direction. Both these anions thus have a positive contribution to the transport number. The flux of HCO_3^- is in the direction of the current and thus contributes negatively. [As a group, the carbonate ions are not moving much, see the discussion in the box below. Effectively they are immobile but transfer a proton to the right.] The contributions of these three ions sum up to unity. At a membrane charge of around $X=1.5$ M, around 75% of the current is carried by OH^- ions, but at $X=4$ M, the contribution of OH^- has dropped to about 25%, with the remainder being what effectively is transport of H^+ , ‘piggy-backing’ with the carbonate ions. These results are presented to illustrate that many intriguing outcomes are possible, and this goes to show that the actual outcome of an experiment (or, of a transport model including acid-base reactions) can not easily be intuited a-priori. Instead, the construction and analysis of a full transport model including all acid-base reactions is highly advised.

How to understand ion transport with simultaneous acid-base reactions. In this section, when referring to the diffusion of ammonia and/or acetate, we discuss this topic as if one ion diffuses in one direction (e.g., the acetic acid neutral molecule), reacts to the other ion (gives off, or takes up, a proton; e.g. to the negative acetate ion), and then this species diffuses back. Though this sounds reasonable, it is not entirely correct. This topic was also addressed at length in Ch. 10. The point is that, for instance for the acetate species, for which the total flux in the membrane of the two ions together is zero, while the acid-base reactions are infinitely fast, it is very hard to use the language that one ion (acetic acid) moves left, the other (acetate anion) moves right. Instead, the acetate entity as a whole basically does not move at all. It might move in the one form leftward for a very short distance (a few nm?), flip to the other form (giving off the proton, or taking up a proton), and move in the reverse direction for a few nm, before it switches back again Effectively, there is no movement of the acetate molecules at all. Of course effectively each individual molecule (tracer molecule) makes a random walk across the membrane, but the language of ions moving in one form rightward across the membrane, reacting at the rightmost boundary, and moving in the other form leftward, is to a large extent misleading, even though it helps in explaining observations and even the output of the numerical code. Thus, we have a useful explanatory framework, but one that in all honesty is not a proper representation

of how in the theory we describe ion transport.

Transport and reactions in electroactive biofilms

Electroactive biofilms are biofilms located on an electrode that are able to conduct electronic charge. We present theory for ion and electron transport and the bioelectrochemical conversions inside a biofilm where organic matter converts anaerobically to CO_2 while producing electrical energy. This chapter describes how to set up a physics-based model for complex coupled processes in bioelectrochemical systems, including ion and electron transport and the biochemical molecular conversions inside the micro-organisms.

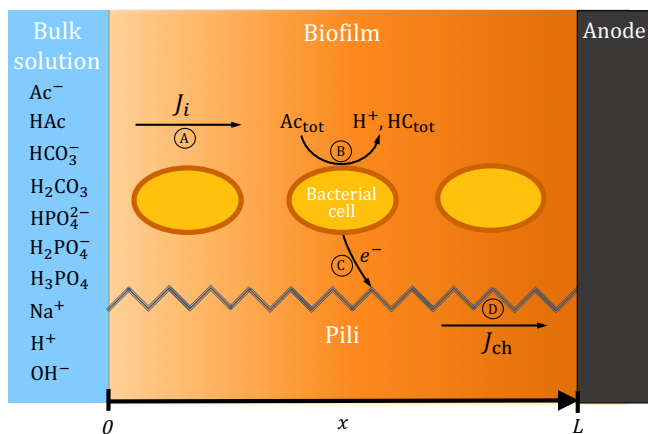


Fig. 18.1: Scheme of the coupled biofilm model, which depicts transport and bioelectrochemical reactions in four steps: (A) ion transport, J_i , across the biofilm, (B) oxidation of substrate in bacteria, (C) electron transfer to a conductive structure, and (D) charge transport, J_{ch} , to the anode.

18.1 Introduction

In a bioelectrochemical system, bacteria attach themselves directly to the surface of electrodes, forming a porous layer called “biofilm”, through which ion transport occurs. The biofilms have electron-conductive properties, with bacteria performing long-distance electron transport over tens to hundreds of micrometers, to deliver current to the electrode. Accordingly, models have so far relied upon empirical knowledge to an important extent. An important example is the Monod equation, which can be used to calculate rates of substrate utilization in biological systems. However, the dynamic processes in a BES, including biochemical reactions, ion and charge transport, can be described in a more fundamental way by a dynamic system of PDEs. In this Chapter, we present a physics-based dynamic description of ion transport, bioelectrochemical reactions, and electron transport inside conductive biofilms on electrodes.

To model an electrochemically active biofilm, we present a mathematical framework that consists of four elements, as shown in Fig. 18.1: (A) transport of substrate and products across the biofilm, (B) oxidation of substrate in the bacteria, (C) electron transfer to a conductive structure, e.g. in the form of pili, and (D) charge transport to the anode.

18.2 Mass transport across the biofilm

We focus on transport of ions and other molecules across a one-dimensional planar biofilm, with simultaneous biochemical reactions. Biofilms consist of a dispersed phase (the bacterial cells) and a continuous aqueous phase (the extracellular space, abbreviated “ES”). We define the porosity of the biofilm, p , as the ratio of the volume of the extracellular space to the total volume of the biofilm, and tortuosity, τ , as the ratio of the average transport distance inside the pores to the geometrical distance. Ion transport across the biofilm is described by the Nernst-Planck equation

$$J_i = -D_{i,e} \left(\frac{\partial c_i}{\partial x} + z_i c_i \frac{\partial \phi}{\partial x} \right) \quad (18.1)$$

where J_i is the molar flux of species i ($\text{mol m}^{-2} \text{s}^{-1}$) across the biofilm, $D_{i,e}$ the effective diffusivity of i in the biofilm ($\text{m}^2 \text{s}^{-1}$), c_i the concentration of i (mol m^{-3} or mM) in the extracellular space, z_i the valence of i (-), ϕ the dimensionless electric potential (-) and x the position in the biofilm (m). Potential ϕ can be converted to a dimensional voltage by multiplying with the thermal voltage, $V_T = RT/F$, where F is the Faraday constant (96485 C mol^{-1}), R the universal gas constant ($8.314 \text{ J K}^{-1} \text{ mol}^{-1}$) and T the temperature (298 K). Transport of components in the biofilm is restricted by the presence of the bacteria and their extracellular substances. Therefore, the effective diffusivity in the biofilm is only a fraction of the value in aqueous solution, and is calculated as $D_{i,e} = D_r D_i$, where $D_r = p/\tau$ is the relative diffusivity ($\text{m}^2 \text{ ES} / \text{m}^2 \text{ biofilm}$) and D_i the diffusivity in free solution ($\text{m}^2 \text{ s}^{-1}$). Mass conservation holds everywhere in the extracellular space, and is given by

$$p \frac{\partial c_i}{\partial t} = -\frac{\partial J_i}{\partial x} + r_i + \gamma_i \quad (18.2)$$

where r_i is the formation rate of species i (mM s^{-1}) due to biochemical reactions in the biofilm, which are described in more detail in Section 18.3, and γ_i is the formation rate of i due to acid-base reactions. For inert species that do not undergo any of these reactions, we have $r_i = \gamma_i = 0$, and for the phosphate system, we have $r_i = 0$.

To describe transport of species that participate in acid-base reactions, we group them in the following way. In our calculation we consider the group containing acetate species (Ac^-) and acetic acid (HAc) (together also called “substrate”); the group containing bicarbonate species (HCO_3^-) and carbonic acid (H_2CO_3), which are the products of the biochemical conversions; and the group of phosphate species (HPO_4^{2-} , H_2PO_4^- and H_3PO_4) which are typically used in experiments to buffer the pH in the biofilm. Finally, the solution contains protons (H^+) and hydroxyl ions (OH^-), and additional unreactive cations, which we jointly describe as Na^+ -ions. We neglect other anions.

For each group of species, we set up a mass balance equation by adding up all balances of all species in a group, and as the summation of the γ -terms within a group is zero, these γ -terms cancel each other out, resulting in

$$p \frac{\partial}{\partial t} [\text{Ac}_{\text{tot}}] = -\frac{\partial}{\partial x} (J_{\text{Ac}^-} + J_{\text{HAc}}) - r_a \quad (18.3)$$

$$p \frac{\partial}{\partial t} [\text{HC}_{\text{tot}}] = -\frac{\partial}{\partial x} (J_{\text{HCO}_3^-} + J_{\text{H}_2\text{CO}_3}) + 2 r_{\text{cat}} \quad (18.4)$$

$$p \frac{\partial}{\partial t} [\text{H}_2\text{P}_{\text{tot}}] = -\frac{\partial}{\partial x} (J_{\text{H}_3\text{PO}_4} + J_{\text{H}_2\text{PO}_4^-} + J_{\text{HPO}_4^{2-}}) \quad (18.5)$$

where we use the notation $[i]$ for concentration (equivalent to the symbol c_i), again with dimension mM, and where $[\text{Ac}_{\text{tot}}]$ is the total concentration of acetate species, $[\text{HC}_{\text{tot}}]$ that of bicarbonate species, and $[\text{H}_2\text{P}_{\text{tot}}]$ that of phosphate species. These concentrations are given by

$$[\text{Ac}_{\text{tot}}] = [\text{HAc}] + [\text{Ac}^-] \quad (18.6)$$

$$[\text{HC}_{\text{tot}}] = [\text{H}_2\text{CO}_3] + [\text{HCO}_3^-] \quad (18.7)$$

$$[\text{H}_2\text{P}_{\text{tot}}] = [\text{H}_3\text{PO}_4] + [\text{H}_2\text{PO}_4^-] + [\text{HPO}_4^{2-}] \quad (18.8)$$

The rate of formation of acetate is given by $-r_a$ (Eq. (18.17)) and of bicarbonate by $+2 r_{\text{cat}}$ (Eq. (18.18)), as discussed in detail in Section 18.3. After setting up these balances, we substitute the acid-base equilibria, as given by

$$\begin{aligned} K_{\text{HAc}} &= \frac{[\text{CH}_3\text{COO}^-][\text{H}^+]}{[\text{CH}_3\text{COOH}]} \\ K_{\text{H}_2\text{CO}_3} &= \frac{[\text{HCO}_3^-][\text{H}^+]}{[\text{H}_2\text{CO}_3]} \\ K_{\text{H}_3\text{PO}_4} &= \frac{[\text{H}_2\text{PO}_4^-][\text{H}^+]}{[\text{H}_3\text{PO}_4]} \\ K_{\text{H}_2\text{PO}_4^-} &= \frac{[\text{HPO}_4^{2-}][\text{H}^+]}{[\text{H}_2\text{PO}_4^-]} \\ K_{\text{W}} &= [\text{OH}^-][\text{H}^+] \end{aligned} \quad (18.9)$$

into the mass balances, Equations (18.3)–(18.5), after which only one ‘master species’ per group remains to be considered in the numerical code. In this way, the numerical code is much simplified as kinetic expressions and constants for these acid-base reactions are not considered. Furthermore, as acid-base reactions are fast compared to diffusion, considering

these reactions would result in a ‘stiff’ set of equations, which is numerically more difficult to solve. Lastly, by grouping ionic species, we do not have to make any assumption when it comes to which ionic species within a group exactly participates in a certain reaction. E.g., we do not have to make any assumption whether the bacteria consume HAc or Ac^- , and whether they produce H_2CO_3 or HCO_3^- .

Besides the mass balances for each group of species, we consider the charge balance in solution, which describes that, at each position in the biofilm, the divergence of the ionic current is equal to the rate of charge transfer from solution to the pili, r_{ch} (mM s^{-1})

$$\sum_i \left(z_i \frac{\partial J_i}{\partial x} \right) = -r_{\text{ch}} \quad (18.10)$$

where i runs over all ionic species, including protons and hydroxyl ions.

The elegance of the use of Equation (18.10) is that in our code no balance needs to be set up related to the ‘alkalinity’, or to protons/hydroxyl ions. This makes the model very transparent to set up. Note that even without explicitly setting up an ‘alkalinity’ balance, local production of protons (or hydroxyl ions) is calculated correctly by the model.

The electroneutrality condition holds everywhere in the biofilm ($x \in [0, L]$, where L is the thickness of the biofilm)

$$\sum_i z_i c_i = 0 \quad (18.11)$$

where i again runs over all ions and where we neglect a possible charge of the bacteria or of the extracellular substances. Next, we define boundary conditions. First, concentrations at the bulk-biofilm boundary (B/BF) are equal to the fixed bulk concentrations

$$c_i|_{B/BF} = c_{B,i} \quad (18.12)$$

where $c_{B,i}$ is the bulk concentration of species i . We neglect any bacterial charge in the electroneutrality balance, and thus a Donnan potential drop does not have to be considered across the B/BF interface. This is different from models for ion-exchange membranes or other membranes with charged nanopores. Secondly, at the biofilm-electrode boundary (BF/E), for each group of ionic species, the sum of the mass fluxes of all species within the group must be zero

$$\sum_j J_j|_{BF/E} = 0 \quad (18.13)$$

where j runs over all ionic species in a group. Eq. (18.13) also holds for the unreactive cations. Furthermore, at the BF/E -boundary the ionic current must be zero

$$\sum_i z_i J_i|_{BF/E} = 0 \quad (18.14)$$

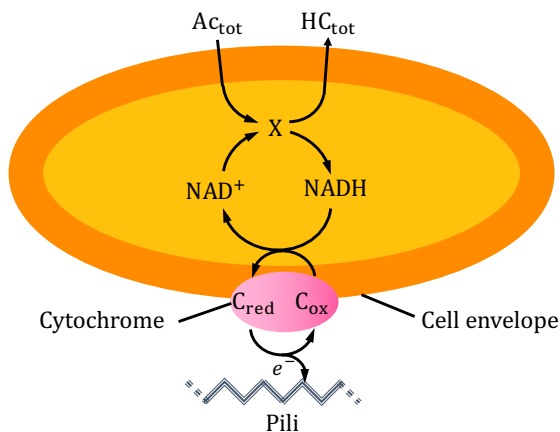


Fig. 18.2: Biochemical conversion of substrate and subsequent electron transfer to the matrix of conductive pili. Acetate (Ac^- or HAc) forms an enzymatic complex, X, with NAD^+ , which is reduced to $NADH$, while bicarbonate species (HCO_3^- or H_2CO_3) are produced. $NADH$ reduces a cytochrome on the outside of the cell, which thereafter transfers its electrons to the conductive pili.

where i runs over all ionic species evaluated in the model.

18.3 Oxidation of substrate in the bacteria

We present here a simplified description of the biochemical reactions associated with oxidation of organic matter (acetate) by bacteria under anaerobic conditions (i.e., in the absence of oxygen), see Fig. 18.2. First, acetate enters the bacterium and forms an enzymatic complex with NAD^+ , a redox component found in all living cells that we use as model electron carrier. Inside the enzyme-substrate complex, that we call “X”, acetate donates its electrons to NAD^+ , in a redox reaction yielding $NADH$ (the reduced form of NAD^+), which remains inside the cell, and bicarbonate ions and protons, which all leave the cell. Next, $NADH$ oxidizes back to NAD^+ , and transfers its electrons to the cytochromes (proteins that can accept electrons) located on the outer membrane of the cell. Finally, the cytochromes transfer the electrons to conductive pili, which conduct the electrons to the anode. In the following sections, we describe in detail how we model these different steps.

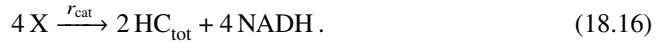
In a bioelectrochemical system, using acetate as a model substrate, the following stoichiometry of conversion is often assumed: $Ac^- + 4H_2O \longrightarrow 2HCO_3^- + 9H^+ + 8e^-$. However, this stoichiometry is only true in a limited pH range. For this reason, we prefer

the numerical approach explained in Section 18.2 that eliminates the need to choose for a particular stoichiometry. In our approach, we only have to implement the chemical information that when one acetate species (Ac^- or HAc) is consumed, two bicarbonate species (HCO_3^- or H_2CO_3) form, together with 8 electrons.

To describe the oxidation of acetate inside the bacteria, we adapt the Butler-Volmer-Monod (BVM) model which offers a simplified description of the underlying biochemical reactions. We modify the BVM model by 1) assuming that the dissociation of the enzyme-substrate complex is irreversible (we remove the k_4 parameter in their model), and 2) adapting it to describe the conversion of acetate to bicarbonate, protons and electrons. This latter modification makes it possible to couple biochemical reactions to the transport of ions. With this approach, the oxidation of one acetate species (the Ac^- ion or the HAc neutral species) is coupled to the reduction of 4 NAD electron carriers by the formation of an enzyme-substrate complex X, according to



while the dissociation of X is described by



In Equation (18.16) the rate of association of Ac_{tot} and NAD^+ into X is given by r_a , and the rate of dissociation of X by r_{cat} (both in mM s^{-1}). Note that Equations (18.15) and (18.16) do not take into account charge neutrality, nor atom balance.

Whereas other BES models rely on empirical expressions such as the double-Monod equation to calculate reaction rates, in our approach, rates of reactions (18.15) and (18.16) are proportional to the product of the concentrations of the reactants, following first-order kinetics

$$r_a = k_a [\text{Ac}]_{\text{tot}} [\text{NAD}^+] - k_d [\text{X}] \quad (18.17)$$

$$r_{\text{cat}} = k_{\text{cat}} [\text{X}]. \quad (18.18)$$

The rate constant for association is denoted by k_a ($\text{mM}^{-1} \text{s}^{-1}$), for dissociation by k_d (s^{-1}), and for ‘‘catalysis’’ by k_{cat} (s^{-1}). Note that the theory can also be used to model a biofilm on a cathode by reversing the reaction scheme (the **lhs** of Eq. (18.15) becomes the **rhs** of Eq. (18.16) and vice-versa). Consequently, Eq. (18.17) is replaced by $r_a = k_a [\text{HC}]_{\text{tot}} [\text{NADH}] - k_d [\text{X}]$. No other modification to the theory is required. The three kinetic constants of reactions (18.15) and (18.16), k_{cat} , k_a and k_d , are related to the classical substrate affinity constant, K_s , by

$$K_s = \frac{k_d + k_{\text{cat}}}{k_a} \quad (18.19)$$

which is also called the Michaelis-Menten constant. Next, we express the change in concentration of redox complex X as the difference between the formation rate, r_a , and the conversion rate, r_{cat} ,

$$\frac{1}{4} \frac{\partial [X]}{\partial t} = r_a - r_{cat} . \quad (18.20)$$

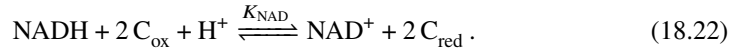
Finally, because the NAD electron carriers do not leave the bacteria, the total concentration, $[NAD]_{tot}$, is position-invariant and constant over time, and is equal to

$$[NAD]_{tot} = [NAD^+] + [NADH] + [X] . \quad (18.21)$$

18.4 Electron transfer to the matrix of conductive pili

18.4.1 Intracellular electron transfer to outer-membrane cytochromes

The mechanism by which electrons are exchanged between the interior of the cell and the extracellular space involves a cascade of redox proteins, such as cytochromes. For simplicity, we model the electron transfer between NADH and the outer-membrane cytochromes as a single step. Cytochromes can be in the reduced state, denoted by C_{red} , or in the oxidized state, C_{ox} . As NADH carries two electrons, the redox reaction between NADH and outer-membrane cytochromes is given by



We hypothesize that reaction (18.22) occurs at a much faster rate than the reaction that produces NADH (reaction (18.16)) and the one that produces C_{ox} (reaction (18.27)). Reaction (18.22) is thus not considered as a limiting step and we assume equilibrium, as given by

$$K_{NAD} = \frac{[NAD^+] [C_{red}]^2}{[NADH] [C_{ox}]^2 [H_1^+]} \quad (18.23)$$

where $[H_1^+]$ is the intracellular proton concentration, which we assume to remain constant at a value of 10^{-4} mM (*i.e.* pH 7). A balance in NAD^+ is given by

$$2 \frac{\partial [NAD^+]}{\partial t} = -8 r_a + r_{cyt} \quad (18.24)$$

where r_{cyt} is the rate of oxidation of cytochromes, to be discussed in the next section.

18.4.2 Extracellular charge transfer from cytochromes to the matrix of conductive pili

We now describe the charge transfer from bacteria to pili. Cytochromes located on the outside of bacteria transfer their electrons directly to the pili at all positions in the biofilm, as represented in Figures 18.1 and 18.2. Like for NAD_{tot} , the total concentration of cytochromes, $[\text{C}]_{\text{tot}}$, is invariant with time and position

$$[\text{C}]_{\text{tot}} = [\text{C}]_{\text{red}} + [\text{C}]_{\text{ox}} \quad (18.25)$$

with a balance over $[\text{C}]_{\text{ox}}$ given by

$$\frac{\partial [\text{C}]_{\text{ox}}}{\partial t} = -r_{\text{cyt}} - r_{\text{ch}}. \quad (18.26)$$

Note that in our model r_{cyt} is a dummy parameter, which cancels out after summing up Eqs. (18.24) and (18.26). The charge transfer from cytochromes to pili is described as a single-electron reaction



where the charge transfer rate, r_{ch} , relates to the redox reaction of cytochromes according to the Butler-Volmer equation, a standard model for electrochemical kinetics that has been shown to be applicable to redox proteins as well,

$$r_{\text{ch}} = k_{\text{red}} [\text{C}]_{\text{ox}} [\text{H}^+] e^{-\alpha \Delta \phi} - k_{\text{ox}} [\text{C}]_{\text{red}} e^{(1-\alpha) \Delta \phi} \quad (18.28)$$

where k_{red} ($\text{mM}^{-1} \text{s}^{-1}$) is the rate constant of the reduction reaction, k_{ox} (s^{-1}) of the oxidation reaction, where α [-] is the transfer coefficient, and where $\Delta \phi = \phi_{\text{pili}}(x) - \phi(x)$, with $\phi_{\text{pili}}(x)$ the dimensionless electric potential in the pili, and $\phi(x)$ the potential of the solution.

18.5 Charge transport to the anode

Finally, we must describe charge transport in the matrix of conductive pili. The current density, J_{ch} (A m^{-2}), is proportional to the biofilm's electronic conductivity σ_{bf} (S cm^{-1}) and the gradient of electric potential across the biofilm, as described by Ohm's law

$$J_{\text{ch}} = -\sigma_{\text{bf}} V_{\text{T}} \frac{\partial \phi_{\text{pili}}}{\partial x}. \quad (18.29)$$

Assuming that pili are not capacitive, no charge accumulates inside. Charge conservation in pili thus implies

$$\frac{\partial J_{\text{ch}}}{\partial x} = r_{\text{ch}} F. \quad (18.30)$$

By substituting Eq. (18.29) into Eq. (18.30) we obtain a final equation for current transfer across the biofilm

$$\sigma_{\text{bf}} V_{\text{T}} \frac{\partial^2 \phi_{\text{pili}}}{\partial x^2} = -r_{\text{ch}} F. \quad (18.31)$$

At the bulk-biofilm boundary (B/BF), no current can pass ($J_{\text{ch}} = 0$), and thus

$$\left. \frac{\partial \phi_{\text{pili}}}{\partial x} \right|_{B/BF} = 0. \quad (18.32)$$

We define the anode overpotential η (V) as the potential in the pili at the biofilm/electrode boundary minus that in the continuous phase at the bulk-biofilm boundary

$$\eta = V_{\text{T}} (\phi_{\text{pili}}|_{BF/E} - \phi|_{B/BF}). \quad (18.33)$$

Electrons transferred from cytochromes to pili eventually leave the biofilm at the anode surface. The current density there is obtained by integrating the charge transfer rate, r_{ch} , over the biofilm thickness

$$I = -F \int_0^L r_{\text{ch}}(x) dx \quad (18.34)$$

where I is the current density at the anode (A m^{-2}).

Redox reactions in environmental chemistry

A solution not only has a temperature, pressure, pH, color, ..., but we can also measure its redox potential, E_h . This potential is a measure of which redox reactions are active. For a mixture of redox-active components at equilibrium, knowing the various electrochemical half reactions, the redox-potential can be calculated, and we show how Pourbaix-diagrams can be constructed.

19.1 Introduction

Electrochemical reactions not only happen at electrodes, but also in solution. Then at least two redox-active species must be present, with one serving as electron donor (reductant) and the other as electron acceptor (oxidant). In water, dissolved oxygen is often the key oxidant, but in the absence of oxygen other species can be the oxidant, such as SO_4^{2-} . Even water itself can be the oxidant (e.g., forming H_2 gas). Organic matter is often the reductant, or a metal such as iron which is oxidized.

The ions can be in many different forms. First, they can be more or less protonated, as regulated by acid-base reactions, described by the well-known equilibrium equations that make use of pK-values. But in addition, ions can be in different 'oxidation states', more or less oxidized. For instance the Fe-atom can exist as Fe^{2+} and Fe^{3+} , as well as metallic Fe, and even as hexavalent iron. Dependent on pH these different oxidation states can associate with OH^- into soluble or insoluble iron (hydr-)oxide substances (or iron-sulfide, or iron-carbonate complexes and deposits).

All of this is regulated by pH and the presence of oxygen (e.g., oxygen 'activity', or oxygen partial pressure), but also other oxidants can play in role in iron oxidation. But instead of trying to measure the oxygen activity, it is possible to use a different property, that can be measured well, namely the redox potential. Indeed, it is possible to measure of a solution with redox active ions the redox potential, similar to how we can measure pH, temperature, pressure,

To this end an electrochemical measurement cell is used with a working electrode made of Pt (WE), and a reference electrode (RE). Some of the redox reactions that can take place in solution will also take place at the WE of the measurement device (a reaction between Fe^{2+} and Fe^{3+} , see Stumm and Morgan (1970), p. 361). This reaction will (try to) push electrons into the WE, thereby changing the electrode potential, and this potential (relative to RE) is measured and is the redox potential, E_h .

The lower E_h , the more electrons have been pushed into the electrode. Apparently the force to push them in is strong (because electrons –on the metallic side of the electrode– do not like negative potentials, so apparently a strong force was present to push them in there anyway). Thus there is a forceful electron donor, or vice-versa, the electron acceptor is 'weak', for instance because the oxygen activity is low. The low E of the WE can also be interpreted that at equilibrium (there is no current running to this WE), the solution side of the EDL must have a high potential versus the metal side, to lure the electrons to come out (to participate in a reduction). Apparently, they do not want to do this as much as a reaction that has a higher E (which doesn't need the large positive potential gain from metal

to solution). Situations with a low E , that would be an anaerobic environment. The reverse is a high value of E_h , and then the oxidizing power of oxidants is strong, for instance there is a high activity of oxygen because there is a significant concentration of dissolved oxygen.

So how to calculate E_h when we know the concentrations of all redox-active species, or vice-versa, if we know E_h , what can we derive of (the ratio between) the various concentrations? This topic is taken up in the next section.

19.2 Calculating the redox potential of a solution

How to calculate the redox potential E_h if we know the composition of a solution? Of course in reality the practical question would be the reverse: what can we learn from a measured value of E_h ?

If we would have a totally unreactive salt solution, say a NaCl solution, blanketed with N_2 -gas, then there just is no E_h to measure. If we now aerate the water (bubble through O_2 -containing gas), then a redox potential should establish, which is the Nernst potential of the reaction of dissolved oxygen gas with water and OH^- ions (i.e., dependent on pH), for which $E_0 = +1.23$ V (vs. SHE) for the reaction $O_2 + 4H^+ + 4e^- \rightarrow 2H_2O$, thus $E = E_0 + V_T \left(\frac{1}{4} \ln p_{O_2} - \ln 10 \cdot \text{pH} \right)$, with the oxygen pressure in bar. This reaction, though slow, will establish the redox potential, thus $E_h = E$ of this reaction. Thus, the higher is the oxygen pressure or the lower is pH, the higher is E_h .¹

If now Fe^{2+} and/or Fe^{3+} ions are added (together with inert anions), what happens next? Let us assume no further species are formed such as iron oxides. Thus we have the reaction $Fe^{3+} + e^- \rightarrow Fe^{2+}$ and of this reaction we have $E = E_0 + V_T \ln [Fe^{3+}] / [Fe^{2+}]$ with $E_0 = +0.77$ V.

In solution the two reactions are as it were short-circuited, so E_{hc} is the same, thus:

$$E_{0,O_2} + V_T/4 \cdot \ln \left(p_{O_2} [H^+]^4 \right) = E_{0,Fe^{3+}/Fe^{2+}} + V_T \ln [Fe^{3+}] / [Fe^{2+}] \quad (19.1)$$

and thus

$$\frac{p_{O_2}^{0.25} [H^+] [Fe^{2+}]}{[Fe^{3+}]} = \exp \left(V_T^{-1} \left(E_{0,Fe^{3+}/Fe^{2+}} - E_{0,O_2} \right) \right) \quad (19.2)$$

with the rhs equal to the numerical value $1.57 \cdot 10^{-8}$. Thus the higher the oxygen pressure, and lower pH, the more Fe will be in the oxidized form, Fe^{3+} . Interestingly, this distribution between Fe^{2+} and Fe^{3+} seems to be independent of the initial ratio of what we added, either

¹In reality, oxygen reduction does not establish this E_0 , but a lower E_h is measured, see Stumm and Morgan, p. 361.

Fe^{2+} or Fe^{3+} . But there is an effect. If we start with only Fe^{2+} and when this is oxidized, and thus oxygen reduced, then H^+ is consumed in this reaction, thus $[\text{H}^+]$ goes down, and thus the final ratio of $\text{Fe}^{2+}/\text{Fe}^{3+}$ ends up nearer to Fe^{2+} than if for instance we would have started at 50%/50% $\text{Fe}^{2+}/\text{Fe}^{3+}$.

Of course, if at the same time we would stabilize pH, by addition of HCl, then the final ratio of $\text{Fe}^{2+}/\text{Fe}^{3+}$ will be independent of the initial ratio of these two ions.

Thus, we know the composition of the solution. But what will the measurement of redox potential lead to? The redox potential is a mixed potential. It depends on all possible half reaction, and on how fast and prominent they are on the electrode of the E_h -sensor. [A reaction can be fast but based on trace ions, it will eventually not contribute much.] In the system just defined, the $\text{Fe}^{2+}/\text{Fe}^{3+}$ have a strong effect on the sensor, and the oxygen reduction does not. Thus, the redox potential completely depends on the Fe half reaction, thus $E_h = E_{\text{hc,Fe}^{3+}/\text{Fe}^{2+}}$. And we know that we can change this ratio between Fe^{3+} and Fe^{2+} by changing the oxygen partial pressure and pH. [This seems to be in contradiction to the Pourbaix diagrams that we will discuss later, where the 'line' between Fe^{2+} and Fe^{3+} is horizontal, i.e., independent of pH. But this simply reflects that when we have equal concentrations of Fe^{2+} and Fe^{3+} , pH will not influence E_h .]

Let us next introduce the possibility of a third Fe-ion, namely FeO_4^{2-} , where Fe is hexavalent. This ion is predicted for all pH values at high E_h , see Fig. 19.1.

— to be continued —

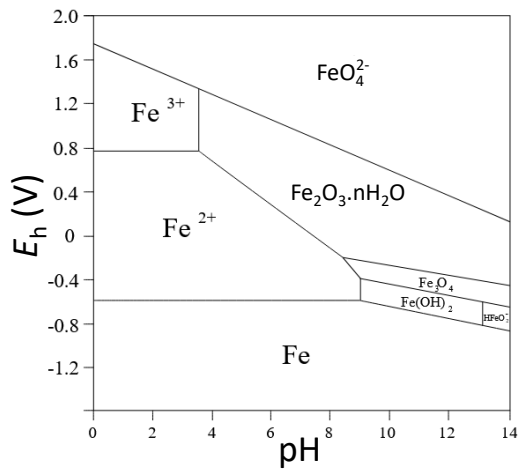


Fig. 19.1: The Pourbaix diagram of iron in water showing the predominant species as function of pH and redox potential E_h .

Part VI

Methods

Overview of electrochemical water desalination

Many methods to desalinate water can be classified as being part of the field of electrochemical processes. In this book well-established key methods were discussed in previous chapters. In this chapter these are briefly summarized focusing on aspects of application. In addition, we briefly describe other methods of electrochemical water desalination.

20.1 Introduction

Water desalination is one of the main applications of the field of electrochemical processes, and for that reason – and the authors' personal interest – this is a key part of this book.

When is a process 'electrochemical'? Or, what is the definition of 'electrochemical' in the context of this book?

As may be inferred from the many topics in this book, to us the definition requires the presence of freely moving ions, thus an electrolyte phase is formed, and there is an additional element such as another phase or material that has a physical-chemical interaction with the electrolyte. This other material is either a charged interface (as a planar wall, or as a porous structure), or an electrode (planar or porous). In addition there can be additional interfaces of the electrolyte, such as the liquid-gas interface.

Thus, in the context of our book title 'Physics of electrochemical processes,' the interactions of the ions with one another and with other dissolved species in the electrolyte, in combination with the processes in or at these aforementioned interfaces, we classify as an electrochemical process.

Interestingly, for a process to be 'electrochemical', in our view the presence of an electrode is not a requirement. One example is the study of ion exchange, which includes the description of ion transport into resin particles and the exchange for other ions. This process is clearly 'electrochemical' following the criteria laid out above. The theory for ion exchange makes use of the same concepts as for other electrochemical processes, such as the Nernst-Planck equation for ion transport, Donnan equilibrium, and electroneutrality. As another example, also the study of the surface tension of an ionizable surface, due to formation of a diffuse layer of ions and the dissociation of surface charges, and the resulting G/L/S contact angle, is part of the field of electrochemical processes.

Indeed, electrochemical processes closely relate to the field of physical chemistry, as long as dissolved ions play a role, and there are additional interfaces such as membranes and/or electrodes. The relevant physics is often based on Poisson's equation applied to electrolytes and interfaces, and the theory furthermore includes ion equilibria or transport, based on (modifications of) the Boltzmann equation and the Nernst-Planck equation.

The phase transition of water containing salt, to either a gas or solid phase, as a method of water desalination (which also includes membrane distillation), can be excluded from the class of electrochemical processes. It can be part of this field if it is established that in the evaporation and freezing of (sometimes highly) saline streams, there is a significant role of the EDL structure or ion transport on the kinetics and thermodynamics of these phase transitions, requiring use of the aforementioned physical theories.

For the desalination of water by methods that are primarily driven by pressure, there is no logical reason to exclude these from fitting under the umbrella of electrochemical processes. And as the chapter on reverse osmosis and nanofiltration (RO and NF) clearly shows, the theories discussed there, to describe ion rejection and desalination, are the same as those used for other desalination methods such as electrodialysis (ED), and ED clearly is a method of electrochemical water desalination. Thus RO and NF fall under the umbrella of electrochemical water desalination as well.

20.2 Core technologies for electrochemical water desalination

The core technologies we identify for electrochemical water desalination are listed in Table III-1 on p. 284, and are discussed in Chapters 15, 11, and 12. In this section these methods are briefly discussed focusing of more technological aspects.

20.2.1 Capacitive Deionization (CDI)

Capacitive deionization (CDI) is a method of water desalination where pairs of capacitive porous film electrodes are used to attract cations into one electrode, and anions in the other, by charging the electrodes negatively and positively, respectively. While electrodes are charged, we produce freshwater from the cell (water with a lower salt concentration than the feedwater). Such film electrodes are typically rather thin, less than 1 mm in thickness, but have a large area, such as $10 \times 10 \text{ cm}^2$ or larger. The capacitive particles in such an electrode (for instance made of NMO (sodium manganese oxide), NiHCF (an example of a Prussian Blue Analogue), or activated carbon) are glued together by a polymer additive, and the electrode structure is furthermore improved by addition of conductive polymer or graphite (carbon black, graphene, or carbon nanotubes) to enhance electron conductivity. The electrodes must have a large fraction of open pore space to allow for ion transport.

While building up an EDL in the electrodes, which raises the voltage inside the electrodes, there is a decay in current across the cell if we work at a constant cell voltage. The decreasing current in time will also lead to lower desalination rates. When the EDL voltage becomes too high and the energy costs of further charging becomes too high, or Faradaic leakage currents develop, the cell voltage is reduced, or the current direction reversed, and cell operation is now in discharge mode and a salt-concentrated stream is produced. This continues until the end of the discharge step, after which a new cycle can start. CDI is thus a cyclic process.

The electrodes in each cell are connected via a ‘current collector’ to the external wiring. The current collector must be electronically conductive, of which an example is graphite paper. The same current collector can be used for two electrodes that are in adjacent cells. Thus a single layer of current collector will have porous electrodes on both sides and each current collector is connected to the external circuit (one is connected to the positive pole of the electrometer, the next to the negative pole, etc.). This is different in the ‘floating’ design, where two adjacent porous electrodes in different cells are electrically insulated from one another by a non-conducting layer, e.g., made of plastic. This insulator blocks passage of current from one cell to the other. With these insulator materials in place, we can again build a stack of many CDI cells, but we only have to charge the end-electrodes, and then automatically all individual cells will charge up and desalinate the water that flow them. In this floating design we must take care of ‘stray’ currents that flow around the cells, through auxiliary stack elements.

Note that when building such a CDI stack, in the design with current collectors between each two electrodes, each cell has an internal sequence that is a mirror-image of the neighbouring cells. This is particularly relevant when ion-exchange membranes are placed in front of the electrodes, and much care must be taken in correctly assembling the cell. For the floating design, each cell has the same sequence, i.e., is a copy (not a mirror-image) of adjacent cells.

The typical CDI design has the water flowing along the electrode, but also flow-through CDI is possible where the water is directed at straight angles *through* the electrode structure [1]. In this case the electrodes must be more open (have a higher hydraulic permeability) by creating larger pores and more porosity, than in the flow-by design. Electrodes can also flow themselves by making use of slurry electrodes in ‘flow-electrode CDI’. On the level of the electrode (particle), the charge-discharge cycle is the same here as for standard film electrodes.

There is a whole range of capacitive materials that can be used in CDI including inorganic components with special charge-discharge characteristics. As long as the electrode voltage is a function of ion loading in the electrode (and thus is a function of stored electronic charge), we can construct an isotherm to describe the data of voltage-charge-salt adsorption (see Ch. 1), and thus an EDL is formed, and the electrode is capacitive. These capacitive electrode materials can also be chemically modified to become highly selective to preferentially take up one ion over another one.

The basic design with two capacitive electrodes can be extended by placing ion-exchange membranes in front of the electrode. In this method called membrane CDI, or MCDI, the performance of the cell is enhanced because the current efficiency is increased, as well as the

salt adsorption capacity. Also longevity of the CDI system is improved. However, the entire stack design needs more volume (or we have less cells per unit stack volume) and becomes more expensive.

For a cell design to classify as MCDI, it can have no more than one membrane per electrode. For more membranes (thus for three membranes per electrode pair or more), two distinct flow channels emerge (namely a distinct diluate flow channel, and a distinct concentrate flow channel), both separate from the electrode compartments. We have now entered a grey zone towards electrodialysis (ED), and we can add more and more membranes, without any further fundamental changes. For ED, electrode performance is of less relevance, but instead the focus is on the study of ion transport in an ED cell.

Desalination by non-capacitive (Faradaic) electrodes is discussed later on in this chapter.

Electrodes can be chemically modified in many ways, to make them more selective to absorb one ion over another. We can also synthesize chemical charge in the electrode. This can then lead to a special operational mode of CDI where during charging (defined here as the step where we invest electrical energy) we do not produce freshwater (as in the standard operational mode), but instead during charging we produce the concentrate stream (ions are pushed out of the electrode), and when we discharge (no electric energy input, or we recover energy), we now desalinate the water. This operational mode is called inverted CDI (*i*-CDI), and how this works can be understood from the effect of the extra chemical charge in the micropores on the EDL structure, see Ch. 2.

When we use electrodes that are highly selective for either anions and cations, and this is the case for many of the intercalation materials that are highly cation-selective, see Ch. 1, a cell design is possible where each electrode is in direct contact with a flow channel, and the two channel-plus-electrode constructs are separated by a membrane (an anion-exchange membrane is used for cation-selective electrodes). In this CDI-design one channel is producing concentrate while at the same time the other channel produces desalinated water. When the current direction is reversed, the concentrate-producing channel now produces diluate, and vice-versa. So this is also a cyclic CDI process, but the freshwater (diluate) and brine (concentrate) are not produced sequentially, but at the same time, coming from different channels.

1. E.N. Guyes *et al.*, "A one-dimensional model for water desalination by flow-through electrode capacitive deionization," *Desalination* **415**, 8–13 (2017).

20.2.2 Electrodialysis

Typically commercial electrodialysis (ED) stacks have 10s to 100s of cell pairs (membrane pairs) and the key element of study is the single cell, which consists of a pair of flow channels, one to produce the freshwater, the other the concentrate. In between each two channels an ion-exchange membrane (IEM) is placed, alternatingly a cation-exchange membrane or an anion-exchange membrane. These membranes are typically 10s of microns thick, are quite porous with an open porosity of 20-40 vol% and the membrane structure is highly charged; per unit volume of pore water, the membrane charge density is as high as 5 M for commercial IEMs.

The use of many cells in a single ED stack implies that 'end-electrode' effects are less relevant. In these end-electrode compartments, often the decomposition of water is used to Faradaically convert electronic current into ionic current (accompanied by the formation of hypochlorite, or hydrogen gas molecules), or in laboratory experiments, a solution with certain dissolved molecules (a redox couple) is used, and this electrode rinse solution is continuously pumped from the anode to cathode and back. Leakage of these molecules into the ED flow channels must be avoided.

Another option is to use capacitive end-electrodes, often rather thick (several mm's or more), such that the ED process can run (at a given current) for tens of minutes before the current direction in the stack is switched, concurrently with switching the direction of the exit flows. This latter option is similar to 'EDR' which is the commercial name of an ED process with switching at this long time scale, to prevent membrane fouling. At the level of a single cell, after a short switching period of 10s of seconds, operation of the cell quickly resumes to continue as before, in steady state. The rinse solution which is continuously pumped between the two end-electrode can also be a slurry of capacitive particles. Then periodic switching of current is not required, but robustness of pumping of a slurry must now be ascertained.

20.2.3 Ion exchange

The method of ion exchange (IEX) was not yet discussed in this book, but is a very relevant water desalination method where ion exchange resin particles exchange ions, for instance cations absorb and protons desorb. This would bring the pH of the water down, i.e., the water is acidified. In a sequel column, or a mixed bed column, anions are exchanged for hydroxyl ions, and in this way the water is no longer acidic, and now (almost) all ions are removed. The absorption column must be replaced or regenerated when it is saturated with anions and cations.

20.2.4 Reverse Osmosis

The No. 1 technology in electrochemical water desalination is reverse osmosis (RO). RO is widely applied worldwide to provide potable water from brackish water sources and from seawater, for human use, industry and agriculture. RO uses asymmetric membranes where a thin top layer is on top of a supporting structure which provides strength against the several MPa's of pressure that are imposed on the membrane.

The design of an RO installation involves the optimization of membrane transport, module operation, and then the design of the layout of many modules in an optimized RO desalination plant. Pressure recovery devices are a key enabling technology to minimize the energy consumption in RO. For seawater desalination the energy consumption of an RO plant can now be limited to a value less than twice the thermodynamic minimum.

Current research of RO does not focus on the reduction of energy, but on many other relevant topics. These topics include: the application of RO for micropollutant removal from surface water; membrane robustness against cleaning; the prediction and optimization of ion selectivity in RO related to sub-optimal rejection of ions that participate in (de-)protonation reactions (ammonia, boric acid); and RO for the treatment of hypersaline streams for zero liquid discharge applications.

20.2.5 Nanofiltration

Nanofiltration (NF) is closely related to reverse osmosis. Many modern NF membranes are made in a similar way as RO membranes, but only the pore size of the material ends up being a little larger. Therefore in NF the rejection for monovalent ions is moderate (for instance 50%) while the rejection for divalent ions is much closer to 100%. However, this difference between the rejection of monovalent and divalent ions cannot define NF, or delineate NF from RO, because in RO this difference between the rejection of mono- and divalent ions is just as distinct. For instance in a study by Zhang *et al.*, ES&T Lett. (2020), the rejection by an RO membrane for monovalent cations is between 97.0 and 98.5% while the rejection for divalent cations is 99.98%. Thus also here for RO we have a desalination effectiveness (defined as 100% minus rejection) that is a factor 100 different between monovalent and divalent cations.

Most distinct is that NF and RO have gone through a very different history. Whereas the study of RO has always been closely related to seawater desalination and developments in polymeric (thin film) membranes and the design of working desalination plants, the field of NF considered a wider range of materials, for instance inorganic membranes of silica and γ -alumina, while membrane materials of recent interest are polyelectrolyte multilayer

membranes, and focused more on lab-scale experiments with ideal salt solutions (with well-defined concentrations of the mixtures of monovalent and divalent ions).

Theoretically, for RO simple black-box theories have traditionally been used, often based on the SD-model or models based on irreversible thermodynamics. NF used physics-based models such as the Teorell-Meyers-Sievers (TMS) model and extensions thereof to include advection (uniform potential model), and further extensions to include special Donnan effects at the pore entrance and exit. Also the extension to include the radial direction of the pore in more detail by the space-charge model was taken up. These physics-based models used in NF describe performance on the basis of microscopic properties such as diffusion coefficients, membrane charge, etc. Instead, the classical RO models have phenomenological parameters as input, parameters that can be quickly derived from measurements but might not have a direct correlation to fundamental properties of the membrane, the ions, and their interaction.

Thus, until recently, at least in the academic field, the two fields were quite distinct in experimental and theoretical approaches.

20.3 Non-electrochemical methods of water desalination

For completeness, let us briefly summarize water desalination methods that use phase transitions as the primary driving force, either by evaporation of water, or by freezing.

20.3.1 Distillation

Multi-effect distillation, multi-stage flash distillation

20.3.2 Membrane distillation and pervaporation

20.3.3 Freezing

incl. eutectic freeze crystallization

20.4 Non-core methods of water desalination

In this section we discuss in no particular order water desalination methods that can be considered to have a niche application or still are in the investigative stage.

20.4.1 Mosaic membranes for water desalination

20.4.2 Forward Osmosis

20.4.3 Shock electrodialysis

20.4.4 Faradaic electrode desalination

A pair of Faradaic electrodes can be used to desalinate water by a Faradaic electrode process [1]. In Faradaic electrodes ions are not stored in the electrode itself, but in a solid salt nearby. The two systems that have been used for this purpose are Ag/AgCl and Zn/ZnCl₂. These Faradaic processes are not described by an isotherm or a capacitance, and there is no EDL formation that relates to the desalination performance.

In Faradaic desalination there is no continuous change in electrode voltage during desalination and thus no finite capacity of the electrode itself. Instead, in this process, as long as bulk metal is available, the Cl⁻-anion can be removed from the water. Thus, these processes are Faradaic because they do not store ions at or in the electrode itself (the outer surface of the Ag or Zn metal in this case), do not have an isotherm describing their characteristics (instead, the electrode potential is described by the Nernst equation, i.e., only dependent on Cl⁻-concentration), and they do not have a capacitance. They can run forever without changes in the electrode potential.¹

In Faradaic electrode desalination, during Cl⁻ absorption, one or more electrons flow away from the metallic phase, which in the examples discussed here is either Ag or Zn, and a metal atom is turned into a cation which then becomes part of the AgCl or ZnCl₂ solid salt that surrounds the metal phase, allowing for one or two Cl⁻ ions from solution to also become part of the solid salt.

Thus a metal ion is oxidized and becomes part of the solid salt phase. Ions in the solid salt must have a (tiny) mobility relatively to one another because Ag⁺ or Zn₂⁺ cations are continuously inserted on one side (near the metal) while Cl⁻ ions are continuously inserted on the other side of this layer. To keep electroneutrality near these outer interfaces, inside the solid salt the two ions must be allowed to have a (very small) velocity relative to one another.

Of course many hybrid methods are possible where one Faradaic electrode is coupled with one capacitive electrode [2], and many other modifications are possible, such as including one or two ion-exchange membranes.

¹In the examples discussed here, the voltage across the salt layer that covers the electrode will increase when they get thicker (also dependent on current).

1. J. Ahn, *et al.* “High performance electrochemical saline water desalination using silver and silver-chloride electrodes,” *Desalination* **476**, 114216 (2020).
2. M. Pasta, C.D. Wessells, Y. Cui, and F. La Mantia, “A desalination battery,” *Nano Lett.* **12**, 839–843 (2012).

20.4.5 Phase-transition electrode desalination

A further modification is water desalination by using phase transition electrodes, or conversion electrodes. The material BiOCl is often used for this purpose, and it can take up Cl^- -ions while transforming into another phase. Because of the differences in shape and volume between the two phases, upon repeated cycling there is severe loss of cohesion of the electrode and loss of electronic connectivity, and thus repeated cycling of such an electrode can be problematic.

20.4.6 Chemical energy driven spontaneous generation of freshwater and electricity

20.4.7 Ion concentration polarization

Numerical methods in electrochemical processes

In electrochemical processes, many problems require numerical evaluation. This can be for steady state problems, as well as for dynamic calculations. With the right approach, such numerical calculations are robust and precise. The codes can be easy to set up and are a pleasure to work with. Setting up such models and evaluating numerical calculations is then a highly gratifying endeavour. Of course this is only the case when the right numerical approaches are used.

In this chapter we explain how to solve mathematical problems in electrochemical processes by methods that can even be programmed in widely available spreadsheet software. We also provide downloadable example files. We demonstrate how to solve ordinary differential equations with mixed boundary conditions using finite difference methods, important for one-dimensional steady state problems. For dynamic problems described by partial differential equations, we describe first- and second-order differentiation methods. We explain how to include in the numerical code information from overall balances and averaged flux equations. Of special interest are methods to include acid-base reactions in solution and electrodes.

21.1 Introduction

Numerical methods are of great use for the theoretical study of electrochemical processes, because there are so many processes of interest that are too complicated to be described by analytical equations. Or, these analytical equations exist, or may exist, but are difficult to derive and/or to interpret. Often analytical solutions are valid in certain ranges, and it must be carefully checked if they are used in the right range. For these reasons, a numerical calculation can be easier to do, and more robust. Ideally, numerical and analytical equations are compared (in limiting situations where this is possible), and only when they give the same outcome, do we accept that they were correctly evaluated (in that limit).

Electrochemical processes are considered more complicated than other processes in chemical engineering where the charge of species does not play a role. Even though that is perhaps true, in this chapter we will nevertheless provide effective and simple tools that enable the modeling of electrochemical processes in a robust and insightful way.

In this chapter we will explain how to write out a numerical problem as a set of algebraic equations (AEs) and show how to solve them. We do not focus on linearization of this set of equations, which is not needed anyway. The only requirement is that there is an equal number of unknowns as there are equations. Of course any physically correct model (when formulated as a set of AEs) has equal numbers of unknowns as equations. Because otherwise the problem is over- or underspecified, which means that either important physical information is missing, or redundant information is provided (a certain equation is already 'included' in other equations), or the model is internally inconsistent, i.e., there are multiple different equations that deal with the same aspect of the model. Interestingly, in setting up the model, much time is invested in finding the exact set of equations for a certain problem. This is especially so because of charge neutrality requirements, constant current, etc. The methods we outline below are the ones that provide the minimum in time lost in finding the right equations that are not redundant, neither miss information. Sets of non-linear AEs will likely have multiple mathematical solutions, but in the physics of electrochemical processes there typically is only one physically realizable solution. If the solution has all concentrations positive, has the various state variables varying gradually from point to point, then you have probably found that one solution. Though this does not prove you did not make an error in the model, at least the first step, to set up and solve a model that at least gives a realistic output, that step you successfully made. The most difficult part is behind you. Now comes the detective work to figure out by looking very critically at the model output if there isn't some error. Every method you can come up with to check your model in yet one more creative way, you must apply (e.g., compare with some simpler model, ideally

also derive analytical equations to compare with.)

Steady-state and equilibrium problems are described by a set of AEs (after discretization along a coordinate direction). The other type of problem we often deal with is dynamic (time-dependent). The partial differential equations (PDEs) that describe a dynamic problem can be discretized in space and then the resulting set of ordinary differential equations (ODEs) together with the auxiliary AEs can be solved in time using the Method-of-Lines by a DAE-solver. (This is a solver for sets of differential and algebraic equations.) Though we have used DAE solvers and still do, in this book we promote a simpler methodology whereby we discretize both in space and in time but in different ways. For the discretization with time there are first and second order methods, but we prefer the first order methods (Crank-Nicolson, and implicit Euler). Of these two methods, we have a preference for the implicit Euler method.

General to all of these methods is that we advise the use of finite difference methods, which are precise and insightful and elegant. This is at least the case when we have a single x -coordinate to consider, and in that case we can make maximum use of overall balances and other integrated properties, as we will explain below.

For calculations in multiple dimensions, finite difference methods will also work fine when the shape of boundaries is ideally suited for the numerical analysis (e.g., the domain is a perfect rectangle), for equilibrium, and for steady state without convection. But in other cases, such as with complicated geometries, convection, and/or for time-dynamic problems, the finite difference method is generally replaced by finite element/finite volume methods.

In this chapter, and throughout this book, we describe many problems that are both position- and time-dependent, also including convection. In all cases the mathematical structure is that the space coordinate is primarily one-dimensional, and we can then use the finite difference method. We also make calculations for flow channels and we then consider two dimensions (and in §12.4 we also refer to a 3D calculation), but in these calculations each of the various space coordinates is treated differently. For instance, in a channel for water desalination by ED or RO, a typical model structure that we set up evaluates the short direction towards the membrane as the key space coordinate for which we solve a set of AEs, while we solve for transport in the long direction (along the membrane) by a sequence of steps in that direction (implicit Euler). That works when in that direction we only need to consider convection, and not diffusion and electromigration. In this way, a 2D or 3D physical problem is solved primarily as a 1D mathematical problem solved sequentially. We will explain below in more detail how we deal with such 2D transport problems, but we first discuss problems that only have one positional coordinate, x , i.e., problems that in space are one-dimensional.

21.2 Solving a set of algebraic equations for a steady state transport problem

A problem that is described as a set of algebraic equations (AEs) can be solved by various methods or approaches (e.g., Schwalbe *et al.*, 2006). In the next box we explain how one such numerical approach can be programmed in readily available spreadsheet software.

Solving multiple algebraic equations in spreadsheet software. We can easily solve \mathcal{N} coupled algebraic equations which have an equal number \mathcal{N} of unknown variables, x_i . For instance, we have two unknowns, x_1 and x_2 , and the two equations

$$\begin{aligned}\sinh(x_1) &= x_2 + 2 \\ x_1 &= 2 \cdot x_2\end{aligned}$$

then, to solve for x_1, x_2 using spreadsheet software (such as Microsoft Excel), we do the following:

1. In two cells we enter guess values for x_1 and x_2 .
2. We rewrite the equations to

$$\begin{aligned}\sinh(x_1) - x_2 - 2 &= 0 \\ x_1 - 2 \cdot x_2 &= 0\end{aligned}$$

and program this left side ('the function') in two cells, as function of the guess values for x_1 and x_2 (see 1.).

3. In two additional cells, we evaluate the square of each function.
4. These two squared numbers are added up in a new cell.
5. This sum-of-squares must become zero, i.e., it must be minimized. To that end we use the 'Solver'-routine in Excel, and minimize this cell under variation of x_1 and x_2 . The example Excel file is available [here](#). The calculated values for x_1 and x_2 turn out to be: $x_1 = 1.78\dots$ and $x_2 = 0.89\dots$

In the remainder of this chapter, what was just discussed we call the ‘solution route’ to find the values of the unknowns, the x_j ’s.

A summary of what we did is as follows. We have N AEs and N unknowns x_j . And in a spreadsheet we provide N cells with guess values for the unknown x_j ’s. And in N other cells the N AEs are programmed, i.e., the ‘functions’ (which each ultimately must equal zero, but as long as the x_j ’s are not yet optimized, don’t). These functions, (i.e., the left sides of AEs written as $\dots = 0$), are squared and the squares are added up. That summed term is minimized under variation of the guess values of x_j . This works fine in Microsoft Excel, where we worked with up to 50 or so unknown x_k ’s (we never tried more). This method is very powerful in solving many problems that can be formulated as sets of AEs, and as we show below, a small extension also allows us to solve dynamic problems. Of course it is relevant to have reasonable good guesses for the x_j ’s; if the guess values are completely off, the solver may not converge to the required solution. Afterwards, check if the values for x_j that you found are realistic.

What is interesting, very interesting, is that it is not the case that always each of the y_j equations has a direct tie to one particular unknown variable x_j . I.e., it is not the case that equation y_3 is there to solve for parameter x_3 . No. All equations are there to solve for all unknowns, in one ‘global’ calculation. Of course, often there is a connection, that a certain mass balance in component i , solved at position j , is there to calculate that concentration at that position, $c_{i,j}$, but this link is not always there. Indeed, equations and unknowns can be quite ‘disconnected’ – it can be the case that we solve for the concentrations of a species i (at multiple positions), even though there are no mass balances explicitly formulated in that species i . This typically is the case for problems with acid-base equilibria. Neither is it the case that ‘we first solve for x_2 , then x_3 ’. No, all functions and unknowns are calculated ‘in one go’ and there is no sequence, or order, or hierarchy. All unknowns are equal.

Then the question is, how to come to a problem formulation in terms of AEs? Let us consider an x -domain that runs from $x=0$ to $x=L$. We make use of the parameter np , this is the number of gridpoints minus 1. We assign the index $j=0$ to the left-most gridpoint, which corresponds to the left boundary, at $x=0$. Thus this left-most gridpoint is the left

boundary of the domain, the left edge. It is *right there*, at the edge.ⁱ The gridpoint $j = np$ is the right-most position in the domain, it is the right edge. These two gridpoints are the *outer gridpoints*. All other gridpoints $\{1 \dots np-1\}$ are the *inner gridpoints*. The distance between gridpoints is $\Delta x = L/np$.

Often, on the outer gridpoints we formulate boundary conditions, but not necessarily so. But what is always the case is that at all inner gridpoints we solve all differential and algebraic equations that may apply. For instance we have the following three equations (mass balances in cation $i = 1$ and anion $i = 2$ in a membrane, and as a third equation we have electroneutrality), that all apply at all inner gridpoints,

$$0 = D_i \frac{\partial^2 c_i}{\partial x^2} + z_i D_i \frac{\partial}{\partial x} \left(c_i \frac{\partial \phi}{\partial x} \right) \quad (21.1)$$

$$c_1 - c_2 + X = 0 \quad (21.2)$$

which could also include chemical reactions, convection, etc., that can be implemented easily.

Interestingly, in this steady-state problem, we can divide all terms in the mass balance by the diffusion coefficient D_i , and then (when there is no reaction or convection) it seems that this problem is independent of the diffusion coefficient. But we will see further on that the two D_i 's are in at least one of the boundary conditions, and thus the complete problem most certainly depends on the D_i 's.

It is imperative to understand that such mass balances, based on second order ODEs, *are only solved at inner gridpoints*, never at the outer gridpoints of a numerical domain. Such differential mass balances apply to a volume, i.e., are valid 'away' from edges. There is no information about conditions *at edges* incorporated in such a differential mass balance. The edges (outer gridpoints) are described by other physical information.

Returning to the ODEs solved at inner gridpoints, the next step is to first evaluate the migration term using partial differentiation, leading to

$$\frac{\partial}{\partial x} \left(c_i \frac{\partial \phi}{\partial x} \right) \rightarrow c_i \frac{\partial^2 \phi}{\partial x^2} + \frac{\partial c_i}{\partial x} \cdot \frac{\partial \phi}{\partial x} \quad (21.3)$$

ⁱIf we have multiple adjacent domains, i.e., numerical domains that are 'in contact', this point at $j = 0$ will also be the rightmost point of a domain that is to the left of the domain we just considered. So the same physical position is represented by a gridpoint $j = 0$ in one domain and $j = np$ in an adjacent domain. Numerically, these two points must be tied to one another by information such as equality of concentration or potential. Often a nanoscopic Donnan layer is 'in between' the two domains, which leads to several AEs tying these two numerical positions to one another. Often also information about equality of fluxes is included, which leads to relations between gradients in concentration or potential in the one and in the other domain.

and then discretize the mass balance by first- and second-order central differencing, resulting for Eq. (21.1) in

$$0 = \frac{c_{i,j-1} - 2c_{i,j} + c_{i,j+1}}{\Delta x^2} + z_i c_{i,j} \frac{\phi_{j-1} - 2\phi_j + \phi_{j+1}}{\Delta x^2} + z_i \frac{c_{i,j+1} - c_{i,j-1}}{2\Delta x} \cdot \frac{\phi_{j+1} - \phi_{j-1}}{2\Delta x}. \quad (21.4)$$

If there is a convection term in the balance, the resulting term $\partial c_i / \partial x$ can be discretized by central differencing, or by an upwind or downwind scheme, i.e.,

$$\frac{\partial c_i}{\partial x} \rightarrow \frac{c_{i,j+1} - c_{i,j-1}}{2\Delta x} \text{ or } \frac{c_{i,j} - c_{i,j-1}}{\Delta x} \text{ or } \frac{c_{i,j+1} - c_{i,j}}{\Delta x}. \quad (21.5)$$

The above equations together are most of the AEs that we need, with at each gridpoint three resulting equations, ‘solving for’ $c_{1,j}$, $c_{2,j}$ and ϕ_j at all points j from 1 to $\text{np}-1$.ⁱⁱ

What can now be quickly observed, is that if we can make the electroneutrality AE explicit in one of these parameters, that we can reduce the number of unknown variables per gridpoint by one; thus per gridpoint one unknown drops out of the numerical solution route. Thus, we want to insert the electroneutrality AE in the other two AEs. For instance, assuming X is a constant, we can rewrite this equation to $c_{2,j} = c_{1,j} + X$, and substitute it for $c_{2,j}$ in the discretized mass balances. We have now removed per gridpoint one equation and one parameter ($c_{2,j}$), and only $c_{1,j}$ and ϕ_j remain.

Let us stress that we suggest to substitute all values of $c_{2,j}$ using this electroneutrality equation *after we discretized the differential equations*. It is also possible to do this before discretization, and then go through the required manipulations of the equations, but often the easiest and most robust method is to substitute one equation into another afterwards.

Note that this substitution does not always have to be made explicitly. In the spreadsheet software that we use, there is no need to explicitly substitute the EN-equation in the other ones. Instead, concentration $c_{2,j}$ has its own computational ‘spreadsheet cell’, and is directly calculated from the (initially unknown, i.e., guessed) value of $c_{1,j}$ by the electroneutrality balance. In this way only $c_{1,j}$ and ϕ_j are unknown variables (at each gridpoint), and an additional calculation provides $c_{2,j}$ at each gridpoint based on (the guess for) $c_{1,j}$. Concentration $c_{2,j}$ (‘slaved to’ $c_{1,j}$) is used in the discretized mass balance equations as an intermediate parameter.

This finalizes the evaluation of equations at all inner gridpoints. On the outer gridpoints, the AEs also apply, but not the ODE mass balances. With one AE (in the example the

ⁱⁱInteresting is that in these discretizations, if the argument is a combination of factors, say $\alpha\beta$, both dependent on x , then we don’t necessarily have to do a partial differentiation. That would result in a summation of a term $\alpha \partial\beta / \partial x$ and a term $\beta \partial\alpha / \partial x$, and then one discretizes each term. Instead we can just as well discretize based on the original argument $\alpha\beta$, for instance to $(\alpha\beta|_{j+1} - \alpha\beta|_{j-1}) / 2\Delta x$.

electroneutrality constraint), that is two extra equations. But the differential mass balances are not solved at the edges; they are only evaluated at inner gridpoints. Thus we are still in need of finding 4 remaining equations. The first one is easy, because working with electrical potentials, it is always the case that we can set the potential to a fixed value at some random point in a domain. For instance, at position $x=0$ we set the potential to zero, thus $\phi_0=0$. Now we are down to 3 equations that are still required. To start, if the problem was based on a certain applied current, J_{ch} , that will lead to one more equation, as we discuss next.

To find this equation, we need to analyze the expression for current J_{ch} , and this current is the same at each position, and is given by a summation over the individual fluxes times the charge number of the ions, thus

$$J_{\text{ch}} = - \sum_i z_i D_i \left(\frac{\partial c_i}{\partial x} + z_i c_i \frac{\partial \phi}{\partial x} \right). \quad (21.6)$$

Now, one can decide to discretize this equation, and solve it at some position in the membrane, either at one of the inner points or at one of the edges. Especially evaluation of such an equation at a boundary is very common, certainly when the flux only involves a diffusional contribution such as $J = - \partial c / \partial x|_{x=0}$.

However, our experience is that ideally we should avoid as much as possible a direct discretization of a flux equation such as Eq. (21.6). Numerical stability of a scheme where we directly discretize Eq. (21.6) is generally poor, and the code is less precise. In addition, solving this flux-equation at one particular position is arbitrary: which position to take? And the calculation becomes 'asymmetric', because this position is given more 'importance' than other positions. Thus, if we can avoid it, we propose to not discretize a flux equation such as Eq. (21.6) directly. Instead, we *integrate* Eq. (21.6) one more time, see Dykstra *et al.* (Water Research, 2017) and Tedesco *et al.* (J. Membrane Sci., 2018). We then obtain

$$J_{\text{ch}} \cdot L_{\text{eff}} = - \sum_i z_i D_i \left(c_{i,\text{np}} - c_{i,0} + \frac{z_i}{2} \sum_{j=1..\text{np}} (c_{i,j-1} + c_{i,j}) \cdot (\phi_j - \phi_{j-1}) \right) \quad (21.7)$$

where in the integration of the electromigration-term we implemented the Trapezoid-rule. We replace membrane thickness L here by L_{eff} for reasons we will explain below. Note that here the diffusion coefficients, D_i , show up, thus they are part of the numerical solution, as predicted.

This gives us 1 more equation. Thus there are 2 equations left to find. If this was a model for a membrane (with fixed charge density X), then likely both boundaries relate via a Donnan balance to a salt concentration just outside the membrane. If these outside concentrations are known, then via these Donnan balances and Boltzmann's law, we know

the concentrations at positions 0 and np just in the membrane. This gives us the final 2 equations. Note that we only have to provide such an equation for one of the ions, because the electroneutrality constraint gives us the concentration of the other ion on these positions. If we would evaluate the Boltzmann relation for both ions, and then also the EN balance, then the problem is overspecified. Instead, one Donnan and one Boltzmann relationship is evaluated at position 0, and the same at position np. Using the standard Donnan balance, and knowing the outside concentration, c_{∞}^* , then we can calculate on each side the Donnan potential $\Delta\phi_D$ by Eq. (2.9) and we then calculate the concentration of one of the ions just in the membrane by the Boltzmann equation $c_i^* = c_{\infty}^* \exp(-z_i \Delta\phi_D)$, where * refers to the edges of the membrane, either on the very left ($x = 0$) or very right side ($x = L$). Thus we introduce two auxiliary variables, $\Delta\phi_D$, and two additional equations. We now have implemented all information and have exactly enough equations to solve for all unknowns.

One extra thing we can now calculate, ‘afterwards’, is the flux of ions through the membrane, J_i , and thus also the transport numbers, T_i . Focusing on the cation (ion type 1, or +), then the steady-state cation flux, given by the Nernst-Planck equation, after working through the integration approach that was also used in Eq. (21.7), becomes

$$J_+ \cdot L_{\text{eff}} = -D_+ \left(c_{+,np} - c_{+,0} + \frac{1}{2} \sum_{j=1..np} (c_{+,j-1} + c_{+,j}) \cdot (\phi_j - \phi_{j-1}) \right). \quad (21.8)$$

We can now also afterwards calculate the transport number as $T_+ = J_+/J_{\text{ch}}$. This calculation is provided as worksheet 1 [here](#).

—

In an extended calculation we add transport in the boundary films that are on each side of the membrane, using Eqs. (7.13) and (7.41). Now the calculation of J_+ and T_+ can no longer be done afterwards, but becomes part of the set of AEs that must be solved. For $z_+ = |z_-| = 1$, Eq. (7.41) becomes

$$J_{\text{ch}} = - \frac{2D_+D_-}{D_- (1 - T_-) - D_+ (1 - T_+)} \frac{\partial c}{\partial x} \Big|_{x=0} \quad (21.9)$$

which we can combine with Eq. (7.13) to arrive at the equation

$$J_{\text{ch}} = \pm (D_{\text{hm}} \tau)^{-1/2} \cdot 2D_+D_- / (D_- (1 - T_-) - D_+ (1 - T_+)) \cdot (c_{\infty} - c_{\infty}^*) \quad (21.10)$$

which becomes part of the calculation, relating (for a given J_{ch}), the unknown concentration in the boundary film, c_{∞}^* , just at the membrane surface, to the transport numbers, T_i .ⁱⁱⁱ Due

ⁱⁱⁱThe + sign is used for the boundary film left of the membrane, and the - is added for the boundary film on the right side.

to this new calculation, the parameter τ , which describes the degree of convection/stirring outside the membrane, becomes part of the full calculation scheme.

Interestingly, in this particular problem, because all fluxes are constant across the membrane, and thus the T_i 's as well, then when τ is the same on the two sides of the membrane, we immediately see that the two terms $c_\infty - c_\infty^*$ that we must evaluate (one on each side of the membrane) are equal in magnitude but opposite in sign. This information can immediately be implemented in the numerical code, and we then only have to solve Eq. (21.10) on one side of the membrane.

Note that the diffusion coefficients in Eq. (21.10) are those in solution. In the equations for the membrane the diffusion coefficients are those inside the membrane, which are lower than in solution. But for steady state, the effect of this reduction can be implemented by using a value of L_{eff} that is larger than the real membrane thickness L . Namely, to account for various effects that reduce the transport rate in the membrane, summarized in a factor mrf, we can use $L_{\text{eff}} = L \cdot \text{mrf}$. Then the D 's in Eq. (21.7) and (21.8) can be the same as in solution.

Thus we now have implicit relationships on the boundaries involving c_∞^* , c_+^* , the current J_{ch} , and the transport numbers, T_i . The transport numbers are not preset constants, but follow from the numerical calculation. We can solve this full model, as we show in worksheet 2 [here](#). Interestingly, this entire steady-state problem of current-driven membrane transport, including two diffusion boundary layers on either side, does not require numerical evaluation of a gradient at the edge of a domain.

Evaluation of gradients on domain boundaries. In some cases, certainly for dynamic calculations, we often do have to evaluate gradients on domain boundaries directly, because they relate to a flux J , without being able to resort to integrated equations or overall balances. We try to avoid such gradient-expressions as much as possible (unless they are zero, which is the case for symmetry at a midplane, or for impermeable walls), but when necessary, we strongly advise the 2-step Backward Differentiation Formula (BDF2). For a left boundary, at a position $x=0$ (where $j=0$), after discretization, we then have

$$\left. \frac{\partial y}{\partial x} \right|_{x=0} \rightarrow -\frac{3y_0 - 4y_1 + y_2}{2 \Delta x}$$

while for a right boundary at $x=L$ (where $i=np$), we have

$$\left. \frac{\partial y}{\partial x} \right|_{x=L} \rightarrow \frac{3y_{np} - 4y_{np-1} + y_{np-2}}{2 \Delta x}.$$

When this gradient is zero, such as is often the case for an impermeable wall, or for a symmetry plane, for instance the midplane of a channel, then these equations are zero (i.e., the expressions above can be set equal to zero) and can be simplified by multiplying with $2\Delta x$.

In the Excel file provided [here](#), the membrane model is implemented with $np=10$. In the worksheet, the current J_{ch} can be varied, as well as the two external salt concentrations, c_∞ , the membrane charge density, X , the two ion diffusion coefficients, the effective membrane thickness, L_{eff} , and the solution ‘stirring parameter’, τ .

Thus, as this example shows, we can rather easily solve steady state transport problems using a self-programmed AE-solver in commercial spreadsheet software, and obtain a code that can handle many different parameter settings. Next we discuss how to deal with dynamic problems.

21.3 Solving a dynamic problem

To solve a dynamic (time-dependent, transient) problem, let us again consider the mass balance of ion i , but now dynamically

$$\frac{\partial c_i}{\partial t} = D_i \left(\frac{\partial^2 c_i}{\partial x^2} + z_i \frac{\partial}{\partial x} \left(c_i \frac{\partial \phi}{\partial x} \right) \right) \quad (21.11)$$

Based on the previous section we know that we can evaluate this equation at all inner gridpoints (after discretization with position), and we know how we can evaluate the right side of this equation at any moment in time, t_k , if the left side would be zero. But also when the left side is some explicit function of concentrations, potentials, at that same time, t_k , we can just have this term join the terms on the right side, and the solution methods of the last section can be applied unchanged. The only question is, how to deal with the left side of this equation to arrive at the situation that we can use the AE solution method already discussed.

Let us first simplify this equation, by replacing the entire right side by f , the ‘function’, which we can evaluate at discrete moments in time, thus we write f_k (with k a ‘time-counter’). When in the Crank-Nicolson method this f_k is evaluated at two moments in time, and averaged, it is the entire right side, the function, that is evaluated and then averaged as a whole. Thus it must be stressed that we do not average the concentration or potential, etc. We only average a complete function f that is evaluated at times $k-1$ and k .

Thus, in general this equation becomes, after discretization in space,

$$\frac{\partial c_{i,j}}{\partial t} = f_j \quad (21.12)$$

where the counter j as before refers to a position between 1 and $np-1$. After discretization, the function f_j is the same as the expression in Eq. (21.4). Thus we can evaluate the right side of Eq. (21.12) at all inner gridpoints.

To deal with the left side, the changes in time, we can use the same BDF2 method that we used for the spatial boundary conditions described in the box above, and discretize in time, resulting in

$$3c_{i,j,k} - 4c_{i,j,k-1} + c_{i,j,k-2} = 2\Delta t f_{j,k} \quad (21.13)$$

where Δt is the time between different timelines, which we call the timestep. This equation shows that when all concentrations (and other state variables) are known at timelines $k-2$ and $k-1$, we have now an equation with variables only to be evaluated for the ‘present’ timeline k . All parameters at this timeline we can solve with the AE solver discussed in the previous section. We just have as extra terms the left side of the equation above, which includes constants (concentrations calculated in previous timelines), and an additional term related to concentrations at time k , which we can shift to the right side of the equation, and we can then follow the solution route explained in the box on p. 458. We start with an initial situation that is known at time zero, and then for the first timeline we must use one of the methods that we will discuss below, and from time $k=2$ onward, we can use this BDF2 method.

This method works well and is accurate. However, the disadvantage is that we cannot easily change the timestep while we go. Thus if at some moment the calculation becomes unstable because the timestep is too large, we can’t just redo the last timeline with an arbitrarily different timestep. And vice-versa, we can’t increase the timestep when the changes in time become very gradual. These limitations can be remedied within the BDF2-method but they require extra programming. Without these adjustments, the BDF2 method requires the timestep to stay the same, which makes it less flexible.

Two methods that are more simple and don’t have this disadvantage, are as follows. In both these methods we can freely change the timestep from one timeline to the next. These two methods are the Implicit (or Backward) Euler method, and the Crank-Nicolson (CN) scheme. CN is more precise with respect to the time-integration, but in our experience is more prone to have difficulties with sharp changes such as shocks. We find that the Implicit Euler method is extremely robust, even when sharp changes develop.

Implicit Euler is actually BDF1, where the previous function was BDF2, and can be

presented as

$$\frac{c_{i,j,k} - c_{i,j,k-1}}{\Delta t} = f_{j,k} \rightarrow 0 = \Delta t f_{j,k} - (c_{i,j,k} - c_{i,j,k-1}) . \quad (21.14)$$

Thus, the equations that we must solve with an AE solver are just slightly different from before, with now an addition term $c_{i,j,k}$ and a constant term $c_{i,j,k-1}$. This method can be used right at the first timeline after an initial condition at $t=0$. While the calculation steps from time t_k to t_{k+1} , we can easily change the timestep and make it longer and shorter as we go.

This implicit (backward) Euler method is also the first of the Adams-Moulton methods ($s=0$). The next Adams-Moulton method ($s=1$) is Crank-Nicolson, which is given by

$$c_{i,j,k} - c_{i,j,k-1} = \frac{1}{2} \Delta t (f_{j,k-1} + f_{j,k}) \quad (21.15)$$

which on the left side is the same as Implicit Euler, but the right side is now an average of the function f_k at the present (new) timeline, and the function at the previous timeline, f_{k-1} . This requires extra programming because this old function must be explicitly calculated and stored, and on a next timeline correctly retrieved and implemented. These extra programming steps are not necessary for the implicit Euler scheme.

Thus, though Crank-Nicolson is a wonderful method, we actually mostly use the Implicit Euler method for time integration. If we must improve on precision, we make smaller steps in time and take more positional gridpoints.

To illustrate the use of the Implicit Euler method, we analyze the dynamics of diffusion and electromigration across a planar layer, just as in the previous example, though now we set the charge density X to zero, thus it is an uncharged layer, and on the right side (where $x=L$, $j=np$) –as if it is an electrode– we impose a transport number for cations of $T_+=1$, i.e., only cations react away at this surface, i.e., an electrode which is impermeable to anions.

On the left side of the layer (where $x=0$, $j=0$), one option is to consider that it is in contact with a bulk phase, and thus we can assume/impose a fixed salt concentration there, thus $c_{i,0,k}$ is known at all times k . Anions and cations can freely move across this left interface, thus between bulk and the transport layer. The other option is to make the calculation considered in §7.6, where the system was assumed to be closed off and the total amount of anions was fixed. This is actually equivalent to stating that also at the left boundary we have $T_+=1$. Because the current is constant across the layer, also the cation flux entering on the left side, is equal to that leaving on the right side.

Most of the elements that were used in the previous steady state calculation can be retained in a dynamic model, such as that at each point we have $c_{2,j,k} = c_{1,j,k}$ because of

electroneutrality. The integrated expression for current J_{ch} is also the same, because current is invariant across the layer, also when the problem is time-dependent. However, *this is not the case* for the integrated ionic fluxes, J_+ and J_- . These individual fluxes are only invariant with position in steady state, but not in a dynamic situation.

An interesting overall balance can be used to calculate the ionic fluxes at each position. We set up here a balance for the anion to calculate J_i . The cation flux is at each point then simply the current J_{ch} minus this anion flux J_- . The particular equation that follows is only valid because the anion flux at $x = L$ is zero. For the anion we evaluate a certain average concentration

$$L_j \frac{\partial \langle c_{i,j} \rangle}{\partial t} = J_{-,j} \quad (21.16)$$

where $\langle c_{i,j} \rangle$ is the average concentration in the layer with thickness $L_j = L \cdot (np - j) / np$ that is to the right of a certain gridpoint j . The change of this average concentration equals the anion flux at that position j . This average concentration at a position j is calculated in a numerical scheme by averaging over the layer from j to np , making use of the Trapezoid rule, that in this case is $\langle c_{i,j} \rangle = 1/(2(np - j)) \sum_{\alpha=j+1..np} (c_{i,\alpha-1} + c_{i,\alpha})$.

In a numerical scheme, we can implement this overall balance to calculate J_- , either when using the CN method or the Implicit Euler scheme. When we use the latter, this results in

$$\langle c_{i,j,k} \rangle - \langle c_{i,j,k-1} \rangle = \Delta t / L_j \cdot J_{-,j,k} \quad (21.17)$$

This method shows that also in this dynamic calculation, using an overall balance (in this case over part of the transport layer), we can calculate both fluxes, J_- and J_+ , and thus also calculate the transport numbers, T_i , at all positions and at all times, and we still did not need to explicitly solve the flux of either of the ions by the Nernst-Planck equation evaluated at that particular point. An Excel file that makes this calculation is provided [here](#). This latter example illustrates how much is possible with overall balances of all kinds, integrating fluxes, and making extensive use of the Trapezoid method to numerically integrate across domains. This is a very powerful method to obtain a robust and accurate numerical code.

21.4 Including Acid-Base equilibria

In Chs. 10 and 17 we described in detail how to include acid-base reactions, and also provided details of an example calculations, for CO_2 adsorption in an amine solution, and for acetate and ammonia diffusion across charged membranes. The key aspect for numerical programming is that when we have two ions between which there is chemical equilibrium,

described for instance by $c_1 \cdot c_2 = K$, then we can use this equation, evaluated at each gridpoint, just like an electroneutrality balance, to remove one concentration from the set of unknown parameters. And with more than one such reaction, more and more ion concentrations can be removed from the numerical code. For instance when we have the proton and hydroxyl ion, and bicarbonate acid, H_2CO_3 , and the bicarbonate ion, HCO_3^- , with two reactions and two associated K -values, we quickly reduce the number of unknown concentrations that must be found by the numerical solution route from 4 to 2 (see box on page 458).

Experimental methods

To characterize processes and materials, a range of useful experimental methods is available in the study of electrochemical processes. In this chapter some of these methods are explained in more detail.

For charged membranes, one of the most common methods to characterize a membrane, is measurement of the membrane potential.

For electrode processes, important is measurement of the polarization curve, which relates current to voltage for a steady state Faradaic process, either for a single electrode or for an electrochemical process, and for capacitive processes we have the galvanostatic intermittent titration technique (GITT) to measure electrode charge versus voltage for equilibrium conditions.

Cyclic Voltammetry (CV) is an experiment that is easy to do but not easy to analyze because it is neither steady state nor equilibrium but it is a dynamic experiment, with all parameters time-dependent. Therefore it is more difficult to extract fundamental knowledge from a CV experiment.

Electrochemical impedance spectroscopy (EIS) is a further extension because a large range of frequencies is probed, at a certain voltage off-sets (but always for a small voltage window). In CV and EIS only the charge-voltage characteristic is probed. These two methods can be applied both for Faradaic and capacitive processes, as well as for mixed-type electrode processes.

22.1 Membrane Potential

One of the most common methods to characterize charged membranes, is measurement of the membrane potential. Here two ‘Luggin’-capillaries are placed on either side of a membrane, in two different electrolyte solutions. Inside the capillaries are two reference electrodes. There is a zero current across the membrane. In the standard method two 1:1 solutions are used with a factor of 10 difference in salt concentration. The system will generate a potential across the membrane with two components. The first is the diffusion potential set up inside the membrane, to ensure that counterions are slowed down and coions made to go faster, such that they have equal fluxes, to ensure that the current through the membrane is zero. In addition, on both membrane/solution interfaces a Donnan potential develops because of the high membrane charge. For a highly charged membrane, one that does not allow coions to go through, and as a consequence neither allows transport of counterions, the ‘ideal’ potential that develops is equal to $V_T \cdot \ln(10)$, which is around $\phi_{m,ideal} = 58$ mV for a factor 10 concentration difference. The ‘permselectivity’, α , is now defined as the measured membrane potential, ϕ_m , over this ideal value,

$$\alpha = \phi_m / \phi_{m,ideal} . \quad (22.1)$$

The value measured for α is always below unity, but often quite close to it, and this is taken as evidence that the membrane must be highly selective to allow counterions passage and block coions. However, this is far from true, as analysed in detail in Tedesco *et al.* (2017). In an actual process, with currents running through the membrane, and also solvent flow, coions can permeate the membrane much more than the measured permselectivity suggests.

Nevertheless, this is an important experiment, relevant to characterize a (new) membrane. Because, if we measure that the permselectivity is well below unity, then the membrane may be leaky or in any case not very selective. However, the reverse is not necessarily the case: if the permselectivity is measured to be close to unity, this does not imply the membrane will retain its ion selectivity in an actual process.

Here we give a brief description of how α can be related to one property of the membrane, namely its charge density, $|X|$. In this analysis we set other contributions to the partitioning coefficient to unity, and only consider electrostatics. We only consider the Donnan potentials on the two faces of the membrane and neglect the internal diffusion potential.

Thus for all ions, on both outer surfaces of the membrane, we have the Boltzmann relationship, $c_{m,i} = c_{\infty,i} \exp(-z_i \Delta\phi_{D,j})$, where j refers to either of the two sides of the membrane (below denoted by sides 1 and 2).

When evaluated for both ions of a 1:1 salt, we know that

$$|\Delta\phi_{D,j}| = \sinh^{-1} \frac{|X|}{2 c_{\infty,j}}. \quad (22.2)$$

The membrane potential has contributions from these two Donnan potentials, and from the diffusion potential in the membrane. If we first neglect the latter, and only consider the Donnan potentials, then the membrane potential is given by $\phi_m = |\Delta\phi_{D,1} - \Delta\phi_{D,2}|$. Instead of using the sinh-functions, this same expression for ϕ_m based only on Donnan potentials, is given as the first part of Eq. (22.5).

For a very high membrane charge, the expression for the membrane potential simplifies to

$$\phi_{m,ideal} = |\ln(c_{1,\infty}/c_{2,\infty})| \quad (22.3)$$

and thus the permselectivity can be calculated as

$$\alpha = \left| \frac{\sinh^{-1}(X/2 c_{\infty,1}) - \sinh^{-1}(X/2 c_{\infty,2})}{\ln(c_{1,\infty}/c_{2,\infty})} \right|. \quad (22.4)$$

If the two salt concentrations are a factor 10 different, the denominator here is $\ln 10$.

The calculation in this section is provided as an Excel file and can be downloaded [here](#). As an example, with $c_{1,\infty} = 50$ mM and $c_{2,\infty} = 500$ mM, from Eq. (22.3) we obtain a dimensionless potential of $\phi_{m,ideal} = 2.30$ and thus with $V_T = 25.6$ mV, we obtain $V_{m,ideal} = 58.9$ mV. If the membrane charge is $|X| = 2$ M, we obtain for the two Donnan potential $\Delta\phi_{D,1} = 3.69$ and $\Delta\phi_{D,2} = 1.44$, and thus $\phi_m = 2.25$ and $V_m = 57.5$ mV, and the permselectivity is $\alpha = 0.975$.

—

A well-known extension of this theory is to include the diffusion potential, i.e., the potential drop across the inner part of the membrane that develops to speed up the slowest ion, with the aim to equalize the two fluxes, which is required to make sure the current through the membrane is zero. This diffusion potential depends on the ratio of diffusion coefficients in the membrane. As discussed in detail in Galama et al. (2015), care is required to correctly evaluate the various \pm -signs, relating to the sign of the fixed charge. The equation below uses the $|\cdot|$ -notation to indicate that $|X|$ must be used as a positive quantity. Furthermore the parameter ω is the sign of the fixed membrane charge, which is positive, i.e., $\omega = +1$, for an AEM, and for a CEM, it is negative, and then we have $\omega = -1$. For both these membrane

types we obtain for the membrane potential, defined as the potential in solution 2 vs. in solution 1.

$$\phi_m = \omega \ln \left\{ \frac{c_{2,\infty}}{c_{1,\infty}} \cdot \frac{|X| + \sqrt{X^2 + 4c_{1,\infty}^2}}{|X| + \sqrt{X^2 + 4c_{2,\infty}^2}} \right\} + \bar{U} \ln \left\{ \frac{-\bar{U}\omega|X| + \sqrt{X^2 + 4c_{1,\infty}^2}}{-\bar{U}\omega|X| + \sqrt{X^2 + 4c_{2,\infty}^2}} \right\} \quad (22.5)$$

where \bar{U} is a ratio of ion diffusion coefficients in the membrane,

$$\bar{U} = \frac{D_+ - D_-}{D_+ + D_-} \quad (22.6)$$

where the D_i 's refer to ion diffusion coefficients in the membrane. This equation derives from the Nernst-Planck equation, without consideration of convection or ion-ion friction.

As Eq. (22.5) shows, when the anion and cation have the same diffusion coefficient in the membrane (irrespective of being counterion or coion), the diffusion potential is zero. This is certainly remarkable: without a current, the system will always help the slower ion, even if it is the counterion, the concentration of which is many magnitudes larger than of the coion.

We make a specific calculation based on the same conditions as in the earlier example, and we now chose a CEM, thus $\omega = -1$, and assume the anion to be twice faster than the cation, then we have $\bar{U} = -0.333$, and we calculate a diffusion potential of 1.38 mV based on the second half of Eq. (22.5), see the Excel file via the link above. The sign of this potential is such that it always helps the slower ions, which in this case are the cations, to move from the high-salinity side to the low-salinity side of the membrane. This is remarkable, that the potential has this sign irrespective of whether the slow ions are the coions or counterions. Thus it is even the case when they are counterions and thus in much higher quantities in the membrane than the anions. One might instead think the diffusion potential should be such as to help the coions, if the aim is to arrive at a zero current, because there are far fewer of them. But that is not how diffusion works: diffusion depends on concentration gradients, not on the magnitude of the concentration, thus coions can easily have the same flux as counterions. Now, for this membrane problem, because of the fixed charge X , and electroneutrality, inside the membrane the concentration gradient for anions and cations is always the same. Thus, if they have the same D_i , they have the same flux, without the necessity of a potential gradient. Only when the D_i 's are different, does a potential gradient need to step in to help the slower ion along (and retard the other ion). These results relate to this particular case of there being just two ions. In multi-ion systems –as mentioned at many points in this book– the situation is generally much more complex.

What is also interesting, is that the diffusion potential is low, much lower than the potential that is built up by the Donnan potentials. However, even this potential of 1.38 mV will

significantly affect the derived permselectivity. In the calculation here, we drop from $\alpha = 0.975$ to 0.952 , which is a value ‘two times as bad’. Thus stated differently, when the cation is twice as slow as the anion, for a CEM, the measured permselectivity may be a significant underestimate of the ‘real’ permselectivity (the one we would obtain if we would only measure the Donnan potentials). In the reverse situation, when the cation is faster than the anion, the membrane potential will be higher, and thus the permselectivity closer to unity. Thus, in a CEM, when cations have a higher diffusion coefficient than anions inside the membrane, the permselectivity that is measured will ‘look better’ than for equal diffusion coefficients, thanks to the diffusion potential that is inside the membrane. Interestingly, when we make the cation much faster than the anion (for a CEM), then the membrane potential approaches the ideal value, given by Eq. (22.3), but it never goes beyond it. Thus, numerical analysis shows that the limit of Eq. (22.5) for $\bar{U} \rightarrow \infty$ when $\omega = -1$, results in Eq. (22.3).

—

The question may be raised if relevant information can be obtained if we measure the permselectivity α for other salts than a 1:1 salt, for instance a 2:2 salt, or a 2:1 or 1:2 salt, or even for salt mixtures with more than two ions of different valencies.

We provide an Excel file [here](#) that provides a method to calculate α for arbitrary compositions of the salt solution on the two sides of the membrane, considering only the two Donnan potentials. For a certain membrane charge X (a signed quantity, i.e., can be both positive or negative), the Excel file provides the value of the membrane potential, the ideal value (if the membrane charge is very high), and the ratio of these two potentials, which is α . The equation used on each side of the membrane is Eq. (2.5), with σ_w replaced by X .

A calculation using this Excel file of a 1:1 salt with one extra divalent ion, results in the observation that ... α can be higher than unity ! This is an interesting result. However, it also suggests that when the aim is to check whether the membrane is intact and charged, there does not seem to be a good rationale for measuring the membrane potential in salt solutions other than a 1:1 salt.

—

Calculation of the membrane potential for an asymmetric (2:1 or 1:2) salt solution including the diffusion potential is more complicated than for a 1:1 salt, and a numerical calculation is required (see Excel file provided).

To calculate the diffusion potential for an asymmetric salt, we use the Nernst-Planck equation. The condition of zero current for a 2:1 salt, like CaCl_2 , leads to

$$-2D_+ \left(\frac{\partial c_+}{\partial x} + 2c_+ \frac{\partial \phi}{\partial x} \right) + D_- \left(\frac{\partial c_-}{\partial x} - c_- \frac{\partial \phi}{\partial x} \right) = 0. \quad (22.7)$$

Local electroneutrality for a 2:1 salt is $2c_+ - c_- + \omega|X| = 0$, and thus $2 \partial c_+ / \partial x = \partial c_- / \partial x$. We can then rewrite Eq. (22.7) to

$$2(D_- - D_+) \frac{\partial c_+}{\partial x} = (\omega|X|D_- + 2c_+(D_- + 2D_+)) \frac{\partial \phi}{\partial x} \quad (22.8)$$

which can be differentiated to

$$2(D_- - D_+) \frac{\partial^2 c_+}{\partial x^2} = \omega|X|D_- \frac{\partial^2 \phi}{\partial x^2} + 2(D_- + 2D_+) \frac{\partial}{\partial x} \left(c_+ \frac{\partial \phi}{\partial x} \right). \quad (22.9)$$

We also use the integration of Eq. (22.8), which is

$$2(D_- - D_+) (c_+^2 - c_+^1) = \omega|X|D_- (\phi^2 - \phi^1) + 2(D_- + 2D_+) \int_1^2 c_+ d\phi \quad (22.10)$$

where 1 and 2 refer to positions at the very edges of the membrane, just inside the membrane. The integral term at the very right is solved numerically using the Trapezoid rule.

Taking the flux expression for the divalent cation, which because of steady state and thus $\nabla J = 0$ results in

$$\frac{\partial^2 c_+}{\partial x^2} + 2 \frac{\partial}{\partial x} \left(c_+ \frac{\partial \phi}{\partial x} \right) = 0. \quad (22.11)$$

We combine this last equation with Eq. (22.9) to arrive at

$$3 \frac{\partial^2 c_+}{\partial x^2} = \omega|X| \frac{\partial^2 \phi}{\partial x^2}. \quad (22.12)$$

These two PDEs are solved at all inner gridpoints to solve for the profiles in c_+ and ϕ .

Results of calculations for the membrane potential for asymmetric salt solutions are presented in Fig. 22.1, which includes the Donnan potentials at the two membrane faces and the diffusion potential that develops inside the membrane. We make calculations for a CEM with two values of the membrane charge, of $|X|=2$ M and 3 M, and consider a 2:1 salt such as CaCl_2 where we assume that the cation diffusion coefficient is half that of the anion. We evaluate the membrane potential for a factor 10 difference between the high salt concentration, c_H , and the low concentration, c_L . We notice in Fig. 22.1 that at low concentrations the membrane potential is in the range of 10-30 mV, to decrease at higher salt

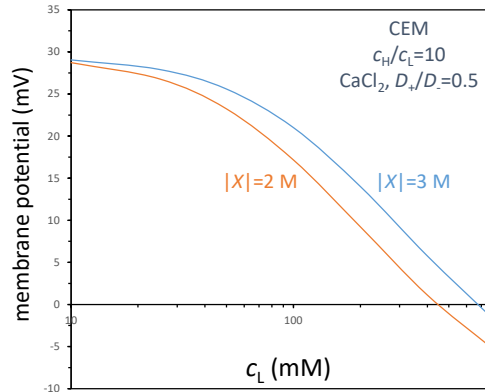


Fig. 22.1: Membrane potential for a cation exchange membrane in a 2:1 salt solution like CaCl_2 with a factor 10 difference in salt concentration for two values of the membrane charge X and as function of the low salt concentration.

concentration, and at sufficiently high salt concentration the membrane potential switches sign. [This sign change can also occur for a 1:1 salt, and is then actually more pronounced.] This switching point shifts to lower salt concentration when the membrane charge density goes down. Note that the membrane potential in Fig. 22.1 is that in the low salinity solution minus in the high salinity solution.

Measuring membrane potentials in symmetric and asymmetric salt solutions can be interesting but the data which come out may be somewhat limited in applicability, for instance because also convection can play a role, driven by the osmotic water transport between the two salt solutions at different concentration. This becomes especially relevant at even higher salt concentration ratios and can lead to the membrane potential even decreasing when the ratio of salt concentrations is beyond 100 (Fig. 8 in Galama et al., 2015). Very thin membranes (less than $10 \mu\text{m}$) are also especially prone to excessive water flow through the membrane, which then also modifies the salt solution concentration just outside the membrane, changing the Donnan potentials.

22.2 Polarization curve for Faradaic processes

Faradaic processes can be characterized in a straightforward and clear way by running a current through the electrode and measuring the electrode voltage. Doing this experiment at many currents, or voltages, results in a complete current - voltage curve, which traditionally

is called the polarization curve. [Note that the same curve is obtained if the experiment is done at various voltage values, and the current measured, or vice-versa, when the current is varied in steps, and the voltage measured. Both lead to the same result, because there is just one current-voltage curve.] The voltage of the electrode is generally measured relative to a reference electrode that is placed near the electrode. The current runs between the electrode under study (the working electrode) and some auxiliary electrode, the counter electrode. The nature of this last electrode is irrelevant, as long as it does not influence the working electrode and reference electrode. Also a full electrochemical cell can be tested, without a reference electrode, and the measured voltage is then the cell voltage, i.e., the voltage between the two electrodes, anode and cathode (no longer is now the vocabulary of working and counter electrode used). Often additional 'indifferent' salt is added to reduce voltages across bulk electrolyte phases, and thus to more closely measure the voltage (and changes in it) in the electrode, and not measure mass transport resistances. Because each data point (one current and the corresponding voltage) is independent of other data, this polarization curve can be constructed bit by bit, with more and more data collection as one goes, in regions of interest. One does not have to measure the data in one rigorous sequence, e.g., from low voltage to high.

22.3 Galvanostatic titration for capacitive processes

Capacitive processes cannot be operated in steady state, thus a polarization curve cannot be recorded, which demonstrates the clear distinction of a capacitive process relative to a Faradaic process. Instead, we can titrate the electrode: we can inject a certain amount of charge (for a certain duration we apply a certain current), let the system equilibrate, and measure the new electrode potential. This is the GITT method which stands for the Galvanostatic Intermittent Titration Technique. GITT can also be reversed: we increase the electrode potential in discrete steps, and after each potential step change we measure the current vs. time (until current goes back to zero). We integrate this current to calculate how much charge flowed into the electrode in response to this step in voltage.

From many such data points we can set up an equilibrium voltage vs. charge curve (titration curve). In such a curve, one reports data points for the charge injected into the electrode as function of voltage (after letting voltage equilibrate). This experiment measures equilibrium properties of the electrode, the EDL, and transport outside the electrode does not influence these equilibrium values of charge and voltage. [Of course the dynamics after each voltage step, or during and after each period of current injection, these can be analyzed, which provides information on the dynamics of the process.]

Ideally, the electrode is purely capacitive for this method to work in an optimal fashion. In that case, after each step change in voltage, the current starts high and then levels off at zero. If it indeed levels off at zero, there is no Faradaic reaction taking place. If it doesn't go back to zero, there is some Faradaic leakage current operating in parallel to the capacitive process. It is possible to separate out the Faradaic process from the capacitive process, but an assumption must then be made, such as that during the entire period at the new voltage the same Faradaic current was running 'in the background'.

One can decide to continue to make steps in voltage or charge, e.g., go to 0.1 V relative to the starting voltage, wait, increase the voltage to 0.2 V, wait, go to 0.3 V, etc., but one can also start at a certain voltage, increase the voltage to 0.1 V, then return to the starting voltage, next go to a voltage of 0.2 V, go back to the starting condition, go to 0.3 V., etc. Thus one returns to some standard situation after each single data point has been measured. This has several advantages, such as that errors in each individual experiment do not accrue. We also have now a check on our own data. Because after having increased the voltage from say 0 V to say 0.2 V and measuring a certain charge that flows to bring the system to equilibrium, when we reduce the voltage again to 0 V, we can evaluate if the same charge now flows back. If these numbers are close, this gives a check that the experiment was done well and Faradaic reactions were minor. (The ratio of these two values of charge, is the Coulombic efficiency.)

Just like for the polarization curve, also with GITT, we don't have to obtain the data points in a predetermined fashion. Instead, we can measure data at will, i.e., we can decide on the fly which voltage or charge to test next. Thus, we do not have to make a rigorous sequence of 0.1 V, 0.2 V, etc., but any random order is fine, collecting more and more data points for this titration curve, based on intermediate data analysis which provides feedback about where more data are of interest.

This experiment can be performed in several very different ways. For instance, it can be done for a certain electrode under study, with the voltage measured relative to a reference electrode, at artificially high salt concentrations. Typically here the method is used where we inject for a certain duration a certain amount of charge, and after relaxation check how much the voltage relative to a reference electrode has changed. A very different approach is to take a complete cell with two electrodes that are considered appropriate for the process (e.g., two porous capacitive electrodes for energy storage or water desalination). Then the voltage between the two electrodes, i.e., the cell voltage, is changed in discrete steps, and the total charge that flows between the two electrodes is measured until equilibrium is established again. In this way an equilibrium charge-vs.-voltage curve for the entire electrochemical cell is measured.

Note that instead of presenting data for electrode charge versus voltage, it can be more

useful to take each increment of charge, when we move from one voltage point to the next, and divide the charge increment by the voltage step.¹ We then have obtained data for the capacitance (expressed in F/g or F/mL) at that value along the curve, and we can then plot capacitance versus charge or versus voltage, see the example of Fig. 1.1 in Ch. 1.

Both methods are commonly used for water desalination with porous electrodes, a method called capacitive deionization (CDI). With the first method, where only a single electrode is tested, typically only the charge is measured versus voltage. However, in a fully operational desalination cell, in addition to measuring the charge, also the total amount of salt removed from the water is measured. In this way important additional information is obtained that can be used to validate an EDL model that is set up to describe the capacitive electrode process.

Thus, in this way not only information is obtained for the voltage-vs.-charge relationship, but also for the dependency of salt adsorption on charge. With these data simultaneously measured, we also obtain information on the equilibrium EDL property called charge efficiency, Λ , which is the ratio of salt adsorption over charge. It must be noted that when a complete cell is measured, all these measured properties are ‘cell-based’ and can only be converted to information pertaining to individual electrodes when an assumption is made. For unmodified microporous carbons a common, and successful, assumption is that of symmetry: the assumption is that for a 1:1 salt the anion behaves similar in the one electrode, as the cation in the other electrode. Or, a very different assumption can be made for cation selective intercalation materials, because here we know that only cations adsorb. With such an assumption in place, information obtained for a full cell can be converted to information on the EDL structure of each separate electrode.

Note that this titration method can be used for any capacitive material, including intercalation materials, or microporous carbons modified with redox functionalities, or secondary batteries (where ions phase-separate inside the electrode). In all these cases the GITT method is an indispensable tool for the characterization of electrodes.

[An interesting phenomenon in CDI is that after a step change in cell voltage, the charge signal rather quickly returns to zero, so it seems that equilibrium is reached. However, the salinity in the flow channel responds much slower and in such an experiment we must wait until the salt concentration levels off before we can take an equilibrium data point (of salt adsorption and charge versus cell voltage).]

Testing of a secondary battery by GITT ideally results for many steps in charge increments, in obtaining the same voltage. This means we are then in the horizontal plateau that is so

¹It is not necessary that these data points were measured in chronological order. They are just an ordered sequence from low to high voltage.

indicative of such a battery, depicted in Fig. 15.2. When after several injections of charge one of the end-points of this plateau is reached, yet more injection of charge now results in the voltage changing to a quite different value. In this plateau, this unvarying voltage –which would also be obtained if we very slowly inject a steady current– might resemble a Faradaic process, as if we could be able to operate the electrode for an infinite time. But this is not the case and the resemblance is only superficial. Because, while in a Faradaic process the electrode in steady state does not change its composition and we can run the process ad infinitum, here, inside the battery electrode, there are dramatic changes under way, with more and more charge and ions stored, like in any capacitive process. It is just that due to the internal phase separation the output voltage is constant in a certain range of charge. Thus, the electrode behaves in what seems to be a Faradaic manner, if only for a brief period of time. This pseudo-Faradaic behavior is discussed more on p. 15.2.1.

22.4 Cyclic Voltammetry

For Faradaic processes, we advise the measurement of the polarization curve, while capacitive processes are described by the equilibrium charge-voltage curve obtained by the GITT method. The first of these two experiments is a steady-state process (no time-dependence on time, but there is transport), the latter is pure equilibrium (no dependencies on time, and no flows).

An experiment that in its analysis is more complicated, is cyclic voltammetry (CV), and that is because it is dynamic. There are flows, and the flows change in time. In CV a certain current is applied for some time after which the current switches and for the same duration the current runs in the opposite direction. While this takes place the electrode potential is measured (the basis of the name voltammetry).

An alternative approach is more common which is to apply a voltage which goes up and then down in a see-saw fashion. In other words, the change in voltage is imposed with a certain ramp, or scan rate (in so many mV/s), first positive (the voltage goes up), and then the scan rate is turned to negative, which makes the voltage go down. In this way many cycles are scanned sequentially. If the voltage is fixed at one or both of the end points of the window that is scanned, a set of curves is obtained that have the same voltage end points. The current is measured as function of time, and plotted versus the voltage (not versus time).

There are many variables that can be changed in such an experiment: there are the two voltages that limit the voltage window, and there is the scan rate by which the voltage is ramped up and down. As function of these three choices, very different curves will be obtained.

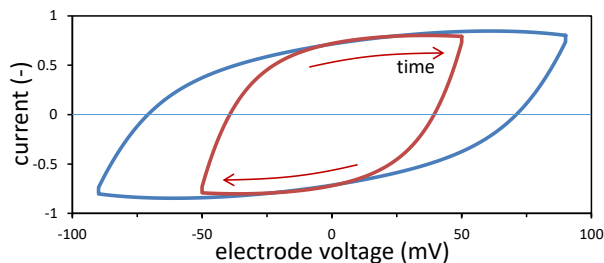


Fig. 22.2: Example diagram of a CV diagram of charging and discharging of a capacitive intercalation electrode.

An important advantage of the CV experiment is that it is easy to do, and available in many laboratories. But a disadvantage is that rigorous analysis of CV curves requires careful analysis, based on a dynamic theory that also includes accumulation of ions and charge near and in the electrodes, also for a purely Faradaic process. This is a reason why analysis of CV curves –and how resulting curves depend on the conditions of the experiments (such as the scan rate and voltage window)– must be undertaken carefully, supported by appropriate mathematical-theoretical tools. Instead, often CV diagrams are heuristically analysed, and information about the electrode process is extracted from several features in the CV diagram, such as its overall shape and the presence of peaks.

In Fig. 22.2 we present examples of the typical rectangular shape for the CV curves of a capacitive material such as the PBA intercalation material discussed in Chs. 1 and 15, using the same parameter settings as in Fig. 1.1. We model the electrode without internal mass transfer limitations. In series to the EDL electrode capacity, described by Eq. (1.23), a linear resistance is placed, as if due to a transport resistance outside the (thin) electrode. The EDL voltage in the electrode and the voltage over the external resistance add up to the measured voltage (which is the x -axis in Fig. 22.2). The entire problem can be described by a single nondimensional parameter, $\mathcal{P} = \gamma \cdot R \cdot \Sigma / V_T^2$, where γ is the scan rate (in V/s), R is the external resistance (in V/A), and Σ is the maximum charge of the electrode (if we could cycle between $0 < \vartheta < 1$; unit C). We do the calculation at two values of \mathcal{P} , and of the voltage window. The CV curve that has the larger window in Fig. 22.2 leads to cycling in intercalation degree in a window of $0.20 < \vartheta < 0.80$ ($\mathcal{P} = 10$). In the smaller window we cycle between $0.33 < \vartheta < 0.67$ ($\mathcal{P} = 5$). The cycle is run through clockwise.

22.5 Electrochemical Impedance Spectroscopy (EIS)

In the method of electrochemical impedance spectroscopy (EIS), a low-amplitude sinusoidally varying voltage signal is imposed to an electrochemical cell, superposed on 'steady' voltage signal (constant, or slowly varying), and the response is recorded, which is the magnitude and phase-shift of the current trace. The period of the response signal (current) is the same as that of the input voltage, i.e., the frequency of the input and output signals are the same. This experiment is done at many frequencies from slow to very fast, and in this way data are obtained that can be plotted in various ways such as a Nyquist plot. Below we will show some examples thereof. EIS is an extremely relevant method for the characterization of all kinds of electronic devices, and electrodes. A novel application is the use of EIS to materials not directly connected to an electronic circuit, such as ion-exchange membranes (IEM). Interestingly, EIS applied to the study of an IEM requires consideration of the changing Donnan layers on the two membrane edges. Neglect thereof results in an effective membrane resistance which decays at low external salt solution. This effective membrane resistance is only representative of the real membrane resistance (which is largely independent of external salt concentration) when tested at high salt concentration, around 1 M salt solution (Díaz and Kamcev, 2021).

When an IEM is placed between two salt solutions and a voltage signal with a certain frequency is applied, the following transport elements must be considered. Unless we are at very high salt concentration, the membrane has a constant conductivity σ_m and we can assume (for now) that the membrane only allows counterions access, i.e., at the membrane outer surfaces we can assume a transport number for counterions of $T_+ = 1$. In the layer in front of the membrane we must solve the dynamics of the salt distribution in the last microns in front of the membrane, by any of the film models discussed in Ch. 7. Here we will use the simplest model and neglect any dispersion effects. We assume a film layer thickness that is large enough that at its 'outside' at all times the concentration is equal to the bulk salt concentration, c_∞ . We assume equal ion diffusion coefficients for the cat- and anion. At the solution-membrane interface, the Donnan equilibrium is established (Donnan EDL model at solution-membrane interface), and the solution salt concentration in this equation is changing throughout the EIS experiment, down in one part of the cycle, up in the other. On the other side of the membrane the same happens, but counter-cyclically. This leads to an additional voltage drop, especially at very low c_∞ which in interpretation of this experiment can be translated as an effective membrane conductivity, steadily dropping the lower the external salt concentration. This effective conductivity must not be confused with the real membrane conductivity which is independent of external salt concentration (below $c_\infty = 1$ M

for an IEM with $|X|$ larger than approx. 2.5 M), see p. 166.

Thus, in conclusion, when EIS is applied to materials not directly part of the electrical circuit, care must be taken in interpreting the data. Counterintuitive results (such as that the membrane resistance is a function of external salt concentration) are best taken as an indication that further system analysis is useful. Or in other words: EIS can provide much useful information of (ion transport in and around) such materials, information that may not be accessible otherwise.

Part VII

Bibliography

General References

- W. Ostwald, *Electrochemistry, History and Theory*, Vol. 1 and Vol. 2, Leipzig (in German) (1896). Translated into English and published by Amerind Publishing, New Delhi (1980).
- A.N. Frumkin, V.S. Bagotskiy, Z.A. Iofa, and B.N. Kobanov, *Kinetics of Electrode Processes*, Moscow (1952). Translated into English by NTIS, Springfield, VA, USA (1967).
- G. Kortüm, *Treatise on Electrochemistry*, Elsevier, Amsterdam (1965).
- D.M. Mohilner, "The electrical double layer," In A.J. Bard, *Electroanalytical Chemistry* **1**, 241–409, Marcel Dekker, New York (1966).
- K.J. Vetter, *Electrochemical Kinetics*, Berlin (1961). Translated into English and published by Academic Press, New York (1967).
- J. O'M. Bockris and A.K.N. Reddy, *Modern Electrochemistry*, Vol. 1 and Vol. 2, Plenum Press, New York (1970).
- T. Erdey-Grúz, *Transport phenomena in aqueous solutions*, Halsted Press, Wiley, New York (1974).
- A.J. Bard and L.R. Faulkner, *Electrochemical methods - Fundamentals and Applications*, Wiley, New York (1980).
- R.F. Probstein, *Physicochemical Hydrodynamics*, Butterworths, Boston (1989).
- K.J. Laidler, "The chemical history of a current," *Can. J. Chem.* **75** 1552–1565 (1997).
- M.R. Wright, "An introduction to aqueous electrolyte solutions," Wiley, Chichester (2007).

Ch. 1 – The extended Frumkin isotherm for the EDL in intercalation materials

- J.T. Davies, "The distribution of ions under a charged monolayer, and a surface equation of state for charged films," *Proc. R. Soc. Lond. A* **208**, 224–247 (1951).
- N.O. Mchedlov-Petrossyan, "The Davies equation of state of ionic surfactant adsorbed monolayer and related problems," *Colloids Surfaces A* **537**, 325–333 (2018).
- P.M. Biesheuvel, W.M. de Vos, and V.M. Amoskov, "Semianalytical Continuum Model for Nondilute Neutral and Charged Brushes Including Finite Stretching," *Macromolecules* **41**, 6254–6259 (2008).
- E. Spruijt, P.M. Biesheuvel, and W.M. de Vos, "Adsorption of charged and neutral polymer chains on silica surfaces: The role of electrostatics, volume exclusion, and hydrogen bonding," *Phys. Rev. E* **91**, 012601 (2015).

K. West, T. Jacobsen, B. Zachau-Christiansen, and S. Atlung, "Determination of the differential capacity of intercalation materials by slow potential scans," *Electrochim. Acta* **28**, 97–107 (1983).

K. Singh, H.J.M. Bouwmeester, L.C.P.M. de Smet, M.Z. Bazant, and P.M. Biesheuvel, "Theory of Water Desalination with Intercalation Materials," *Phys. Rev. Appl.* **9**, 064036 (2018).

Ch. 2 – The Donnan model: the EDL in small pores

P.M. Biesheuvel, "Theory of expansion of porous carbon electrodes in aqueous solutions according to the Donnan model," arXiv:1702.05310 (2017).

P.M. Biesheuvel, "Activated carbon is an electron-conducting amphoteric ion adsorbent," arXiv:1509.06354 (2015).

P.M. Biesheuvel, M.E. Suss, and H.V.M. Hamelers, "Theory of water desalination by porous electrodes with fixed chemical charge," arXiv:1506.03948 (2015).

L. Zhang, P.M. Biesheuvel, and I.I. Ryzhkov, "Theory of ion and water transport in electron-conducting membrane pores with pH-dependent chemical charge," *Phys. Rev. Appl.* **12**, 014039 (2019).

Collagen and the Donnan equilibrium in mixtures of salts

L.-N. Niu *et al.*, "Collagen intrafibrillar mineralization as a result of the balance between osmotic equilibrium and electroneutrality," *Nature Materials* **16**, 370–378 (2016).

Sh.-T. Li and E.P. Katz, "An Electrostatic Model for Collagen Fibrils. The Interaction of Reconstituted Collagen with Ca^{++} , Na^+ , and Cl^- ," *Biopolymers* **15**, 1439–1460 (1976).

Ch. 3 – The EDL for a planar surface: The Gouy-Chapman-Stern model

O. Stern, "ZUR THEORIE DER ELEKTROLYTISCHEN DOPPELSCHICHT," *Zeitschrift für Elektrochemie* **30**, 508–516 (1924).

I. Langmuir, "Repulsive Forces between Charged Surfaces in Water, and the Cause of the Jones-Ray Effect," *Science* **88**, 430–432 (1938).

R. Ellis, "Die Eigenschaften von Ölemulsionen. Teil II. Beständigkeit und Grösse der Kügelchen," *Z. Physik. Chem.* **80**, 597–616 (1912).

D.C. Grahame, "Diffuse Double Layer Theory for Electrolytes of Unsymmetrical Valence Types," *J. Chem. Phys.* **21**, 1054–1060 (1953).

K.M. Joshi, R. Parsons, "The diffuse double layer in mixed electrolytes," *Electrochim. Acta* **4**, 129–140 (1961).

D.M. Mohilner, "THE ELECTRICAL DOUBLE LAYER PART I. ELEMENTS OF DOUBLE-LAYER THEORY," *Electroanal. Chem.* **1**, 241–409 (A.J. Bard (ed.), Dekker, NY (1966).

P.M. Biesheuvel, "Electrostatic free energy of interacting ionizable double layers," *J. Colloid Interface Sci.* **275**, 514–522 (2004).

P.M. Biesheuvel, A.A. Franco, and M.Z. Bazant, "Diffuse charge effects in fuel cell membranes," *J. Electrochem. Soc.* **156**, B225–B233 (2009).

R. Zhao, M. van Soestbergen, H.H.M. Rijnaarts, A. van der Wal, M.Z. Bazant and P.M. Biesheuvel, "Time-dependent ion selectivity in capacitive charging of porous electrodes," *J. Colloid Interface Sci.* **384**, 38–44 (2012).

F. Liu, R.M. Wagterveld, B. Gebben, M.J. Otto, P.M. Biesheuvel, and H.V.M. Hamelers, "Carbon nanotube yarns as strong flexible conductive capacitive electrodes," *Colloids Interface Sci. Comm.* **3**, 9–12 (2014).

Ch. 4 – Ion volume effects in electrochemical processes

J.J. Bikerman, "Structure and capacity of electrical double layer," *Philos. Mag.* **33** 384–397(1942).

H.S. Frank and P.T. Thompson, "A point of view on ion clouds," Ch. 8 in *The structure of electrolytic solutions*, W.J. Hamer (Ed.), Wiley, New York (1959).

P.M. Biesheuvel and M. van Soestbergen, "Counterion volume effects in mixed electrical double layers," *J. Colloid Interface Sci.* **316**, 490–499 (2007).

E. Spruijt and P.M. Biesheuvel, "Sedimentation dynamics and equilibrium profiles in multicomponent mixtures of colloidal particles," *J. Phys. Condens. Matter* **26**, 075101 (2014).

P.M. Biesheuvel, "The activity coefficient of z:1 ionic solutions scales with the cube root of salt concentration," Arxiv:2012.12194 (2020).

J.G. Gamaethiralalage, K. Singh, S. Sahin, J. Yoon, M. Elimelech, M.E. Suss, P. Liang, P.M. Biesheuvel, R.L. Zornitta, and L.C.P.M. de Smet, "Recent advances in ion selectivity with capacitive deionization," *Energy & Environm. Sci.* **14**, 1095–1120 (2021).

Ch. 5 – The energy of an electrical double layer

D.Y.C. Chan and D. Mitchell, "The free energy of an electrical double layer," *J. Colloid Interface Sci.* **95**, 193–197 (1983).

E.M. Blokhuis, Y. Shilkrot, and B. Widom, "Young's law with gravity," *Mol. Phys.* **86**, 891–899 (1995).

F. Zhou *et al.*, "Polyelectrolyte Brush Amplified Electroactuation of Microcantilevers," *Nano Letters* **8**, 725–730 (2008).

E. Virga, E. Spruijt, W.M. de Vos, and P.M. Biesheuvel, "Wettability of Amphoteric Surfaces: The Effect of pH and Ionic Strength on Surface Ionization and Wetting," *Langmuir* **34**, 15174–15180 (2018).

S.H. Kim *et al.*, "Harvesting electrical energy from carbon nanotube yarn twist," *Science* **357**, 773–778 (2017).

E. Virga, W.M. de Vos, and P.M. Biesheuvel, "Theory of gel expansion to generate electrical energy," *EPL (Europhysics Letters)* **120**, 46002 (2017).

Ch. 6 – The interaction forces between colloidal particles

H. Reerink, *The rate of coagulation as a criterion of the stability of silver iodide sols*, PhD thesis, Utrecht University (1952).

J. Gregory, "Approximate expression for the interaction of diffuse electrical double layers at constant charge," *J. Chem. Soc. Faraday Trans. II* **69**, 1723–1728 (1973).

W.B. Russel, D.A. Saville, and W.R. Schowalter, *Colloidal dispersions*, Cambridge University Press (1989).

R. Ettelaie and R. Buscall, "Electrical double layer interactions for spherical charge regulating colloidal particles," *Adv. Coll. Interf. Sci.* **61**, 131–160 (1995).

P.M. Biesheuvel, "Simplifications of the Poisson–Boltzmann Equation for the Electrostatic Interaction of Close Hydrophilic Surfaces in Water," *J. Colloid Interface Sci.* **238**, 362–370 (2001).

P.M. Biesheuvel, "Dynamic Charge Regulation Model for the Electrostatic Forces between Ionizable Materials," *Langmuir* **18**, 5566–5571 (2002).

B.C. Yu, P.M. Biesheuvel, and F.F. Lange, "Compact formation during colloidal isopressing," *J. Am. Ceram. Soc.* **85**, 1456–1460 (2002).

P.M. Biesheuvel, "Electrostatic free energy of interacting ionizable double layers," *J. Coll. Interf. Sci.* **275**, 514–522 (2004).

L. Koopal, W. Tan, and M. Avena, "Equilibrium mono- and multicomponent adsorption models: From homogeneous ideal to heterogeneous non-ideal binding," *Adv. Colloid Interf. Sci.* **280**, 102138 (2020).

Ch. 7 – Solute Transport

P.V. Danckwerts, "Significance of liquid-film coefficients in gas absorption," *Ind. Eng. Chem.* **43**, 1460–1467 (1951).

K.S. Spiegler, "Transport processes in ionic membranes," *Trans. Faraday Soc.* **54**, 1408–1428 (1958).

J. Newman, *Electrochemical Systems*, Prentice-Hall (1983).

P.M. Biesheuvel, "Two-fluid model for the simultaneous flow of colloids and fluids in porous media," *J. Colloid Interface Sci.* **355**, 389–395 (2011).

Ch. 8 – Electrokinetics

R. Schlögl, "Zur Theorie der anomalen Osmose," *Z. Phys. Chem.* **3** 73–102 (1955).

A. A. Sonin, "Osmosis and ion transport in charged porous membranes: A macroscopic, mechanistic model," in *Charged Gels and Membranes I*, E. Sélégny (Ed.), D. Reidel, Dordrecht, pp. 255–265 (1976).

V. Sasidhar and E. Ruckenstein, "Electrolyte osmosis through capillaries," *J. Colloid Interface Sci.* **82**, 439–457 (1981).

M.W. Verbrugge and R.F. Hill, "Ion and Solvent Transport in Ion-Exchange Membranes. I. A Macrohomogeneous Mathematical Model." *J. Electrochem. Soc.* **137** 886–893 (1990).

J.A.M. Kuipers, K.J. van Duin, F.P.H. van Beckum, and W.P.M. van Swaaij, "A numerical model of gas-fluidized beds," *Chem. Eng. Sci.* **47**, 1913–1924, 1992).

P.B. Peters, R. van Roij, M.Z. Bazant, and P.M. Biesheuvel, "Analysis of electrolyte transport through charged nanopores," *Phys. Rev. E* **93**, 053108 (2016).

Ch. 9 – Heating and cooling in electrochemical systems

I. Langmuir, "The relation between contact potentials and electrochemical action," *Trans. Am. Electrochem. Soc.* **29**, 125–x.x (1916).

P.M. Biesheuvel, D. Brogioli, and H.V.M. Hamelers, "Electrostatic cooling in Ion-Exchange Membranes," *Arxiv:1402.1448* (2014).

M. Janssen, E. Griffioen, P.M. Biesheuvel, R. van Roij, and B. Ern , “Coulometry and calorimetry of electric double layer formation in porous electrodes,” *Phys. Rev. Lett.* **119**, 166002 (2017).

S. Porada, H.V.M. Hamelers, and P.M. Biesheuvel, “Electrostatic cooling at electrolyte-electrolyte junctions,” *Phys. Rev. Res.* **1**, 033195 (2019).

Ch. 10 – Combined mass transport and chemical reactions

G. Astarita, D.W. Savage, and A. Bisio, “Gas Treating with Chemical Solvents,” Wiley, N.Y. (1983).

J.E. Dykstra, P.M. Biesheuvel, H. Bruning and A. ter Heijne, “Theory of ion transport with fast acid-base equilibrations in bioelectrochemical systems,” *Phys. Rev. E* **90**, 013302 (2014).

J.E. Dykstra, A. ter Heijne, S. Puig, and P.M. Biesheuvel, “Theory of transport and recovery in microbial electrosynthesis of CO₂ towards acetate,” *Electrochimica Acta* **379**, 138029 (2021).

Part III – Membrane Processes for Water Desalination

S.K. Patel, C.L. Ritt, A. Deshmukh, Z. Wang, M. Qin, R. Epsztein, and M. Elimelech, “The relative insignificance of advanced materials in enhancing the energy efficiency of desalination technologies,” *Energy Environ. Sci.*, **13**, 1694–1710 (2020).

P.M. Biesheuvel, S. Porada, M. Elimelech, and J.E. Dykstra, “Tutorial review of reverse osmosis and electrodialysis,” *J. Membrane Sci.*, **647** 120221 (2022).

Ch. 11 – Reverse Osmosis and Nanofiltration

K.S. Spiegler, “Transport processes in ionic membranes,” *Trans. Faraday Soc.* **54**, 1408–1428(1958).

L. Dresner, “Stability of the Extended Nernst-Planck Equations in the Description of Hyperfiltration through Ion-Exchange Membranes,” *J. Phys. Chem.* **76**, 2256–2267 (1972).

L. Dresner, “SOME REMARKS ON THE INTEGRATION OF THE EXTENDED NERNST-PLANCK EQUATIONS IN THE HYPERFILTRATION OF MULTICOMPONENT SOLUTIONS,” *Desalination* **10**, 27–46 (1972).

E.H. Bresler and L.J. Groome, “on equations for combined convective and diffusive transport of neutral solute across porous membranes,” *Am. J. Physiol.* **241** F469–F476 (1981).

V.M. Starov and N.V. Churaev, “Separation of electrolyte solutions by reverse osmosis,” *Adv. Colloid Interface Sci.* **43**, 145–167 (1993).

Y.S. Oren and P.M. Biesheuvel, “Theory of ion and water transport in reverse osmosis membranes,” *Phys Rev. Appl.* **9**, 024034 (2018).

Ch. 12 – Electrodialysis

A.A. Sonin and R.F. Probstein, “A hydrodynamic theory of desalination by electrodialysis,” *Desalination* **5**, 293–329 (1968).

M. Tedesco, H.V.M. Hamelers, and P.M. Biesheuvel, "Nernst-Planck transport theory for (reverse) electro dialysis: I. Effect of co-ion transport through the membranes," *J. Membrane Sci.* **510**, 370–381 (2016).

M. Tedesco, H.V.M. Hamelers, and P.M. Biesheuvel, "Nernst-Planck transport theory for (reverse) electro dialysis: II. Effect of water transport through ion-exchange membranes," *J. Membrane Sci.* **531**, 172–182 (2017).

M. Tedesco, H.V.M. Hamelers, and P.M. Biesheuvel, "Nernst-Planck transport theory for (reverse) electro dialysis: III. Optimal membrane thickness for enhanced process performance," *J. Membrane Sci.* **565**, 480–487 (2018).

Ch. 13 – The difference between Faradaic and non-Faradaic electrode processes

D.C. Grahame, "MATHEMATICAL THEORY OF THE FARADAIC ADMITTANCE," *J. Electrochem. Soc.* **99**, 370C–385C (1952).

P.M. Biesheuvel, S. Porada, and J.E. Dykstra "The difference between Faradaic and non-Faradaic electrode processes," ArXiv:1809.02930 (2018).

Ch. 14 – Electrode Kinetics

A. Frumkin, "WASSERSTOFFÜBERSpannung UND STRUKTUR DER DOPPELSCHICHT," *Z. Phys. Chem.* **164**, 121– (1933).

M.T.M. Koper, N.P. Lebedeva, and C.G.M. Hermse, "Dynamics of CO at the solid/liquid interface studied by modeling and simulation of CO electro-oxidation on Pt and PtRu electrodes," *Faraday Discuss.* **121**, 301–311 (2002).

L.I. Antropov, *Kinetics of electrode processes and null points of metals*, Council of Scientific & Industrial Research, New Delhi (1960).

Ch. 15 – Porous electrodes

R. de Levie, "ON POROUS ELECTRODES IN ELECTROLYTE SOLUTIONS," *Electrochim. Acta* **8**, 751–780 (1963).

K. West, T. Jacobsen, and S. Atlung, "Modeling of porous insertion electrodes with liquid electrolyte," *J. Electrochem. Soc.* **129**, 1480–1485 (1982).

W. Dreyer, J. Jamnik, C. Guhlke, R. Huth, J. Moškon, and M. Gaberšček, "The thermodynamic origin of hysteresis in insertion batteries," *Nature Materials* **9**, 448–453 (2010).

J.E. Dykstra, K.J. Keesman, P.M. Biesheuvel, and A. van der Wal, "Theory of pH changes in water desalination by capacitive deionization," *Water Research* **119**, 178–186 (2017).

T.M. Mubita, S. Porada, P.M. Biesheuvel, A. van der Wal, and J.E. Dykstra, "Capacitive deionization with wire-shaped electrodes," *Electrochim. Acta* **270**, 165–173 (2018).

T.M. Mubita, J.E. Dykstra, P.M. Biesheuvel, S. Porada, A. van der Wal, "Selective adsorption of monovalent anions in microporous carbons," *Water Research* **164**, 114885 (2019).

Ch. 19 – Redox reactions in environmental chemistry

W. Stumm and J.J. Morgan, *Aquatic Chemistry*, Wiley, New York (1970).

Ch. 21 – Numerical methods in electrochemical processes

D. Schwalbe, H.A. Kooijman, and R. Taylor, "Solving Stiff Differential Equations and Differential Algebraic Systems with Maple V," *Maple Tech.*, 347–53 (1996).

Ch. 22 – Experimental methods

A.H. Galama, J.W. Post, H.V.M. Hamelers, V.V. Nikonenko, and P.M. Biesheuvel, "On the origin of the membrane potential arising across densely charged ion exchange membranes: How well does the Teorell-Meyer-Sievers theory work?," *J. Membrane Sci. Res.* **2**, 128–140 (2015).

Glossary

⊙ **Anode** - The electrode to which the anions move, and where cations move away from, i.e., the electrode to which electronic charge flows from the external circuit, i.e., the electrode that ‘produces’ electrons, i.e., electrons are flowing out of this electrode through the conducting phase (i.e., wires). This definition suffices for a steady state process. In a cyclic process, the definition is very tricky.ⁱⁱ

⊙ **Anode-/cathode-/working-potential** - The potential as measured (often in a three-electrode setup) between a metal wire connecting an electrode under study and a reference electrode.

⊙ **Battery** - A battery is a technological term for all devices that store electrical energy. The first battery was a capacitive device, the Leyden Jar, and (to describe that several were put together) was called a battery by Benjamin Franklin in 1748. Other batteries that are capacitive are the modern-day Li-ion battery. Also Faradaic energy storage devices can be called a battery, such as the lead-acid car battery.

⊙ **Binary salt (solution)** - A salt or electrolyte solution with only one type of cation and one type of anion. The valencies of the two ions and their diffusion coefficients can be different, i.e., if a solution only contains Ca^{2+} -ions and Cl^- -ions, this is a binary (salt) solution. A solution prepared from NaCl only, is also a binary salt. See entries for *symmetric salt* and *1:1 salt*.

⊙ **Bulk (phase)** - The phase located next to an interface that is in some sense ‘larger’ than the

ⁱⁱIn a cyclic process we must define the key process step. In CDI this is the salt removal or charging step. (For a more detailed discussion of terms such as ‘charging step’, see entry below.) In this step we define which electrode is the anode, and which is the cathode. When we now go to the discharge step, we do not change around the anode/cathode definition. Instead, the physical object (‘piece of material’) that was the anode during charging, we also call the anode during discharge. For a battery or supercapacitor, discharge is the key step, and we define anode/cathode based on the discharge step.

interface and in which the concentration and potential show smaller changes with position and time than in the interface. Often to describe the bulk phase, the symbol ' ∞ ' is used, referring to 'of infinite extent', which (from the point of view of the interface or layer next to which bulk is located) is indeed how the bulk phase is perceived. In a bulk phase at each position we can assume local electroneutrality. See [website](#) for more information.

⊙ **Capacitance of an EDL, of an electrode** - The slope of the curve of electrode charge with electrode potential. Capacitance is a function of electrode potential and charge, it is not just a single number. The capacitance is an equilibrium property of the electrode, thus to be measured in an experiment that approaches equilibrium (for instance using the galvanostatic intermittent titration technique).

⊙ **Capacitive Deionization, CDI** - A method of water desalination using cycles of charging and discharging a pair of capacitive porous electrodes. Can also be called Battery Deionization (BDI) or Battery Desalination.

⊙ **Capacitive electrode process** - An electrode process in which the electrode structure (gradually) changes when current flows across the electrode. Thus (except for the case of phase separation inside the EDL), one will see the electrode potential continue to change.

⊙ **Capacity of an EDL, of an electrode** - The measurable property of a capacitive electrode as the change in charge of the electrode when the electrode potential is changed from one to the other value (potential window), often divided by volume or mass of the electrode. If reference is made to 'the' capacity, this refers to the maximum, or limiting, value, i.e., an even larger potential window will not change the measured capacity. Measured for equilibrium.

⊙ **Capacity of an electrode pair** - The measurable property of a pair of capacitive electrodes as the charge (in one region of one of the electrodes) at one non-zero value of the cell voltage relative to the charge when the cell voltage is zero.

⊙ **Cathode** - The electrode where cations flow to, and where anions move away from, i.e., the electrode where electrons arrive at. This definition suffices for a steady state process. For cyclic processes, see an earlier footnote.

⊙ **Cell voltage** - The measurable voltage between two electrodes. For a constant current, the cell voltage changes in time when the composition of the electrolytes or other phases changes, or because the electrode structure changes.

⊙ **Charge** - An amount, often with dimension C (coulomb). By dividing with Faraday's number, F ($F = 96485$ C/mol), charge expressed in C is converted to charge expressed in mol(es). Charge can be positive and negative, and charge can flow. The flow of charge is called a current. Part of an ionic solution (electrolyte) can contain charge, *ionic charge*, and likewise in a metal there can be charge. This charge would then be called ionic charge or electronic charge, respectively. Important to note is that a positive electronic charge in some

region, means there is a deficit of electrons there. And the statement that at some position ‘the electronic charge goes up,’ means electrons leave this region. See also entries *EDL charge* and *Electrode charge*.

⊙ **Charge transfer electrode** - An electrode where electrons or ions (i.e., charged particles) are transferred across the full electrode in an ongoing electrode reaction, where at least one reacting species (ion, atom, electron) is transferred from one bulk phase outside the electrode to another bulk phase outside the electrode. A better term would have been charged *species* transfer electrode. In any case it is an electrode in a Faradaic electrode process.

⊙ **Charging step / Discharge step** - In cyclic electrochemical processes, such as water desalination by CDI, in a full cycle there is a period of charging the cell, and a period where the cell is discharged. These periods can be called ‘steps’, as in: charging step, and discharge step. A certain electronic condition is changed at the moments we go from one step to the other, such as changing the current direction, or a change in the setpoint of the cell voltage. For certain CDI designs it is not so obvious what part of the cycle is to be defined as the charging step and which as the discharge step. It is then customary that the charging step is when the electrical energy input is larger than in the discharge step. Note that the time frame (starting time to end time) of a charging step does not coincide with the time period that desalinated water flows out of a CDI device. With more than two steps in a cycle, multiple of these steps can be called charging, other discharge.

⊙ **Chemical equilibrium** - Equilibrium related to transport or reactions of species (such as ions). For instance referring to an EDL structure where it can be assumed that the structure of the EDL (as defined by concentration and potential profiles) does not depend on transport processes, e.g., the EDL structure does not depend directly on how much current runs through the EDL. Such an EDL structure quickly adapts to external changes to form a (new) equilibrium structure. The advantage of being able to assume an equilibrium structure, is that the equations describing the structure significantly simplify compared to those required for transport. || That an EDL is at equilibrium does not mean ions do not exchange between the EDL and adjacent bulk phases. Instead, there is certainly mobility and exchange, but for each n ions of one type leaving the EDL, n ions of the same type also come back.ⁱⁱⁱ Chemical equilibrium also relates to chemical reactions between species, at some position in solution, being described by an equilibrium reaction. Note that under the Chemical Equilibrium assumption there can still be a transport or conversion with reactions going from reactants

ⁱⁱⁱIf an EDL has say Na^+ cations as counterions, and it is at equilibrium, and we now bring it in contact with a solution with K^+ -cations, the Na^+ ions in the EDL are exchanged for K^+ . But if K^+ and Na^+ behave in the same way, have the same properties, even then we can say that during the exchange, in some respects the EDL always was at chemical equilibrium.

A to products B. Only in The Equilibrium State are these transport processes or conversions zero.

⊙ **Coion (also written as co-ion)** - The ion of the same charge sign as the charge of the surface or porous structure. Often at a lower concentration compared to outside the EDL or porous structure.

⊙ **Conductivity** - The (ionic) conductivity, or conductance, of an ionic solution is often described by the symbol σ or κ , and has the unit S/m (with S for Siemens) or $(\Omega \cdot \text{m})^{-1}$, where $S = 1/\Omega = A/V$. Often Ω is called (and written as) 'Ohm'. The volumetric resistance ρ of an electrolyte solution is $\rho = 1/\sigma$ with unit $\Omega \cdot \text{m}$, see p. 165 and p. 248. Conductors (metals) have a certain *electronic* conductivity.

⊙ **Conductor, or metal** - A conducting phase, or conductor, conducts electrons not ions. It will be the wires connecting electrodes to a power source or other type of electrometer. There is no background charge. || The terms 'Ion conductor', and 'ion conductivity' relate to the electrolyte phase.

⊙ **Convection** - Convection is the mechanism by which solutes, such as ions, are dragged along with the moving fluid.

⊙ **Coulombic efficiency** - For a cyclic process of charging and discharge, such as in CDI, the ratio of 'returned charge' (the charge expressed in C, transferred between the electrodes during the discharge step), over 'charge input' (the charge transferred between the electrodes during the charging step). A dimensionless number, less than unity.

⊙ **Counterion** - The ion of opposite charge sign to the (fixed) charge of a surface or porous material. Often therefore at an enhanced concentration compared to outside the EDL or porous structure.

⊙ **Current efficiency** - For a membrane the ratio of the total molar flow rate (of all ions added together), over the current density. A dimensionless number. Only used when all ions are monovalent.

⊙ **Dielectric** - A dielectric (material) is a material, or a layer, that does not *contain* any type of charged species, neither electrons nor ions. In the context of the dielectric capacitor, it is also implied that it does not *conduct* any type of charge. The Stern layer, a theoretical approach in EDL modelling, in some regards is considered in the same way, i.e., to block transfer of ions or electrons. However, in electrode reaction modeling (Frumkin-equation) it nevertheless is looked upon as the layer across which ions or electrons hop from one phase to the other. A synonymous term is *insulator* or insulating layer.

⊙ **Dialysis** - This is a process where a selective membrane is placed between two solutions with different solute composition (e.g., different salt concentration), and solutes (salts) and water flows through the membrane only because of concentration differences, without an

applied pressure difference or current. Also call the osmosis experiment.

⊙ **Diffuse double layer** - An erroneous term, conflating diffuse layer and EDL. What is meant is: diffuse layer.

⊙ **Diffuse layer** - A theoretical element of an EDL model, relating to the profiles in ion concentration and electric potential in an electrolyte that develop because of a balance of electrostatic and entropic forces. The thickness of the diffuse layer relates to the Debye length, which decreases with increasing salt concentration, and also decreases with increasing valency of the ions.

⊙ **Diffuse layer potential, Donnan potential** - Both these potentials are denoted by ϕ_D . In a Gouy-Chapman-(Stern) model, this is the electric potential across the diffuse layer, thus the potential at the Stern plane relative to outside the EDL. In an extended Donnan model for ion-containing micropores, ϕ_D is likewise the potential inside the micropore volume, relative to outside the EDL/micropore. For membranes, at the solution/membrane interface, Donnan potential refers to the electric potential difference between inside the membrane (micro-)pores and just outside the membrane, thus across the full EDL that is the solution/membrane interface.

⊙ **Dynamic** - A dynamic process is not at steady state, thus some or all process elements change in time. Note that for many processes it is often the case that certain elements are in chemical equilibrium (for instance the EDL structure), other elements are in steady state (transport through a microporous membrane, or a mass transfer film), and yet other elements are dynamical (accumulation of salts in reservoirs). Which modelling approach to choose, and how to combine these elements, are key aspects of electrochemical process modelling and design.

⊙ **EDL, or electrical double layer** - The EDL is the structure at the interface between bulk phases (i.e., it *is* the interface), in situations where at least some charged species such as ions are involved. Across the EDL there is a voltage difference, and within the EDL are regions of opposite charge. On the two sides outside the EDL there are two charge neutral bulk phases. These phase either contain charge carriers (ions in an electrolyte, or electrons in a conductor) or do not (insulator). When we compare the field strength, E , in the EDL (very dependent on position in the EDL) with that in bulk, then we note that in the two bulk phases E is very low, or zero, and it is much higher in the EDL. The EDL as a whole is charge neutral.

⊙ **EDL charge** - If an EDL is overall charge neutral, how can it be we generally use the term 'EDL charge' and related concepts such as the capacitance of an EDL? The answer is that these terms, such as EDL charge, refer to one of the regions of the EDL. For instance, it refers to the region that can be associated with the (electron-)conducting phase (inside the

EDL), thus related to the electronic charge stored in the EDL. See also entries *Charge* and *Electrode charge*.

⊙ **Electrical field (strength)** - see *Field strength*.

⊙ **Electrochemical water desalination** - The group of water desalination methods that makes use of elements of electrochemical processes, such as ion transport, charged media, and electroneutrality. Examples are reverse osmosis, capacitive deionization, and electrodialysis.

⊙ **Electrode** - A special type of EDL, namely formed at the interface of a (semi-)conductor and electrolyte. The EDL is an interface (see entry about *Interface*) and includes several regions of opposite charge that are within this region where conductor and electrolyte are in contact. On one side of the electrode is the charge-neutral bulk metallic phase, and on the other side the charge-neutral bulk electrolyte. The processes at an electrode can be capacitive or Faradaic. A Faradaic process involved transfer of ions or electrons across this interface. This is the formal, theoretical, definition of an electrode. In an oxidation reaction, an electron is liberated from ions *all within* the electrode, and the electron then leaves the electrode to go into the bulk metal phase. In all electrodes current flows across the electrode (across the EDL) and is unchanged in 'numerical value'. However, its nature changes, from ionic to electronic (or the reverse). [That we can assign a direction is only because it was decided that a flow of electrons relates to a negative current; a flow of cations a positive current, etc. Other than because of this arbitrary convention, there is no 'real' direction to the current and there is not an intrinsic physical reason to say that in some experiment electronic current became ionic current, or the reverse. We can only do that because we decided that a flow of anions or electrons contributed to a negative current.] Thus an electrode is an interface that changes the nature of a current flow, from ionic to electronic (or vice-versa), but the current remains unchanged in a numerical sense.

⊙ **Electrode^{TC}** - The technological convention (TC) of the word electrode refers to the piece of metal that is brought in contact with electrolyte. In this convention, in an oxidation reaction an electron 'goes into the electrode.' *In this book we will not use the index 'TC' and thus the word 'electrode' can have both meanings.*

⊙ **Electrode charge** - The charge in an electrode, by which is meant the charge in one or more of the regions of the electrode. It does not refer to the electrode charge as a whole, because the electrode as a whole is always charge-neutral, and thus the total charge is zero. Often refers to a difference in charge between two situations (e.g., moments in time; 'the charge was increased by 5 C'), and generally refers to the charge on the metallic (electron-conducting) side. See also entries *EDL charge* and *Electrode charge*.

⊙ **Electrode potential** - The potential across the electrode. Note, the electrode is the EDL

structure at the interface of (multiple) phases, at least one of which conducts electronic charge and at least one of which conducts ions. The electrode potential is a function of the electrode (EDL) charge.

⊙ **Electrode reaction** - The reaction in an electrode, which involves electrons, and atoms and molecules coming from nearby non-metallic bulk phases, of which one phase at least is an electrolyte phase. Often the electrode reaction involves reactant species adsorbed to the surface and the reaction product is also an adsorbed species, which subsequently desorbs. An example is the oxidation of an adsorbed H-atom, to a proton, H^+ , while releasing an electron into the electrode. Reactions in an electrode (e.g., between adsorbed species) that do not involve electronic charge are not called an electrode reaction. We do not need two electrodes to have an electrode reaction. When we have a single electrode, for instance a reference electrode, or even just a piece of metal, and we bring it into contact with an electrolyte, an electrode reaction may occur and charge builds up in the EDL. So for a brief period an electrode reaction took place. Also in a dynamic process with two electrodes (with possibly one electrode capacitive) we can have electrode reactions. The two electrode reactions on the two electrodes can have different rates. The two electrode reactions do not need to add up perfectly from two half-cell reactions into one overall reaction, see also §14.1. An important distinction is between the (rate of the) ‘electrode reaction in the direction of reduction’, R_R , and ‘reduction (reaction)’, ϱ_R , and similarly for the difference between ‘electrode reaction in the direction of oxidation’, R_O , and ‘oxidation (reaction)’, ϱ_O , see Eq. (15.4) for the difference, which is that $R_R = -R_O = \varrho_R - \varrho_O$.

⊙ **Electrolyte** - A phase that contains ions, ions that move around because of diffusional and electrostatic forces. In a liquid electrolyte there is also convective transport of ions. In contrast, in a solid electrolyte, or solid salt, like AgCl that forms a crystal structure, anions and cations can move relative to one another. There is only a frictional factor that describes the resistance of this movement of cations relative to anions. There is no solvent in such a solid electrolyte. In between these two cases are electrolyte phases that do contain solvent but the solvent and ions are highly restricted in their motion. For instance, inside the pores of an intercalation material, or inside the pores of other (micro-)porous structure, such as in porous carbons, or inside the pores of a hydrated ion-exchange membrane or other gel-like structure built up of charged polymer, there is solvent through which ions can pass, but similar to a solid salt we have a rigid structure of charged atomic constituents. Perhaps these materials should be called semi-electrolytes.

⊙ **Electrometer** - The name for all devices that can impose and record currents and voltages applied to an electrochemical cell. The term captures specific terminology such as voltmeter, power source, battery, load, potentiostat, galvanostat, etc.

- ⊙ **Electron acceptor** - a species that (is able to) take(s) up an electron, thereby being reduced; its charge becomes more negative. So before the reaction happens, it is in the oxidized state, afterwards it is in the reduced state. This could be at an electrode, but this terminology more generally refers to redox reactions in solution. Then, while species A is the electron acceptor, another species D donates the electron. While species A is reduced, species D is oxidized. Thus, species A is the oxidant (the reaction leads to another species being oxidized).
- ⊙ **Electron donor** - a species that (is able to) give(s) off an electron, thereby being oxidized; its charge becomes more positive. So as long as the reaction hasn't happened yet, it is in the reduced state, afterwards it is in the oxidized state. This could be at an electrode, but this terminology more generally refers to redox reactions in solution. Thus, while species D is the electron donor, another species A accepts the electron. While species D is oxidized, species A is reduced. Thus, species D is the reductant (the reaction leads to another species being reduced).
- ⊙ **The equilibrium state** - A situation where there are no net flows, no fluxes, no net reactions. Reactions can go back and forth, but there are no net conversions.
- ⊙ **Faradaic electrode process** - An electrode process that with current flowing, can go on forever, because the structure of the electrode does not change in time. Ions and electrons entering the electrode (the EDL) from one bulk phase adjacent to the electrode, also leave the EDL again to the same, or to another, bulk phase. Thus, ions or electrons transfer across the EDL in a Faradaic process.
- ⊙ **Faradaic reaction** - An electrode reaction, a 'half-reaction' where participating ions, atoms, molecules, on the reactant side and product side, all potentially can come from outside the electrode, and leave the electrode again (possibly after further (non-electrode) reactions in the electrode).
- ⊙ **Field Strength** - The field strength, \mathbf{E} , is a vector quantity that is the negative of the gradient of the electric potential, $\mathbf{E} = -\nabla V$. When only one spacial coordinate needs to be considered, x , we have $E = -\partial V/\partial x$. In this book we general use the dimensionless potential $\phi = V/V_T$, where V_T is the 'thermal voltage' given by $V_T = RT/F$ and thus $E = -V_T \partial \phi/\partial x$.
- ⊙ **Flux** - The flow of a species divided by the perpendicular surface area through which the flow is directed, thus with unit mol/s divided by m^2 , resulting in the unit $\text{mol}/(\text{m}^2 \cdot \text{s})$. In transport studies with porous materials careful attention is required to distinguish *interstitial* and *superficial* flow rates, fluxes, and velocities.
- ⊙ **Hydrostatic (hydraulic) pressure** - The pressure at some point in an electrolyte phase. The hydrostatic pressure can be measured as the pressure required to create a small extra

volume inside the phase at that position. The difference in hydrostatic pressure between inside and outside a charged (polymer) network exerts an expansive force on the network.

⊙ **Interface** - The region formed when two different phases or materials are brought in contact. The interface is not an ‘mathematical’ infinitely thin 2D layer, i.e., it is not a *surface*. Instead, it has an extension, a thickness. Others have then proposed the term ‘interphase’ but we stick to using the more common term ‘interface.’

⊙ **Ionic current (density)** - The current carried by ions. Current (density) can have unit A, A/m² or mol/m²/s.

⊙ **Mechanical equilibrium** - The (near-)equality of the forces responsible for flow of fluid. In bulk solution this would be constancy of hydrostatic pressure. In an EDL this would be constancy of the total pressure (hydrostatic pressure minus osmotic pressure). When EDLs are at chemical equilibrium, it is reasonable to assume they are also at mechanical equilibrium, see entry *Chemical equilibrium*.

⊙ **Migration or Electromigration** - The movement of an ion or other charged solute inside an electrolyte phase or charged porous structure because of a local non-zero electrical field. One of various driving forces that can act on an ion.

⊙ **Osmotic pressure** - Not really a pressure in the sense that the hydrostatic pressure is. Nothing happens in a solution at high osmotic pressure. One can create a small ‘cavity’ or ‘bubble’ of volume inside an electrolyte, at a cost unrelated to the local osmotic pressure. The osmotic pressure in a phase is simply a function of the concentrations of all freely moving solutes (and a function other contributions to the chemical potential of the solutes, such as excess, volumetric, effects).

⊙ **Oxidant, oxidizing species** - see entry *electron acceptor*.

⊙ **Partition coefficient** - The partition coefficient, Φ_i , also called solubility, S_i , describes the concentration of a species (solute, ion) i in a phase/environment $j=1$ relative to another phase $j=2$, thus $\Phi_i = c_{i,1}/c_{i,2}$. Here for instance $j=1$ is a membrane and $j=2$ an electrolyte solution. The calculation is based on equality of chemical potential, μ_i , for the species between two positions on either side of the interface. Thus a *difference* in a certain contribution to μ_i matters. (A difference for species i between phases 1 and 2.) Three possible contributions are discussed next, leading to $\Phi_i = \Phi_{\text{aff},i} \cdot \Phi_{\text{exc},i} \cdot \Phi_{\text{D},i}$. When one of these Φ_i -values is larger than unity, then apparently that term results in a preference for the solute or ion to be in phase 1 rather than in phase 2. Vice-versa, a value less than unity implies there is an energetic penalty for the ion or solute to be in phase 1 (instead of in phase 2), and thus it will still be there, but at a lower concentration. These three contributions are:

1. the effect of ‘affinity,’ described by $\Phi_{\text{aff},i}$, which is the result of a difference in chemical interaction of the solute with the two phases, with the local environments.

2. the effect of volume of the solutes, described by $\Phi_{\text{exc},i}$, which is the excess contribution, due to volumetric interactions of a solutes with one another and with solid constituents fixed in place (e.g., the polymer structure of a membrane, or another matrix). Interestingly, the solute under study, i , may be infinitely small ('volumeless'), but still the presence of other solutes, or the matrix can influence this excess contribution for species i .
 3. the Donnan effect which is due to the requirement of electroneutrality in both phases, where typically one of the phases also has a permanent charge. The Donnan effect, described by $\Phi_{\text{D},i}$, influences the distribution of an ion between phases, and is generally described by a Boltzmann-type electrostatic term, $\exp(-z_i\Delta\phi)$, replacing the more general $\Phi_{\text{D},i}$ -notation.
- ⊙ **Porous electrode** - A porous electrode is a multi-phase material of the following constituting phases: an electroneutral region of water and ions (electrolyte); an electron-conducting (and electron-containing) phase; and a structural matrix to provide mechanical strength. The interface of electrolyte and conductor, i.e., the EDL, is often formed inside sub-nm diameter 'micropores', which are electrolyte-filled pores inside an electron-conducting matrix.
 - ⊙ **Potential** - Often referring to the electric potential at some position relative to another position, then with symbol ϕ , often dimensionless (i.e., multiplication with the thermal voltage leads to a 'voltage' with unit V). But potential can also refer to the chemical potential of an ion or other solute, often denoted by μ_i . Chemical potential refers not just to an ideal entropic term $\ln c_i$, but instead is a summation over all sources that can change the 'potential' of a molecule, including volumetric and affinity effects, charge, and also gravitational effects can be included in the chemical potential of a solute. One can add the adjective 'total' to make it clear a summation of many contributions to the chemical potential are considered.
 - ⊙ **Reductant, reducing species** - see entry *electron donor*.
 - ⊙ **Round trip efficiency** - An efficiency number between 0 and 1, describing how much energy (unit J) is provided by an energy storage device during use (discharge), relative to the energy required to recharge the device.
 - ⊙ **Semi-conductor** - Like a metal, a semi-conductor also has electrons as charge carriers, but in addition the material has fixed charges ('p-doping' or 'n-doping'). The conductivity is much lower than in a metal.
 - ⊙ **Space-charge region** - The same as diffuse layer, often applied for the diffuse layer inside a semi-conductor.
 - ⊙ **Stern layer** - A theoretical element of an EDL model. The Stern layer is a constant-capacitance element envisioned to be located between the diffuse layer and the charged surface. It does not contain charge itself. Its thickness can be assumed to relate to the

(hydrated) radii of counterions, because that represents the closest-approach distance of the centers of the counterions to the surface. A typical value used in colloid science would be $C = 0.2 \text{ F/m}^2$. Also called Helmholtz layer.

⊙ **Stern plane (Outer Helmholtz plane)** - Also a theoretical element of an EDL model, being the surface, the theoretical dividing plane, between the Stern layer and the diffuse layer. It is not a plane that contains counterions, as it is unfortunately often depicted in textbooks. It is simply the closest approach distance for the centers of ions to approach the charged surface. (In very advanced EDL models, there can possibly be consideration of specific adsorption of ions in this plane.)

⊙ **Surface** - Mathematical two-dimensional plane without a thickness.

⊙ **Steady state** - A very important word describing how in a process there are flows and reactions, but at any location there are no observable (macroscopic) changes *in time* of state variables such as concentration, pressure, and temperature. In a theory, this means that accumulation terms $\partial/\partial t$ in mass and heat balances can be set to zero.

⊙ **Symmetric salt (solution)** - This is a salt solution where all ions are monovalent, or all are divalent, or all trivalent. Out of all cations, there can be several types of cations (all with the same valency), and the same for all ions in solution. The 1:1 salt (solution) describes a symmetric salt where all ions are monovalent. See entries *binary salt (solution)* and *1:1 salt (solution)*.

⊙ **Transference number** - The ratio of an ion's $z_i^2 D_i c_i$ over the sum of that term evaluated for all ions in the system, at a particular position (e.g. different in a membrane, compared to in solution). The symbol t_i is used. Each ion's transference number is between 0 and 1. The summation over all t_i 's is unity.

⊙ **Transport number** - The ratio of flux of ion i times its valency z_i , over the ionic current density, see p. 170, for which the symbol T_i is used. The transport number is dimensionless (the current density is expression in $\text{mol/m}^2/\text{s}$). It will depend on position and time. Inside a (one-dimensional, planar) membrane, operating in steady-state, and without reactions, the T_i 's are invariant across the membrane. Transport numbers can be less than zero and larger than one. The sum of all transport numbers of all ions in the system, is unity. Sometimes transport numbers and transference numbers are the same.

⊙ **Valency** - The valency of an ion, z_i , or an ion's charge, is a discrete number, such as +1, +2, or -1 or -2, etc. It does not have a unit. And it is 'signed', that is, it is a positive number for a cation, and a negative number for an anion. In some problems it makes sense to include the possibility that an ion has valency 0, and still call it an ion. Thus bicarbonate is a monovalent anion and when protonated becomes the uncharged carbonic acid 'ion'.

⊙ **1:1 salt (solution)** - A salt solution where all ions are monovalent. A 1:1 binary salt

(solution) has a more restricted meaning because a 1:1 binary salt (solution) contains only one type of anion and one type of cation, and both are monovalent). Examples are KCl and NaCl. [Or, there may be more than one type of cation in a real solution, but we treat it in a theoretical model as if it is a 1:1 salt.] See entries *binary salt (solution)* and *symmetric salt (solution)*.

Technical conventions

In this book the following conventions are often followed:

1. Two parameters x and y are *linearly* related when they relate according to $y = a \cdot x + b$, with a and b constants. In addition, variables x and y are *proportional* to one another when $b = 0$. Thus a proportional relationship is a special type of linearity, i.e., a proportional relation is also linear, but a linear relationship is not necessarily showing proportionality between x and y . When x and y relate according to $y = x + b$, i.e., $a = 1$, this is a specific type of linearity, for which there is no specific term but we can write ‘are the same (i.e., are equal) but for a constant offset b ’, or ‘are linearly related with slope 1.’ See below at item 26.
2. Often we define an axis, a positional coordinate, which we generally give the symbol x . By default this coordinate axis runs ‘left to right’ in the descriptions that we use, i.e., it points ‘to the right’. To us the following three statements mean the same thing, namely that a flux, or velocity, or current (density), is positive, or that it has a positive value, or that it ‘points to the right’.
3. If we then define a difference in a parameter, Y , often denoted by ΔY , this is generally the value of the parameter on a position (more to the) right, minus its value at a position more to the left, i.e., a ΔY is always defined ‘right minus left’ in the axis convention just defined. Potentials in an EDL model, such as for the Donnan, diffuse layer, or Stern potential, are always defined more inside the EDL or more inside the porous structure (membrane) relative to ‘more outside’, which in the end is the outside electrolyte phase. Thus always defined as ‘(more) inside minus (more) outside.’ The electrode potential, V_e , is the electric potential inside a metallic phase relative to (i.e., minus) that in the adjacent electrolyte phase (between two positions that both are outside the EDL).
4. The words ‘electric’ and ‘electrical’ can refer to the electron-conducting phase (e.g., metal), as well as to electrolyte. i.e., they have a broad meaning also encompassing the electrolyte. Thus ‘electric(al) current’ can also refer to the ionic current in solution.
5. However, the word ‘electronic’ does refer to the electron-conducting, metallic, phase. Thus electronic charge or electronic current is charge or current in the ‘wires’ or other external circuit elements. Note that ‘electronic charge’ or ‘electronic current’ is not defined as the flux of electrons,

i.e., the negative charge carriers. Instead, all currents, ionic and electronic, describe the flow of charge. Thus with a coordinate axis x pointing 'to the right' (see point 1 above), a positive current means that there is a net transport of positive charge carriers to the right, or negative charge carriers to the left. This goes both for ionic current, as well as for electronic current. Thus when we write that there is a certain electronic current of $I = 5$ A flowing from left to right through a wire to an anode, we can mentally depict this as a flow of $I/F \sim 50 \mu\text{mol/s}$ of electrons flowing in the opposite direction, out of this anode through the wire.

6. Note that we use both the terms current and current density to refer to a current in A/m^2 . Sometimes a current (density) is also in $\text{mol}/(\text{m}^2\cdot\text{s})$ (with symbol J_{ch} or J_F then often used), and multiplying by Faraday's number converts this current to A/m^2 . Sometimes current has the unit of A for the overall (integrated) current running across an electrode (from a connecting wire into electrolyte). In all these cases the symbol I is often used.

7. We use the word adsorption and absorption somewhat interchangeably without sticking to a formal distinction where adsorption is at a surface, and absorption inside a volumetric medium. This distinction is not always easy to make, and therefore we use both words in a flexible way.

8. When writing ordinary and partial differential equations, we prefer the use of ∂ over d if only for aesthetic reasons. We do not switch from ∂ to d when we go from a PDE to an ODE.

9. When we use the word 'potential' this most often refers to an electric(al) potential, i.e., a voltage, often in dimensionless units.

10. In many sections we discuss energies and pressures with units of mol/m^3 , while chemical potentials are dimensionless. All these quantities can be multiplied by RT to return to the usual dimensions of $\text{Pa}=\text{J/m}^3$ and J/mol . Sometimes a dimensionless chemical potential, μ_i , is described as: 'the chemical potential of species i is $5 kT$ ' but note that formally this means $\mu_i = 5$.

11. A word we very often use is 'ion', which is a dissolved and charged species in water (or in another electrolyte). It will be hydrated (when in water), i.e., have for instance 4 or 6 tightly bound water molecules surrounding it (especially for cations; for anions, ion hydration and the structure of this water shell is less pronounced). This entire entity is what in most cases we call the ion. For instance, if we refer to the volume of an ion in water, it is that of the ion plus its hydration shell, i.e., of the hydrated ion.

12. In general the water (which is the electrolyte that we focus on), contains anions (negatively charged ions) and cations (positively charged ions), and in addition there can be neutral species of all sorts. One example is when bicarbonate, HCO_3^- , is protonated to the neutral carbonic acid, H_2CO_3 . In this book, because so much of the theory equally applies to charged as well as such neutral species (solutes), please understand that 'ions' then not only refers to anions and cations, but also to species with a charge equal to zero. Thus, also H_2CO_3 can be called an ion, it just happens to have a zero charge, exactly in between the charge of anions and cations.

13. We use the term proton, or H^+ , as shorthand for the hydronium ion, H_3O^+ . Thus, where officially a reaction of H_3O^+ and OH^- involves two water molecules, in this shorthand method it seems to be

just one. This has no effect on resulting equations, because the concentration of water is not part of any of the equations anyway. (There are thermodynamic equations in relation to Gibbs formation energies where care is required, with the Gibbs energy of the proton set to zero, and the Gibbs energy of H₂O included.)

14. Charge is often in C or C/m² or C/m³, sometimes in mol/m², or mol/m³. The Faraday number makes the conversion between the C-based and mol-based charge.

15. Concentrations are denoted as c or as [...], and both notations have the same meaning. For volumetric concentrations the official unit is mol/m³ which is the same as mM. We also use M, and remember this is mol/L. When we present theory and calculation results, we are not introducing factors such as 10³ to address that a concentration in M or μM must be converted correctly, for instance to mol/m³. (We neither do that for other conversions for instance between nm and μm .) Concentrations can also be in (μ)mol/m² for a concentration per surface area. When using these ‘mol-based’ concentrations, in theory we then often make use of the gas constant, R , and Faraday’s constant, F . It is possible to translate to concentration in numbers per volume or area, by making use of Avogadro’s number, N_{av} (unit mol⁻¹). These concentrations are often denoted by n and for energies we then use the Boltzmann constant k_{B} , and the electronic charge e , instead of R and F , i.e., $n_{\infty} = c_{\infty} \cdot N_{\text{av}}$, $k_{\text{B}} = R/N_{\text{av}}$, and $e = F/N_{\text{av}}$.

16. We use the words ‘unit’ and ‘dimension’ interchangeably.

17. A multiplication between scalar quantities, or a scalar and a vector, is often denoted without an operator, such as in: $a b$. Alternatively, also the operators $*$, \times and \cdot are used in this book. In addition, we use the operator \cdot to describe the inner product of two vectors, such as in $\mathbf{I} \cdot \mathbf{E}$.

18. When we include acid-base reactions, involving (de-)protonation of ions, ions can be neutralized. For instance the bicarbonate ion can be protonated to a neutral carbonic acid molecule. In problems involving such neutralized species, we call all species ions. Thus some types of ions have a charge (valency) that is positive or negative, and for some ions valency is zero.

19. In water the concentration and fluxes of H₃O⁺- and OH⁻-ions are often of relevance. Instead of writing H₃O⁺ for the hydronium ion, we often use the shorthand of writing proton, or H⁺-ion.

20. The words increase, decrease, lower, higher, up, and down, are ambivalent for properties that can be both negative and positive. For all these words two meanings are possible, either referring to: 1. the numerical value moving left or right on the number scale, for instance a change from +1 to -2 is then a decrease, but 2. these words can also refer to a change in the magnitude of a numerical value. In that second meaning a change from -2 to -1 is a decrease. We try to avoid ambiguities and for instance in the latter case use the terminology ‘becomes less negative’. A useful term to indicate that a parameter (still a scalar quantity) can be both positive and negative, is to write that it ‘is signed’ or ‘has a sign’.

21. The words larger, smaller, more, less do not have the ambiguity just pointed out. They refer to the magnitude of a property going up or down, without consideration of a change in sign or direction. I.e., to write that a velocity becomes smaller, or becomes less, would never mean that it goes from +2 m/s to -1 m/s.

22. Interesting is what it means when we write or say ‘there is no current’ or ‘in the absence of current’. Most likely the intention is to convey there actually is information, namely that the *current is zero*. A transport model will use this information somewhere in the (numerical) solution. So there certainly ‘is’ a current conceptually, it just happens to have the numerical value of zero (it is zero). Similar is ‘We assume there is no Stern capacitance.’ or ‘We neglect the Stern capacitance.’ In this case we do not set the value of this capacitance to zero, but to infinity because only then is it ineffective. Thus in this case stating ‘we assume there *is* no capacitance’ relates to assigning an infinitely high value to it.
23. Somewhat different is a statement such as ‘the EDL has no volume.’ Here the intention is probably to inform that a proposed theory or model does not make use of volume as a relevant concept (but perhaps something else, such as area).
24. An interesting problem is the fact that pK and pH are both used as symbols for certain properties, in the same way that T is used as symbol for temperature, but at the same time pH and pK are the ‘written-out’ names of that property, i.e., ‘pH’ is both equivalent to ‘temperature’ and to ‘ T ’. Thus we could end up with a sentence such as: ‘In the vicinity of the surface, pH is around pH 7.5.’ This is not ideal, but we are not the ones who created this situation, so we consider it to be allowed to write it in this way. An alternative could be ‘..., the acidity is around pH 7.5.’ You may notice that with pH (and pK, and likewise other non-dimensional properties such as Re or Pe) one can leave out the =-sign between symbol and numerical value as in the above examples. This one would not do in general. For instance, for temperature, for instance, one would keep the =-sign, as in ‘..., temperature is $T = 30\text{ }^{\circ}\text{C}$.’ For pK we have a similar situation, and can end up writing ‘.. pK is pK 12.’ This is not ideal, but again, we are not the ones who created this situation. Other options could be ‘... the pK-value is pK 12’ or ‘... the equilibrium constant is pK 12.’ In all cases we desire to avoid a situation where a numerical value is not preceded by its associated symbol. Thus, we advise against writing: ‘The temperature was $12\text{ }^{\circ}\text{C}$ ’ or ‘... pH was 7.5.’
25. It is also ambivalent if we should use ‘the’ in relation to pH or pK. Our advise is to try and avoid the use of ‘the’ and thus we advise against writing ‘The pH ...’ This is because of the double meaning of pH as ‘written-out name’ and as symbol. In the same way we also wouldn’t write ‘The T is going up.’ But it cannot always be avoided, for instance at the start of a sentence, where we might have to use ‘The pH ...’ A way out can be ‘The pH-value’ or ‘the pK-value’. Nothing is ideal in this regard, which is something we have to live with. We did not create this situation.
26. Another intriguing problem in explaining physical theories is to describe that two sides of an equation are different, or are the same, or likewise that a parameter x and a parameter y ‘are the same’. A specific example we use on p. 170 is that we explain how transference numbers and transport numbers are fundamentally different physical properties, but still ‘can be the same’. This sound contradictory, parameters are different but also the same. Of course the meaning is that for certain conditions, these different entities have *the same numerical value*. Sometimes we do use this latter phrasing, that ‘they have the same (numerical) value’ but for readability we can also write ‘are the same’ or ‘they are equal’ when for a dedicated reader the intended meaning is clear.

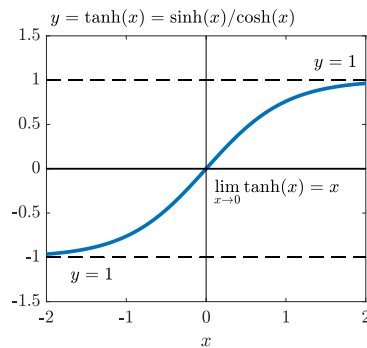
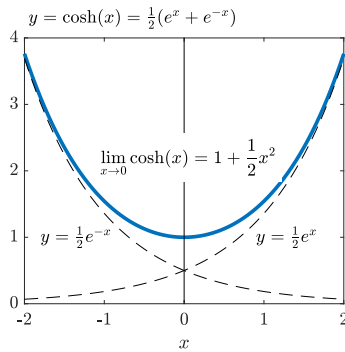
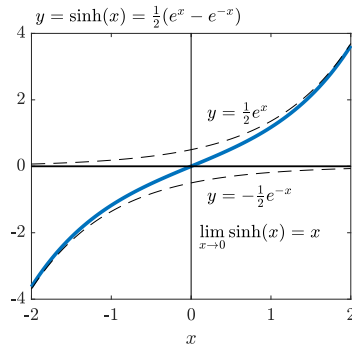
27. If we have an equation $a=b$, and if we arrive at physical information that tells us that the factor 'a' is zero (or because we make this assumption), then it is common to say that 'we set the left side of this equation to zero' and continue with $0=b$. Of course with this new information it is the case that we set both sides of the equation to zero, because each side is the same, that is why it is an equation. And actually, with the knowledge that $a=0$, we indeed typically continue the derivation based on $0=b$, i.e., what we effectively do is set b to zero, not a ! Now that we have pointed out that the standard way of phrasing how equations are manipulated is somewhat ambiguous, we can continue using it nonetheless. Thus with a mass balance $\partial c/\partial t = D \partial^2 c/\partial x^2$, we can say that we assume steady state, thus set the left side to zero, and continue with $D \partial^2 c/\partial x^2 = 0$. Note also that the following terminologies can all be used to mean the same: 'the left side,' 'the left-hand side (LHS)' or just 'on the left' or even 'left' (and of course the same for the right side, etc.).

28. 'Amphoteric' is a complicated word. In the context of charged surfaces the meaning is quite clear as a surface that can be charged positive and negative, see a box on p. 83. However, for ionic solutions the situation is much more ambivalent, where it has been associated with the capability 'of a compound' or 'of a substance' to act both as base and as acid. And it is not clear if by 'compound' and 'substance' reference is made to a family or group of ions (such as the entire group of three carbonate-related species), or whether reference is to a specific ion, such as the bicarbonate ion. The definition is only clear if it refers to specific ions, such as the bicarbonate ion, which indeed can react as acid and as base, and thus is amphoteric, while for instance the carbonate ion is not. In this book we do not use the term 'amphoteric' for ions or groups of ions in solution, but only use it to refer to materials or surfaces that can charge positively and negatively (as function of pH), see box on p. 83.

29. In science, the word 'problem' does not relate to something problematic, but instead it refers to the situation in front of one that must be dealt with, and that has been transformed into something tangible, tractable, doable, like a puzzle that hopefully can be solved. Merriam-Webster defines this meaning of the word as 'a question raised for inquiry, consideration, or solution.' Thus in this book we use the word 'problem' to describe many of the theoretical tasks that we first lay out and then tackle.

Hyperbolic functions

In the theory of electrochemical processes, the hyperbolic functions are used very frequently. Therefore we summarize in the figures below their most important characteristics, including limits for $x \rightarrow 0$ and $x \rightarrow -\infty, \infty$.





The authors at Tsinghua University, Beijing, May 2019.*

P. M. (Maarten) Biesheuvel
*Wetsus, European Centre of Excellence
for Sustainable Water Technology
Leeuwarden, The Netherlands*

J. E. (Jouke) Dykstra
*Environmental Technology
Wageningen University
Wageningen, The Netherlands*

For comments, corrections, and questions, you can email the authors at
authors@physicsofelectrochemicalprocesses.com